

# Nanobiomaterials in Tissue Engineering

Materials for Biomedical Engineering

# Nanobiomaterials in Tissue Engineering

Edited by

**Alina-Maria Holban**

*Faculty of Biology, University Politehnica of  
Bucharest, Bucharest, Romania*

**Alexandru Mihai Grumezescu**

*Faculty of Applied Chemistry and Materials Science,  
University Politehnica of Bucharest, Bucharest, Romania*



Elsevier

Radarweg 29, PO Box 211, 1000 AE Amsterdam, Netherlands

The Boulevard, Langford Lane, Kidlington, Oxford OX5 1GB, United Kingdom

50 Hampshire Street, 5th Floor, Cambridge, MA 02139, United States

Copyright © 2019 Elsevier Inc. All rights reserved.

No part of this publication may be reproduced or transmitted in any form or by any means, electronic or mechanical, including photocopying, recording, or any information storage and retrieval system, without permission in writing from the publisher. Details on how to seek permission, further information about the Publisher's permissions policies and our arrangements with organizations such as the Copyright Clearance Center and the Copyright Licensing Agency, can be found at our website: [www.elsevier.com/permissions](http://www.elsevier.com/permissions).

This book and the individual contributions contained in it are protected under copyright by the Publisher (other than as may be noted herein).

#### Notices

Knowledge and best practice in this field are constantly changing. As new research and experience broaden our understanding, changes in research methods, professional practices, or medical treatment may become necessary.

Practitioners and researchers must always rely on their own experience and knowledge in evaluating and using any information, methods, compounds, or experiments described herein. In using such information or methods they should be mindful of their own safety and the safety of others, including parties for whom they have a professional responsibility.

To the fullest extent of the law, neither the Publisher nor the authors, contributors, or editors, assume any liability for any injury and/or damage to persons or property as a matter of products liability, negligence or otherwise, or from any use or operation of any methods, products, instructions, or ideas contained in the material herein.

#### British Library Cataloguing-in-Publication Data

A catalogue record for this book is available from the British Library

#### Library of Congress Cataloging-in-Publication Data

A catalog record for this book is available from the Library of Congress

ISBN: 978-0-12-816909-4

For Information on all Elsevier publications  
visit our website at <https://www.elsevier.com/books-and-journals>



Working together  
to grow libraries in  
developing countries

[www.elsevier.com](http://www.elsevier.com) • [www.bookaid.org](http://www.bookaid.org)

*Publisher:* Matthew Deans

*Acquisition Editor:* Gwen Jones

*Editorial Project Manager:* Emma Hayes

*Production Project Manager:* Debasish Ghosh

*Cover Designer:* Greg Harris

Typeset by MPS Limited, Chennai, India

# List of Contributors

**Geeta Aggarwal**

Delhi Pharmaceutical Sciences and Research University, Government of NCT of Delhi, New Delhi, India

**Mudasir Ahmad**

Biopolymer Research Laboratory, Department of Chemistry, Jamia Millia Islamia, New Delhi, India

**Suhail Ahmad**

Biopolymer Research Laboratory, Department of Chemistry, Jamia Millia Islamia, New Delhi, India

**M. Teresa P. Amorim**

Centre for Textile Science and Technology (2C2T), Department of Textile Engineering, University of Minho, Campus of Azurém, Guimarães, Portugal

**Ecaterina Andronescu**

Department of Oxide Materials and Nanomaterials, Faculty of Applied Chemistry and Materials Science, Politehnica University of Bucharest, Bucharest, Romania

**Maria Filomena Barreiro**

Laboratory of Separation and Reaction Engineering - Laboratory of Catalysis and Materials (LSRE-LCM), Bragança Polytechnic Institute, Bragança, Portugal; Centro de Investigação de Montanha (CIMO), Instituto Politécnico de Bragança, Campus de Santa Apolónia, Bragança, Portugal

**Sonali Batra**

University Institute of Pharmaceutical Sciences, Panjab University, Chandigarh, India

**Amandeep Brar**

Department of Microbiology, School of Life Sciences, Central University of Rajasthan Bandarsindri, Kishangarh, India

**L. Calabrese**

Department of Engineering, University of Messina, Messina, Italy

**Juan-Ramón Campos-Cruz**

National Institute of Technology of Mexico/Aguascalientes Institute of Technology, Aguascalientes, Mexico

**Thakur Prasad Chaturvedi**

Faculty of Dental Science, Institute of Medical Sciences, Banaras Hindu University, Varanasi, India

**Marieta Costache**

Department of Biochemistry and Molecular Biology, Faculty of Biology, University of Bucharest, Bucharest, Romania



**Madalena Maria Dias**

Laboratory of Separation and Reaction Engineering - Laboratory of Catalysis and Materials (LSRE-LCM), Faculty of Engineering, University of Porto, Porto, Portugal

**F. Fabiano**

Department of Biomedical Sciences, Dentistry and Morphological and Functional Imaging, University of Messina, Messina, Italy

**Helena P. Felgueiras**

Centre for Textile Science and Technology (2C2T), Department of Textile Engineering, University of Minho, Campus of Azurém, Guimarães, Portugal

**Anton Fikai**

Faculty of Applied Chemistry and Material Science, Politehnica University of Bucharest, Bucharest, Romania

**Bianca Galateanu**

Department of Biochemistry and Molecular Biology, Faculty of Biology, University of Bucharest, Bucharest, Romania

**Alexandru Mihai Grumezescu**

Department of Oxide Materials and Nanomaterials, Faculty of Applied Chemistry and Materials Science, Politehnica University of Bucharest, Bucharest, Romania

**Sung Soo Han**

School of Chemical Engineering, Yeungnam University, Gyeongsan, South Korea; Department of Nano, Medical and Polymer Materials, Yeungnam University, Gyeongsan, South Korea

**Ariana Hudita**

Department of Biochemistry and Molecular Biology, Faculty of Biology, University of Bucharest, Bucharest, Romania

**Saiqa Ikram**

Biopolymer Research Laboratory, Department of Chemistry, Jamia Millia Islamia, New Delhi, India

**Anuj Kumar**

School of Chemical Engineering, Yeungnam University, Gyeongsan, South Korea; Department of Nano, Medical and Polymer Materials, Yeungnam University, Gyeongsan, South Korea

**Ashish Kumar**

School of Materials Science and Technology, Indian Institute of Technology (Banaras Hindu University), Varanasi, India

**Manish Kumar**

Department of Microbiology, School of Life Sciences, Central University of Rajasthan Bandarsindri, Kishangarh, India

**Jose Carlos Lopes**

Laboratory of Separation and Reaction Engineering - Laboratory of Catalysis and Materials (LSRE-LCM), Faculty of Engineering, University of Porto, Porto, Portugal

**Paramjot Maman**

Chitkara College of Pharmacy, Chitkara University, Patiala, India

**Kaiser Manzoor**

Biopolymer Research Laboratory, Department of Chemistry, Jamia Millia Islamia, New Delhi, India

**Manju Nagpal**

Chitkara College of Pharmacy, Chitkara University, Patiala, India

**Alexandra Elena Oprea**

Faculty of Applied Chemistry and Material Science, Politehnica University of Bucharest, Bucharest, Romania

**Lalit M. Pandey**

Department of Biosciences and Bioengineering, Indian Institute of Technology Guwahati, Guwahati, India

**Nidhi Pareek**

Department of Microbiology, School of Life Sciences, Central University of Rajasthan Bandarsindri, Kishangarh, India

**Roxana C. Popescu**

Department of Life and Environmental Physics, “Horia Hulubei” National Institute for Physics and Nuclear Engineering, Magurele, Romania;  
Department of Oxide Materials and Nanomaterials, Faculty of Applied Chemistry and Materials Science, Politehnica University of Bucharest, Bucharest, Romania

**Rajiv Prakash**

School of Materials Science and Technology, Indian Institute of Technology (Banaras Hindu University), Varanasi, India

**E. Proverbio**

Department of Engineering, University of Messina, Messina, Italy

**Norma-Aurea Rangel-Vázquez**

National Institute of Technology of Mexico/Aguascalientes Institute of Technology, Aguascalientes, Mexico

**Ricardo Rangel-Vázquez**

PCC, Haciendas Ave., Aguascalientes, Mexico

**Gabriela Ruphuy**

Laboratory of Separation and Reaction Engineering - Laboratory of Catalysis and Materials (LSRE-LCM), Faculty of Engineering, University of Porto, Porto, Portugal; Laboratory of Separation and Reaction Engineering - Laboratory of Catalysis and Materials (LSRE-LCM), Bragança Polytechnic Institute, Bragança, Portugal

**Lokesh Saharan**

Humanoid, Biorobotics and Smart Systems (HBS) Laboratory, Department of Mechanical Engineering, The University of Texas at Dallas, Richardson, TX, United States

**Varun Saxena**

Department of Biosciences and Bioengineering, Indian Institute of Technology Guwahati, Guwahati, India

**Sumit Sharma**

University Institute of Pharmaceutical Sciences, Panjab University, Chandigarh, India

**Ishani Shukla**

Department of Industrial & Management Engineering, Indian Institute of Technology Kanpur, Kanpur, India

**Yonas Tadesse**

Humanoid, Biorobotics and Smart Systems (HBS) Laboratory, Department of Mechanical Engineering, The University of Texas at Dallas, Richardson, TX, United States

**Rajul Vivek**

Faculty of Dental Science, Institute of Medical Sciences, Banaras Hindu University, Varanasi, India

**V. Vivekanand**

Centre for Energy and Environment, Malaviya National Institute of Technology, Jaipur, India

# Series Preface

In the past few decades there has been growing interest in the design and implementation of advanced materials for new biomedical applications. The development of these materials has been facilitated by multiple factors, especially the introduction of new engineering tools and technologies, emerging biomedical needs, and socioeconomic considerations. Bioengineering is an interdisciplinary field encompassing contributions from biology, medicine, chemistry, and materials science. In this context, new materials have been developed or reinvented to fulfill the need for modern and improved engineered biodevices.

A multivolume series, *Materials for Biomedical Engineering* highlights the most relevant findings and discusses key topics in this impressive research field.

Volume 1. *Bioactive Materials: Properties and Applications*, offers an introduction to bioactive materials, discussing the main properties, applications, and perspectives of materials with medical applications. This volume reviews recently developed materials, highlighting their impact in tissue engineering and the detection, therapy, and prophylaxis of various diseases.

Volume 2. *Thermoset and Thermoplastic Polymers*, analyzes the main applications of advanced functional polymers in the biomedical field. In recent years there has been a revolution in thermoplastic and thermosetting polymers with medical and biological uses, which are currently being developed for medical devices, drug delivery, tailored textiles, packaging, and tissue engineering.

Volume 3. *Absorbable Polymers*, describes the main types of polymers of different compositions with bioabsorbable and biodegradable properties. The biomedical applications of such materials are reviewed and the most innovative findings are presented in this volume.

Volume 4. *Biopolymer Fibers*, highlights the applications of polymeric fibers of natural biological origin in biomedical engineering. Such materials are of great utility in tissue engineering and biodegradable textiles.

Volume 5. *Inorganic Micro- and Nanostructures* and Volume 6. *Organic Micro- and Nanostructures*, deal, respectively, with the preparation and properties of inorganic and organic nanostructured materials with biomedical applications.

Volume 7. *Hydrogels and Polymer-Based Scaffolds*, discusses the recent progress made in the field of polymeric materials designed as scaffolds and tools for tissue engineering. The technological challenges and advances in their production, as well as current applications in the production of scaffolds and devices for regenerative medicine are presented.

Volume 8. *Bioactive Materials for Antimicrobial, Anticancer, and Gene Therapy*, offers an updated perspective regarding new bioactive materials with potential in the therapy of severe diseases such as infections, cancer, and genetic disorders.

Volume 9. *Nanobiomaterials in Tissue Engineering*, provides valuable examples of recently designed nanomaterials with powerful applications in tissue engineering and artificial organ approaches.

Volume 10. *Nanomaterials-Based Drug Delivery*, discusses the most investigated types of nanoparticles and nanoengineered materials with an impact in drug delivery. Applications for drug-therapy, and examples of such nanoscale systems are included in this volume.

This series was motivated by the need to offer a scientifically solid basis for the new findings and approaches relevant to the biomedical engineering field. This scientific resource collects new information on the preparation and analysis tools of diverse materials with biomedical applications, while also offering innovative examples of their medical uses for diagnoses and therapies of diseases. The series will be of particular interest for material scientists, engineers, researchers working in the biomedical field, clinicians, and also innovative and established pharmaceutical companies interested in the latest progress made in the field of biomaterials.

**Michael R. Hamblin<sup>1</sup> and Ioannis L. Liakos<sup>2</sup>**

<sup>1</sup>*Harvard Medical School, Boston, MA, United States*

<sup>2</sup>*Istituto Italiano di Tecnologia, Genoa, Italy*

# Preface

Tissue engineering (TE) has emerged as a promising alternative in the treatment of malfunctioning or lost organs and tissues. Over the last few decades, TE has demonstrated an unquestionable potential to regenerate damaged tissues and organs. Some tissue-engineered solutions have recently entered the clinic, but most of the pathologies of interest are still far from being solved. The purpose of this volume is to present the newest advances registered in the field on nanobiomaterials with direct applications in TE and regenerative medicine.

This volume is an international collection, containing 15 chapters prepared by outstanding authors, as follows:

Chapter 1, Nanobiomaterials for tissue engineering, by Ariana Hudita et al., presents different combinations of natural and synthetic polymers currently dominant as scaffolding materials in the TE field and that by various nanofabrication methods are capable of generating nanofiber scaffolds that bear a remarkable resemblance to the natural extracellular matrix (ECM). Nanoparticles used as drug delivery reservoirs loaded with biologically active molecules that can facilitate and accelerate the regeneration process can be also combined with other nanoelements for designing and fabricating TE scaffolds that can be subsequently employed in different TE applications.

Chapter 2, Resorbable biomaterials: role of chitosan as a graft in bone tissue engineering, by Kaiser Manzoor et al., discusses the recent development and future perspectives in the field of natural biopolymers such as chitosan and polyaminosaccharide, which widely take part as bone substitute, having suitable biomedical properties like biocompatibility, antiinflammatory, antimicrobial activity, biodegradability and nontoxicity, immunogenicity, controlled release behavior, mucoadhesive nature, and economic feasibility.

Chapter 3, Novel twisted and coiled polymer artificial muscles for biomedical and robotics applications, by Lokesh Saharan and Yonas Tadesse, describes twisted and coiled polymer (TCP) muscles that are made out of highly drawn polymer fibers such as nylon 6, nylon 6,6, and polyethylene, following specific material processing steps. The biomedical devices powered with TCP muscles can address the challenges associated with design and applications such as high actuation performance at lower material cost, which in turn improve the quality of life for patients.

Chapter 4, Electrospun nanofibers for tissue engineering applications, by Alexandra Elena Oprea et al., focuses on the artificial materials provided by TE to support three-dimensional tissue formation. To obtain proper tissue regeneration, it is important that the scaffold for TE application simulate the functional and also mechanical properties of ECM. Amongst the large numbers of scaffolding techniques, electrospinning is a remarkable one, which is able to produce nonwoven fibrous structures with dimensional constituents comparable to those of ECM fibers.

Chapter 5, Recent advances of chitosan composites in artificial skin: the next era for potential biomedical application, by Sumit Sharma and Sonali Batra, focuses on the chitosan composites explored for restoring damaged tissues and enhancing healing process by promoting rate of vascularization. Different techniques used for physicochemical modulation and variation in mechanical properties are being used to prepare biocompatible composites, which mimic the ECM and pave a promising pathway to biomaterial fabrication.

Chapter 6, Resorbable polymer fiber reinforced composites in biomedical application, by Paramjit Maman et al., defines the concept of composites and biocomposites and describes the use of biodegradable resorbable polymers for the formation of bioresorbable composites by combining with different reinforcing elements. The fabrication and mechanisms behind these modifications are presented and biomedical applications in context of bone tissue repair are discussed.

Chapter 7, Possibilities and perspectives of chitosan scaffolds and composites for tissue engineering, by Manish Kumar et al., emphasizes the assessment of chitosan scaffolds and composites for engineering of blood vessels, bone, articular and tracheal cartilage, skin, skeletal muscle, neural tissue, etc. Relationships of polymers' structural properties to their employment in tissue have been presented. Challenges and opportunities to improve polymer properties for fabrication of cost-effective materials for TE and regenerative medicine are summarized here.

Chapter 8, Hydroxyapatite: an inorganic ceramic for biomedical applications, by Varun Saxena et al., discusses the bioactive properties of hydroxyapatite, its modification by various elemental doping and substitutions along with the plausible applications such as drug delivery, dental applications, stem cell differentiation, treatment of osteomyelitis, and as a coating material by revisiting representative experimental results of several references along with some possible strategies to resolve the shortcomings of this polymer.

Chapter 9, Mechanical behavior of hydroxyapatite-based dental resin composites, by F. Fabiano et al., reviews conservative dental composites; the physical, mechanical and chemical properties of hydroxyapatite filled composites (e.g., by varying hydroxyapatite filler content, filler morphologies, etc.); and offers a critical overview of the literature. In addition, adequate polymerization of restorative composite is a fundamental factor to obtain optimal clinical performances. Key components on the potential applicative implications of hydroxyapatite-based dental resin composite and to define a systematic experimental selection of different methods to analyze the effect on mechanical and physical–chemical properties of hybrid ceramic-based composites are discussed.

Chapter 10, Molecular study of simulated body fluid and temperature on polyurethane/graphene polymeric nanocomposites: calcium carbonate and polymethyl methacrylate (PMMA) using dynamics modeling by Monte Carlo for applications in bone regeneration, by Juan-Ramón Campos-Cruz et al., describes the approaches to designing new biomaterials with specific properties by analyzing the behavior at the nanoscale. The authors have developed different models of computer simulation as molecular dynamics, dynamics of quasi-classical spin,

Langevin's and Boltzmann's equations, such as Monte Carlo simulations, which are performed through a repeating random sampling and simultaneously a statistical analysis is performed to obtain better results.

Chapter 11, New insights into nanohydroxyapatite/chitosan nanocomposites for bone tissue regeneration, by Gabriela Ruphuy et al., reveals the newest progress made on the use of nanohydroxyapatite/chitosan nanocomposites for their application in hard tissue regeneration.

Chapter 12, Production of polymer–bioactive glass nanocomposites for bone repair and substitution, by Helena P. Felgueiras and M. Teresa P. Amorim, reviews new trends in bioactive glass (BG) for bone and tissue regeneration. The most promising BG–polymer combinations and the advantages introduced in bone regeneration by these composites are enumerated, and this chapter explores some of the most commonly used synthesis techniques applied to the production of BG–polymer composites.

Chapter 13, Bioactive glass–based composites in bone tissue engineering: synthesis, processing, and cellular responses, by Anuj Kumar and Sung Soo Han, reviews the synthesis and processing of BGs and their use with various polymers as composite bone materials for load-bearing capacity and excellent cell viability during bone tissue regeneration.

Chapter 14, Mechanical and wear properties of nano titanium based dental composite resin, by Rajul Vivek et al., summarizes the study of mechanical and wear properties of PMMA resins modified by nano-Ti fillers along with the recent gist of other dentistry materials. The main purpose in conservative dentistry has been to restore the missing tooth substance by a restorative material with harmonizing significant properties like mechanical, physical, thermal, and wear properties.

Chapter 15, In vitro and in vivo technologies: an up to date overview in tissue engineering, by Roxana C. Popescu et al., presents an up to date overview of the in vitro and in vivo technologies in the TE field, with applications in the development of better tumor models for the study of mechanisms and possible therapeutic approaches.

**Alina-Maria Holban<sup>1</sup> and Alexandru Mihai Grumezescu<sup>2</sup>**

<sup>1</sup>*Faculty of Biology, University Politehnica of Bucharest, Bucharest, Romania*

<sup>2</sup>*Faculty of Applied Chemistry and Materials Science, University Politehnica of Bucharest, Bucharest, Romania*



# Nanobiomaterials for tissue engineering

# 1

**Ariana Hudita, Bianca Galateanu and Marieta Costache**

*Department of Biochemistry and Molecular Biology, Faculty of Biology, University of Bucharest, Bucharest, Romania*

## 1.1 INTRODUCTION

Tissue engineering (TE) represents a cutting edge branch of regenerative medicine, which relies on the latest progresses reported in cell biology, material science, and biomedical engineering to develop a proper biological substitute capable of restoring, maintaining, or improving the genuine function of a defective tissue (Walmsley et al., 2015).

Regardless of the numerous definitions available for TE, it is widely acknowledged that the key elements that represent the foundation of this field are represented by cells, scaffolds, and growth factors (Pereira et al., 2011) that are generally known as the “tissue engineering triad.” However, recent studies imply a TE scaffold-free approach, which promotes the lack of the tridimensional (3D) exogenous support material required for tissue regeneration. Indeed, the modern scaffoldless approach contradicts the basic principles of traditional TE, but this regenerative strategy comes with a poor mechanical support for tissue regeneration and so it addresses a significant limited number of tissue defects, focusing mainly on defective cartilages or vascular regeneration. Thereby, for the most part scaffolds are placed in the spotlight of the regenerative medicine field as they generally represent a mandatory element to obtain an engineered tissue.

Modern approaches in TE and regenerative medicine envisage the integration of nanotechnology in the development of nanostructured biomaterials with superior regenerative potential. The quite recent integration of nanotechnology into medicine is referred to as nanomedicine and it brings exciting opportunities to the development of innovative approaches in the field of drugs delivery systems development, imaging techniques, TE, and regenerative medicine. Nanotechnology enables the design and fabrication of nanoscaled biocompatible scaffolds and further controls the release of biological factors in space and time, controlling in this way the cell behavior to finally generate implantable tissues.

In vivo, cells within tissues are surrounded by an extracellular matrix (ECM), a natural web of hierarchically organized nanofibers (Stevens and George, 2005),

which provides support to the cells and directs their behavior. Furthermore, the ECM plays a key role in activating and regulating the storage and release of a wide range of biological active factors (Taipale and Keski-Oja, 1997) like growth factors for example. Recent advances in nanotechnology envisage the design and development of a nanoscale biomimetic microenvironment, which provides an analog to native ECM to cells. Consequently, nanostructured materials are able to mimic tissue-specific bioenvironments by designing bioconstructs with specific biochemical, mechanical, and electrical properties. Therefore *de novo* tissue can be engineered by employing these nanostructures for enhanced cell adhesion, growth, and differentiation. Additionally, the interaction of the cells with these biomimetic nanopatterns triggers dynamic ECM changes and also can induce the differentiation of stem cells without the addition of exogenous soluble biochemical factors (Kim et al., 2012). Nanosized materials, on the other hand, have attracted much attention for medical applications primarily due to their large surface to mass ratio that offers them unique features like the ability to adsorb and carry compounds, chemical reactivity, energy absorption, and biological mobility (Murthy, 2007).

Independent of the chosen material or fabrication method, the scaffold is designed based on a minimal number of characteristics that support its prospective use for *in vitro* production of engineered tissue and further *in vivo* applications. Briefly, a scaffold needs to be biocompatible, biodegradable, and consistent with the mechanical requirements of the tissue that is targeted for regeneration or replacement (Zhou and Lee, 2011).

Therefore the art of generating an ideal engineered tissue relies on obtaining the appropriate blend of the TE tools available to produce a final bioconstruct with mechanical, physical, and biological proprieties as close as possible to the native characteristics of the defective tissue. Since *in vivo* the cells are shielded within an ECM, the design process is usually based on the most promising biomaterials capable to mimic the ECM of the damaged tissue.

---

## 1.2 APPLICATIONS OF NANOENGINEERED SCAFFOLDS IN REGENERATIVE MEDICINE

Numerous studies show that the interaction between cells and their microenvironment may trigger the cytoskeleton's reorganization (Dinescu et al., 2015) as well as specific cell signaling that regulates the fate of the cell. In this context, nanostructured scaffolds that mimic the tissue-specific microenvironment (similar biochemical, mechanical, electrical properties and topography to those of native tissues) have attracted much attention in nanotechnology for TE and regenerative medicine as they are able to enhance cell adhesion, proliferation, and stem cell differentiation (Yang et al., 2014). Consequently, these nanodevices seem to be able to direct cellular behavior from cell adhesion to gene expression.

ECM-like architectures are produced by various methods such as nanopatterning, electrospinning, self-assembly, conjugation of adhesion molecules to the matrix, etc. (Kim et al., 2010a). Additional incorporation of nanomaterials like carbon nanotubes (CNTs), nanowires, or nanoparticles (NPs) in these architectures modulate the properties of the biomaterial (Dvir et al., 2011). For example, Galateanu et al. (2015) described the development of a bacterial cellulose and magnetic NPs nanocomposite biomaterial for efficient chronic wounds healing, while You et al. (2011) published a paper describing the development of an electrically conductive hybrid hydrogel scaffold based on gold NPs synthesized throughout a polymer template gel. Nanotopographical variations in the cell adhesion substrate can regulate differentiation of human mesenchymal stem cells towards adipocytes, chondrocytes, or osteocytes (Ahn et al., 2014; Dinescu et al., 2014, 2015).

Understanding the mechanisms regulating the pathways involved in cell–matrix interactions is crucial for designing further improved biomimetic nanoscaffolds that can even release bioactive agents in a controlled manner.

---

### 1.3 NANOSTRUCTURED POLYMERS AS TISSUE ENGINEERING SCAFFOLDS

As aforementioned, scaffolds play a pivotal role in the development of novel engineered tissues that aim to restore, replace, or regenerate impaired tissues (Rouchi and Mahdavi-Mazdeh, 2015). The choice of the material underlying the scaffold synthesis is dependent on the final application as it is essential to match the native biological and structural characteristics of the damaged tissue that requires regeneration or replacement. Despite the variety of materials available at the moment for scaffold fabrication (Ratner et al., 2004), biopolymers represent the favorite selection for developing biological substitutes for regenerative purposes. The main biocompatible and biodegradable polymers used for TE applications include natural polymers such as collagen, chitosan, silk, alginate, fibrin, gelatin, or synthetic polymers, counting among the most used polylactic acid (PLA), polyglycolic acid (PGA), poly- $\epsilon$ -caprolactone (PCL), poly(lactic-co-poly(glycolic acid)) (PLGA), poly(L-lactic acid), polyacrylamide, polyurethane (PU), polyethylene terephthalate, polymethyl methacrylate, polyethylene oxide, and polyvinyl alcohol (PVA).

Based on the rapid development of the nanotechnologies currently available for producing nanoscaled scaffolds, polymers can be used as bulk material to produce bi- (2D) or 3D nanoscaled systems in form of nanocomposites, nanogels, or nanofibers. Among these formulations, polymers are currently being intensively used for obtaining nanofibrous scaffolds, through different synthesis strategies such as electrospinning, self-assembly, or phase separation. Electrospinning technique (Li et al., 2002) is currently the most intensively used method for obtaining

polymeric nanofibers due to the fact that it is a relative easy method and offers increased flexibility of the input material. Even if the scaffolds fabricated by electrospinning resemble the natural ECM in terms of morphology, they usually present a smooth surface and fail to provide cells the nanostructure topography that features *in vivo* the natural collagen nanofibrils; this matter can easily impact in a negative manner cell attachment, growth, and proliferation (Fang et al., 2013; Fiedler et al., 2013), so during the scaffolding process other reinforcement strategies can be used to tailor the biological response of cells during scaffold interaction.

### 1.3.1 NATURAL AND SYNTHETIC POLYMERS

To benefit from their enhanced biocompatibility, natural polymers have been widely used for nanostructured polymeric scaffold synthesis. The use of natural polymers as part of the scaffold manufacturing process represent a smart approach since they exhibit several important advantages beyond their excellent biocompatibility (Sabir et al., 2009). Natural polymers are biologically active, therefore they are more likely to promote cellular adhesion and sustain cellular proliferation and differentiation towards the cellular type needed. More, natural polymers are biodegradable and the degradation rate can be easily customized by cross-linking with different agents to adjust the scaffold degradation rate consistent with the targeted application. However, issues like immunogenicity and their poor mechanical properties that limit their TE applications still need to be addressed (Sano et al., 2003; Saravanan et al., 2016).

The most common option for generating nanostructured scaffolds from the vast variety of natural polymers available is collagen, since this protein is the predominant structural protein in the ECM and it can be easily isolated and purified. Collagen exhibits several unique characteristics that convert this protein into an ideal material for scaffold fabrication such as excellent biocompatibility, immunogenicity, and a natural capacity to promote cellular adhesion and proliferation. Thus collagen has been exhaustively used for biomedical scaffold applications such as wound healing (Ma et al., 2003), cartilage regeneration (Vazquez-Portalatin et al., 2016; Mohan et al., 2018; Halili et al., 2018) bone TE (Montalbano et al., 2018; Wang et al., 2018a; He et al., 2018), and neural and vascular reconstructive strategies (Ding et al., 2011; Yan et al., 2018; Schuh et al., 2018). With the help of the current nanotechnologies available, collagen can easily be reconstituted into nanofibrous structures that mimic the native ECM of the tissues. Gelatin, a derivative of collagen obtained by hydrolysis is becoming lately more appealing than collagen since it presents a lower antigenicity as compared with its precursor, but can still naturally facilitate cellular adhesion, proliferation, and differentiation (Malafaya et al., 2007).

Pristine collagen was successfully employed in studies aiming at nerve tissue regeneration scaffold fabrication. For example, Timnak and colleagues synthesized a nanofibrous porous scaffold based on collagen and chondroitin sulfate

using electrospinning as method for generating polymeric nanofibers. The use of chondroitin sulfate as glycosaminoglycan component of the final composite obtained was sustained by the potential of this biological molecule to support and accelerate tissue regeneration and to promote cell–scaffold interaction (Shaoping et al., 2005, 2007). More, for increasing the biocompatibility of the scaffold, genipin was preferred as cross-linking agent at the expense of the widely used glutaraldehyde due to its significant reduced cytotoxicity. The potential of the scaffold to sustain cellular attachment and to sustain cellular viability and proliferation was investigated using the SK-N-MC human neuroblastoma cell line as in vitro cell culture model. Results showed that the novel scaffold obtained presents a good biocompatibility and easily allowed the attachment of the human neuroblastoma cells. Also, controlling the orientation of the polymeric fibers throughout the synthesis process presented a positive impact upon the cellular outgrowth orientation (Timnak et al., 2011).

Silk fibroin (SF) represents a fibrous protein that can be easily isolated from silk, apart from its secondary globular component sericin. Even if a large spectrum of natural sources is available for harvesting SF, *Bombyx mori* is extensively used as the primary isolation source at the moment. Generally, for TE applications SF was subjected to a scaffold prefabrication step called degumming (Kim et al., 2017a) to be totally cleansed from sericin, which can alter its noncytotoxic potential. Although degumming was initially an essential step in scaffold fabrication protocols, recent studies report sericin as a biocompatible material for TE, since it generates toxic effects only in combination with SF. Properly degummed SF is a promising candidate for TE applications since it distinguishes excellent mechanical proprieties, unlikely from other natural polymers. SF is a biocompatible and biodegradable polymer, which triggers a minimal inflammatory response upon implantation (Faokhi et al., 2016; Ju et al., 2016). The degradable rate of SF scaffold is slow due to the in vivo proteolytic activity, but it can be customized depending on the targeted TE application by modifying different mechanical settings of the scaffold synthesis procedure (Horan et al., 2004). SF has been successfully employed in different TE applications such as cardiovascular TE (Zhang et al., 2010a).

To increase the mechanical and biological proprieties of the human amniotic membrane (HAM) as bioengineered skin substrate, the deepithelized HAM was reinforced with electrospun SF nanofibers. The novel bilayer scaffold obtained has shown superior mechanical and in vitro biological proprieties as compared with pristine HAM, being a good candidate for skin TE (Arasteh et al., 2016).

A micro/nanoporous pattern of a SF scaffold was obtained by Xiao et al. (2017) that presented a modified salt-leaching process for generating novel SF scaffolds that presented an enhanced potential for stimulating cell proliferation and differentiation of bone marrow mesenchymal stem cells as compared with SF scaffolds obtained by conventional methods.

A simple SF/hydroxyapatite (HAp) scaffold can promote osteoblast adhesion and sustain the early stage osteogenic differentiation (Wei et al., 2011). Recently,

Niu et al. fabricated a potential bone TE scaffold composed by a mix of nanofibrous SF with HAp NPs and bone-morphogenetic protein 2 (BMP-2) to boost the osteoinductive potential of the synthesized scaffold. The addition of HAp and BMP-2 upgrades the mechanical characteristic of simple SF scaffold and intensifies the bioactivity of the scaffold; the bone-marrow stem cells (BMSCs) succeeded to attach to the surface and presented an excellent viability, followed by successful in vitro osteogenic differentiation (Niu et al., 2017).

Other biocompatible and biodegradable natural polymers have been intensively used for TE scaffold fabrication. Chenghong et al. (2017) fabricated an electrospun cellulose nanofiber scaffold improved with nanoHAp for bone tissue regeneration that showed good biocompatibility, with low cytotoxicity even at high concentrations of nanoHAp.

Zang et al. synthesized bacterial cellulose (BC) tubes from *Gluconacetobacter xylinum* using for the first time polydimethylsiloxane as fabrication mold. This method seems to be viable for obtaining tubular scaffolds for vascular TE as the obtained scaffolds presented good mechanical properties and high thermal stability, together with great biocompatibility as revealed by the in vitro viability and proliferation assays performed on vessel-connected cell cultures (endothelial cells, smooth cells, and fibroblasts). The in vivo results sustained the scaffold biocompatibility and reveal that the BC tubes lack ability to induce an immune response (Zang et al., 2015).

For fabricating antibacterial wound dressings, which is extremely useful to amplify the regeneration process, Liakos et al. (2017) fabricated electrospun fiber pads of cellulose acetate combined with different essential oils that presented great antimicrobial properties when tested against microbial species that are constantly present in infections and particularly difficult to treat, while Tabaii and Emtiazi (2018) synthesized nontoxic bacterial cellulose membranes impregnated with silver NPs that presented great biocompatibility and hold great promise in enhancing the antibacterial activity of classical antibiotics such as gentamicin.

Synthetic polymers, mainly PGA, PLA, and PCL, have also been employed in designing TE scaffolds, since the costs involved for scaffold fabrication are reduced compared with the exclusively natural polymeric scaffolds and also because they are easier to process. More, the mechanical properties of synthetic polymer based scaffolds are on the whole superior as compared with natural ones, but they lack ability to provide the necessary biological cues for cell adhesion, usually due to their hydrophobic nature. Even if the degradation products are represented by metabolites naturally present in the human body, the acid nature of the degradation products can still trigger inflammation reaction, but usually the immune reactions cannot be compared in magnitude with those activated by natural polymers (Liu et al., 2012). Mainly due to their lack of bioactivity, synthetic polymers are blended with polymers isolated from natural sources for a synergistic effect that can improve the final mechanical and biological performance of the TE scaffold fabricated or functionalized with bioactive elements for the same purpose (He et al., 2009; Liu et al., 2012; Guo et al., 2015).

### 1.3.2 BLENDED POLYMERS FOR SMART HYBRID SCAFFOLD FABRICATION

Thus to fabricate an ideal scaffold for TE applications, the latest trend is to efficiently blend natural and synthetic polymers to fully benefit from the strengths of both classes of polymers. Generally, the synthetic polymer based scaffolds present excellent mechanical proprieties required for different TE applications, but lack ability to encourage cellular adhesion and usually exhibit poor biocompatibility. In contrast, natural polymers produce highly biocompatible and bioactive scaffolds that provide cells biological cues for attachment and further sustain cellular proliferation and differentiation. Therefore several recent studies have been carried out on fused natural and synthetic polymers scaffolds that can increase the odds to obtain ECM-like constructs in terms of mechanical and biological proprieties. This approach has been successfully used for a large number of TE applications.

For example, Shen et al. evaluated the synergic effect of combining two nanoscaled strategies for obtaining an effective scaffold intended for dentin TE; it has been shown that PLA, used frequently for periodontitis treatment (Wu et al., 2010; Li et al., 2013) produces an inflammatory response generated by its degradation products (Wu et al., 2015) and also presents a poor hydrophilicity that can alter the scaffold potential to sustain cell adhesion, proliferation, and differentiation (Kim et al., 2006; Khorasani et al., 2008). Indeed, endorsing the PLA nanofibers with chitosan NPs overcomes these drawbacks.

For skin regeneration purposes, Sharif and colleagues successfully fabricated a collagen-coated PCL scaffold that showed a significantly improved cell adhesion and proliferation support for human endometrial stem cells as compared with simple PCL scaffold (Sharif et al., 2018).

Electrospun nanofibers generated from bacterial cellulose have been used as reinforcement of PVA-based scaffolds (Palaninathan et al., 2018), obtaining increased biocompatibility confirmed by L929 mouse fibroblast adhesion and proliferation for the final PVA/bacterial cellulose scaffold that can be further employed in different TE applications.

A novel PCL/collagen/nanobioglass was highlighted as an excellent candidate in nerve tissue regeneration as it promotes the in vitro capacity of endometrial stem cells to adhere and proliferate (Mohamadi et al., 2017).

Even if several studies that confirm the benefits of using nanofibrous scaffolds and sustain their prospective use in TE are available, this approach presents disadvantages that can hamper the design of a final ECM-mimicking 3D scaffold. Regardless of the choice of material for fabrication, the conventional nanofibrous scaffold obtained provide a superficial porous structure consisting of pores of very small size that can obstruct the cellular migration process within the scaffold (Kim et al., 2010b; Sisson et al., 2010;) and diminish the cellular infiltration, which leads to fabricating a scaffold that is capable only of generating 2D bioconstructs. To overcome this issue nanostructured polymers can be easily merged



with microstructured ones (Tuzlakoglu et al., 2011), usually using dual extrusion electrospinning technique.

For instance, Kim et al. fabricated a composite scaffold blending micro-PCL with nano-SF to promote bone regeneration. Compared with the simple microfibrous PCL scaffold, the addition of nano-SF considerably improved the bioactivity of the novel scaffold synthesized in terms of cellular adhesion, proliferation, and osteogenic differentiation of human mesenchymal stem cells. More, when implanted *in vivo* in the calvarial defects of rabbits the scaffold stimulated new bone formation (Kim et al., 2015).

Also for bone tissue regeneration, Kwak et al. used nanofibrous collagen in the design of a hybrid nano/microscaffold to enhance the scaffold potential to stimulate cell attachment and sustain proliferation and differentiation. Microfibrous PLGA meshes were alternated with nanofibrous meshes of collagen and endorsed or not with nanorods of HAp and showed a significantly increased potential in sustaining cellular adhesion, proliferation, and osteogenic differentiation of MC3T3-E1 cells as compared with the simple PLGA scaffold (Kwak et al., 2016).

Sarkar and teammates fabricated a layered nano/microfibrous chitosan/collagen scaffold as dermal substitute. The future use of this scaffold with combined micro- and nanoarchitecture in skin TE was sustained by the excellent biocompatibility established *in vitro* on fibroblasts and keratinocytes (Sarkar et al., 2013).

### 1.3.3 OTHER NANOSTRATEGIES COMBINED WITH POLYMERIC SCAFFOLDS

Even if the polymeric scaffolds are intensively used in TE, the scaffolding process needs to be dynamically adapted to the diverse and growing needs of regenerative medicine so it is important to take advantage of other promising materials available that can boost the performance of the synthesized scaffolds. In this view, different materials such as CNTs or carbon nanofibers (CNFs), HAp, and NPs have been exploited for nanocomposite designing and processing, usually for TE applications that require high mechanical strength. For fabrication of polymeric based hybrid scaffolds, the amount of CNTs or CNFs embedded in the final construct needs to be carefully selected and optimized since it can affect the fiber diameter, the overall mechanical properties, and the biological yield in terms of cell adhesion, proliferation, or differentiation. For scaffolding, CNTs can be used in form of single sheets of graphite known as single-walled CNTs, but the preferred option remains the multiwalled carbon nanotubes (MWCNTs) that are constructed by multiple concentric graphite cylinders and present larger diameters than the single-walled type (Lin et al., 2004).

The CNTs and CNFs are hollow nonbiodegradable materials, with outstanding physical properties, characterized by nanosizes, the CNTs being smaller (1–30 nm) in diameter as compared with CNFs (50–200 nm). Both nanostructures are widely



used for biomedical applications in nanocomposite designing and synthesis, usually as reinforcement agents for polymeric scaffolds targeting hard TE applications. Despite their popularity for osteoinductive scaffold synthesis, CNTs have been used successfully as tissue scaffolds for cardiac constructs (Wickham et al., 2014; Ren et al., 2017; Ho et al., 2017; Sun et al., 2017) or nerve regeneration (Kuzmenko et al., 2016; Singh et al., 2016; Vallejo-Giraldo et al., 2016; Lv et al., 2017; Lee et al., 2018).

Since CNTs/CNFs-based nanocomposites are mechanically robust, it is not surprising that most of the applications developed are aimed at bone tissue regeneration. By external electrical stimulus the osteoblasts' biological activity, adhesion, proliferation potential, and osteogenic differentiation process can be modulated so the great conductivity of CNTs can be exploited to improve the osteoblasts' performance (Meng et al., 2013). More, CNTs can be easily functionalized with a vast variety of biomolecules to diminish their cytotoxic potential and proinflammatory potential, making the CNTs a remarkable biocompatible nanomaterial for TE (Dumortier et al., 2006).

Abdorreza et al. (2017) synthesized a gelatin/chitosan scaffold reinforced with functionalized MWCNTs that presented good porosity, superior mechanical properties, and facilitated biomineralization, being a suitable candidate for bone TE.

Shrestha and colleagues fabricated an electrospun PU scaffold reinforced with functionalized MWCNTs and zinc oxide (ZnO) NPs that presented a remarkable mechanical profile, with enhanced electrical conductivity. The biocompatibility of the nanocomposite was highlighted by MC3T3-E1 preosteoblasts behavior showing that the scaffold stimulates cellular adhesion, proliferation, and differentiation and sustains cellular survival. Addition of functionalized MWCNTs, together with ZnO NPs significantly enhanced the alkaline phosphatase activity (ALP) and collagen I secretion, confirming the capacity of the nanocomposite to promote osteogenic differentiation of MC3T3-E1 preosteoblasts. More, the novel nanocomposite was found to present antibacterial activity and to promote biomineralization, validating this scaffold as a proper osteoinductive candidate (Shrestha et al., 2017).

For reinforcement purposes, a PCL polymeric scaffold was decorated with MWCNTs and presented satisfactory biocompatibility as revealed by the viability assays performed in vitro on rat bone marrow-derived stroma cells. More, the presence of CNTs in the composite scaffold facilitated osteogenic differentiation as suggested by the elevated levels of the bone marker ALP and enhanced the mechanical properties of the nanocomposite as compared with neat PCL scaffolds. As clearly pointed by Pan et al. (2012), the CNT levels need to be thoroughly adjusted since they can impact the scaffold potential to promote cellular proliferation and differentiation. More recently, a PCL/CNTs scaffold with a unique shish-kebab structure was synthesized. Inspired by previous studies that described different variations of the shish-kebab structure and also highlighted the positive effect of this pattern upon cellular attachment and propagation (Li et al., 2005, 2006; Wang et al., 2013), Wu et al. fabricated a shish-kebab-structured

CNTs/PCL original scaffold, by screening different concentrations of CNTs to select the optimal one for the desired nanotopography. The resulting scaffold exhibited an excellent biological performance as they allowed MG-63 cells to attach and further enhanced their proliferation potential (Wu et al., 2017).

Carboxyl functionalized MWCNTs were blended with PLGA using solvent casting technique and the biological activity of the obtained nanocomposite was evaluated *in vitro* on rat bone marrow-derived mesenchymal stem cells. Functionalizing the MWCNTs appeared to improve the final pattern of the composite, since it allowed a better dispersion of the CNTs in the polymeric matrix in contrast to simple MWCNTs and also exhibited superior mechanical attributes. In terms of biological effects, the functionalized MWCNTs promoted cellular attachment, growth, and stimulated osteogenic differentiation (Lin et al., 2011).

A chitosan HAp mixed scaffold was grafted with functionalized MWCNTs, clearly stimulated cellular adhesion and proliferation, showing a twofold increase of the MG-63 cells followed by notable mechanical proprieties, in comparison with simple chitosan (Venkatesan et al., 2011).

McKeon-Fisher et al. fabricated a scaffold designed for skeletal muscle TE by shuffling electrospun PCL nanofibers, MWCNTs, and a binary polymeric hydrogel based on PVA and PLA. The mixed scaffold presented superior conductivity and displayed a slightly elevated ratio of attached cells. Even if the addition of CNTs boosts the mechanical proprieties over those of rat and pig skeletal muscle, the original nanocomposite is a promising agent for skeletal muscle repair (McKeon-Fischer et al., 2011).

An original hybrid scaffold based on electrospun mixture of poly(3-hydroxybutyrate) (PHB), chitosan, and MWCNTs functionalized with carboxylic acid on knitted degummed silk randomly was evaluated in terms of physical and mechanical characteristics. A higher concentration of 1% MWCNTs was preferred for further use in TE, based on great tensile strength, good porosity, and enhanced hydrophilicity, but a biocompatibility evaluation needs to be performed to evaluate if the 1% MWCNTs are suitable for cell adhesion and growth (Mirmusavi et al., 2018).

Graphene oxide (GO) is another versatile carbon-based material in fashion especially for bone TE applications (Cicuéndez et al., 2017; Kim et al., 2017b, 2018a), but its cytotoxicity still remains a barrier in developing GO-based scaffolds. The GO-based materials exhibit generally poor biocompatibility as they decrease cell viability by activating death protease caspase-3 and subsequently inducing a necrotic cellular status (Zhang et al., 2010b; Qu et al., 2013), together with an increment of the oxidative stress. Thus pristine GO scaffolds need to be functionalized to surpass their cytotoxicity, a modern strategy being the addition of hydrophilic nontoxic polyethylene glycol coatings that improve the physical properties of GO and also create a friendly environment for cellular survival (Yang et al., 2013; Chu et al., 2018).

Bioceramics are highly popular for TE scaffolds development as they can tailor the biological quality of the final constructs, especially by enhancing

osteoinductivity for bone-like scaffolds. Naturally, HAp is found in the inorganic phase of the ECMs of hard tissues so it can be a smart choice of reinforcing agent for enhancing the osteogenic capacity of hard tissue TE scaffolds. Different derivatives of HAp have been successfully employed in scaffolding processing such as biodegradable PCL/SF/HAp porous scaffold with superior osteoconductive and osteoinductive proprieties synthesized by supercritical foaming (Diaz-Gomez et al., 2017); biocompatible cellulose/HAp scaffold with great mechanical proprieties and ECM-like measurements (Ao et al., 2017); a nHA/PLGA scaffold that presented improved in vivo bone formation for femur bone defects in a rabbit model at lower amounts of HAp, showing the importance of optimizing the HAp amounts for TE applications (He et al., 2016); an electrospun PCL/nanocellulose fibrous scaffold was decorated with a layer of HAp by simulated body fluid immersion (Si et al., 2016); simple collagen matrices embedded with HAp microspheres that significantly increased cell viability and can be also used as drug-delivery vehicles (Cholas et al., 2016); or an osteoblast conditioning gelatin/HAp nanocomposite that positively impacts the osteoblasts' behavior in terms of viability and proliferation and is capable of almost fully regenerating bone defects within 3 months as shown in vivo on critical size bone defects created on rat calvarium (Samadikuchaksaraei et al., 2016).

For a prospective use in magnetic field—assisted TE, designing and processing scaffolds can also involve magnetic materials. Scaffold enrichment with magnetic materials, generally in the form of magnetic NPs, are extremely useful to guide cells to the defective sites or to accelerate the regeneration process (Qu et al., 2018). Scaffolds with magnetic proprieties can be further used for different applications such as nerve regeneration (Li et al., 2002), cardiac TE (Sun et al., 2018) bone repair (Hu et al., 2018), or wound healing (Galateanu et al., 2015).

Traditionally, the field of nanomedicine encompasses the use of NPs as smart nanocarriers that are capable of rejuvenating the classical therapeutic strategies currently available for cancer management (Radu et al., 2017; Kabary et al., 2018; Jin et al., 2018; Wu et al., 2018; Li et al., 2018) due to the capacity of the nanosized delivery systems to offer protection against degradation of the encapsulated therapeutic agents and further enable their sustained and controlled release. The encapsulated drugs can be either classical chemotherapeutic agents or novel synthesized molecules with potential anticancer effects and can be loaded alone or in different combinations to take advantage of their potential synergistic anticancer effect. More, NPs have been used for improving antibacterial and antifungal approaches (Popescu et al., 2017; Limban et al., 2018; Wang et al., 2018b; Kim et al., 2018b) or improving the current imaging techniques available (Sheng et al., 2014). Thus NPs acquire a great potential mainly as drug carriers and their outstanding benefits as potential TE tools have been used in a secondary role. However, to fulfill the TE's principal scope, NPs can easily decorate the scaffold surfaces or can be embedded in the scaffold body and further used as delivery vehicles for different biological molecules that can facilitate cellular adhesion, proliferation,

and differentiation and overall accelerate and sustain the regeneration process, and recent studies sustain the positive impact of NPs-based approaches upon their prospective use in TE applications (Modaresifar et al., 2017; Piran et al., 2018; Hasan et al., 2018; Yao et al., 2018; Qu et al., 2018; Arslan et al., 2018; Raftery et al., 2018).

---

## **1.4 DNA NANOTECHNOLOGY, A PROMISING APPROACH IN TISSUE ENGINEERING**

Bionanotechnology researchers are approaching new techniques for attaching DNA nanoarrays to cell surfaces for various reasons including cell labeling; the targeted delivery of drugs, NPs, or CNTs; or even gene silencing. Another approach in this field is to engineer microtissues of cell/cell networks by using self-hybridizing properties of single stranded DNA molecules. DNA origami is a structural DNA-based nanotechnology that was developed during the past 30 years and that consists of the use of programmed combinations of short complementary oligonucleotides to fold a large single strand of DNA into 2D and even 3D architectures (Kearney et al., 2017). The ability to precisely pattern and orient protein molecules with nanometer precision may enable researchers to study intricate protein–protein interactions and construct novel biomaterials for applications such as TE.

DNA origami can be used to develop a wide range of particle shapes and sizes and for this reason is an excellent candidate for the study of, and application in, drug delivery and TE. Recently, DNA nanotechnology applications combining DNA with proteins or cellulose offer promising solutions for creating biomimetic ordered structures with potential use in biomedical applications.

---

## **1.5 CONCLUSIONS AND FURTHER PERSPECTIVES**

For the development of an ideal scaffold, the conventional fabrication methods must be adapted to the latest progresses reported in TE-linked research areas. Natural and synthetic polymers represent an appealing choice for scaffold fabrication due to their remarkable biocompatibility and combined with nanofabrication methods such as electrospinning or self-assembly hold great promise in generating a synthetic duplicate of the ECM that promotes and sustains tissue regeneration. Likewise, inserting in scaffolds different NPs loaded with biologically active molecules such as growth factors or differentiation inducers that intensify the regeneration process represents another promising nanosized approach for TE applications. Thus inserting nanoscaled elements in the scaffold design and fabrication process enhances the scaffold's potential to bear resemblance to the natural ECM and leads to a significantly increased potential of the novel synthesized

scaffold to facilitate cellular adhesion and to further sustain proliferation and differentiation.

In conclusion, both the regulation of cellular behavior through nanotechnology as well as the benefits of nanoscale are crucial aspects demonstrating the great promise that nanoengineering holds in biomedicine. Notably, the technologies presented generate nanotopographic surfaces and nanofeatured scaffolds with great promise in further improvement of regenerative outcomes. 3D nanostructured biomaterials-based scaffolds hold a promising future for successful TE applications.

---

## REFERENCES

- Abdorreza, S., Mesgar, Z.M., Setareh, K., 2017. Improvement of mechanical proprieties and in vitro bioactivity of freeze-dried gelatin/chitosan scaffolds by functionalized carbon nanotubes. *Int. J. Poly. Mater. Poly. Biomater.* 67 (5), 267–276.
- Ahn, E.H., Kim, Y., Kshitiz, An, S.S., Afzal, J., Lee, S., 2014. Spatial control of adult stem cell fate using nanotopographic cues. *Biomaterials* 35 (8), 2401–2410.
- Ao, C., Niu, Y., Zhang, X., He, X., Zhang, W., Lu, C., 2017. Fabrication and characterization of electrospun cellulose/nano-hydroxyapatite nanofibers for bone tissue engineering. *Int. J. Biol. Macromol.* 97, 568–573.
- Arasteh, S., Kazemnejad, S., Khanjani, S., Heidari-Vala, H., Akhondi, M.M., Mobini, S., 2016. Fabrication and characterization on nano-fibrous bilayer composite for skin regeneration application. *Methods* 99, 3–12.
- Arslan, A., Çakmak, S., Gümüşderelioğlu, M., 2018. Enhanced osteogenic activity with boron-doped nanohydroxyapatite-loaded poly(butylene adipate-co-terephthalate) fibrous 3D matrix. *Artif. Cells Nanomed. Biotechnol.* Available from: <https://doi.org/10.1080/21691401.2018.1470522>.
- Chenghong, A., Yan, N., Zhang, X., He, X., Zhang, W., Lu, C., 2017. Fabrication and characterization of electrospun cellulose/nanohydroxyapatite nanofibers for bone tissue engineering. *Int. J. Biol. Macromol.* 97, 568–573.
- Cholas, R., Padmanabhan, K., Gervaso, F., Udayan, G., Monaco, G., Sannio, A., et al., 2016. Scaffolds for bone regeneration made of hydroxyapatite microspheres in a collagen matrix. *Mater. Sci. Eng. C Mater. Biol. Appl.* 63, 499–505.
- Chu, J., Panpan, S., Yan, W., Fu, J., Yang, Z., He, C., et al., 2018. PEGylated graphene oxide-mediated quercetin-modified collagen hybrid scaffold for enhancement of MSCs differentiation potential and diabetic wound healing. *Nanoscale* 10, 9547–9560.
- Cicuéndez, M., Silva, V.S., Hortigüela, M.J., Matesanz, M.C., Vila, M., Portolés, M.T., 2017. MC3T3-E1 pre-osteoblast response and differentiation after graphene oxide nanosheet uptake. *Coll. Surf. B Biointer.* 158, 33–40.
- Díaz-Gomez, L., García-González, C.A., Wang, J., Yang, F., Aznar-Cervantes, S., Cenis, J. L., 2017. Biodegradable PCL/fibroin/hydroxyapatite porous scaffolds prepared by supercritical foaming for bone regeneration. *Int. J. Pharm.* 527 (1–2), 115–125.
- Dinescu, S., Galateanu, B., Lungu, A., Radu, E., Nae, S., Iovu, H., et al., 2014. Perilipin expression reveals adipogenic potential of hADSCs inside superporous polymeric cellular delivery systems. *BioMed Res. Int.* 2014, 830791.

- Dinescu, S., Galateanu, B., Radu, E., Hermenean, A., Lungu, A., Stancu, I.C., 2015. A 3D porous gelatin-alginate-based-IPN acts as an efficient promoter of chondrogenesis from human adipose-derived-stem-cells. *Stem Cells Int.* 2015, 252909.
- Ding, T., Lu, W.W., Zheng, Y., Li, Z.Y., Pan, H.B., Luo, Z., 2011. Rapid repair of rat sciatic nerve injury using a nanosilver-embedded collagen scaffold coated with laminin and fibronectin. *Regen. Med.* 6 (4), 437–447.
- Dumortier, H., Lacotte, S., Pastorin, G., Marega, R., Wu, W., Bonifazi, D., et al., 2006. Functionalized carbon nanotubes are non-cytotoxic and preserve the functionality of primary immune cells. *Nano Lett.* 6 (7), 1522–1528.
- Dvir, T., Timko, B.P., Kohane, D.S., Langer, R., 2011. Nanotechnological strategies for engineering complex tissues. *Nat. Nanotechnol.* 6 (1), 13–22.
- Fang, M., Goldstein, E.L., Matich, E.K., Orr, B.G., Holl, M.M.B., 2013. Type I collagen self-assembly: the roles of substrate and concentration. *Langmuir* 29 (7), 2330–2338.
- Faokhi, M., Mottaghitalab, F., Shokrgozar, M.A., Kaplan, D.L., Kim, H.W., 2016. Prospects of peripheral nerve tissue engineering using nerve guide conduits based on silk fibroin protein and other biopolymers. *Int. Mat. Rev.* 1–25.
- Fiedler, J., Ozdemir, B., Bartholoma, J., Plettl, A., Brenner, R.E., Ziemann, P., 2013. The effect of substrate surface nanotopography on the behavior of multipotent mesenchymal stromal cells and osteoblasts. *Biomaterials* 34 (35), 8851–8859.
- Galateanu, B., Bunea, M.C., Stanescu, P., Vasile, E., Casarica, A., Iovu, H., et al., 2015. In vitro studies of bacterial cellulose and magnetic nanoparticles smart nanocomposites for efficient chronic wounds healing. *Stem Cells Int.* 2015, 195096.
- Guo, B., Lei, B., Li, P., Ma, P.X., 2015. Functionalized scaffolds to enhance tissue regeneration. *Regen. Biomater.* 2 (1), 47–57.
- Halili, A.N., Kürüm, B., Karahan, S., Hasirci, V., 2018. Collagen based multilayer scaffolds for meniscus tissue engineering: in vivo test results. *Biomater. Med. Appl.* 2, 1.
- Hasan, A., Waibhaw, G., Saxena, V., Pandey, L.M., 2018. Nano-biocomposite scaffolds of chitosan, carboxymethyl cellulose and silver nanoparticle modified cellulose nanowhiskers for bone tissue engineering applications. *Int. J. Biol. Macromol.* 111, 923–934.
- He, L., Liu, B., Xipeng, G., Xie, G., Liao, S., Quan, D., 2009. Microstructure and properties of nano-fibrous PCL-b-PLLA scaffolds for cartilage tissue engineering. *Eur. Cell. Mater.* 18, 63–74.
- He, S., Lin, K.F., Sun, Z., Song, Y., Zhao, Y.N., Wang, Z., et al., 2016. Effects of nano-hydroxyapatite/poly (DL-lactic-co-glycolic acid) microsphere-based composite scaffolds on repair of bone defects: evaluating the role of nano-hydroxyapatite content. *Artif. Organs.* 40 (7), 128–135.
- He, X., Fan, X., Feng, W., Chen, Y., Guo, T., Wang, F., 2018. Incorporation of microfibrillated cellulose into collagen-hydroxyapatite scaffold for bone tissue engineering. *Int. J. Biol. Macromol.* 115, 385–392.
- Ho, C.M., Mishra, A., Lin, P.T., Ng, S.H., Yeong, W.Y., Kim, Y.J., et al., 2017. 3D printed polycaprolactone carbon nanotube composite scaffolds for cardiac tissue engineering. *Macromol. Biosci.* 17 (4), 1600250.
- Horan, R.L., Antle, K., Collette, A.L., Wang, Y., Huang, J., Moreau, J.E., et al., 2004. In vitro degradation of silk fibroin. *Biomaterials* 26, 3385–3393.
- Hu, S., Zhou, Y., Zhao, Y., Xu, Y., Zhang, F., Gu, N., et al., 2018. Enhanced bone regeneration and visual monitoring via superparamagnetic iron oxide nanoparticle scaffold in rats. *J. Tissue Eng. Regen. Med.* 12 (4), e2085–e2098.

- Jin, M., Jin, G., Kang, L., Chen, L., Gao, Z., Huang, W., 2018. Smart polymeric nanoparticles with pH-responsive and PEG-detachable properties for co-delivering paclitaxel and surviving siRNA to enhance antitumor outcomes. *Int. J. Nanomed.* 13, 2405–2426.
- Ju, H.W., Lee, O.J., Lee, J.M., Moon, B.M., Park, H.J., Park, Y.R., 2016. Wound healing effect of electrospun silk fibroin nanomatrix in burn model. *Int. J. Biol. Macromol.* 85, 29–39.
- Kabary, D.M., Helmy, M.W., Elkhodairy, K.A., Fang, J.Y., Elzoghby, A.O., 2018. Hyaluronate/lactoferrin layer-by-layer coated lipid nanocarriers for targeted co-delivery of rapamycin and berberine to lung carcinoma. *Coll. Surf. B Biointer.* 169, 183–194.
- Kearney, C.J., Lucas, C.R., O'Brian, F.J., Castro, E.C., 2017. DNA origami: folded DNA nanodevices that can direct and interpret cell behavior. *Adv. Mater.* 28 (27), 5509–5524.
- Khorasani, M.T., Mirzadeh, H., Irani, S., 2008. Plasma surface modification of poly (L-lactic acid) and poly (lactic-co-glycolic acid) films for improvement of nerve cells adhesion. *Radiat. Phys. Chem.* 77 (3), 280–287.
- Kim, C.H., Khil, M.S., Kim, H.Y., Lee, H.U., Jahng, K.Y., 2006. An improved hydrophilicity via electrospinning for enhanced cell attachment and proliferation. *J. Biomed. Mater. Res.* 78, 283–290.
- Kim, D.H., Lee, H., Lee, Y.K., Nam, J.M., Levchenko, A., 2010a. Biomimetic nanopatterns as enabling tools for analysis and control of live cells. *Adv. Mater.* 22 (41), 4551–4566.
- Kim, S.J., Jang, D.H., Park, W.H., Min, B.M., 2010b. Fabrication and characterization of 3-dimensional PLGA nanofiber/microfiber composite scaffolds. *Polymer* 51 (6), 1320–1327.
- Kim, D.H., Provenzano, P.P., Smith, C.L., Levchenko, A., 2012. Matrix nanotopography as a regulator of cell function. *J. Cell. Biol.* 197 (3), 351–360.
- Kim, B.S., Park, K.E., Kim, M.H., You, H.K., Lee, J., Park, W.H., 2015. Effect of nanofiber content on bone regeneration of silk fibroin/poly(e-caprolactone)nano/microfibrous composite scaffolds. *Int. J. Nanomed.* 10, 485–502.
- Kim, H.D., Kim, J., Koh, R.H., Shim, J., Lee, J.C., Kim, T., et al., 2017a. Enhanced osteogenic commitment of human mesenchymal stem cells on polyethylene glycol-based cryogel with graphene oxide substrate. *ACS Bio. Sci. Eng.* 3 (10), 2470–2479.
- Kim, H.J., Kim, M.K., Lee, K.H., Nho, S.K., Han, M.S., Um, I.C., 2017b. Effect of degumming methods on structural characteristics and properties of regenerated silk. *Int. J. Biol. Macromol.* 104 (A), 294–302.
- Kim, J., Kim, H.D., Park, J., Lee, E., Kim, E., Lee, S.S., et al., 2018a. Enhanced osteogenic commitment of murine mesenchymal stem cells on graphene oxide substrate. *Biomater. Res.* 22, 1.
- Kim, B., Pang, H.B., Kang, J., Park, J.H., Ruoslahti, E., Sailor, M.J., 2018b. Immunogene therapy with fusogenic nanoparticles modulates macrophage response to *Staphylococcus aureus*. *Nat. Commun.* 9 (1), 1969.
- Kuzmenko, V., Kalogeropoulos, T., Thunberg, J., Johannesson, S., Hägg, D., Enoksson, P., et al., 2016. Enhanced growth of neural networks on conductive cellulose-derived nanofibrous scaffolds. *Mater. Sci. Eng. C Mater. Biol. Appl.* 1 (58), 14–23.
- Kwak, S., Haider, A., Gupta, C.K., Kim, S., Kang, I.K., 2016. Micro/nano multilayered scaffolds of PLGA and collagen by alternately electrospinning for bone tissue engineering. *Nano Res. Lett.* 11, 323.



- Lee, S.J., Zhu, W., Nowicki, M., Lee, G., Heo, D.N., Kim, J., 2018. 3D printing nano conductive multi-walled carbon nanotube scaffolds for nerve regeneration. *J. Neural Eng.* 15 (1), 016018.
- Li, W., Laurencin, C.T., Caterson, E.J., Tuan, R.S., Ko, F.K., 2002. Electrospun nanofibrous structure: a novel scaffold for tissue engineering. *J. Biomed. Mater. Res.* 60, 613–621.
- Li, C.Y., Li, L.Y., Cai, W.W., Kodjie, S.L., Tenneti, K.K., 2005. Nanohybrid shish-kebabs: periodically functionalized carbon nanotubes. *Adv. Mater.* 17 (9), 1198–1202.
- Li, C.Y., Li, L.Y., Ni, C.Y., 2006. Polymer crystallization-driven, periodic patterning on carbon nanotubes. *J. Am. Chem. Soc.* 128 (5), 1692–1699.
- Li, H., Wang, Q., Xiao, Y., Bao, C., Li, W., 2013. 25-Hydroxyvitamin D (3)-loaded PLA microspheres: in vitro characterization and application in diabetic periodontitis models. *AAPS Pharm. Sci. Tech.* 14, 880–889.
- Li, Y., Yang, H., Yao, J., Yu, H., Chen, X., Zhang, P., et al., 2018. Glutathione-triggered dual release of doxorubicin and camptothecin for highly efficient synergistic anticancer therapy. *Coll. Surf. B Biointer.* 169, 273–279.
- Liakos, I.L., Holban, A.M., Carzino, R., Lauciello, S., Grumezescu, A.M., 2017. Electrospun fiber pads of cellulose acetate and essential oils with antimicrobial activity. *Nanomaterials* 7 (4). Available from: <https://doi.org/10.3390/nano7040084>.
- Limban, C., Missir, A.V., Caproiu, M.T., Grumezescu, A.M., Chirfiriuc, M.C., Bleotu, C., 2018. Novel hybrid formulations based on thiourea derivatives and core@shell  $\text{Fe}_3\text{O}_4@\text{C}_{18}$  nanostructures for the development of antifungal strategies. *Nanomaterials* 8, 47.
- Lin, Y., Taylor, S., Li, H., Fernando, S.K.A., Qu, L., Wang, W., et al., 2004. Advances towards bioapplications of carbon nanotubes. *J. Mater. Chem.* 14 (4), 527–541.
- Lin, C., Wang, Y., Lai, Y., Yang, W., Jiao, F., Zhang, H., et al., 2011. Incorporation of carboxylation multiwalled carbon nanotubes into biodegradable poly (lactic-co-glycolic acid) for bone tissue engineering. *Coll. Surf. B Biointer.* 83 (2), 367–375.
- Liu, X., Holzwarth, J.M., Ma, P.X., et al., 2012. Functionalized synthetic biodegradable polymer scaffolds for tissue engineering. *Macromol. Biosci.* 12 (7), 911–919.
- Lv, Z.J., Liu, Y., Miao, H., Leng, Z.Q., Guo, J.H., Liu, J., 2017. Effects of multiwalled carbon nanotubes on electrospun poly(lactide-co-glycolide)-based nanocomposite scaffolds on neural cells proliferation. *J. Biomed. Mater. Res. B Appl. Biomater.* 105 (5), 934–943.
- Ma, L., Gao, C., Mao, Z., Zhou, J., Shen, J., Hu, X., et al., 2003. Collagen/chitosan porous scaffolds with improved biostability for skin tissue engineering. *Biomaterials* 24 (26), 4833–4841.
- Malafaya, P.B., Silva, G.A., Reis, R.L., 2007. Natural-origin polymers as carriers and scaffolds for biomolecules and cell delivery in tissue engineering applications. *Adv. Drug. Deliv. Rev.* 59 (4–5), 207–233.
- McKeon-Fischer, K.D., Flagg, D.H., Freeman, J.W., 2011. Coaxial electrospun poly( $\epsilon$ -caprolactone) multiwalled carbon nanotubes and polyacrylic acid/polyvinyl alcohol scaffold for skeletal muscle tissue engineering. *J. Biomed. Mater. Res. Part A* 99A, 493–499.
- Meng, S., Ouabhia, M., Zhang, Z., 2013. Electrical stimulation modulates osteoblast proliferation and bone protein production through heparin bioactivated conductive scaffold. *Bioelectromagnetics* 34 (3), 189–199.



- Mirmusavi, M.H., Karbasi, S., Semnani, D., Kharazi, A.Z., 2018. Characterization of silk/poly-3-hydroxybutyrate-chitosan-multi-walled carbon nanotube micro–nano scaffold: a new hybrid scaffold for tissue engineering applications. *J. Med. Signals. Sen.* 8 (1), 46–52.
- Modaresifar, K., Hadjizadeh, A., Niknejad, H., 2017. Design and fabrication of GelMA/chitosan nanoparticles composite hydrogel for angiogenic growth factor delivery. *Artif. Cells. Nanomed. Biotechnol.* Available from: <https://doi.org/10.1080/21691401.2017.1392970>.
- Mohamadi, F., Ebrahimi-Barough, S., Reza Nourani, M., Ali Derakhshan, M., Goodarzi, V., Sadegh Nazockdast, M., 2017. Electrospun nerve guide scaffold of poly (ε-caprolactone)/collagen/nanobioglass: an in vitro study in peripheral nerve tissue engineering. *J. Biomed. Mater. Res. Part A* 105A, 1960–1972.
- Mohan, R., Mohan, N., Vaikkath, D., 2018. Hyaluronic acid dictates chondrocyte morphology and migration in composite gels. *Tissue Eng. Part A*. Available from: <https://doi.org/10.1089/ten.TEA.2017.0411>.
- Montalbano, G., Fiorilli, S., Caneschi, A., Vitale-Brovarone, C., 2018. Type I collagen and strontium-containing mesoporous glass particles as hybrid material for 3D printing of bone-like materials. *Materials* 11 (5), 700.
- Murthy, S.K., 2007. Nanoparticles in modern medicine: state of the art and future challenges. *Int. J. Nanomed.* 2 (2), 129–141.
- Niu, B., Li, B., Gu, Y., Shen, X., Liu, Y., Chen, L., 2017. In vitro evaluation of electrospun silk fibroin/nano-hydroxyapatite/BMP-2 scaffolds for bone regeneration. *J. Biomat. Sci.* 28, 257–270.
- Palaninathan, V., Raveendran, S., Rochani, A.K., Chauhan, N., Sakamoto, Y., Ukai, T., et al., 2018. Bioactive bacterial cellulose sulfate electrospun nanofibers for tissue engineering applications. *J. Tissue Eng. Regen.* Available from: <https://doi.org/10.1002/term.2689>.
- Pan, L., Pei, X., He, R., Wan, Q., Wan, J., 2012. Multiwall carbon nanotubes/polycaprolactone composites for bone tissue engineering application. *Coll. Surf. B Biointer.* 93, 226–234.
- Pereira, H., Frias, A.M., Oliveira, J.M., Espregueira-Mendes, J., Reis, R.L., 2011. Tissue engineering and regenerative medicine strategies in meniscus lesions. *Arthroscopy* 27, 1706–1719.
- Piran, M., Vakilian, S., Piran, M., Mohammadi-Sangcheshmeh, A., Hosseinzadeh, S., Ardeshirylajimi, A., 2018. In vitro fibroblast migration by sustained release of PDGF-BB loaded in chitosan nanoparticles incorporated in electrospun nanofibers for wound dressing applications. *Artif. Cells. Nanomed. Biotechnol.* Available from: <https://doi.org/10.1080/21691401.2018.1430698>.
- Popescu, R.C., Andronescu, E., Vasile, B.S., Trusca, R., Boldeiu, A., Mogoanta, L., 2017. Fabrication and cytotoxicity of gemcitabine-functionalized magnetite nanoparticles. *Molecules* 22 (7), 1080.
- Qu, G., Liu, S., Zhang, S., Wang, L., Wang, X., Sun, B., et al., 2013. Graphene oxide induces toll-like receptor 4 (TLR4)-dependent necrosis in macrophages. *ACS Nano* 7, 5732–5745.
- Qu, M., Xiao, W., Tian, J., Wang, S., Li, H., Liu, X., 2018. Fabrication of superparamagnetic nanofibrous poly (L-lactic acid)/γ-Fe<sub>2</sub>O<sub>3</sub> microspheres for cell carriers. *J. Biomed. Mater. Res. B Appl. Biomater.* Available from: <https://doi.org/10.1002/jbm.b.3414>.

- Radu, I.C., Hudita, A., Zaharia, C., Stanescu, P.O., Vasile, E., Iovu, H., 2017. Poly (hydroxybutyrate-co-hydroxyvalerate) (PHBHV) nanocarriers for silymarin release as adjuvant therapy in colorectal cancer. *Front. Pharmacol.* 8, 508.
- Raftery, R.M., Mencía-Castaño, I., Sperger, S., Chen, G., Cavanagh, B., Feichtinger, G., et al., 2018. Delivery of the improved BMP-2-advanced plasmid DNA within a gene-activated scaffold accelerates mesenchymal stem cell osteogenesis and critical size defect repair. *J. Control Release*. Available from: <https://doi.org/10.1016/j.jconrel.2018.05.022>.
- Ratner, B.D., Hoffman, A.S., Schoen, F.J., Lemons, J.E., 2004. *Biomaterials science, An Introduction to Materials in Medicine*, 1-32, second ed. Elsevier Academic Press, San Diego, CA, pp. 137–151.
- Ren, J., Xu, Q., Chen, X., Li, W., Guo, K., Zhao, Y., et al., 2017. Superaligned carbon nanotubes guide oriented cell growth and promote electrophysiological homogeneity for synthetic cardiac tissues. *Adv. Mater.* 29 (44), 1702713.
- Rouchi, H., Mahdavi-Mazdeh, M., 2015. Regenerative medicine in organ and tissue transplantation: shortly and practically achievable? *Int. J. Organ Transplant Med.* 6 (3), 93–98.
- Sabir, M.I., Xu, X., Li, L., 2009. A review on biodegradable polymeric materials for bone tissue engineering applications. *J. Mater. Sci.* 44, 5713–5724.
- Samadikuchaksaraei, A., Gholipourmalekabadi, M., Erfani Ezadyar, E., Azami, M., Mozafari, M., Johari, B., et al., 2016. Fabrication and in vivo evaluation of an osteoblast-conditioned nano-hydroxyapatite/gelatin composite scaffold for bone tissue regeneration. *J. Biomed. Mater. Res. A*. 104 (8), 2001–2010.
- Sano, A., Maeda, M., Nagahara, S., Ochiya, T., Honma, K., Itoh, H., 2003. Atelocollagen for protein and gene delivery. *Adv. Drug Deliv. Rev.* 55 (12), 1651–1677.
- Saravanan, S., Leena, R.S., Selvamurugan, N., 2016. Chitosan based biocomposite scaffolds for bone tissue engineering. *Int. J. Biol. Macromol.* 93, 1354–1365.
- Sarkar, S.D., Farrugia, B.L., Dargaville, T.R., Dhara, S., 2013. Chitosan–collagen scaffolds with nano/microfibrous architecture for skin tissue engineering. *J. Biomed. Mater. Res. Part A* 101 (12), 3482–3492.
- Schuh, C.M.A.P., Day, A.G.E.D., Redl, H., 2018. An optimized collagen-fibrin blend engineered neural tissue promotes peripheral nerve repair. *Tissue Eng. Part A*. Available from: <https://doi.org/10.1089/ten.TEA.2017.0457>.
- Shaoping, Z., Wee, E.T., Xiao, Z., Roger, B., Seeram, R., et al., 2005. Formation of collagen-glycosaminoglycan blended nanofibrous scaffolds and their biological properties. *Biomacromolecules* 6, 2998–3004.
- Shaoping, Z., Wee, E.T., Xiao, Z., Roger, B., Seeram, R., Lin Yue, L.Y., 2007. Development of a novel collagen-GAG nanofibrous scaffold via electrospinning. *Mater. Sci. Eng.* 27 (C), 262–266.
- Sharif, S., Ai, J., Azami, M., Verdi, J., Atlasi, M.A., Shirian, S., et al., 2018. Collagen-coated nano-electrospun PCL seeded with human endometrial stem cells for skin tissue engineering applications. *J. Biomed. Mater. Res. Part B* 106 (4), 1578–1586.
- Sheng, Y., Liao, L.D., Thakor, N.V., Tan, M.C., 2014. Nanoparticles for molecular imaging. *J. Biomed. Nanotechnol.* 10 (10), 2641–2676.
- Shrestha, B.K., Shrestha, S., Prasa, A., 2017. Bio-inspired hybrid scaffold of zinc oxide-functionalized multi-wall carbon nanotubes reinforced polyurethane nanofibers for bone tissue engineering. *Mater. Design.* 133, 69–81.

- Si, J., Cui, Z., Wang, Q., Liu, Q., Liu, C., 2016. Biomimetic composite scaffolds based on mineralization of hydroxyapatite on electrospun poly ( $\epsilon$ -caprolactone)nanocellulose fibers. *Carbohydr. Polym.* 143, 270–278.
- Singh, N., Chen, J., Koziol, K.K., Hallam, K.R., Janas, D., Patil, A.J., 2016. Chitin and carbon nanotube composites as biocompatible scaffolds for neuron growth. *Nanoscale* 21 (8), 8288–8299.
- Sisson, K., Zhang, C., Farach-Carson, M.C., Chase, D.B., Rabolt, J.F., 2010. Fiber diameters control osteoblastic cell migration and differentiation in electrospun gelatin. *J. Biomed. Mater. Res.* 94A, 1312–1320.
- Stevens, M.M., George, J.H., 2005. Exploring and engineering the cell surface interface. *Science* 310 (5751), 1135–1138.
- Sun, H., Zhou, J., Huang, Z., Qu, L., Lin, N., Liang, C., 2017. Carbon nanotube-incorporated collagen hydrogels improve cell alignment and the performance of cardiac constructs. *Int. J. Nanomed.* 12, 3109–3120.
- Sun, T., Shi, Q., Huang, Q., Wang, H., Xiong, X., Hu, C., 2018. Magnetic alginate microfibers as scaffolding elements for the fabrication of microvascular-like structures. *Acta Biomater.* 66, 272–281.
- Tabaïi, M.J., Emtiazi, G., 2018. Transparent nontoxic antibacterial wound dressing based on silver nano particle/bacterial cellulose nano composite synthesized in the presence of tripolyphosphate. *J. Drug Deliv. Sci.* 44, 244–253.
- Taipale, J., Keski-Oja, J., 1997. Growth factors in the extracellular matrix. *FASEB J.* 11 (1), 51–59.
- Timnak, A., Yousefi Gharebaghi, F., Pajoum Shariati, R., Bahrami, S.H., Javadian, S., Hojjati Emami, S.H., et al., 2011. Fabrication of nano-structured electrospun collagen scaffold intended for nerve tissue engineering. *J. Mater. Sci. Mater. Med.* 22 (6), 1555–1567.
- Tuzlakoglu, K., Santos, M.I., Neves, N., Reis, R.L., 2011. Design of nano-and microfiber combined scaffolds by electrospinning of collagen onto starch-based fiber meshes: a man-made equivalent of natural extracellular matrix. *Tissue Eng. Part A* 17 (3–4), 463–473.
- Vallejo-Giraldo, C., Pugliese, E., Larrañaga, A., Fernandez-Yague, M.A., Britton, J.J., Trotier, A., et al., 2016. Polyhydroxyalkanoate/carbon nanotube nanocomposite: flexible electrically conducting elastomers for neural applications. *Nanomed. Lond.* 11 (19), 2547–2563.
- Vazquez-Portalatin, N., Kilmer, C.E., Panitch, A., Liu, J.C., 2016. Characterization of collagen type I and II blended hydrogels for articular cartilage tissue engineering. *Biomacromolecules* 17, 3145–3152.
- Venkatesan, J., Qian, Z.J., Ryu, B.M., Kumar, N.A., Kim, S.K., 2011. Preparation and characterization of carbon nanotube-grafted-chitosan-natural hydroxyapatite composite for bone tissue engineering. *Carbohydr. Polym.* 83 (2), 569–577.
- Walmsley, G.G., McArdle, A., Tevlin, R., Momeni, A., Atashroo, D., Hu, M.S., et al., 2015. Nanotechnology in bone tissue engineering. *Nanomed.* 11, 1253–1263.
- Wang, X.F., Salick, M.R., Wang, X.D., Cordie, T., Han, W.J., Peng, Y.Y., et al., 2013. Poly(epsilon-caprolactone) nanofibers with a self-induced nanohybrid shish-kebab structure mimicking collagen fibrils. *Biomacromolecules* 14 (10), 3557.
- Wang, K.K., Shin, E.P., Lee, H.J., Jung, S.J., Hwang, J.K., Heo, I., et al., 2018a. Target-oriented photofunctional nanoparticles (TOPFNs) for selective photodynamic inactivation of methicillin-resistant *Staphylococcus aureus* (MRSA). *J. Photochem. Photobiol. B* 183, 184–190.

- Wang, Y., Hua, Y., Zhang, Q., Yang, J., Li, H., Li, Y., 2018b. Using biomimetically mineralized collagen membranes with different surface stiffness to guide regeneration of bone defects. *J. Tissue Eng. Regen. Med.* 1–11.
- Wei, K., Li, Y., Kim, K.O., Najagawa, Y., Kim, B.S., Abe, K., et al., 2011. Fabrication of nano-hydroxyapatite on electrospun silk fibroin nanofiber and their effects in osteoblastic behavior. *J. Biomed. Mater. Res. A* 97 (3), 272–280.
- Wickham, A.M., Islam, M.M., Mondal, D., Phopase, J., Sadhu, V., Tamas, E., et al., 2014. Polycaprolactone-thiophene-conjugated carbon nanotube meshes as scaffolds for cardiac progenitor cells. *J. Biomed. Mater. Res. B Appl. Biomater.* 102 (7), 1553–1561.
- Wu, D., Chen, X., Chen, T., Ding, C., Wu, W., Li, J., 2015. Substrate-anchored and degradation-sensitive anti-inflammatory coatings for implant materials. *Sci. Rep.* 5, 11105.
- Wu, S.Y., Chen, Y.T., Chen, C.W., Chi, L.Y., Hsu, N.Y., Hung, N.Y., et al., 2010. Comparison of clinical outcomes following guided tissue regeneration treatment with a polylactic acid barrier or a collagen membrane. *Int. J. Periodontics Restorative Dent.* 30 (2), 173–179.
- Wu, T., Chen, X., Sha, J., Peng, Y.Y., Ma, Y.L., Xie, L.S., 2017. Fabrication of shish-kebab-structured carbon nanotube/poly(e-caprolactone) composite nanofibers for potential tissue engineering applications. *Rare Metals*. Available from: <https://doi.org/10.1007/s12598-017-0965-y>.
- Wu, S.T., Fowler, A.J., Garmon, C.B., Fessler, A.B., Ogle, J.D., Grover, K.R., et al., 2018. Treatment of pancreatic ductal adenocarcinoma with tumor antigen specific-targeted delivery of paclitaxel loaded PLGA nanoparticles. *BMC Cancer* 18 (1), 457.
- Xiao, L., Liu, S., Yao, D., Ding, Z., Fan, Z., Lu, Q., et al., 2017. Fabrication of silk scaffolds with nanomicroscaled structures and tunable stiffness. *Biomacromolecules* 18 (7), 2073–2079.
- Yan, J., Hu, K., Xiao, Y., Zhang, F., Han, L., Pan, S., 2018. Preparation of recombinant human-like collagen/fibroin scaffold and its promoting effect on vascular cells biocompatibility. *J. Bioact. Compat. Polym.* Available from: <https://doi.org/10.1177/0883911518769680>.
- Yang, K., Gong, H., Shi, X., Wan, J., Zhang, Y., Liu, Z., 2013. In vivo biodistribution and toxicology of functionalized nano-graphene oxide in mice after oral and intraperitoneal administration. *Biomaterials* 34, 2787–2795.
- Yang, H.S., Ieronimakis, N., Tsui, J.H., Kim, H.N., Suh, K.Y., Reyes, M., et al., 2014. Nanopatterned muscle cell patches for enhanced myogenesis and dystrophin expression in a mouse model of muscular dystrophy. *Biomaterials* 35 (5), 1478–1486.
- Yao, Q., Liu, Y., Selvaratnam, B., Koodali, R.T., Sun, H., 2018. Mesoporous silicate nanoparticles/3D nanofibrous scaffold-mediated dual-drug delivery for bone tissue engineering. *J. Control Release* 279, 69–78.
- You, J.O., Rafat, M., Ye, G.J., Auguste, D.T., 2011. Nanoengineering the heart: conductive scaffolds enhance connexin 43 expression. *Nano Lett.* 11 (9), 3643–3648.
- Zhang, K., Mo, X., Huang, C., He, C., Wang, H., 2010a. Electrospun scaffolds from silk fibroin and their cellular compatibility. *J. Biomed. Mater. Res. A* 93 (3), 976–983.
- Zhang, Y., Ali, S.F., Dervishi, E., Xu, Y., Li, Z., Casciano, D., et al., 2010b. Cytotoxicity effects of graphene and single-wall carbon nanotubes in neural pheochromocytoma 18 derived PC12 cells. *ACS Nano* 4, 3181–3186.

- Zang, S., Zhang, R., Chen, H., Lu, Y., Zhou, J., Chang, X., et al., 2015. Investigation of artificial blood vessels prepared from bacterial cellulose. *Mater. Sci. Eng. C* 46, 111–117.
- Zhou, H., Lee, J., 2011. Nanoscale hydroxyapatite particles for bone tissue engineering. *Acta Biomater.* 7, 2769–2781.

---

## FURTHER READING

- Liu, Z., Zhu, S., Liu, L., Ge, J., Huang, L., Sun, Z., et al., 2017. A magnetically responsive nanocomposite scaffold combined with Schwann cells promotes sciatic nerve regeneration upon exposure to magnetic field. *Int. J. Nanomed.* 12, 7815–7832.
- Morrison, R.J., Nasser, H.B., Kashlan, K.N., Zopf, D.A., Milner, D.J., Flanagan, C.L., et al., 2018. Co-culture of adipose-derived stem cells and chondrocytes on three-dimensionally printed bioscaffolds for craniofacial cartilage engineering. *The Laryngoscope*. Available from: <https://doi.org/10.1002/lary.27200>.
- Shen, R., Xu, W., Xue, Y., Chen, L., Ye, H., Zhong, E., et al., 2018. The use of chitosan/PLA nano-fibers by emulsion electrospinning for periodontal tissue engineering. *Artif. Cells Nanomed. Biotech.* Available from: <https://doi.org/10.1080/21691401.2018.1458233>.
- Tangm, Y.P., Yang, X.L., Hang, B.J., Li, J.T., Huang, L., Xu, Z.N., 2016. Efficient production of hydroxylated human-like collagen via the co-expression of three key genes in *Escherichia coli* origami (DE3). *Appl. Biochem. Biotechnol.* 178, 1458–1470.

# Resorbable biomaterials: role of chitosan as a graft in bone tissue engineering

# 2

**Kaiser Manzoor, Mudasir Ahmad, Suhail Ahmad and Saiqa Ikram**

*Biopolymer Research Laboratory, Department of Chemistry, Jamia Millia Islamia,  
New Delhi, India*

## 2.1 INTRODUCTION

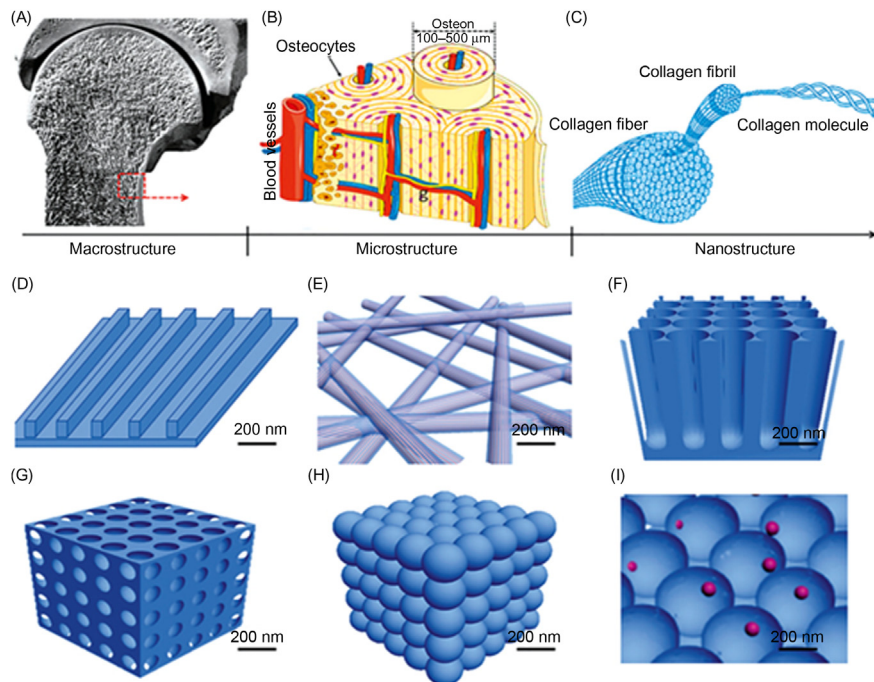
In adult humans, bone tissue can be categorized into two types: trabecular, constituting about 20% of the total skeleton, and cortical bone, amounting to 80% of the total skeleton (Hill, 1998; Sikavitsas, et al., 2001). Cortical bone is only 10% porous and includes femur, tibia, short bones, and flat; however the trabecular bones are 50%–90% porous, arranged in a honeycomb fashion, and include vertebral bones. Three types of cells are mainly involved in growth, development, and maintenance of the bone tissue: osteoblasts, osteocytes, and osteoclasts, the main features of which are listed in Table 2.1 (Bilezikian, 1996; Ducey et al., 2000; Mackie, 2003) (Fig. 2.1, Gong, T. et al., 2015).

Bone tissue forms the main portion of the body. In addition to providing mechanical support and allowing proper movement of the organs, it is also the manufacturing unit of the red blood cells (RBCs). Its composition includes ~65%–70% mineral part, which includes calcium, phosphorous, hydroxyapatite, and ~30%–35% organic part, including glycoproteins, proteoglycans, and sialoproteins (Gong et al., 2015, Fig. 2.2; Sommerfeldt and Rubin, 2001).

There has been a vast increase in in sports for various reasons, for example, health consciousness or adventure. This has led to increase in bone related diseases as well as in bone fractures, which in turn has provided the opportunity for the researchers to develop bone substitutes to cure these diseases and fractures. Researchers have developed a lot of materials from various sources such as metals, polymers, injectable cements porous solids, etc. Every year there are about two million cases worldwide with issues related to bone deformations and bone fractures (Greenwald and Garino, 2001). The available treatment consists of the use of allograft or the autologous bone, both of which involve second surgeries at the extraction site and highlight the need for the advent of alternative treatment procedures (Mahendra and Maclean, 2007; Arrington et al., 1996; Younger and Chapman, 1989). Allograft bone is constituted of a specially treated bone obtained from cadavers or live donors. The main disadvantage of allograft bone

**Table 2.1** Composition of the Bone: Characteristics and Functions

Cells	Characteristics	Function
Osteoblasts	<ul style="list-style-type: none"> <li>Osteoblasts arise from mesenchymal stem cells cuboidal in shape, polarized and located at the bone surface</li> <li>Slightly basophilic due to the presence of a large amount of rough endoplasmic reticulum</li> </ul>	<ul style="list-style-type: none"> <li>Synthesis and regulation of bone ECM deposition and mineralization</li> <li>Respond to mechanical stimuli</li> <li>Synthesize cross-linked collagen, osteocalcin, and osteopontin proteins</li> </ul>
Osteocytes	<ul style="list-style-type: none"> <li>Contains a single nucleus that is located toward the vascular side and has one or two nucleoli and a membrane</li> <li>Stellate shaped</li> <li>Possess fewer organelles than the osteoblasts</li> </ul>	<ul style="list-style-type: none"> <li>Calcification of the osteoid matrix</li> <li>Transmit signals over long distances, mechanosensor cells of the bone</li> <li>Blood-calcium homeostasis</li> <li>Endocrine regulator of phosphate metabolism</li> </ul>
Osteoclasts	<ul style="list-style-type: none"> <li>Osteoclasts are found in pits in the bone surface</li> <li>Polarized cells</li> <li>Multinucleated cells</li> </ul>	<ul style="list-style-type: none"> <li>Bone resorption</li> <li>Osteoclasts' rough endoplasmic reticulum is sparse, and the Golgi complex is extensive Cathepsin K, cysteine protease mainly expressed in osteoclasts is responsible for degradation proteins.</li> </ul>

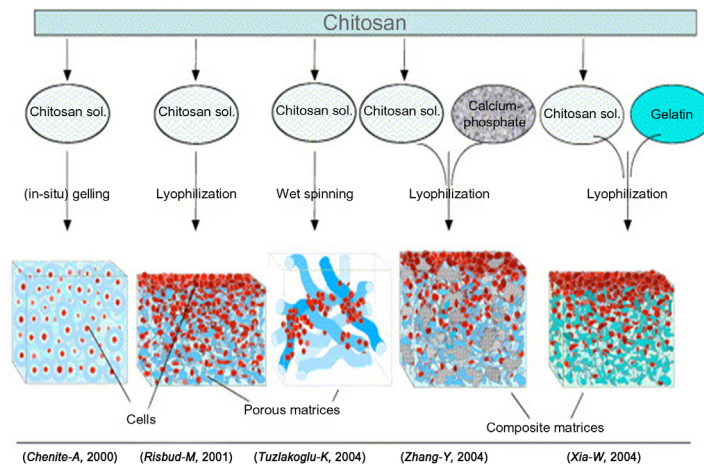


**FIGURE 2.1**

Structures of bone: (A) cortical, (B) consecutive osteon units, (C) collagen fibers, (D) nanofibers, (E) nanotubers, (F) nanopores, (G) nanospheres, (H) nanocomposites, and (I) nanocomposites with structural components.

*Reprinted with permission from NCBI.*



**FIGURE 2.2**

Use of chitosan for various tissue engineering purposes.

*Reprinted with permission from Elsevier.*

transplantation is the immunological response from the recipient and the transmission of diseases like HIV, gonorrhea, syphilis, and other communicable diseases (Hofmann et al., 1995). Deproteinized bones have been used for overcoming the problems arising from the transmission of diseases. Bovine bones can for example be completely deproteinized and sintered over 1000°C to remove all the organic matter (Wenz et al., 2001). Alternatively resorbable synthetic materials with improved biological and chemical properties can be developed for bone graft substitutes with higher performance. A wide range of materials have been proposed such as titanium, tantalum, magnesium, iron, polymers like polyglycolides, polycaprolactones, ceramics, polylactides, and polyurethanes like silicate based glasses, calcium sulfate hemihydrate, and calcium phosphates (Albee, 1920; Huang et al., 2014; Heini and Berlemann, 2001; Schnürer et al., 2003; Vaccaro and Madigan, 2002). The materials based on calcium phosphate have been most important due to their composition similarity with natural bone, so they have been studied as bone substitutes for the last century (Hench, 2013; Klawitter and Hulbert, 1971; Roberts and Brilliant, 1975; Roy and Linnehan, 1974). Bone graft substitutes mainly consist of the granules or porous blocks, however some other injectable fluids have also been developed that harden later on. The ability of bone graft tissue to be injected allows its vast application, for example, in the treatment of bone fractures by minimally invasive technique. As far as the replacement of the damaged or fractured bone is concerned, a mature bone should ideally be the replacement alternative to prevent the transient loss of the mechanical strength. This results in stabilization of bone graft substitutes, which are mechanically unstable with nonresorbable metallic material. It thus becomes



important to increase the resorption rate of bone graft substitutes so that the healing time of the fractured bone is minimized. Basically the word *resorbable* is used for the materials that will disappear after the function they are deemed to perform is complete, irrespective of the mechanism by which they are removed from the action site. Resorption rate exhibits an important role in quality of the bone graft material. The resorption rate is mainly controlled by two methods, one of which involves the optimization of the geometry of the material (Bohner and Baumgart, 2004). Presence of the pores or channels with approximate diameter of 0.05 mm enables blood vessel invasion and cells allowing material biodegradation and growth of the damaged bone (Karageorgiou and Kaplan, 2005; Lu et al., 1999). Modification of the chemistry of the material will also affect the resorption rate of the material, for example, change in crystallinity of the polymer or inclusion of more degradable sequences in the polymer network will greatly affect its functionality. The resorption mechanism of the materials used for bone graft substitute is found to be diverse with materials like gypsum disappearing by simple dissolution while there is hydrolytic removal of polylactides and glycosides (Bohner, 2008; Gogolewski et al., 1993). Metal-based composites are decomposed through corrosion while the biopolymers like chitosan and cellulose are dissolved flowing into the lymph nodes (Witte et al., 2006; Peuster et al., 2006). Enzymatic degradation is also common for polymers such as collagen, hyaluron, and fibrin glue (Eglin and Alini, 2008). Osteoclasts are responsible for the resorption of the material like  $\beta$ -tricalcium phosphate (Eggli et al., 1988).

Among all the materials used as bone graft substitutes, calcium phosphates are most important because the degradation products of these can be used in new bone formations besides being considered as a drug. As known, calcium and phosphate are used in regulation of the bone metabolism. Regulation of osteoblast production, osteopontin, apoptosis, and mineralization rate is prominently carried out by phosphate ions. Proliferation of osteoblasts and the regulation of osteoclasts is found to be regulated by calcium ions (Kanatani et al., 1991; Meleti et al., 2000; Wu et al., 2003; Zaidi et al., 1989; Nakade et al., 2001; Wang et al., 1999). So far the application of calcium phosphate compounds has rarely been studied for drug delivery purposes although they are used for delivery of various therapeutic agents. The main objective is the loading of the drug on the calcium phosphate bone graft substitutes during synthesis following their release on resorption. Most of the work is related to the Si-based hydroxyapatite substitutes but the work is being carried out for other ions like zinc and strontium. The composition of the calcium phosphate substitutes affects the change in solubility and structure as well as its release and resorption.

The synthesis of bone graft substitute is a new field of research and has expanding opportunities. Anticipations are to be met in the future research for the synthesis of the graft substitutes capable of load bearing for reconstruction of bone in arthroplasty or reinforcement in osteoporotic bones as the number of people who are active in old age is increasing. There is need for the exploration of cheaper and safer alternatives with ability to induce bone formation in heterotopic implantation (Habibovic and de Groot, 2007).

---

## 2.2 PROPERTIES OF SUBSTITUTES TO ACT AS BONE GRAFTS

Bone provides the main structural support to the body besides being a sink for various minerals, RBCs, and other essential nutrients. A comparison of different properties between the natural bone and the artificial bone graft substitutes is shown in [Table 2.2](#).

For replacement of the fractured or damaged bone, the material should possess the following features.

### 2.2.1 BIOCOMPATIBILITY

The developed bone graft substitutes must not prompt the immune responses from the host tissue and should be well integrated with it. These properties are essential for nutrient transport and minerals besides the diffusion of the gases and other metabolic wastes produced within the structure.

### 2.2.2 POROSITY

The scaffolds must possess a highly porous interconnected geometry with larger surface area/volume ratios for proper growth of cells and its uniform distribution throughout the whole of the structure. It must also possess the micropores for allowing the capillary in-growth and neovascularization with the surrounding cells. Extent of porosity, however, always affects the other properties of the material such as mechanical strength and therefore is to be maintained in a balanced way.

### 2.2.3 PORE SIZE

Size of the pores of the material is an important property that affects the application for bone graft substitute. If the pores in the scaffold are small it will result in neovascularization of the inner areas of the scaffold, and inhibition of the cellular penetration and extracellular matrix production. It has been reported that the effective pore size for bone graft substitutes should be in the range of 200–900  $\mu$  (Yang et al., 2001; Boccaccini et al., 2005; Vunjak-Novakovic and Freed, 1998; Burg et al., 2000). However, macroporous grafts have also been reported but such scaffolds are mechanically less stable.

### 2.2.4 SURFACE PROPERTIES

Both chemical and topographical properties such as adhesion and proliferation of the scaffolds are affected by the surface properties of the materials. The ability of the material to interact with the proteins and adhere to other surfaces depends on

**Table 2.2** Comparison of Physical Properties Between Natural Bone and Other Degradable and Nondegradable Materials (Eglin and Alini, 2008; Athanasiou et al., 2001; Yaszemski et al., 1996; Tamimi et al., 2012; Claes 1992; Blackburn et al., 1992; Tan et al., 2013; Armentano et al., 2010; Witte et al., 2008; Giannoudis et al., 2005)

Material	Compressive Strength (MPa)	Tensile Strength (MPa)	Young's Modulus (GPa)	Elongation (%)	Degradation Time (months)	Loss of Total Strength (months)	Application
<b>A. Bone</b>							
Human cortical	131–224	35–283	17–20	1.07–2.10	Natural bone remodeling	None	Autograft and allograft used for defect filling, alveolar ridge augmentation, sinus
Human cancellous	5–10	1.5–38	0.05–0.1	0.5–3	Natural bone remodeling	0.5–1	Augmentation, dental ridge preservation (Khoury, 1999; Block and Degen, 2004; Bolander and Balian, 1986; Araujo et al., 2013; Sterio et al., 2013; Whittaker et al., 1989; Valentini and Abensur, 1997; Guerrero and Al-Jandan, 2012; Avila et al., 2010; Sohn et al., 2009)
<b>B. Degradable</b>							
Collagen	0.5–1	50–150	0.002–5	3	2–4	1–4	Carriers (sponges) for BMP (Jo et al., 2015; Cha et al., 2014; Geiger et al., 2003), composite with HA (John et al., 2001), membranes for GBR (Chung et al., 1990; Matilina, 2014), scaffolds (Liu and Ma, 2004)
	1.7–3.4	35–75	2–18	1–2	4–6	<3	Chitosan scaffolds, microgranules, composite materials, VBA, membranes, xerogels (Silva et al., 2007; Lee et al., 2006, 2010; Zhao et al., 2008; Ambrose et al., 2015)
Poly glycolic acid	340–920	55–80	5–7	15–20	3–4	1	Internal fixation, graft material, scaffold, composite (Silva et al., 2007; Lee et al., 2006, 2010; Zhao et al., 2008; Ambrose et al., 2015; Törmälä, 1992; Linhart et al., 2001)
Poly-L-lactic acid	80–500	45–70	2.7	5–10	>24	3	Carrier for BMP, scaffolds, composite with HA (Niu et al., 2009; Xiong et al., 2001; Higashi et al., 1986; Razak et al., 2012; Vert, 2005; Nejati et al., 2008; Lagoa et al., 2008)
D,L-Polylactic acid	15–25	90–103	1.9	3–10	12–16	4	Fracture fixation, interference screws (Warden et al., 1999; Bozic et al., 2001; Ignatius and Claes, 1996)
L-Polylactic acid	20–30	100–150	2.7	5–10	>24	3	Fracture fixation, interference screws, scaffolds, bone graftmaterial (Törmälä, 1992; Xiong et al., 2001;

Poly(lactic glycolic acid)	40–55	55–80	1.4–2.8	3–10	1–12	1	Leenslag et al., 1987; Vainionpaa et al., 1987; Nam and Park, 1999; Nie et al., 2015)
Hydroxyapatite	500–1000	40–200	80–110	0.5–1	>24	>12	Interference screws, microspheres, and carriers for BMP, scaffolds, composite (Ji et al., 2010; Gavenis et al., 2010; Fei et al., 2008; Sheikh et al., 2016)
Magnesium	65–1000	135–285	41–45	2–10	0.25	<1	Scaffolds, composites, bone fillers (granules and blocks), pastes, vertebroplasty, drugdelivery, coatings (Balçik et al., 2007; Quarto et al., 2001; Mardziah et al., 2009; Thian et al., 2006; Noshi et al., 2000; Oonishi, 1991; Cook et al., 1988; Sopyan et al., 2007; Heise et al., 1990; Kumar et al., 2015; Domic-Cule et al., 2015; Singh and Majumdar, 2014)
							Implants, osteosynthesis devices, plates, screws, ligatures, and wires (Shadanbaz and Dias, 2012; Staiger et al., 2006; Wong et al., 2010; Zeng et al., 2008; Waizy et al., 2013; Gu and Zheng, 2010; Witte, 2010; Liu et al., 2014; Lyndon et al., 2014; Chaya et al., 2015a, 2015b; Jiang et al., 2015; Wong, 2015; Zhou et al., 2015; Khakbaz et al., 2014; Tang et al., 2013)

### C. Nondegradable

Titanium alloy	900	900–1000	110–127	10–15	No	None	Implants, plates, screws, BMP carriers, orthognathic surgery, mid-facial fracture treatment (Van Der Stok et al., 2015; Mikos et al., 2014; Tomlinson et al., 2015; Al-Moraissi and Ellis, 2015; Kang et al., 2014; Mazzoni et al., 2015; Paeng et al., 2012; Buijs et al., 2012)
Stainless steel	500–1000	460–1700	180–205	10–40	No	None	Implants, plates, mini-plates, screws (Bhatnagar et al., 2013; Bender et al., 2012; Chew et al., 2012)
Bioglass	40–60	120–250	0–1	35	No	None	Bone defect fillers (Vallittu et al., 2015; Kokubo, 1991; Rahaman et al., 2011; Hench, 2013; Balani et al., 2014; Fiorilli et al., 2015; Bagheri et al., 2015)

the surface morphology of the scaffolds. The fibrin matrix will be held more by a rough surface than that of a smooth surface. It has been explored that rougher surface will hold the fibrin matrix better than a smooth one and hence will facilitate the migration of osteogenic cells to the surface of the material.

### 2.2.5 OSTEOINDUCTION

Induction of stem cells and osteoprogenitor cells to the bone healing site and stimulation of the osteogenic differentiation is called osteoconduction (Albrektsson and Johansson, 2001). For large portion bone regeneration, natural osteoinduction combined with a biodegradable scaffold is not sufficient and hence requires the scaffold to be osteoinductive by itself.

### 2.2.6 MECHANICAL STABILITY AND BIODEGRADABILITY

The artificial bone graft substitutes must possess sufficient mechanical strength to bear the hydrostatic pressures and maintain the gaps in between for proper cell growth and proliferation (Leong et al., 2003). As bones are always under stress, the implants must mechanically match the natural bones to mimic their function. Besides, the developed scaffold must be biodegradable and must be resorbed by the time the injured bone is regenerated completely.

---

## 2.3 CHITOSAN-BASED MATERIAL FOR BONE GRAFT SUBSTITUTES

Currently the bone graft substitutes are focused on the restoration of the damaged tissue by transplantation of the cells combined with supportive scaffolds and biomolecules. In recent years considerable attention has been paid towards the chitosan-based materials and their application in the bioengineering fields because of their properties such as antibacterial action, lower foreign body reaction, and ability to be molded into various porous scaffolds that are suitable for cell growth and osteoconduction. The gelling properties of chitosan allow it for a controlled delivery of the morphogenic and other pharmaceutical agents and its cationic nature allows it be used in targeted gene delivery (Martino et al., 2005).

Chitosan, a deacetylated derivative of chitin obtained from shells of marine crustaceans and cell walls of fungi, is a linear polysaccharide, composed of glucosamine and N-acetyl glucosamine linked in a  $\beta$  (1–4) manner insoluble in aqueous solutions above pH 7, however in dilute acids protonated amino groups facilitate the solubility of the molecule (Dornish et al., 2001; Athanasiou et al., 2001; Madhally and Matthew, 1999). The cationic nature of chitosan is primarily responsible for its interaction with the biological systems like negatively charged molecules, proteoglycans, and glycosaminoglycan, besides chitosan and chitin

both being chemoattractive to neutrophils causing stimulatory effect on macrophages. The biodegradation of the chitosan is based on the degree of deacetylation; the higher the degree of deacetylation, the lower will be its biodegradation, which is mainly carried out by lysozymes while other proteolytic enzymes show very low biodegradation activity. Chitosan has the ability to be molded into porous scaffolds by freezing and lyophilization to form gels as shown in Fig. 2.2 (Hu et al., 2004; Risbud and Bhowmik, 2000; Chow and Khor, 2000).

Mechanical properties of chitosan scaffold are largely influenced by the pore size and their orientation; it has been observed that elastic modulus is greatly reduced (0.1–0.5 MPa) in porous membranes as compared with nonporous membranes (5–7 MPa) (Suh and Matthew, 2000). The intrinsic antibacterial property of chitosan has been a major factor for its application in bioengineering materials. Due to its cationic nature, chitosan associates easily with the anions present on the bacterial cell wall thereby suppressing biosynthesis. Furthermore it also disrupts the mass transport in the bacterial cell wall, finally leading to the death of bacteria. Chitosan has been blended with a large number of other materials such as alginate, hydroxyapatite, hyaluronic acid, calcium phosphate, poly-L-lactic acid, and other growth factors for potential application in orthopedics, with which it offers application in broader areas of tissue engineering (Hu et al., 2004).

Chitosan has provided a vast opportunity for researchers for application in bone tissue engineering due to its biodegradability, biocompatibility, antimicrobial action as well as its ability to promote growth and deposition of mineral rich matrix by osteoblasts in culture (Seol et al., 2004; Seeherman et al., 2003). Chitosan–calcium phosphate (CCP) composites have been widely used as bone graft substitutes (Zhang and Zhang, 2001, 2002a).

### 2.3.1 CHITOSAN–CALCIUM PHOSPHATE BASED SUBSTITUTES

Calcium phosphate cements have been able to replace a defective bone and have been resorbed effectively because they harden to form the solid bone hydroxyapatite and conform to complex cavity shapes. However, the lower strength of the calcium phosphate cements and their macroporosity limits their application in craniofacial and orthopedic repairs, which can be overcome by their complexation with other biopolymers. Zhang and Zhang (2002b) have developed a 3D macroporous calcium phosphate bioceramic scaffold with porous chitosan sponges embedded in it. The embedded chitosan sponge increased the mechanical strength of the ceramic scaffold by reinforcing the matrix besides preserving the osteoblast phenotype. Similar scaffolds consisting of  $\beta$ -tricalcium phosphate and calcium phosphate, and macroporous chitosan incorporated with hydroxyapatite and calcium phosphate with porosity of 100  $\mu\text{m}$  as a bone graft substitute, have been synthesized (Zhang et al., 2003). The calcium phosphate cements are suitable for bone repair and regeneration because after implantation in bone defects they are rapidly integrated into the bone structure, after which they are transformed into new bone by the action of osteoblasts and osteoclasts. Chitosan is usually mixed

with other bone graft substitutes as adjuvant while keeping intact the chemicophysical properties like mechanical strength and setting time suitable for surgical use. Chitosan added with calcium phosphate cements increases the injectability and the strength of the material, many of which are used for non-load-bearing bone defects (Leroux et al., 1999; Gutowska et al., 2001). On addition of phosphorylated chitosan to the calcium phosphate it was found to be biocompatible, osteoinductive, bioresorbable, and remoldable for its application in filling bone defects in radius and tibia (Wang et al., 2002).

### 2.3.2 CHITOSAN HYDROXYAPATITE BASED BONE GRAFT SUBSTITUTES

Chitosan, because of its cationic nature and faster degradation rate, binds easily to the growth factors for their release in controlled fashion. Chitosan linked with imidazole group further enhances its cationic nature, induces bone formation, and fills up critical size bone defects (Park et al., 2000; Lee et al., 2000, 2002; Muzzarelli et al., 1994). Chitosan has been used for the modification of the surface properties of the bone graft substitutes to enhance the attachment of the osteoblasts (Lee et al., 2002). Chitin hydroxyapatite composite proved to be osteoconductive and exhibited a rapid neovascularization and rapid degradation. Furthermore the synthesized composite showed an enhanced mechanical strength and bending modulus making it suitable for application for curing of long bone fractures (Ge et al., 2004; Kawakami et al., 1992). Proliferation and attachment of the osteoblasts is found to be enhanced by the titanium surface-modified chitosan with silane glutaraldehyde. These coatings exhibited an increase in the dissolution in both acidic as well as in neutral solutions (Bumgardner et al., 2003; Wang et al., 2004). The osteoconductive behavior of hydroxyapatite is optimized by degradable matrices besides allowing bone in-growth into the implant in which matrix is gradually resorbed. Chitosan bonded hydroxyapatite composite had an optimized tensile strength and elongation behavior to help the cells and blood vessels penetrate through the matrix. In addition these scaffolds can be molded easily during the operation and are injectable. For increasing their injectability several other additives can be added such as lactic acid, chitosan, glycerol, glycerophosphate, etc. Recently an injectable bone substitute has been proposed that consists of citric acid and chitosan in solution phase and tetracalcium phosphate, dicalcium phosphate anhydrous, and calcium sulfate hemihydrate powders as solid components. Chitosan oligosaccharides enhanced the cement biocompatibility as an approximate twofold increase in cell proliferation. The combination of gelatin and chitosan oligosaccharides provided benefits due to synergistic effects in terms of antiwashout properties and biological activity (Song et al., 2009). Due to its susceptibility to lysozymes and immunostimulating properties chitosan enhances the physiological bone formation and healing processes effectively.

The disruption of bone architecture and vascular network due to fracture causes decrease in the nutrient supply and oxygen as well as reduces mechanical strength. The inflammatory response is accompanied by the activation of macrophages and infiltration of platelets that release various cytokines, which are involved in initiation of the bone repair process. New bone is produced by the differentiation of postfracture periosteal osteoprogenitor cells and osteoblasts. Fibroblast growth factors and bone morphogenetic proteins are involved in the process to provide crucial nutrient supplies to the cells. The technological and chemical versatility of chitosan make it possible to prepare elaborated composites for bone regeneration. Durable integration is required between the metallic support and healthy bone in an orthopedic implant for bone fracture. Apatite coated titanium alloys conjugated with chitosan provide an excellent attachment between the bone marrow stromal cells and increase the proliferation of osteoblasts. For the stimulation of the stem cells to form osteoblasts and osteoclasts chitosan, N-carboxymethyl chitosan, polylactic acid (PLA), are proving excellent. For efficient bone formation chitosan acts as a scaffolding device.

### 2.3.3 CHITOSAN-ALGINATE SCAFFOLDS

Bioactive ceramics have the composition that resembles that of a bone and hence allows osteogenesis to occur while supporting adhesion to the host bone (Jarcho, 1981). Despite their compatible biological properties these have clinical limitations because of their low biodegradability and brittleness. Chitosan is comparatively biodegradable, biocompatible, nonantigenic, nontoxic, and biofunctional. In addition chitosan is hydrophilic due to which it helps in adhesion of cells, proliferation, and shows minimum response to foreign body. However chitosan is mechanically less stable and is unable to maintain the shape of a transplant (Shanmugasundaram et al., 2001). Therefore a scaffold is needed to be developed that besides having the advanced biological properties like biocompatibility, biodegradability, etc. also provides the mechanical strength to the bone graft substitute. Alginate is a biopolymer that undergoes instant gel formation and also has hydrophilic, biocompatible, biodegradable nature and is most often used in bone tissue engineering (Gutowska et al., 2001; Becker et al., 2001). A natural polymer based complex scaffold has been prepared from chitosan and alginate that has significantly increased the mechanical strength. This scaffold has been found highly stable due to strong ionic interactions between the amine group of chitosan and the carboxylic group of the alginate. The scaffold synthesized has the porosity of approximately 90% besides a compressive modulus and yield strength of 8.16 and 0.46 MPa, respectively. Furthermore unlike chitosan-based scaffolds chitosan-alginate scaffolds can be fabricated not only in acidic solutions but also in neutral and basic solutions also, the feature providing favorable incorporation of proteins with least risk of denaturation for sustained release (Li et al., 2005).



### 2.3.4 CHITOSAN POLYLACTIC ACID SUBSTITUTE

Recently chitosan-based materials have been applied to spine tissue engineering such as spine fusion, nucleus pulposus regeneration, and gene therapy. To bone graft during spinal fusion procedures several factors are to be taken into consideration, which depend on the type and position of the graft. Some of the grafts are supposed to possess load-bearing ability because of their exposure to the high compressive force. For such purposes a graft prepared from chitosan combined either with PLA or PEG-PLA was prepared and applied for spinal fusion. Many useful derivatives of chitosan have been prepared by graft copolymerization. For controlling the surface morphology and function of the cells in bone tissue engineering chitosan grafted with PLA has been found to be very effective. The graft proved to be excellent due to its biodegradability, stiffness, plasticity, and its ability to release the growth factor and support cells. In addition the graft has a macroporous structure and predictable degradation rate, which allowed the linking of the growth factors and supports osteogenic cells involved in spinal fusion (Boden, 2002; Saito and Takaoka, 2003; Alden et al., 2002). The scaffolds from chitosan-PLA degrade very quickly because the tensile strength of the developed graft reduces to half within 2 weeks of implantation (Ikada, 2006).

---

## 2.4 SUMMARY

Use of biomaterials in tissue engineering dates back to 3500 BC, when silk, linen, silk, flax, hair, grass, and animal gut were used as fibrous joints. By this time a large number of synthetic and natural biomaterials have been explored for use in medical applications. The biomedical field has been revolutionized by the development of the new generation biodegradable and biocompatible polymeric materials especially after the development of synthetic resorbable material Dexon in the 1960s. The significance of the bioresorbable material over the permanent biostable implants is the biocompatible issues and immunological responses arising in case of the latter. The degradation of the bioresorbable material over time provides the regain of the natural properties such as mechanical strength and steady growth. The biocompatibility of the resorbable material includes its nontoxicity, noninflammatory, noncarcinogenicity, and nonimmunogenicity, which render it useful for the bone graft substitutes and other biomedical applications. Due to complex behavior of the synthetic bioresorbable material there have been developments for the use of natural polymeric materials due to their efficient bioactivity as well as their biodegradability.

Chitosan, being a versatile polymer due to its biocompatibility, biodegradability, and antimicrobial properties, has been extensively used in the fields of tissue engineering. Chitosan can be molded into various shapes, becoming a potential material to be used as bone graft substitute. Furthermore the increase in the mechanical strength of the chitosan scaffolds and bioresorbability, on

hybridization with other natural materials like calcium hydroxide, hydroxyapatite, etc. makes it perfect material for bone implants. Moreover the interaction of chitosan with DNA molecules increases its ability to be used in gene therapy of orthopedic defects.

## REFERENCES

- Al-Moraissi, E.A., Ellis, E., 2015. Biodegradable and titanium osteosynthesis provide similar stability for orthognathic surgery. *J. Oral Maxillof. Surg.* 73 (9), 1795–1808.
- Albee, F.H., 1920. Studies in bone growth: triple calcium phosphate as a stimulus to osteogenesis. *Ann. Surg.* 71 (1), 32–39.
- Albrektsson, T., Johansson, C., 2001. Osteoinduction, osteoconduction and osseointegration. *Eur. Spine J.: Offic. Publ. Eur. Spine Soc. Eur. Spinal Deformity Soc. Eur. Sect. Cerv. Spine Res. Soc.* 10 (Suppl. 2), S96–S101.
- Alden, T.D., et al., 2002. Bone morphogenetic protein gene therapy. *Spine* 27 (16 Suppl. 1), S87–S93.
- Ambrose, C.G., et al., 2015. Polymers in orthopaedic surgery. In: Puoci, F. (Ed.), *Advanced Polymers in Medicine*. Springer International Publishing, Cham, pp. 129–145. Available from: [http://dx.doi.org/10.1007/978-3-319-12478-0\\_5](http://dx.doi.org/10.1007/978-3-319-12478-0_5).
- Araujo, P.P.T., et al., 2013. Block allograft for reconstruction of alveolar bone ridge in implantology: a systematic review. *Implant Dentis.* 22 (3), 304–308.
- Armentano, I., et al., 2010. Biodegradable polymer matrix nanocomposites for tissue engineering: a review. *Polym. Degrad. Stabil.* 95 (11), 2126–2146. Available from: <http://www.sciencedirect.com/science/article/pii/S0141391010002430>.
- Arrington, E.D., et al., 1996. Complications of iliac crest bone graft harvesting. *Clin. Orthop. Relat. Res.* 329, 300–309.
- Athanasiou, K.A., et al., 2001. Basic science of articular cartilage repair. *Clin. Sports Med.* 20 (2), 223–247.
- Avila, G., et al., 2010. Clinical and histologic outcomes after the use of a novel allograft for maxillary sinus augmentation: a case series. *Implant Dentis.* 19 (4), 330–341.
- Bagheri, Z.S., et al., 2015. Osteogenesis and cytotoxicity of a new Carbon Fiber/Flax/Epoxy composite material for bone fracture plate applications. *Mater. Sci. Eng. C* 46, 435–442.
- Balani, K., et al., 2014. Surface engineering and modification for biomedical applications. *Biosurfaces*. John Wiley & Sons, Inc, pp. 201–238. Available from: <http://dx.doi.org/10.1002/9781118950623.ch7>.
- Balçık, C., et al., 2007. Early weight bearing of porous HA/TCP (60/40) ceramics in vivo: a longitudinal study in a segmental bone defect model of rabbit. *Acta Biomater.* 3 (6), 985–996.
- Becker, T.A., Kipke, D.R., Brandon, T., 2001. Calcium alginate gel: a biocompatible and mechanically stable polymer for endovascular embolization. *J. Biomed. Mater. Res.* 54 (1), 76–86.
- Bender, S., et al., 2012. Mechanical characterization and modeling of graded porous stainless steel specimens for possible bone implant applications. *Int. J. Eng. Sci.* 53, 67–73. Available from: <http://www.sciencedirect.com/science/article/pii/S0020722512000158>.

- Bhatnagar, A., et al., 2013. Comparative analysis of osteosynthesis of mandibular anterior fractures following open reduction using “stainless steel lag screws and mini plates”. *J. Maxillofac. Oral Surg.* 12 (2), 133–139. Available from: <http://www.ncbi.nlm.nih.gov/pmc/articles/PMC3682007/>.
- Bilezikian, J.P., 1996. *Principles of Bone Biology*, Academic Press, San Diego, CA.
- Blackburn, J., et al., 1992. Mechanical properties of microcallus in human cancellous bone. *J. Orthop. Res.: Offic. Public. Orthop. Res. Soc.* 10 (2), 237–246.
- Block, M.S., Degen, M., 2004. Horizontal ridge augmentation using human mineralized particulate bone: preliminary results. *J. Oral Maxillof. Surg.* 62 (Supple), 67–72. Available from: <http://www.sciencedirect.com/science/article/pii/S0278239104007335>.
- Boccaccini, A.R., et al., 2005. Biodegradable and bioactive polymer/bioglass® composite foams for tissue engineering scaffolds. *Current Research in Advanced Materials and Processes*. Materials Science Forum. Trans Tech Publications, pp. 499–506.
- Boden, S.D., 2002. Overview of the biology of lumbar spine fusion and principles for selecting a bone graft substitute. *Spine* 27 (16 Suppl. 1), S26–S31.
- Bohner, M., 2008. *Degradation Rate of Bioresorbable Materials*. Woodhead Publishing Limited, Cambridge.
- Bohner, M., Baumgart, F., 2004. Theoretical model to determine the effects of geometrical factors on the resorption of calcium phosphate bone substitutes. *Biomaterials* 25 (17), 3569–3582.
- Bolander, M.E., Balian, G., 1986. The use of demineralized bone matrix in the repair of segmental defects. Augmentation with extracted matrix proteins and a comparison with autologous grafts. *J. Bone Joint Surg. Am. Vol.* 68 (8), 1264–1274.
- Bozic, K.J., et al., 2001. Mechanical testing of bioresorbable implants for use in metacarpal fracture fixation. *J. Hand Surg.* 26 (4), 755–761.
- Buijs, G.J., et al., 2012. A randomized clinical trial of biodegradable and titanium fixation systems in maxillofacial surgery. *J. Dental Res.* 91 (3), 299–304. Available from: <http://www.ncbi.nlm.nih.gov/pubmed/22269272>.
- Bumgardner, J.D., et al., 2003. Chitosan: potential use as a bioactive coating for orthopaedic and craniofacial/dental implants. *J. Biomater. Sci. Polym. Ed.* 14 (5), 423–438.
- Burg, K.J., Porter, S., Kellam, J.F., 2000. Biomaterial developments for bone tissue engineering. *Biomaterials* 21 (23), 2347–2359.
- Cha, J.-K., et al., 2014. Sinus augmentation using BMP-2 in a bovine hydroxyapatite/collagen carrier in dogs. *J. Clin. Periodontol.* 41 (1), 86–93.
- Chaya, A., Yoshizawa, S., Verdelis, K., Noorani, S., et al., 2015a. Fracture healing using degradable magnesium fixation plates and screws. *J. Oral Maxillof. Surg.* 73 (2), 295–305.
- Chaya, A., Yoshizawa, S., Verdelis, K., Myers, N., et al., 2015b. In vivo study of magnesium plate and screw degradation and bone fracture healing. *Acta Biomater.* 18, 262–269.
- Chew, K.K., et al., 2012. Corrosion resistance study of electrophoretic deposited hydroxyapatite on stainless steel for implant applications. *Key Engineering Materials*. Trans Tech Publications, pp. 141–146. Available from: <http://www.scopus.com/inward/record.url?eid=2-s2.0-84859056792&partnerID=40&md5=535302c23ff2a6b33aa9deec026e8ecb%5Cnhttp://www.scientific.net/KEM.507.141>.
- Chow, K.S., Khor, E., 2000. Novel fabrication of open-pore chitin matrixes. *Biomacromolecules* 1 (1), 61–67.

- Chung, K.M., et al., 1990. Clinical evaluation of a biodegradable collagen membrane in guided tissue regeneration. *J. Periodontol.* 61 (12), 732–736.
- Claes, L.E., 1992. Mechanical characterization of biodegradable implants. *Clin. Mater.* 10 (1), 41–46. Available from: <http://www.sciencedirect.com/science/article/pii/0267660592900836>.
- Cook, S.D., et al., 1988. Hydroxyapatite-coated titanium for orthopedic implant applications. *Clin. Orthop. Relat. Res.* 232, 225–243.
- Dornish, M., Kaplan, D., Skaugrud, O., 2001. Standards and guidelines for biopolymers in tissue-engineered medical products: ASTM alginate and chitosan standard guides. American Society for Testing and Materials. *Ann. NY Acad. Sci.* 944, 388–397.
- Ducy, P., Schinke, T., Karsenty, G., 2000. The osteoblast: a sophisticated fibroblast under central surveillance. *Science* (New York, NY) 289 (5484), 1501–1504.
- Dumic-Cule, I., et al., 2015. Biological aspects of segmental bone defects management. *Int. Orthop.* 39 (5), 1005–1011.
- Eggli, P.S., Muller, W., Schenk, R.K., 1988. Porous hydroxyapatite and tricalcium phosphate cylinders with two different pore size ranges implanted in the cancellous bone of rabbits. A comparative histomorphometric and histologic study of bony ingrowth and implant substitution. *Clin. Orthop. Relat. Res.* 232, 127–138.
- Eglin, D., Alini, M., 2008. Degradable polymeric materials for osteosynthesis: tutorial. *Eur. Cells Mater.* 16, 80–91.
- Fei, Z., et al., 2008. Preparation and property of a novel bone graft composite consisting of rhBMP-2 loaded PLGA microspheres and calcium phosphate cement. *J. Mater. Sci. Mater. Med.* 19 (3), 1109–1116.
- Fiorilli, S., et al., 2015. Electrophoretic deposition of mesoporous bioactive glass on glass-ceramic foam scaffolds for bone tissue engineering. *J. Mater. Sci.: Mater. Med.* 26 (1), 1–12.
- Gavenis, K., et al., 2010. BMP-7-loaded PGLA microspheres as a new delivery system for the cultivation of human chondrocytes in a collagen type I gel: the common nude mouse model. *Int. J. Artif. Organs* 33 (1), 45–53.
- Ge, Z., et al., 2004. Hydroxyapatite-chitin materials as potential tissue engineered bone substitutes. *Biomaterials* 25 (6), 1049–1058.
- Geiger, M., Li, R.H., Friess, W., 2003. Collagen sponges for bone regeneration with rhBMP-2. *Adv. Drug Deliv. Rev.* 55 (12), 1613–1629.
- Giannoudis, P.V., Dinopoulos, H., Tsiridis, E., 2005. Bone substitutes: an update. *Injury* 36 (Suppl. 3), S20–S27.
- Gogolewski, S., et al., 1993. Tissue response and in vivo degradation of selected polyhydroxyacids: polylactides (PLA), poly(3-hydroxybutyrate) (PHB), and poly(3-hydroxybutyrate-co-3-hydroxyvalerate) (PHB/VA). *J. Biomed. Mater. Res.* 27 (9), 1135–1148.
- Gong, T., Xie, J., Liao, J., Zhang, T., Lin, S., Lin, Y., 2015. Nanomaterials and bone regeneration. *Bone Res.* 3, 15029. Available from: <https://doi.org/10.1038/boneres.2015.29>.
- Greenwald, A.S., Garino, J.P., 2001. Alternative bearing surfaces: the good, the bad, and the ugly. *J. Bone Joint Surg.* 83 (2 Suppl. 2), S68–S72. Available from: [http://jbjs.org/content/83/2\\_suppl\\_2/S68](http://jbjs.org/content/83/2_suppl_2/S68).
- Gu, X.N., Zheng, Y.F., 2010. A review on magnesium alloys as biodegradable materials. *Front. Mater. Sci. China* 4 (2), 111–115. Available from: <https://doi.org/10.1007/s11706-010-0024-1>.
- Guerrero, J.S., Al-Jandan, B.A., 2012. Allograft for maxillary sinus floor augmentation: a retrospective study of 90 cases. *Implant Dentis.* 21 (2). Available from: <http://journals>.

- lww.com/implantdent/Fulltext/2012/04000/Allograft\_for\_Maxillary\_Sinus\_Floor\_Augmentation\_\_12.aspx.
- Gutowksa, A., Jeong, B., Jasionowski, M., 2001. Injectable gels for tissue engineering. *Anatom. Rec.* 263 (4), 342–349.
- Habibovic, P., de Groot, K., 2007. Osteoinductive biomaterials—properties and relevance in bone repair. *J. Tissue Eng. Regenerat. Med.* 1 (1), 25–32.
- Heini, P.F., Berlemann, U., 2001. Bone substitutes in vertebroplasty. *Eur. Spine J.: Offic. Public. Eur. Spine Soc. Eur. Spinal Deform. Soc. Eur. Sect. Cerv. Spine Res. Soc.* 10 (Suppl. 2), S205–S213.
- Heise, U., Osborn, J.F., Duwe, F., 1990. Hydroxyapatite ceramic as a bone substitute. *Int. Orthop.* 14 (1990), 329–338.
- Hench, L.L., 2013. Chronology of bioactive glass development and clinical applications. *New J. Glass Ceram.* 3 (2), 67–73. Available from: <http://www.scirp.org/journal/PaperInformation.aspx?PaperID=30885&#abstract>.
- Higashi, S., et al., 1986. Polymer-hydroxyapatite composites for biodegradable bone fillers. *Biomaterials* 7 (3), 183–187. Available from: <http://www.sciencedirect.com/science/article/pii/0142961286900992>.
- Hill, P.A., 1998. Bone remodelling. *Br. J. Orthod.* 25 (2), 101–107. Available from: <http://www.ncbi.nlm.nih.gov/pubmed/9668992>.
- Hofmann, G.O., et al., 1995. Infections and immunological hazards of allogeneic bone transplantation. *Arch. Orthop. Trauma Surg.* 114 (3), 159–166. Available from: <https://www.scopus.com/inward/record.uri?eid=2-s2.0-0028955038&doi=10.1007%2FBF00443390&partnerID=40&md5=8577369fb32c065edec675be756a60ea>.
- Hu, Q., et al., 2004. Preparation and characterization of biodegradable chitosan/hydroxyapatite nanocomposite rods via in situ hybridization: a potential material as internal fixation of bone fracture. *Biomaterials* 25 (5), 779–785. Available from: <http://www.sciencedirect.com/science/article/pii/S0142961203005829>.
- Huang, Q., Wang, L., Wang, J., 2014. Mechanical properties of artificial materials for bone repair. *J. Shanghai Jiaotong Univ. (Sci.)* 19 (6), 675–680. Available from: <https://doi.org/10.1007/s12204-014-1565-8>.
- Ignatius, A.A., Claes, L.E., 1996. In vitro biocompatibility of bioresorbable polymers: poly (L, DL-lactide) and poly(L-lactide-co-glycolide). *Biomaterials* 17 (8), 831–839.
- Ikada, Y., 2006. Challenges in tissue engineering. *J. R. Soc. Interf.* 3 (10), 589–601. Available from: <http://www.ncbi.nlm.nih.gov/pmc/articles/PMC1664655/>.
- Jarcho, M., 1981. Calcium phosphate ceramics as hard tissue prosthetics. *Clin. Orthop. Relat. Res.* 157, 259–278.
- Ji, Y., et al., 2010. BMP-2/PLGA delayed-release microspheres composite graft, selection of bone particulate diameters, and prevention of aseptic inflammation for bone tissue engineering. *Ann. Biomed. Eng.* 38 (3), 632–639.
- Jiang, G., et al., 2015. Fabrication of graded porous titanium-magnesium composite for load-bearing biomedical applications. *Mater. Design* 67, 354–359. Available from: <http://www.sciencedirect.com/science/article/pii/S0261306914009790>.
- Jo, J.-Y., et al., 2015. Sequential delivery of BMP-2 and BMP-7 for bone regeneration using a heparinized collagen membrane. *Int. J. Oral Maxillof. Surg.* 44 (7), 921–928.
- John, A., et al., 2001. A trial to prepare biodegradable collagen-hydroxyapatite composites for bone repair. *J. Biomater. Sci. Polym. Ed.* 12 (6), 689–705.
- Kanatani, M., et al., 1991. Effect of elevated extracellular calcium on the proliferation of osteoblastic MC3T3-E1 cells: its direct and indirect effects via monocytes. *Biochem. Biophys. Res. Commun.* 181 (3), 1425–1430.

- Kang, I.G., et al., 2014. Comparison of titanium and biodegradable plates for treating mid-facial fractures. *J. Oral Maxillof. Surg.* 72 (4), p. 762.e1–4.
- Karageorgiou, V., Kaplan, D., 2005. Porosity of 3D biomaterial scaffolds and osteogenesis. *Biomaterials* 26 (27), 5474–5491. Available from: <http://www.sciencedirect.com/science/article/pii/S0142961205001511>.
- Kawakami, T., et al., 1992. Experimental study on osteoconductive properties of a chitosan-bonded hydroxyapatite self-hardening paste. *Biomaterials* 13 (11), 759–763.
- Khakbaz, H., et al., 2014. Self-dissolution assisted coating on magnesium metal for biodegradable bone fixation devices. *Mater. Res. Express* 1 (4), 45406. Available from: <http://stacks.iop.org/2053-1591/1/i=4/a=045406?key=crossref.520b4cf9a0fa2f874042379f591aa4eb>.
- Khoury, F., 1999. Augmentation of the sinus floor with mandibular bone block and simultaneous implantation: a 6-year clinical investigation. *Int. J. Oral Maxillof. Implants* 14 (4), 557–564.
- Klawitter, J.J., Hulbert, S.F., 1971. Application of porous ceramics for the attachment of load bearing internal orthopedic applications. *J. Biomed. Mater. Res.* 5 (6), 161–229. Available from: <https://doi.org/10.1002/jbm.820050613>.
- Kokubo, T., 1991. Bioactive glass ceramics: properties and applications. *Biomaterials* 12 (2), 155–163. Available from: <http://www.sciencedirect.com/science/article/pii/S014296129190194F>.
- Kumar, A., Biswas, K., Basu, B., 2015. Hydroxyapatite-titanium bulk composites for bone tissue engineering applications. *J. Biomed. Mater. Res. Part A* 103 (2), 791–806.
- Lagoa, A.L.C., et al., 2008. A strut graft substitute consisting of a metal core and a polymer surface. *J. Mater. Sci. Mater. Med.* 19 (1), 417–424.
- Lee, Y.M., et al., 2000. Tissue engineered bone formation using chitosan/tricalcium phosphate sponges. *J. Periodontol.* 71 (3), 410–417.
- Lee, J.-Y., et al., 2002. Enhanced bone formation by controlled growth factor delivery from chitosan-based biomaterials. *J. Control. Release* 78 (1–3), 187–197. Available from: <http://www.sciencedirect.com/science/article/pii/S0168365901004989>.
- Lee, J.-Y., et al., 2006. Enhanced bone formation by transforming growth factor- $\beta$ 1-releasing collagen/chitosan microgranules. *J. Biomed. Mater. Res. Part A* 76A (3), 530–539. Available from: <https://doi.org/10.1002/jbm.a.30434>.
- Lee, E.-J., et al., 2010. Silica xerogel-chitosan nano-hybrids for use as drug eluting bone replacement. *J. Mater. Sci. Mater. Med.* 21 (1), 207–214.
- Leenslag, J.W., et al., 1987. Resorbable materials of poly(L-lactide). VII. In vivo and in vitro degradation. *Biomaterials* 8 (4), 311–314.
- Leong, K.F., Cheah, C.M., Chua, C.K., 2003. Solid freeform fabrication of three-dimensional scaffolds for engineering replacement tissues and organs. *Biomaterials* 24 (13), 2363–2378.
- Leroux, L., et al., 1999. Effects of various adjuvants (lactic acid, glycerol, and chitosan) on the injectability of a calcium phosphate cement. *Bone* 25 (2, Suppl. 1), 31S–34S. Available from: <http://www.sciencedirect.com/science/article/pii/S8756328299001301>.
- Li, Z., et al., 2005. Chitosan-alginate hybrid scaffolds for bone tissue engineering. *Biomaterials* 26 (18), 3919–3928. Available from: <https://doi.org/10.1016/j.biomaterials.2004.09.062>.
- Linhart, W., et al., 2001. Biologically and chemically optimized composites of carbonated apatite and polyglycolide as bone substitution materials. *J. Biomed. Mater. Res.* 54 (2), 162–171.

- Liu, X., Ma, P.X., 2004. Polymeric scaffolds for bone tissue engineering. *Ann. Biomed. Eng.* 32 (3), 477–486.
- Liu, C., et al., 2014. Preclinical investigation of an innovative magnesium-based bone graft substitute for potential orthopaedic applications. *J. Orthop. Transl.* 2 (3), 139–148. Available from: <http://www.sciencedirect.com/science/article/pii/S2214031X14000497>.
- Lu, J.X., et al., 1999. Role of interconnections in porous bioceramics on bone recolonization in vitro and in vivo. *J. Mater. Sci.: Mater. Med.* 10 (2), 111–120. Available from: <https://doi.org/10.1023/A:1008973120918>.
- Lyndon, J.A., Boyd, B.J., Birbilis, N., 2014. Metallic implant drug/device combinations for controlled drug release in orthopaedic applications. *J. Control. Release* 179 (1), 63–75.
- Mackie, E.J., 2003. Osteoblasts: novel roles in orchestration of skeletal architecture. *Int. J. Biochem. Cell Biol* 35 (9), 1301–1305.
- Madhally, S.V., Matthew, H.W., 1999. Porous chitosan scaffolds for tissue engineering. *Biomaterials* 20 (12), 1133–1142.
- Mahendra, A., Maclean, A.D., 2007. Available biological treatments for complex non-unions. *Injury* 38 (Suppl. 4), S7–S12.
- Mardziah, C.M., Sopyan, I., Ramesh, S., 2009. Strontium-doped hydroxyapatite nanopowder via sol-gel method: effect of strontium concentration and calcination temperature on phase behavior. *Artif. Organs* 23 (2), 105–113.
- Martino, A.D.I., Sittering, M., Risbud, M.V., 2005. Chitosan: a versatile biopolymer for orthopaedic tissue-engineering. *Biomaterials* 26 (30), 5983–5990. Available from: <http://www.sciencedirect.com/science/article/pii/S0142961205002309>.
- Matilina, K., 2014. Barrier Membranes for Tissue Regeneration and Bone Augmentation Techniques in Dentistry. Pan Stanford Publishing, Singapore.
- Mazzoni, S., et al., 2015. Computer-aided design and computer-aided manufacturing cutting guides and customized titanium plates are useful in upper maxilla waferless repositioning. *J. Oral Maxillof. Surg.* 73 (4), 701–707.
- Meleti, Z., Shapiro, I.M., Adams, C.S., 2000. Inorganic phosphate induces apoptosis of osteoblast-like cells in culture. *Bone* 27 (3), 359–366. Available from: <http://www.sciencedirect.com/science/article/pii/S875632820000346X>.
- Mikos, A.G. et al., 2014. Combined space maintenance and bone regeneration system for the reconstruction of large osseous defects. Available from: <http://www.freepatentsonline.com/y2015/0081034.html>.
- Muzzarelli, R.A.A., et al., 1994. Stimulatory effect on bone formation exerted by a modified chitosan. *Biomaterials* 15 (13), 1075–1081. Available from: <http://www.sciencedirect.com/science/article/pii/0142961294900930>.
- Nakade, O., et al., 2001. Effect of extracellular calcium on the gene expression of bone morphogenetic protein-2 and -4 of normal human bone cells. *J. Bone Mineral Metabol.* 19 (1), 13–19.
- Nam, Y.S., Park, T.G., 1999. Porous biodegradable polymeric scaffolds prepared by thermally induced phase separation. *J. Biomed. Mater. Res.* 47 (1), 8–17.
- Nejati, E., Mirzadeh, H., Zandi, M., 2008. Synthesis and characterization of nano-hydroxyapatite rods/poly(l-lactide acid) composite scaffolds for bone tissue engineering. *Compos. Part A: Appl. Sci. Manufact.* 39 (10), 1589–1596. Available from: <http://www.sciencedirect.com/science/article/pii/S1359835X0800153X>.
- Nie, L., et al., 2015. Macroporous biphasic calcium phosphate scaffolds reinforced by poly-L-lactic acid/hydroxyapatite nanocomposite coatings for bone regeneration. *Biochem. Eng. J.* 98, 29–37. Available from: <http://www.sciencedirect.com/science/article/pii/S1369703X15000601>.



- Niu, X., et al., 2009. Porous nano-HA/collagen/PLLA scaffold containing chitosan microspheres for controlled delivery of synthetic peptide derived from BMP-2. *J. Control. Release: Offic. J. Control. Release Soc.* 134 (2), 111–117.
- Noshi, T., et al., 2000. Enhancement of the in vivo osteogenic potential of marrow/hydroxyapatite composites by bovine bone morphogenetic protein. *J. Biomed. Mater. Res.* 52 (4), 621–630.
- Oonishi, H., 1991. Orthopaedic applications of hydroxyapatite. *Biomaterials* 12 (2), 171–178. Available from: <http://www.sciencedirect.com/science/article/pii/014296129190196H>.
- Paeng, J.Y., et al., 2012. Comparative study of skeletal stability between bicortical resorbable and titanium screw fixation after sagittal split ramus osteotomy for mandibular prognathism. *J. Cranio-Maxillof. Surg.* 40 (8), 660–664.
- Park, Y.J., et al., 2000. Platelet derived growth factor releasing chitosan sponge for periodontal bone regeneration. *Biomaterials* 21 (2), 153–159.
- Peuster, M., et al., 2006. Long-term biocompatibility of a corrodible peripheral iron stent in the porcine descending aorta. *Biomaterials* 27 (28), 4955–4962.
- Quarto, R., et al., 2001. Repair of large bone defects with the use of autologous bone marrow stromal cells. *New Eng. J. Med.* 344 (5), 385–386.
- Rahaman, M.N., et al., 2011. Bioactive glass in tissue engineering. *Acta Biomater.* 7 (6), 2355–2373.
- Razak, S.I.A., Sharif, N., Rahman, W., 2012. Biodegradable polymers and their bone applications: a review. *Int. J. Basic Appl. Sci.* 12 (1), 31–49.
- Risbud, M.V., Bhonde, R.R., 2000. Polyacrylamide-chitosan hydrogels: in vitro biocompatibility and sustained antibiotic release studies. *Drug Deliv.* 7 (2), 69–75.
- Roberts, S.C.J., Brilliant, J.D., 1975. Tricalcium phosphate as an adjunct to apical closure in pulpless permanent teeth. *J. Endodontics* 1 (8), 263–269.
- Roy, D.M., Linnehan, S.K., 1974. Hydroxyapatite formed from coral skeletal carbonate by hydrothermal exchange. *Nature* 247 (5438), 220–222.
- Saito, N., Takaoka, K., 2003. New synthetic biodegradable polymers as {BMP} carriers for bone tissue engineering. *Biomaterials* 24 (13), 2287–2293. Available from: <http://www.sciencedirect.com/science/article/pii/S0142961203000401>.
- Schnürer, S.M., et al., 2003. Bone substitutes. *Der Orthopäde* 32 (1), 2–10. Available from: <https://doi.org/10.1007/s00132-002-0407-9>.
- Seeherman, H., Li, R., Wozney, J., 2003. A review of preclinical program development for evaluating injectable carriers for osteogenic factors. *J. Bone Joint Surg. Am.* Vol. 85–A (Supp 1), 96–108.
- Seol, Y.-J., et al., 2004. Chitosan sponges as tissue engineering scaffolds for bone formation. *Biotechnol. Lett.* 26 (13), 1037–1041. Available from: <https://doi.org/10.1023/B:BILE.0000032962.79531.f0>.
- Shadanbaz, S., Dias, G.J., 2012. Acta Biomaterialia Calcium phosphate coatings on magnesium alloys for biomedical applications: a review. *Acta Biomater.* 8 (1), 20–30. Available from: <https://doi.org/10.1016/j.actbio.2011.10.016>.
- Shanmugasundaram, N., et al., 2001. Collagen-chitosan polymeric scaffolds for the in vitro culture of human epidermoid carcinoma cells. *Biomaterials* 22 (14), 1943–1951.
- Sheikh, F.A., et al., 2016. Hybrid scaffolds based on PLGA and silk for bone tissue engineering. *J. Tissue Eng. Regenerat. Med.* 10 (3), 209–221.
- Sikavitsas, V.I., Temenoff, J.S., Mikos, A.G., 2001. Biomaterials and bone mechanotransduction. *Biomaterials* 22 (19), 2581–2593.
- Silva, G.A., Ducheyne, P., Reis, R.L., 2007. Materials in particulate form for tissue engineering. 1. Basic concepts. *J. Tissue Eng. Regenerat. Med.* 1 (1), 4–24.



- Singh, A.B., Majumdar, S., 2014. The composite of hydroxyapatite with collagen as a bone grafting material. *J. Adv. Med. Dental Sci. Res.* 2, 53–55.
- Sohn, D.-S., et al., 2009. Histomorphometric evaluation of mineralized cancellous allograft in the maxillary sinus augmentation: a 4 case report. *Implant Dentis.* 18 (2), 172–181.
- Sommerfeldt, D.W., Rubin, C.T., 2001. Biology of bone and how it orchestrates the form and function of the skeleton. *Eur. Spine J.: Offic. Public. Eur. Spine Soc. Eur. Spinal Deformity Soc. Eur. Sect. Cerv. Spine Res. Soc.* 10 (Suppl. 2), S86–S95.
- Song, H.-Y., Esfakur Rahman, A.H.M., Lee, B.-T., 2009. Fabrication of calcium phosphate-calcium sulfate injectable bone substitute using chitosan and citric acid. *J. Mater. Sci. Mater. Med.* 20 (4), 935–941.
- Sopyan, I., et al., 2007. Porous hydroxyapatite for artificial bone applications. *Sci. Technol. Adv. Mater.* 8 (1–2), 116–123. Available from: <http://www.sciencedirect.com/science/article/pii/S1468699606002348>.
- Staiger, M.P., et al., 2006. Magnesium and its alloys as orthopaedic biomaterials: a review. *Biomaterials* 27 (9), 1728–1734. Available from: <http://www.sciencedirect.com/science/article/pii/S0142961205009014>.
- Sterio, T.W., et al., 2013. A prospective, multicenter study of bovine pericardium membrane with cancellous particulate allograft for localized alveolar ridge augmentation. *Int. J. Periodon. Restorat. Dentis.* 33 (4), 499–507.
- Suh, J.-K.F., Matthew, H.W.T., 2000. Application of chitosan-based polysaccharide biomaterials in cartilage tissue engineering: a review. *Biomaterials* 21 (24), 2589–2598. Available from: <http://www.sciencedirect.com/science/article/pii/S0142961200001265>.
- Tamimi, F., Sheikh, Z., Barralet, J., 2012. Dicalcium phosphate cements: brushite and monetite. *Acta Biomater.* 8 (2), 474–487. Available from: <http://www.sciencedirect.com/science/article/pii/S1742706111003497>.
- Tan, L., et al., 2013. Biodegradable materials for bone repairs: a review. *J. Mater. Sci. Technol.* 29 (6), 503–513. Available from: <http://www.sciencedirect.com/science/article/pii/S1005030213000558>.
- Tang, J., et al., 2013. Surface coating reduces degradation rate of magnesium alloy developed for orthopaedic applications. *J. Orthop. Transl.* 1 (1), 41–48. Available from: <http://www.sciencedirect.com/science/article/pii/S2214031X13000053>.
- Thian, E.S., et al., 2006. Novel silicon-doped hydroxyapatite (Si-HA) for biomedical coatings: an in vitro study using acellular simulated body fluid. *J. Biomed. Mater. Res. Part B Appl. Biomater.* 76 (2), 326–333.
- Tomlinson, A.W., et al., 2015. Mechanical performance in axial compression of a titanium polyaxial locking plate system in a fracture gap model. *Vet. Comparat. Orthop. Traumatol.* 28 (2), 88–94.
- Törmälä, P., 1992. Biodegradable self-reinforced composite materials; manufacturing structure and mechanical properties. *Clin. Mater.* 10 (1), 29–34. Available from: <http://www.sciencedirect.com/science/article/pii/0267660592900814>.
- Vaccaro, A.R., Madigan, L., 2002. Spinal applications of bioabsorbable implants. *Orthopedics* 25 (Suppl. 10), s1115–s1120.
- Vainionpää, S., et al., 1987. Strength and strength retention in vitro, of absorbable, self-reinforced polyglycolide (PGA) rods for fracture fixation. *Biomaterials* 8 (1), 46–48.
- Valentini, P., Abensur, D., 1997. Maxillary sinus floor elevation for implant placement with demineralized freeze-dried bone and bovine bone (Bio-Oss): a clinical study of 20 patients. *Int. J. Periodon. Restorat. Dentis.* 17 (3), 232–241.

- Vallittu, P.K., Närhi, T.O., Hupa, L., 2015. Fiber glass-bioactive glass composite for bone replacing and bone anchoring implants. *Dental Mater.* 31 (4), 371–381. Available from: <http://www.sciencedirect.com/science/article/pii/S0109564115000172>.
- Van Der Stok, J., et al., 2015. Full regeneration of segmental bone defects using porous titanium implants loaded with BMP-2 containing fibrin gels. *Eur. Cells Mater.* 29, 141–154.
- Vert, M., 2005. aliphatic polyesters: great degradable polymers that cannot do everything. *Biomacromolecules* 6 (2), 538–546. Available from: <https://doi.org/10.1021/bm0494702>.
- Vunjak-Novakovic & Freed, 1998. Culture of organized cell communities. *Adv. Drug Deliv. Rev.* 33 (1–2), 15–30.
- Waizy, H., et al., 2013. Biodegradable magnesium implants for orthopedic applications. *J. Mater. Sci.* 48 (1), 39–50. Available from: <https://doi.org/10.1007/s10853-012-6572-2>.
- Wang, D., et al., 1999. Isolation and characterization of MC3T3-E1 preosteoblast subclones with distinct in vitro and in vivo differentiation/mineralization potential. *Journal of Bone Mineral Res: Offic. J. Am. Soc. Bone Mineral Res.* 14 (6), 893–903.
- Wang, J., de Boer, J., de Groot, K., 2004. Preparation and characterization of electrodeposited calcium phosphate/chitosan coating on Ti6Al4V plates. *J. Dental Res.* 83 (4), 296–301.
- Wang, X., et al., 2002. Bone repair in radii and tibias of rabbits with phosphorylated chitosan reinforced calcium phosphate cements. *Biomaterials* 23 (21), 4167–4176.
- Warden, W.H., et al., 1999. Magnetic resonance imaging of bioabsorbable polylactic acid interference screws during the first 2 years after anterior cruciate ligament reconstruction. *Arthrosc.: J. Arthrosc. Relat. Surg.: Offic. Publicat. Arthrosc. Assoc. North Am. Int. Arthrosc. Assoc.* 15 (5), 474–480.
- Wenz, B., Oesch, B., Horst, M., 2001. Analysis of the risk of transmitting bovine spongiform encephalopathy through bone grafts derived from bovine bone. *Biomaterials* 22 (12), 1599–1606. Available from: <http://www.sciencedirect.com/science/article/pii/S0142961200003124>.
- Whittaker, J.M., et al., 1989. Histological response and clinical evaluation of heterograft and allograft materials in the elevation of the maxillary sinus for the preparation of endosteal dental implant sites. Simultaneous sinus elevation and root form implantation: an eight-month aut. *J. Oral Implantol.* 15 (2), 141–144.
- Witte, F., et al., 2006. In vitro and in vivo corrosion measurements of magnesium alloys. *Biomaterials* 27 (7), 1013–1018.
- Witte, F., et al., 2008. Degradable biomaterials based on magnesium corrosion. *Curr. Opin. Solid State Mater. Sci.* 12 (5–6), 63–72. Available from: <http://www.sciencedirect.com/science/article/pii/S1359028609000357>.
- Witte, F., 2010. The history of biodegradable magnesium implants: a review. *Acta Biomater.* 6 (5), 1680–1692. Available from: <http://www.sciencedirect.com/science/article/pii/S1742706110000966>.
- Wong, H.M., et al., 2010. A biodegradable polymer-based coating to control the performance of magnesium alloy orthopaedic implants. *Biomaterials* 31 (8), 2084–2096. Available from: <http://www.sciencedirect.com/science/article/pii/S0142961209013556>.
- Wong, S., 2015. Investigation on Mg-Mn-Zn alloys as potential biodegradable materials for orthopaedic applications. HKU Theses Online (HKUTO). Available from: <http://hdl.handle.net/10722/208603>.

- Wu, X., et al., 2003. Requirement of calcium and phosphate ions in expression of sodium-dependent vitamin C transporter 2 and osteopontin in MC3T3-E1 osteoblastic cells. *Biochim. Biophys. Acta (BBA) –Molec. Cell Res.* 1641 (1), 65–70. Available from: <http://www.sciencedirect.com/science/article/pii/S016748890300065X>.
- Xiong, Z., et al., 2001. Fabrication of porous poly(l-lactic acid) scaffolds for bone tissue engineering via precise extrusion. *Scripta Mater.* 45 (7), 773–779. Available from: <http://www.sciencedirect.com/science/article/pii/S1359646201010946>.
- Yang, S., et al., 2001. The design of scaffolds for use in tissue engineering. Part I. Traditional factors. *Tissue Eng.* 7 (6), 679–689.
- Yaszemski, M.J., et al., 1996. Evolution of bone transplantation: molecular, cellular and tissue strategies to engineer human bone. *Biomaterials* 17 (2), 175–185.
- Younger, E.M., Chapman, M.W., 1989. Morbidity at bone graft donor sites. *J. Orthop. Trauma* 3 (3), 192–195.
- Zaidi, M., et al., 1989. “Calcium-activated” intracellular calcium elevation: a novel mechanism of osteoclast regulation. *Biochem. Biophys. Res. Commun.* 163 (3), 1461–1465. Available from: <http://www.sciencedirect.com/science/article/pii/0006291X89911431>.
- Zeng, R., et al., 2008. Progress and challenge for magnesium alloys as biomaterials. *Adv. Eng. Mater.* 10 (8), B3–B14. Available from: <https://doi.org/10.1002/adem.200800035>.
- Zhang, Y., Zhang, M., 2001. Synthesis and characterization of macroporous chitosan/calcium phosphate composite scaffolds for tissue engineering. *J. Biomed. Mater. Res.* 55 (3), 304–312.
- Zhang, Y., Zhang, M., 2002a. Calcium phosphate/chitosan composite scaffolds for controlled in vitro antibiotic drug release. *J. Biomed. Mater. Res.* 62 (3), 378–386.
- Zhang, Y., Zhang, M., 2002b. Three-dimensional macroporous calcium phosphate bioceramics with nested chitosan sponges for load-bearing bone implants. *J. Biomed. Mater. Res.* 61 (1), 1–8.
- Zhang, Y., et al., 2003. Calcium phosphate—chitosan composite scaffolds for bone tissue engineering. *Tissue Eng.* 9 (2), 337–345. Available from: <http://www.liebertonline.com/doi/abs/10.1089/107632703764664800>.
- Zhao, H., et al., 2008. Fabrication and properties of mineralized collagen-chitosan/hydroxyapatite scaffolds. *Polym. Adv. Technol.* 19 (11), 1590–1596. Available from: <https://doi.org/10.1002/pat.1174>.
- Zhou, J., et al., 2015. A novel multilayer model with controllable mechanical properties for magnesium-based bone plates. *J. Mater. Sci.: Mater. Med.* 26 (4), 164.

# Novel twisted and coiled polymer artificial muscles for biomedical and robotics applications

# 3

**Lokesh Saharan and Yonas Tadesse**

*Humanoid, Biorobotics and Smart Systems (HBS) Laboratory, Department of Mechanical Engineering, The University of Texas at Dallas, Richardson, TX, United States*

## 3.1 INTRODUCTION

### 3.1.1 DESCRIPTION

Artificial muscle is the name given to those materials that contract and relax like the skeletal muscle upon the application of external stimuli. The stimuli could be a chemical or physical stimulus (Tondu, 2015). There have been several methods of creating artificial muscles based on different working mechanisms. Some of the most common ones are electrochemical actuation, electrostatic actuators, piezoelectric, carbon nanotube (CNT), shape memory alloys (SMAs), pneumatic muscles (PMs), and composites. Artificial muscle has attracted the attention of many researchers, after the long usage of engines and motors for powering mechanical systems. Artificial muscles have been used for the design and development of biomedical devices and biomimetic robots. However, the ideal biomimetic robots require specially designed actuators that can replicate the behavior of natural muscle. Natural muscles are impeccably capable of sensing, acting, and calculating. Such replica of an artificial muscle is required for biomedical and robotic applications that have advanced and higher performance. In this development, most of the artificial muscles faced a limitation on one or another front and hence mainly failed to compete with mammalian muscles. This has led to further curiosity and recently accelerated research in the field of artificial muscles. Recently, Haines et al. introduced a better alternative to expensive existing artificial muscles with better performances. The muscles are made by twisting and coiling and some heat treatment, so we call them twisted and coiled polymer (TCP) muscles (Haines et al., 2014a). These muscles have a large strain ( $\sim 50\%$ ), high power to weight ratio comparable to that of a jet engine (5.26 kW), and can lift 100 times greater load than human muscle. We will explain the fabrication process of these novel muscles in a later section. The

muscles can be made using commercially available materials used for sewing thread or fishing lines such as nylon 6, nylon 6,6, or polyethylene precursor fibers.

### 3.1.2 FABRICATION OF BASIC TWISTED AND COILED POLYMER MUSCLES

The typical muscle fabrication process is shown in Fig. 3.1(i). The precursor fiber of a certain length (usually thrice the desired length of the muscle) is tied on one side to a motor and the other side to a linearly guided dead weight (M) of optimum value (depending of type and thickness of the material) and the motor is rotated. The dead weight is used to keep the thread in tension during the twist insertion. The precursor fiber decreases in length as it is twisted. During the twist insertion, after a sufficient number of twists get into the fiber and it can no longer take more twists, the fiber starts coiling on its own axis or one can coil the twisted fiber over a mandrel (shown in the inset figure). The fully coiled structure is shown in Fig. 3.1(i)d. Since twist insertion builds up stresses in the fiber, the fiber is annealed above 105°C either by resistive heating (Fig. 3.1(i)e) or using a furnace (Fig. 3.1(i)f). The muscle is finally trained for actuation by applying voltage under a load until consistent actuation is obtained. Some fabrication and performance results are presented in IMECE 2016 (Saharan and Tadesse, 2016a).

### 3.1.3 STRUCTURES AND WORKING PRINCIPLES OF TWISTED AND COILED POLYMER MUSCLES

TCP muscles were invented by the understanding of the molecular structure of the polymeric precursor fibers. According to Haines et al. (2014a), these fibers are composed of highly flexible and oriented (in fiber direction) polymeric chains. These fibers are semicrystalline in nature and have a small negative thermal coefficient in the crystalline region, but they are capable of significant reversible contractions in noncrystalline regions when heated because they are less conformationally constrained in the noncrystalline region. This can result in 4% of strain for nylon 6,6 precursor fiber (Haines et al., 2014a), which is comparable to Ni-Ti SMA wires. This effect can be amplified by adding twist into the fiber, which makes them chiral. The amount of twist inserted and chirality largely affects the material behavior.

Chirality plays a significant role in actuation behavior of the TCP. The term *chirality* is derived from the Greek word for hand,  $\chi\epsilon\iota\rho$  (“their”). As seen in Fig. 3.1(ii), tensile actuation of the material is dependent on the fiber bias angle where positive and negative tensile actuation are according to the chirality of the fiber. The heterochiral structure exhibits extensional motion, whereas the homo-chiral coiled fibers contracts upon heating.

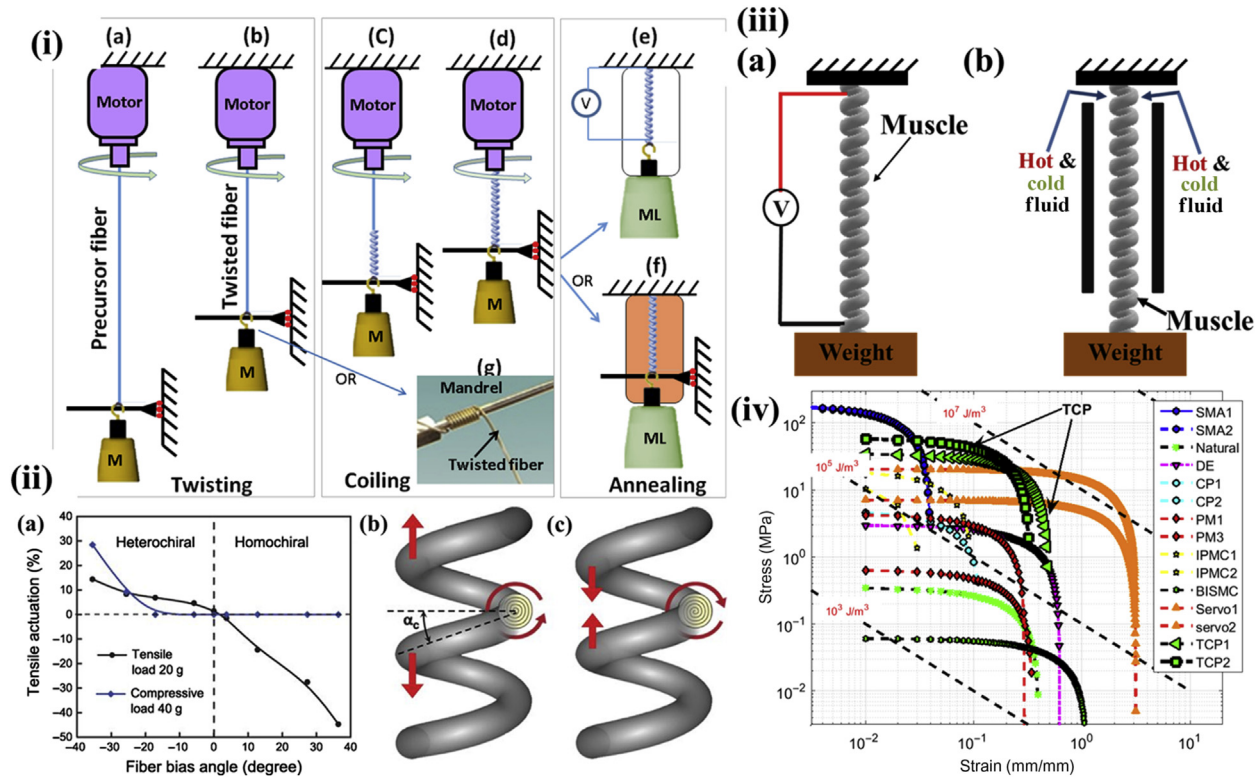


**FIGURE 3.1**

(i) Fabrication process of TCP and actuation of TCP muscles: (a,b) twisting, (c,d) self-coiling, (e,f) training, and (g) twisting and coiling on mandrel. (ii) Chirality and actuation mechanism: (a) comparison of the heterochiral and homochiral tensile and compressive actuation, (b) heterochiral coiling and actuation mechanism, and (c) homochiral coiling and actuation mechanism. (iii) Mechanism of actuation of the TCP muscles using (a) electrothermally and (b) hot and cold fluid. (iv) Comparison of TCP actuators with other actuator technologies, blocking stress-strain and energy density (Haines et al., 2014a; Tadesse, 2013). CP, Conducting polymer; SMA, shape memory alloy; DE, dielectric elastomer; PM, pneumatic muscle; BISM, bioinspired muscle; BMF, biomimetic fiber SMA; IPMC, ionic polymer-metal composite; Servo, small RC servo HS81; Natural, skeletal muscles; TCP, twisted and coiled polymer muscle.

Figure adapted from (ii) Haines, C.S., Lima, M.D., Li, N., Spinks, G.M., Foroughi, J., Madden, J.D., et al., 2014a. Artificial muscles from fishing line and sewing thread. *Science* 343, 868–872. (iv) Tadesse, Y., Wu, L., Saharan, L.K., 2016. Musculoskeletal system of bio-inspired robotic systems. *Mech. Eng.* 138.

When the chirality of the precursor fiber and coils matches (which is called homochirality), then the actuator will contract whereas opposite chirality (heterochirality) leads to expansion of the muscle. Fig. 3.1(ii) shows the homochiral and heterochiral muscles and their behavior. The muscle can be fabricated with desired chirality as per requirement. The actuation is a reversible contraction and it depends on the material's physical properties, for example, nylon 6,6 has a large thermal contraction (4%–34%) between 20°C and 240°C due to its high melting point when compared with polyethylene having a temperature range of 20°C–130°C providing smaller contractions (0.3%–16%) (Haines et al., 2014a). Human muscle has a contraction of 20%, which is less than 34% provided by nylon 6,6 based TCP muscle. These capabilities make these muscles a distinct candidate for application in orthosis, prosthetics, robotics, and many other biomedical applications.

Fig. 3.1(iii) shows the different mechanisms of actuating the TCP muscles, which can be either hot air blown to the surface of the structure, or hot and cold fluid supplied in a confined space to transfer heat to the polymer structure or by applying voltage across the polymer composite. For the electrical actuation, a conductor or metal coating of the polymer is a necessary condition.

### 3.1.4 COMPARISON WITH OTHER SOFT ACTUATORS

TCP muscle is a great alternative to conventional actuators such as DC motors, pneumatic, and hydraulic muscles including the SMA. TCP muscle has a tremendous power to weight ratio. It has impeccable qualities when comparing them on various parameters such as cost, availability, working principle, and application. This muscle requires polymeric fibers such as nylon 6, nylon 6,6, and polyethylene as precursor material, which are readily available in many places at very low cost. The muscle requires heat as an input, which can be provided using some fluid like water, or it can be actuated electrothermally, which makes its application versatile from the actuator, a sensor to energy harvester. Along with the qualities above, this material can be easily manufactured anywhere with easily available tools by following the standard procedure. The fabrication process will be explained in later sections along with performance characteristics.

The important performance parameters for comparison of the muscle are the stress and strain (Smith et al., 2011; Tadesse, 2013). Stress produced implies the amount of force per unit area ( $\sigma = F/A$ ) of the actuator. Strain ( $\epsilon = \Delta l/l$ ) is defined as the amount of the displacement produced by the actuators per unit of its length. Strain enables us to find the suitable actuator for a given application. The comparative chart for the actuators performance [Fig.3.1(iv) (Tadesse et al., 2016)] in terms of stress–strain and energy per unit volume for actuators suitable for soft robotics, humanoids, and prosthetics is of utmost important. The chart shows the SMA being the highest in energy density  $10^5$ – $10^7$  J/m<sup>3</sup> (diagonal lines) and stresses of greater than 100 MPa. SMA was considered to be the best option for low-frequency applications until it was challenged by recently invented



coiled and twisted polymeric muscles. SMA is expensive, difficult to fabricate, and it has limitations such as high hysteresis (Haines et al., 2014a,b; Wu et al., 2015b; Madden et al., 2004; Tadesse, 2013), which can be replaced by TCP muscles.

The only limitation of TCP muscles is efficiency when compared with the DC motors. The efficiency of the muscle is slightly above 1%. Lower efficiency can make actuators power hungry, which can lead to the demand for large battery packs. Efficiency issue can be easily dealt with by using a locking mechanism. Locking mechanisms are the devices that help robotic manipulators, prosthetic hands or orthotic devices to hold a certain position by mechanically locking the position. These devices are helpful in robotic, prosthetic (Saharan and Tadesse, 2016c), and orthotic applications.

---

## 3.2 DETAILED FABRICATION OF THE TWISTED AND COILED POLYMERIC MUSCLES

TCP muscle can be fabricated by following the right procedure on the precursor fiber. Single twisted and coiled muscle is called 1-ply muscle. Multiple 1-ply muscle can be plied together to create 2-ply, 3-ply, or more plied muscles. Typically, 1-ply, 2-ply, and 3-ply muscles have been reported and studied widely in the literature. Mainly two types of precursor fibers have been described in the literature. Silver-coated precursor fibers (Haines et al., 2014a; Saharan and Tadesse, 2016a; Wu et al., 2016a; Cho et al., 2016) (such as mono or multifilament nylon 6,6) are used to fabricate the muscles, which can be driven electrothermally. Silver-coated fibers have a thin coating of the silver on the precursor fiber, which helps to generate heat in the muscle by application of electrical potential (Joules effect). Such muscles can be used along with batteries on mobile devices. Silver coating or painting can also be applied to the muscle during twist insertion for the precursor fibers with no silver coating on them (Mirvakili et al., 2014). Another type of muscles can be precursor fibers without silver coating on them (Haines et al., 2014a; Wu et al., 2015a; Saharan and Tadesse, 2016b). Without the silver coating, the muscle is actuated by alternating flow of hot and cold fluid such as water. Also, recently, Semochkin (2016) has presented a device to manufacture the TCP muscle with a heater wire in an automated manner. Both types of the muscles have similar type of the procedure for fabrication. The procedure involves twist insertion under a certain load followed by coiling.

### 3.2.1 TWISTING

Twist insertion is a process in which a load of optimum values is tied to the precursor fiber on one end and the other end is tied to a motor that rotates at a certain speed. As described above, twist insertion will bring chirality to the



muscle, which amplifies the linear stroke. Typically three times the length of precursor fiber is desired of the intended muscle length. The amount of weight used as a preload or stress (Haines et al., 2014a) and twist insertion speed (Saharan and Tadesse, 2016a) will affect the properties of the fiber. For example, 10, 16, and 35 MPa stresses during the coiling can give different spring indices of the muscle of 1.7, 1.4, and 1.1, respectively, for a 127  $\mu\text{m}$ , nylon 6,6 monofilament precursor fibers, according to Haines et al. For a silver-coated multifilament nylon 6,6 of 200  $\mu\text{m}$  diameter, twist insertion (Wu et al., 2016a; Tadesse et al., 2016; Saharan and Tadesse, 2016a) was reported at 9.9 MPa. Load or weight on the muscle during twist insertion plays an important role since too much weight can break the fiber during twist insertion whereas less weight can cause snarling in the fibers. Different combination of weight and speed would give a different properties (Saharan and Tadesse, 2016a). Fig. 3.2(i) shows a typical TCP muscle fabrication process of 1-ply muscle and plying together 1-ply muscles for making 2-ply muscles. The process (a) to (b) in the figure is the twisting process using an electric motor at the top and a dead weight at the bottom. The weight is constrained to translate only. The weight is not simply hung; it is supported by a guide for the linear displacement at the fiber is twisted. These properties can be managed for various applications by varying fabrication process. The total amount of twist inserted in the precursor fiber affects the performance of the muscle. A large number of twists will create high-performance muscle. The twisting will lead to self-coiling.

### 3.2.2 COILING

Once the fiber is twisted extremely, it will start coiling on its own. The coil could start from the top or the bottom along the axis. The process from (b) to (c) in Fig. 3.2(i) is the coiling process, where an increased diameter is seen for the coiled structure. Twist insertion will make the precursor fiber stiffer where more twist will cause coiling of the muscle about the axis of rotation. This coiling is a result of extreme twist insertion. The packing density of the coil will be determined by the amount of stress during the coiling. Another type of coiling is mandrel coiling (Wu et al., 2015c; Haines et al., 2014a). After twist insertion, a mandrel can be used to wrap the twisted muscle around it. Various shapes for mandrel coiling can be used to create spring structures of varying shapes and sizes. A cylindrical muscle can be obtained by wrapping the muscle around a cylindrical rod (Haines et al., 2014a) whereas a cone can create a conical shaped muscle (Haines et al., 2016) and mandrel coiling will facilitate a large stroke at the cost of the stresses produced by the muscle. Coiled muscle will try to unwind due to internal stresses.

Muscle is largely driven by the torsion of twisting and untwisting of the fiber under the influence of the temperature; the same amount of twist inserted in two different fibers would cause the same amount of tensile untwist. According to the

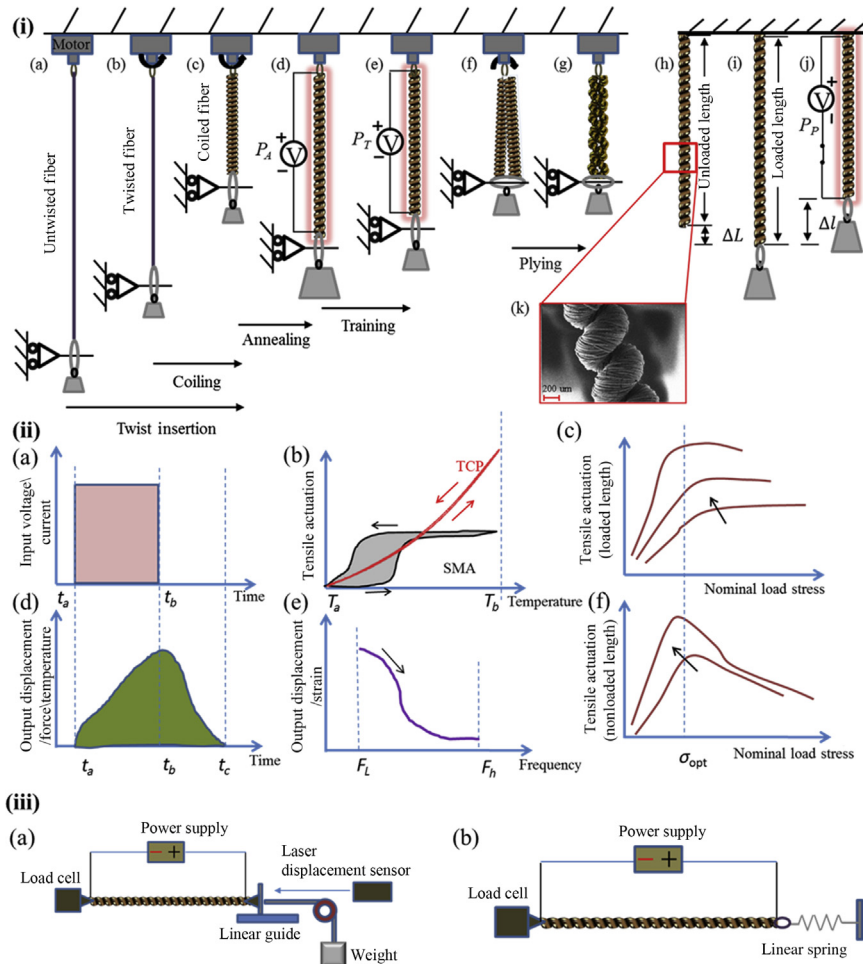


**FIGURE 3.2**

(i) Illustration of the fabrication process for TCP muscles: (a) The top end of the precursor fiber is attached to the motor and the bottle end was hooked with a dead weight, which keeps the precursor fiber straight and taut. (b) The twist is inserted in the fiber after the motor starts rotating in a counterclockwise direction. (c) The twisted nylon fibers form continuous, regular coils throughout the thread length. (d) A 1-ply muscle is annealed by electrothermal heating. (e) The muscle is then receiving training by electrothermal heating. (f) A 2-ply muscle is formed by plying two-coiled 1-ply muscles together during the motor's clockwise rotating direction. (g) After finishing annealing and training, TCP muscle contracts upon receiving heating. (h) unloaded length of the finished 1-ply muscle, (i) change in length of the muscle due to an applied constant load, (j) the actuation behavior of the muscle upon application of electrical power, (k) SEM image of the unloaded 1-ply muscle. (ii) Typical characteristics of TCP muscles based on current knowledge on the material. (a) Input voltage and current supplied versus time; (b) the corresponding displacement, force, and temperature profile of the actuator; (c) tensile actuation versus temperature of TCP compared with SMA actuator; (d) strain versus frequency relation; (e) tensile actuation under loaded length versus nominal applied stress; and (f) tensile actuation under nonloaded length versus nominal applied stress. (iii) Displacement/strain measurement of a TCP muscle (a) under static load and (b) under dynamic load.

(i) Figure adapted from Wu, L., Jung De andrade, M., Saharan, L., Rome, R., Baughman, R.H., Tadesse, Y., 2016a. Compact and low-cost humanoid hand powered by nylon artificial muscles. *Bioinspirat. Biomim.* (submitted).

study by Haines et al. (2016), coiling due to twist insertion happens beyond a critical torque,  $\tau_c$ , which is given by Ross (1977):

$$\tau_c = \sqrt{2EIF} \quad (3.1)$$

where  $E$  is the young's modulus of the material ( $\text{N/m}^2$ ),  $I$  is the second moment of area of a fiber of circular diameter ( $D$ ) given by  $\pi D^4/16$  ( $\text{m}^4$ ), and  $F$  is the tensile load applied on the material for twist insertion ( $\text{N}$ ).

For the coils made under a tensile load  $F$ , the same stress  $\sigma$ , is given by:

$$\sigma = F/A, \text{ where } A = \pi D^2/4 \quad (3.2)$$

Critical twist to coil,  $T_c$  is given by:

$$T_c = \frac{\tau_c}{2\pi JG'} \quad (3.3)$$

where  $T_c$  is the critical twist torque required for coiling (Turns/m),  $J$  is the polar moment of inertia given by  $= \pi D^4/32$  for a cylindrical fiber ( $\text{m}^4$ ), and  $G'$  is the shear modulus of fiber material ( $\text{N/m}^2$ ).

Now combining (3.1) and (3.3) will give us the twist required to coil a fiber:

$$T_c = \frac{2\sqrt{2\sigma E}}{\pi D G'} \quad (3.4)$$

This equation shows us that for the same tensile loading, twist required to coil a cylindrical fiber is inversely proportional to the fiber diameter. Irrespective of the coiling method or coiling parameter, the samples should maintain the twisted and coiled structure. Therefore, annealing is required for the muscle to retain the shape.

### 3.2.3 ANNEALING (HEAT TREATMENT)

Coiling is a cold working process on the muscle. This process will induce stresses in the structure. To keep the shape of the structure, annealing is essential. Annealing is a heat treatment process that relieves stresses in the structure, and enables to maintain the shape and obtain desired properties. As we have described in the previous section, two different types of the muscles, one with the silver coating on it and another one without silver coating, are the common electrothermally actuated muscles. These types of the muscles can be annealed differently. Silver-coated muscles can be annealed electrothermally. Muscle without metal coating can be annealed in a heated environment or in a furnace.

Fig. 3.2(i)d shows an annealing setup for silver-coated TCP muscle. This can be called electrothermal annealing, by applying a voltage or electrical power across the muscle. For muscles made of commercially available conductive sewing thread (Shieldex 260151023534oz) (Saharan and Tadesse, 2016a) were annealed by using voltage equal to one volt per unit length of the muscle. Another parameter is electrical current annealing. Typically, 0.6, 0.7, and 0.8 A

magnitude of the current can be used for electrothermal annealing of the 1-ply, 2-ply, and 3-ply muscles. Electrothermal annealing is mostly done in cycles. Typically, 12 power cycles for 20–40 seconds are good enough depending on material and number of plies.

The other approach is annealing in a furnace for bare precursor fiber. For example, a coiled muscle fabricated using 400  $\mu\text{m}$  nylon fishing line in a furnace at 180°C for 90 minutes (Saharan and Tadesse, 2016b). Some researchers prefer to anneal in a medium other than air. For example, Kianzad et al. (2015a) have used nitrogen for annealing of the muscle. Nitrogen annealing is good, especially in the case of silver-coated precursor fibers since nitrogen avoids the oxidation of the silver on the muscle surface, which is directly related to the life and performance of the muscle. The heat-treated structure needs to be trained for the specific application and completes the fabrication process.

### 3.2.4 TRAINING

Training of the muscle is required to obtain reversible actuation cycle under a load. Fig. 3.2(i)e shows the annealing process. For this purpose, the annealed structure undergoes multiple on and off cycles for the amount of load for which it is going to be used. For example, if the muscle is required to be used to open and close a valve, it has a known amount of force required to open the valve. The training load is also a function of spring index of the muscle. Monofilament, nonsilver-coated muscles with comparatively larger diameter are stiffer and require more force to obtain better coil spacing. So, the muscle can be trained on a dead weight equal to the amount of force required to open and close the valve. Another parameter to decide here is what kind of muscle are we using? If we are using an electrothermal muscle, we need a power supply and a stop watch to train the muscle. Another option could be a computer controlled power supply, which can give electrical power cycles through a computer program. Muscle without silver coating may require an arrangement for alternating hot and cold water switching mechanism. Hot air blower can also be used but that would not be a great option for control of the hot air flow and heat loss can potentially be an issue. Once a particular method of training is selected, the number of cycles, load, and magnitude of stimuli (voltage/hot fluid) are determined accordingly. Some training cycles presented are as follows: 12–15 power cycles of training with 50% duty cycle are sufficient for the training of the muscles (Saharan and Tadesse, 2016a).

Another possible training method could be training under dynamic loadings such as springs. Dynamic loading is a special case for loading since the force keeps on increasing or decreasing with the displacement. For example, spring force ( $F = kx$ ) is a function of the amount of extension of the spring. In such cases, the muscles should be trained for the maximum amount of force required. One of the training techniques yet to be explored is dynamic training. In dynamic

**Table 3.1** TCP Muscle Fabrication Parameters Used in a Study (Saharan and Tadesse, 2016a)

Property	1-Ply	2-Ply	3-Ply
Precursor fiber diameter ( $\mu\text{m}$ )	200	200	200
Precursor fiber length	711	850	711 (three 1-ply)
Coil diameter, $d$ ( $\mu\text{m}$ )	920	1260	1720
Coiled length (mm)	192	244	192 (3 quantity)
No. of twist per mm	1.14	1.14	1.14
Total no. of twists	810	$936 \times 2$	$810 \times 3$
No. of annealing cycles, (voltage)	12 (60 s each)	12 (60 s each)	12 (60 s each)
No. of training cycles	12 (30 s each)	12 (30 s each)	12 (30 s each)
Annealing voltage based on length (V/inch)	1.1	1.1	1
Length used for performance testing (mm)	95	90	92

training, one can use a spring of variable stiffness or variable weight. Evidence of such training is not present in the literature yet.

The entire process of fabricating 2-ply muscle is shown in Fig. 3.2(i) from twisting, coiling, annealing, training, and actuation testing. Another fabrication process is also presented that compares the 1-ply, 2-ply, and 3-ply muscles as shown in Table 3.1 (Saharan and Tadesse, 2016a), where two 1-ply muscles are plied together to form 2-ply muscle. In such case, a higher load than the load used to make 1-ply muscle was used. Similarly, 3-ply muscles are made following the same analogy.

Different manufacturing methods as shown in Table 3.2 were described by various researchers. Haines et al. have described wide variety of precursor fibers and their performance.

### 3.3 CHARACTERISTICS AND PROPERTIES OF TWISTED AND COILED POLYMER MUSCLES

As with any other materials, the performance characteristics and properties of TCP muscles are dependent on the fabrication procedure/parameters, type of raw material, and working environment. These muscles can have two degrees of motion: linear motion and rotary motion. They produce strain linearly and rotate about their central axis due to twisting and untwisting of the fibers. Linear strain is significant and is of utmost importance. The rotary motion has less force generation capability and it has not gained much attention from researchers.

**Table 3.2** Various Muscle Fabrication Parameters Used by Different Investigators ([Saharan and Tadesse, 2016a](#))

Authors	Type of Muscle	Stresses/Load	Fiber Diameter ( $\mu\text{m}$ )	Annealing Time/Cycle	Annealing Temperature	Method	Medium
<a href="#">Haines et al. (2014a)</a>	Fishing line/silver-coated nylon	Variable (diameter dependent)	76–2450	Variable	Variable	Constant temp.	Air
<a href="#">Wu et al. (2015a)</a>	Fishing line	900 g	800	2 h	180°C	Constant temp.	Air
<a href="#">Yip and Niemeyer (2015)</a>	Silver-coated nylon	50 g	720	20 cycles	150°C	Joule heating	Air
<a href="#">Cherubini et al. (2015)</a>	Silver-coated nylon	25 MPa	500	1 h	150°C	Constant temp.	Air
<a href="#">Moretti et al. (2015)</a>	Silver-coated nylon	25 MPa	500	1 h	150°C	Constant temp.	Air
<a href="#">Kianzad et al. (2015a)</a>	Silver-coated nylon	21 MPa	294	30 min	180°C	Constant temp.	Nitrogen
<a href="#">Mirvakili et al. (2014)</a>	Silver painted nylon	1–9 N	180/296	20 cycles	N/A	Joule heating	Air
<a href="#">Tadesse et al. (2016)</a>	Silver-coated nylon	120 g	180	30 cycles	Variable	Joule heating	Air
<a href="#">Saharan and Tadesse (2016a,b,c)</a>	Silver-coated nylon	125 g	200	Varying	Variable	Joule heating	Air

The linear strain is also a function of the type of chirality of the muscle. As discussed in the earlier section, the homochiral muscles would show linear contraction whereas heterochiral muscles would show linear expansion. Both types of linear strains have their importance and application in the biomedical and soft robotics fields. Important characteristics of artificial muscles are stress generation or force, strain or displacement, input power, output energy or power, efficiency, frequency of operation, life cycle, repeatability, and cost. Most of these parameters are quantified and we will present here some results presented in the literature. We also discussed how these parameters are measured to synchronize with other input stimuli such temperature to understand the muscles. Time domain stress and strain have been measured by some researchers (Saharan and Tadesse, 2016a; Tadesse et al., 2016; Haines et al., 2014a; Wu et al., 2016a) in literature. We will discuss here strain and force measurement for the 2-ply and 3-ply muscles.

The key characteristic curves of TCP muscles are shown in Fig. 3.2(ii). A square wave voltage is shown in Fig. 3.2(ii)a for electrically actuated TCP muscles with starting time  $t_a$  and end time  $t_b$ , the corresponding outputs of the muscle (displacement, force, and temperature) will have a profile as shown in Fig. 3.2(ii)b. The magnitudes will increase until the voltage is turned off at  $t_b$ ; this is the heating phase of the muscle. Then, the profile starts decreasing until time  $t_c$ ; this is the cooling phase. Fig. 3.2(ii)c shows a typical plot of tensile actuation versus temperature plot compared with SMA actuators that have large hysteresis. Fig. 3.2(ii)d is the output displacement or strain versus frequency. The decrease in strain at high frequency is common to all smart materials. Another characteristic curve is the tensile actuation versus nominal applied stress. Fig. 3.2(ii)e shows an increase at the initial stage and relatively constant tensile actuation afterwards as the applied load is increased. This tensile actuation is based on the normalization with respect to loaded length. The loaded length is increasing as the applied load is stretching the material axially. Fig. 3.2(ii)f shows a characteristic curve where the initial length for tensile actuation is nonloaded length. In this case, the tensile actuation versus applied load increases initially and decreases at optimum applied load. Note that the nonloaded length is shorter than the loaded length; as a result the strain magnitude will be different for the two cases.

The profiles shown in Fig. 3.2(ii) are based on the current development of the materials and some of the measurement can be done to determine properties under different circumstances. We will discuss displacement/strain, force/stress, frequency, and microscope images of the TCP muscles.

### 3.3.1 STRAIN AND FORCE MEASUREMENT

Strain is the ratio of the change in length to the original length of an actuator. It is often expressed in percentage. There are two different types of strain measurement, under a constant load measurement or under a variable load. Fig. 3.2(iii)a shows the experimental setup for the strain measurement under the constant

loading and Fig. 3.2(iii)b is the strain under variable load or spring. The setup includes displacement sensor, load cell, power supply, linear guide for initial pre-stress and a load. The strain is given by the following equation:

$$\varepsilon = \frac{L_f - L_i}{L_f} 100\% \quad (3.5)$$

where  $L_f$  is the final length of the actuator after the application of stimuli.  $L_i$  is the initial length of the actuator before the stimulus is applied. If the loaded or unloaded length of the actuator is used for the strain calculation, the strain profile will be different as noted earlier in Fig. 3.2(ii)e and f.

The power supplied to the muscle during actuation (usually electrical power is given) is described in terms of the power applied to the muscle per length of the muscle, which is normalized power  $P_N$ .

$$P_N = \frac{VI}{L_i} \quad (3.6)$$

where  $V$  is the voltage,  $I$  is the current supplied to the muscle, and  $L_i$  is the initial length of the muscle before actuation and loaded length.

First, let us discuss the actuation response of the silver-coated muscles. Wu et al. (2016a) have used a laser displacement sensor (Keyence LK-G152) to measure the strain against the fixed hanging weight. Two different results are presented in Fig. 3.3(i) for 2-ply and 3-ply muscles. Fig. 3.3(i)a shows the tensile actuation of a 2-ply muscle under a loading of 200 g weight (Wu and Tadesse, 2016). This result is for applied electrical power of 23.7% duty cycle and a period of 70 seconds. Three different power cycles were presented in Fig. 3.3(i)a for 0.18, 0.22, and 0.25 W/cm. Maximum actuation was 14% for 0.25 W/cm for a 2-ply muscle. In a similar experiment for 3-ply muscle for 200 g loading, three different power cycles of 0.21, 0.27, and 0.33 W/cm were used.

Actuation response for the nonsilver-coated muscles is also present in the literature. In a study, Wu et al. have presented the tensile actuation of the water driven muscle. Fig. 3.3(ii) shows the response of a 1-ply fishing line muscle actuated by hot water that varies from 60°C to 99°C. The maximum tensile actuation is around 23% at 99°C of water when loaded with 200 g of weight (Wu and Tadesse, 2016).

The tensile actuation strain as a function of temperature change was investigated for various material. Fig. 3.3(iii) shows the comparison of the tensile actuation of the different materials presented by Haines et al. (2014a) in *Science* when they introduced the TCP muscle for the first time. In the inset, tensile actuation of the precursor fiber was also reported without twisting and coiling. The large graph is the effect of extreme twisting and coiling of the polymer muscles. Silver-coated nylon 6,6, nylon 6, and polyethylene are some of the materials investigated.

In a recent study, Haines et al. (2016) have shown 200% actuation of the TCP muscles that are spiral in shape. A result from the publication is shown in the



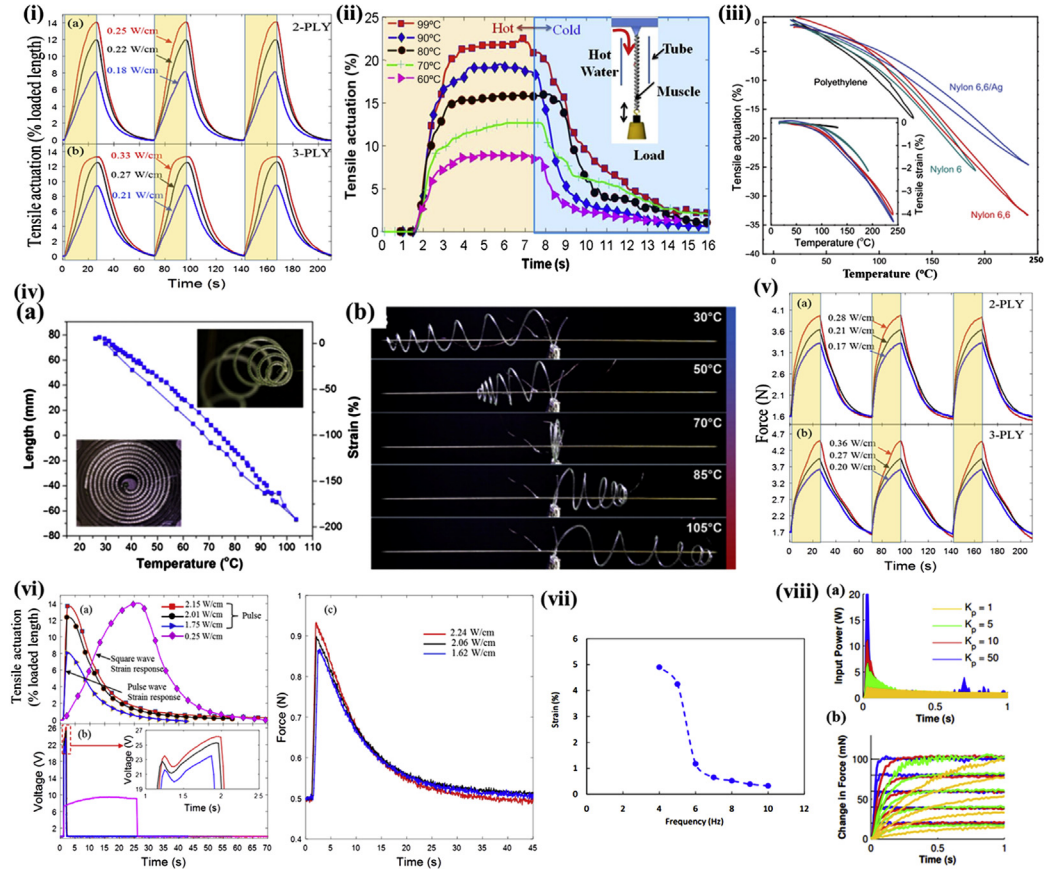


**FIGURE 3.3**

(i) Showing the percentage actuation for a TCP muscle (a) for 2-ply and (b) for 3-ply muscle. (ii) Tensile actuation of a coiled fishing line muscle actuated using hot and cold water with 200 g of load. (iii) Tensile actuation comparison of TCP muscle based on different materials.

(Continued)

- ◀ Inset is the comparison of actuation of the different precursor fiber. (iv) Twist on artificial muscle shows the 200% tensile actuation of a TCP muscle: (a) strain versus temperature and (b) optical picture of the muscle when actuated electrically. (v) Force measurement for three power cycles obtained from a Futek load cell (LBS-200) under the loading of an extension spring: (a) for 2-ply muscle; (b) for 3-ply muscle. (vi) Results for a pulsed actuation experiments using three different power cycles: (a) tensile actuation in comparison with a square wave actuation; (b) voltage input; (c) force response for similar power input cycles. (vii) The frequency response of silver plated sew thread TCP under a load of 25 MPa. (viii) Effect of closed loop controller on the TCP muscle: (a) input power and (b) change in force.

Figure adapted from (i) Wu, L., Jung De andrade, M., Saharan, L., Rome, R., Baughman, R.H., Tadesse, Y., [2016a](#). Compact and low-cost humanoid hand powered by nylon artificial muscles. *Bioinspirat. Biomim.* (submitted). (ii) Wu, L., De andrade, M.J., Rome, R.S., Haines, C., Lima, M.D., Baughman, R.H., et al., 2015a. Nylon-muscle-actuated robotic finger. In: *SPIE Smart Structures and Materials + Nondestructive Evaluation and Health Monitoring, International Society for Optics and Photonics*, 94310I-94310I-12. (iii) Haines, C.S., Lima, M.D., Li, N., Spinks, G.M., Foroughi, J., Madden, J.D., et al., 2014a. Artificial muscles from fishing line and sewing thread. *Science* 343, 868–872. (iv) Haines, C.S., Li, N., Spinks, G.M., Aliev, A.E., Di, J., Baughman, R.H., [2016](#). New twist on artificial muscles. *Proc. Natl Acad. Sci.*, 201605273. (v) Wu, L., Jung De andrade, M., Saharan, L., Rome, R., Baughman, R.H., Tadesse, Y., [2016a](#). Compact and low-cost humanoid hand powered by nylon artificial muscles. *Bioinspirat. Biomim.* (submitted). (vi) Wu, L., Jung De andrade, M., Saharan, L., Rome, R., Baughman, R.H., Tadesse, Y., [2016a](#). Compact and low-cost humanoid hand powered by nylon artificial muscles. *Bioinspirat. Biomim.* (submitted). (vii) Mirvakili, S.M., Ravandi, A.R., Hunter, I.W., Haines, C.S., Li, N., Foroughi, J., et al., [2014](#). Simple and strong: twisted silver painted nylon artificial muscle actuated by Joule heating. In: *SPIE Smart Structures and Materials + Nondestructive Evaluation and Health Monitoring, International Society for Optics and Photonics*, 90560I-90560I-10. (viii) Yip, M.C., Niemeyer, G., [2015](#). High-performance robotic muscles from conductive nylon sewing thread. In: *Robotics and Automation (ICRA), 2015 IEEE International Conference on. IEEE*, pp. 2313–2318.

Fig. 3.3(iv). According to the explanation in the publication, there are two reasons, which limit the actuation of the muscle. The first reason is the amount of twist inserted in the muscle. Since these are the torsional muscles, the amount of twist determines the tensile stroke (Aziz et al., 2016). The second reason could be the coils being constrained by the adjacent coils. The second one is more prevalent than the former (Haines et al., 2016). As can be seen from the figure, this is a special case of the TCP muscle, that is, conical. Therefore, each coil is free to move and they pass through each other to cause displacement more than 100%. The figure clearly shows that muscle from one end to the other travels from +80 to −80 mm.

### 3.3.2 FORCE MEASUREMENT

Stress generated by the muscle shows the capability and the application area where the muscle can be used. Stresses can be calculated by measuring the force generated by the muscle. There are several studies that presented the force generated by the muscle. Force measurement typically requires a load cell. In our previous studies, we have used Omega LCL-010, Futek LBS-200 load cells, or just hanging a dead weight. Force generated by single, double, and triple plied muscles would typically be lying in the range on 0–5 N based on the number of plies, material, and applied power. Force generated is typically large for the larger diameter precursor fibers. Force generated would also drop significantly for mandrel coiled muscles. Again, both the different types of loading will generate different types of stresses in the muscle. Static loading would generate constant stress. For example, a muscle of 1.35 mm diameter (typical diameter of a 200  $\mu\text{m}$  multifilament, 2-ply muscle) under 150 g (1.5 N), 200 g (2 N), and 300 g (3 N) would be 1, 1.37, and 2.05 MPa, respectively. Several cases of the static loading were reported by Haines et al. (2014a). Similarly, we can load different types of muscle with static loads for constant stresses. Dynamic loading using a spring was presented (Wu et al., 2016a) in one of our previous studies.

The stress generated by the actuator  $\sigma$  can be obtained from the following equation:

$$\sigma = \frac{F - F_a}{A} = \frac{F_{\text{eff}}}{A} = \frac{4F_{\text{eff}}}{\pi D^2} \quad (3.6)$$

where  $F$  is the force obtained from measurement during actuation;  $F_a$  is the applied force or prestress in the muscle;  $F_{\text{eff}}$  is the effective force, which is the difference between generated and the applied force/load;  $A$  is the cross sectional area of the muscle; and  $D$  is the diameter of the muscle. The muscle is assumed to have circular cross section.

Results for 2-ply muscles for the three different power cycles of 0.17, 0.21, and 0.28 W/cm are in Fig. 3.3(v)a for three cycles each. The results are very consistent and repeatable. The force starts at 1.6 N, which is a small amount of prestress required for the muscle. So, the effective force for 0.28 W/cm is 2.5 N,

which is highest for this power density. Similarly, results for 3-ply muscle, the force is shown in Fig. 3.3(v)b. A slightly higher prestress of 1.7 N was used to obtain approximately 3.1 N of force. If we compare the 0.28 and 0.27 W/cm applied power for the 2-ply and 3-ply muscles from the figure, we can conclude that 2-ply has generated the slightly higher force for the same power. Hence, we can conclude that 2-ply muscles are more efficient than 3-ply muscle.

### 3.3.3 FREQUENCY MEASUREMENT AND PULSED ACTUATION

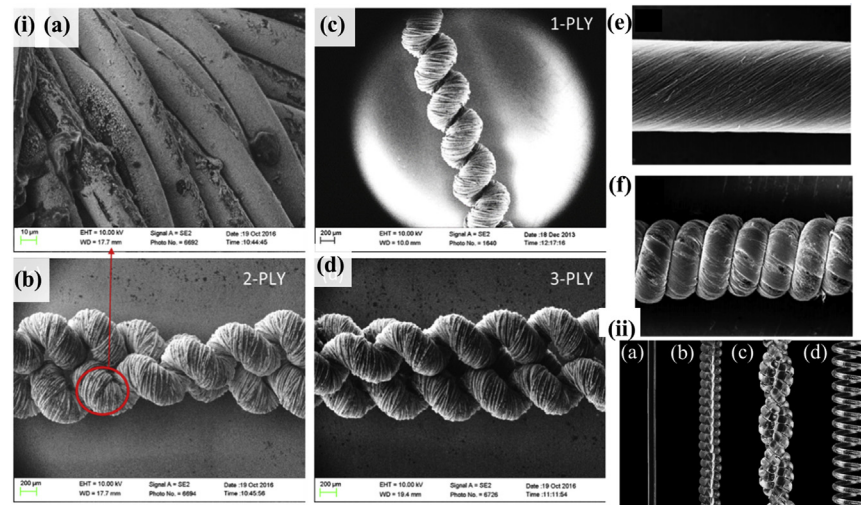
Typically, results reported in the literature have shown the slow frequency response of the TCP muscles. Since these muscles work on heat transfer, theoretically and practically the frequency is limited by how fast they are heated and cooled. High-temperature pulses and forced cooling can provide a high frequency of actuation. In their initial study Haines et al. (2014a) showed the response of nonsilver-coated muscle at 1 Hz by switching the hot and cold water alternatively. In the same study, authors reported silver-coated muscles actuation at 5 Hz when submerged in water. In our study, which was described in the previous section (Wu et al., 2016a), we studied the higher frequency of response in the muscle where actuation required 1 second of an electrical pulse on a 2-ply muscle at 50 g weight. Results for the strain and force response are shown in Fig.3.3(vi).

Fig. 3.3(vi) shows the result of the response of three distinct power cycles of 1.75, 2.01, and 2.15 W/cm for 1 second. The 2.15 W/cm power cycle has the same response as 0.25 W/cm for a longer period. The voltage waveform of the muscle input can also be observed from the figure. It shows some change in resistance due to pulse input. The force response of the muscle is also given in Fig. 3.3(vi)c. This pulsed actuation force measurement was performed for dynamic loading. We can observe from the figure a significant decrease in the muscle performance regarding force generation.

In a different study, Mirvakili et al. have shown the high-frequency response of the silver-coated sewing thread based TCP muscle as shown in Fig. 3.3(vii). Authors tested the muscle for 5–10 Hz to show the frequency response of the muscle to a pulse of 45 V. We can see from the figure how the frequency response of the muscle has decreased significantly at 6 Hz. Strain becomes almost zero for 10 Hz. In another study, following feedback control theory, Yip and Niemeyer (2015) showed that the response time of such actuator (the authors called them SCPs) can surpass that of skeletal muscle. They showed a 28-ms response time for a feedback gain of 50 as shown in Fig. 3.3(viii) (blue).

### 3.3.4 MICROSCOPY

Microscopic images will help us in understanding of the structure and shape of the muscle. Fig. 3.4(i) shows the SEM images of 1-ply, 2-ply, and 3-ply muscles, silver-coated nylon. Fig. 3.4(i)a shows the magnified view of the 2-ply muscle

**FIGURE 3.4**

(i) SEM images of 1-ply, 2-ply and 3-ply silver-coated TCP muscles: (a) magnified view of 2-ply muscle in (c); (b) 1-ply muscle; (c) 2-ply muscle; (d) 3-ply muscle; (e) CNT wrapped nylon 6,6 of 126  $\mu\text{m}$  diameter filament and (f) after the coiling. (ii) Examples of the TCP muscles without silver coating and the precursor structures using nylon 6,6 monofilament (a) nontwisted fiber, (b) twist insertion in the fiber, (c) 2-ply muscle formed from the coil in (b); and (d) a mandrel coiled.

(i) Figures (a)–(d) adapted from Wu, L., Jung De andrade, M., Saharan, L., Rome, R., Baughman, R.H., Tadesse, Y., 2016a. Compact and low-cost humanoid hand powered by nylon artificial muscles. *Bioinspirat. Biomim.* (submitted) and Figures (e) and (f) are adapted from Haines, C.S., Lima, M.D., Li, N., Spinks, G.M., Foroughi, J., Madden, J.D., et al., 2014a. Artificial muscles from fishing line and sewing thread. *Science* 343, 868–872. (ii) Figure adapted from Haines, C.S., Lima, M.D., Li, N., Spinks, G.M., Foroughi, J., Madden, J.D., et al., 2014a. Artificial muscles from fishing line and sewing thread. *Science* 343, 868–872.

presented in Fig. 3.4(i)c. We can observe the flaking of the silver from the surface and damage of some of the filaments. This phenomenon has a direct impact on the life and performance consistency of the muscle. Fig. 3.4(i)b is the 1-ply muscle showing the helically wound structure as a result of twisting and coiling. Fig. 3.4(i)c and d show the magnified view of the 2-ply and 3-ply muscles. We can say that coils from the adjacent coiled structure can restrict the torsional movement of the fibers, which in turn results in a decrease in tensile actuation. From our studies, we observed that with increasing number of muscle plies, its force generated increases and tensile stroke decreases. Fig. 3.4(i)e is a different structure where a CNT sheet is wrapped on a nylon 6,6 monofilament of diameter 126  $\mu\text{m}$  before coiling. Such wrapping enables the muscle to heat up fast due to the high thermal conductivity of CNT. Fig. 3.4(i)f is the coiled structure of the CNT wrapped nylon1-ply muscle.

The structures of the nylon 6,6 monofilament fiber (Fig. 3.4(ii)a) and TCP muscles without silver coating (Fig. 3.4(ii)b–d) (bare nylon) are illustrated in Fig. 3.4(ii) using optical imaging. We can see the difference in coil spacing between self-coiled (Fig. 3.4(ii)b) and mandrel coiled (Fig. 3.4(ii)d) muscles. The latter have large spacing between coils compared to the former. Such coils have a large axial contraction ( $\sim 49\%$  in some cases). Fig. 3.4(ii)c shows an optical image of 2-ply muscle.

### 3.4 BIOMEDICAL APPLICATIONS OF TWISTED AND COILED POLYMER

The TCP muscles are getting a number of applications in biomedical, orthotics, prosthetics, and medical textiles. Some of these applications have been explored and presented in the literature. Some potential applications are yet to be discovered. Other smart materials that received attention for biomedical and robotics applications are electroactive polymers (Carpi and Smela, 2009). The most widely explored application of TCP muscle is in prosthetic hands since these actuators are comparable to SMAs that have been explored for biomedical applications (Yoneyama and Miyazaki, 2008).

#### 3.4.1 PROSTHETIC HANDS

There are a large number of amputees living across the globe. Most of them cannot afford the expensive prostheses, such as myoelectric prostheses, which cost somewhere between \$20,000 and \$100,000 (McGimpsey and Bradford, 2008; van der Riet et al., 2013). As described by Haines et al. (2014a) the TCP actuators have a tensile stroke more than mammalian muscles ( $\sim 20\%$ ). Hence, we can design a device based on these muscles that can help improve the life of amputees. Biomimetic design can help restore all kinds of prehensile and nonprehensile movements of the hand. Prehensile motions are related to wrapping the hand around objects and grasping whereas nonprehensile motions are mostly gestures and movements that do not involve holding and grasping of the objects. Before understanding the design of prosthetic hands, let us understand the anatomy of the hand.

**Human hand grasping and gripping:** The natural human hand is comprised of bones and muscles. Wrapping, holding, and grasping of an object is termed as a prehensile movement. There are six different types of prehensile movements (Taylor and Schwarz, 1955): (1) cylindrical: thumb and finger wrap around a cylindrical object such as glass or pipe; (2) hook (snap): grasping something using fingers only without using palm or thumb, for example, holding and pulling a door handle; (3) tip pinch: holding by the type of thumb tip by pressing something against the tip of other fingers, for example, holding a screw head; (4)

palmar: grasping something with curled fingers and palm, for example, holding a brush; (5) spherical grasp: holding something against finger and thumb pads such as a ball; (6) lateral grip: holding something using thumb and index finger such as holding a key.

**Human hand description:** The human hand is made up of four fingers and a thumb. The human hand contains 27 bones (ElKoura and Singh, 2003, Taylor and Schwarz, 1955). Finger bones are called phalanges and these facilitate flexion—extension and abduction—adduction motion. Flexion motion refers to the bending or curling of the finger to take some shape. Extension motion is the returning of the flexed finger to rest position. Abduction and adduction motion is defined by left and right movement from the midline of the finger. Finger phalanges are termed as the distal, the middle, and the proximal phalange. The thumb has five degrees of freedom (DoF), one for interphalangeal joint, two for metacarpophalangeal (MCP) and two for carpometacarpal joint. The other four fingers all have three joints and four degrees of freedom. The MCP joint has two DoF, which includes abduction and adduction motion. The other two distal interphalangeal and the proximal interphalangeal have one DoF each. Due to its five DoF, the thumb can reach each finger to facilitate precision grip.

In one of our recent studies (Arjun et al., 2016), we showed a completely customizable and 3D printable prosthetic hand (Fig. 3.5(i)) that was designed and developed using TCP muscles. The cost of the complete device was around \$170 excluding the electronics. The key advantages of the TCP muscles are their low material cost (as low as \$5/kg) compared with SMA (more than \$3000/kg) and the low hysteresis (1.2°C for TCP and 27°C for SMA). The prosthetic hand was tested extensively and was able to grasp all sorts of daily used objects. The prototype was of an adult size human hand. This hand used beading wire routed through guides to the wrist via palm. Then, the tendons were connected with the TCP muscle in the palm. Since the 3D printed plastic parts had hard surface, which causes slippage of the objects during handling, a silicone coating on the finger pads was added to improve grasping. The device was designed in SolidWorks and could be easily 3D printed and assembled. The 3D printed structure was very light in weight and easily customizable depending on the need (the notion of personalized medicine). The prosthetic hand design used brass pulleys to accommodate longer muscle lengths. All the above made the prosthetic device ergonomic. Parameters for the prototypes are given in Table 3.3.

Grasping experiments of the prosthetic hand were also done using trials of objects of different shapes and sizes and are shown in Fig. 3.5(ii). This hand can help improving the quality of life of the millions of the amputees worldwide and can be a viable alternative to all those expensive prosthetic devices.

Another example of the prosthetic/humanoid/robotic hand was presented in one of our recent studies (Wu et al., 2016a). This hand mimics a 7-year-old child's hand and it was also developed using the TCP muscles. It is a suitable alternative for child amputees. This lightweight and compact hand has



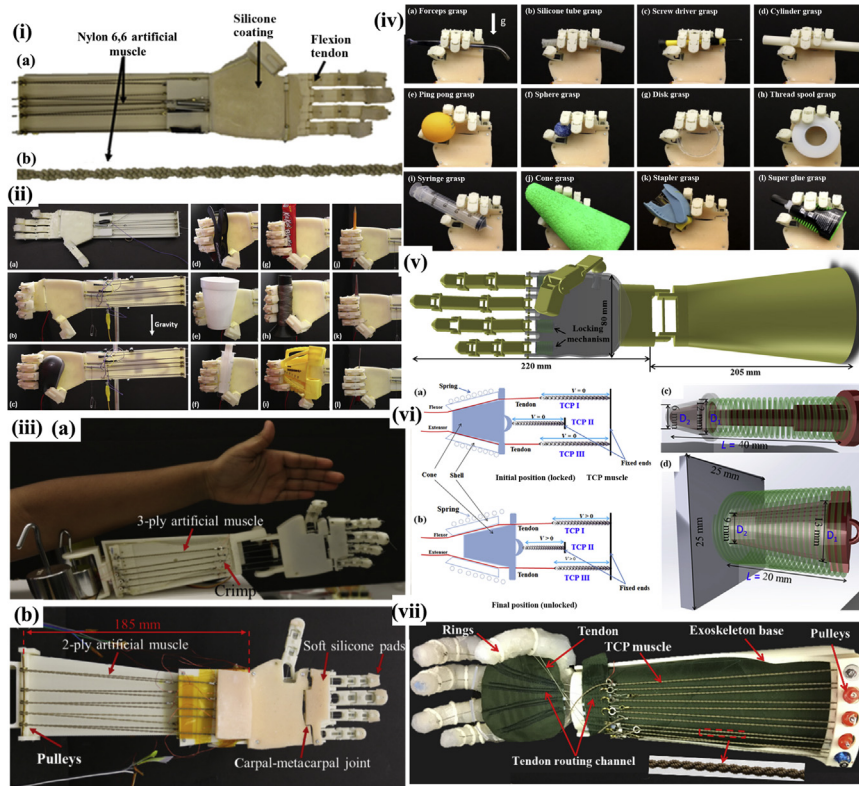


**FIGURE 3.5**

(i) Examples of 3D printed prototype of prosthetic hand developed using TCP muscles for adult hand: (a) 3D printed prototype and (b) a 2-ply TCP muscle used for the development. (ii) Grasping capability of prosthetic hand developed using TCP muscles: (a) picture of the second prototype kept on a tabletop view, and (b)–(l) successful grasping of objects: side view, while gravity is downward. (iii) TCP hand prototype: (a) comparison with an 8-year-old child's hand; (b) description of various parts of the hand (Wu et al., 2016a). (iv) Grasping configurations on the TCP hand, prototype II: (a)–(l) gravity is in the same direction for all images as shown in (a). (v) CAD model of prosthetic/robotic hand with locking mechanism. (vi) Locking mechanism for TCP muscles: (a,b) Schematic diagram explaining working principle of the locking mechanism; (c,d) CAD model of two different designs (Saharan and Tadesse, 2016c). (vii) iGrab orthotic device developed using TCP muscle mounted on a biomimetic testbed hand.

Figure adapted from (i) Arjun, A., Saharan, L., Tadesse, Y., 2016. Design of a 3D printed hand prosthesis actuated by nylon 6-6 polymer based artificial muscles. In: 12th Conference on Automation Science and Engineering, August 21–24, 2016, The Worthington Renaissance Hotel Fort Worth, TX. IEEE Robotics & Automation Society. (ii) Arjun, A., Saharan, L., Tadesse, Y., 2016. Design of a 3D printed hand prosthesis actuated by nylon 6-6 polymer based artificial muscles. In: 12th Conference on Automation Science and Engineering, August 21–24, 2016, The Worthington Renaissance Hotel Fort Worth, TX. IEEE Robotics & Automation Society. (iv) Wu, L., Jung De andrade, M., Saharan, L., Rome, R., Baughman, R.H., Tadesse, Y., 2016a. Compact and low-cost humanoid hand powered by nylon artificial muscles. *Bioinspirat. Biomim.* (submitted). (v) Saharan, L., Tadesse, Y., 2016c. Robotic hand with locking mechanism using TCP muscles for applications in prosthetic hand and humanoids. In: *SPIE Smart Structures and Materials + Nondestructive Evaluation and Health Monitoring, International Society for Optics and Photonics*, 97970V-97970V-9. (vii) Saharan, L., De andrade, M.J., Saleem, W., Baughman, R.H., Tadesse, Y., 2017. iGrab: hand orthosis powered by twisted and coiled polymer muscles. *Smart Mater. Struct.*, 26, 105048.



**Table 3.3** Summary of Main Design Features of Prosthetic Hand Developed Using TCP Muscles

	Design I	Design II
Total size in (mm)	450 × 160 × 27	440 × 110 × 25
Number of muscles	5	5
Number of joints	15	15
Mass of the prototype (g)	231	290
Avg. length of muscles (mm)	340	340
Springs/elastic materials	Tension springs to allow muscle to actuate	Tension springs and five rubber band as extension tendon
Maximum angle (degrees)	85	157

*Adapted from Arjun, A., Saharan, L., Tadesse, Y., 2016. Design of a 3D printed hand prosthesis actuated by nylon 6-6 polymer based artificial muscles. In: 12th Conference on Automation Science and Engineering, August 21–24, 2016, The Worthington Renaissance Hotel Fort Worth, TX. IEEE Robotics & Automation Society.*

five fingers, has 16 DoF overall with 15 DoF for fingers and 1 DoF for palm. The palm design of the hand was given special attention to facilitate grasping in such a small sized hand. The hand was 122 mm × 64 mm × 1 mm in length, breadth, and thickness. Fig. 3.5(iii) shows the prototype of the hand. The fingers are more rectangular unlike the previous hand, which has trapezoidal finger design. Again, this hand also has silicone pads to facilitate grip with the basic difference being on the fingers and the palm, extra joint in the palm. Similar to the adult size hand, this design also accommodates brass pulleys to allow the longer length of muscle fibers. This child-size hand has two designs as well. One is using custom-made springs on the fingers to facilitate return (extension) motion whereas the other uses passive rubbers to facilitate the extension motion. The hand was able to grasp several objects as can be seen from Fig. 3.5(iv). Being a small size hand, grasping of the hand is versatile as can be seen from Table 3.4. Objects have different shapes and sizes.

Other examples of hand applications (robotic/prosthetic/humanoid) can be seen from literature. For instance, Yip and Niemeyer (2015) have presented a hand developed using TCP muscles that features a closed loop control system.

One more example of the TCP muscle actuated robotic finger was presented by Wu et al. (2015a). They do not show a fully developed hand but the interesting thing about the prototype is that it is not working on electrothermally actuated muscles. This finger works based on nonsilver coated TCP muscles. Authors used alternative switching of hot and cold water to actuate the muscle. The idea of using fluids for transferring energy and making muscles work is very biomimetic

**Table 3.4** The Various Objects the TCP Hand Could Grasp

Name	Silicone Tube	Screw Driver	Ping Pong Ball	Sphere	Disk
Mass (g)	8.0	7.0	2.7	0.5	4.5
Size (mm)	$L = 115$ , $D = 10$	$L = 110$	$D = 40$	$D = 22$	$D = 60$ , $T = 6$
Name	Thread pool	Syringe	Cone	Stapler	Super glue
Mass (g)	33.0	14.0	4.0	38.0	26.0
Size (mm)	$D = 56$ , $T = 20$	$L = 125$ , $D = 21$	$D_{\max} = 8$ , $D_{\min} = 26$ , $H = 155$	$L \times W \times H = 60 \times 33 \times 46$	$L \times W \times H$ : $13 \times 44 \times 63$

*L, length; W, width; H, height; T, thickness; D, diameter.*

in nature. Again, as we have described earlier, the only drawback for the device is the energy efficiency. The efficiency of the muscle is close to 1%. To tackle the issue, we need to add some device or mechanics that can save energy. In one of our studies, we have developed a prosthetic hand with locking mechanism. We showed a study (Saharan and Tadesse, 2016c) that was mostly based on design and characterization of a prosthetic hand with energy efficiency. Fig. 3.5(v) shows the CAD design of the prosthetic hand with locking mechanism.

Like the human hand, TCP muscles also need a continuous supply of energy to maintain a certain position. For example, if we are holding a cup of tea, the muscles need to keep feeding power to hold the cup. A smarter solution can be designing a locking mechanism, which can maintain the final position until asked to release it. The locking mechanism can be designed for retaining a certain position for the manipulator to save energy. Fig. 3.5(vi) shows the two different designs of the locking mechanism that were presented in Saharan and Tadesse (2016c).

There are two different designs of the locking mechanism. The first one is thin but longer in length, whereas the second one is slightly thicker but the length is half of the original device. The working mechanism of both the locking mechanisms is the same. The device is essentially made up of three parts: a cone, a shell, and a spring. The spring holds the cone in the hollow shell and keeps it pressing against the shell walls. Therefore, when tendons are routed through the shell, the cone will squeeze the tendon. The cone with the help of spring exerts enough pressure on the tendons to hold their position. The schematic diagram in Fig. 3.5(vi)c and d shows the working of the locking mechanism. From Fig. 3.5(vi)a and b, we can see three different TCP muscles. TCP I and TCP III are the extensor and flexor muscles for the prosthetic/robotic hand. These two muscles can be powered on and off to move the finger in the desired direction. TCP II is the muscle that can control the locking and unlocking position of the mechanism.

The authors have performed experiments on the locking mechanism to show the efficacy of the mechanism. This locking mechanism works well up to 4N of force. Another possible case for locking mechanism development could be a ratchet mechanism that is yet to be explored for this muscle.

### 3.4.2 ORTHOTIC HAND

Orthotic devices or wearable robotic systems are devices that help people with muscular disorders restore their body part functions. There are millions of people across the globe who have lost their motor ability due to neural disorders, accidents, or strokes. Researchers are working on a wide variety of orthotic devices such as hand, arms shoulder, foot, hip, and back. Orthotic devices are meant to improve the quality of life of the affected people. Traditionally most of the orthotic devices rely on DC motors, and pneumatic and hydraulic actuators. Some researchers have tried using SMA as an alternate. Not to mention, most of these conventional methods are heavy and/or costly. In our recent study ([Saharan et al., 2017](#)), we used TCP muscle for the development of ergonomic orthotic devices, which is light in weight, and customizable based on the need ([Fig. 3.5\(vii\)](#)). An orthotic device for wrist was also designed and studied recently by [Sutton et al. \(2016\)](#) and [Sharma et al. \(2017\)](#).

### 3.4.3 FECAL INCONTINENCE TREATMENT

Fecal incontinence (FI) is the involuntary loss of bowel contents or unintentional loss of stool due to muscle disorders. This is a muscle disorder that could be caused due to age related or neural disorders. This can cause stigma and affect the quality of life for the affected person. According to [Fattorini et al. \(2016\)](#), about 45% of retired people are affected by this disease. FI can be treated using artificial sphincter implant. Naturally, the FI can be dealt with by external anal sphincter muscle (EAS). According to Fattoini's recent study, most of the artificial sphincters are not able to provide a complete solution. Hence, we can see that currently there is no proper solution to the problem. TCP muscles might be used to design such a device.

### 3.4.4 VARIABLE STIFFNESS ACTUATORS

Human muscles ability to vary stiffness helps in walking and catching actions ([Kianzad et al., 2015b](#)). Variable stiffness structures can mimic the controllable stiffness property of the natural muscle. Such structures can help developing prosthetics and orthotic devices for a human arm and leg. Most of the current actuators cannot vary their stiffness while recruiting in the assistive devices. Hence, the device cannot fully replicate the natural motion of the limb. Kianzad et al. developed a variable stiffness actuator (VSA), like a pinnate muscle by recruiting TCP muscles at an angle of 20 degrees from central tendon as shown in [Fig. 3.6\(i\)](#).

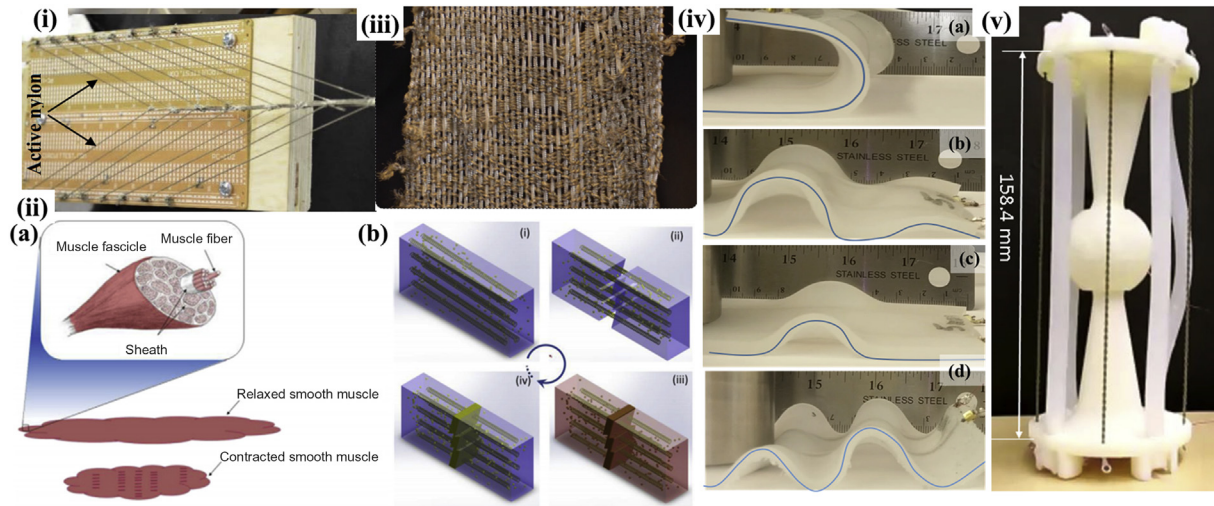


**FIGURE 3.6**

(i) TCP actuators are patterned in pennate structure. (ii) Self-healing structure concept: (a) structure of the natural muscle; (b) schematic of on demand healing process. [b(i)] A polymer composite sample reinforced by polymer artificial muscle (light golden coiled fiber) and thermoplastic particle in a matrix (blue); [b(ii)] crack initiated by external load during service life; [b(iii)] crack closed by thermally activated TCP and healed by healing agent; [b(iv)] solid wedge formed after cool down, establishing continuity between healing agent and the matrix. (iii) Fabric woven from coiled nylon threads (extending vertically). (iv) (a–d) TCP muscles embedded in silicone skin at different geometries in response to varied voltage and actuation conditions. (v) 3D printed prototype of artificial musculoskeletal system actuated by 2-ply TCP muscles.

Figure adapted from (i) Kianzad, S., Pandit, M., Lewis, J.D., Berlingeri, A.R., Haebler, K.J., Madden, J.D., 2015b. Variable stiffness structure using nylon actuators arranged in a pennate muscle configuration. In: *SPIE Smart Structures and Materials + Nondestructive Evaluation and Health Monitoring, International Society for Optics and Photonics*, 94301Z-94301Z-5. (ii) Zhang, P., Li, G., 2015. Healing-on-demand composites based on polymer artificial muscle. *Polymer*, 64, 29–38. (iv) Almubarak, Y., Toliver, A., Tadesse, Y., 2016. Twisted and coiled polymer (TCP) muscles embedded in silicone elastomer for use in soft robot. *Int. J. Intellig. Robot. Appl.* (v) Tadesse, Y., Wu, L., Saharan, L.K., 2016. Musculoskeletal system of bio-inspired robotic systems. *Mech. Eng.* 138.

Pennate muscles are those that can produce higher force and low displacement. These muscles will be joining the central tendon at an angle.

The artificial VSA structure contains 16 muscles, as seen in [Fig. 3.6\(i\)](#). These muscles are actuated using pulse width modulation (PWM). Results show that stiffness of the structure can be varied from 503 N/m at a resonance frequency of 1.4 Hz to an active state of 1480 N/m with the resonance frequency of 3.1 Hz. The stiffness of the structure can be varied using a number of muscles active at a certain time. The VSA described above was made up of silver-coated TCP muscles. Similar, structure can also be created using nonsilver-coated muscles with different stiffness range. Such VSA can have a wide variety of application in the development of future orthotics and prosthetics.

TCP muscle can provide a potential solution for the future artificial FI implants. According to [Haines et al. \(2014a\)](#); polyethylene based TCP muscle can provide up to 16% of actuation for applied temperature between 20°C and 130°C. Normal human body temperature is usually 37°C. Along with utilizing 17°C of body heat, we can potentially design a device that senses the bowel pressures with appropriate sensors. Then, TCP muscle can act as an artificial EAS. It is also possible to utilize a battery to power the muscle. The battery can be charged using body heat through the pyroelectric material. Pyroelectric materials ([Potnuru and Tadesse, 2014](#)) have the capability to convert heat into electrical voltage/energy. Though there is no device, available designed on this concept but it is feasible. There are many energy harvesting devices that should be explored for use in powering biomedical devices ([Priya and Inman, 2009](#)).

### 3.4.5 SELF-HEALING COMPOSITES

Biomimetic structures have capabilities of healing-on-demand on their own, a concept that enables structures to close cracks or areas of damage by filling the defects. Self-healing composites have application in biomedical field such as an implants for the body and wound healing. Similar structures can be developed using TCP muscles. [Zhang and Li \(2015\)](#) have shown the application of the TCP of muscle in such a biomimetic structure shown in [Fig. 3.6\(ii\)](#). The composite structure was made up of EPON Resin 862 as composite matrix cured using diethylenetriamine for 3 days at 25°C. This structure is a thermoplastic host with thermoplastic powder (the CAPA 6506 powder) in it. Fishing line based TCP muscles are used in the structure. Upon testing for three-point damage due to bending, the structure was healed for a 10-minute heating. The TCP muscle can bring the damaged areas close to each other upon heating. At the same time, the thermoplastic agent will melt and fill the cracks. During the study, three different types of TCP were used with a spring index of 1.7, 2.4, and 3.2, respectively. However, spring index does not have a significant effect on the healing process but prestrain of the muscle has the effect on the healing efficiency. Results show that 60% of healing efficiency was achieved at 60% of prestrain; it was also

found that the process is quite repeatable, low cost, with high efficiency and excellent flexibility.

### 3.4.6 MEDICAL TEXTILES

Medical textiles are a vast field that includes the use of fabric in artificial ligaments, artificial kidneys, artificial cartilage, and vascular grafts and bandages (Rajendran et al., 2016). TCP muscle can find many applications in this area since it can be made or configured in different forms. Fig. 3.6(iii) shows a fabric woven of TCP muscles that open/close pores in the fabric depending on the surrounding temperature and enables to cool the wearer's body.

Another application is the use of the TCP muscles woven fabrics in the support bandages. Support bandages help the broken bones and torn muscles for recovery. We have support bandages for some body parts such as hand, fingers, back, knee, foot, and thigh. TCP muscle woven fabric can have variable stiffness based on the need as discussed in an earlier section. It can also help the body part keep warm on demand. Such fabric can make support bandages with multiple utilities in a cost-effective way.

---

## 3.5 ROBOTIC APPLICATION OF TWISTED AND COILED POLYMER

### 3.5.1 TWISTED AND COILED POLYMER MUSCLE EMBEDDED IN SILICONE

We have discussed earlier the capability of TCP muscle as a soft actuator. These actuators when embedded in silicone can change their shape entirely. A study by Almubarak et al. (2016) showed that the TCPs embedded in silicone skins could mimic the flexible appendage of certain animals. Fig. 3.6(iv) shows the comparison of the natural creatures and their analogical motion created by TCP muscles embedded in silicone. From the figure, we can see how skin can take the shape of an elephant trunk; it can replicate a caterpillar motion, a string ray motion, and an electric ghost knife fish. This attribute of the silicone embedded TCP can be utilized for soft implants as well, specifically, near the organs where hard implants can cause damage and potentially can cause infection.

### 3.5.2 ARTIFICIAL MUSCULOSKELETAL SYSTEMS

Musculoskeletal systems (MSs) are building blocks of the biological systems. Hence, they can also be used as a building block of future robotic and prosthetic systems. Recently, a MS based on TCP muscle was introduced by Tadesse et al. (2016). Fig. 3.6(v) gives a glimpse of the future building block for biomimetic systems. This MS is designed based on a ball-and-socket joint. Most of the joints

of the human body are different forms of the ball-and-socket joint. Nevertheless, most of the robotic systems currently do not have a controlled ball-and-socket joints. This is because it is difficult to control ball-and-socket joint using conventional actuators. Though, multiple hydraulic and PMs can do the job. But again, the system would be heavy and perhaps designing a prosthetic based on such a joint is not possible. TCP muscles are linear actuators with high power to weight ratio and fit well for such systems. Hence, authors designed, assembled, and studied the system. Another aspect of this device is that it can be designed to be “printed in the assembly.” Hence, it makes them highly customizable for different sizes. Printing in assembly helps reduce the assembly time (Wu et al., 2016b).

New types of TCP muscles/actuators along with sample MSs are also introduced (Wu et al., 2018), bundled type of muscles (Simeonov et al., 2018), more work on feedback control (Masuya et al., 2018), and fuzzy based control for humanoid applications (Jafarzadeh et al., 2018) are some of the recent demonstrations that will be expected to continue in the next few years.

---

## ACKNOWLEDGMENT

The authors would like to acknowledge the support of the Office of Naval Research (ONR), Young Investigator Program, under the grant number N00014-15-1-2503.

---

## REFERENCES

- Almubarak, Y., Tadesse, Y., 2017. Twisted and coiled polymer (TCP) muscles embedded in silicone elastomer for use in soft robot. *Int. J. Intell. Robot. Appl.* 1 (3), 352–368. Available from: <https://doi.org/10.1007/s41315-017-0022-x>.
- Arjun, A., Saharan, L., Tadesse, Y., 2016. Design of a 3D printed hand prosthesis actuated by nylon 6-6 polymer based artificial muscles. In: 12th Conference on Automation Science and Engineering, August 21–24, 2016, The Worthington Renaissance Hotel Fort Worth, TX. IEEE Robotics & Automation Society.
- Aziz, S., Naficy, S., Foroughi, J., Brown, H.R., Spinks, G.M., 2016. Controlled and scalable torsional actuation of twisted nylon 6 fiber. *J. Polym. Sci. B: Polym. Phys.* 54 (13), 1278–1286. Available from: <https://doi.org/10.1002/polb.24035>.
- Carpi, F., Smela, E. (Eds.), 2009. *Biomedical applications of electroactive polymer actuators*. John Wiley & Sons, ISBN: 978-0-470-77305-5.
- Cherubini, A., Moretti, G., Vertechy, R., Fontana, M., 2015. Experimental characterization of thermally-activated artificial muscles based on coiled nylon fishing lines. *AIP Adv.* 5, 067158.
- Cho, K.H., Song, M.G., Jung, H., Park, J., Moon, H., Koo, J.C., et al., 2016. A robotic finger driven by twisted and coiled polymer actuator. *SPIE Smart Structures and Materials + Nondestructive Evaluation and Health Monitoring*. International Society for Optics and Photonics, 97981J-97981J-7.



- Elkoura, G., Singh, K., 2003. Handrix: animating the human hand. Proceedings of the 2003 ACM SIGGRAPH/Eurographics Symposium on Computer Animation. Eurographics Association, pp. 110–119.
- Fattorini, E., Brusa, T., Gingert, C., Hieber, S.E., Leung, V., Osmani, B., et al., 2016. Artificial muscle devices: innovations and prospects for fecal incontinence treatment. *Ann. Biomed. Eng.* 44, 1355–1369.
- Haines, C.S., Lima, M.D., Li, N., Spinks, G.M., Foroughi, J., Madden, J.D., et al., 2014a. Artificial muscles from fishing line and sewing thread. *Science* 343, 868–872.
- Haines, C.S., Lima, M.D., Li, N., Spinks, G.M., Foroughi, J., Madden, J.D.W., et al., 2014b. Artificial muscles from fishing line and sewing thread. *Science* 343, 868–872.
- Haines, C.S., Li, N., Spinks, G.M., Aliev, A.E., Di, J., Baughman, R.H., 2016. New twist on artificial *muscles*. *Proc. Natl. Acad. Sci.* 113 (42), 11709–11716. Available from: <https://doi.org/10.1073/pnas.1605273113>.
- Jafarzadeh, M., Gans, N., Tadesse, Y., 2018. Control of TCP muscles using Takagi–Sugeno–Kang fuzzy inference system. *Mechatronics* 53, 124–139.
- Kianzad, S., Pandit, M., Bahi, A., Ravandi, A.R., Ko, F., Spinks, G.M., et al., 2015a. Nylon coil actuator operating temperature range and stiffness. *SPIE Smart Structures and Materials + Nondestructive Evaluation and Health Monitoring. International Society for Optics and Photonics*, 94301X-94301X-6.
- Kianzad, S., Pandit, M., Lewis, J.D., Berlingeri, A.R., Haebler, K.J., Madden, J.D., 2015b. Variable stiffness structure using nylon actuators arranged in a pennate muscle configuration. *SPIE Smart Structures and Materials + Nondestructive Evaluation and Health Monitoring. International Society for Optics and Photonics*, 94301Z-94301Z-5.
- Madden, J.D., Vandesteeg, N.A., Anquetil, P.A., Madden, P.G., Takshi, A., Pytel, R.Z., et al., 2004. Artificial muscle technology: physical principles and naval prospects. *Ocean. Eng. IEEE J.* 29, 706–728.
- Masuya, K., Ono, S., Takagi, K., Tahara, K., 2018. Feedforward control of twisted and coiled polymer actuator based on a macroscopic nonlinear model focusing on energy. *IEEE Robot Autom. Lett.* 3 (3), 1824–1831. Available from: <https://doi.org/10.1109/LRA.2018.2801884>.
- McGimpsey, G., Bradford, T.C., 2008. Limb prosthetics services and devices. Bioengineering Institute Center for Neuroprosthetics Worcester Polytechnic Institution White Paper.
- Mirvakili, S.M., Ravandi, A.R., Hunter, I.W., Haines, C.S., Li, N., Foroughi, J., et al., 2014. Simple and strong: twisted silver painted nylon artificial muscle actuated by Joule heating. *SPIE Smart Structures and Materials + Nondestructive Evaluation and Health Monitoring. International Society for Optics and Photonics*, 90560I-90560I-10.
- Moretti, G., Cherubini, A., Vertechy, R., Fontana, M., 2015. Experimental characterization of a new class of polymeric-wire coiled transducers. *SPIE Smart Structures and Materials + Nondestructive Evaluation and Health Monitoring. International Society for Optics and Photonics*, 94320P-94320P-9.
- Potnuru, A., Tadesse, Y., 2014. Characterization of pyroelectric materials for energy harvesting from human body. *Integrat. Ferroelect.* 150, 23–50.
- Priya, S., Inman, D.J., 2009. *Energy Harvesting Technologies*. Springer.
- Rajendran, S., Anand, S., Rigby, A., 2016. Textiles for healthcare and medical applications. *Handb. Tech. Textiles Tech. Textile Appl.* 2, 135.
- Ross, A., 1977. Cable kinking analysis and prevention. *J. Eng. Ind.* 99, 112–115.
- Saharan, L., Tadesse, Y., 2016. Fabrication parameters and performance relationship of twisted and coiled polymer muscles. *ASME. International Mechanical Engineering*



- Congress and Exposition, American Society of Mechanical Engineers, V014T11A028-V014T11A028.
- Saharan, L., Tadesse, Y., 2016b. A novel design of thermostat based on fishing line muscles. ASME. International Mechanical Engineering Congress and Exposition, American Society of Mechanical Engineers, V014T07A019-V014T07A019.
- Saharan, L., Tadesse, Y., 2016c. Robotic hand with locking mechanism using TCP muscles for applications in prosthetic hand and humanoids. SPIE Smart Structures and Materials + Nondestructive Evaluation and Health Monitoring. International Society for Optics and Photonics, 97970V-97970V-9.
- Saharan, L., De andrade, M.J., Saleem, W., Baughman, R.H., Tadesse, Y., 2017. iGrab: hand orthosis powered by twisted and coiled polymer muscles. *Smart Mater. Struct.* 26, 105048.
- Semochkin, A.N., 2016. A device for producing artificial muscles from nylon fishing line with a heater wire. In: *Assembly and Manufacturing (ISAM)*, 2016 IEEE International Symposium on, IEEE, pp. 26-30.
- Sharma, A., Saharan, L., Tadesse, Y., 2017. 3-D printed orthotic hand with wrist mechanism using twisted and coiled polymeric muscles. ASME 2017 International Mechanical Engineering Congress and Exposition. American Society of Mechanical Engineers, V003T04A057-V003T04A057.
- Simeonov, A., Henderson, T., Lan, Z., Sundar, G., Factor, A., Zhang, J., et al., 2018. Bundled super-coiled polymer artificial muscles: design, characterization, and modeling. *IEEE Robot. Autom. Lett.* 3, 1671–1678.
- Smith, C., Villanueva, A., Joshi, K., Tadesse, Y., Priya, S., 2011. Working principle of bio-inspired shape memory alloy composite actuators. *Smart Mater. Struct.* 20, 012001.
- Sutton, L., Moein, H., Rafiee, A., Madden, J.D. & Menon, C., 2016. Design of an assistive wrist orthosis using conductive nylon actuators. In: *Biomedical Robotics and Biomechanics (BioRob)*, 2016 6th IEEE International Conference on. IEEE, pp. 1074-1079.
- Tadesse, Y., 2013. Electroactive polymer and shape memory alloy actuators in biomimetics and humanoids. SPIE Smart Structures and Materials + Nondestructive Evaluation and Health Monitoring. International Society for Optics and Photonics, 868709-868709-12.
- Tadesse, Y., Wu, L., Saharan, L.K., 2016. Musculoskeletal system for bio-inspired robotic systems. *Mech. Engin. Mag. Sel. Art.* 138 (03), S11–S16. Available from: <https://doi.org/10.1115/1.2016-Mar-8>.
- Taylor, C.L., Schwarz, R.J., 1955. The anatomy and mechanics of the human hand. *Artif. Limbs* 2, 22–35.
- Tondu, B., 2015. What Is an Artificial Muscle? A Systemic Approach. *Actuators*. Multidisciplinary Digital Publishing Institute, pp. 336–352.
- Van Der riet, D., Stopforth, R., Bright, G., Diegel, O., 2013. An overview and comparison of upper limb prosthetics. *AFRICON*, 2013. IEEE, pp. 1–8.
- Wu, L., Tadesse, Y., 2016. Musculoskeletal system for bio-inspired robotic systems based on ball and socket joints. ASME. International Mechanical Engineering Congress and Exposition, American Society of Mechanical Engineers, V04AT05A020-V04AT05A020.
- Wu, L., De andrade, M.J., Rome, R.S., Haines, C., Lima, M.D., Baughman, R.H., et al., 2015a. Nylon-muscle-actuated robotic finger. SPIE Smart Structures and Materials + Nondestructive Evaluation and Health Monitoring. International Society for Optics and Photonics, 94310I-94310I-12.

- Wu, L., Jung De andrade, M., Rome, R.S., Baughman, R.H., Tadesse, Y., 2015b. Nylon-muscle-actuated robotic finger. In: SPIE Biological-Inspired Systems and Bio-MEMS, San Digeo, CA.
- Wu, L., Jung De andrade, M., Rome, R.S., Haines, C., Lima, M.D., Baughman, R.H. et al., 2015c. Nylon-muscle-actuated robotic finger. pp. 94310I-94310I-12.
- Wu, L., Jung De andrade, M., Saharan, L., Rome, R., Baughman, R.H., Tadesse, Y., 2016a. Compact and low-cost humanoid hand powered by nylon artificial muscles. *Bioinspirat. Biomim.* (submitted).
- Wu, L., Larkin, M., Potnuru, A., Tadesse, Y., 2016b. HBS-1: a modular child-size 3D printed humanoid. *Robotics* 5, 1.
- Wu, L., Chauhan, I., Tadesse, Y., 2018. A novel soft actuator for the musculoskeletal system. *Adv. Mater. Technol.* 3, 1700359.
- Yip, M.C., Niemeyer, G., 2015. High-performance robotic muscles from conductive nylon sewing thread. In: *Robotics and Automation (ICRA), 2015 IEEE International Conference on.* IEEE, pp. 2313-2318.
- Yoneyama, T., Miyazaki, S., 2008. *Shape Memory Alloys for Biomedical Applications.* Elsevier.
- Zhang, P., Li, G., 2015. Healing-on-demand composites based on polymer artificial muscle. *Polymer* 64, 29–38.

# Electrospun nanofibers for tissue engineering applications

**Alexandra Elena Oprea<sup>1</sup>, Anton Ficai<sup>1</sup> and Ecaterina Andronescu<sup>2</sup>**

*<sup>1</sup>Faculty of Applied Chemistry and Material Science, Politehnica University of Bucharest, Bucharest, Romania <sup>2</sup>Department of Oxide Materials and Nanomaterials, Faculty of Applied Chemistry and Materials Science, Politehnica University of Bucharest, Bucharest, Romania*

## 4.1 INTRODUCTION

At present, a big challenge for surgeons and tissue engineers is represented by reconstruction and regeneration of human tissues and organs. All this can be possible using biomaterials, cells, and growth factors. Regenerative engineering includes advanced material science, stem cell science, nanotechnology, and developmental biology and represents the next multidisciplinary archetype to design complex tissues (Jiang et al., 2015; Mason and Dunnill, 2008).

One of the most important challenges in this domain is to mimic meticulously the hierarchical structure and properties of the extracellular matrices (ECMs) of the natural tissues (Khorshidi et al., 2016). A strategy to create biomaterials with nanoscale topographical appearance, micro- and macroscale gradient structures, and biological fields to interact with target growth factors and cells is needed to meet the demand for successful tissue regeneration (Jiang et al., 2015; Khorshidi et al., 2016).

In the field of nanotechnology, the most researched physical forms of nanomaterials are nanofibers, nanoparticles, nanowires, and nanotubes.

Nanofibers principally have accumulated a lot of interest from academia and industry owing to their high surface area-to-volume ratio, high aspect ratio, flexibility to tailor surface properties, and functionalities and superior mechanical properties. Furthermore, nanofibers as building blocks for nanomembranes or nanodevices find prospects for application in the domains of biomedical research, filtration, energy storage, sensors, catalysis, drug delivery, textiles, and electronics (Jiang et al., 2015; Srivastava, 2017).

Different methods have been published in literature for the production of nanofibers, for example, phase separation (Katsogiannis et al., 2015), melt blowing (Nayak et al., 2015), drawing (Guo et al., 2017), template synthesis (Zhang et al., 2014), self-assembly (Zheng et al., 2016), and also electrospinning (ES)

technique (Hu et al., 2014; Sridhar et al., 2015). Among all these methods and techniques, ES is one of the most adaptable techniques to obtain nanofibers having a diameter in the range of 50–1000 nm. ES technique has gathered a lot of attention in the past two decades based on its main advantage to produce nanofibers from a large variety of materials (ceramics, polymers, and metals) in a rapid and controlled mode (Srivastava, 2017; Agarwal et al., 2008).

Polymeric nanofibers are obtained by direct ES of polymer solution or melt. Nevertheless, composite nanofibers are prepared by incorporating inorganic nanostructured materials in polymeric nanofibers. Ceramic nanofibers are obtained by ES of metal salts using a polymer as matrix. Finally, the polymer is removed by calcination or dissolution (Sill and von Recum, 2008). ES technique furnishes increased flexibility to make nanofibers of various morphologies and functionalities that have been investigated for different applications (Srivastava, 2017; Agarwal et al., 2008).

Electrospun fibers represent a promising approach for tissue-engineering (TE) scaffolds that provide the cells an environment that mimics the native ECM. Fibers with different properties can be obtained by ES conforming to the demands of the tissue to be restored (Braghirolli et al., 2014; Rogina, 2014).

ES generate ultrathin fibers with diameters ranging from a few micrometers to tens of nanometers. Recent studies have demonstrated that the ES technology can be used to produce organ components and restore injured tissues. ES for tissue regeneration supports a complete overview of this new strategy to tissue repair and regeneration and studies how it is being employed within the biomaterials domain (Sill and von Recum, 2008; Braghirolli et al., 2014; Wang and Ryan, 2011).

It is predictable that research into the ES field will become highly interdisciplinary in the near future. Especially in regard to its application in TE, more research is necessary to demonstrate the effect of nanofibers on the biochemical pathways and cellular signaling mechanisms that control cell morphology, differentiation, growth, proliferation, motility, and genotype. Understanding into how the natural ECM components secreted by cells restore the biodegradable polymeric scaffolds is also desired (Wang and Ryan, 2011; Okutan et al., 2014).

---

## 4.2 THE ELECTROSPINNING PROCESS

The basis of ES process was first designed by Formhals in the 1930s, and it regained major attention in the 1990s (Sun et al., 2014).

In a conventional ES process a high voltage is utilized to form an electrically charged jet of polymer solution or melt polymer, which dries or solidifies on extrusion and results in a polymer fiber. To complete this process three main components are needed: a high-voltage power supply, a capillary tube with a spinneret, and a collector, which is normally earthed. Usually, the spinneret is

connected to a syringe, which supplies the polymer solution, and the solution can be charged through the spinneret at a regular rate by using a syringe pump. The pendant drop of the polymer solution at the nozzle of the spinneret becomes statically charged when a high voltage is used, also, the induced charges are uniformly distributed over the surface. The surface tension of the droplet would usually develop into a sphere at equilibrium (Hu et al., 2014). The accumulation of charge may lead to a protrusion that may appear on the end of the droplet, deforming the droplet into a conical shape called the Taylor cone (Yousefzadeh, 2017). When the field strength is increased, the repulsive electrostatic force overcomes the surface tension and a charged jet of fluid is ejected from the tip of the Taylor cone when a detracting value is achieved. The polymer solution is released as a jet, which then suffers a stretching and whipping process that leads to the formation of a long thin thread. Solid polymer fibers having diameters ranging from micrometers to nanometers are produced and are put in a grounded collecting metal screen or drum. The ES process has advanced in recent years and it has been discussed in detail (Wang and Ryan, 2011; Chu and Seeger, 2014).

The ES technique has shown an electrified fluid dynamics related problem. For an improved control of the structure, morphology, and mass production of the electrospun nanofibers, it is important to understand quantitatively how the ES process changes the fluid solution through a millimeter diameter capillary tube into solid micro/nanofibers, which are four to five orders of magnitude smaller in diameter (Chu and Seeger, 2014). Currently, theoretical and experimental studies have shown that the ES process normally has three main stages: (1) jet initiation and elongation of the charged jet along a straight line; (2) growth of electrical bending instability (also known as whipping instability) (Šimko and Lukáš, 2016) and further elongation of the jet, which may or may not be attended by the jet branching and/or splitting; (3) solidification of the jet into micro/nanofibers and deposition on collector (Sun et al., 2014; Ahmed et al., 2015).

In this process, the type of collector used is an important element that may affect the morphology of the collected fibers (Thenmozhi et al., 2017). A simple collector plate will design an unraveled mat of fibers in a random orientation, whereas other particularly constructed collectors can accumulate aligned fibers. For specialized collectors such as spinning disks, drums, and mandrels, the speed of rotation is an important factor that may affect the fiber deposition rate. If the collector is moving faster than the deposition of the fibers, the fibers will stretch or break into small fragments as the fiber sticks to the collector and is increased away. The type of the fiber orientation may influence the configuration of the collector (Robb and Lennox, 2011). The configuration of the collector depends on the type of fiber orientation desired. For aligned fibers, the speed of collector rotation needs to be calibrated to the polymer deposition rate and can be accomplished using a variable speed motor, such as an overhead stirrer, or a variable speed drill to drive the collector (Robb and Lennox, 2011; Cai et al., 2017).

ES has the special ability to form ultrafine fibers of various materials in different fibrous assemblies. Due to their submicrometer size, electrospun fibers can realize a highly porous mesh and their large surface area-to-volume ratio enhance performance for very many applications (Wang and Ryan, 2011). The main advantages of the ES technique include the production of fibers a few nanometers to micrometers in diameter, high porosity, and large surface areas, which can imitate the ECM structure in terms of the chemistry and dimensions (Braghirolli et al., 2014).

### 4.2.1 MULTIJETS FROM A SINGLE NEEDLE

Multijets from a single needle were seen for the first time during ES of polybutadiene using a single homemade stainless steel needle with a grooved tip mounted on a glass syringe (Wang and Ryan, 2011). Normally, a single jet is observed to form from the Taylor cone under application of an electric field in single-needle electrospinning (SNE), and the formation of multijets in the preceding case is attributed to either blockage of a needle tip or inconsistency in the electric field distribution. Multijets in an SNE may be formed by jet splitting, i.e., the formation of two or more secondary jets from the emanating primary jet. This has been accomplished by applying large axial electric fields to the fluid or by using a curved collector (Braghirolli et al., 2014; Wang and Ryan, 2011; Srivastava, 2016).

### 4.2.2 MULTIJETS FROM MULTIPLE NEEDLES

A challenge in ES is represented by the slow rate of production. To boost it, a strategy that has been adopted by researchers is to grow the number of needles allowing multijets to be formed. In such multiple needle electrospinning (MNE) set-ups, the configuration in which needles are organized is an important model parameter that needs thorough consideration as the needles can be arranged linearly or in many other 2D forms, for example, circular, elliptical, or hexagonal. The final outcome may be affected by the number of needles and the needle gauge, also, different reports for fabrication of nanowebs and enhancement of production rates have been published where all the aforementioned parameters are varied to obtain the desired results. The MNE set-ups normally need a large operating space, and to prevent strong charge repulsion between the emanating jets, the relative distance among the needles is to be carefully constructed (Echegoyen et al., 2017). The distance between needles is influenced by the needle gauge as well as on the properties of a solution to be electrospun. Also, other issues must be consigned to obtain efficient operation in MNE set-ups, for example, needle clogging or nonworking needles, nonuniform electric field on needle tips at different positions, fiber deposition across the web, and jet instability (Srivastava, 2016).

### 4.2.3 MULTIJETS FROM NEEDLELESS SYSTEMS

The issues associated with MNE can be solved by using a needleless ES system where numerous polymeric jets are formed from a free liquid surface (Liu et al., 2016). This can be realized as the waves of an electrically conductive liquid self-organize on a mesoscopic scale and finally form jets when the intensity of the applied electric field passes over an onset value (Srivastava, 2016). The result is in the formation of multijets from a needleless system, and was announced by Yarin and Zussman (2004).

Their work (Yarin and Zussman, 2004) refers to a combination of normally aligned electric and magnetic fields acting on a two-layer system comprised of a ferromagnetic suspension as the lower layer, and a polymeric solution as the upper layer. Several steady spikes of poly(ethylene oxide) (PEO) are shaped at the free surface of the magnetic fluid by usage of the magnetic field. With the inclusion of a polymer layer and the utilization of high voltage, some disorders are seen at the free surface of the polymer layer. Multiple jets begin to eject toward the grounded collector when the voltage is raised above the threshold level (Yarin and Zussman, 2004). Various reports on multijet needleless ES to obtain nanowebs out of several polymers have been published in recent years (Zhang et al., 2016). Multijet ES from a single droplet has also been reported (Zhou et al., 2009).

### 4.2.4 MELT ELECTROSPINNING

Lorrain and Manley did the pioneering work on melt ES, which needs a provision to melt the polymer in addition to other parts, identical to solution ES (Srivastava, 2016). Manufacturing of nanofibers of different polymers [e.g., polylactic acid (PLA, Luu et al., 2003), PAA (Kim et al., 2005), polyethylene terephthalate (Ma et al., 2005), polycaprolactone (PCL) and PEG-b-PCL (Detta et al., 2010)] and different means [e.g., heating ovens (Zhou et al., 2006), heat guns (Dalton et al., 2007), laser melting devices (Ogata et al., 2007), and electric heating (Hochleitner et al., 2015)] to melt the polymer have been described by several research groups. Excepting the factors that govern fiber uniformity and morphology in solution ES, the temperature of the spinneret and viscosity of the polymer melt need consideration in melt ES. The technique has shown many advantages over solution ES, such as no usage of organic solvents, ease of polymeric fiber blends fabrication, high throughput due to no loss of mass by solvent evaporation, and suitability to polymers having no proper solvent at room temperature. Even if this technique has several advantages, the requirement of a heating system to melt the polymer, low conductivity of the melt, and electric discharge associated with the melt are some limitations of the technique (Teo and Ramakrishna, 2006). Due to the high viscosity of the melt and rapid solidification of the polymer jet among the needle tip and the collector, it is very hard to achieve fibers with diameters in the nanometer range (Srivastava, 2016; Lyons et al., 2004).

---

### 4.3 ELECTROSPINNING FOR TISSUE ENGINEERING

TE is an inspiring domain that involves engineering and biological knowledge to create or restore tissue and organs. It uses three main tools: cells, biomaterials, and biomolecules (Braghirolli et al., 2014).

The architecture of an engineered tissue substitute has an important role in modulating tissue growth (Gouma and Han, 2017). The perfect scaffold must fulfill a number of often conflicting demands: appropriate levels and sizes of porosity allowing for cell migration; sufficient surface area; a variety of surface chemistries that promote cell adhesion, growth, migration, and differentiation; and also a degradation rate that closely matches regeneration rate of the desired natural tissue (Khorshidi et al., 2016). While a various range of TE matrices have been designed, a few types of synthetic scaffolding show important promise. Structures composed of the thin fibers produced by ES fall into this class as determined by the widespread use of the process (Lannutti et al., 2007; Hasan et al., 2014).

ES represent a facile and adaptable method that produces scaffolds obtained by nano and microfibers, which offer a proper microenvironment for cellular development by mimicking the native ECM (Braghirolli et al., 2014).

Even if they have many advantages and are extensively used, electrospun scaffolds have some practical limitations, such as scarce cell infiltration and inadequate mechanical strength for load-bearing applications. Various research groups have offered different solutions to overcome the above-mentioned limitations (Khorshidi et al., 2016).

#### 4.3.1 BONES, CARTILAGE, AND TENDON TISSUE REGENERATION

ES process is a rapidly emerging technology for the development of bone TE (Khorshidi et al., 2016). The electrospun fiber matrix presents a structure similar to the ECM of bone, ensuring cells with a comparable environment for attachment and proliferation. The characteristics of prospective scaffolds for bone tissue repair are dominant to the success of the scaffold. ES furnishes advantageous scaffold properties like high random fiber orientation, porosity, and the capability to fabricate biodegradable polymeric scaffolds (Hasan et al., 2014). A lot of studies have been focused on the incorporation of bioactive materials, for instance hydroxyapatite (HAp) and bioactive glass into polymeric nanofibers to raise the osteoblast response (Bassi et al., 2011).

A promising method for preparation of electrospun HAp covered cellulose nanofiber scaffold (HAp/CMC) for TE applications was reported in 2016 by Yamaguchi et al. (2016). The cellulose nanofibers (CNFs) were obtained by deacetylation of cellulose acetate nanofibers. Thence, the fibers were transformed to sodium carboxy methyl cellulose (Na-CMC). The sodium carboxy methyl CNFs mat was then coated with HAp for bone regeneration applications. The



HAp-coated carboxy methyl CNFs demonstrated various morphology by concentration of NaOH at carboxymethylation process and  $\text{HCO}_3^-$  of simulated body fluid (SBF), and the mineralization time. It was proved that the obtained HAp-coated CMC nanofiber scaffolds can support the development of TE for bone regeneration.

Another research showed that electrospun nanocomposite of Poly (H-caprolactone) scaffolds incorporating bioactive glass present superior performance in cell attachment and proliferation for bone tissue remodeling (Otadi and Mohebbi-Kalhari, 2015). Electrospun PCL-bioactive glass (BGs) nanocomposites were obtained using ES technique. Three different bioactive glasses were selected based on a  $\text{SiO}_2$ -CaO-SrO- $\text{P}_2\text{O}_5$  system, with exchange of SrO content substituted for CaO, and the other glass was 45S5. The results demonstrated that bioactive glass with a satisfying dispersion and distribution in the nanofibers' structure increases the mechanical properties correlated with pure PCL, but the 45S5 presents a weak nanocomposite structure.

Bioactive glasses doped with therapeutic metal ions (i.e., copper or strontium) integrated into the gelatin/polycaprolactone (Gt/PCL) fibrous mats using ES technique support the foundation for further studies with regard to production of multifunctional scaffolds for bone TE applications (Gönen et al., 2016). The HAp presents the ability of forming fiber mats that could affect their bioactivity, which is relevant and very important for bone regeneration. The electrospun nanocomposite fiber mats represent promising scaffolds as they blend the great bioactivity of bioactive glasses, the valuable effects of therapeutic metallic ions on bone growth, and an interconnected porous structure of electrospun nanofibers that can be capable to promote cell invasion, cell adhesion, and vascularization.

Vashisth and Bellare (2018) obtained a biomimetic hybrid scaffold comprising both micro- and nanoscale characteristics by mimicking the natural bone matrix. To mimic the nanostructure of bone, core-sheath nanofibers of Gt/PCL enclosed with HAp nanocrystals were prepared using a versatile ES method. The materials were obtained as nonwoven sheets. Then, the coaxial nanofibers were reinforced in the design of tightly coiled spiral rings in a matrix of hydrogel to imitate the osteon structure of cortical bone. The reinforcement of nanofibrous rings into the hydrogel matrix improved the global mechanical properties of hydrogel, cellular responses, and surface biomineralization.

Disorder and injury in articular cartilage makes it a major health care target for restoration and regeneration (Wall and Board, 2014). ES method of nanofibrous scaffolds possesses a lot of aspects that correspond to the production of structures with various 3D architectures that fit the demands of cartilage repair (Hardingham, 2011).

The use of an extensive range of synthetic (Li et al., 2002) and natural polymers (Hu et al., 2014; Kong and Ziegler, 2014; Noh et al., 2006) has been recommended for TE cartilage such as: polyglycolic acid, polylactic-co-glycolic acid, PCL, PCL nano with PLA macro, collagen II (COL II), PLA, chitin/chitosan, silk, etc. This has included biodegradable synthetic polymers extensively used to

obtain implanted medical devices, like poly(lactide-*co*-glycolide), poly(l-lactic acid) (PLLA), and PCL, which all enjoy FDA (Food and Drug Administration) authorization for use in vivo. Not long ago, attention on these was focused on PCL as it has a slower in vivo degradation rate with a half-life of months, which is better fit to cartilage repair than a half-life of only a few weeks or less (Hardingham, 2011).

Wang et al. (2017a) synthesized a cartilage phase by connecting the ES techniques, freeze-drying, and water vortex collecting. The nanofibers were synthesized from poly (L-lactic acid)-co-poly ( $\epsilon$ -caprolactone) (PLLA-CL) and COL I using the ES process. Then the obtained nanofibers were drawn into a water vortex and collected by a rotating mandrel. Also, the tests support a favorable benefit of cartilage oligomeric matrix protein in cartilage TE and clinical cartilage restoration and regeneration.

It was demonstrated that core-shell structured nanofibers with P(LLA-CL) and collagen as the sheath and bovine serum albumin/rhTGF- $\beta$ 3 as the core can be obtained using coaxial ES technique (Wang et al., 2017b). The authors prepared a bioactive nanofibrous scaffold charging recombinant human transforming growth factor- $\beta$ 3 (rhTGF- $\beta$ 3) by coaxial ES method, which might stimulate the chondrogenic differentiation of WMSCs (Wharton's jelly of human umbilical cord) for cartilage restoration in trachea repair. Coaxial ES was completed by applying a usual needle ES setup, a high power supply (BGG DC high-voltage generator), and two digitally controlled syringe pumps (KDS200). Besides this, the particular equipment for coaxial ES was designed by a nozzle with an inner needle coaxially placed inside an outer one.

ES method was also utilized to produce nanosized fibers based on sodium alginate (SA), soy protein isolated (SPI), and PEO loading with vancomycin antibacterial drug (Wongkanya et al., 2017). Aqueous solutions of vancomycin-loaded SA/PEO/SPI were satisfyingly electrospun to obtain uniform fibers with diameter range of 60–600 nm. The composition of polymer mixture clearly influenced the fiber morphology and, as a consequence, the drug release activity. The prepared electrospun SA/PEO/SPI fibers could act as a biomedical material providing considerable advantages including drug encapsulation and controlled release, antibacterial properties, and compatibility with cells (Wongkanya et al., 2017).

The disc- ES technique was also used to produce fibrous scaffolds for tissue regeneration. The technique is composed by a rotating metal disc spinneret, a solution barrel, a high-voltage direct-current power generator supply, and finally a rotating collector. With aid of this method, Li et al. (2016) fabricated poly ( $\epsilon$ -caprolactone)/gelatin fibrous (PCL/GT) scaffolds. The applied voltage was set to 50 kV, collecting distance 25 cm, and the rotating speed of the disc was 10 rpm. After disc- ES method, the prepared nanofiber was conserved in vacuum at room temperature for 72 hours to eliminate the solvent residue. The study's results indicated the capacity of disc-electrospun poly( $\epsilon$ -caprolactone)/gelatin fibrous scaffold with multiscale architecture in the application of TE regeneration.

Chitosan/poly(vinyl alcohol)/graphene oxide (GO) composite nanofibers were obtained using ES method. The GO was utilized as filler considering its satisfying antibacterial activity and great biocompatibility (Cao et al., 2017). The prepared solution was electrospun at 18 kV and the tip-to-collector distance was established at 16 cm to obtain a spun composite nanofiber. The spun nanofiber was maintained in an oven at 50°C for approximately 24 hours, followed by curing at 120°C for about 10 minutes. The biocompatibility studies showed that chitosan/PVA/GO represent a proper material to maintain the most adequate environment for the growth of ATDC5 cells. Thus, the chitosan/PVA/GO nanofiber can be used as a potential alternative for artificial cartilage.

The specific properties of triazole and tyrosine ring enclosed in fibrous scaffolds incorporated with gelatin were also studied to obtain electrospun nanofibers for cartilage TE (Agheb et al., 2017). The homogeneous solution of gelatin-tyrosine-triazole (GTT) was transferred into syringe. A positive voltage (20 kV) was applied to the needle using a high-voltage power supply. The distance between the collector and needle was fixed to 20 cm. The solution flow rate was set at 0.8 mL/h. The electrospun samples were put in a vacuum oven overnight at 40°C to eliminate any possible residual solvents. The authors claim that the electrospun nanofibers of modified GTT could promote chondrocyte adhesion, and might have the capability of being used in cartilage tissue regeneration.

It is obvious that electrospun nanofibers could provide an environment adequate to promote advanced chondrocyte growth and differentiation to form a cartilage matrix. Currently, the clinical delivery of cartilage repair is based on injecting cells without scaffolds and this has accomplished certain success (Hardingham, 2011).

All body tendons are exposed to direct damage generated by accidental lacerations, or injuries caused by sports. Moreover, the tendons could be affected by diseases, such as osteoarthritis. It was proposed that tendon diseases could be generated by inflammation of tissue, that is, “tendonitis” (Bosworth, 2011).

Coaxial ES, one of the adjusted ES techniques, introduced by Loscertales et al., could produce core-shell nanofibers that can contain both hydrophilic and hydrophobic polymers (Xie et al., 2008). The coaxial ES technique can be utilized to produce core-shell structure with special physicochemical properties and important characteristics. This modified ES method could be used for this purpose because of the construction of a multichannel spinneret presenting inner core and outer shell channels for production of a core-shell structure (Shalumon et al., 2018; Moghe and Gupta, 2008). HA/PEO/ibuprofen/PEG/PCL/AgNP (IP/PAA) core-shell nanofibrous membranes containing HAp and ibuprofen in the core and embedded silver nanoparticles in the polyethylene glycol/polycaprolactone (PEG/PCL) shell were successfully obtained to imitate the tendon sheath by the coaxial ES method (Shalumon et al., 2018). The PEG/PCL/AgNP (PPA) prepared solution was used as the shell solution, while HA/PEO/ibuprofen (HI) solutions with different ibuprofen concentrations (HI0, HI10, HI30, HI50, respectively) were used in the core component. Gross view tests, histology, and biomechanical

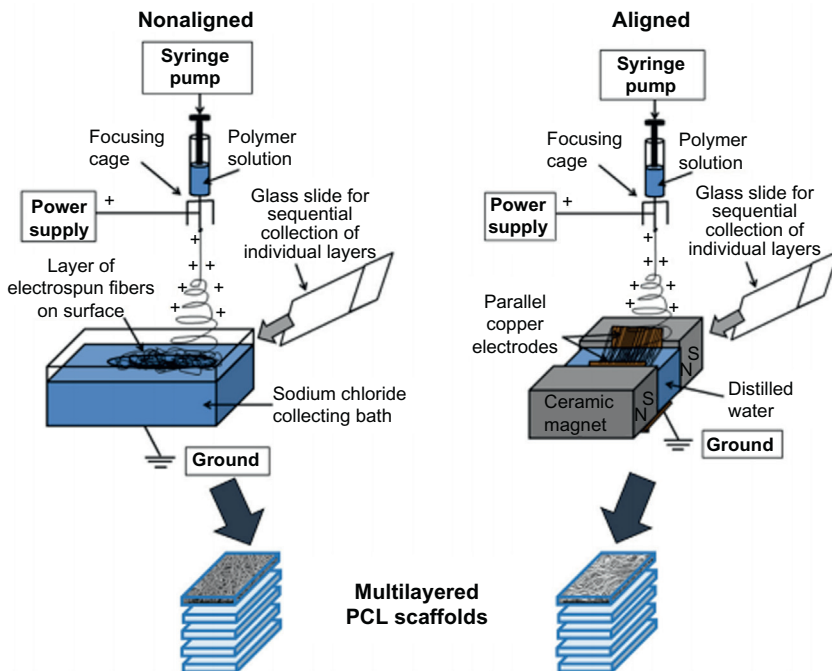
analysis in a rabbit flexor digitorum profundus tendon model proved the superior peritendinous antiadhesion barrier properties of the HI30/PPA membrane through the combined effect of HAp, ibuprofen, and silver nanoparticles (Shalumon et al., 2018).

Novel nanofibrous biotextiles, which copy the ECM of natural tendon with regard to structure and inherent nanoscale organization, have been produced by electrospun PCL and textile weaving technology (Wu et al., 2017). An electrospun nanofiber yarn-forming system utilized two oppositely positioned metal needles. Positive and negative voltages were applied to generate nanofibers. One rotating neutral metal disc (NMD) and one static neutral hollow metal rod (NHMR) were disposed oppositely in the middle of two needles. The NMD and the NHMR are used to collect nanofibers and further convert them into yarns. The nanofibrous scaffolds present a 3D aligned microstructure and larger pore size. These characteristics are favorable for cell proliferation, orientation, infiltration, and the expression of tendon fibroblast-associated markers. The PCL nanofiber yarn represents a promising alternative for tissue engineered scaffolds, especially for tendon regeneration.

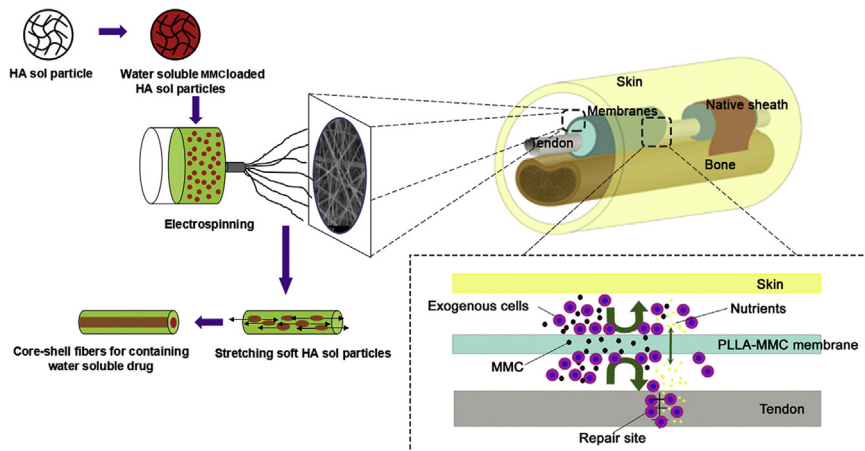
Sequential ES was used to fabricate biomimetic dual-layer organic/inorganic integrated fibrous membranes (Li et al., 2017). On the surface of nanoHAp/poly-L-lactic acid (n-HA/PLLA) fibrous layer was formed a layer composed by apatite nanoparticles after incubation in SBF, and the PLLA layer retained its original properties. The upper layer of PLLA fibers could induce tendon regeneration, while the lower layer of n-HA/PLLA formed a scaffold with a fiber structure and mineral deposition mimetic at the tendon-to-bone insertion site. The tests results showed that combination of nanoHAp and poly-L-lactic acid could serve as a novel treatment approach for improving the tendon–bone healing.

Orr et al. (2015) developed a multilayered ES method that provides a prescribed alignment of each layer in a clinically relevant patch size, and also evaluates the capacity of these aligned scaffolds to generate complete cellular infiltration, tenogenic ECM formation, and development of tensile mechanical properties by human adipose-derived stem cells compared with nonaligned multilayered scaffolds. Aligned layers were collected sequentially from the surface of the saline bath every 3 minutes onto a 5 cm × 7.5 cm glass slide, for a total of 140 layers—approximately 1 mm. Nonaligned layers were collected sequentially from the surface of the saline bath every 2 minutes using a 5 cm × 7.5 cm glass slide, for a total of 70 layers—approximately 1 mm. The parameters were selected to prepare similar scaffold thickness and fiber diameters between aligned and nonaligned scaffolds. Each scaffold was dried at room temperature and then stored at room temperature protected from light until use (Orr et al., 2015) (Figs. 4.1 and 4.2).

Compared with nonaligned scaffolds, aligned electrospun polymer scaffolds demonstrate considerable anisotropy and exert a higher tenogenic effect. The authors evaluated if multilayered aligned scaffolds improved collagen alignment, tendon-related gene expression, and mechanical properties correlated to

**FIGURE 4.1**

Schematic representation of ES apparatus for nonaligned and aligned electrospun scaffolds (Orr et al., 2015).

**FIGURE 4.2**

Schematic representation of production of MMC-loaded PLLA fibrous membranes by hyaluronan (HA) micro-sol ES (Zhao et al., 2015).

multilayered nonaligned scaffolds. Both aligned and nonaligned multilayered scaffolds determined cell infiltration and ECM deposition in the full thickness of the scaffold after 28 days of culture. Aligned scaffolds showed a large increased expression of tenomodulin compared with nonaligned scaffolds and displayed aligned collagen fibrils all over the full thickness, the presence of which may promote the increased yield stress and Young's modulus of cell-seeded aligned scaffolds along the axis of fiber alignment (Orr et al., 2015).

Zhao et al. (2015) obtained excellent mitomycin C (MMC)-loaded PLLA micro-sol electrospun fibrous membranes, which can perform controlled release of water-soluble MMC. The membrane could inhibit fibroblast adhesion and proliferation and promote cell apoptosis in vitro. Further, it could inhibit tissue adhesion surrounding tendon without detrimental effect for the healing process of damaged tendon by mediating fibroblast apoptosis as well as syntheses of collagen and  $\alpha$ -smooth muscle actin in vivo. Hence, it has possible clinical character as antiadhesion materials for tendon healing.

The ES technique seems to be a convenient method for developing scaffolds that simulate the tendon structure, especially 3D scaffolds that imitate the tendon's collagen fibrous bundles and hierarchical organization. The electrospun fibers effortlessly support cell attachment, proliferation, and grant guidance to the cells if using surface treatments of synthetic materials, like PCL, for directing cellular orientation. The choice of solvent and material guarantee important attention as the tensile features are considerably modified and are of significant importance in this tissue application (Bosworth, 2011; James et al., 2011).

### 4.3.2 SKIN TISSUE REGENERATION

The usage of electrospun nanofibers for skin has received a great importance in treating patients who suffer from acute burn injuries and chronic nonhealing wounds like venous ulcers, diabetic ulcers, pressure ulcers, and many more besides. At present, available skin substitutes that improve the tissue function have had limited success rate. TE has been researched to create a scaffold that copies entirely the ECM in its function and structure (Zhou et al., 2007). Lately, ES has become known as an important method in the fabrication of scaffolds because of its singular ability to generate nanofibers with appropriate mechanical, physical, and biological properties that contribute to cell growth, differentiation, migration, and proliferation (Subramanian et al., 2011).

Cold plate electrospinning (CPE) represents an efficient and facile method to produce 3D silk fibroin nanofibers avoiding the intrinsic limitation of traditional (TE) and salt-leaching electrospinning (SLE). ES using a cold plate is able to produce nanofibers with higher porosity than those prepared using the classical ES and SLE techniques. Thus, the 3D nanofiber scaffolds produced by CPE presented a controlled thickness and high porosity. Also, the cell attachment and infiltration studies recommend the obtained scaffolds to be used for artificial skin reconstruction due to easy contouring of facial shape (Sheikh et al., 2015).

This technique could be applied to simplify the fabrication of biomaterials with the same shapes and morphologies; especially, such nanofibers are highly attractive for developing structures that resemble the dermis, nose, or ear or for repairing other facial defects (Sheikh et al., 2015).

Dong et al. (2016) developed an in situ deposition of customized nanofibrous dressing using a different handy e-spinning technique that simply uses a battery and a converter to support the operating high voltage. Mesoporous silica nanoparticles loaded with silver nanoparticles (Ag-MSNs) were synthesized by the cocondensation method in intensely dilute sodium hydroxide solution, which could regularly release silver ions, and had longlasting antibacterial activity. After e-spinning, the obtained materials were characterized to evaluate basic properties, such as surface morphology and structure, thermal stability, and hydrophobic nature, and also to assess their potential as wound dressing. The antimicrobial activity of the in situ e-spun membranes was realized using a disk agar diffusion test. The in vitro and in vivo tests confirmed the bioavailability and antimicrobial activity of Ag-MSNs/PCL nanofibers to promote skin wound healing (Dong et al., 2016).

Electrospun nanofibers are considered as favorable scaffolds for TE as a result of ECM imitating factor appearing in a controllable 3D nanofibrous structure. The CPE technique can simplify the production of this class of biomaterials to design structures that could simulate the dermis (Sheikh et al., 2015).

#### 4.3.3 OTHER TISSUE ENGINEERING APPLICATION OF ELECTROSPUN NANOFIBERS

Muscle is distinctive of all of the tissues due the fact that it develops its own force, exhibiting a unique challenge in TE. New tissue developed from the scaffold must not only have structural integrity, it must also be capable to adapt the protein-based changes necessary for contraction and force generation (McKeon-Fischer and Freeman, 2011).

Electrospun scaffolds induce the arrangement of muscle cells in only one direction and can promote the necessary organization of the cells to produce a functional skeletal muscle. By utilizing a conductive component in the scaffold, electrical stimulation together with mechanical stimulation can be mixed to simplify skeletal muscle organization (McKeon-Fischer and Freeman, 2011; Fasolino et al., 2017).

Functional nerve regeneration is a complex and difficult process. The regeneration of nerve tissue by electrospun nanofibrous grafts could represent a way to fix a few clinical problems, like the restricted availability of allogeneic tissue that can be used in nerve conduits to accomplish most favorable mechanical properties and the size essential for joining and regeneration. The ES technique could represent a promising method to fabricate some specific scaffold that could be used in nerve tissue regeneration (Wang et al., 2011; Dinis et al., 2015).



TE is becoming progressively a promising approach to design biologically influenced cellular microenvironments to guide cell growth, differentiation, and functional tissue organization. All this could be possible with recent advances in developmental and stem cell biology (Simonet et al., 2011).

Using ES methods can obtain most of the tissue demands defined for heart valve TE (Kluin et al., 2017; Namdari and Eatemadi, 2016). Because the different ES methods are not always compatible, combining them is difficult. For example, adding bioactive factors generally reduces the ES possibilities and results in less flexibility in scaffold design. However, to produce a functional heart valve, these methods must be integrated into one complex 3D heart valve scaffold, formed by a three-layered structure (Fallahiarezoudar et al., 2015). Each of these layers should perfectly contain tailored bioactivity and mechanical characteristics. Many efforts are being attempted to find the best combination and concentration of the different bioactive factors and their implementation into the electrospun structure at the specifically locations (Simonet et al., 2011).

The utilization of ES techniques/electrospun biomaterials, in combination with in vitro TE or in vivo regenerative engineering approach, carries ambiguous promise for routine bladder augmentation or substitution. The main challenges include identification of appropriate elastic/biodegradable polymers and scaffold structures that pair the physical and biological demands of the bladder (Baker and Southgate, 2011).

Current treatments for diseases and trauma of dental and oral structures depend on durable materials like amalgam or synthetic materials, and also autologous tissue grafts. An archetype strategy was possible by utilizing electrospun nanofibers for tooth restoration and dento-oral regeneration (Zafar et al., 2016; Hughes, 2016). Use of electrospun fibers and their scaffolds in dento-oral applications include some considerations, including the type of material, the fiber orientation, the porosity, surface modification, and obviously tissue application (Seo et al., 2016). The selection of materials involves both natural and synthetic materials and a mixture of both. Also, the surface of the scaffold could be modified by osteoconductive components, which can support an optimal combination of mechanical and biomimetic properties (Rehman and Khan, 2011).

Due to simplicity and versatility of ES technique, multifunctional electrospun nanofibers are easily accessible providing superior therapeutic treatment for the wound (Zhao et al., 2014; Pilehvar-Soltanahmadi et al., 2018). The electrospun nanofibers present two distinct characteristics compared with traditional wound dressings. The first is represented “biomimetic effect” where nanofibers mimic the natural ECM. Nanofibers can act as biomimetic scaffolds, which support cell growth and tissue regeneration at the wound site. The second characteristic is focused on the “size effect” where nanofibers furnish large surface areas due to their reduced fiber diameters. The advantages of nanofibers as wound dressings include improved hemostasis, satisfied absorbency, ability to maintain a moist environment by the absorption of exudates, semipermeability to prevent bacterial invasion, superior conformability to cover the wound, and efficient drug delivery



behavior with sustained release profile (Abrigo et al., 2014). It has been shown not only that simple therapeutic or bioactive agents can be incorporated into nanofibers during ES, but also some complex compositions (e.g., multicomponent nanofibers) and structures/architectures (e.g., core-shell nanofibers). This opens up particular avenues for the design and production of next generation wound healing materials with ideal and multiple functionalities (Hayes and Su, 2011).

---

## 4.4 CONCLUSIONS

ES technique represents an effective and economical method for obtaining continuous fibers with a diameter range from hundreds of nanometers to tens of micrometers from a concentrated solution or melt under an intense electric field. The electrospun fibers present a lot of advantages, such as large surface area-to-volume ratios, high aspect ratios, and very porous structures. The morphology of electrospun fibers could mimic the natural collagen fibrils of the ECM.

The major concerns in ES method are represented by low production rate, scale-up, and the usage of organic solvents in the process. Some novel strategies, including multijets from multiple needles or needleless systems and also melt/emulsion ES, have been developed to overcome such challenges. Nevertheless, the issues associated with these systems must be consigned to make them commercially more feasible.

In recent years, ES method has considerably determined the growth of the field of nanotechnology, providing an efficient and easy method to produce nanofibers and other nanodevices based on them. With an important ability to commercialize and open up new research areas, ES remains the most advantageous method to obtain nano- and microfibers in various patterns.

Out of all the studied methods to obtain nano- and microfibers, ES is still the most investigated and focused-upon technique, with more than 18,000 publications (source—Scopus) to date on this field.

---

## REFERENCES

- Abrigo, M., McArthur, S.L., Kingshott, P., 2014. Electrospun nanofibers as dressings for chronic wound care: advances, challenges, and future prospects. *Macromol. Biosci.* 14 (6), 772–792.
- Agarwal, S., Wendorff, J.H., Greiner, A., 2008. Use of electrospinning technique for biomedical applications. *Polymer* 49 (26), 5603–5621.
- Agheb, M., et al., 2017. Novel electrospun nanofibers of modified gelatin-tyrosine in cartilage tissue engineering. *Mater. Sci. Eng. C* 71, 240–251.
- Ahmed, F.E., Lalia, B.S., Hashaiekh, R., 2015. A review on electrospinning for membrane fabrication: challenges and applications. *Desalination* 356, 15–30.

- Baker, S.C., Southgate, J., 2011. 11—Bladder tissue regeneration. *Electrospinning for Tissue Regeneration*. Woodhead Publishing, pp. 225–241.
- Bassi, A., et al., 2011. 5—Bone tissue regeneration. *Electrospinning for Tissue Regeneration*. Woodhead Publishing, pp. 93–110.
- Bosworth, L.A., 2011. 8—Tendon tissue regeneration. *Electrospinning for Tissue Regeneration*. Woodhead Publishing, pp. 148–167.
- Braghirolli, D.I., Steffens, D., Pranke, P., 2014. Electrospinning for regenerative medicine: a review of the main topics. *Drug Discov. Today* 19 (6), 743–753.
- Cai, X., et al., 2017. Electrospinning of very long and highly aligned fibers. *J. Mater. Sci.* 52 (24), 14004–14010.
- Cao, L., et al., 2017. Fabrication of chitosan/graphene oxide polymer nanofiber and its biocompatibility for cartilage tissue engineering. *Mater. Sci. Eng. C* 79, 697–701.
- Chu, Z., Seeger, S., 2014. Superamphiphobic surfaces. *Chem. Soc. Rev.* 43 (8), 2784–2798.
- Dalton, P.D., et al., 2007. Electrospinning of polymer melts: phenomenological observations. *Polymer* 48 (23), 6823–6833.
- Detta, N., et al., 2010. Melt electrospinning of polycaprolactone and its blends with poly (ethylene glycol). *Polym. Int.* 59 (11), 1558–1562.
- Dinis, T., et al., 2015. 3D multi-channel bi-functionalized silk electrospun conduits for peripheral nerve regeneration. *J. Mech. Behav. Biomed. Mater.* 41, 43–55.
- Dong, R.-H., et al., 2016. In situ deposition of a personalized nanofibrous dressing via a handy electrospinning device for skin wound care. *Nanoscale* 8 (6), 3482–3488.
- Echegoyen, Y., et al., 2017. High throughput electro-hydrodynamic processing in food encapsulation and food packaging applications. *Trends Food Sci. Technol.* 60, 71–79.
- Fallahiazroudar, E., et al., 2015. A review of: application of synthetic scaffold in tissue engineering heart valves. *Mater. Sci. Eng. C* 48, 556–565.
- Fasolino, I., et al., 2017. 5-Azacytidine-mediated hMSC behavior on electrospun scaffolds for skeletal muscle regeneration. *J. Biomed. Mater. Res. Part A* 105 (9), 2551–2561.
- Gönen, S.Ö., Erol Taygun, M., Küçükbayrak, S., 2016. Fabrication of bioactive glass containing nanocomposite fiber mats for bone tissue engineering applications. *Compos. Struct.* 138, 96–106.
- Gouma, P.-I., Han, D., 2017. Electrospun bioscaffolds that mimic the topology of extracellular matrix. *Nanomedicine in Cancer*. Pan Stanford, pp. 185–196.
- Guo, Y., et al., 2017. Polymer composite with carbon nanofibers aligned during thermal drawing as a microelectrode for chronic neural interfaces. *ACS Nano* 11 (7), 6574–6585.
- Hardingham, T., 2011. 6—Cartilage tissue regeneration. *Electrospinning for Tissue Regeneration*. Woodhead Publishing, pp. 111–126.
- Hasan, A., et al., 2014. Electrospun scaffolds for tissue engineering of vascular grafts. *Acta Biomater.* 10 (1), 11–25.
- Hayes, T.R., Su, B., 2011. 15—Wound dressings. *Electrospinning for Tissue Regeneration*. Woodhead Publishing, pp. 317–339.
- Hochleitner, G., et al., 2015. Additive manufacturing of scaffolds with sub-micron filaments via melt electrospinning writing. *Biofabrication* 7 (3), 035002.
- Hu, X., et al., 2014. Electrospinning of polymeric nanofibers for drug delivery applications. *J. Control. Release* 185, 12–21.
- Hughes, S.M., 2016. *Electrospun PCL Nanofibers Incorporated With Natural and Synthetic Calcium Hydroxyapatite Particles for Tooth Regeneration*. Wichita State University.

- James, R., et al., 2011. Tendon tissue engineering: adipose-derived stem cell and GDF-5 mediated regeneration using electrospun matrix systems. *Biomed. Mater.* 6 (2), 025011.
- Jiang, T., et al., 2015. Electrospinning of polymer nanofibers for tissue regeneration. *Progress Polym. Sci.* 46, 1–24.
- Katsogiannis, K.A.G., Vladisavljević, G.T., Georgiadou, S., 2015. Porous electrospun polycaprolactone (PCL) fibres by phase separation. *Eur. Polym. J.* 69, 284–295.
- Khorshidi, S., et al., 2016. A review of key challenges of electrospun scaffolds for tissue-engineering applications. *J. Tissue Eng. Regenerat. Med.* 10 (9), 715–738.
- Kim, B., et al., 2005. Poly (acrylic acid) nanofibers by electrospinning. *Mater. Lett.* 59 (7), 829–832.
- Kluin, J., et al., 2017. In situ heart valve tissue engineering using a bioresorbable elastomeric implant—from material design to 12 months follow-up in sheep. *Biomaterials* 125, 101–117.
- Kong, L., Ziegler, G.R., 2014. Fabrication of pure starch fibers by electrospinning. *Food Hydrocolloids* 36, 20–25.
- Lannutti, J., et al., 2007. Electrospinning for tissue engineering scaffolds. *Mater. Sci. Eng. C* 27 (3), 504–509.
- Li, W.J., et al., 2002. Electrospun nanofibrous structure: a novel scaffold for tissue engineering. *J. Biomed. Mater. Res. Offic. J. Soc. Biomater. Japan. Soc. Biomater. Austr. Soc. Biomater. Kor. Soc. Biomater.* 60 (4), 613–621.
- Li, D., et al., 2016. A comparison of nanoscale and multiscale PCL/gelatin scaffolds prepared by disc-electrospinning. *Colloids Surf. B Biointerf.* 146, 632–641.
- Li, X., et al., 2017. Flexible bipolar nanofibrous membranes for improving gradient microstructure in tendon-to-bone healing. *Acta Biomater.* 61, 204–216.
- Liu, Z., Chen, R., He, J., 2016. Active generation of multiple jets for producing nanofibres with high quality and high throughput. *Mater. Design* 94, 496–501.
- Luu, Y., et al., 2003. Development of a nanostructured DNA delivery scaffold via electrospinning of PLGA and PLA–PEG block copolymers. *J. Control. Release* 89 (2), 341–353.
- Lyons, J., Li, C., Ko, F., 2004. Melt-electrospinning part I: processing parameters and geometric properties. *Polymer* 45 (22), 7597–7603.
- Ma, Z., et al., 2005. Surface engineering of electrospun polyethylene terephthalate (PET) nanofibers towards development of a new material for blood vessel engineering. *Biomaterials* 26 (15), 2527–2536.
- Mason, C., Dunnill, P., A brief definition of regenerative medicine, *Regen. Med.* 3 (1), 2008, 1–5.
- McKeon-Fischer, K.D., Freeman, J.W., 2011. 7—Muscle tissue regeneration. *Electrospinning for Tissue Regeneration*. Woodhead Publishing, pp. 127–147.
- Moghe, A., Gupta, B., 2008. Co-axial electrospinning for nanofiber structures: preparation and applications. *Polym. Rev.* 48 (2), 353–377.
- Namdari, M., Eatemadi, A., 2016. Nanofibrous bioengineered heart valve—application in paediatric medicine. *Biomed. Pharmacother.* 84, 1179–1188.
- Nayak, R., et al., 2015. Structural and mechanical properties of polypropylene nanofibres fabricated by meltblowing. *J. Textile Inst.* 106 (6), 629–640.
- Noh, H.K., et al., 2006. Electrospinning of chitin nanofibers: degradation behavior and cellular response to normal human keratinocytes and fibroblasts. *Biomaterials* 27 (21), 3934–3944.
- Ogata, N., et al., 2007. Poly (lactide) nanofibers produced by a melt-electrospinning system with a laser melting device. *J. Appl. Polym. Sci.* 104 (3), 1640–1645.

- Okutan, N., Terzi, P., Altay, F., 2014. Affecting parameters on electrospinning process and characterization of electrospun gelatin nanofibers. *Food Hydrocolloids* 39, 19–26.
- Orr, S.B., et al., 2015. Aligned multilayered electrospun scaffolds for rotator cuff tendon tissue engineering. *Acta Biomater.* 24, 117–126.
- Otadi, M., Mohebbi-Kalhari, D., 2015. Evaluate of different bioactive glass on mechanical properties of nanocomposites prepared using electrospinning method. *Proc. Mater. Sci.* 11, 196–201.
- Pilehvar-Soltanahmadi, Y., et al., 2018. An overview on application of natural substances incorporated with electrospun nanofibrous scaffolds to development of innovative wound dressings. *Mini Rev. Med. Chem.* 18 (5), 414–427.
- Rehman, I.U., Khan, A.S., 2011. 13 - Dental regeneration. *Electrospinning for Tissue Regeneration*. Woodhead Publishing, pp. 280–297.
- Robb, B., Lennox, B., 2011. 3 - The electrospinning process, conditions and control. *Electrospinning for Tissue Regeneration*. Woodhead Publishing, pp. 51–66.
- Rogina, A., 2014. Electrospinning process: versatile preparation method for biodegradable and natural polymers and biocomposite systems applied in tissue engineering and drug delivery. *Appl. Surf. Sci.* 296, 221–230.
- Seo, S.-J., Kim, H.-W., Lee, J.-H., 2016. Electrospun nanofibers applications in dentistry. *J. Nanomater.* 2016.
- Shalumon, K.T., et al., 2018. Multi-functional electrospun antibacterial core-shell nanofibrous membranes for prolonged prevention of post-surgical tendon adhesion and inflammation. *Acta Biomater.*
- Sheikh, F.A., et al., 2015. 3D electrospun silk fibroin nanofibers for fabrication of artificial skin. *Nanomed. Nanotechnol. Biol. Med.* 11 (3), 681–691.
- Sill, T.J., von Recum, H.A., 2008. Electrospinning: applications in drug delivery and tissue engineering. *Biomaterials* 29 (13), 1989–2006.
- Šimko, M., Lukáš, D., 2016. Mathematical modeling of a whipping instability of an electrically charged liquid jet. *Appl. Math. Model.* 40 (21–22), 9565–9583.
- Simonet, M., et al., 2011. 10—Heart valve tissue regeneration. *Electrospinning for Tissue Regeneration*. Woodhead Publishing, pp. 202–224.
- Sridhar, R., et al., 2015. Electrosprayed nanoparticles and electrospun nanofibers based on natural materials: applications in tissue regeneration, drug delivery and pharmaceuticals. *Chem. Soc. Rev.* 44 (3), 790–814.
- Srivastava, R., 2016. Indian Institute of Technology Delhi, New Delhi, India. *Electrospun Nanofibers*. Elsevier, p. 399.
- Srivastava, R., 2017. Electrospinning of patterned and 3D nanofibers. *Electrospun Nanofibers*. Elsevier, pp. 399–447.
- Subramanian, A., Krishnan, U.M., Sethuraman, S., 2011. 14—Skin tissue regeneration. *Electrospinning for Tissue Regeneration*. Woodhead Publishing, pp. 298–316.
- Sun, B., et al., 2014. Advances in three-dimensional nanofibrous macrostructures via electrospinning. *Progress Polym. Sci.* 39 (5), 862–890.
- Teo, W.E., Ramakrishna, S., 2006. A review on electrospinning design and nanofibre assemblies. *Nanotechnology* 17 (14), R89.
- Thenmozhi, S., et al., 2017. Electrospun nanofibers: new generation materials for advanced applications. *Mater. Sci. Eng. B* 217, 36–48.
- Vashisth, P., Bellare, J.R., 2018. Development of hybrid scaffold with biomimetic 3D architecture for bone regeneration. *Nanomed. Nanotechnol. Biol. Med.*

- Wall, A., Board, T., 2014. The biological effect of continuous passive motion on the healing of full-thickness defects in articular cartilage. An experimental investigation in the rabbit. *Classic Papers in Orthopaedics*. Springer, pp. 437–439.
- Wang, L., Ryan, A.J., 2011. 1—Introduction to electrospinning. *Electrospinning for Tissue Regeneration*. Woodhead Publishing, pp. 3–33.
- Wang, C., et al., 2011. 9—Nerve tissue regeneration. *Electrospinning for Tissue Regeneration*. Woodhead Publishing, pp. 168–201.
- Wang, C., et al., 2017a. Cartilage oligomeric matrix protein improves in vivo cartilage regeneration and compression modulus by enhancing matrix assembly and synthesis. *Colloids Surf. B Biointerf.* 159, 518–526.
- Wang, J., et al., 2017b. Evaluation of the potential of rhTGF- $\beta$ 3 encapsulated P(LLA-CL)/collagen nanofibers for tracheal cartilage regeneration using mesenchymal stems cells derived from Wharton's jelly of human umbilical cord. *Mater. Sci. Eng. C* 70, 637–645.
- Wongkanya, R., et al., 2017. Electrospinning of alginate/soy protein isolated nanofibers and their release characteristics for biomedical applications. *J. Sci. Adv. Mater. Dev.* 2 (3), 309–316.
- Wu, S., et al., 2017. Living nanofiber yarn-based woven biotextiles for tendon tissue engineering using cell tri-culture and mechanical stimulation. *Acta Biomater.* 62, 102–115.
- Xie, J., et al., 2008. Encapsulation of protein drugs in biodegradable microparticles by coaxial electrospray. *J. Colloid Interf. Sci.* 317 (2), 469–476.
- Yamaguchi, K., et al., 2016. Highly dispersed nanoscale hydroxyapatite on cellulose nanofibers for bone regeneration. *Mater. Lett.* 168, 56–61.
- Yarin, A., Zussman, E., 2004. Upward needleless electrospinning of multiple nanofibers. *Polymer* 45 (9), 2977–2980.
- Yousefzadeh, M., 2017. Modeling and simulation of the electrospinning process. *Electrospun Nanofibers*. Elsevier, pp. 277–301.
- Zafar, M., et al., 2016. Potential of electrospun nanofibers for biomedical and dental applications. *Materials* 9 (2), 73.
- Zhang, W., et al., 2014. Nanowire-directed templating synthesis of metal-organic framework nanofibers and their derived porous doped carbon nanofibers for enhanced electrocatalysis. *J. Am. Chem. Soc.* 136 (41), 14385–14388.
- Zhang, J., et al., 2016. Preparation of self-clustering highly oriented nanofibers by needleless electrospinning methods. *Fibers Polym.* 17 (9), 1414–1420.
- Zhao, R., et al., 2014. Electrospun chitosan/sericin composite nanofibers with antibacterial property as potential wound dressings. *Int. J. Biol. Macromol.* 68, 92–97.
- Zhao, X., et al., 2015. Optimization of intrinsic and extrinsic tendon healing through controllable water-soluble mitomycin-C release from electrospun fibers by mediating adhesion-related gene expression. *Biomaterials* 61, 61–74.
- Zheng, Z., et al., 2016. Cell environment-differentiated self-assembly of nanofibers. *J. Am. Chem. Soc.* 138 (35), 11128–11131.
- Zhou, H., Green, T.B., Joo, Y.L., 2006. The thermal effects on electrospinning of polylactic acid melts. *Polymer* 47 (21), 7497–7505.
- Zhou, Y., et al., 2007. Electrospun water-soluble carboxyethyl chitosan/poly (vinyl alcohol) nanofibrous membrane as potential wound dressing for skin regeneration. *Biomacromolecules* 9 (1), 349–354.
- Zhou, F.-L., Gong, R.-H., Porat, I., 2009. Three-jet electrospinning using a flat spinneret. *J. Mater. Sci.* 44 (20), 5501–5508.

# Recent advances of chitosan composites in artificial skin: the next era for potential biomedical application

**Sumit Sharma and Sonali Batra**

*University Institute of Pharmaceutical Sciences, Panjab University, Chandigarh, India*

## 5.1 INTRODUCTION

Skin plays important functions in our body such as providing protection from pathogenic invasion and ultraviolet rays by acting as physical and mechanical barrier, regulating body temperature, providing elastic ability with sensory receptors permitting body movement, and consisting of exocrine and endocrine glands for excretion and vitamin D synthesis. All these properties of skin make the skin injuries (due to burns or accidents resulting in severe skin damage) a very serious subject of concern for early recovery and regeneration. Serious skin damage requires immediate medical assistance to avoid further serious complications and even death. Third degree burns and deep tissue damage are often associated with complications like bacterial infections, hypovolemia due to excessive blood loss, and hypothermia due to loss of body heat. Recovery of human skin is a time consuming and complex process and hence it requires a mechanism that can speed the healing or induce regenerative process. Skin comprises epidermis, dermis, and hypodermis regions, and the reconstruction of skin requires mainly epidermal and dermal equivalents to hasten the regeneration activity. An ideal tissue engineering material composite must have key properties like biocompatibility, hydration capacity, gaseous permeation, antibacterial properties, and mechanical strength that mimic the dry and moist skin microenvironment. Treatment of skin wounds has been practiced since time immemorial such as preventing blood loss and electrolyte disturbances using dressing materials. Various dressing materials are used for wound dressing and they are mainly classified as biological, synthetic, and biological cum synthetic. Biological skins used for wound dressing like pigskin, alloskin, cadaveric skin allograft, etc. provide more adherence and natural

extracellular matrix for promoting fast restoration. In spite of these advantages certain drawbacks like high antigenicity, ethical issues, and possibility of high degree of cross contamination render them as unsuitable materials for medical applications. Certain synthetic polyester polymers are studied with living tissues for novel drug delivery and treatment of inflammation (Kaur et al., 2017). Similarly synthetic materials like silicone, nylon, poly lactic acid, polycaprolactone, and polylactic-co-glycolic acid provide good mechanical strength, elastic properties, and less degree of contaminations but they are not able to provide natural extracellular microenvironment that imparts natural tissue recovery. On the other hand, dual properties of biological and synthetic skin material composites like chitosan/collagen, chitosan/gelatin, etc. serve the purpose of an ideal artificial skin biomaterial.

Commercially certain artificial skin substitutes and wound dressing materials are available (Table 5.1), fabricated with respect to the type of wound and tribology of skin. Due to their promising results in tissue engineering and increased use there seems to be a new era in material composites and skin equivalents for tissue engineering. Prior knowledge about the biocompatibility, skin texture, mechanical properties, sensory processing mechanisms, healing procedures, and growth factors like fibrovascular in growth are the prerequisites for designing an artificial skin substitute (Derler and Gerhardt, 2012). There are certain essential requirements to be considered before fabrication of an artificial skin substitute, which include biocompatibility of the material, meaning that it should not lead to acute or chronic reaction. Material should be biodegradable so that growing tissue can replace the applied external skin substitute. It should have adherent properties so that it allows cell proliferation and mechanical properties to provide strength to damaged or growing tissues. Table 5.1 enlists the commercially available pharmaceutical formulations for wound healing.

The general approach for skin regeneration is to develop a dermal substrate seeded with keratinocytes or other growing cells and applied to the damaged skin area where cells undergo mitosis and the process of regeneration starts. Chitosan-based composites form a matrix that provides a base for epidermal layer and desired extracellular microenvironment that promotes the natural biological process of regeneration. A general process of skin regeneration using chitosan-based composite is depicted in Fig. 5.1. Studies have reported that chitosan-based skin substitutes can facilitate cell differentiation, repair of wounds, and allow secretion of inflammatory mediators such as cytokines, prostaglandins, etc. (Sharma and Sinha, 2018; Jayakumar et al., 2011; Shahabuddin et al., 1990). Chitosan is obtained from chitin, which is the second most abundant polysaccharide after cellulose and is a common constituent of cell walls in invertebrates, insects, crustaceans, and various marine species. Chitosan itself is not in abundance but can easily be derived from deacetylation of chitin. Varying degree of deacetylation and availability from different sources leads to acquiring different properties with respect to solubility and mechanical properties. Chitosan is a linear polysaccharide composed of *N*-acetyl D-glucosamine and D-glucosamine

**Table 5.1** Enlisted Commercial Formulations for Wound Healing and Tissue Regeneration Globally

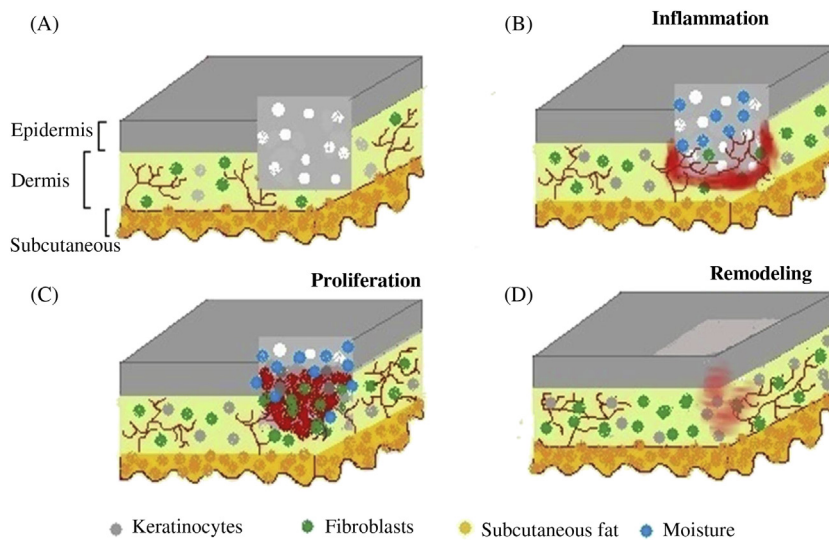
Product Name	Category	Composition	Description	Applications	Marketed by
ChitoFlex PRO	Hemostatic dressing	Chitosan	<ul style="list-style-type: none"> <li>• Can be stuffed into the wound to control excessive bleeding</li> <li>• Available in size 1 × 3"</li> </ul>	<ul style="list-style-type: none"> <li>• Acute trauma wounds</li> <li>• Wound debridement</li> <li>• Surgical site incisions, Pacemaker pockets</li> </ul>	Tricol Biomedical Inc.
Beschitin	Emollient and wound healing agent	Chitin	Better permeability and water absorption	<ul style="list-style-type: none"> <li>• As dressing for nasal and skin wounds</li> <li>• Promotes granulation</li> <li>• Avoids scar formation</li> </ul>	Unitika
Biobrane	Biosynthetic wound dressing	Nylon, silicone, and porcine extracellular matrix	Collagen peptides incorporated in nylon mesh to which silicone membrane is bonded	Partial thickness burns	Bertek Pharmaceuticals
Dermagraft	Skin substitute	Allogenic neonatal fibroblast cells in polyglycolic acid mesh	<ul style="list-style-type: none"> <li>• Absorbable extracellular matrix</li> <li>• Biodegradable and contains no silicon</li> </ul>	Full thickness in diabetic foot ulcers greater than 6 weeks	Organogenesis Inc.
Integra	Dermal substitute	Silicone membrane	Glycosaminoglycans with bovine collagen peptides are incorporated in silicone membrane	Burns and reconstructive surgery	Integra LifeSciences Corporation
Permacol	Dermal substitute	Porcine-based collagen peptides	<ul style="list-style-type: none"> <li>• Promotes tissue in growth</li> <li>• Nonimmunogenic</li> </ul>	<ul style="list-style-type: none"> <li>• Ventral hernia repair and abdominal wall reconstruction</li> </ul>	Bard Medical

*(Continued)*



**Table 5.1** Enlisted Commercial Formulations for Wound Healing and Tissue Regeneration Globally *Continued*

Product Name	Category	Composition	Description	Applications	Marketed by
Transcyte	Allogenic temporary skin substitute	Nylon and collagen	Collagen coated on nylon and seeded with neonatal fibroblastsIntegrates with tissue and promotes in growth	Mid dermal to indeterminate depth partial thickness burns	Shire Regenerative Medicine
Apligraf	Bilayered skin substitute	Type I collagen	Fibroblasts and neonatal keratinocytes in type I collagen matrix with cytokines	Full thickness diabetic foot ulcers	Organogenesis Inc.
TraumaStat	Absorbent	Chitosan, polyethylene and silica	Polyethylene fibers coated with chitosan and incorporated silica	Hemostatic	Ore-Medix
Vulnosorb	Super absorbent foam	Chitosan and collagen	Microcrystalline chitosan is mixed with collagen	<ul style="list-style-type: none"> <li>• Controls severe bleeding</li> <li>• Provides moisture in the wound</li> </ul>	Tesla Pharma
ChitoPack C	Fibrous form	Chitosan acetate	Cotton like chitosan is used for fabrication	Regeneration of deep wounds up to subcutaneous layer	Eiasi Co.
ChitoPack S	Sponge	Chitin	Freeze dried chitin dispersion	<ul style="list-style-type: none"> <li>• Promotes granulation</li> <li>• Severe tissue injuries</li> <li>• Avoids scar formation</li> </ul>	Eiasi Co.
Syvek-Patch	Fibrous form	Chitin	Nonwoven microfibers of chitin	Hemostatic	Marine Polymer Technologies
Tegasorb	Gel	Chitosan	Oval-shaped polyurethane membrane composed of dispersed chitosan which forms hydrocolloid mass	Healing of deep wounds	3M

**FIGURE 5.1**

A general description on functioning of artificial skin in wound healing.

amino acid units. To be labeled as chitosan, chitin must be 60% deacetylated, which is done under high alkaline conditions and by enzymatic hydrolysis (Croisier and Jerome, 2013; Jayakumar et al., 2010a; Venkatesan and Kim, 2010). Chitosan being a biopolymer having well recognized applications in tissue engineering and cellular level regeneration has been given considerable attention nowadays for fabricating artificial skin. The structure of chitosan is somewhat analogous to the structure of growth factors and proteins and peptides (collagen and keratin) found in skin tissues, which was found to be important for stimulating natural physiological reactions required for tissue repair and cell regeneration during tissue damage (Parvez et al., 2012). The use of chitosan is widely recognized in novel drug delivery and biomedical applications such as in making of prostheses, artificial skins and implants, etc. (Sharma et al., 2014; Salati et al., 2011; LogithKumar et al., 2016).

## 5.2 ANATOMY OF SKIN

The skin is a complex membrane that acts a shield for internal organs and performs various vital functions like:

- **Heat regulation:** The blood vessels and sweat glands are responsible for regulation of body temperature during changes in temperature externally and

physical exertion. For instance constriction of blood vessels prevents heat loss whereas dilation leads to cooling effect by altering the blood flow through the skin. In addition to this sweat glands regulate the body temperature by evaporation of sweat through the surface of skin.

- **Sensory function:** Skin is comprised of several sensory and motor nerve fibers and their endings. Sensory nerves mediate the sensation of touch, pain, temperature, and itching sensations whereas motor nerves mediate smooth muscle activity, sweat glands secretion, and arterioles.
- **Secretions:** Skin is responsible for secretion of sebum, which prevents excessive water loss through the skin and keep it moisturized. Also this protects from bacterial and fungal infections. Skin also contains precursors for vitamin D synthesis.

Skin has a stratified organization with varied thickness, structural integrity, and composition. It is a dynamic tissue the composition and form of which changes with certain factors like region, age, and external factors. Despite all the aforesaid functions of skin, it is also responsible for expressing certain intense emotions in the form of blushing, gooseflesh, and paleness. Skin is categorized mainly in three layers: epidermis, dermis, and subcutaneous.

### 5.2.1 SUBCUTANEOUS LAYER

Subcutaneous layer is a specialized layer of skin and is the deepest of the three. It is responsible for storing fat, nutrients, and energy. This layer is also referred to as the hypodermis layer, which means “below the dermis,” and is well vascularized. The thickness of this layer is due to fat tissue, which is thick on the buttocks, palms, and soles of the feet, by virtue of which it prevents the internal organs from physical and thermal shock. Appendages like deep hair follicles, sebaceous and sweat glands grow in this layer. It is difficult to identify a demarcation line between the dermis and hypodermis. The distribution of fat in subcutaneous tissue is regulated by certain hormones like testosterone, estrogen, insulin, etc. and of course genes ([Dreno, 2009](#)).

### 5.2.2 DERMIS

The dermis is an amorphous connective tissue mainly comprising of collagen fibers that provide the essential tensile strength to the skin, elastic fibers made of elastin (amorphous protein) that provides elastic nature, and reticular fibers referred to as immature collagen fibers. Dermis is also composed of cellular components like fibroblasts, which are responsible for formation of collagen fibers. Mast cells and lymphocytes are known to be responsible for dilation of vessels and immunogenic reactions. The base of the dermis is difficult to identify with histological examination and is rich in polysaccharides, proteins, and growth and

immune factors (McLafferty et al., 2012). Hyaluronic acid is a mucopolysaccharide present in minimal amount but accumulates in pathologic conditions. The role of the dermis is to hold water to keep the skin moist and thermal regulation. Dermis is also comprised of sensory nerves and receptors. The dermis with epidermal layers together contributes to development of epidermal appendages and remodeling of tissue. The extracellular matrix of dermis contains mainly glycosaminoglycans, which forms the major bulk and supports the structural proteins (collagen and elastin) to preserve moisture. This function of glycosaminoglycans keeps the dermis and epidermis in a viable condition by maintaining the collagen and elastin in good form.

### 5.2.3 EPIDERMIS

The epidermis refers to the outermost layer of skin, which is approximately 100  $\mu\text{m}$  thick. Epidermis layer renews itself around every 28 days. Epidermis further includes five stratified layers; from outer layer to inner layer:

- horny layer also known as stratum corneum,
- stratum lucidum,
- stratum granulosum also referred to as granular layer,
- stratum spinosum, and
- stratum basale.

Horny layer represents the outermost layer of skin mainly comprised of dead keratinocytes, which impart a frictional property to the skin. In between the keratinocytes lipids and fatty acids are present, which together act as cement and impart moisturizing effect. In addition to this this layer prevents invasion of microorganisms, allergens, and ultraviolet light. Sebaceous and sweat gland secretions consist of fatty acids and salts due to which skin has slightly acidic pH (4.5–6.5). Stratum lucidum layer is commonly present in palms, fingertips, and soles of feet. Going deeper is a granular layer that comprises hard fibers by virtue of which it provides strength to skin and act as a protective barrier. The cells present in this usually tend to die due to insufficient access of nutrients from subcutaneous layer as they lie far from this nutrient store. Further the stratum spinosum is where mostly polygonal flat shaped keratinocytes are present. Stratum basale is the epidermal layer next to the dermis where new keratinocytes regenerate through cell mitosis and replace the dead keratinocytes in the epidermis. This layer is identified with the presence of cube shaped cells. The regeneration power of the keratinocytes in this layer gets weakened with aging. In addition to this a melanin pigment is secreted by melanocytes present in this layer. The pigment along with keratinocytes migrates to the upper layers of the epidermis. This pigment provides protection from ultraviolet light and imparts color to the skin.

## 5.3 CHITOSAN COMPOSITES

### 5.3.1 CHITOSAN COMPOSITES AS SPONGES

Sponges are a type of 3D scaffolds that are soft and have porous structure that provides a guiding template for the skin repair process. Sponges have greater porosity, which provides advantages of absorbing wound exudates (more than 20% of its dry weight) and better cell interconnection yet remain soft and flexible due to microporosity (Croisier and Jerome, 2013). The application of chitosan-based matrix biomaterial composites is best suited to large dressing areas particularly in severe skin damages or urgent recovery required during skin grafting (Denkbass et al., 2004). Studies have suggested that chitosan is an excellent material for skin tissue engineering because it has a porous structure due to which it allows gas permeation, enhanced water absorbing capacity, cell interaction and incorporation of drugs, growth factors, seeding of stem cells or DNA molecules. These attributes make the substitute suitable for wound healing as these properties prevent bacterial infections and prevent wounds from becoming dehydrated. In addition to this, *N*-acetyl-D-glucosamine, a product formed on chitosan degradation, stimulates fibroblast proliferation, which further accelerates the synthesis of extracellular matrix of skin (Jayakumar et al., 2011). Selective natural polymers like collagen, hyaluronic acid, chondroitin sulfate, and gelatin form promising biomaterial composites with chitosan for wound healing (Anisha et al., 2013). The utility of using sponge as a skin substitute is that it provides a hydrated microenvironment at wound the interface, which is essential for early tissue recovery without leaving scars. Otherwise it takes a very long time (years) for a scar to diminish from the site of recovery. The scar looks distinguishable on the normal skin surface and has randomly arranged epidermal cells and collagen fibers as represented in Fig. 5.2.

Chitosan/gelatin composites as sponges have been investigated as a promising substitute for wound dressings. The combination of these two polymers is favored because of their good mechanical properties and thermostability. Gelatin has good water absorbing ability and film forming properties while chitosan has hemostatic

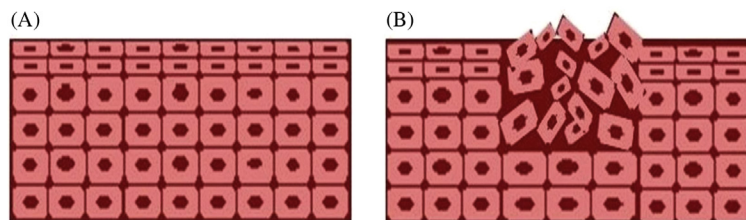


**FIGURE 5.2**

Architectural difference between (A) normal tissue and (B) recovered tissue with scar formation.

and antibacterial ability. Both of these polymers are biocompatible, which avoids allergic reactions, and are biodegradable materials, and therefore leave no scars on healing. In terms of texture gelatin-based membrane has rough surface while chitosan has comparatively plain surface. Composites of these polymers in the right composition yield the most suitable porous scaffold to be used as dermal equivalent. Biocompatibility of chitosan/gelatin sponge was explained by cytotoxic studies performed on L929 cell lines. It was inferred that around 140% of cells were viable after 72 hours of incubation of L929 cells with chitosan/gelatin sponge and it was found to be superior when compared with only chitosan or gelatin made sponge. Improved mechanical properties of the sponge with comparatively better Young's modulus and tensile strength from chitosan or gelatin alone were observed. Considerably high water absorbing capacity and retention time of chitosan/gelatin sponge was estimated as compared with chitosan or gelatin alone. Also chitosan/gelatin sponge loaded with growth factors was found to be relatively better than the sponge without growth factors as it accelerated the healing process. All these findings explain the characteristics of ideal skin substitute for wound dressings (Lu et al., 2016). Additionally it is important to consider the best suitable ratio of chitosan and gelatin to fabricate an ideal biocomposite for soft tissue regeneration. It is reported that artificial skin membrane made from a mixture of chitosan and gelatin in the ratio of 3:10 showed good mechanical properties with high tensile strength and elongation at break. Increase in chitosan (up to 3%) with constant gelatin concentration improves mechanical property but after a particular point (above 3%) it shows reduced mechanical strength. Therefore 3:10 proportion of chitosan:gelatin was found to be optimum for flexible and strong biomaterial to be used as artificial skin substitute in the context of mechanical properties. Moreover in terms of antimicrobial effects, 3:10 proportion showed relatively higher zone of inhibition than pure chitosan, gelatin, and other ratios of composites (5:10 and 7:10) against *Bacillus* sp. and *Candida* sp. (Parvez et al., 2012).

Chitosan/collagen biocomposite is also suggested as a potential skin substitute for rapid wound healing. Collagen (Types I, IV, and VII) being a major component of skin protein represents approximately 70% of dry skin mass and because of better cellular affinity is preferred for fabrication of skin substitutes (Debels et al., 2015). But the drawback of using collagen alone is its rapid biodegradation and poor mechanical properties (Rothamel et al., 2005). Various synthetic polymers have been studied to fabricate a composite with collagen to increase the shelf life and better mechanical properties but allergic reactions and cytotoxicity predominate. To overcome biocompatibility, biodegradability issues, and improving mechanical properties, chitosan is blended with collagen. In vitro biodegradation studies have shown that biostability of collagen can be improved without the use of synthetic cross-linkers by forming a composite with chitosan and collagen, which can serve the purpose. Moreover it has been evident from full thickness wound model on albino rats that medicated chitosan/collagen composite leaves no scar after 28 days of wound healing period. Also no pus formation was observed

in wounds treated with chitosan/collagen scaffold (medicated and nonmedicated) implying that chitosan itself has antibacterial activity (Mahmoud and Salama, 2016).

### 5.3.2 CHITOSAN COMPOSITES AS HYDROGELS

Hydrogels have the ability to soak up a large amount of fluid yet still remain insoluble. Due to excessive water content they are soft and are biocompatible with living tissues whereas the solid behavior of gel provides a physical support and mimics the nature of soft tissue. Due to the soft and flexible nature of hydrogels it ensures minimal damage to surrounding living tissues. The porosity of hydrogels can be altered easily depending on the extent of crosslinking in the gel structure. Moreover porous structure of hydrogels also allows incorporation of various micro- and macromolecules that enhance the tissue healing. Hydrogels also act as a reservoir and provide a localized drug concentration when used as tissue substitute. All these properties of chitosan hydrogels have increased the interest for chitosan-based hydrogels to be used as skin substitutes and also in various biomedical applications like cellular immobilization, supporting material for cell adhesion, drug delivery, etc. (Croisier and Jerome, 2013; Hoare and Kohane, 2008).

Treatment of burns requires effective dressing materials to cure both dermal and epidermal tissues. But in instances of burn care, a major criterion is to prevent proliferation of bacterial infections. Antibacterial hydrogel dressings with natural polymers are preferred so as to prevent damage during the change of the dressings. A study shows that chitosan–alginate hydrogel provides adequate mechanical properties required for stable dressing material. In this, gelatin-based antibacterial drug (tetracycline hydrochloride) loaded microspheres were prepared. These microspheres when incorporated in chitosan–alginate (4:1) hydrogels showed significant antibacterial effect against *Escherichia coli* and *Staphylococcus aureus*. The tetracycline loaded microspheres embedded in hydrogel showed better sustained release of the drug for 4 days as compared with the hydrogel without medicated microspheres. The steady release of the drug was up to 14 days, which makes the use of such hydrogel-based composite an effective antibacterial biocomposite to be used in wound dressing. Use of microspheres in the hydrogel provides a double barrier for the release of water soluble drug. Hydrogel-based systems are efficient for wound dressings as they easily reform according to the shape of wound providing an edge over other forms of skin substitute (Chen et al., 2017).

### 5.3.3 CHITOSAN COMPOSITES AS NANOFIBERS

Skin is composed of two layers: the overlying epidermis, which contains mainly keratinocytes, and underlying dermis layer, which has high density of soft and moist fibrous network of fibroblasts, collagen, and polysaccharides (Sarkar et al., 2013).

This fibrillar extracellular matrix acts as a reservoir for living cells and endorses cell adherence, which further aids in cell signaling and chemotaxis. In this way cell proliferation occurs normally and leaves no scar formation after tissue regeneration. But in case of severe damage to skin or large wounds due to third degree burns or chemical exposure, removal of skin at full thickness often leaves scars after surgery or healing. So in view of skin tissue engineering it is desired to fabricate extracellular fibrillar matrix that mimics the living skin tissue with great emphasis on cell adherence and stimulate normal cell proliferation so as to speed up the healing process. In addition to this biocompatibility and biodegradability should also be considered during fabrication of artificial fibrillar tissue matrix so as to avoid unnecessary inflammatory responses and signs of scars on total recovery. During recent years chitosan-based micro- and nanofibers have been explored with potential wound healing results ([Han et al., 2010](#); [Ahmed and Ikram, 2016](#); [Jayakumar et al., 2010b](#)). A study based on fabrication of chitosan/collagen fibrillar network as a substitute to skin extracellular matrix within the micro- and nanorange has been explored successfully for wound healing application. Collagen is most commonly opted for skin substitutes due to the main protein component of connective tissue in mammals. It has been noted that in diabetes or skin damages (due to third degree burns or chemical exposures) the reepithelialization process is very weak and skin takes a long time to heal. This is attributed to the presence of matrix metalloproteinase (MMP), which occurs due to persistent inflammatory reactions that denature both viable and nonviable collagen already present in skin. Therefore a fiber-based matrix scaffold has been fabricated using collagen, which supplements the scarcity of depleted collagen due to MMP activity and helps in tissue restoration on wound closure. A lyophilized fibrous scaffold was developed with underlying cross-linked type 1 collagen matrix blended with chitosan electrospun layer. Generally potential mechanical and degradation limitations of collagen are overcome by making composites with glycosaminoglycans. Here in this study incorporation of chitosan contributes to the availability of glycosaminoglycans. In addition to this chitosan induces cellular response and promotes fibroblasts to form collagen for wound healing. Wound healing study on human skin equivalent clearly indicates that cross-linked chitosan alone was unable to induce keratinocytes migration. On the other hand chitosan/collagen-based scaffolds showed clear signs of presence of keratinocytes onto the scaffold and human skin equivalent indicating the acceptance by the host tissue and supporting reepithelialization ([Sarkar et al., 2013](#)).

Wound healing is a continuous process that involves three main stages: preliminary inflammation, tissue reconstruction for wound closure, and reviving of physiological and functional activity of tissue. Hence apart from desired mechanical and biodegradability certain growth factors are also been added to promote skin regeneration in case of large wounds and chronic wounds. A problem associated in this approach with conventional wound dressings is the degradation of growth factors or seeded germ cells, denaturation of incorporated proteins/peptides, and leakage of loaded above-said components along with wound exudates



(Xie et al., 2013). Therefore for full thickness wounds with severe bleeding, an ideal artificial skin substitute must ensure the stability, viability, and prevent leakage of incorporated wound healing enhancers in dry and wet conditions. Apart from collagen (a natural protein), gelatin, and other natural polysaccharides like arginine, cellulose is widely accepted to form nanofibers coupled with chitosan to mimic native skin (Antunes et al., 2015; Wu et al., 2014). Gelatin is a source of amino acids like proline, hydroxyproline, and glycine, which means abundant amino and carboxyl groups are responsible for enhanced hydrophilic character and nonantigenicity. Studies have shown that gelatin activates macrophages and have potential hemostatic activity. Gelatin is also used as dressing material, absorbent for absorbing plasma exudates and adhesive (Dhandayuthapani et al., 2010). Gelatin when coupled with chitosan leads to increase in hydrophilicity of chitosan, which further supports cell adhesion, migration of cells between the micro/nanofibrous structures, and excellent cytocompatibility. Moreover electrostatic interaction between positive charge on chitosan and negative charge on gelatin reduces the ionic interaction of chitosan with negatively charged cell membrane. Due to decrease in net charge it will increase the cell migration between the micro/nanofibrous mat, which provides a natural mechanical framework for reconstruction of skin tissue and results in scar free skin recovery (Jafari et al., 2011).

### 5.3.4 CHITOSAN COMPOSITES AS CONDUCTIVE MEMBRANE/FILMS

Skin membrane along with living cells and proteins/peptides also comprises the peripheral nervous system, which is responsible for tactile property (sensation of touch, pain, and temperature) of skin. The peripheral nerve system is deep seated in the skin and comprises mainly nerves and Schwann cells responsible for the motor activity or electrical signaling between brain and skin receptors. Skin damage at the dermal level due to large wounds or physical trauma may result in nerve defects. These sensory nerve defects either take a very long time to recover or cause permanent loss of sensory stimulus. Various approaches have been adopted to repair the nerve defects occurring in large wounds including autologous nerve grafting, acellular nerve allografts and biological or synthetic nerve guidance channels. But these are associated with certain complications like numbness, abnormal functionality, and drawbacks like unable to repair normal sensory activity in large gaps (Zhang et al., 2014). However it has been proposed that optimum electrical stimulation in conductive artificial skin structures incorporated with Schwann cells have shown promising significance in nerve cell regeneration (Shi et al., 2008; Wood and Willits, 2006; McKenzie et al., 2006). An experiment has been performed on nerve regeneration using a biodegradable conductive membrane. Chitosan composite with polypyrrole was used to develop a conductive membrane of 0.4 mm thickness. Polypyrrole, a synthetic polymer, was selected due to its high electrical conductivity and biocompatibility. However this polymer is nonbiodegradable in nature and has rigid conjugated molecular

structure making it unsuitable for developing artificial skin membrane. Hence a biodegradable artificial conductive skin membrane was prepared using 2.5% (w/w) polypyrrole and 97.5% (w/w) chitosan (~90% deacetylated) impregnated with Schwann cells. Schwann cells play an important role in the growth of axons and releasing nerve growth factors. MTT cell viability has shown that electrical stimulus of 100 mV promotes the cell growth of Schwann cells after 12 and 24 hours of incubation with Schwann cells derived from sciatic nerves of newborn SD rats when compared with and without electrical stimulus. Also results obtained from RT-PCR and western blotting suggested that electrical stimulus through chitosan/polypyrrole conductive membrane significantly increases the expression and secretion of neurotrophins like nerve growth factor and  $\beta$ -brain derived neurotrophic factor in Schwann cells. All this evidence supports the fact that chitosan-based conductive skin substitute with optimum electrical stimulation generates nerve regeneration and skin sensory restoration ([Huang et al., 2010](#)).

---

## 5.4 CHARACTERIZATION

### 5.4.1 PORE SIZE AND POROSITY

Every organ has a characteristic pore size by virtue of which the structural and functional activity of organ is determined. For instance the porosity of skin is responsible for the presence of different cells (fibroblasts, keratinocytes, melanocytes, etc.), sensory receptors (Pacinian corpuscles, Ruffini's corpuscles, free nerve endings, Merkel's disks, Meissner's corpuscles, etc.), and glands (sebaceous and sweat). Apart from all these, porous structure provides a space for migration of cells, and water and gaseous exchange, which are necessary to maintain skin viability and mechanical properties. Studies have proposed that pore size of the artificial skin must be within a range of 100–200  $\mu\text{m}$  and porosity must be more than 90% to mimic the native skin membrane structurally as well as functionally ([Han et al., 2014b](#)). In addition to this the suggested range of pore size and porosity is required for seeding of stem cells or growth factors, proper supply of oxygen, nutrients, and room for growing new cells. Porosity of developed artificial skin also determines the water uptake capacity. Chitosan and its composites for artificial skin generally have intrinsic water absorbing capacity due to which films/membranes/fibrous mats swell and reduce the space in between, which is vital for neotissue regeneration also to maintain the viability of seeded living cells. Therefore the porosity holds an importance in such situations and enhances the water uptake capacity of chitosan-based films/membranes/fibrous mats/sponges. The adopted method to determine the porosity is to soak developed artificial skin with known dimension into the known volume of ethanol for 24 hours. Then calculate the volume of dry artificial skin with known dimensions. Also weigh the artificial skin both in dry and wet conditions. The percentage porosity is then calculated using the given mathematical expression represented in

the following equation, where  $W_f - W_i/\rho$  signifies the actual volume of pores in the known size of artificial skin.

$$\% \text{Porosity} = \frac{W_f - W_i}{\rho \times V} \times 100$$

where  $W_f$  is the weight of soaked artificial skin,  $W_i$  is the weight of dry artificial skin,  $\rho$  is the density of absolute alcohol, and  $V$  is the calculated volume of dry artificial skin of known geometry.

### 5.4.2 MECHANICAL STRENGTH

The mechanical strength of artificial skin holds a vital role in maintaining a desired architectural integrity both in dry and wet conditions. Chitosan has poor mechanical strength in wet conditions, which are essential in the applications of artificial skin. This drawback of chitosan is attributed to its swelling characteristic in wet conditions. Chitosan has good water adsorption property but it is beneficial to some extent when used as load bearing artificial skin in the form of films/sponges (Oh and Hwang, 2013). Excessive adsorption of fluid swells the polymer and affects the tensile strength, elongation at break, gaseous exchange, and pore size of artificial skin. As a consequence cell migration into the wound, proliferation, and natural tissue remodeling get affected. Also being a bioresorbable material the developed artificial skin may be subjected to degradation after application by hydrolysis, temperature decomposition, etc., which reduces the strength and cell attachment. In addition to this instability of chitosan artificial skin in wet conditions influences the drug release, viability of incorporated cells, and growth factors. As discussed earlier, studies have proposed that the mechanical behavior of chitosan can be improvised as per requirement by making composites with natural or synthetic polymers in appropriate composition to minimize the fluid absorption capacity of chitosan and enhanced mechanical stability in wet conditions (Li et al., 2009; Oh and Hwang, 2013). Mechanical strength for artificial skin must satisfy the following requirements both in dry and wet conditions:

- Optimum flexibility to acquire the shape of wound to provide scar free healing.
- Sufficient strength to attach and adhere on the wound surface.
- Optimum elasticity so as to conform on wound surface in proportion to the applied force.
- Adequate structural integrity so as to maintain the required porous behavior and ability to be removed easily on healing particularly in wet conditions.

During wound healing growing tissue penetrates into the artificial skin structure. Due to this the artificial skin should provide satisfactory tissue adhesion and should not be detached from the wound surface until healing is complete. As discussed earlier the chitosan-based skin substitutes are degraded due to hydrolysis and thermal exposure. Therefore with the passage of time during wound healing

chitosan-based artificial skin is exposed to fluid retention and swelling and undergoes degradation slowly, and hence its tensile strength gets reduced. So, for the development of chitosan-based skin substitute, it should be optimized for tensile strength under various possible degradative treatments that are most likely to occur during wound healing. Also the artificial skin should be peeled off without any discomfort and damage to the recovered skin. All these factors are necessary for the production of skin substitute having an optimal functional life required according to the wound condition to be treated. Studies have been done to optimize the mechanical strength of chitosan composites for biomedical applications in terms of tensile strength, Young's modulus, and elongation at break and ensure a gold standard in the field of artificial skin for better cell attachment and proliferation (Kang et al., 2010). These parameters give an indication of flexibility, elasticity, and physical strength to be used in skin substitutes. Optimum elasticity and high percentage of elongation at break is said to be suitable for soft nerve tissue regeneration. Viscoelasticity is another characteristic parameter of materials that warrants important consideration for the materials to be used as an ideal skin substitute and supposed to mimic the natural skin during wound healing. Human skin tissue has the property to regain its natural shape after removal of stress but not instantaneously. While other materials undergo structural deformations under stress and regain their original structure immediately on removal of stress. This immediate recovery represents the elastic nature of the materials while in case of skin tissue the slow recovery is attributed to its viscoelastic property. Viscoelasticity can be defined as combination of viscous and elastic behavior under the influence of stress. Skin tissue has a microporous structure comprising of water along with fatty components that impart a viscous nature and collagen fibers that impart tensile strength by virtue of which it shows viscoelastic nature. In concrete terms it is explained as when strain is removed skin tissue acquires its original shape after a definite time. This property is important in living skin tissues because skin consists of various continuous migrating living and dead cells. In addition to these various growth factors, nutrients and glands are situated inside the skin. Therefore during physical activity or continuous changes in stress-strain, the viscoelastic nature allows all skin components remain undisturbed, providing time and space to adjust normally, hence maintaining the normal architectural integrity of the skin. This shows that an artificial skin to be used for wound healing must possess viscoelastic nature so as to provide a natural environment for wound healing and perform similar mechanical functions as natural human skin tissue. Chitosan with molecular weight greater than 310 kD has higher tensile strength as compared with low molecular weight chitosan (50–190 kD) (Sarasam and Madihally, 2005). Chitosan has water absorbing property after which it turns into a viscous consistency and ultimately shows a viscoelastic nature. In vitro studies have also been performed to estimate and validate the tensile strength of chitosan composites for the use as skin substitute in dry and wet conditions. For instance chitosan composite with gelatin has been studied for tensile strength in tissue engineering. It was reported that in dry

conditions gelatin had three times greater tensile strength than chitosan while the situation is totally reversed in wet conditions. Also it has been observed that increase in gelatin content increases the stiffness of membrane developed from chitosan/gelatin composite in dry form. Whereas in wet form increase in gelatin had reduced the stiffness in the membrane and membrane of gelatin polymer alone had 20 times lower stiffness as compared with chitosan/gelatin composite in a ratio of 1:3 (Huang et al., 2005). In a study, a composite of chitosan was fabricated with nanofibrillar cellulose to enhance the mechanical strength of chitosan. It has been suggested evidently that the ultimate strength of chitosan composite was increased with increase in nanofibrillar cellulose concentration (Wu et al., 2014). In concrete terms chitosan composites provide microtensile strength to ensure better elasticity and flexibility during biodegradation and wet conditions.

### 5.4.3 BIOCOMPATIBILITY

Biocompatibility needs a special attention before developing any form of artificial skin substitute. The incompatibility between native skin and substitute may lead to immunogenic reactions, which could produce acute or chronic inflammatory responses that may worsen the existing condition of the wound. Many results have been reported signifying the biocompatibility of chitosan and chitosan-based composites with human skin, fibroblast cells (L929 and HFFF2 cells), and human embryonic stem cells (Luangbudnark et al., 2012; Ebnesajjad, 2012; Han et al., 2014a; Casimiro et al., 2017). Mainly the cytocompatibility of chitosan is demonstrated by MTT (3-(4,5-dimethylthiazol-2-yl)-2,5-diphenyltetrazolium bromide) or XTT (2,3-Bis-(2-methoxy-4-nitro-5-sulfophenyl)-2H-tetrazolium-5-carboxanilide salt) assay, brine shrimp lethality bioassay method, alamarBlue cell viability assay, and acridine orange/ethidium bromide assay. Studies have strongly recommended that chitosan and chitosan composites (chitosan/collagen, chitosan/gelatin, and chitosan cellulose) as skin substitutes supports cell viability, cell proliferation, revascularization, and reepithelialization.

---

## 5.5 WOUND HEALING MODELS STUDIED FOR CHITOSAN COMPOSITES

Current perspectives to understand the complex biological processes of wound healing and evaluate the effectiveness of artificial skin are based on various in vivo models. Specifically to identify important key mechanisms and validate new engineered strategies for clinical treatment. A general overview of wound healing processes using artificial skin is illustrated in Fig. 5.1. *Wound* is defined as a physical damage in which skin is peeled off at a certain level or broken. Wounds are mainly classified by two categories:

1. Wound thickness: Superficial (involves epidermis and upper dermis), partial (involves skin loss up to lower dermis), full thickness (involves skin loss up to subcutaneous tissue) and deep complex wounds (involves damage up to body cavity).
2. Wound age: Fresh (physical trauma) and chronic (due to ulcers, diabetes, or bacterial and fungal infections).

Further wound healing involves mainly three stages: (1) initial inflammation, which involves inflammatory responses, that is, secretion of macrophages, cytokines, and histamines that remove infection and activate the tissue regeneration cascade; (2) proliferation, which involves migration of keratinocytes, development of granular tissue, and wound closure; and (3) maturation, where collagen fibers are strengthened and revascularization takes place. Lastly formation of appendages and nerve tissue regeneration occur as they grow at a slow rate. Recently much development has been seen in numerous wound healing models to decipher the potential of currently designed new therapies and understanding the detailed mechanism of tissue regeneration for future research. Moreover to reflect various wound healing complications specifically in chronic wounds such as bacterial infections, ulcerations, dehiscence, and ischemia. A detailed description of various types of wound models for clinical experimentation is given in literature (Davis, 2008; Davidson, 2001; Perez and Davis, 2008). New developments in chitosan composites have been studied in numerous *in vitro* and *in vivo* models and have established the potential clinical significance at various stages of wound healing.

### 5.5.1 IN VIVO MODELS

The *in vivo* model widely advanced the understanding of wound healing mechanisms as it involves daily photographic analysis to profile wound closure and histopathological analysis to understand macroscopic changes during healing. Moreover transgenic models provide information about the role of specific genes in tissue repair unlike in *in vitro* models. However *in vitro* culturing of human keratinocytes and *ex vivo* study of wound healing face controversy due to ethical issues (Shevchenko et al., 2010). The *in vivo* wound healing models studied with chitosan composites as artificial skin are described in further subsections.

#### 5.5.1.1 Full thickness wound model

Surgical incision and excision are made at the dorsal trunk skin of rats or rabbits to cause a full thickness wound and skin loss. The full thickness wound can be defined as damage to the skin up to subcutaneous tissue level (loss of epidermis and dermis) or beyond (exposing muscle, bones, tendons, etc.). In this model normal healing of wounds can be described as initial fibrin clot formation at margins and at the base of the wound, and further the invasion of granular tissues into and migration of epithelial tongue.

Chitosan composite with gelatin has been studied using full thickness wound model on New Zealand rabbits. A surgical excision was done to remove skin of around 2.5 cm depth. Skin has layered architecture and this model helps to view the macroscopic changes that occur on tissue repair. On histological examination, edema and exudates were evident till the third day. On the seventh day growth of dermis and epidermis with vascularization was observed. On day 15, a complete reepithelialization was observed with presence of significant blood capillaries and organized collagen fibers similar to that of normal tissue (Lu et al., 2016). Similarly full thickness model on irradiated skin at high dose (10 Gy) to impair normal wound healing was studied on irradiated rats to assess wound healing property of chitosan as biomaterial in impaired wounds. Skin was removed using a sterile blade of size 10 and creating a full thickness wound of dimension  $1 \times 1 \text{ cm}^2$  on the dorsal side in postradiated skin of rats using source skin distance technique. The irradiation was done to mimic the wound healing conditions as in pressure ulcers (stages II–IV) or dermal ulcers with full thickness wound. Investigators suggested that chitosan dermal and skin substitute contributes to complete wound healing with minimum scar appearance when compared with DuodermCGF (Mohd Hilmi et al., 2013).

#### **5.5.1.2 Split thickness model**

Split thickness model is usually practiced to study the rate of reepithelialization where a substantial surface of dermis is removed such that the epidermal appendages remain intact. Usually skin is removed at depth of around 100–1500  $\mu\text{m}$  using device dermatome or electrically. This wound model does not suit well in specimens with dense hair growth like in rats or rabbits. Therefore hairless strains are preferred to understand the rate of reepithelialization such as pig. These features prove this model to be useful for evaluating surface agents, growth factors, wound dressings, and topical applications that accelerate reepithelialization. In a clinical study of 17 human patients (13 males and 4 females) a prototype of carboxymethylchitosan was examined for hemostatic activity using split thickness model. The hemostatic potential of chitosan derivative was compared with two marketed formulations (SPONGOSTAN and Algisite-M) for the treatment of wound size 1.5 inch  $\times$  0.1 mm (width  $\times$  depth) at donor sites using split thickness. It was observed that chitosan-based prototype showed maximum absorption of blood as compared with marketed formulations. This is attributed to its porous structure and chemical nature of carboxymethylchitosan. Also evidently reported with wound image analysis chitosan prototype accelerates the clotting cascade and faster recovery. The possible explanation suggested for this is interaction between carboxyl groups of carboxymethylchitosan and clotting factors that promote tissue recovery and prevents blood loss (Janvikul et al., 2013).

---

## 5.6 CHALLENGES

In spite of the recent advancement and results reported for the chitosan as an effective dermis/epidermal substitute there are certain limitations that have to be addressed for relevant clinical applications in tissue engineering. Following are some of the important challenges that have to be confronted for the development of ideal skin substitute so as to provide a guiding template for precise and automated manner of tissue regeneration:

- Currently commercially as well as reported innovations available for skin substitutes are unable to promote hair growth and hair glands on recovered skin. This requires a great understanding with appropriate knowledge of skin anatomy and physiological condition.
- Great emphasis is required to develop a skin substitute that promotes vascularization along with wound closure and high quality skin replacement.
- Chitosan is derived from chitin, which is further obtained from a variety of sources like crustaceans, mollusks, insects, etc. Therefore due to variable sources there are irregularities in the characteristic properties of chitosan, which ultimately reduces the batch reproducibility and hinders the industrial viability for manufacturing of chitosan-based skin substitutes.
- Chitosan is brittle in nature and hence requires forming a composite or blending with other suitable polymers in an optimized composition to get the desired structural and functional activity for an ideal skin substitute. This optimization of desired physicochemical characterization requires good amount scientific information as it varies from polymer to polymer combining with chitosan and various forms like film/membrane, fibrous mats, 3D scaffolds, and extracellular matrix systems.
- Variation in *N*-acetyl-D-glucosamine units due to variable source of chitin results in irregular degree of deacetylation from batch to batch, which makes it cumbersome for the industry to yield chitosan with uniform characteristics.
- Molecular weight of chitosan has also to be considered with prime importance as it further signifies the physicochemical behavior of the polymer and interaction with other polymers.
- Although several reports exist that suggest that chitosan promotes cell adherence, cell proliferation, and migration of cells, chitosan composite as bioresorbable material for wound healing applications must have the property to stimulate the coagulation cascade to prevent excessive loss of blood during severe burns, deep cuts, or removal of complete layer of skin. This could be achieved by enhancing the tissue–polymer interaction and incorporating inflammatory cytokines that produce continuous inflammatory stimulus and contribute to activation of coagulation cascade. The problem associated with



this idea is that cytokines are sensitive proteins that may get denatured on storage or due to protein–polymer incompatibility.

- On the basis of currently available information about chitosan, chitosan composites, as well as other polymeric skin substitutes, there is no developed biomaterial available that provides tactile sensation to the recovered skin. This holds a great responsibility on skin substitutes in case of high-degree damage to the skin where patients lose their sense of touch perception even after total wound healing and skin replacement.

---

## 5.7 FUTURE PERSPECTIVES

Chitosan has always been the polymer of choice for wound dressings or artificial skin with certain modifications in hydrophilicity, solubility, and mechanical properties. These modifications are generally achieved in the form of blends, composites with other suitable polymers, and derivatives with chemical modifications. Moreover advances in chemical modification of the chitosan polymer and biomanufacturing processes including addition of drugs, growth factors, and native cells/DNA have emerged as a potential bioresorbable skin substitute for tissue regeneration. Chitosan is preferred mostly in biomedical applications particularly in tissue engineering due to its unique properties. For instance chitosan has antibacterial property because of its positively charged structure, which interacts with negatively charged cell membrane of bacteria and stops its growth. Moreover the wide acceptance of this polymer in the domain of tissue engineering is due to its biocompatibility and biodegradability. As a consequence in view of wound healing many results have been discussed, suggesting the scar free recovery in various wound models including full thickness removal of skin tissue and sustaining cell viability. The mechanical properties of chitosan from the perspective of tensile strength, flexibility, and elongation at break have been widely reported suggesting the importance in providing the stable structural integrity during the neotissue development. The porosity and swelling behavior of chitosan have also been highlighted and reported to have important role in skin tissue regeneration as it has a vital role in migration of cells like keratinocytes, nutrients, and growth factors and provides a natural microenvironment for cell growth. Chitosan is also reported to have adhesive properties that support cell adhesion and aid in wound closure, which prevents excessive blood loss due to deep cut or third degree burns. All these intrinsic properties of chitosan mentioned hitherto can also be tailored by forming composites or blends with other suitable polymers as desired for various forms like matrix, micro/nanofibrous mats, sponges, film or membranes, etc. to emulate the native skin extracellular milieu.

## REFERENCES

- Ahmed, S., Ikram, S., 2016. Chitosan based scaffolds and their applications in wound healing. *Achieve. Life Sci.* 10, 27–37.
- Anisha, B.S., Sankar, D., Mohandas, A., Chennazhi, K.P., Nair, S.V., Jayakumar, R., 2013. Chitosan–hyaluronan/nano chondroitin sulfate ternary composite sponges for medical use. *Carbohydr. Polym.* 92, 1470–1476.
- Antunes, B.P., Moreira, A.F., Gaspar, V.M., Correia, I.J., 2015. Chitosan/arginine–chitosan polymer blends for assembly of nanofibrous membranes for wound regeneration. *Carbohydr. Polym.* 130, 104–112.
- Casimiro, M.H., Lancastre, J.J., Rodrigues, A.P., Gomes, S.R., Rodrigues, G., Ferreira, L. M., 2017. Chitosan-based matrices prepared by gamma irradiation for tissue regeneration: structural properties vs. preparation method. *Top. Curr. Chem. (J.)* 375, 5.
- Chen, H., Xing, X., Tan, H., Jia, Y., Zhou, T., Chen, Y., et al., 2017. Covalently antibacterial alginate–chitosan hydrogel dressing integrated gelatin microspheres containing tetracycline hydrochloride for wound healing. *Mater. Sci. Eng. C Mater. Biol. Appl.* 70, 287–295.
- Croisier, F., Jerome, C., 2013. Chitosan-based biomaterials for tissue engineering. *Eur. Polym. J.* 49, 780–792.
- Davidson, J.M., 2001. Experimental animal wound models. *Wounds Compend. Clin. Res. Practice* 13, 9–23.
- Davis, S., 2008. Animal models of wound healing. *Wounds Compend. Clin. Res. Practice* 20, 1–2.
- Debels, H., Hamdi, M., Abberton, K., Morrison, W., 2015. Dermal matrices and bioengineered skin substitutes: a critical review of current options. *Plast. Reconstr. Surg. Glob. Open* 3, e284.
- Denkbaz, E.B., Ozturk, E., Ozdemir, N., Kececi, K., Agalar, C., 2004. Norfloxacin-loaded chitosan sponges as wound dressing material. *J. Biomater. Appl.* 18, 291–303.
- Derler, S., Gerhardt, L.C., 2012. Tribology of skin: review and analysis of experimental results for the friction coefficient of human skin. *Tribol. Lett.* 45, 1–27.
- Dhandayuthapani, B., Krishnan, U.M., Sethuraman, S., 2010. Fabrication and characterization of chitosan–gelatin blend nanofibers for skin tissue engineering. *J. Biomed. Mater. Res. B Appl. Biomater.* 94, 264–272.
- Dreno, B., 2009. Anatomy and physiology of skin and cutaneous annexes. *Ann. Dermatol. Venereol.* 136 (Suppl. 6), S247–S251.
- Ebnesajjad, S., 2012. *Handbook of Biopolymers and Biodegradable Plastics: Properties, Processing and Applications*. Elsevier/William Andrew.
- Han, C.M., Zhang, L.P., Sun, J.Z., Shi, H.F., Zhou, J., Gao, C.Y., 2010. Application of collagen–chitosan/fibrin glue asymmetric scaffolds in skin tissue engineering. *J. Zhejiang Univ. Sci. B* 11, 524–530.
- Han, F., Dong, Y., Su, Z., Yin, R., Song, A., Li, S., 2014a. Preparation, characteristics and assessment of a novel gelatin–chitosan sponge scaffold as skin tissue engineering material. *Int. J. Pharm.* 476, 124–133.
- Han, F., Dong, Y., Su, Z., Yin, R., Song, A.H., Li, S.M., 2014b. Preparation, characteristics and assessment of a novel gelatin–chitosan sponge scaffold as skin tissue engineering material. *Int. J. Pharm.* 476, 124–133.

- Hoare, T.R., Kohane, D.S., 2008. Hydrogels in drug delivery: progress and challenges. *Polymer* 49, 1993–2007.
- Huang, Y., Onyeri, S., Siewe, M., Moshfeghian, A., Madihally, S.V., 2005. In vitro characterization of chitosan–gelatin scaffolds for tissue engineering. *Biomaterials* 26, 7616–7627.
- Huang, J.H., Hu, X.Y., Lu, L., Ye, Z., Zhang, Q.Y., Luo, Z.J., 2010. Electrical regulation of Schwann cells using conductive polypyrrole/chitosan polymers. *J. Biomed. Mater. Res. Part A* 93A, 164–174.
- Jafari, J., Emami, S.H., Samadikuchaksaraei, A., Bahar, M.A., Gorjipour, F., 2011. Electrospun chitosan–gelatin nanofibrous scaffold: fabrication and in vitro evaluation. *Biomed. Mater. Eng.* 21, 99–112.
- Janvikul, W., Thavornnyutikarn, B., Kosorn, W., Surattanawanich, P., 2013. Clinical study of chitosan-derivative-based hemostat in the treatment of split-thickness donor sites. *Maejo Int. J. Sci. Technol.* 7, 385–395.
- Jayakumar, R., Menon, D., Manzoor, K., Nair, S.V., Tamura, H., 2010a. Biomedical applications of chitin and chitosan based nanomaterials—a short review. *Carbohydr. Polym.* 82, 227–232.
- Jayakumar, R., Prabakaran, M., Nair, S.V., Tamura, H., 2010b. Novel chitin and chitosan nanofibers in biomedical applications. *Biotechnol. Adv.* 28, 142–150.
- Jayakumar, R., Prabakaran, M., Sudheesh kumar, P.T., Nair, S.V., Tamura, H., 2011. Biomaterials based on chitin and chitosan in wound dressing applications. *Biotechnol. Adv.* 29, 322–337.
- Kang, Y.O., Yoon, I.S., Lee, S.Y., Kim, D.D., Lee, S.J., Park, W.H., et al., 2010. Chitosan-coated poly(vinyl alcohol) nanofibers for wound dressings. *J. Biomed. Mater. Res. B Appl. Biomater.* 92, 568–576.
- Kaur, M., Sharma, S., Sinha, V.R., 2017. Polymer based microspheres of aceclofenac as sustained release parenterals for prolonged anti-inflammatory effect. *Mater. Sci. Eng.: C* 72, 492–500.
- Li, Q., Zhou, J., Zhang, L., 2009. Structure and properties of the nanocomposite films of chitosan reinforced with cellulose whiskers. *J. Polym. Sci. Part B Polym. Phys.* 47, 1069–1077.
- Logithkumar, R., Keshavnarayan, A., Dhivya, S., Chawla, A., Saravanan, S., Selvamurugan, N., 2016. A review of chitosan and its derivatives in bone tissue engineering. *Carbohydr. Polym.* 151, 172–188.
- Lu, B., Wang, T., Li, Z., Dai, F., Lv, L., Tang, F., et al., 2016. Healing of skin wounds with a chitosan–gelatin sponge loaded with tannins and platelet-rich plasma. *Int. J. Biol. Macromol.* 82, 884–891.
- Luangbudnark, W., Viyoch, J., Laupattarakasem, W., Surakunprapha, P., Laupattarakasem, P., 2012. Properties and biocompatibility of chitosan and silk fibroin blend films for application in skin tissue engineering. *ScientificWorldJournal* 2012, 697201.
- Mahmoud, A.A., Salama, A.H., 2016. Norfloxacin-loaded collagen/chitosan scaffolds for skin reconstruction: preparation, evaluation and in-vivo wound healing assessment. *Eur. J. Pharm. Sci.* 83, 155–165.
- Mckenzie, I.A., Biernaskie, J., Toma, J.G., Midha, R., Miller, F.D., 2006. Skin-derived precursors generate myelinating Schwann cells for the injured and dysmyelinated nervous system. *J. Neurosci.* 26, 6651–6660.
- Mclafferty, E., Hendry, C., Alistair, F., 2012. The integumentary system: anatomy, physiology and function of skin. *Nurs. Stand.* 27, 35–42.

- Mohd Hilmi, A.B., Halim, A.S., Jaafar, H., Asiah, A.B., Hassan, A., 2013. Chitosan dermal substitute and chitosan skin substitute contribute to accelerated full-thickness wound healing in irradiated rats. *Biomed. Res. Int.* 2013, 795458.
- Oh, D.X., Hwang, D.S., 2013. A biomimetic chitosan composite with improved mechanical properties in wet conditions. *Biotechnol. Prog.* 29, 505–512.
- Parvez, S., Rahman, M.M., Khan, M.A., Khan, M.A.H., Islam, J.M.M., Ahmed, M., et al., 2012. Preparation and characterization of artificial skin using chitosan and gelatin composites for potential biomedical application. *Polym. Bull.* 69, 715–731.
- Perez, R., Davis, S.C., 2008. Relevance of animal models for wound healing. *Wounds* 20, 3–8.
- Rothamel, D., Schwarz, F., Sager, M., Herten, M., Sculean, A., Becker, J., 2005. Biodegradation of differently cross-linked collagen membranes: an experimental study in the rat. *Clin. Oral Implants Res.* 16, 369–378.
- Salati, A., Keshvari, H., Karkhaneh, A., Taranejoo, S., 2011. Design and fabrication of artificial skin: chitosan and gelatin immobilization on silicone by poly acrylic acid graft using a plasma surface modification method. *J. Macromol. Sci. Part B* 50, 1972–1982.
- Sarasam, A., Madhally, S.V., 2005. Characterization of chitosan–polycaprolactone blends for tissue engineering applications. *Biomaterials* 26, 5500–5508.
- Sarkar, S.D., Farrugia, B.L., Dargaville, T.R., Dhara, S., 2013. Chitosan–collagen scaffolds with nano/microfibrous architecture for skin tissue engineering. *J. Biomed. Mater. Res. A* 101, 3482–3492.
- Shahabeddin, L., Berthod, F., Damour, O., Collombel, C., 1990. Characterization of skin reconstructed on a chitosan-cross-linked collagen–glycosaminoglycan matrix. *Skin Pharmacol.* 3, 107–114.
- Sharma, S., Sinha, V.R., 2018. Current pharmaceutical strategies for efficient site specific delivery in inflamed distal intestinal mucosa. *J. Control Release* 272, 97–106.
- Sharma, S., Lohan, S., Murthy, R.S., 2014. Formulation and characterization of intranasal mucoadhesive nanoparticulates and thermo-reversible gel of levodopa for brain delivery. *Drug Dev. Ind. Pharm.* 40, 869–878.
- Shevchenko, R.V., James, S.L., James, S.E., 2010. A review of tissue-engineered skin bioconstructs available for skin reconstruction. *J. R. Soc. Interface* 7, 229–258.
- Shi, G., Rouabhia, M., Meng, S., Zhang, Z., 2008. Electrical stimulation enhances viability of human cutaneous fibroblasts on conductive biodegradable substrates. *J. Biomed. Mater. Res. A* 84, 1026–1037.
- Venkatesan, J., Kim, S.K., 2010. Chitosan composites for bone tissue engineering—an overview. *Mar. Drugs* 8, 2252–2266.
- Wood, M., Willits, R.K., 2006. Short-duration, DC electrical stimulation increases chick embryo DRG neurite outgrowth. *Bioelectromagnetics* 27, 328–331.
- Wu, T., Farnood, R., O'Kelly, K., Chen, B., 2014. Mechanical behavior of transparent nanofibrillar cellulose–chitosan nanocomposite films in dry and wet conditions. *J. Mech. Behav. Biomed. Mater.* 32, 279–286.
- Xie, Z., Paras, C.B., Weng, H., Punnakitakashem, P., Su, L.C., Vu, K., et al., 2013. Dual growth factor releasing multi-functional nanofibers for wound healing. *Acta Biomater.* 9, 9351–9359.
- Zhang, P., Lu, X., Chen, J., Chen, Z., 2014. Schwann cells originating from skin-derived precursors promote peripheral nerve regeneration in rats. *Neural Regen Res.* 9, 1696–1702.

# Resorbable polymer fiber reinforced composites in biomedical application

Paramjot Maman<sup>1</sup>, Manju Nagpal<sup>1</sup> and Geeta Aggarwal<sup>2</sup>

<sup>1</sup>Chitkara College of Pharmacy, Chitkara University, Patiala, India <sup>2</sup>Delhi Pharmaceutical Sciences and Research University, Government of NCT of Delhi, New Delhi, India

## 6.1 INTRODUCTION

Composites are the materials that are made from the combination of two or more separate materials having different chemical and physical properties, such that their combination produces a material having characteristics different from the individual components (Maghaireh et al., 2017). The properties of matter are significantly affected by its dimensions. Nanosized materials in the 21st century represent a highly promising field because of their novel properties and controlled structures (Jog and Burgess, 2017). A variety of composite systems like 1D (Stojanovic et al., 2016), 2D (Yan et al., 2017), 3D (Wang et al., 2017a), amorphous materials at micro- and nanoscale have been prepared and been used to get promising results. The classification of composites and types of materials for their preparation is shown in Fig. 6.1. The individual properties of the elements (two or more than two) from which composites are made up and their combination effects need to be recognized first, to understand the applications and actual use of composites prepared (Liu et al., 2017). Usually, a composite consists of bulk material, called matrix, and a small mass of another material mainly used for strengthening, increasing the power, potency, and stiffness of the bulk material. This strengthening is mainly in fiber form. Such composites are also known as polymer matrix composites and fiber reinforced polymers (Qi et al., 2015). Such composites contain resins that act as polymeric matrix materials and different varieties of fibers like carbon, silk, glass, aramid, etc. for reinforcing matrix properties.

In composites resin systems are combined with fibers like glass (Zhang et al., 2016a), carbon (Gholizadeh et al., 2017), and aramid (Patterson and Sodano, 2016) whose main function is to reinforce the resin system properties. The resin matrix, on application of stress, spreads the load to each of the individual fibers, which further protects the fibers from abrasion and impact related damage. Better molding power into different shapes, high strength, better stiffness, high

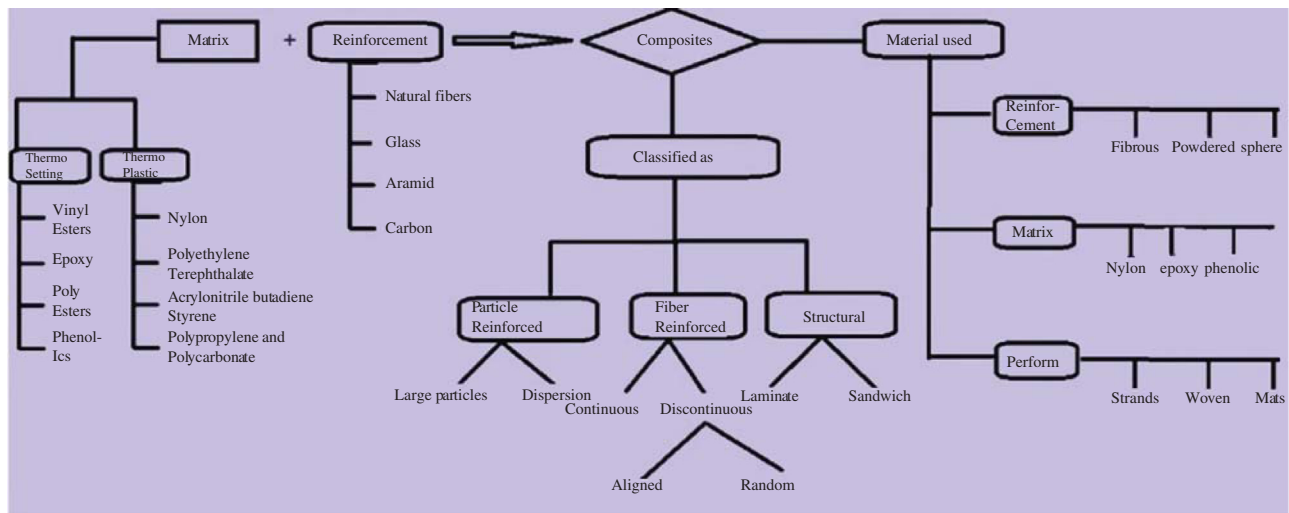


**FIGURE 6.1**

Classification of composites and types of materials for preparation.

resistance against environmental damages, and some other benefits create the resultant composite better than the metals (Iliut et al., 2016).

The composite's properties are mainly affected by:

- properties of the fiber,
- orientation of the fibers in the composite (Hu et al., 2016),
- ratio of fiber to resin used in preparation of composite (fiber volume fraction) (Guner and Dericioglu 2016),
- geometry of the fibers in the composite (Wada 2016), and
- properties of the resin.

---

## 6.2 BIOCOMPOSITES

Biomedical composites or biocomposites are terms used for blending of natural fibers (which can be wood fibers like hard wood or soft wood, can be nonwood fibers like sugar cane, jute, flax, banana, pineapple, rice straw, hemp, sisal, oil palm) with biodegradable polymers (can be obtained from either renewable or nonrenewable resources) (Nouri et al., 2015). The term *biocomposites* can also be used for those composite materials in which at least one constituent ought to be biodegradable or biobased. Biocomposites in which both the components are of bioorigin and biodegradable are known as green composites (Saravanan et al., 2016).

After more than 45 years of success of implants, the claim of using different devices based on resorbable polymers is increasing day by day in the pharmaceutical and medical fields. As a result, with time a new generation of resorbable polymeric composites has been discovered that could be a better alternative to nonresorbable polymeric composites and can be used to replace various types of metal based implants (Barth et al., 2016). The most important benefit of using implants manufactured from resorbable polymers is their ability to perform the same function in body as that of tissue (temporary functioning), which is not possible in implants manufactured from metallic or nonresorbable materials. The strength of resorbable implant should be high to function appropriately in between healing time. That is why the integrity of such implants combined with the reinforcing fibers allow the tissue to serve its usual function along with better healing time. Such resorbable polymers lead to controlled drug release from implants by diffusion and also help in achieving better mechanical strength required to do its appropriate function (Del Campo et al., 2016). Some examples of fibers obtained from natural sources are shown in Fig. 6.2.

After 1966, a lot of research work was published on engineered composites that were found to be helpful in treating bone fractures, hip joint fractures, dentistry, etc. Some engineered composites having biomedical applications include:

1. metal matrix composites (Del Campo et al., 2016),
2. polymer matrix composites (Rodrigues et al., 2017),

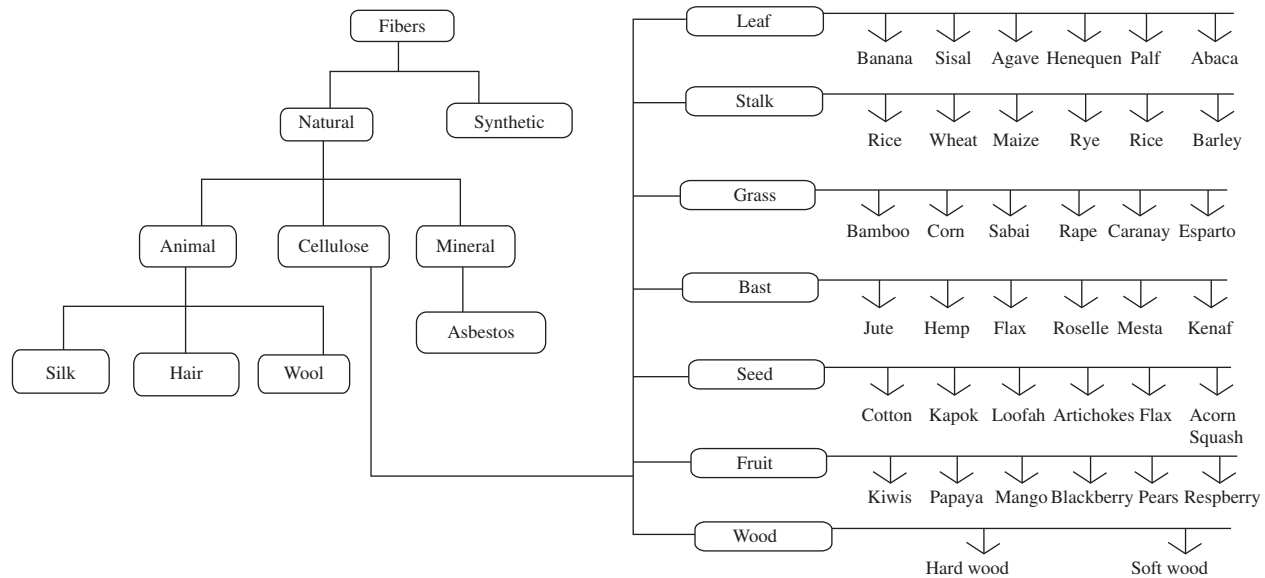


**FIGURE 6.2**

Classification of fibers obtained from natural sources.



3. reinforced plastic composites,
4. ceramic matrix composites (Zhang et al., 2016a,b), and
5. composites containing building materials such as concrete and cement.

Chemical cleavage of polymer's backbone occurs after its implantation, which results in immediate decrease in length of polymeric chain. When the polymeric chain achieves a specific chain length (which depends upon the polymer's nature and its use) or goes down it, then the integrity of implant decreases rapidly. This time point is known as the strength retention period (Ayala et al., 2015). After this, the mass of the implant starts decreasing after reduction in chain length of polymer.

Factors that affects the rate of degradation of polymeric chain are (1) polymer chain length, (2) hydrophilicity, and (3) crystallinity.

Mechanical properties of these composites can be easily altered by optimization of resorbable polymer concentration, reinforcement element, ratio to be used, method of preparation, nature of resorbable polymer, etc. Suitable mechanical strength can be achieved depending upon these parameters. Some of the properties of resorbable polymers are shown in Table 6.1.

Fibers obtained from natural sources can also be used for preparation of composites. Some examples of natural polymers obtained from plants (Karimi et al., 2016; Barari et al., 2016; Idrovo Encalada et al., 2016) and animals (Yi et al., 2016; Shao et al., 2016; Lazar et al., 2016) that can be used for preparation of composites and their mechanical strengths are shown in Table 6.2.

---

## 6.3 BIOCOMPOSITES PREPARED BY USING RESORBABLE POLYMERIC FIBERS

There are various polymeric fibers that possess resorbable property and can be used to prepare biocomposites.

### 6.3.1 POLYLACTIDE

Poly(lactic acid) (PLA), also known as polylactide, is one of most important biodegradable polyesters. Recently, this polymer has been widely used in various medical fields like orthopedic devices (Chen et al., 2016), wound management (Suh et al., 2014), drug delivery (Chen et al., 2014), tissue engineering (Lih et al., 2016), etc. Polylactide polymer was synthesized by using lactic acid monomers. These monomers can be prepared by using two methods as shown in Fig. 6.3. These lactic acid monomers can be polymerized by using different methods, for example, polycondensation, azeotropic dehydration reactions, ring opening polymerization, etc. (Salerno et al., 2016). This results in synthesis of PLA from lactic acid monomers. Some physical and mechanical properties of polylactide are shown in Table 6.3.

**Table 6.1** Properties of Some Resorbable Polymers

S. No.	Polymer	Grade	Glass Transition Temperature (°C)	Specific Melting Point (°C)	Young's Modulus of Elasticity	Degradation Time (in Months)
1	ε-Caprolactone	12	−60	55–65	0.2–0.4	>24
2	Poly (DL-lactic-co-glycolic acid)	5010	50	—	3.1–3.9	1–2
3	Poly D-lactide	20	55	—	3.2–3.7	12–15
4	Polyglycolide	20	40	215–225	6.5–7.0	6–13
5	Poly lactide	38	60	180–190	3.2–3.7	>24

**Table 6.2** Mechanical Properties of Natural Polymers Used for Preparation of Composites

S. No.	Fibers	Young's Modulus of Elasticity (GPa)	Tensile Strength (MPa)	Percentage of Elongation Required for Breakage (%)
<b>Fibers Obtained From Human Tissues</b>				
1	Skin	4–9	7.5–8.0	75–80
2	Heart valves	—	0.5–2.5	10–15.3
3	Elastic cartilage	—	2–5	25–33
4	Hard tissue obtained from bone	15–22	120–165	1–5
5	Tendon	1–5	55–160	8–15
6	Hard tissue obtained from tooth	15–20	120–160	1–5
7	Aorta	—	0.05–1.1	75–82
8	Fibrocartilage	159.1 MPa	10.4	20–35
9	Ligament	303.0 MPa	29.5	—
10	Intraocular lens	5.6 MPa	2.6	—
11	Arterial tissue (longitudinal section)	—	0.1	—
12	Arterial tissue (transverse section)	—	1.1	—
13	Articular cartilage	10.5 MPa	27.5	—
<b>Fibers Obtained From Plants</b>				
1	Hemp	30–75	310–900	1.5–6
2	Banana	25–30	530–920	2–5
3	Pineapple	65–85	170–1700	2–4
4	Wool	2–5	120–175	20–40
5	Flax	25–80	300–1600	2–10
6	Cotton	5–15	250–810	3–10
7	Jute	10–65	200–900	2–8
8	Ramie	45–130	350–950	2–8
9	Kenaf	2–3	300–1200	3–5
10	Sisal	9–22	150–280	20–30

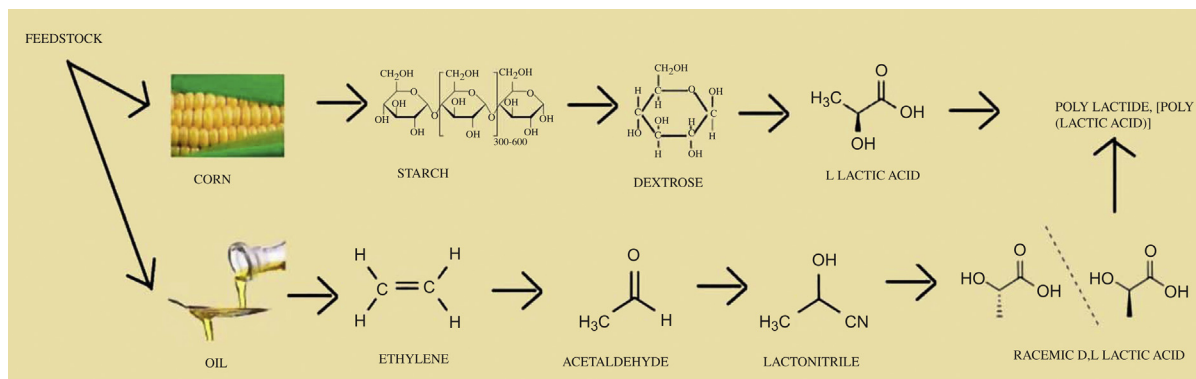


**FIGURE 6.3**

Preparation of polylactide polymer.

**Table 6.3** Physical/Mechanical Properties of Polylactic Acid

S. No.	Physical/Mechanical Properties	Values	Units
1	Specific gravity	1.24	Unitless
2	Tensile strength at break	53	MPa
3	Tensile modulus	3.5	GPa
4	Notched izod impact	16	J/m
5	Tensile yield strength	60	MPa

#### 6.3.1.1 Biodegradation of polylactic acid

Biodegradation and photodegradation of PLA composites in which starch is used as reinforced material have been studied by [Copinet et al. \(2003\)](#) and composites containing PLA/starch/PLA films were designed. After exposure to UV light at 315 nm, the decrease in molecular weight and glass transition temperature of the polymers and separation of starch and PLA films was observed. The percentage of degradation was found to be 92.4%–93.4% in its liquid medium. However, degradation percentage was less in inert medium, which was found to be 80%–83%. Some additives can be added to reduce this degradation of composites. Improvement in mechanical properties of PLA/starch composites can be done by using peroxides and anhydrides in their catalytic amounts. However, environmental conditions like temperature, pH, humidity, production, storage, transportation, etc. also affect the biodegradation of PLA composites.

Body enzymes like trypsin and elastase also contribute in degradation of PLA. Such body microbes and enzymes act on PLA polymer and biodegrade it into proteinous materials. The PLA composites' degradation can be increased by adding nanoclays, which enhance its biodegradation by enzymes because of their affinity towards the clays ([Salerno et al., 2016](#); [Jain et al., 2016](#)).

#### 6.3.1.2 Medical applications of polylactic acid composites

##### Tissue engineering

Tissue engineering is a multidisciplinary field aimed at finding solutions for dangerous medical conditions like organ failure and loss of tissue. PLA and its copolymers, and their composites with natural fibers as reinforcing elements, are widely used in tissue engineering. PLA is a polyester polymer and it dissolves in the body by simple hydrolysis of its ester backbone, which results in production of degradation products that are nontoxic and not harmful to the body. Moreover, it is a biocompatible polymer. All these features make it a better candidate for medical applications ([Zhou et al., 2016](#)). However, PLA has very poor mechanical properties, which are required for application in medical applications. Hence, to get better results, PLA mechanical properties need to be modified, which can be done by using three methods: (1) by blending of polymer ([Zhong et al., 2012](#)), (2) by combining the polymer with reinforcing materials resulting in composites formation, or (3) by copolymerization method ([Salimi et al., 2014](#)).

Composites of PLA were prepared by combining with octadecylamine as reinforcing material in nanoforms. They were prepared by dissolving PLA in chloroform in a beaker and dispersing octadecylamine nanodiamonds in chloroform in a separate beaker. After this both chloroform containing solutions were mixed in single beaker and chloroform evaporated by rota evaporator leaving a layer of PLA/octadecylamine composites. It was seen that the prepared composites exhibited better mechanical properties like better Young's modulus and better hardness as compared with native PLA, when around 10% of octadecylamine was added in the PLA polymer. This enhancement in mechanical properties occurs because of excellent affinity between the PLA and octadecylamine (Stloukal et al., 2015). The toxicity and biocompatibility studies showed no significant change as compared with PLA, making it better for use in tissue engineering as compared with native PLA.

Bone morphogenetic proteins (BMPs) are biological active molecules that have capability to produce new bones. They can be combined with biomaterials and can be used clinically. PLA and BMP composites were clinically used to treat demineralized bone. PLA polymer having low molecular weight is mixed with BMP to produce composite using BMP as reinforcing material. When this PLA-BMP composite is implanted on the host bone, then with the biodegradation of composite (PLA matrix), new bone cells produced. The results proved it a promising candidate for treating bone disorders (Eğri and Eczacıoğlu, 2017). A scaffold was also prepared using PLA and BMP composites, which on insertion proved that the prepared scaffold can induce bone formation within 2 weeks without any toxic effects.

### Wound management

PLA in combination with its copolymers has recently been widely used in wound management in the form of surgical sutures, preventing postoperative adhesion and healing dental extraction wounds, etc. Polymeric blends of PLA were successfully prepared to treat postoperative adhesions. In this study, PLA polymer was blended with the polytrimethylene carbonate polymer in a solution in which both the polymers were mixed in optimized ratio and dissolved in presence of acetoacetate salt. After this, the excess of solvent was removed after pouring the polymeric solution on Teflon plate to obtain a thin layer of composites. The thin layer was collected and tested for its mechanical and thermal properties. The results showed that the mechanical properties such as Young's modulus, tensile strength, and glass transition temperature of prepared blends was lower as compared with pure PLA, however the flexibility of prepared blends was higher as compared with pure PLA (Saini et al., 2016). This increase in flexibility and decrease in mechanical properties make the PLA blends more suitable to freely cover the whole wound, which was not possible in case of pure PLA. The toxicity studies proved the PLA blends to be nontoxic to human skin. PLA surgical dressing (Boonkong et al., 2013) materials were also used to reduce the chances of wound formation during mandibular third molar extraction making it a

suitable candidate to treat dental wound healing. PLA containing stents were also successfully prepared to treat ureteral war injuries (Al-Azzawi and Koraitim 2014; Williams and Jezior 2013). These PLA stents after application on injuries degrade slowly and get removed from the body easily without any toxic effects.

#### Drug delivery system

A large number of biodegradable polymers, because of their better encapsulation, biocompatibility, biodegradability, and low toxicity properties, were widely used in drug delivery systems to deliver the drug from days to weeks to months to even years. The examples of these polymers are PLA, gelatin, polycaprolactone, etc. (Hami et al., 2017). Polymeric degradation occurs mainly by three ways, namely erosion, swelling, and diffusion. Polylactic acid is a polyester polymer having ester backbone. Such polymers are mainly degraded by hydrolysis in presence of water. Their degradation mainly starts after penetration of the water into the polymeric device. After this, hydrolysis of polymer starts, which leads to breakage of ester bonds randomly by hydrolytic ester cleavage further resulting in complete degradation of polymeric device. This erosion can be bulk or surface erosion as shown in Fig. 6.4 depending upon the type of polymer and polymeric device used.

PLA polymer is widely used in encapsulation of large number of molecules such as drugs like antipsychotic drugs, oridonins, dermatotherapy, hormones, proteins etc. to achieve controlled release of active moiety. For example, Paclitaxel drug is loaded in polylactic-co-glycolic acid polymer and final formulation is converted in nanoform using solvent-evaporation method. The results showed better loading efficiency and better encapsulation efficiency. A sustained release of drug from the nanoparticles was also obtained.

PLA and PLGA (poly (lactic-co-glycolic acid)) composite nanoparticles were also prepared by solvent-evaporation method to deliver human growth hormone

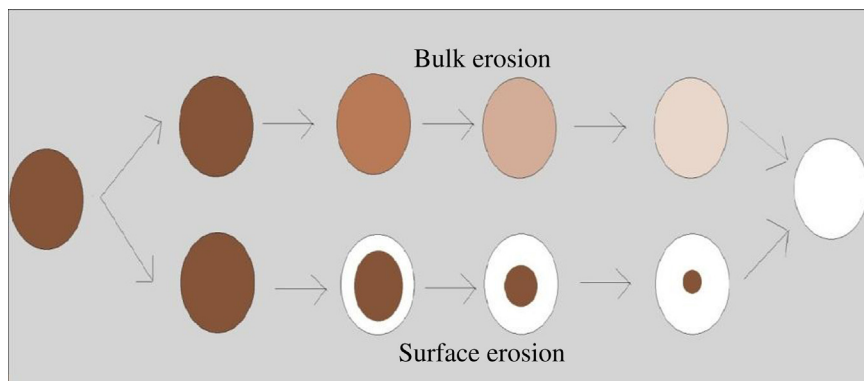


**FIGURE 6.4**

Comparison of bulk and surface erosion of PLA by hydrolytic cleavage.

in controlled release (Kim and Park 2004). The final formulated nanoformulation showed better morphology with good stability of encapsulated protein. The formulation also showed high encapsulation efficiency of protein. Because of better encapsulation and better controlled release of hormone with high stability, the prepared nanoparticles proved promising candidates for delivering human growth hormone.

Microparticles of 17- $\beta$ -estradiol valerate were prepared by solvent-evaporation method using PLA to achieve sustained release of active moiety. The encapsulation efficiency of final prepared microparticles was found to be more than 80%. In vitro release of hormone from the microparticles was also found to be sustained. In vivo study was also conducted to check the degradation of microparticles. The final microparticles showed better efficiency yield and morphological characteristics making them a promising candidate for achieving controlled and sustained release of 17- $\beta$ -estradiol (Hong et al., 2011).

### Orthopedic system

These days, use of biodegradable polymers for orthopedic devices has gained huge popularity as compared with nonbiodegradable polymers. Before their discovery titanium devices were used for this purpose. But after a few days of application, a second surgery procedure was required to remove the titanium from the body. To avoid this step, biodegradable polymers have been incorporated and in a single application, these get completely degraded within the body such that there is no need for a second surgery. Usually, PLA polymer has been mainly used to produce biodegradable pins, plates, sutures, screws, etc. during surgery. These are widely used in surgeries where mechanical strength and rigidity are not required. But for those surgeries where hardness is required, the PLA composites have been used in which their function is modified by using reinforcing material (Zhou et al., 2012). To impact strength and mechanical stiffness, PLA biodegradable polymers were also given in combination with metals whose amount is modified within limits for use in fractures. These proved beneficial during the surgery of various orthopedic areas like foot, shoulders, hand, elbow, wrist, ankle, pelvis, knee fractures, zygomatic fractures, etc.

It has been seen that mechanical properties of PLA can be modified by using both D and L form of PLA in a ratio of 15:85. The resultant composites of PLA showed increased mechanical properties and were used in manufacturing of plates and screws for fixation of fracture. The results proved that the PLA composites can be used for fracture fixation without need of any additional support. Some hydrophobic polymers like poly (orthoesters) can be biodegraded by surface erosion. To achieve better degradation rates, lactide groups can be added with these polymers. With addition of lactide groups in orthoesters, carboxylic acids being released during hydrolysis which enhance the degradation of orthoesters. In vivo studies showed that scaffold obtained from poly (orthoesters) were able to maintain their structural integrity for about 6–12 weeks after applying for bone tissue



engineering. Whereas, scaffolds obtained from PLGA were able to maintain their structural integrity for 4–6 weeks (Asti and Gioglio, 2014).

### **6.3.1.3 Polylactide based microcomposites using different reinforcing materials**

Microcomposites of poly (L-lactide) and clay as a reinforcing material were successfully prepared to deliver antineoplastic drug, 6-mercaptopurine, for reduction of its cell toxicity and improving its in vitro drug release. The drug-loaded microcomposite spheres were prepared by using ion exchange method. The final prepared polylactide composites showed controlled drug release because of partial diffusion of loaded drug through the clay's swollen matrix. The final formulation showed less dose related cytotoxicity as compared with native drug suggesting it a promising candidate for controlled release of antineoplastic drugs (Iqbal et al., 2015).

Microcomposites of poly (L-lactic acid) reinforced by materials like absorbable calcium phosphate, nonabsorbable carbon, fibers like chitin, poly (glycolic acid) were prepared for fixing bone fracture. The microcomposites prepared by chitin and poly (glycolic acid) showed lower Young's modulus and high ductility as compared with microcomposites prepared by using calcium phosphate. Chitin fibers in composites retained about 87% of tensile strength and about 130% of Young's modulus even after 25 days. During in vitro hydrolysis test, the fiber matrix interfacial shear strength for different prepared microcomposites was checked, which was found to be 49% after 15 days for PLA and nonabsorbable carbon microcomposites, and 46% after 6 days for absorbable calcium PLA microcomposites. For fibers it was found to be 28.3 MPa for chitin PLA microcomposites. The final results showed that poly (glycolic acid) and chitin fibers based microcomposites had better mechanical properties and can be used for bone fractures, but are unable to provide stiffness equal to bone plates (Slivka et al., 1997).

Microcomposites of PLA and talc were prepared by using melt mixing method. The prepared microcomposites showed improved mechanical and thermal properties as compared with native PLA. This is because of the better stiffness, toughening, and strengthening nature of talc. However, when these microcomposites were investigated for their stability by applying ultraviolet irradiation and humidity as per ISO 4892-3 for 100, 200, and 300 hours, the molecular weight and mechanical properties got drastically reduced because of degradation of microcomposites by photolysis and hydrolysis (Battezzore et al., 2011).

Microcomposites of PLA and cellulose were prepared by blending the PLA polymer with cellulose fiber materials to modify the mechanical properties of the native PLA. The final results showed that the microcomposites prepared from high molecular weight PLA showed better mechanical properties as compared with microcomposites, which are prepared by polymerization of lactide group with cellulosic fibers. The Young's modulus of microcomposites containing 25% of fibers got improved by 53% as compared with native PLA. Further increase in the fiber content up to 35% led to the reduction of Young's modulus (Birgit et al., 2006).

Microcomposites and nanocomposites of PLA combined with clay as reinforcing element were prepared by using melt-blending method in which about 3% weight of sodium montmorillonite (Kaewprapan and Phattanasudee, 2012) was loaded. Both polymers, that is, PLA and clay, showed excellent affinity and bonding power with each other as proved by X-ray diffraction (XRD) studies. The thermogravimetric analysis (TGA) showed that the nanocomposites showed better thermal stability and reduced flammability as compared with the microcomposites in air (Lu et al., 2015).

#### ***6.3.1.4 Polylactide based nanocomposites using different reinforcing materials***

Polymeric nanocomposites are the composites with materials with at least one constituent phase having dimensions in the nanoscale range, that is, less than 100 nm. The nanocomposites with nanoscale fillers showed better optical, mechanical, thermal, magnetic, and electrical properties. Depending upon the size and shapes of nanofillers they can be further divided into 1D, 2D, and 3D nanofillers. Single dimensional nanofillers have plate-like shapes, for example, silicates, graphene sheets, smectic clays, etc. 2D nanofillers have diameter below 100 nm and examples include carbon nanotubes, nanosized cellulose, etc. 3D nanofillers exhibit 3D dimensions and have diameter less than 100 nm and examples include metal oxides, oligomeric silsesquioxane, etc.

Nanocomposites of PLA and sepiolite were prepared by Fukushima et al. (2012) using melt blending of polymers. Sepiolite is a magnesium silicate fiber having microporous dimensions. Size of these fibers varies extensively, but mostly it lies between 10 and 5000 nm in length and 10 and 30 nm in breadth, and about 5 and 10 nm in thickness. It has excellent water retention property and hence is widely used as filter aid, catalyst carrier, absorbent, bleaching agent, etc. Transmission electron microscopy (TEM) analysis of prepared nanocomposites showed better dispersion of small bundles and needles. Improvements in thermomechanical properties of prepared nanocomposites were observed. Polymeric properties of PLA were enhanced in prepared nanocomposites because of better dispersibility. The nanocomposites also showed better fire resistance property.

Nanocomposites of PLA and halloysite were also prepared to enhance the thermal, mechanical, crystallization, and fire stabilization properties of polymer. Halloysite is very much similar to kaolinite with respect to its composition. Halloysite is considered to be a cheaper alternative to silicates and nanotube carbon because of its better length to diameter ratio, nanoscale lumen, and low density of hydroxyl groups on its surface. High performance nanocomposites using halloysite and PLA were prepared by using melt-blending method, which showed better tensile strength and Young's modulus of elasticity. It was seen that 6% halloysite containing PLA nanocomposites showed tensile strength of 70 MPa and Young's modulus of elasticity of 2800 MPa. Targeted use of these nanocomposites for engineering applications can be possible because of their better dispersion capability (Du et al., 2010; Marney et al., 2008).

Various researchers prepared cellulose- and PLA-based nanocomposites. But because of the hydrophilic nature of nanocellulose and hydrophobic nature of matrix, that is, PLA, this makes it difficult to formulate diffusible composites, which results in aggregations of nanocellulose particles. That is why various methods and chemical strategies have been developed to reduce the interfacial compatibility between nanocelluloses and PLA polymer. [Oksman et al. \(2006\)](#) prepared a suspension of PLA and cellulosic nanocomposites by treating with *N,N*-dimethylacetamide and lithium chloride with the intention of swelling of nanocrystals of cellulose. The prepared suspension was added in polymer using melt extrusion process. *N,N*-dimethylacetamide resulted in degradation of nanocomposites hence was replaced by polyvinyl alcohol as processing aid. The prepared nanocomposites in both cases showed poor mechanical and thermal properties because of its phase separation having continuous PLA phase. Later on, coating of prepared nanocomposites was performed to enhance its stability but results remained unfruitful.

Some researchers also tried to prepare nanocomposites of carbon nanotubes ([Spitalsky et al., 2010](#)) and PLA by using a large number of techniques like in situ polymerization, solvent-evaporation method, and melt-blending but due to low solubility of carbon nanotubes in PLA and most of the organic solvents, chemical modification of carbon nanotubes is required through oxidation processes. To obtain better dispersion and improved solubility of carbon nanotubes in PLA, surface functionalization of PLA was performed by functional groups modification like COOH or OH, which were introduced at the surface of carbon nanotubes through oxidation processes. These functional moieties further interact with ester linkage of PLA via hydrogen bonding to prepare PLA-based nanocomposites. The effect of surface functionalization on the thermal stability and rheology of PLA nanocomposites was investigated. The results showed better dispersion of nanocomposites within PLA matrix proved by TEM analysis. However, small carbon nanotube bundles were also visible within the composites ([Wu et al., 2008, 2010a,b](#)).

Researchers also tried to prepare PLA-graphene nanocomposites. Graphene is thin honeycomb-like 2D shaped material that is made up of carbon atoms. Graphene as nanofillers gives more promising applications as polymeric nanocomposites because of its unique electronic and structural individuality. To achieve better dispersion of graphene in PLA polymeric materials, it was modified by using compatibilization process as used in carbon based nanocomposites like chemical modifications, noncovalent and covalent functionalizations. [Kim and Jeong \(2010\)](#) prepared PLA and modified graphene nanocomposite by melt-blending method and checked its mechanical and electrical properties, morphology, and thermal stability. The nanocomposite showed thickness of 15 nm and better homogeneous dispersion as seen in SEM and XRD patterns. The thermal degradation and Young's modulus of prepared nanocomposites increased with graphene up to 3% weight.

Silver-PLA nanocomposites were successfully prepared by using extrusion technology under high shear environment. The final prepared nanocomposites showed better thermal properties and good tensile strength. However, TEM images showed aggregates of silver nanoparticles, which correspond to use other alternatives to improve better dispersion of silver in PLA for future use. When the size of silver is reduced from micro- to nanosize, increase in its total surface area occurs, which results in increase in its antibacterial efficiency. Nanosized silver shows better healing and hygienic properties than native silver.

Kamyar et al. (2010) after chemical reduction of silver by using sodium borohydride and silver nitrate, prepared nanosized silver having diameter in range of 3–5 nm, which was mixed with PLA to prepare nanocomposites using two solvents namely chloroform and dimethyl formamide. The final synthesized silver nanoparticles dispersed in PLA colloidal solution of chloroform were found to be stable for longer period of time without precipitation. Prepared nanocomposites showed strong antibacterial activity both against Gram-negative and Gram-positive bacteria. Afterward, nanosized silver containing nanofibers were also prepared using PLA through electrospinning method. Prepared fibers showed better antibacterial property against *Staphylococcus aureus* and *Escherichia coli* (98.5% and 94.2%, respectively). Silver nanoparticles have natural ability to complex with nitrogen, oxygen, sulfur, or other functional groups found in bacterial enzymes. This results in cell metabolism and destabilization of cell wall of bacteria. Silver-PLA nanocomposites were also prepared by using solution processing methods.

Titanium and zinc oxide nanocomposites were also prepared by using PLA to enhance its mechanical properties and thermal stability (Hanemann and Szabó, 2010). A fine distribution and dispersion of zinc and titanium oxide nanoparticles were noticed through TEM images. The resulting nanocomposites showed high brittleness. Nanosized titanium dioxide dispersed in PLA matrix showed better photodegradability, improvement in toughness, acceptable targeting towards cancerous cells, and better kinetics of crystallization. It was found that direct mixing of nanosized titanium dioxide with PLA yields aggregates of titanium dioxide in the matrix. Hence, some surface treatments of nanoparticles were required to improve dispersion of nanosized titanium dioxide into PLA matrix by using propionic acid. Surface treatment of nanoparticles with lactic acid also results in better dispersion in PLA matrix.

PLA-silica nanocomposites were also prepared using melt compounding method. By this method, nanocomposites containing about 1%–10% of silica at 175°C were prepared successfully. The final nanocomposites showed better thermal stability and better protection against nitrogen and oxygen gases. However, with increased amount of silica, that is, above 10%, aggregates of silica nanoparticles can be seen through TEM images. L-Lactic acid, epoxidized soybean oil could be used to obtain better dispersion of silica nanoparticles (Huang et al., 2009; Wen et al., 2011). Table 6.4 depicts various polylactide based microcomposite and nanocomposites using reinforcing materials.

**Table 6.4** Polylactide Based Micro- and Nanocomposites Using Different Reinforced Materials

S. No.	Matrix Material	Reinforcing Material	Purpose	Inference	Reference
<b>Poly lactide-Based Microcomposites Using Different Reinforcing Materials</b>					
1	Poly (L-lactide)	Clay	For controlled release of 6-mercaptopurine	<ul style="list-style-type: none"> <li>Final microcomposites prepared by ion exchange method</li> <li>Better in vitro drug release</li> <li>Reduced cytotoxicity of drug</li> <li>High stability</li> <li>Controlled release of drug</li> </ul>	<a href="#">Iqbal et al. (2015)</a>
2	Poly (L-lactide)	<ul style="list-style-type: none"> <li>Nonabsorbable carbon</li> <li>Absorbable calcium</li> <li>Chitin</li> <li>Poly (glycolic acid)</li> </ul>	Microcomposites for fixing bone fractures	<ul style="list-style-type: none"> <li>Prepared microcomposites were tested using microbond and fragmentation method.</li> <li>The fiber matrix interfacial shear strength of all prepared microcomposites was tested.</li> <li>The final results showed that poly (glycolic acid) and chitin fibers based microcomposites had better mechanical properties and can be used for bone fractures.</li> </ul>	<a href="#">Slivka et al. (1997)</a>
3	Poly lactide	Talc	For evaluating effect of talc on properties of polylactide	<ul style="list-style-type: none"> <li>Prepared by melt mixing method.</li> <li>Improved mechanical properties.</li> <li>Improved thermal properties because of talc's stiffness and strengthening properties.</li> <li>A sudden reduction in mechanical properties was seen after providing stress conditions for 100, 200, and 300 h as per ISO 4892-3.</li> </ul>	<a href="#">Battegazzore et al. (2011)</a>

*(Continued)*

**Table 6.4** Polylactide Based Micro- and Nanocomposites Using Different Reinforced Materials *Continued*

S. No.	Matrix Material	Reinforcing Material	Purpose	Inference	Reference
4	Poly lactide	Cellulose	For modification in the mechanical properties of native PLA	<ul style="list-style-type: none"><li>• Microcomposites prepared by three methods: blending, polymerization with fibers alone, polymerization with high molecular weight PVA.</li><li>• Microcomposites containing 25% of fibers showed improved Young's modulus of elasticity.</li><li>• Microcomposites containing more than 35% of fibers showed reduction in Young's modulus of elasticity.</li></ul>	<a href="#">Birgit et al. (2006)</a>
5	Poly lactide	Clay	For testing affinity and stability of polymers after combination	<ul style="list-style-type: none"><li>• Microcomposites and nanocomposites were prepared by melt-blending method.</li><li>• XRD studies showed better affinity between PLA and clay polymers.</li><li>• TGA studies proved better thermal stability and reduced flammability of nanocomposites as compared with microcomposites.</li></ul>	<a href="#">Lu et al. (2015), Kaewprapan and Phattanasuddee (2012)</a>
<b>Polylactide-Based Nanocomposites Using Different Reinforcing Materials</b>					
1	Poly lactide	Sepiolite	To improve thermomechanical properties of polymer	<ul style="list-style-type: none"><li>• Prepared by using melt-blending method.</li><li>• TEM analysis of showed better dispersion of small bundles and needles.</li><li>• Improved thermomechanical properties.</li><li>• Better dispersibility.</li><li>• The prepared nanocomposites also showed better fire resistance property.</li></ul>	<a href="#">Fukushima et al. (2012)</a>

2	Poly(lactide)	Halloysite	To enhance the thermal, mechanical, crystallization, and fire stabilization properties of polymer	<ul style="list-style-type: none"> <li>• Prepared by using melt-blending method.</li> <li>• Showed better tensile strength and Young's modulus of elasticity.</li> <li>• About 6% halloysite containing PLA nanocomposites showed tensile strength of 70 MPa and Young's modulus of elasticity of 2800 MPa.</li> <li>• Targeted use of these nanocomposites for engineering applications is possible.</li> </ul>	<a href="#">Du et al. (2010), Marney et al. (2008)</a>
3	Poly(lactide)	Cellulose	To get dispersion of cellulose nanocomposites in PLA matrix	<ul style="list-style-type: none"> <li>• Prepared by treating PLA and cellulose with <i>N,N</i>-dimethylacetamide and lithium chloride.</li> <li>• Better dispersion of nanocomposites in PLA matrix.</li> <li>• Coating of prepared nanocomposites was performed to enhance its stability.</li> </ul>	<a href="#">Oksman et al. (2006)</a>
4	Poly(lactide)	Carbon nanotubes	To get better dispersion of carbon nanotubes in PLA matrix.	<ul style="list-style-type: none"> <li>• To obtain better dispersion and improved solubility of carbon nanotubes in PLA, surface functionalization of PLA was performed by functional groups modification like COOH or OH.</li> <li>• These functional moieties interact with ester linkage of PLA through hydrogen bonding.</li> <li>• Surface functionalization resulted in better thermal stability and rheology of PLA nanocomposites.</li> <li>• The results showed better dispersion of nanocomposites within PLA matrix proved by TEM analyses.</li> </ul>	<a href="#">Spitalsky et al. (2010), Wu et al. (2010a,b)</a>

(Continued)

**Table 6.4** Polylactide Based Micro- and Nanocomposites Using Different Reinforced Materials *Continued*

S. No.	Matrix Material	Reinforcing Material	Purpose	Inference	Reference
5	Poly lactide	Graphene	To enhance the thermal, mechanical, stability along with better dispersion properties of polymer	<ul style="list-style-type: none"><li>• To achieve better dispersion of graphene in PLA polymeric materials, it was modified by using compatibilization process like chemical modifications, noncovalent and covalent functionalizations.</li><li>• PLA and modified graphene nanocomposites were prepared by melt-blending method.</li><li>• Nanocomposites showed thickness of 15 nm and better homogeneously dispersion as found through SEM and XRD patterns.</li><li>• The thermal degradation and Young's moduli of prepared nanocomposites increased with graphene up to 3% weight.</li><li>• With increase in concentration aggregates were obtained.</li></ul>	<a href="#">Kim and Jeong (2010)</a>
6	Poly lactide	Silver	To obtain better thermal and tensile strength.	<ul style="list-style-type: none"><li>• Chemical reduction of silver was done by using sodium borohydride and silver nitrate to prepare nanosized silver.</li><li>• Nanosized silver having diameters in range of 3–5 nm, which was mixed with PLA to prepare nanocomposites.</li><li>• The final synthesized silver nanoparticles found to be stable for longer period of time without precipitation.</li><li>• Prepared nanocomposites showed strong antibacterial activity wide spectrum bacteria.</li><li>• Nanofibers of silver showed better antibacterial property against <i>S. aureus</i> and <i>E. coli</i> (98.5% and 94.2%, respectively).</li></ul>	<a href="#">Kamyar et al. (2010)</a>



7	Poly lactide	Titanium dioxide/ zinc oxide	To enhance its mechanical properties and thermal stability	<ul style="list-style-type: none"> <li>• Titanium dioxide nanocomposites were prepared by using PLA.</li> <li>• A fine distribution and dispersion of zinc and titanium oxide nanoparticles were noticed through TEM images.</li> <li>• The resulting nanocomposites showed high brittleness.</li> <li>• Surface treatments of nanoparticles were required to improve dispersion of nanosized titanium dioxide into PLA matrix by using propionic acid to inhibit agglomeration.</li> <li>• Surface treatment of nanoparticles with lactic acid also results in better dispersion in PLA matrix.</li> </ul>	<a href="#">Hanemann and Szabó (2010)</a>
8	Poly lactide	Silica	To obtain better thermal stability and better protection against nitrogen and oxygen gases	<ul style="list-style-type: none"> <li>• PLA-silica nanocomposites were also prepared using melt compounding method.</li> <li>• The final nanocomposites showed better thermal stability and better protection against nitrogen and oxygen gases.</li> <li>• With increased amount of silica, i.e., above 10%, aggregates of silica nanoparticles can be seen through TEM images.</li> <li>• L-Lactic acid, epoxidized soybean oil could be used to obtain better dispersion of silica nanoparticles.</li> </ul>	<a href="#">Huang et al. (2009)</a> , <a href="#">Wen et al. (2011)</a>

Raghunath et al. (2018) have successfully prepared biobased nanocomposites by blending the combination of epoxidized soybean oil and polylactic acid in different compositions in the ratio of epoxidized soybean oil:polylactic acid 5:95, 10:90, 15:85, 20:80, and 25:75 by weight percent. The final optimized nanocomposites were prepared by using composition of epoxidized soybean oil:polylactic acid in the ratio of 80:20. The nanocomposites were prepared by using solvent casting method. The final results showed appropriate and acceptable mechanical strength of the polylactic acid and tensile measurements. Scanning electron microscopy (SEM) confirmed the nanostructure of the composites and thermal properties like  $T_c$ ,  $T_m$ ,  $T_g$ . The degradation temperature of selected polymers was tested by using TGA. The electroactive nature of prepared nanocomposites was confirmed by “U”-shaped bending test. All results showed the prepared nanocomposites more stable and better as compared with commercial available nanocomposites with appropriate polylactic acid concentration.

In general, most of the recently prepared biobased and biodegradable nanosized composites containing poly lactide were prepared by using extrusion technology under high shear environment, solvent casting method, solvent-evaporation or extrusion method, and melt compounding method. However, these days, a new technology has been discovered to prepare better nanocomposites with appropriate mechanical strength and thermal properties. These nanocomposites can be prepared by using the principal of stereochemistry. The stereocomplexation between the polylactic acid and starch can produce better and stronger nanocomposites. Previously, the hydrogen bonding interactions between the starch and polylactic acid polymers were used. The strength of these nanocomposites was found to be weaker than that of stereocomplexed polymers. Benali et al. (2018) have successfully prepared the nanocomposites by using poly lactide and poly (glycidyl-methacrylate) copolymers. The size-exclusion chromatography analysis and NMR spectroscopic studies have successfully confirmed a complete formation of copolymer synthesis. The nanocomposites were prepared by using melt-processed method by compression molding using stereochemistry principle. The prepared nanocomposites showed better thermogravimetric and differential scanning calorimetry (DSC) results. The results showed that these supramolecular interactions due to the stereocomplexation between the polylactide matrix and poly (glycidyl-methacrylate) matrix showed a synergetic effect, which helped to preserve the nanoplatelets and their morphological geometry during melt processing procedure. This makes the prepared nanocomposites better in morphological strength, thermogravimetric test, better morphological structure, and better stability. This makes these nanocomposites better candidates as compared with the other prepared nanocomposites.

### 6.3.2 COLLAGEN

Collagen is the most plentiful protein found in the human body. It is the major component of bone, cartilage, ligament, tendon, blood vessels, and skin. Collagen

consists of triamino blocks of glycine-proline-hydroxyproline amino acids polypeptide strands. To date, about 30 distinct types of collagen have been discovered. Collagen is a biodegradable protein that has acceptable mechanical strength, better biocompatibility, and enzymatic degradability, making it useful in various medical applications (Kim et al., 2016, 2017).

Various researchers have used collagen in different forms of drug delivery like nanosponges, nanotubes, powders, injectables, nanosheets, etc. Catgut is one of the most commonly used suture materials for medical purposes in which collagen is the major component. Collagen has a tensile strength of about 92.5 MPa. This ability of collagen makes it suitable for use in bone tissue engineering. Bone is composed of organic phase, that is, collagen, and mineral phase, that is, calcium phosphate in the form of hydroxyapatite. The collagen found in human bone is responsible for the viscoelasticity and toughness of bone. Researchers are trying to develop a biomimetic composite that will show balance between both biological and biomechanical properties.

A large number of composites have been prepared using collagen. Composites prepared by adding hydroxyapatite and collagen have properties to mimic the natural bone's composition. Recently Angiotech Pharmaceuticals marketed a synthetic bone graft substitute called Collagraft, which is composed of collagen and hydroxyapatite granules. Collagraft got FDA approval and has been used clinically.

The mechanical and thermal properties of different human tissues like bones, tendons, and ligaments directly depend on the arrangement of their constituent components. Type I collagen is an abundantly found protein all over the human body especially in bones, tendons, and ligaments (about 66% of all proteins present in humans) and is mainly responsible for its tensile stress bearing ability. The way by which collagen molecules are assembled in fibers represents the mechanical properties of different human tissues.

Atomic force microscopy (AFM) is a recently used micromanipulation technique that helps in measuring the mechanical properties of materials at the nano- and micron-scale. As per AFM studies, a single fiber of collagen has a diameter of about 10–500 nm. At structural levels including fibers, fibrils, collagen molecules, even at higher levels like fascicles, collagen has a highly organized structure, which differentiates it from most of other proteins. The Young's modulus of collagen fiber was found to be 1–8 GPa at its dry stage, which is similar to human tendons, and it is found to be 0.15–1 GPa at its hydrated state.

Collagen usually exhibits viscoelastic properties, which means the mechanical and thermal behavior of collagen molecules is rate dependent. This viscoelastic property is very important for healthy functioning of human tissue. Moduli of elasticity of collagen-based tendon molecules change with change in strain rates. Wu et al. (2010a,b) found that the elastic moduli of tendons by applying strain rates of 0.6% per second, 1.5% per second, 5% per second were  $427 \pm 10$ ,  $653 \pm 21$ , and  $837 \pm 11$  MPa, respectively. Lynch et al. (2003) investigated that

the elastic modulus of collagen fascicles get changed from  $160 \pm 49$  to  $216 \pm 68$  MPa with increase in strain rate (from 0.01% per second to 1% per second). The bending moduli and shear modulus of collagen fibrils was found to be 1.0–3.9 GPa and  $33 \pm 2$  MPa, respectively, at ambient conditions. But when these collagen fibrils were immersed in phosphate buffer, both bending moduli and shear modulus of collagen fibrils got reduced to 0.07–0.17 GPa and  $2.9 \pm 0.3$  MPa, respectively.

Fu et al. (2017) prepared scaffold composites by using polymers collagen and chitosan in which mesenchymal stem cells are seeded for tissue engineered heart valve. Prepared biodegradable collagen chitosan composites were used to produce tissue engineered valves for heart. The prepared scaffold composites were found to be cytocompatible, and the seeded mesenchymal stem cells of bone marrow were easily differentiated from endothelial cells. The tissue engineered valves showed positive results for both endothelial cell as well as smooth muscle actin cells. Electron microscopy showed the similarity in shapes of seeded cells to endothelial cells, smooth muscle cells, and fibroblasts. In vitro studies showed that the biological activity of seeded cells in collagen chitosan composites scaffold was retained after being cultured.

Xie recently prepared the nanocomposites by using graphene oxide and silk fibroin. The nanocomposites were prepared by using melt solvent method, which exhibits high mechanical strengths alternatively at nanoscale. The mechanical nature of prepared nanocomposites is evaluated through microscale ballistic characterization with the help of  $7.6 \mu\text{m}$  sized diameter silica at high speed by using 400 m/s speed. The volume of the reinforcing material, which is graphene oxide, varies from 0% to 32% in size. The penetration energy of these prepared nanocomposites increases depending upon the distribution of used graphene oxide, which was isolated by partial overlapping of continuous sheets of graphene oxide (Xie et al., 2018). This makes the nanocomposites a better candidate as compared with the others because the continuous sheets of graphene oxide showed better mechanical strength and better thermostability.

Wang et al. (2017b) studied the effect of combination of three different types of starches namely normal starch, waxy maize starch, and high amylose content starch on collagen properties. SEM showed that by using amylose and normal starch, tensile strength of composites increased. Addition of more starch resulted in decreased solubility in water. DSC thermograms studies showed improved thermal stability of all prepared composites. XRD studies proved decrease in crystallinity of starch and collagen on heating. FTIR spectra showed increase in intermolecular interactions between both polymers in all prepared composites (i.e., starch and collagen) on heating.

Kim et al. (2016, 2017), prepared biocomposites scaffold by using fibrin and collagen to check its tissue regenerative property. Fibrin and collagen, both polymers, are widely used for medical applications mainly in surgery because of their tissue regeneration property. Combination of fibrin and collagen resulted in composite formation, which showed synergistic tensile mechanical properties as

compared with its native isolated proteins. This increase in tensile mechanical strength may be because of change in polymeric network density and enhancement in crisscrossing between polymeric structures. Formation of bundles of polymeric fibers may also be a reason for this synergistic phenomenon. The results proved this fibrin–collagen combination to be promising for use in tissue regeneration in form of sealants, sponges, or scaffolds with predictable mechanical and tensile properties by optimizing the ratio of both polymers to be used in formation of composites.

Lewandowska et al. (2016) prepared porous composites by using collagen, chitosan, and hyaluronic acid by lyophilization process. Properties of composites prepared by collagen and chitosan were modified by adding hyaluronic acid in different concentrations (1%, 2%, and 5%). The results showed improved thermal stability and mechanical properties with insignificant effect on cell morphology. Fibroblast cells showed modified proliferation rate after incubation in 3-(4,5-dimethylthiazolyl-2)-2,5-diphenyltetrazolium bromide assay. Biological studies proved the 3D composites to be nontoxic.

Kanda et al. (2016) prepared composites of collagen and octacalcium phosphate to treat bone defects because of its bone regeneration ability. Prepared composites were implanted in 11 male dogs' premolar teeth. The results showed implantation of prepared collagen and octacalcium phosphate composites in the alveolar region helps in preserving the alveolar ridge and does not cause any disturbance in permanent tooth eruption.

Caliari et al. (2012) prepared composite based on bioactive collagen glycosaminoglycan scaffold. The prepared scaffold has micron scale porosity, which was supported by polycaprolactone frame having millimeter scale porosity. The permeability, thermal stability, mechanical properties, and bioactivity of prepared composite was found to be satisfactory. The use of polycaprolactone supporting frame helped the composites in enhancing its modulus by 6000-fold as compared with scaffold alone. High specific surface area can be achieved by assimilation of mineral scaffold with prepared composites, which resulted in increased attachment stem cells.

Gurumurthy et al. (2016) prepared composites scaffold containing collagen and elastin like polypeptide as reinforcing element. The composites showed acceptable tensile strength, toughness, and elastic modulus. The prepared composites showed the viability of the human adipose stem cells for more than 22 days in its culture period. Composites containing about 15 mg/mL of elastin like polypeptide and 6 mg/mL of collagen showed the best tensile, mechanical strength, and elastic modulus. Various collagen-based nanocomposites have been summarized in Table 6.5.

### 6.3.3 SILK

To develop novel and successful reinforcement in resorbable biocomposites, silk fibers obtained from silkworms and spiders can be a better substitute. Although

**Table 6.5** Various Collagen-Based Nanocomposites

S. No.	Polymer 1	Polymer 2	Final Preparation	Result	Reference
1	Hydroxyapatite	Collagen	Nanocomposites	The collagen fibers and hydroxyapatite nanocrystals get cross-linked with each other by self-organization mechanism such that they mimic human bone. The prepared composites gave better bioresorbability and mechanical strength making it suitable for bone disorders.	<a href="#">Brasinika et al. (2016)</a>
2	Gold	Collagen	Nanocomposites	The prepared gold and collagen nanocomposites showed laser facilitated treatment of ruptured intestine. By using the prepared composites, the tensile strength of ruptured intestine becomes 68% through laser treatment, which was closer to native healthy intestine. This makes the prepared formulation as promising candidate for ruptured intestinal treatment.	<a href="#">Wang et al. (2016)</a>
3	Silica	Collagen	Nanocomposites	The prepared silica collagen nanocomposites were found to give sustained release of loaded biomolecules like genes, proteins, DNA, peptides, etc. through prepared hydrogel. Such nanocomposites make promising carrier for local gene delivery to encourage tissue repair.	<a href="#">Wang et al. (2015)</a>
4	Cellulose	Collagen	Nanocomposites	Prepared nanocomposites of bacterial cellulose and collagen type I was used for tissue repair. The tensile strength and elastic modulus of prepared nanocomposites decreases after sterilization as compared with native bacterial cellulose. The prepared nanocomposites can be considered as better alternative for bone tissue engineering.	<a href="#">Torres et al. (2012)</a>
5	Silica	Collagen	Nanocomposites	The prepared nanocomposites of silica and collagen showed great potential for corneal replacement. The results showed improved mechanical and tensile strength nanocomposites and better corneal replacement results. The final prepared nanocomposites preparation can be considered as better alternative for other applications like drug delivery, gene delivery, protein peptide delivery, etc. with sustained release.	<a href="#">DiVito et al. (2012)</a>
6	Hydroxyapatite	Collagen	Nanocomposites	The nanocomposites of hydroxyapatite and collagen were prepared by using coprecipitation method using glutaraldehyde as cross-linking agent. SEM and FTIR showed self-organization of prepared nanocomposites with drying process responsible for altering its tensile and shear strength.	<a href="#">Itoh et al. (2004)</a>
7	Silica	Collagen	Nanocomposites	Drug sodium Ibandronate was loaded in silica collagen nanocomposites. For its stability and better release pattern. The hydrogels prepared from composite nanoparticles showed drug release for over 10 days. The formulation showed promoting effect on differentiation of cells by increasing activity of enzyme alkaline phosphatase.	<a href="#">Alvarez et al. (2015)</a>

many different types of reinforcing agents are used in preparation of composites, the increasing demands for natural fibers to achieve sustainable release resulted in use of silk fibers. It was observed that the reinforcement caused by silk fibers is much better as compared with various other fibers obtained from plants or human organs. They are even better than synthetic fibers like glass fibers used in textiles.

This is because most of the fibers form bundles by combining with each other and they are cylindrical in shape, which does not allow proper fitting of fibers with matrix polymer. While in case of silk fibers, they do not form bundles like other plant fibers, but rather they retain their individual filament or thread-like geometry and are smooth and long (ability to reach up to 1500 m). These fibers are triangular in shape irrespective of other plant fibers, which are mostly spherical in shape. This triangular geometry gives better fitting of silk fibers as compared with other plant fibers (Vollrath 2000).

Natural fibers' use in biocomposites increases day by day because of high market activity and heavy demand for sustainable and controlled released materials. Silk fibers obtained from either spiders or silkworms are considered as ideal fibers for preparation of composites because the silk fibers have compressibility, triangular cross-sections, and long thread-like structures (Morin and Alam, 2016). Silk not only gives more compressibility benefits but also has better compactibility than glass fibers. Silk fibers have natural ability to withstand twisting and bending without producing any breaks, which makes them better than any other plant fibers. This property also helps in enhancing the mechanical properties of composite (Zhu et al., 2015).

PLGA (polylactic glycolic acid) silk composite nanofibrous scaffold was prepared by using electrospun technique with varying concentrations of different materials to be used for tissue engineering. Silk fibroin, PLGA, and scaffolds have good biocompatibility with body's neurons. The average diameter of the prepared fibers was found to be  $280 \pm 26$  to  $168 \pm 21$  nm having high porosity, tensile strength, and hydrophilicity. The tensile strength of prepared nanofibers was found to be  $1.76 \pm 0.32$  MPa. The results proved the final preparation to be effective for biocomposite formulation (Wang et al., 2011).

---

## 6.4 PATENT LITERATURE ON BIOCOMPOSITES

A number of patents have been published and filed related to the application of composite materials in various biomedical and drug delivery applications, for example, bone material substitutes, dental applications, as a substitute for dermal tissue, scaffolds, surgical repairing, wound healing, etc. Various patents with their description have been depicted in Table 6.6.

**Table 6.6** Patent Literature on Various Composites and Their Description

Patent No.	Title	Description	Reference
US 2012/0010146 A1	Composite containing collagen and elastin as a dermal expander and tissue filler	An injectable composition having dermal filling and tissue expanding activity comprises (1) a quantity of elastin sufficient to bring about dermal filling and tissue expansion and (2) a pharmaceutically acceptable carrier, was reported. The composition further comprised of collagen and other alternatives, hyaluronic acid, if present can be cross-linked, either intramolecularly or intermolecularly.	<a href="#">Han et al. (2012)</a>
US 2011/0264119 A1	Medical implant including a 3D mesh of oxidized cellulose and a collagen sponge	The invention described a bioresorbable implant comprising of a bioresorbable porous layer including biopolymer foam and defining first pores, a bioresorbable porous 3D mesh made from a microbial cellulose and defining second pores, wherein the bioresorbable porous layer is disposed in the bioresorbable porous 3D mesh. Also the method of making a bioresorbable implant was discussed.	<a href="#">Yves et al. (2011)</a>
US 2011/0217388 A1	Devices and methods for the regeneration of bony defects	This invention described the method for producing a composite bone graft material for regenerating bony defects in the body. The invention had further discussed the methods for the production of bioactive glass particles used in the composite that have been surface treated to allow for the production of a highly porous composite that can hold significant amounts of body fluid or other molecules that will aid in the regenerative process. The method of surface treatment allowed for the manufacture of a suitable implantable composite while retaining the unique osteostimulative properties that are associated with bioactive glass particles.	<a href="#">Greenspan and Katta (2011)</a>



US 2009/0018655A1	Composite implant for surgical repair	The invention disclosed the biocompatible implants that combine a scaffold material for supporting long term repair of a soft tissue with an elongated member such as a suture for aiding in placement of the scaffold during a surgical procedure as well as for immediate mechanical reinforcement of a repair site. The components of an implant were combined such that a longitudinal load placed upon a composite structure can be borne primarily by the elongated member and the scaffold material is isolated from the longitudinal load. Thus, the scaffold material of a composite could be protected from damage due to applied loads and stresses during and following a surgical procedure.	<a href="#">Brunelle et al. (2009)</a>
US 2007/0218038A1	Stabilized, sterilized collagen scaffolds with active adjuncts attached	The invention was related to the bioimplants comprised of biological tissues having conjugated thereto adjunct molecules. The biological tissues were sterilized with a chemical sterilizing agent, such as a water-soluble carbodiimide. The processes of making the bioimplants included a process in which an adjunct molecule was conjugated to a biological tissue during the sterilization process.	<a href="#">Nataraj et al. (2007)</a>
US 2007/0065943 A1	Cell-support matrix having narrowly defined uniformly Vertically and nonrandomly organized porosity and pore density and a method for preparation thereof	A cell-support matrix having narrowly defined uniformly vertically and nonrandomly organized porosity and pore density and a method for preparation was discussed. The matrix was suitable for preparation of cellular or acellular implants for growth and de novo formation of an articular hyaline-like cartilage. A gel-matrix composite system comprising collagen-based matrix having a narrowly defined porosity capable of inducing hyaline-like cartilage production from chondrocytes in vivo and in vitro, was studied.	<a href="#">Smith et al. (2007)</a>

(Continued)

**Table 6.6** Patent Literature on Various Composites and Their Description *Continued*

Patent No.	Title	Description	Reference
US 2006/0263417 A1	Electrospun blends of natural and synthetic polymer fibers as tissue engineering scaffolds	Nonwoven fibrous scaffolds made by electrospinning from the synthetic biodegradable polymer such as, for example, poly(lactic-co-glycolic acid) (PLGA) and natural proteins, such as, for example, gelatin (denatured collagen) and elastin and a method of preparation had been reported.	<a href="#">Peter et al. (2006)</a>
US 2006/0233887 A1	Bioactive material for use in stimulating vascularization	The invention was related to a bioactive material, particularly one that comprises SiO <sub>2</sub> and CaO and optionally Na <sub>2</sub> O and/or for use in stimulating vascularization and pharmaceutical compositions, wound dressings, tissue constructs, and delivery systems that include such a bioactive material.	<a href="#">Richard (2006)</a>
US 2006/0189516 A1	Method for producing cross-linked hyaluronic acid–protein biocomposites	The invention was concerned with a new method for producing cross-linked hyaluronic acid–protein biocomposites in various shapes. In the process, a polysaccharide solution and a protein solution were mixed under moderate pH values in presence of salts to form a homogenous solution, which can be processed into various shapes, such as membrane, sponge, fiber, tube, microgranular and so on. After that, the homogenous solution was subjected to a cross-linking reaction in organic solvent containing weak acid to produce an implantable biocomposite material having excellent biocompatibility, biodegradability, prolonged enzymatic degradation time, and good physical properties.	<a href="#">Yang et al. (2006)</a>

US 2006/0172918 A1	Composite biomaterials	The invention provided novel composite biomaterials having excellent bioadaptability and bone inductivity and a process for producing the same. The composite biomaterials comprised of hydroxyapatite, collagen, and alginate and have microporous structures in which the c-axis of the hydroxyapatite is oriented along the collagen fibers.	<a href="#">Shinichi et al. (2006)</a>
US 2006/0067969 A1	Multiphased, biodegradable, and osteointegrative composite Scaffold for biological fixation of musculoskeletal soft tissue to bone	Methods and apparatuses were studied for musculoskeletal tissue engineering in the invention. For example, a scaffold apparatus was provided that comprises microspheres of selected sizes and/or composition. The microspheres were layered to have a gradient of microsphere sizes and/or compositions. The scaffold provided a functional interface between multiple tissue types.	<a href="#">Helen et al. (2006)</a>
US 2005/0053638A1	Organic/inorganic composite biomaterials and process for producing the same	The invention provided organic/inorganic composite biomaterials constituted by composites of hydroxyapatite and collagen and having an average fiber length of 60 $\mu\text{m}$ or longer, and a process for producing the same in which the calcium ion and phosphate ion concentrations in the reaction vessel are optimized through regulation of the concentration of a starting material and the flow rate. The organic/inorganic composite biomaterials had mechanical strength and a biodegradation rate suitable for artificial bones through the introduction of cross-linking therein.	<a href="#">Junzo et al. (2005)</a>
US 2005/0004599 A1	Nonlight-activated adhesive composite, system, and methods of use thereof	The invention provided a nonlight-activated adhesive composite, method, and system suitable for medical and surgical applications. The composite included a scaffold and a nonlight-activated adhesive. The scaffold and the nonlight-activated adhesive included biological, biocompatible, biodegradable materials.	<a href="#">McNally-Heintzelman et al. (2005)</a>

(Continued)

**Table 6.6** Patent Literature on Various Composites and Their Description *Continued*

Patent No.	Title	Description	Reference
US 2004/0236371 A1	Light-activated adhesive Composite, system, and methods of use thereof	The invention provided a light-activated adhesive composite suitable for medical and surgical applications. The composite included a scaffold and a light-activated adhesive, such as a laser tissue solder. The scaffold included a biological, biocompatible, or biodegradable material, such as PLGA or SIS.	<a href="#">McNally-Heintzelman et al. (2004)</a>
US 2004/0131562 A1	Biomimetic organic/inorganic composites, processes for their production, and methods of use	The subject invention concerned a composite comprising an organic fluid-swellable, fibrous matrix, such as collagen, and a mineral phase, such as calcium carbonate or phosphate mineral phase, for use as a biomimetic of bone. In another aspect, the subject invention concerned a process for making a composite involving the inclusion of acidic polymers to a supersaturated mineralizing solution, to induce an amorphous liquid-phase precursor to the inorganic mineral, which was then absorbed (pulled by capillary action) into the organic matrix. Advantageously, once solidified, a high mineral content could be achieved, with the inorganic mineral crystals embedded within the collagen fibers (intrafibrillarly) and oriented such that they are aligned along the long axes of the fibers of the organic matrix, thereby closely mimicking the natural structure of bone. It further included the method of treating a patient suffering from a bone defect by applying a biomimetic composite to the bone defect site.	<a href="#">Laurie et al. (2004)</a>

US 2004/0124564 A1	Process for preparing a chemically modified Fibrin-fibrillar protein (FFP) Composite sheet	The invention was related to a process for the preparation of a novel chemically modified FFP composite sheet for medical application and the FFP composite prepared thereby. The FFP sheet found potential use as a dressing aid in the treatment of various external wounds of different nature, which included cut wounds, burn wounds, and even ulcers in animals and human beings.	Sheik et al. (2004)
US 2003/0232198 A1	Immobilized bioactive hydrogel matrices as surface coatings	The invention was directed to a stabilized bioactive hydrogel matrix coating for substrates, such as medical devices. The invention provided a coated substrate comprising a substrate having a surface, and a bioactive hydrogel matrix layer overlying the surface of the medical device, the hydrogel matrix comprising a first high molecular weight component and a second high molecular weight component, the first and second high molecular weight components each being selected from the group consisting of polyglycans and polypeptides, wherein at least one of the first and second high molecular weight components was immobilized (e.g., by covalent cross-linking) to the surface of the substrate.	Francis et al. (2003)
US 2003/0225355A1	Composite material for wound repair	A composite comprising a barrier material and a support material used for wound or tissue repair was studied. Benefits included decreased adhesion to organs or other structures adjacent to the repair site, limited fluid flux, increased vascularization and cellular infiltration, decreased inflammation, and reduced scar tissue formation.	Charles (2003)

(Continued)

**Table 6.6** Patent Literature on Various Composites and Their Description *Continued*

Patent No.	Title	Description	Reference
US 2003/0118560 A1	Composite biocompatible matrices	A composite matrix having two layers was studied. The first layer included at least about 5 dry weight percent flexibility modifying agent. The second layer included at least about 5 dry weight percent less flexibility modifying agent than the first layer. A valved prosthesis with flexible leaflets supported by a wall can be formed from the composite materials. In some embodiments, the wall of the prosthesis included a first layer with at least about 60 wt% collagen and a second layer with at least about 25 wt% collagen and at least about 5 wt% elastin. The leaflets preferably included a first layer with at least about 60 wt% collagen and a second layer with at least about 25 wt% collagen and at least about 5 wt% proteoglycans.	<a href="#">Sheila and Matthew (2003)</a>
US 7,226,611 B2	Glycosaminoglycan/collagen Complexes and use thereof	The invention offered a novel material that combines cell-adhesive proteins such as collagen with glycosaminoglycan polymers to construct an environment similar to an extracellular matrix, capable of controlling differentiation and proliferation of cells. A glycosaminoglycan-functionalized polymer protein composite produced by combining a cell-adhesive protein with a glycosaminoglycan-functionalized polymer obtained by incorporating a carbohydrate chain containing a structure corresponding to at least a portion of a glycosaminoglycan backbone into a vinyl polymer main chain, as well as a cell culture substrate and a material for tissue reconstruction treatments comprising the composite, was reported.	<a href="#">Hirofumi et al. (2007)</a>

US 7,211,275 B2	Composite materials for controlled release of water Soluble products	Composite materials comprising a water-soluble compound adsorbed onto a basic inorganic material and a biodegradable polymer that yields acidic degradation products were described and methods of producing these and methods of their use were also included. These composite materials were designed to provide controlled release of the water-soluble molecule.	<a href="#">Jackie and Tseh-Hwan (2007)</a>
US 7,087,227 B2	Cartilage composites and methods of use	The invention described neocartilage compositions characterized by having multiple layers of cells, which are surrounded by a substantially continuous insoluble glycosaminoglycan and collagen-enriched hyaline extracellular matrix, and which neocartilage phospholipids are advantageously enriched in antiinflammatory <i>n</i> -9 fatty acids, particularly 20:3 <i>n</i> -9 eicosatrienoic or Mead acid. The methods of growing neocartilage in substantially serum-free growth media and methods of producing a conditioned growth media containing compounds effective to enhance neocartilage formation. The neocartilage compositions were useful as implants and as replacement tissue for damaged or defective cartilage and as a model system for studying articular cartilage disease and response to natural and synthetic compounds.	<a href="#">Hustun (2006)</a>
US 6,527,810 B2	Bone substitutes	A strong, porous article used as a bone substitute material was offered. The article comprised a continuous strong framework structure having struts defining interstices that interconnect the bulk volume, and may have ceramic or osteoconductive material occupying at least a portion of the same bulk volume as the framework structure. The osteoconductive materials were a resilient material that serves to distribute stresses within the article.	<a href="#">James et al. (2003)</a>

(Continued)

**Table 6.6** Patent Literature on Various Composites and Their Description *Continued*

Patent No.	Title	Description	Reference
US 6,509,031 B1	System for polymerizing collagen and collagen composites in situ for a tissue compatible wound sealant, delivery vehicle, binding agent, and/or chemically modifiable matrix	The invention described the materials and methods for cross-linking, in situ, proteins, including collagen, with peroxidase, including horseradish peroxidase, to form biocompatible semisolid gels useful in a number of biological and food product applications.	<a href="#">Douglas et al. (2003)</a>
US006110484A	Collagen-polymer matrices with differential biodegradability	The invention offered a biomedical implant comprising a biomedical matrix material and a biodegradable porosifying agent. As the porosifying agent degraded in situ, an implant with an interconnecting network was formed. The resultant mechanically stable implant allowed for tissue and fluid influx into the matrix.	<a href="#">David (2000)</a>
US005425770A	Calcium phosphate/ateloptide collagen compositions for bone repair	Processes for the preparation of compositions used in conductive bone repair were disclosed. The compositions contained a mixture consisting essentially of either a calcium phosphate particulate mineral component or particulate hydroxyapatite in admixture with a telopeptide reconstituted fibrillar collagen. The method comprised of mixing a dispersion of the collagen and mineral, the latter of which was present in dry particulate form, followed by molding and drying the composition in a mold to obtain a dried composition.	<a href="#">Karl et al. (1995)</a>
4,841,962	Collagen matrix/polymer film composite dressing	A wound dressing was disclosed that was comprised of a cross-linked collagen matrix; a bioabsorbable adhesive coated on one surface of the collagen matrix; a multilayer polymer film imparting preselected moisture vapor and gas transmissivity to the dressing, secured to the opposite surface of the collagen matrix; and an adhesive securing the collagen matrix to the polymer film.	<a href="#">Richard et al. (1989)</a>



4,280,954	Cross-linked collagen-mucopolysaccharide composite materials	Composite materials were disclosed which were formed by contacting collagen with a mucopolysaccharide and subsequently covalently cross-linking the resultant composite. These composite materials possessed a balance of mechanical, chemical, and physiological properties that make them useful in surgical sutures and prostheses of controlled biodegradability (resorption) and controlled ability to prevent development of a foreign body reaction and many are also useful in applications in which blood compatibility is required.	<a href="#">Ioannis et al. (1981)</a>
CN1406632A	Collagen-based composite sponge and production thereof	A collagen-based composite sponge for medical purpose was prepared from collagen, chitosan and glycerin through dissolving collagen in solution of acetic acid, dissolving chitosan in solution of acetic acid, proportionally mixing them with glycerin, freezing at $-10^{\circ}\text{C}$ to $-80^{\circ}\text{C}$ for 1–5 days for 20–100 min in gas generator, washing with aqueous solution of glycerin and vacuum drying.	<a href="#">X et al. (2003)</a>
EP0230023A2	Pharmaceutical compositions for the enhancement of wound healing	The invention described a pharmaceutical composition comprising of sulfated oligosaccharides, particularly mono- and disaccharides, or their salts to enhance healing of wounds. Preferred saccharides are those having three or more sulfate groups, with persulfation being most preferred. Preferred salts were the soluble salts most preferably the alkali metal salts, particularly potassium and sodium salts. Sucrose octasulfate was the most preferred material. The saccharide may be present in any form, including liquids, gels, or time release polymers. The saccharide preferably was present in combination with collagen.	<a href="#">Michaeli (1978)</a>

(Continued)

**Table 6.6** Patent Literature on Various Composites and Their Description *Continued*

Patent No.	Title	Description	Reference
JPH07236688A	Composite material of bioabsorptive plastic and collagen	The invention offered a highly strong composite body while keeping the property in which the immunogenetic property possessed by collagen is extremely low and excellent in the penetration or activity of cells for tissue regeneration by covering at least a part of a sponge material consisting of collagen with bioabsorptive plastic.	<a href="#">Akiyama (1995)</a>
WO2013091001A1	A peptide hydrogel composite	The invention was related to polymers that were especially useful as hydrogels and to use of these hydrogels for repair or restoration of tissue. The polymers and hydrogels of the current invention could be used for the repair or restoration of cartilage, especially articular cartilage. The polymers comprised of at least a monomer for binding water, a monomer for imparting mechanical properties, and a monomer for binding to an extracellular protein.	<a href="#">Dehghani et al. (2013)</a>
WO2006029571A1	Photochemically cross-linked collagen scaffolds and methods for their preparation	The invention described a method for producing collagen-based scaffolds with improved characteristics, which broadens the usage of collagen in tissue engineering. The method comprised of reconstitution of 3D collagen matrices from collagen monomer solution and cross-linking the matrix with a light source in the presence of a photosensitizing reagent. The cross-linked products could be in any shape and form and used in the dry or wet state, for applications including but not limited to tissue engineering and controlled drug delivery.	<a href="#">Barbara and So (2006)</a>

---

## 6.5 RECENT ADVANCES AND FUTURE PROSPECTS

Various studies on the use of composites in medical applications are going on to date and improving day by day with modifications in different aspects. After the use of synthetic polymers for composite preparations, the use of biodegradable polymers started expanding because of their better compatibility with body. Later, the use of resorbable biodegradable polymers gained more popularity because once inserted, there is no need for further operations as the implant gets dissolved within body fluids without causing any toxic effects. Presently the concept of biocomposites or green composites is being highly used for achieving controlled and sustained drug delivery of sensitive drugs. Such green biocomposite preparations are useful in obtaining sustained release of various biomolecules like gene delivery, protein peptide delivery, deoxy-ribose nucleic acid (DNA) delivery, enzymes delivery, vaccines delivery, drug molecules delivery, etc. with their enhanced thermal and chemical stability. Recently this technique was also used in aerosol formulations (dry powder inhalers) (Paul et al., 2007). The use of single polymeric material for medical applications makes it difficult to fulfill all requirements needed for an ideal medical ingredient. Hence, combination of polymers is required to achieve all ideal requirements for any formulation, giving the role and use of biocomposites a bright future.

---

## 6.6 CONCLUSION

Use of single polymeric materials for medical applications makes it difficult to fulfill all requirements for an ideal medical ingredient. Hence, various studies on use of composites in medical applications are ongoing, in which the thermomechanical properties of polymers are modified by combining with reinforcing elements. With time, the use of biodegradable polymers as composites in medical applications has gained more popularity as compared with nonbiodegradable ones because of their resorbable property. The most commonly used resorbable polymers include polylactic acid, silk, and collagen, which are reinforced by different elements to get desired thermomechanical properties, Young's moduli, tensile strength, etc. This increase in tensile mechanical strength is mainly because of change in polymeric network density and enhancement in cross-linking between both polymeric structures. Formation of bundles of polymeric fibers may also be a reason for these enhanced thermomechanical properties. Such biodegradable composite preparations can also be considered as better alternatives for biomedical applications, particularly sustained release of various biomolecules like gene delivery, protein peptide delivery, DNA delivery, enzymes delivery, vaccines delivery, drug molecules delivery, etc., with their enhanced thermal stability.

## REFERENCES

- Akiyama, H., 1995. Composite material of bioabsorptive plastic and collagen. JPH07236688A.
- Al-Azzawi, I.S., Koraitim, M.M., 2014. Urethral and penile war injuries, the experience from civil violence in Iraq. *Arab. J. Urol.* 122, 149–154.
- Alvarez, G.S., Echazu, M.I., et al., 2015. Synthesis and characterization of ibandronate-loaded silica nanoparticles and collagen nanocomposites. *Curr. Pharm. Biotechnol.* 167, 661–667.
- Asti, A., Gioglio, L., 2014. Natural and synthetic biodegradable polymers, different scaffolds for cell expansion and tissue formation. *Int. J. Artif. Organs.* 373, 187–205.
- Ayala, P., Caves, J., et al., 2015. Engineered composite fascia for stem cell therapy in tissue repair applications. *Acta Biomater.* 26, 1–12.
- Barari, B., Omrani, E., et al., 2016. Mechanical, physical and tribological characterization of nano-cellulose fibers reinforced bioepoxy composites, an attempt to fabricate and scale the ‘Green’ composite. *Carbohydr. Polym.* 147, 282–293.
- Barbara, P.C., So, K., 2006. Photochemically crosslinked collagen scaffolds and methods for their preparation. WO2006029571A1.
- Barth, J., Akritopoulos, P., et al., 2016. Efficacy of osteoconductive ceramics in bioresorbable screws for anterior cruciate ligament reconstruction, a prospective intrapatient comparative study. *Orthop. J. Sports Med.* 45, 2325967116647724.
- Battegazzore, D., Bocchini, S., Frache, A., 2011. Crystallization kinetics of poly(lactic acid)-talc composites. *eXPRESS Polym. Lett.* 10, 849–858.
- Benali, S., Farid, K., Djahida, L., Rosica, M., Youssef, H., Driss, L., et al., 2018. Supramolecular approach for efficient processing of polylactide/starch nanocomposites. *ACS Omega* 3 (1), 1069–1080.
- Birgit, B., Dorgan, J.R., Knauss, D.M., 2006. Reactively compatibilized cellulosic polylactide microcomposites. *J. Polym. Environ.* 14, 49–58.
- Boonkong, W., Petsom, P., et al., 2013. Rapidly stopping hemorrhage by enhancing blood clotting at an opened wound using chitosan/poly(lactic acid)/polycaprolactone wound dressing device. *J. Mater. Sci. Mater. Med.* 246, 1581–1593.
- Brasinika, D., Tsigkou, O., et al., 2016. Bioinspired synthesis of hydroxyapatite nanocrystals in the presence of collagen and l-arginine, candidates for bone regeneration. *J. Biomed. Mater. Res. B Appl. Biomater.* 1043, 458–469.
- Brunelle, J., Siegel, J., Nguyen, C., Yantzer, B., Sander, T., 2009. Composite implant for surgical repair. US 2009/0018655A1.
- Caliari, S.R., Weisgerber, D.W., et al., 2012. The influence of collagen-glycosaminoglycan scaffold relative density and microstructural anisotropy on tenocyte bioactivity and transcriptomic stability. *J. Mech. Behav. Biomed. Mater.* 11, 27–40.
- Charles, E.B., 2003. Composite material for wound repair. US 2003/0225355A1.
- Chen, J., Sheu, A.Y., et al., 2014. Polylactide-co-glycolide microspheres for MRI-monitored transcatheter delivery of sorafenib to liver tumors. *J. Control. Release* 184, 10–17.
- Chen, W.C., Chen, C.L.K., et al., 2016. Comparison and preparation of multilayered polylactic acid fabric strengthen calcium phosphate-based bone substitutes for orthopedic applications. *J. Artif. Organs* 191, 70–79.
- Collagen based composite sponge and production thereof. CN1406632A, 2003.

- Copinet, A., Bertrand, C., Longieras, A., Coma, V., Couturier, Y., 2003. Photodegradation and biodegradation study of a starch and polylactic acid coextruded material. *J. Polym. Environ.* 11, 4.
- David, H.S., 2000. Collagen-polymer matrices with differential biodegradability. US6110484A.
- Dehghani, F., Weiss, A., Wei, H., Mithieux, S., Fathi, A., 2013. A peptide hydrogel composite WO2013091001A1.
- Del Campo, R., Savoini, B., et al., 2016. Processing and mechanical characteristics of magnesium-hydroxyapatite metal matrix biocomposites. *J. Mech. Behav. Biomed. Mater.* 69, 135–143.
- DiVito, M.D., Rudisill, S.G., et al., 2012. Silica hybrid for corneal replacement, optical, biomechanical, and ex vivo biocompatibility studies. *Invest. Ophthalmol. Vis. Sci.* 5313, 8192–8199.
- Douglas, R.M., Ian, R. Tizard, J.T., Keeton, J.F., 2003. Prochaska System for polymerizing collagen and collagen composites in situ for a tissue compatible wound sealant, delivery vehicle, binding agent and/or chemically modifiable matrix. US6,509, 031 B1.
- Du, M., Guo, B., Jia, D., 2010. Newly emerging applications of halloysite nanotubes, a review. *Polym. Int.* 59, 574–582.
- Eğri, S., Eczacıoğlu, N., 2017. Sequential VEGF and BMP-2 releasing PLA-PEG-PLA scaffolds for bone tissue engineering: I. Design and in vitro tests. *Artif. Cells Nanomed Biotechnol* 45 (2), 321–329.
- Francis, V.L., Richard C.K., Ronald S.H., 2003. Immobilized bioactive hydrogel matrices as surface coatings. US 2003/0232198 A1.
- Fu, J.H., Zhao, M., et al., 2017. Degradable chitosan-collagen composites seeded with cells as tissue engineered heart valves. *Heart Lung Circ.* 261, 94–100.
- Fukushima, K., Fina, A., Geobaldo, F., Venturello, A., Camino, G., 2012. Properties of polylactic acid nanocomposites based on montmorillonite, sepiolite and zirconium phosphonate. *eXPRESS Polym. Lett.* 11, 914–926.
- Gholizadeh, S., Moztaizadeh, F., et al., 2017. Preparation and characterization of novel functionalized multiwalled carbon nanotubes/chitosan/beta-glycerophosphate scaffolds for bone tissue engineering. *Int. J. Biol. Macromol* 97, 365–372.
- Greenspan, D.C., Katta, S., 2011. Devices and methods for the regeneration of bony defects. US 2011/0217388 A1.
- Guner, S.N., Dericioglu, A.F., 2016. Nacre-mimetic bulk lamellar composites reinforced with high aspect ratio glass flakes. *Bioinspir. Biomim.* 121, 016002.
- Gurumurthy, B., Bierdeman, P.C., et al., 2016. Composition of elastin like polypeptide-collagen composite scaffold influences in vitro osteogenic activity of human adipose derived stem cells. *Dent. Mater.* 3210, 1270–1280.
- Hami, Z., Rezayat, S.M., Gilani, K., Amini, M., Ghazi Khansari, M., 2017. In vitro cytotoxicity and combination effects of the docetaxel conjugated and doxorubicin conjugated poly (lactic acid) poly (ethylene glycol) folate based polymeric micelles in human ovarian cancer cells. *J. Pharm. Pharmacol.* 69 (2), 151–160.
- Han, B., Nimni, M.E., Monica, S., 2012. Composite containing collagen and elastin as a dermal expander and Tissue filler. US2012/0010146 A1.
- Hanemann, T., Szabó, D.V., 2010. Polymer-nanoparticle composites, from synthesis to modern applications. *Materials* 3, 3468–3517.
- Helen, H.L., Jeffrey, S., Kathie, D., 2006. Multi-phased, biodegradable osteointegrative composite scaffold for biological fixation of musculoskeletal soft tissue to bone. US 2006/0067969 A1.

- Hirofumi, Y., Masayuki, I., Yoshio, S., Katsuaki, O., Masato, S., 2007. Glycosaminoglycan/collagen complexes and use thereof. US7,226,611 B2.
- Hong, L., Krishnamachari, Y., et al., 2011. Intracellular release of 17-beta estradiol from cationic polyamidoamine dendrimer surface-modified poly lactic-co-glycolic acid microparticles improves osteogenic differentiation of human mesenchymal stromal cells. *Tissue Eng. Part C Methods* 173, 319–325.
- Hu, J.X., Ran, J.B., et al., 2016. Carboxylated agarose CA-silk fibroin SF dual confluent matrices containing oriented hydroxyapatite HA crystals, biomimetic organic/inorganic composites for tibia repair. *Biomacromolecules* 177, 2437–2447.
- Huang, J.W., Hung, Y.C., Wen, Y.L., Kang, C.C., Yeh, M.Y., 2009. Polylactide/nano and microscale silica composite films. I. Preparation and characterization. *J. Appl. Polym. Sci.* 112, 1688–1694.
- Huston, D.A., 2006. Cartilage composites and methods of use. US7,087,227 B2.
- Idrovo Encalada, A.M., Basanta, M.F., et al., 2016. Carrot fiber CF composite films for antioxidant preservation, particle size effect. *Carbohydr. Polym.* 136, 1041–1051.
- Iliut, M., Silva, C., et al., 2016. Graphene and water-based elastomers thin-film composites by dip-moulding. *Carbon N.Y.* 106, 228–232.
- Ioannis, V.Y., Philip, L.G., Chor, H., Frederick, H.S., John, F.B., 1981. Cross-linked collagen-mucopolysaccharide composite materials. US4,280,954.
- Iqbal, Q., Bernstein, P., et al., 2015. Quantitative analysis of mechanical and electrostatic properties of polylactic acid fibers and polylactic acid-carbon nanotube composites using atomic force microscopy. *Nanotechnology* 2610, 105702.
- Itoh, S., Kikuchi, M., et al., 2004. Development of a hydroxyapatite/collagen nanocomposite as a medical device. *Cell Transpl.* 134, 451–461.
- Jackie, Y.Y., Tseh-Hwan, Y., 2007. Composite materials for controlled release of water soluble products. US7,211,275 B2.
- Jain, D.S., Bajaj, A.N., et al., 2016. Thermosensitive PLA based nanodispersion for targeting brain tumor via intranasal route. *Mater. Sci. Eng. C Mater. Biol. Appl.* 63, 411–421.
- James, R.J., Jeffrey, G.M., Wesley, D.J., 2003. Bone substitutes. US6,527,810 B2.
- Jog, R., Burgess, D.J., 2017. Pharmaceutical amorphous nanoparticles. *J. Pharm. Sci.* 1061, 39–65.
- Junzo, T., Masanori, K., Noriichi, I., Yoshinobu, M., 2005. Organic/inorganic composite biomaterials and process for producing the same. US2005/0053638A1.
- Kaewprapan, K., Phattanasuddee, S., 2012. Synthesis and characterization of polylactic acid/montmorillonite nanocomposites by *in situ* polycondensation catalyzed by non-metal-based compound. *J. Nanosci. Nanotechnol.* 121, 781–786.
- Kamyar, S., Bin Ahmad, M., Yunus, W.M.Z.W., Ibrahim, N.A., Jokar, M., Darroudi, M., 2010. Silver/poly lactic acid nanocomposites, preparation, characterization, and antibacterial activity. *Int. J. Nanomed.* 5, 573–579.
- Kanda, N., Matsui, K., et al., 2016. Implantation of octacalcium phosphate collagen composites OCP/Col after extraction of canine deciduous teeth achieved undisturbed permanent tooth eruption. *Arch. Oral. Biol.* 72, 179–186.
- Karimi, S., Abdulkhani, A., et al., 2016. Effect of cellulosic fiber scale on linear and non-linear mechanical performance of starch-based composites. *Int. J. Biol. Macromol.* 91, 1040–1044.

- Karl, A.P., Bruce, B.P., George, H.C., Thomas, L.S., Diana, H., 1995. Calcium phosphate/atelo peptide collagen compositions for bone repair. US5,425,770A.
- Kim, H.K., Park, T.G., 2004. Comparative study on sustained release of human growth hormone from semi-crystalline poly-L-lactic acid and amorphous poly(D,L-lactic-co-glycolic acid) microspheres, morphological effect on protein release. *J. Control. Release* 981, 115–125.
- Kim, I.H., Jeong, Y.G., 2010. Polylactide/exfoliated graphite nanocomposites with enhanced thermal stability, mechanical modulus, and electrical conductivity. *J. Polym. Sci. Part B Polym. Phys.* 48, 850–858.
- Kim, O.V., Litvinov, R.I., Chen, J., Chen, D.Z., Weisel, J.W., Alber, M.S., 2017. Compression-induced structural and mechanical changes of fibrin-collagen composites. *Matrix Biol.* 60, 141–156.
- Kim, V., Litvinov, I., Weisel, W., Alber, S., 2016. Compressive mechanics of collagen-fibrin composites and their structural alterations. Supplement 1. 110, 338.
- Laurie, B.G., Matthew, J.O., Elliot P.D., Sivakumar M., Donna, L.W., 2004. Biomimetic organic/inorganic composites, processes for their production, and methods of use US 2004/0131562 A1.
- Lazar, M.A., Rotaru, H., et al., 2016. Evaluation of the biocompatibility of new fiber-reinforced composite materials for craniofacial bone reconstruction. *J. Craniofac. Surg.* 277, 1694–1699.
- Lewandowska, K., Sionkowska, H., et al., 2016. Surface and thermal properties of collagen/hyaluronic acid blends containing chitosan. *Int. J. Biol. Macromol.* 92, 371–376.
- Lih, E., Park, K.W., et al., 2016. Biomimetic porous PLGA scaffolds incorporating decellularized extracellular matrix for kidney tissue regeneration. *ACS Appl. Mater. Interfaces* 833, 21145–21154.
- Liu, S., Li, H., et al., 2017. Preparation and properties of *in situ* growth of carbon nanotubes reinforced hydroxyapatite coating for carbon/carbon composites. *Mater. Sci. Eng. C Mater. Biol. Appl.* 70Pt (1), 805–811.
- Lu, J., Hou, R., et al., 2015. Development and characterization of drug-loaded biodegradable PLA microcarriers prepared by the electrospraying technique. *Int. J. Mol. Med.* 361, 249–254.
- Lynch, H.A., Johannessen, W., et al., 2003. Effect of fiber orientation and strain rate on the nonlinear uniaxial tensile material properties of tendon. *J. Biomech. Eng.* 125, 726–731.
- Maghaireh, G.A., Taha, N.A., et al., 2017. The silorane-based resin composites, a review. *Oper. Dent.* 421, E24–E34.
- Marney, D.C.O., Russell, L.J., Wu, D.Y., Nguyen, T., Cramm, D., Rigopoulos, N., et al., 2008. The suitability of halloysite nanotubes as a fire retardant for nylon 6. *Polym. Degrad. Stabil.* 93, 1971–1978.
- McNally-Heintzelman, K.M., Heintzelman, D.L., Bloom, J.N., Duffy, M.T., 2004. Light activated adhesive composite system, and methods of use thereof. US 2004/0236371 A1.
- McNally-Heintzelman, K.M., Heintzelman, D.L., Bloom, J.N., Duffy, M.T., 2005. Non-light activated adhesive composite, system, and methods of use thereof. US 2005/0004599 A1.
- Michaeli, D., 1978. Pharmaceutical compositions for the enhancement of wound healing. EP0230023A2.
- Morin, A., Alam, P., 2016. Comparing the properties of *Bombyx mori* silk cocoons against sericin-fibroin regummed biocomposite sheets. *Mater. Sci. Eng. C Mater. Biol. Appl.* 65, 215–220.

- Nataraj, C., Ritter, G., Sander, T., 2007. Stabilized, sterilized collagen scaffolds with active adjuncts attached. US 2007/0218038A1.
- Nouri, L., Bendjama, Z., et al., 2015. Optimization of a novel biocomposite synthesis Ammi Visnaga extraction waste/alginate for Cd<sup>2+</sup> biosorption. *Int. J. Biol. Macromol.* 80, 588–595.
- Oksman, K., Mathew, A.P., Bondeson, D., Kvien, I., 2006. Manufacturing process of cellulose whiskers/polylactic acid nanocomposites. *Compos. Sci. Technol.* 66, 2776–2784.
- Patterson, B.A., Sodano, H.A., 2016. Enhanced interfacial strength and UV shielding of aramid fiber composites through ZnO nanoparticle sizing. *ACS Appl. Mater. Interfaces* 849, 33963–33971.
- Paul, M., Daniela, T., Matthew, C., Hak, C., 2007. Recent advances in understanding the influence of composite-formulation properties on the performance of dry powder inhalers. *Phys. B Condensed Matter.* 394, 315–319.
- Peter, I.L., Li, M., Mark M., Ko, F., 2006. Electrospun blends of natural and synthetic polymer fibers as tissue engineering scaffolds. US 2006/0263417 A1.
- Qi, Y., Xiong, W., et al., 2015. Experimental study of the flexural and compression performance of an innovative pultruded glass-fiber-reinforced polymer-wood composite profile. *PLoS One* 1010, e0140893.
- Raghunath, S., Kumar, S., et al., 2018. PLA/ESO/MWCNT nanocomposite: a study on mechanical, thermal and electroactive shape memory properties. *J. Polym. Res.* 25, 120–126.
- Richard, M.D., 2006. Bioactive material for use in stimulating vascularization. US 2006/0233887 A1.
- Richard, A.B., Frederick, H.S., James, M.P., John, D'A., 1989. Collagen matrix/polymer film Composite dressing. US 4,841,962.
- Rodrigues, M.C., Xavier, T.A., Arana-Chavez, V.E., Braga, R.R., 2017. Polymer-based material containing calcium phosphate particles functionalized with a dimethacrylate monomer for use in restorative dentistry. *J. Biomater. Appl.* 31 (6), 871–877. 2017.
- Saini, P., Arora, M., et al., 2016. Polylactic acid blends in biomedical applications. *Adv. Drug Deliv. Rev.* 107, 47–59.
- Salerno, A., Guarino, V., et al., 2016. Bio-safe processing of polylactic-co-caprolactone and polylactic acid blends to fabricate fibrous porous scaffolds for in vitro mesenchymal stem cells adhesion and proliferation. *Mater. Sci. Eng. C Mater. Biol. Appl.* 63, 512–521.
- Salimi, K., Yilmaz, M., et al., 2014. Controlled graft copolymerization of lactic acid onto starch in a supercritical carbon dioxide medium. *Carbohydr. Polym.* 114, 149–156.
- Saravanan, S., Leena, R.S., et al., 2016. Chitosan based biocomposite scaffolds for bone tissue engineering. *Int. J. Biol. Macromol.* 93 (Pt B), 1354–1365.
- Shao, W., He, J., et al., 2016. Coaxial electrospun aligned tussah silk fibroin nanostructured fiber scaffolds embedded with hydroxyapatite-tussah silk fibroin nanoparticles for bone tissue engineering. *Mater. Sci. Eng. C Mater. Biol. Appl.* 58, 342–351.
- Sheik, E.N., Mandyam, D.R., Radhakrishnan, G., Bhabendra, N.D., Ummadisetty, V., Chellan R., et al., 2004. Process for preparing a chemically modified fibrin-fibrillar protein (FFP) composite sheet. US2004/0124564A1.
- Sheila, J.K., Matthew, F.O., 2003. Composite biocompatible matrices. US 2003/0118560 A1.
- Shinichi, S., Toshimasa U., Junzo T., Kenichi S., Tetsuya T., 2006. Composite biomaterials. US 2006/0172918 A1.



- Slivka, M.A., Chu, C.C., et al., 1997. Fiber-matrix interface studies on bioabsorbable composite materials for internal fixation of bone fractures. I. Raw material evaluation and measurement of fiber-matrix interfacial adhesion. *J. Biomed. Mater. Res.* 364, 469–477.
- Smith, R.L., Laurence J.B.T., Akihiko K., Hans P., 2007. Ingemar Claesson, cell-support matrix having Narrowly defined uniformly vertically and non-randomly organized porosity and pore. US 2007/0065943 A1.
- Spitalsky, Z., Tasis, D., Papagelis, K., Galiotis, C., 2010. Carbon nanotube–polymer composites, chemistry, processing, mechanical and electrical properties. *Progress Polym. Sci.* 35, 357–401.
- Stloukal, P., Pekarova, S., et al., 2015. Kinetics and mechanism of the biodegradation of PLA/clay nanocomposites during thermophilic phase of composting process. *Waste Manage.* 42, 31–40.
- Stojanovic, Z.S., Ignjatovic, N., et al., 2016. Hydrothermally processed 1D hydroxyapatite, Mechanism of formation and biocompatibility studies. *Mater. Sci. Eng. C Mater. Biol. Appl.* 68, 746–757.
- Suh, D.H., Lee, S.J., et al., 2014. The safety and efficacy of poly-L-lactic acid on sunken cheeks in Asians. *J. Cosmet. Laser. Ther.* 164, 180–184.
- Torres, F.G., Commeaux, S., et al., 2012. Biocompatibility of bacterial cellulose based biomaterials. *J. Funct. Biomater.* 34, 864–878.
- Vollrath, F., 2000. Strength and structure of spiders' silks. *J. Biotechnol.* 742, 67–83.
- Wada, H., 2016. Structural mechanics and helical geometry of thin elastic composites. *Soft Matter.* 1235, 7386–7397.
- Wang, G., Hu, X., et al., 2011. Electrospun PLGA-silk fibroin-collagen nanofibrous scaffolds for nerve tissue engineering. *In Vitro Cell Dev. Biol. Anim.* 473, 234–240.
- Wang, X., Helary, C., et al., 2015. Local and sustained gene delivery in silica-collagen nanocomposites. *ACS Appl. Mater. Interfaces* 74, 2503–2511.
- Wang, S., Zhao, X., et al., 2016. Biologically inspired polydopamine capped gold nanorods for drug delivery and light-mediated cancer therapy. *ACS Appl. Mater. Interfaces* 837, 24368–24384.
- Wang, J., Fang, F., Yuan, T., Yang, J., Chen, L., Yao, C., Sun, D., 2017a. Three-dimensional graphene/single-walled carbon nanotube aerogel anchored with SnO<sub>2</sub> nanoparticles for high performance lithium storage. *ACS Appl. Mater. interfaces* 9 (4), 3544–3553.
- Wang, K., Wang, W., et al., 2017b. Mechanical properties and solubility in water of corn starch-collagen composite films, effect of starch type and concentrations. *Food Chem.* 216, 209–216.
- Wen, X., Zhang, K., Wang, Y., Han, L., Han, C., Zhang, H., et al., 2011. Study of the thermal stabilization mechanism of biodegradable poly(l-lactide)/silica nanocomposites. *Polym. Int.* 60, 202–210.
- Williams, M., Jezior, J., 2013. Management of combat-related urological trauma in the modern era. *Nat. Rev. Urol.* 109, 504–512.
- Wu, D., Wu, L., Zhang, M., Zhao, Y., 2008. Viscoelasticity and thermal stability of polylactide composites with various functionalized carbon nanotubes. *Polym. Degrad. Stabil.* 93, 1577–1584.
- Wu, D., Wu, L., Zhou, W., Sun, Y., Zhang, M., 2010a. Relations between the aspect ratio of carbon nanotubes and the formation of percolation networks in biodegradable polylactide/carbon nanotube composites. *J. Polym. Sci. Part B Polym. Phys.* 48, 479–489.

- Wu, D., Wu, L., Zhou, W., Zhang, M., Yang, T., 2010b. Crystallization and biodegradation of polylactide/carbon nanotube composites. *Polym. Eng. Sci.* 50, 1721–1733.
- Xie, W., Tadepalli, S., Park, S.H., Kazemi, M.A., Jiang, Q., Lee, J.H., et al., 2018. Extreme mechanical behavior of nacre-mimetic graphene-oxide and silk nanocomposites. *Nano Lett.* 18 (2), 987–993.
- Yan, D., Zhao, H., et al., 2017. The rational designed graphene oxide-Fe<sub>2</sub>O<sub>3</sub> composites with low cytotoxicity. *Mater. Sci. Eng. C Mater. Biol. Appl.* 72, 659–666.
- Yang, C.L., Chen, J.H., Tsai, S.W., Shih, H.N., Shih, L.Y., 2006. Methods for producing cross-linked hyaluronic acid-protein bio-composites. US 2006/0189516 A1.
- Yi, M., Sun, H., et al., 2016. Flexible fiber-reinforced composites with improved interfacial adhesion by mussel-inspired polydopamine and polymethyl methacrylate coating. *Mater. Sci. Eng. C Mater. Biol. Appl.* 58, 742–749.
- Yves, B., Sébastien, L., Olivier, L., Philippe G., 2011. Medical implant including a 3d Mesh of oxidized cellulose and a collagen sponge. US2011/0264119 A1.
- Zhang, J., Wang, J., et al., 2016a. Noncontact detection of Teflon inclusions in glass-fiber-reinforced polymer composites using terahertz imaging. *Appl. Opt.* 5536, 10215–10222.
- Zhang, L., Shan, X., et al., 2016b. Process and microstructure to achieve ultra-high dielectric constant in ceramic-polymer composites. *Sci. Rep.* 6, 35763.
- Zhong, T., Deng, C., et al., 2012. Studies of *in situ*-forming hydrogels by blending PLA-PEG-PLA copolymer with silk fibroin solution. *J. Biomed. Mater. Res. A* 1008, 1983–1989.
- Zhou, H., Lawrence, J.G., et al., 2012. Fabrication aspects of PLA-CaP/PLGA-CaP composites for orthopedic applications, a review. *Acta Biomater.* 86, 1999–2016.
- Zhou, J.F., Wang, Y.G., et al., 2016. Preparation of polypyrrole-embedded electrospun polylactic acid nanofibrous scaffolds for nerve tissue engineering. *Neural Regen. Res.* 1110, 1644–1652.
- Zhu, B., Li, W., et al., 2015. E-spun composite fibers of collagen and dragline silk protein, fiber mechanics, biocompatibility, and application in stem cell differentiation. *Biomacromolecules* 161, 202–213.

# Possibilities and perspectives of chitosan scaffolds and composites for tissue engineering

**Manish Kumar<sup>1</sup>, Amandeep Brar<sup>1</sup>, V. Vivekanand<sup>2</sup> and Nidhi Pareek<sup>1</sup>**

<sup>1</sup>*Department of Microbiology, School of Life Sciences, Central University of Rajasthan Bandarsindri, Kishangarh, India* <sup>2</sup>*Centre for Energy and Environment, Malaviya National Institute of Technology, Jaipur, India*

## 7.1 INTRODUCTION

Over the last three decades, tissue engineering has drawn much attention from researchers in diverse disciplines, for example, biology, medicine, engineering, and material sciences, for the treatment of damaged or lost human tissue and organs. Tissue engineering can be defined as the exploitation of biological, chemical, and engineering principles in the repair, restoration, and regeneration of living tissues using biomaterials, cells, and factors alone or in combination. One of the important challenges in the field of tissue engineering is the development of the suitable biodegradable materials and scaffolds for cell seeding and tissue growth. The challenge can be accomplished by the employment of natural biopolymer for fabrication of scaffolds and composites for tissue engineering (Nwe et al., 2009).

Scaffolds are used to support the tissue or organ in their damage recovery or regeneration. In the present era of tissue engineering, scaffold and composite based tissue engineering is one of the well-studied approaches. Scaffolds or composites serve as structural support and initial temporary extracellular matrix (ECM) for cells to adhere, proliferate, differentiate, and mature. Additionally, the scaffolds may act as a carrier for bioactive molecules, growth factors, and cells to heal the defect. After tissue generation in the scaffold matrix, the matrix degrades gradually to complete the healing process. Biomaterials are required to have certain properties to be exploited for medical applications, for example, material chemistry, molecular weight, solubility, lubricity, surface energy, water absorption, degradation, and erosion. Development of polymeric scaffolds is of prime concern due to their high surface-to-volume ratio, high porosity with very small pore size, biodegradation and mechanical properties (Dhandayuthapani et al., 2011). In this regard, the natural bioactive polymers have been proved as novel

assets as they possess the properties of an ideal tissue engineering scaffolds, that is, the scaffold should degrade in a controlled manner to match the natural ECM formation, can gradually transfer the structural and functional roles to the newly formed tissue, and finally can be easily resorbed and metabolized (Jiang et al., 2012). Various classes of the natural bioactive polymers, that is, proteins (silk, collagen, gelatin, fibrinogens, elastin, keratin, actin, and myosin), polysaccharides (cellulose, amylose, dextran, chitin, and glycosaminoglycans), and polynucleotides (DNA, RNA) (Dhandayuthapani et al., 2011) have been explored to produce potential biodegradable matrices for tissue engineering. Among the natural polymers, chitosan, that is, the deacetylated product of chitin has shown enormous potentiality in tissue engineering as a scaffold material.

Chitosan is the deacetylated form of chitin with degree of deacetylation (DD) more than 50% and soluble in aqueous acidic media. It is a semicrystalline polymer in solid state. Being biocompatible, biodegradable, renewable, and with the ability to be molded into different forms, chitosan has been exploited for a wide range of biomedical applications, for example, antimicrobial, immunologic, antitumoral, hemostatic, anticoagulant, hypocholesterolemic, healing, and drug delivery. In the human body, chitosan can be degraded by the hydrolytic activity of the enzyme lysozyme, present in the body fluid. Degradability of chitosan is greatly determined by its DD, molecular weight, and crystallinity. The nontoxic nature of chitosan makes it cytocompatible, which results in better cell adhesion and proliferation. Chitosan also shows excellent processability, and can be easily fabricated into different forms, for example, films, sponges, microspheres, nanofibers, hydrogels, etc. (Dash et al., 2011).

Large numbers of chitosan scaffolds have been prepared for clinical use to repair and regenerate lost or damaged tissue and organs. These scaffolds are prepared from different types of fabrication techniques, for example, freeze-gelation, lyophilization, phase separation, and electrospinning. Each fabrication process is utilized to synthesize the desired chitosan scaffold on the basis of their specific utilization. Currently, plenty of research is going on to improve the properties of chitosan scaffolds to enhance their applicability in the tissue engineering. This includes the combination of other natural and synthetic polymers, incorporation of nanoparticles, and growth factors. Biomedical researchers have gained progress in the utilization of chitosan membranes for development of wound healing and wound dressing materials, for example, IDRA hydrogel. Scant amount of literature is available on employment of chitosan scaffolds for repair and regeneration of the liver and nerve tissues. Utilization of chitosan scaffolds for bone tissue repair has also gaining increased attention of the researchers. In the bone tissue engineering, there are three key ingredients: (1) harvested cells, (2) recombinant signaling molecules, and (3) three-dimensional matrices. The three-dimensional matrices, that is, scaffolds promote and direct the growth of the new bone cells and facilitate the attachment of new cells to intrinsic tissues by degrading slowly and growing afterward (Jamalpoor, 2015). Additionally, researchers are also exploring the ability of chitosan scaffolds and composites for drug delivery and gene therapy.

In this decade, significant advances have been made in the employment of chitosan scaffolds for biomedical applications. The advancement has not only been limited to the improvement of the biological properties of chitosan-based scaffolds but also in the fabrication techniques along with the applications in the biomedical sector. The chapter is intended to illustrate various chitosan scaffolds and composites in the field of tissue engineering and regenerative medicine. The chapter presents a detailed review on the commonly used scaffold fabrication techniques, different forms of chitosan scaffolds used in tissue engineering, as well as the latest development in the application of the chitosan scaffolds.

---

## 7.2 SCAFFOLD

In the present era of tissue engineering and regenerative medicine research, scaffolds have proven to be an important asset. Scaffolds are commonly made up of polymeric biomaterials, which provide a structural support for cell attachment and subsequent development. Scaffolds perform a range of vital functions: (1) promoting cell–biomaterial interactions, cell adhesion and ECM deposits; (2) permitting the sufficient transport of gases, nutrients, and regulatory factors for cell survival, proliferation, and differentiation; (3) breaking down at a controllable rate that is close to the regeneration rate of tissue of interest; and (4) creating minimal inflammation (Rodríguez-Vázquez et al., 2015; Langer and Tirrell, 2004). Scaffolds meet the above functional demands of tissue engineering and regenerative medicine due to their mechanical and biological properties, for example, pore size, water absorption, sensitivity to lysozyme degradation, mechanical strength, and cellular activities. To attain the requirements of an ideal scaffold a polymer should not induce acute or chronic response, should be biodegradable, possess surface properties for cell attachment, should have suitable mechanical properties for handling, can be manufactured into variety of forms, and should have ability to mimic the damaged tissue (Wei and Ma, 2004; Croisier and Jérôme, 2013).

Dhandayuthapani et al. (2011) proposed various characteristics required for the fabrication of scaffold into six major groups. These are as follows:

1. External geometry. This is mainly related to the physical characteristics (macrostructure and microstructure) and interconnectivity that helps to mimic the ECM. The mimicking of ECM using biomaterials is the most promising approach for scaffold based tissue engineering.
2. Surface properties, which include chemical as well as topographical characteristics that help in controlling the cellular adhesion and proliferation. The surface properties of the scaffold can be modified to enhance the biomaterial performance.
3. Porosity and pore size. Average pore size, pore size distribution, pore volume, pore interconnectivity, pore shape, and pore wall roughness are the imperative parameters in scaffold design. These parameters deliver a biocompatible

network into which the adjacent tissue is induced and act as a temporary template for tissue regeneration.

4. Biocompatibility, which refers to the ability of a biomaterial to accomplish its desired roles without causing any uninvited local or systemic effects in the host.
5. Degradation rate; scaffold should degrade by programmed period to be replaced by newly grown tissue from the adhered cells.
6. Mechanical properties. Tissue scaffold must have appropriate mechanical properties in term of strength, elasticity, adsorption, and chemical degradation for the rapid generation. The aforementioned novel scaffold material assets can be accomplished by chitosan, a biocompatible and biodegradable natural polymer.

### 7.3 CHITOSAN

Chitosan is a partially deacetylated product of chitin, which is found abundantly in invertebrates, fungi, and yeast. Chitosan is composed of (1 → 4)-2-acetamido-2-deoxy-β-D-glucan (*N*-acetyl-D-glucosamine) and (1 → 4)-2-amino-2-deoxy-β-D-glucan (D-glucosamine) subunits arranged in a linear fashion. The overall process of conversion of chitin into chitosan includes critical steps like deproteinization, demineralization, decoloration, and deacetylation. The difference between the chemical structure of chitin and chitosan as well as the summarized production process of chitosan can be easily understood via Fig. 7.1. Molecular weight of chitosan varies from 300 to >1000 kDa with a deacetylation between 30% and

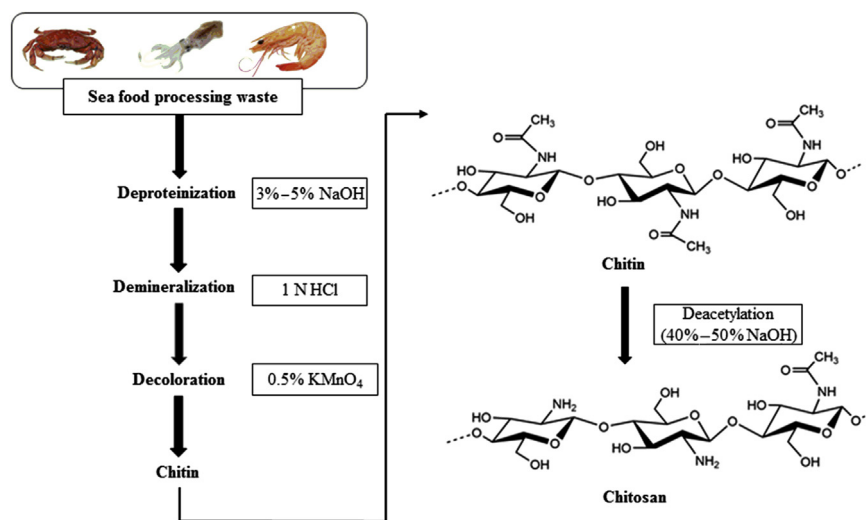


FIGURE 7.1

Preparation of chitin and chitosan.

95% (Rodríguez-Vázquez et al., 2015). This large extent of range is owing to the variations in the origin and procedure of preparations. The amount of deacetylation largely depends upon the manufacturing process conditions. Chitosan is a highly reactive polysaccharide due to its functionality provided by amino group and hydroxyl group. The free amino group in the polymer chain provides a free positive charge to chitosan and also determines the DD. This positive charge enables chitosan to interact with diverse negatively charged molecules. Other characteristics, for example, biodegradability, reactivity, solubility, and absorption are impacted by the amount of protonated amino groups in the polymer chain. Due to these properties, chitosan has wide applications in the medical field, for example, as wound dressing (Stephen-Haynes et al., 2014), blood anticoagulant (Balan and Verestiuc, 2014), hypocholesterolemic agent (Dash et al., 2011), and antithrombogenic and drug delivery systems (Kumar, 2000). In addition, chitosan has found applications in various other fields, for example, wastewater treatment (Liu and Bai, 2014), food and feed additives (Luo and Wang, 2013), cosmetics (Jimtaisong and Saewan, 2014), and textiles (Vakili et al., 2014).

---

## 7.4 CHITOSAN AS BIOMATERIAL: PROPERTIES

Chitosan has several remarkable properties that offer unique opportunities for biomedical applications. These properties include biodegradability, antimicrobial activity, porosity, water absorption capacity, etc., that put together chitosan as one of the most demanding biomaterial of the medical and pharmaceutical sectors.

### 7.4.1 MUCOADHESIVE

Mucoadhesion is the phenomenon of adhesive attachment between two materials in which one must be a mucus or mucous membrane. The major components of mucus are mucin glycoproteins, lipids, inorganic salts, and water. Mucin is the major structure forming component of mucus membrane, resulting in the characteristic adhesive property (Sogias et al., 2008). In an acidic medium, chitosan amino groups are positively charged and thus can interact with negatively charged residue, that is, sialic acid in mucin. The DD is directly proportional to mucoadhesion; as the chitosan DD increases, the number of positive charge also increases and this results in improved mucoadhesive properties (Dyawanapelly et al., 2016; He et al., 1998). The mechanism behind the formation of mucoadhesive bond depends on the nature of the mucous membrane and mucoadhesive materials, the type of formulation, the attachment process, and the subsequent environment of the bond (Smart, 2005). Mansuri et al. (2016) suggested mucoadhesion as a promising approach in drug delivery. The study reported that the mucoadhesion is affected by mucin turnover rate, molecular weight of the polymer, pH at which polymer substrate interacts, concentration of polymer, flexibility of polymer chains, and the stereochemistry of the polymer. Dyawanapelly et al. (2016)

studied processes to improve the mucoadhesive properties of chitosan and chito-oligosaccharides for mucosal delivery of proteins.

### 7.4.2 HEMOSTATIC

Hemostasis is natural physical response of the body against bleeding or hemorrhage. Chitosan has been reported as a novel hemostatic agent. The hemostatic activity of chitosan is also related to the presence of positive charge on the chitosan backbone. The mechanism of hemostatic effect of chitosan is still not so clear. But on the basis of up-to-date research it can be concluded that the positive charge of chitosan attributes to its hemostatic activity, which allows it to interact with the negatively charged red blood cell membrane (Park et al., 2004; Croisier and Jérôme, 2013). Researchers have suggested three possible ways of controlling bleeding through chitosan: (1) plasma sorption, in which chitosan can absorb up to 300% liquid from its primary weight, resulting in the concentration of erythrocytes and platelets at injured places; (2) erythrocytes coagulation, in which cross-linking of chitosan with erythrocytes results in enhanced erythrocytes coagulation; and (3) platelet adhesion, aggregation, and activation, which is considered as the main reason for hemostatic activity of chitosan. According to this mechanism, chitosan films induce platelet adhesion, aggregation and activation of intrinsic blood coagulation (Fan et al., 2012; Maksym, 2015). Song et al. (2014) reported the preparation of porous hemostatic chitosan sponges using ammonium bicarbonate particles through supercritical fluid technology. The prepared chitosan sponge possesses >90% hemostatic efficiency as compared with the commercially used Avitene. Recently, various researchers reported the applicability of chitosan alone or in combination with other compounds as a hemostatic agent (Crofton et al., 2016; Mao et al., 2016; Feng et al., 2016).

### 7.4.3 ANTIMICROBIAL

Chitosan has been reported to possess remarkable activity against different groups of microorganisms (Oyervides-Muñoz et al., 2017). Several mechanisms have been suggested to explain the antimicrobial action and two of them are widely accepted. According to the first mechanism, the positively charged chitosan interacts with negatively charged group at the cell surface, which results in the alteration of its permeability. This alteration prevents essential materials from entering the cell and/or lead to the leaking of the fundamental solutes out of the cell. On the other hand, the second mechanism proposes that chitosan binds with the cellular DNA via protonated amino groups and results in the inhibition of the microbial RNA synthesis (Martins et al., 2014; Sudarshan et al., 1992). Goy et al. (2016) reported that *N,N,N*-trimethyl chitosan shows antimicrobial activity against both Gram-positive *Staphylococcus aureus* and Gram-negative *Escherichia coli*. They also found that chitosan is more active against the Gram-positive bacteria. Venkatesan et al. (2014) prepared



chitosan–carbon nanotube hydrogels by freeze-drying method. The prepared hydrogel showed greater activity against *S. aureus* and *E. coli* with an increase in the concentration of the chitosan–carbon nanotube. Antimicrobial properties of chitosan have been explored by various researchers (Nesic et al., 2017; Sun et al., 2017; Han et al., 2016; Chien et al., 2016).

#### 7.4.4 BIODEGRADABLE

Applicability of chitosan as an ideal drug delivery agent depends on its metabolic fate in the body or biodegradation (Bernkop-Schnürch and Dünnhaupt, 2012; Felt et al., 1998). Due to its easily biodegradable of chitosan has been the prime concern of biomedicine researchers (Li et al., 2014; Timashev et al., 2016). Chitosan can be degraded by both thermal and enzymatic means. In addition to this, the rate of degradation of the chitosan is inversely proportional to the degree of crystallinity. Chitosan can be degraded by a broad range of hydrolytic enzymes. In vivo chitosan degradation has been reported by proteases and lysozymes (Dash et al., 2011; Kean and Thanou, 2011). Chitinase is also involved in the degradation of chitin up to a certain extent. There are only eight human chitinases that have been identified with three of them having enzymatic activity on chitosan (Funkhouser and Aronson, 2007). The biodegradation of chitosan led to the formation of nontoxic and more medically applicable oligosaccharides (Das et al., 2015; Li et al., 2016).

#### 7.4.5 BIOCOMPATIBLE

A novel biomaterial must be biocompatible (it should not show any adverse reactions when coming into contact with the body) to be utilized in biomedical applications. A biocompatible material must be able to recognize and cooperate with the body, without producing any adverse effects. Chitosan meets with all the demands of a biomaterial. Clinical tests have proven that chitosan does not result in any inflammatory or allergic reactions after implantation, injection, topical application, or ingestion in the human body (Svirshchevskaya et al., 2016; Thorat et al., 2014). The compatibility of chitosan depends on the physiological medium and DD. DD has been observed to be directly proportional to the biocompatibility. The Food and Drug Administration (FDA) has also approved chitosan for use in wound dressings (Chatelet et al., 2001; Wedmore et al., 2006). Remarkable research work has been performed to improve the biological and mechanical properties of chitosan and chitosan-based biomaterials for tissue engineering (Albanna et al., 2013; Gopi et al., 2014; Sámano-Valencia et al., 2014).

The aforementioned properties promote the utilization of chitosan for biomedical and pharmaceutical applications. Chitosan-based scaffolds have been widely explored as potential materials for bone tissue growth, wound healing, and regeneration of skin, bone, and cartilage. The following section of this chapter will focus on the potential application of chitosan scaffold and composites in tissue engineering.

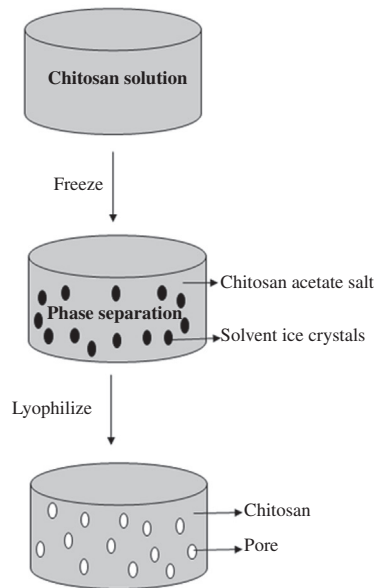
## 7.5 CHITOSAN SCAFFOLD

At present there is a growing demand from tissue and organ substitutes with a rapid reduction in the availability of organs for transplantation, so tissue engineering is providing hope to patients. In this regard, polymeric scaffolds are gaining a lot of attention due to their unique properties such as high surface-to-volume ratio, high porosity with very small pore size, biodegradation, mechanical strength, and biocompatibility. Chitosan scaffolds, being biodegradable and biocompatible, fulfill the required properties for specific tissue engineering applications. Chitosan has been processed into various 3D and 2D scaffolds forms, for example, hydrogels, nanoparticles, beads, bandages, membranes, nanogels, films, and nanofibers (Croisier and Jérôme, 2013; Dhandayuthapani et al., 2011). Various forms of chitosan scaffolds have been investigated in the field of tissue engineering or regenerative medicine with the help of different fabrication techniques like freeze-gelation, electrospinning, phase separation, etc. The major types of fabrication techniques are described diagrammatically through Fig. 7.2. The latest reports in the fabrication of chitosan scaffolds and composites have also been summarized with their tissue application in Table 7.1. These fabrication techniques provide chitosan scaffolds the necessary shape for use in different tissues and organs to serve the healing and regeneration purposes. In the following paragraphs, we are going to discuss the different forms of chitosan scaffolds with their preparation methods.

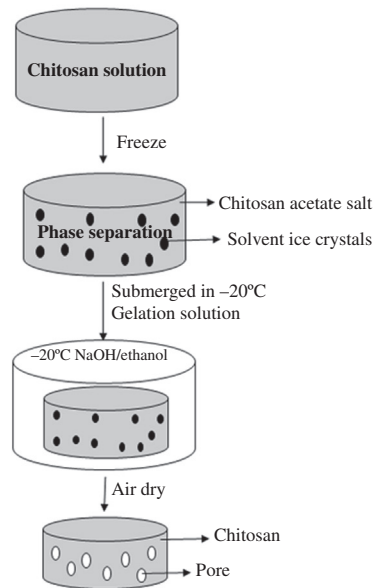
### 7.5.1 CHITOSAN HYDROGEL

Chitosan hydrogels are three-dimensional covalently cross-linked polymer networks consisting of both solid and liquid phase. The solid phase content is less, that is, approximately 10% of the total volume of the hydrogel, and the rest of the volume is water or adjuvants. The solid content of the gel enables it to soak up or absorb large quantities of water. Chitosan hydrogels are degradable, can be processed under mild conditions, and have several mechanical and structural properties similar to many tissues and ECM (Drury and Mooney, 2003). The high water content of hydrogels makes them compatible with living tissues. The viscoelastic nature of hydrogels minimizes the risk of damage to the surrounding host tissues. In addition to these, hydrogels are also able to mimic the functional and morphological characteristics of the damaged tissues (Hoffman, 2012). Chitosan hydrogels forms, for example, either physical association networks or cross-linked networks (Hennink and Van Nostrum, 2012). Nie et al. (2015) constructed the oriented structure of chitosan hydrogel in multilayered form. Chitosan has been observed to play dual roles of the inner electrolyte and supporting medium in the process. Xu et al. (2017) reported the fabrication of self-cross-linking chitosan by using sodium chloride and phosphate buffer saline (pH = 7.4) in the place of strong bases like sodium hydroxide due to the fact that strong bases can affect

### Lyophilization and phase separation



### Freeze gelation



### Electrospinning

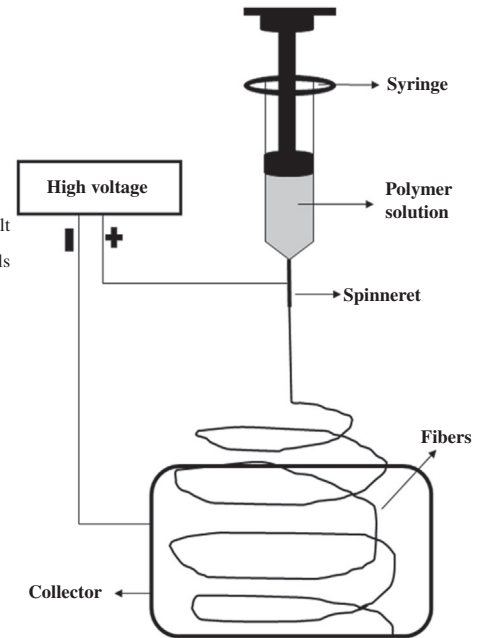


**FIGURE 7.2**

Fabrication techniques for chitosan scaffolds.

**Table 7.1** Chitosan Scaffolds and Composites: Fabrication Techniques and Tissue Applications

Polymer	Fabrication Method	Scaffold Type	Tissue Application	Reference
Chitosan + chitin nanocrystal	Freeze drying	Composite	Bone	Liu et al. (2016a)
Chitosan + poly(ethylene glycol) + ciprofloxacin hydrochloride	Freeze-gelation	Composite	Skin	Sinha et al. (2013)
Chitosan + gelatin	Freeze drying	Sponge	Skin	Han et al. (2014)
Chitosan + poly(D,L-lactic-co-glycolic)	Solution casting	Membrane	Nerve	Soltani et al. (2016)
Chitosan + collagen + norfloxacin	Freeze drying	Sponge	Skin	Mahmoud and Salama (2016)
Chitosan + gelatin + nanohydroxyapatite	Freeze drying	Composite	Bone	Dan et al. (2016)
Chitosan + starch	Freeze drying	Composite	Bone	Shahriarpanah et al. (2016)
Chitosan + polycaprolactone	Electrospinning	Nanofiber	Liver	Semnani et al. (2017)
Chitosan + silk + poly(3-hydroxybutyrate)	Electrospinning	Nanofiber	Cartilage	Karbasi et al. (2016)
Chitosan + poly-epsilon-caprolactone	Salt leaching	Sponge	Cartilage	(Filová et al., 2016)

biocompatibility and sometimes can also destroy the bioactive factors or drug payload of the hydrogels. This work also suggested that the microstructure of hydrogels and their physical properties can be adjusted by altering various parameters, that is, concentration, temperature, pH, and ionic strength. Some recent studies also reported fabrication of chitosan hydrogels with remarkable biological properties like enhanced antimicrobial activity and cytocompatibility (Lu et al., 2017; Chen et al., 2017; Wang et al., 2017).

### 7.5.1.1 Physical association network

Chitosan constructs a stable hydrogel by forming a physical association network. The interchain interactions of the network are strong enough to form semipermanent junction points and are also capable of exchanging water molecules with the hydrated polymer network (Berger et al., 2004). The physical network occurs as the result of four major physical interactions, for example, ionic, polyelectrolyte, interpolymer complex, and hydrophobic associations. The ionic interaction results in the ionic complexes, which are formed by interactions between the cationic chitosan and negatively charged molecules or anionic metals (Ma et al., 2016). The different forms of hydrogels can be achieved by introducing manipulation in these interactions. Polyelectrolyte interactions are stronger than hydrogen bonding and avoid the use of organic precursors, catalysts, or reactive agents.

Chitosan—polyelectrolyte networks can be developed with DNA, anionic polysaccharides, proteins, and synthetic anionic polymers. These complexes are dependent on charge density, solvent, ionic strength, pH, and temperature in the term of stability. In addition to these, hydrogels can also be formed by interpolymer complexation, that is, formation of polymer blends of chitosan and other water-soluble polymers. These polymer mixtures form junction points in the form of crystallites and interpolymer complexation after lyophilization or a series of freeze—thaw cycles. Moreover, hydrophobic association also forms transient hydrogels that are dependent on environmental temperature. For the occurrence of a hydrophilic—hydrophobic transition, the temperature of the system should be below the lower critical solution temperature. Thus, chitosan solution with low viscosity at room temperature can form a gel above the lower critical solution temperature. This makes them a suitable carrier matrix in biomedical and pharmaceutical applications.

#### **7.5.1.2 Cross-linked networks**

The cross-linked hydrogels are formed by the covalent bonding between the polymer chains. This bonding results in irreversible gelation, so the cross-linked hydrogels are more stable than the physically associated chitosan hydrogels. But, this approach requires chemical modification in the primary structure of the chitosan, so there is chance of alteration in the initial property of chitosan. In addition to this, there is a simple way to obtain irreversible chitosan hydrogels, that is, by using dialdehyde cross-linkers like glyoxal and glutaraldehyde. These cross-linkers react fast with the amino groups of the chitosan D-glucosamine units in comparison to the hydroxyl groups of the chitosan (Croisier and Jérôme, 2013). These hydrogels can also be obtained by attaching photoreactive or enzyme-sensitive molecules on the chitosan, followed by UV or sensitive enzyme exposure. Their properties are dependent on cross-linking density and the ratio of cross-linker molecules to the moles of polymer repeating units. This type of cross-linked network has advantage of better control on pore size, chemical functionalization, dissolution, and degradation over the physical association networks. Two major methods of obtaining cross-linked networks are chemical cross-linking and interpenetrating networks. The chemical cross-linking forms a permanent hydrogel network by using covalent bonding between the polymer chains. The active sites ( $-\text{NH}_2$  and  $-\text{OH}$ ) on the chitosan can form several linkages, including amide and ester bonding as well as Schiff base formation. The small molecule cross-linkers, polymer—polymer reactions between activated functional groups, photosensitive agents, and enzyme-catalyzed reactions can also be utilized to fabricate these networks (Dash et al., 2011; Zhang et al., 2015). On the other hand, an interpenetrating network is formed when a cross-linked chitosan network is allowed to swell in an aqueous solution of monomers followed by its polymerization. There are also semiinterpenetrating networks, which involves one cross-linked polymer network with another polymer in the linear state (Dragan, 2014).

### 7.5.2 CHITOSAN SPONGES

Sponges are soft and flexible porous foams. These are three-dimensional porous scaffolds with an open porosity and interconnected micropore network. These porous solid structures have capacity of absorbing 20 times more fluids than their dry weight as a result of their microporosity. Being soft and flexible they offer good cell interaction and stimulation of ECM resulting in the effective interaction of cells to the environment (Jayakumar et al., 2011). Sponge scaffolds perform additional vital functions like (1) providing a physical surface to cells to lay their own ECM, (2) ability to inhibit cell growth of adherent contact-inhibited cells, (3) providing better nutrient transport to the center of the device via their porous interconnecting channel network, and (4) eliminating the large clusters to avoid the development of a necrotic center (Ma and Zhang, 2001).

Ability of chitosan sponges to soak up the wound exudates makes them one of the most applicable agents in wound healing or tissue regeneration (Ding et al., 2017). In addition to wound healing chitosan sponges have been potentially utilized in tissue engineering (Chaochai et al., 2016). Freeze drying or lyophilization is the main process for preparation of chitosan sponges. This process first involves freezing of the chitosan solution followed by sublimation of the solvent under condensed pressure (Wang et al., 2016b). Iviglia et al. (2016a) engineered a biphasic calcium phosphate scaffold for the effective treatment of periprosthetic infection and bone dental defects. The researchers used scaffold coated with pectin/chitosan through polyelectrolyte coating. In another work conducted by Ikeda et al. (2014), chitosan sponges for tissue engineering were developed by thermally induced phase separation methods. They prepared the sponges with an average diameter of pore size 158.5, 142.5, and 74.5  $\mu\text{m}$  for 1%, 2%, and 4% chitosan, respectively. Preparation and application of chitosan sponges for biomedical applications has been recently practiced by various researchers (Guo and Li, 2016; Lu et al., 2016).

### 7.5.3 CHITOSAN FILMS

Chitosan films are 2D scaffolds with specific affinity towards wound dressing as they fulfill the demands of highly efficient dressing materials, for example, they are nonallergic, nontoxic, allow gas exchange, can keep the environment moist, and can protect the wound against microbial infections. The most common method of preparing a novel chitosan film is immersion precipitation phase-inversion method. The top layer of films contains skin surface and the interconnected micropores prevent bacterial penetration and dehydration of wound surface. The spongy sublayer provides high adsorption capacity (Jayakumar et al., 2011). Researchers have also tried to improve the properties of chitosan films using nitrogen or argon plasma, ozone or UV irradiation, or introduction of silica particles or ethylene glycol (Silva et al., 2008; Clasen et al., 2006). The films' ductility can be improved by blending and chemical modification of chitosan.

The chitosan membrane incorporated with zeolitic imidazolate framework-7 showed better pervaporation performance for the separation of water and ethanol (Kang et al., 2013). Alhwaige et al. (2013) successfully blended chitosan to benzoxazine polymer in aqueous media to enhance the mechanical properties of the films, that is, they exhibit greater tensile strength. The surface properties of chitosan films can be upgraded by the heterogeneous chemical modifications. Radhakumary et al. (2011) developed a thermosensitive film by combining thiolated chitosan, poly(*N*-isopropyl acrylamide), and ciprofloxacin, which can be easily removed upon decreasing the temperature.

The thin films have been proved to have better surface properties. Thin chitosan films can be designed by two processes: Langmuir–Blodgett and layer-by-layer deposition. These techniques control chitosan film thickness, composition, morphology, and roughness. For the Langmuir monolayer formation, a solution in an organic volatile solvent of an amphiphilic water-insoluble macromolecule is spread on the surface of water. When this organic solvent is evaporated, the hydrophilic part of the amphiphile is anchored to the aqueous subphase and the hydrophobic part is directed towards air. In the Langmuir–Blodgett process, the Langmuir monolayer is transported onto a solid support to get a multilayered film (Croisier and Jérôme, 2013; Roberts, 2013). On the other hand the layer-by-layer technique is based on the alternated adsorption of materials bearing complementary charged or functional groups in aqueous medium (Croisier and Jérôme, 2013). Li et al. (2013) reported the formation of antimicrobial *N*-halamine modified films by the bonding of *N*-halamine onto chitosan. Takara et al. (2015) studied the influence of NaOH treatment on the macromolecular structure and chitosan film properties. The study also introduced employment of mild treatment conditions to obtain better quality chitosan films. Recently, various researchers have reported diverse processes for chitosan film formation with better biological and mechanical properties (Liu et al., 2017; Petrova et al., 2017).

#### 7.5.4 CHITOSAN NANOFIBERS

Chitosan nanofibers are of the prime concern in the biomedical research due to their range of applications in drug release, dental use, tissue engineering, and as catalysts and enzyme carriers. The first report on preparation of chitosan nanofibers was accounted in 1926 (Pillai et al., 2009). Initially, mostly fibers were produced by using dry and wet spinning from acetic acid solution but nowadays the most common and effective method of chitosan nanofibers production is electrospinning. Electrospinning is the process of conversion of viscoelastic solution into a nanofiber using high electrostatic force. This technique produces polymer nanofibers with diameter in the range of a few nanometers to microns, depending on the conditions of processing. The electrospinning technique uses high voltage to create an electrically charged jet of polymer solution. These jets dry to form nanofibers, which are collected on a collector plate. These mats of fibers are highly porous, having high specific surface area, and have capability of

mimicking the natural ECM. However, since chitosan is a polyelectrolyte, in acidic medium repulsive forces are generated between charged species within the polymer backbone. This phenomenon negatively affects the continuous formation of fibers and results in the formation of particles (Min et al., 2004; Jayakumar et al., 2010). The morphology of electrospun structure can be determined by various adjustable parameters, that is, (1) flow rate of the polymer solution through the syringe, (2) concentration of the polymer solution, (3) voltage applied to the needle, and (4) the working distance between the needle and the collecting plate (Balagangadharan et al., 2017).

Several studies reported production of pure electrospun chitosan fibers using trifluoroacetic acid and dichloromethane mixtures (Ohkawa et al., 2004; Sangsanoh and Supaphol, 2006). However, blending is considered as the most commonly reported process to fabricate chitosan fibers. Chen and Huang (2016) synthesized water-soluble *N*-maleoyl functional chitosan using neutral deionized water as a spinning solvent via electrospinning. The study also reported potentiality of the tetracycline hydrochloride loaded nanofibers in wound dressing. A novel chitosan–polyethylene oxide nanofibrous mat was designed by Fazli et al. (2016) to get the controlled release of hydrocortisone and imipenem or cilastatin drugs. In this study, chitosan–polyethylene oxide nanocomposite nanofibrous mat containing 3% ZnO nanoparticles and 2% hydrocortisone, 3% imipenem/cilastatin was utilized. An 82% increase in the hydrocortisone release and decrease in the release rate of imipenem/cilastatin was reported in the research. The antibacterial properties of nanofibers could be enhanced by complexing positively charged chitosan with an anionic hydroxypropyl betacyclodextrin citric acid polymer with triclosan (Ouerghemmi et al., 2016). In this research work, they performed the electrospinning by using two oppositely charged polyelectrolytes, which results in the better stability of the material in aqueous media. Deepthi et al. (2016a) developed a tendon construct of electrospun aligned poly(L-lactic acid) nanofibers by electrospinning and chitosan–collagen hydrogel layering. Alginate coated chitosan–collagen nanofiber scaffold was found suitable for flexor tendon regeneration under immobilized conditions. In another study conducted by Kaya et al. (2016) chitosan nanofibers were developed from *Drosophila melanogaster* with a diameter of  $40.0073 \pm 12.35$  nm through the electrospinning of *Drosophila* chitosan. This study also proved the potentiality of the organism as a raw material for nanofibers production. Other researchers have also reported incorporation of chitosan nanofibers with other materials like glutaraldehyde (Abdelgawad et al., 2017) and triclosan (Nesic et al., 2017) to enhance biomedical properties.

### 7.5.5 CHITOSAN NANOCOMPOSITE

Advancement of chitosan composites as scaffold material in tissue engineering is becoming more attractive due to their properties, which can be engineered to accomplish the mechanical and physiological demands of the host tissue by regulating the volume fraction, morphology, and arrangement of the reinforcing phase



(Rezwan et al., 2006). Composites can be prepared by various processes, for example, (1) solution casting, (2) in situ techniques, (3) electrospinning, and (4) freeze-drying. In the solution casting method, composites are attained by precipitation or casting a solution mixture. The solution mixture is prepared by dissolving filler and chitosan polymer through mechanical stirring or sonication at suitable temperatures. The most effective in situ techniques dispersed the filler materials in monomers in the presence or absence of solvent followed by addition of dispersion curing agents or hardener for polymerization at suitable temperature. The electrospinning technique uses a high-voltage power supply, a syringe containing the polymer solution, and a collector plate. While in the freeze-drying technique, the homogenized mixture of polymer and filler solution is poured into a copper mold and quenched in liquid nitrogen, prior to freeze drying to remove the solvents (Mahanta and Maiti, 2016).

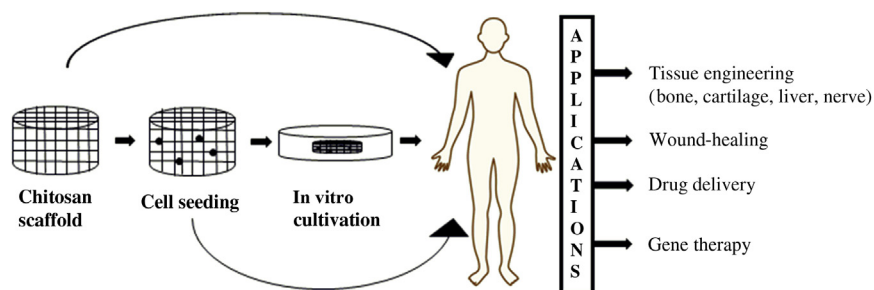
Composite scaffolds are mostly formulated by two or more polymers utilizing unique properties of both the polymers. Chitosan matrix can be combined with other materials to achieve better tissue engineering properties. In bone tissue engineering, chitosan matrix can be combined with osteogenic materials like hydroxyapatite, calcium phosphates and sulfates, alginate, etc. (Anitha et al., 2014; Dahlan et al., 2012; Weir and Xu, 2010; Zo et al., 2012). The mechanical strength of chitosan composites can be enhanced by grafting chitosan polymer with carbon nanotubes (Yan et al., 2016). Dan et al. (2016) reported the development of a three-dimensional chitosan–gelatin/nanohydroxyapatite biocomposite and observed significant effects of hydroxyapatite on the physicochemical and biological properties of the scaffold. There was a remarkable decrease in the swelling and degradation characteristics on addition of hydroxyapatite with an improvement in the cell attachment and cell growth. A group of researchers has also shown the utilization of chitosan–chitin nanocrystal composite scaffolds in tissue engineering (Liu et al., 2016a). The nanocrystals (300 nm in length and 20 nm in width) were evenly dispersed in the chitosan solution and upon utilizing with osteoblast cells gave excellent biocompatibility and low cytotoxicity.

---

## 7.6 APPLICATIONS OF CHITOSAN SCAFFOLDS

### 7.6.1 TISSUE ENGINEERING

Tissue engineering is a highly interdisciplinary field that combines the principles and methods of life sciences, chemical sciences, and engineering to repair, restore, or regenerate living tissues using biomaterials. Scaffold supports the in vitro seeding and cell proliferation. Being biodegradable, nontoxic, and with ease of formulations in a different variety of forms like gels, powder and films, chitosan scaffolds have a vast range of applications in tissue engineering (Dash et al., 2011; Jiang et al., 2012). To date, many tissue analogs have been reported, for example, bone, liver, cartilage, nerve via tissue engineering technology. The

**FIGURE 7.3**

Chitosan scaffolds mechanism of employment and applications in tissue engineering.

basic principle behind the utilization of scaffold in tissue engineering has been represented in Fig. 7.3 with applications. Basically, chitosan scaffolds can be inserted directly in the body or with the incorporation of the cell seeding. In both cases, it serves its functions and the selection of the process is application dependent. Due to the wide range of applicability chitosan scaffold has been utilized tremendously by the researchers in recent times. As a result of this, there is a large number of patents filed worldwide on the fabrication methods of chitosan scaffolds and their applications in the field of tissue engineering. Some of the recent patent publications (source: <https://patents.google.com/>) in the field of chitosan-based scaffolds and composite for tissue engineering purpose are presented in Table 7.2. In the forthcoming section we will review in detail the applications of chitosan scaffold in different sectors, for example, tissue engineering of bone, cartilage, liver, and nerves as well as wound healing, drug delivery, and gene therapy.

### 7.6.1.1 Cartilage tissue engineering

Cartilage is a connective tissue made up of a dense matrix of collagen and elastic fibers. In the human body, cartilage is present in three structurally different forms, that is, hyaline cartilage, fibrocartilage, and elastic cartilage. Articular/hyaline cartilage is a smooth and white tissue that covers the articular surface of bones in synovial joints. It provides a smooth lubricating surface for frictionless joint movements by absorbing shocks and distributing load. The number of patients with articular cartilage lesions has been increased nowadays due to increasing osteoarthritis or trauma. In adults, the avascular nature of the articular cartilage limits its self-generation. Hence, regeneration of articular cartilage via tissue engineering has fascinated researchers. Successful cartilage tissue engineering is based on four factors, for example, scaffolds, growth factors, cells, and the mechanical milieu (Jiang et al., 2012; Kessler and Grande, 2008). Natural articular cartilage matrix contains water (80%) and structural macromolecules (20%) including collagens, proteoglycans, and noncollagenous proteins. The chitosan scaffolds

**Table 7.2** Recent Patents on Employment of Chitosan Scaffolds in Tissue Engineering

S. No.	Title	Patent No.	Publication Date	Reference
1	High strength chitin composite material and method of making	US20160296665A1	October 13, 2016	<a href="#">Ingber and Fernandez (2016)</a>
2	Bioactive grafts and composites	US20150125508A1	January 16, 2015	<a href="#">Govil and Gamboa (2015)</a>
3	Dendritic macroporous hydrogels prepared by crystal templating	US20160237235A1	August 18, 2016	<a href="#">Zawko and Schmidt (2016)</a>
4	Graphene hydrogel and methods of using the same	US20130230496 A1	September 05, 2013	<a href="#">Mohapatra and Wang (2013)</a>
5	Tannin-chitosan composites	US20140134238A1	February 04, 2014	<a href="#">Reed et al. (2014)</a>
6	Durable hemostatic scaffold	US20150105319A1	December 19, 2013	<a href="#">Janmey et al. (2013)</a>
7	Processing of acylchitosan hydrogels	US20130276669A1	March 26, 2013	<a href="#">Freier (2015)</a>
8	Biocompatible and bioabsorbable derivatized chitosan compositions	US20140275291A1	September 18, 2014	<a href="#">McGrath et al. (2014)</a>

provide a framework that facilitates new tissue growth with better mechanical characteristics that match to the native tissue. Various glycosaminoglycans showed structural similarity to the chitosan scaffolds in articular cartilage.

Chitosan composites scaffolds prepared by coprecipitating chitosan with calcium and phosphate have proved useful in tissue engineering. These scaffolds are capable of enhancing the formation of a continuous layer of neocartilage when coated with type I collagen ([Gottipati and Elder, 2016](#)). Researchers are also interested in the formation of injectable scaffolds for cartilage tissue engineering. A group of researchers developed injectable chitosan hyaluronic acid hydrogels consisting of methacrylated glycol chitosan and hyaluronic acid via photo cross-linking with a riboflavin photoinitiator under visible light. The preparation has been observed to increase cell proliferation and cartilaginous ECM production by encapsulated chondrocytes and has high potential in the treatment of cartilage damage ([Park et al., 2013](#)). The mechanical properties of hydrogels can be enhanced for tissue engineering by the addition of other fibers. [Mirahmadi et al. \(2013\)](#) added degummed chopped silk fibers and electrospun silk fibers to the thermosensitive chitosan/glycerophosphate hydrogels. The blending of scaffolds enhanced the hyaline cartilage regeneration. An elastic microporous gelatin/

chondroitin-6-sulfate/hyaluronan cryogel scaffold was prepared to mimic the composition of the native cartilage ECM (Kuo et al., 2015). The study also reported growth arrest and enhanced glycosaminoglycans type II collagen secretion by chondrocytes, which indicates the redifferentiation of chondrocytes in chitosan cryogel. Man et al. (2016) used hybrid scaffold for cartilage injury repair in rabbit. The researchers transplanted the allogenic chondrocytes with chitosan hydrogel-demineralized bone matrix hybrid scaffold and effectively repaired rabbit cartilage injury in a one-step operation. Scaffold-mediated cartilage tissue engineering has been practiced by various researchers to explore the opportunities for their employment in tissue regeneration (Brunger et al., 2014; Li and Hu, 2015; Johnstone et al., 2013; Kock et al., 2012).

### 7.6.1.2 Bone tissue engineering

One of the major clinical problems in osteology is to repair and replace the injured or lost bone. Scaffolds have been observed to play crucial roles as they maintain the structural defects and restore the bone functions (Levengood and Zhang, 2014). To be used in bone tissue engineering the scaffolds should possess the following properties: (1) biocompatibility, to integrate with host tissues deprived of any immune responses; (2) mechanical strength, to face the surrounding forces; (3) biodegradability; and (4) osteoconductivity, for permitting cell infiltration and proliferation, neovascularization, and nutrient transport (Khan et al., 2008). Chitosan scaffolds meet the above-mentioned criteria. Their biocompatibility reduces the local inflammation and porous structure helps in osteoconduction (Hutmacher, 2000). Although feasibility and osteocompatibility have been well demonstrated in pure chitosan scaffolds, there are still some limitations to be considered to develop novel chitosan scaffolds (Logithkumar et al., 2016). These limitations include less osteoconductivity and mechanical strength. Therefore, researchers have now been focused on the incorporation of a variety of polymers or bioceramics in the scaffolds to improve their applications in bone tissue regeneration.

Uswatta et al. (2016) used an injectable spherical chitosan scaffold prepared from chitosan, sodium tripolyphosphate, and nanohydroxyapatite to improve the compressive strength of bone regeneration. The diameter of the scaffold used in the study was in the range of 0.9–1.3 mm and the pore size ranges from 2 to 10  $\mu\text{m}$ . They also showed that the osteoblast adhesion and proliferation on the scaffold was supported by the increase in the amount of nanohydroxyapatite. Zazakowny et al. (2016) also prepared the injectable scaffolds by genipin cross-linked collagen or collagen/chitosan hydrogels containing titanium oxide nanoparticles. Muzzarelli et al. (2015) discussed the various aspects of the genipin-cross-linked chitosan scaffolds. Shakir et al. (2016) synthesized a nanocomposite system by the incorporation of  $\beta$ -cyclodextrin with chitosan and nanohydroxyapatite through coprecipitation. The study also reported that the orchestrated organic or inorganic nanocomposites show advanced cell viability and osteogenesis, controlled

biodegradation, and increased antibacterial activity. Development and employment of magnetic scaffolds for bone tissue engineering has attracted the attention of researchers. Aliramaji et al. (2017) developed silk fibroin/chitosan-based magnetic scaffolds by freeze casting method. Iviglia et al. (2016b) developed a pectin–chitosan hydrogel incorporated with ceramic particles. The incorporation of ceramic particles makes the biomaterial more stable at different pH, increases the compressive elastic modulus, toughness, and tensile strength. The study also reported high proliferation and adhesion activity in SAOS-2 human osteoblastic cell line. The carboxylated starch-chitosan can be used as composite scaffolds in bone regeneration. Starch addition improved the mineralization, compressive strength, carboxyl content, and swelling ratio of the composites (Shahriarpanah et al., 2016). Dan et al. (2016) prepared a biocomposite three-dimensional scaffold by using chitosan–gelatin and nanohydroxyapatite. The presence of hydroxyapatite in scaffold negatively affected the swelling and degradation characteristics of the scaffold whereas it exhibited positive impacts on cell attachment and growth. Muthukumar et al. (2016) used the collagen/chitosan composite scaffold incorporated with the Korean traditional medicinal ginseng compound K for bone tissue engineering. The in vitro analysis of the scaffold has proved its biocompatibility along with supporting the MG-63 cells growth. Employment of chitosan composites as novel scaffold has been advocated by various researchers (Sundaram et al., 2016; Ran et al., 2016; Saravanan et al., 2016; Deepthi et al., 2016b; Yang et al., 2016). Polysaccharides based nanohybrid scaffolds have been observed to promote adhesion and proliferation of osteoblasts along with the growth improvements (Fan et al., 2016).

### 7.6.1.3 Liver tissue engineering

The liver performs various crucial roles in our body such as metabolism as well as storage, synthesis, and release of carbohydrates, vitamins, lipids, and proteins, along with detoxification, inactivation of endogenous and exogenous substances, and activation of precursor molecules. Due its many functions, the liver also faces a number of possible injuries including viral infections, alcohol abuse, surgical resection of tumors, and acute drug induced hepatic failure. The available treatment for liver failure is transplantation, but due to the insufficient donor organs for transplantation there is an urgent need to develop new therapies for liver diseases (Jiang et al., 2015). The bioartificial modes based on the utilization of chitosan scaffold have been proposed as a potential solution for liver failure.

Galactosylated chitosan has been proved to be effective in liver tissue engineering. Wang et al. (2016a) reported the influence of the degree of substitution of galactose on cell attachment and mechanical stability. In this study, they reported enhancement in the cell attachment of hepatocytes on the galactosylated chitosan and lactose-modified chitosan films with an increase in the galactose moieties and reduction in the mechanical stability of the lactose-modified chitosan. Due to the enhancement in cell attachment and biocompatibility the lactose-modified chitosan scaffold can be a utilized as a promising material for tissue engineering. Employment of spongy biocomposite agarose–chitosan scaffold is

another strategy for liver tissue engineering. This scaffold led to increase in the cellular metabolic activity as predicted by the primary hepatocytes proliferation analysis in the in vitro condition. The presence of higher level of hepatic functions and expression of hepatic biomarker (hepatic cytochrome P450) shows the potentiality of in vitro liver tissue model generation (Tripathi and Melo, 2015). Perfect ECM is crucial for maintaining a high level of liver-specific functions in tissue engineering. Chen et al. (2012) prepared a highly porous scaffold from oxidized alginate covalently cross-linked with galactosylated chitosan and evaluated its in vitro biocompatibility. They observed the morphology of the hepatocytes cultured on the scaffold to be spheroidal with the formation of the multicellular aggregates in a perfect integration manner, indicating the applicability of the synthetic scaffold for liver tissue engineering. Similarly, Deng et al. (2015) reported xyloglucan as a synthetic ECM for human hepatoma cell line (HepG2) cell attachment and found considerable effects of it on the adherent behavior. The adherent property of the surface coated with xyloglucan was directly dependent on the concentration of the xyloglucan used in the coating. During the analysis, the researchers observed that the xyloglucan could be effectively employed to enhance cell interactions as well as the cell clusters formation of HepG2. Some researchers also used hierarchical channel networks in tissue engineering scaffold to manufacture metabolically demanding liver tissue with thick and complex structure. Gong et al. (2014) constructed chitosan–gelatin scaffolds having three-dimensional channels through the indirect solid freeform fabrication and freeze-drying technique. The in vitro studies of chitosan–gelatin with HepG2 showed much higher proliferating activity with channel network than without channels. Du et al. (2014) encapsulated cells within a separate domain in multicomponent hydrogel fibers and formed tissue constructs in 3D pattern. They also showed that the presence of endothelial cells in the scaffold could improve the hepatocyte functions in vitro, whereas in partial hepatectomy mouse model it facilitates vascularization of the scaffold. Researchers are also paying attention to the utilization and development of microporous cryogels in liver tissue engineering as hepatocyte carriers (Jain et al., 2015). In addition to this, the biomedical researchers are also working on chitosan composite hollow fiber membranes for liver tissue engineering (Teotia et al., 2015). These hollow fiber membranes can assist devices for bioartificial liver application. Teotia et al. (2015) reported polysulfone–chitosan hollow fiber membrane formation by phase-inversion technique and found better hemocompatibility of the modified composite membrane to the native membranes.

#### **7.6.1.4 Nerve tissue engineering**

The repairing or regeneration of the injured nerve is still a challenging clinical aspect. It not only affects the nervous system but also results in the malfunctioning of the other parts of the body. The present strategies apply either bridging by grafting and tubulization or end-to-end suturing of the nerve stumps (Dash et al., 2011). Autologous nerve graft is one of the most promising techniques for the regeneration of large nerve gaps. However, some limitations are there with the

grafting technique, for example, need of multiple surgeries and loss of functions at the donor site. So, the interest of the biomedical researchers is in the utilization of biomaterials that can compete the demands of the nerve tissue engineering. Due to their biocompatibility, biodegradability, excellent processability, and neuroprotective properties, chitosan-based scaffolds are considered as one of the potential biomaterials to repair nerve tissue injuries (Jiang et al., 2012).

The conductive porous scaffolds can be used in the regeneration of the peripheral nerves. Baniasadi et al. (2015) developed conductive porous scaffolds by incorporating conductive polyaniline/graphene nanoparticles into a chitosan/gelatin matrix. In this study the researchers calculated the various nerve regeneration parameters, for example, porosity, proper electrical conductivity, controlled biodegradability, and the appropriate mechanical property. The study revealed that electrical conductivity and the mechanical properties are directly proportional, whereas the swelling ratio, porosity, and biodegradability are inversely proportional to the incorporation of the polyaniline and graphene content in the scaffold matrix. The researchers also proposed the utilization of polyaniline/graphene (2.5 wt.%) suitable for scaffold material in nerve tissue engineering. Masaeli et al. (2013) reported the use of poly(hydroxy alkanoate) composite nanofibrous scaffolds for nerve tissue engineering. The study represented the combined approach of polymeric scaffold and cells for nerve regeneration. Additionally, the work also supported the utilization of type I collagen in nanofibers for improved cell differentiation. Wrobel et al. (2014) conducted the in vitro evaluation of cell-seeded chitosan films in the engineering of the peripheral nerve tissue. They found that the chitosan films permit neurite outgrowth from disconnected sensory neurons, which revealed their extensive applicability as grafts in nerve tissue engineering. Alhosseini et al. (2012) used a large pore size electrospun polyvinyl alcohol/chitosan nanofibrous scaffold for nervous tissue engineering and repair. The research showed an enhancement in the proliferation and viability of nerve cells by addition of chitosan in the polyvinyl alcohol scaffolds, which resulted in better biocompatibility of the scaffolds. Poly(glycerol sebacate)-based nanofibers prepared through electrospinning, function as the biomimetic scaffold that offers vital chemical and structural cues for nerve regeneration (Hu et al., 2017). The scaffold was able to induce the neurite outgrowth of the nerve stem cells and promote cell proliferation and biocompatibility. Nawrotek et al. (2016) reported the electrodeposition (chitosan solution) based fabrication method of epineurium-mimicking tubular conduits for peripheral nervous tissue engineering. These conduits were able to fulfill the requirements of peripheral nerve implants. The chitosan/graphene membranes and poly(D,L-lactic-co-glycolic acid)/graphene membranes can be considered for the nerve tissue engineering as the MTT assay resulted in the highest proliferation after 72 hours with chitosan (1.5%) graphene membrane (Soltani et al., 2016). Akhavan (2016) has also proposed the potential of graphene scaffold in nerve tissue engineering. Hu et al. (2013) successfully repaired a 50-mm-long median nerve defect in rhesus monkey by the combination of tissue engineering and stem cell therapy. The nerve graft used in this clinical



research was chitosan-based nerve graft using marrow mesenchymal stem cells. Chitosan/silk fibroin-based and Schwann cell-derived hybrid scaffolds have also explored for nerve tissue engineering (Gu et al., 2014).

### 7.6.2 WOUND HEALING

Although the body has a spontaneous wound healing process, this can be impaired in case of acute or chronic wounds. In such cases, materials based on biopolymers like chitosan can enhance and imitate the normal and epidermal wound healing process. The dermal wound healing follows four steps of inflammation, migration, proliferation, and maturation (Dreifke et al., 2015). ECM is also considered to play an important role in the wound healing process. The ECM has roles in orchestrating and guiding cell phenotype, adhesion, migration, and proliferation (Patrulea et al., 2015; Hynes, 2009). Chitosan-based materials have been proved to be an ideal wound healing agent as they not only protect wounds from microbial infections but they also promote the healing process. A number of chitosan-based materials produced from different formulations have been employed in wound healing. One of the major advantages of using chitosan-based materials in wound healing is that chitosan produces less scarring (Patrulea et al., 2015).

Chitosan scaffold can result in better wound healing and dressing agents when it is incorporated with other materials especially with antibiotics or compounds having antimicrobial activity. Poly(ethylene glycol)/chitosan scaffold loaded with ciprofloxacin hydrochloride showed quicker and more regulated wound healing (Sinha et al., 2013). The polyethylene glycol incorporation in the scaffold increased the drug loading up to 5.4% with enhanced drug release up to 35% in comparison to the chitosan alone (20%). This work was also validated experimentally on mice models where faster cell growth was observed during the healing process. Mahmoud and Salama (2016) also used Norfloxacin with collagen/chitosan scaffold for the shin reconstruction and in vivo wound healing. These norfloxacin loaded scaffolds were synthesized by freeze-drying technique. The prepared scaffold was capable of 100% drug release within 24 hours. The study also suggested the better wound healing process and tissue regeneration in case of treated or drug loaded chitosan scaffolds. Similarly, in a research work conducted by Morgado et al. (2017) ibuprofen was used for loading onto the poly(vinyl alcohol)/chitosan scaffolds. The researchers reported the application of ibuprofen in faster skin regeneration. The in vivo studies showed that the presence of the scaffold loaded with ibuprofen prevented scab formation and extreme inflammation, resulting in faster wound healing. Karri et al. (2016) used curcumin (antiinflammatory agent) loaded chitosan nanoparticles with collagen–alginate hybrid scaffold for diabetic wound healing. The nanohybrid scaffold resulted in better water uptake, biocompatibility, and sustained drug availability in vitro while in vivo faster wound healing process was observed. Lu et al. (2017) synthesized a sponge-like nano Ag/ZnO-loaded chitosan composite dressing through the lyophilization process. The composite has high porosity, swelling, blood clotting, and



antibacterial activity. The *in vivo* studies on mice demonstrated enhanced wound healing and reepithelialization along with collagen deposition. In a similar way, [Ding et al. \(2017\)](#) developed a spongy bilayer dressing from chitosan-Ag nanoparticles and chitosan–*Bletilla striata* polysaccharides. This bilayer composite was capable of inhibiting complete microbial invasion. This dressing was able to accelerate the healing rate of cutaneous wounds in mice with a better epidermization and less inflammation. [Vedakumari et al. \(2017\)](#) has fabricated chitosan–fibrin composite scaffolds infused with quercetin. The prepared scaffold was able to accelerate the wound healing process in albino rats.

### 7.6.3 DRUG DELIVERY

Drug delivery is a process of administering a drug in a human or animal body to achieve therapeutic effect. Drugs can be delivered by various routes, for example, oral, ocular, nasal, vaginal, buccal, parental, and intravesical ([Bernkop-Schnürch and Dünnhaupt, 2012](#)). Chitosan-based systems appear as promising auxiliary agents in drug delivery. Chitosan scaffolds have been widely explored for the delivery of proteins/peptides, growth factors, antiinflammatory drugs, antibiotics, anticancer drugs, vaccines, etc. ([Tiwari et al., 2012](#); [Dash et al., 2011](#)). The polymeric nanofibers can be fabricated by the simple and versatile electrospinning method for the drug delivery applications. [Hu et al. \(2014\)](#) discussed in detail the various setups and process parameters of electrospinning and drug releasing kinetics.

Chitosan-based scaffolds have also been proved as an ideal growth factor delivery system. Growth factors may be small proteins or peptides that support the growth and differentiation of cells. Through their study [Sivashankari and Prabakaran \(2016\)](#) demonstrated that the scaffolds capable of delivering growth factors encourage tissue repair and regeneration more quickly than scaffolds without growth factors. [Fazli et al. \(2016\)](#) through electrospinning technique synthesized a novel chitosan–polyethylene oxide nanofibrous mat containing ZnO nanoparticle with the capability of releasing hydrocortisone and imipenem/cilastatin drugs simultaneously. In the wound dressing application, the release of hydrocortisone was capable of inhibiting inflammation and the presence of imipenem/cilastatin antibiotics and ZnO nanoparticles could inhibit infections. [Cao et al. \(2015\)](#) reported the utilization of fish collagen/chitosan/chondroitin sulfate scaffolds in the delivery of growth factors for skin tissue engineering. *In vivo* studies employing these scaffolds suggested that they exhibit good biocompatibility and promote fibroblast cell proliferation along with skin tissue regeneration. Chitosan when grafted with other materials has been observed to improve the controlled drug delivery. [Mahanta et al. \(2015\)](#) grafted chitosan with diisocyanate terminated polyurethane and reported better bio- and hemocompatibility as depicted by platelet aggregation, cell viability, cell adhesion, and hemolysis studies as compared with chitosan alone. [Doty et al. \(2014\)](#) reported dual delivery of vancomycin and recombinant human bone morphogenetic protein-2 through a composite chitosan

and calcium sulfate scaffold. The study proposed the dual ability of the scaffold delivery systems in fighting infections as well as growth factor delivery. In vitro the scaffold was observed to be able to deliver both antibiotic and growth factor. Skop et al. (2013) developed a heparin cross-linked chitosan-based delivery system for central nervous system repair. The chitosan-based microsphere and films were capable of delivering neural stem cells and required growth factors. The MTT assay and microscopic analysis discovered that the prepared scaffold was better in sustaining survival and growth of neural stem cells as compared with the standard culture conditions. Chitosan bionanocomposite beads have also been utilized in drug delivery. Ribeiro et al. (2014) synthesized a drug delivery system using chitosan/layered double hydroxide biohybrid beads that were coated with pectin for the treatment of colon disease. The coating confirms in vitro stability of both chitosan and the hydroxide at the acidic pH of the gastric fluid. Bae et al. (2013) studied a well-established pharmaceutical excipient as a scaffold. In the study, they used thiolated chitosan scaffold for the delivery of bone morphogenetic protein-2 for osteogenic differentiation and bone formation. The in vivo experiments showed enhanced bone formation (1.8-fold) after four weeks of transplantation. Kumari and Singh (2013) prepared chitosan-Au-Fe<sub>3</sub>O<sub>4</sub> hybrid nanoparticle based nanohybrid scaffold for controlled drug delivery and tissue engineering applications. The cell proliferation profile of the prepared nanohybrid also predicted its applicability as a suitable substrate in drug delivery. In another study, researchers used bioglass-based scaffolds in incorporation with polycaprolactone and chitosan coating for the drug delivery (Yao et al., 2013). The bioglass was prepared by replication technique using 45S5 bioglass powder and the loading was done with vancomycin. The study demonstrated complete drug release in 24 hours in case of bare scaffold while in the case of coated scaffold it took 11 days. The research proved the potential of the coated scaffolds as ideal drug carrier. Recently, chitosan nanofibers and chitosan-based polyelectrolyte complexes have also been explored for drug delivery (Luo and Wang, 2014; Chen and Huang, 2016).

#### 7.6.4 GENE THERAPY

Gene therapy is a technique of introduction of foreign genetic material into a target cell to exert a therapeutic effect. It requires targeted transfer of genes into suitable cells and subsequently inside the nucleus. The mode of nucleic acid delivery may be viral or nonviral and their effect is delivery method dependent. Naked nucleic acid injection has low transfection efficiency both in vitro as well as in vivo. Viral vector gene delivery relies on capsid proteins to transfer the gene of interest into cytoplasm followed by the transportation to the nucleus and subsequent expression. The most common viral vectors are adenovirus, retrovirus, lentivirus, and adeno-associated viruses. Whereas, nonviral vector generally includes lipid-based carriers, inorganic nanoparticles, and polymers. The nonviral gene transfer is usually performed with plasmid DNA (Kim et al., 2016). The viral vectors displayed high transfection efficiency but also have

immunogenicity and toxicity. On the other hand, the nonviral vectors are nonimmunogenic and safe but have lower transfection efficiency. The limitations can be satisfied by the application of chitosan-based gene delivery system. An ideal nucleic acid transfer vector should provide protection from nucleases, have ability to reach the target cell, must enable delivery across the target cell membrane, facilitate appropriate intracellular trafficking of the nucleic acid, and in the case of plasmid DNA, facilitate the crossing of the nuclear membrane (Pack et al., 2005; Raftery et al., 2013). Chitosan-based systems especially chitosan scaffold have the ability to counter the aforesaid demands of a novel and model vector.

Raftery et al. (2015) developed a collagen-based scaffold as a gene activated scaffold with potential in a range of tissue engineering applications. In this study the potentiality of chitosan as a gene delivery vector was analyzed by using mesenchymal stem cells and the reported transfection efficiency was of >45% was comparable to the no-viral gold standard vector, polyethyleneimine. The optimized incorporation of chitosan nanoparticles into collagen-based scaffolds could sustain the transgene expression up to 28 days. The study proposed that the variations in the composition of scaffolds and the gene can enhance the potentiality of the therapeutic applications. Kwon et al. (2013) coated adenovirus with chitosan followed by the chemical conjugation of polyethylene glycol and folic acid. The in vivo study demonstrated that the conjugation improves the efficiency and safety profiles and thus can be used as a therapeutic agent to target folate receptor positive cancer. Chitosan-based nanoparticles can also be utilized in the targeted delivery of small interfering RNA. Poly(ethylene glycol)-modified chitosan with small interfering RNA nanoparticles can reduce the growth of xenograft tumors of 4T1 cells and prevent metastasis (Sun et al., 2016). Lee et al. (2016) reported the suppression of the tumor growth by activating the tumor suppressor p53 gene with the help of magnetic thymine-imprinted chitosan nanoparticles. Liu et al. (2016b) synthesized polyethyleneimine-grafted carboxymethyl chitosan for gene delivery. The prepared copolymer was observed to have little impact on the aggregation, morphology or lysis of red blood cells or on blood coagulation when injected with amount <0.05 mg/mL. The study suggested it as a strong candidate for the effective and safe nonviral vector delivery. Wang et al. (2015) used 3D porous chitosan-alginate scaffolds for the evaluation of nanoparticle mediated tumor targeting and gene delivery to prostate cancer. This work provided strong indication that the in vitro cell culture system can serve as a valuable three-dimensional model to mimic the in vivo tumor microenvironment structure and thus can precisely forecast in vivo targeting efficiency. Bae et al. (2016) synthesized scaffold by grafting glycol chitosan with low molecular weight polyethyleneimine and utilized it as a gene carrier for human adipose-derived mesenchymal stem cells. The conjugated polymer endosomal escape analysis demonstrated that it can be used in effective gene delivery.

## 7.7 CONCLUSIONS

Tissue engineering and regenerative medicine are considered as one of the fastest growing disciplines in medical research in the present decade. The disciplines are taking advantage of various fields, for example, medicine, materials, science, cell biology, and biomedical engineering. The key aim of tissue engineering is to offer the patients suffering from tissue damage or organ failure a chance to enjoy a normal functioning body by developing the biological substitutes to repair, restore, or regenerate the living human tissues. Although a considerable amount of research has been done on tissue engineering, still there is plenty of room available for further research. Chitosan scaffolds have been proved as an excellent biomaterial for tissue engineering applications owing to their biodegradability, biocompatibility, and mechanical properties. Further investigations are required to develop well-designed scaffolds with optimized level of properties needed in tissue engineering. Development of chitosan-based scaffolds and composites as the artificial extracellular matrices has great potential in tissue engineering.

## REFERENCES

- Abdelgawad, A.M., El-naggar, M.E., Hudson, S.M., Rojas, O.J., 2017. Fabrication and characterization of bactericidal thiol-chitosan and chitosan iodoacetamide nanofibres. *Int. J. Biol. Macromol.* 94, 96–105.
- Akhavan, O., 2016. Graphene scaffolds in progressive nanotechnology/stem cell-based tissue engineering of the nervous system. *J. Mater. Chem. B* 4, 3169–3190.
- Albanna, M.Z., Bou-Akl, T.H., Blowytsky, O., Walters, H.L., Matthew, H.W., 2013. Chitosan fibers with improved biological and mechanical properties for tissue engineering applications. *J. Mech. Behav. Biomed. Mater.* 20, 217–226.
- Alhosseini, S.N., Moztarzadeh, F., Mozafari, M., Asgari, S., Dodel, M., Samadikuchaksaraei, A., et al., 2012. Synthesis and characterization of electrospun polyvinyl alcohol nanofibrous scaffolds modified by blending with chitosan for neural tissue engineering. *Int. J. Nanomed.* 7, 25.
- Alhwaige, A.A., Agag, T., Ishida, H., Qutubuddin, S., 2013. Biobased chitosan/polybenzoxazine cross-linked films: preparation in aqueous media and synergistic improvements in thermal and mechanical properties. *Biomacromolecules* 14, 1806–1815.
- Aliramaji, S., Zamanian, A., Mozafari, M., 2017. Super-paramagnetic responsive silk fibroin/chitosan/magnetite scaffolds with tunable pore structures for bone tissue engineering applications. *Mater. Sci. Eng. C* 70, 736–744.
- Anitha, A., Sowmya, S., Kumar, P.S., Deepthi, S., Chennazhi, K., Ehrlich, H., et al., 2014. Chitin and chitosan in selected biomedical applications. *Progress Polym. Sci.* 39, 1644–1667.
- Bae, I.-H., Jeong, B.-C., Kook, M.-S., Kim, S.-H., Koh, J.-T., 2013. Evaluation of a thiolated chitosan scaffold for local delivery of BMP-2 for osteogenic differentiation and ectopic bone formation. *BioMed Res. Int.* 2013, 1–10. Article ID 878930.

- Bae, Y., Lee, Y.H., Lee, S., Han, J., Ko, K.S., Choi, J.S., 2016. Characterization of glycol chitosan grafted with low molecular weight polyethylenimine as a gene carrier for human adipose-derived mesenchymal stem cells. *Carbohydr. Polym.* 153, 379–390.
- Balagangadharan, K., Dhivya, S., Selvamurugan, N., 2017. Chitosan based nanofibers in bone tissue engineering. *Int. J. Biol. Macromol.* 104, 1372–1382.
- Balan, V., Verestiuc, L., 2014. Strategies to improve chitosan hemocompatibility: a review. *Eur. Polym. J.* 53, 171–188.
- Baniasadi, H., Sa, A.R., Mashayekhan, S., 2015. Fabrication and characterization of conductive chitosan/gelatin-based scaffolds for nerve tissue engineering. *Int. J. Biol. Macromol.* 74, 360–366.
- Berger, J., Reist, M., Mayer, J.M., Felt, O., Gurny, R., 2004. Structure and interactions in chitosan hydrogels formed by complexation or aggregation for biomedical applications. *Eur. J. Pharm. Biopharm.* 57, 35–52.
- Bernkop-Schnürch, A., Dünnhaupt, S., 2012. Chitosan-based drug delivery systems. *Eur. J. Pharm. Biopharm.* 81, 463–469.
- Brunger, J.M., Huynh, N.P., Guenther, C.M., Perez-Pinera, P., Moutos, F.T., Sanchez-Adams, J., et al., 2014. Scaffold-mediated lentiviral transduction for functional tissue engineering of cartilage. *Proc. Natl Acad. Sci.* 111, E798–E806.
- Cao, H., Chen, M.-M., Liu, Y., Liu, Y.-Y., Huang, Y.-Q., Wang, J.-H., et al., 2015. Fish collagen-based scaffold containing PLGA microspheres for controlled growth factor delivery in skin tissue engineering. *Colloids Surf. B Biointerf.* 136, 1098–1106.
- Chaochai, T., Miyaji, H., Yoshida, T., Nishida, E., Furuike, T., Tamura, H., 2016. Preparation of chitosan-gelatin based sponge cross-linked with GlcNAc for bone tissue engineering. *J. Chitin Chitosan Sci.* 4, 1–8.
- Chatelet, C., Damour, O., Domard, A., 2001. Influence of the degree of acetylation on some biological properties of chitosan films. *Biomaterials* 22, 261–268.
- Chen, C.-K., Huang, S.-C., 2016. Preparation of reductant-responsive N-maleoyl-functional chitosan/poly (vinyl alcohol) nanofibers for drug delivery. *Mol. Pharm.* 13, 4152–4167.
- Chen, F., Tian, M., Zhang, D., Wang, J., Wang, Q., Yu, X., et al., 2012. Preparation and characterization of oxidized alginate covalently cross-linked galactosylated chitosan scaffold for liver tissue engineering. *Mater. Sci. Eng. C* 32, 310–320.
- Chen, H., Xing, X., Tan, H., Jia, Y., Zhou, T., Chen, Y., et al., 2017. Covalently antibacterial alginate-chitosan hydrogel dressing integrated gelatin microspheres containing tetracycline hydrochloride for wound healing. *Mater. Sci. Eng. C* 70, 287–295.
- Chien, R.-C., Yen, M.-T., Mau, J.-L., 2016. Antimicrobial and antitumor activities of chitosan from shiitake stipes, compared to commercial chitosan from crab shells. *Carbohydr. Polym.* 138, 259–264.
- Clasen, C., Wilhelms, T., Kulicke, W.-M., 2006. Formation and characterization of chitosan membranes. *Biomacromolecules* 7, 3210–3222.
- Crofton, A., Chrisler, J., Hudson, S., Inceoglu, S., Petersen, F., Kirsch, W., 2016. Effect of plasma sterilization on the hemostatic efficacy of a chitosan hemostatic agent in a rat model. *Adv. Ther.* 33, 268–281.
- Croisier, F., Jérôme, C., 2013. Chitosan-based biomaterials for tissue engineering. *Eur. Polym. J.* 49, 780–792.
- Dahlan, K., Dewi, S.U., Nurlaila, A., Soejoko, D., 2012. Synthesis and characterization of calcium phosphate/chitosan composites. *Int. J. Basic Appl. Sci.* 12, 50–57.

- Dan, Y., Liu, O., Liu, Y., Zhang, Y.-Y., Li, S., Feng, X.-B., et al., 2016. Development of novel biocomposite scaffold of chitosan-gelatin/nanohydroxyapatite for potential bone tissue engineering applications. *Nanosc. Res. Lett.* 11, 487.
- Das, S.N., Madhuprakash, J., Sarma, P., Purushotham, P., Suma, K., Manjeet, K., et al., 2015. Biotechnological approaches for field applications of chitooligosaccharides (cos) to induce innate immunity in plants. *Crit. Rev. Biotechnol.* 35, 29–43.
- Dash, M., Chiellini, F., Ottenbrite, R., Chiellini, E., 2011. Chitosan—a versatile semi-synthetic polymer in biomedical applications. *Progress Polym. Sci.* 36, 981–1014.
- Deepthi, S., Sundaram, M.N., Kadavan, J.D., Jayakumar, R., 2016a. Layered chitosan-collagen hydrogel/aligned PLLA nanofiber construct for flexor tendon regeneration. *Carbohydr. Polym.* 153, 492–500.
- Deepthi, S., Venkatesan, J., Kim, S.-K., Bumgardner, J.D., Jayakumar, R., 2016b. An overview of chitin or chitosan/nano ceramic composite scaffolds for bone tissue engineering. *Int. J. Biol. Macromol.* 93, 1338–1353.
- Deng, X., Cao, Y., Yan, H., Yang, J., Xiong, G., Yao, H., et al., 2015. Enhanced liver functions of HepG2 cells in the alginate/xyloglucan scaffold. *Biotechnol. Lett.* 37, 235–240.
- Dhandayuthapani, B., Yoshida, Y., Maekawa, T., Kumar, D.S., 2011. Polymeric scaffolds in tissue engineering application: a review. *Int. J. Polym. Sci.* 2011, 1–19. Article ID 290602.
- Ding, L., Shan, X., Zhao, X., Zha, H., Chen, X., Wang, J., et al., 2017. Spongy bilayer dressing composed of chitosan–Ag nanoparticles and chitosan–*Bletilla striata* polysaccharide for wound healing applications. *Carbohydr. Polym.* 157, 1538–1547.
- Doty, H.A., Leedy, M.R., Courtney, H.S., Haggard, W.O., Bumgardner, J.D., 2014. Composite chitosan and calcium sulfate scaffold for dual delivery of vancomycin and recombinant human bone morphogenetic protein-2. *J. Mater. Sci. Mater. Med.* 25, 1449–1459.
- Dragan, E.S., 2014. Design and applications of interpenetrating polymer network hydrogels. A review. *Chem. Eng. J.* 243, 572–590.
- Dreifke, M.B., Jayasuriya, A.A., Jayasuriya, A.C., 2015. Current wound healing procedures and potential care. *Mater. Sci. Eng. C* 48, 651–662.
- Drury, J.L., Mooney, D.J., 2003. Hydrogels for tissue engineering: scaffold design variables and applications. *Biomaterials* 24, 4337–4351.
- Du, C., Narayanan, K., Leong, M.F., Wan, A.C., 2014. Induced pluripotent stem cell-derived hepatocytes and endothelial cells in multi-component hydrogel fibers for liver tissue engineering. *Biomaterials* 35, 6006–6014.
- Dyawanapelly, S., Koli, U., Dharamdasani, V., Jain, R., Dandekar, P., 2016. Improved mucoadhesion and cell uptake of chitosan and chitosan oligosaccharide surface-modified polymer nanoparticles for mucosal delivery of proteins. *Drug Deliv. Translat. Res.* 2011, 1–15.
- Fan, W., Yan, W., Xu, Z., Ni, H., 2012. Erythrocytes load of low molecular weight chitosan nanoparticles as a potential vascular drug delivery system. *Colloids Surf. B Biointerf.* 95, 258–265.
- Fan, T., Chen, J., Pan, P., Zhang, Y., Hu, Y., Liu, X., et al., 2016. Bioinspired double polysaccharides-based nanohybrid scaffold for bone tissue engineering. *Colloids Surf. B: Biointerf.* 147, 217–223.

- Fazli, Y., Shariatnia, Z., Kohsari, I., Azadmehr, A., Pourmortazavi, S.M., 2016. A novel chitosan-polyethylene oxide nanofibrous mat designed for controlled co-release of hydrocortisone and imipenem/cilastatin drugs. *Int. J. Pharm.* 513, 636–647.
- Felt, O., Buri, P., Gurny, R., 1998. Chitosan: a unique polysaccharide for drug delivery. *Drug Dev. Industr. Pharm.* 24, 979–993.
- Feng, C., Li, J., Wu, G.S., Mu, Y.Z., Kong, M., Jiang, C.Q., et al., 2016. Chitosan coated diatom silica as hemostatic agent for haemorrhage control. *ACS Appl. Mater. Interf.* 8, 34234–34243.
- Filová, E., Jakubcová, B., Danilová, I., Kostáková, E.K., Jarosikova, T., Chernyavskiy, O., et al., 2016. Polycaprolactone foam functionalized with chitosan microparticles—a suitable scaffold for cartilage regeneration. *Physiol. Res.* 65, 121.
- Freier, T., 2015. Processing of acylchitosan hydrogels. Google Patents.
- Funkhouser, J.D., Aronson, N.N., 2007. Chitinase family GH18: evolutionary insights from the genomic history of a diverse protein family. *BMC Evolut. Biol.* 7, 1.
- Gong, H., Agustin, J., Wootton, D., Zhou, J.G., 2014. Biomimetic design and fabrication of porous chitosan–gelatin liver scaffolds with hierarchical channel network. *J. Mater. Sci. Mater. Med.* 25, 113–120.
- Gopi, D., Nithiya, S., Shinyjoy, E., Rajeswari, D., Kavitha, L., 2014. Carbon nanotubes/ carboxymethyl chitosan/mineralized hydroxyapatite composite coating on ti-6al-4v alloy for improved mechanical and biological properties. *Industr. Eng. Chem. Res.* 53, 7660–7669.
- Gottipati, A., Elder, S.H., 2016. Composite chitosan-calcium phosphate scaffolds for cartilage tissue engineering. *Chitin and Chitosan for Regenerative Medicine*. Springer.
- Govil, A. P., Gamboa, C., 2015. Bioactive grafts and composites. Google Patents.
- Goy, R.C., Morais, S.T., Assis, O.B., 2016. Evaluation of the antimicrobial activity of chitosan and its quaternized derivative on *E. coli* and *S. aureus* growth. *Revista Brasileira de Farmacognosia* 26, 122–127.
- Gu, Y., Zhu, J., Xue, C., Li, Z., Ding, F., Yang, Y., et al., 2014. Chitosan/silk fibroin-based, Schwann cell-derived extracellular matrix-modified scaffolds for bridging rat sciatic nerve gaps. *Biomaterials* 35, 2253–2263.
- Guo, M., Li, X., 2016. Development of porous Ti6Al4V/chitosan sponge composite scaffold for orthopedic applications. *Mater. Sci. Eng. C* 58, 1177–1181.
- Han, F., Dong, Y., Su, Z., Yin, R., Song, A., Li, S., 2014. Preparation, characteristics and assessment of a novel gelatin–chitosan sponge scaffold as skin tissue engineering material. *Int. J. Pharm.* 476, 124–133.
- Han, S., Sung, H., Lee, G., Jun, J., Son, M., Kang, M., 2016. Chitosan-based film of tyrothricin for enhanced antimicrobial activity against common skin pathogens including *Staphylococcus aureus*. *J. Microbiol. Biotechnol.* 26, 953–958.
- He, P., Davis, S.S., Illum, L., 1998. In vitro evaluation of the mucoadhesive properties of chitosan microspheres. *Int. J. Pharm.* 166, 75–88.
- Hennink, W., Van Nostrum, C.F., 2012. Novel crosslinking methods to design hydrogels. *Adv. Drug Deliv. Rev.* 64, 223–236.
- Hoffman, A.S., 2012. Hydrogels for biomedical applications. *Adv. Drug Deliv. Rev.* 64, 18–23.
- Hu, N., Wu, H., Xue, C., Gong, Y., Wu, J., Xiao, Z., et al., 2013. Long-term outcome of the repair of 50 mm long median nerve defects in rhesus monkeys with marrow



- mesenchymal stem cells-containing, chitosan-based tissue engineered nerve grafts. *Biomaterials* 34, 100–111.
- Hu, X., Liu, S., Zhou, G., Huang, Y., Xie, Z., Jing, X., 2014. Electrospinning of polymeric nanofibers for drug delivery applications. *J. Control. Release* 185, 12–21.
- Hu, J., Kai, D., Ye, H., Tian, L., Ding, X., Ramakrishna, S., et al., 2017. Electrospinning of poly (glycerol sebacate)-based nanofibers for nerve tissue engineering. *Mater. Sci. Eng. C* 70, 1089–1094.
- Hutmacher, D.W., 2000. Scaffolds in tissue engineering bone and cartilage. *Biomaterials* 21, 2529–2543.
- Hynes, R.O., 2009. The extracellular matrix: not just pretty fibrils. *Science* 326, 1216–1219.
- Ikeda, T., Ikeda, K., Yamamoto, K., Ishizaki, H., Yoshizawa, Y., Yanagiguchi, K., et al., 2014. Fabrication and characteristics of chitosan sponge as a tissue engineering scaffold. *BioMed Res. Int.* 2014, 1–8. Article ID 786892.
- Ingber, D.E., Fernandez, J.G., 2016. High strength chitin composite material and method of making. Google Patents.
- Iviglia, G., Cassinelli, C., Bollati, D., Baino, F., Torre, E., Morra, M., et al., 2016a. Engineered porous scaffolds for periprosthetic infection prevention. *Mater. Sci. Eng. C* 68, 701–715.
- Iviglia, G., Cassinelli, C., Torre, E., Baino, F., Morra, M., Vitale-Brovarone, C., 2016b. Novel bioceramic-reinforced hydrogel for alveolar bone regeneration. *Acta Biomater.* 44, 97–109.
- Jain, E., Damania, A., Shakya, A.K., Kumar, A., Sarin, S.K., Kumar, A., 2015. Fabrication of macroporous cryogels as potential hepatocyte carriers for bioartificial liver support. *Colloids Surf. B Biointerf.* 136, 761–771.
- Jamalpoor, Z., 2015. Chitosan: a brief review on structure and tissue engineering application. *J. Appl. Tissue Eng.* 1, 3–7.
- Janmey, P., Uibo, R., Veski, P., Laidmäe, I., 2013. Durable haemostatic scaffold. Google Patents.
- Jayakumar, R., Tamura, H., Nair, S., Furuike, T., 2010. Perspectives of Chitin and Chitosan Nanofibrous Scaffolds in Tissue Engineering. INTECH Open Access Publisher.
- Jayakumar, R., Prabakaran, M., Kumar, P.S., Nair, S., Tamura, H., 2011. Biomaterials based on chitin and chitosan in wound dressing applications. *Biotechnol. Adv.* 29, 322–337.
- Jiang, T., Deng, M., Abdel-Fattah, W.I., Laurencin, C.T., 2012. Chitosan-based biopharmaceutical scaffolds in tissue engineering and regenerative medicine. *Chitosan-Based Systems for Biopharmaceuticals: Delivery, Targeting and Polymer Therapeutics*. Wiley, pp. 393–427.
- Jiang, T., Singh, B., Cho, Y., Akaike, T., Cho, C., 2015. Liver tissue engineering using functional marine biomaterials. *Funct. Mar. Biomater. Proper. Appl.* 91, 91–106.
- Jimtaisong, A., Saewan, N., 2014. Utilization of carboxymethyl chitosan in cosmetics. *Int. J. Cosmetic Sci.* 36, 12–21.
- Johnstone, B., Alini, M., Cucchiari, M., Dodge, G.R., Eglin, D., Guilak, F., et al., 2013. Tissue engineering for articular cartilage repair—the state of the art. *Eur. Cell. Mater.* 25, e67.
- Kang, C.-H., Lin, Y.-F., Huang, Y.-S., Tung, K.-L., Chang, K.-S., Chen, J.-T., et al., 2013. Synthesis of ZIF-7/chitosan mixed-matrix membranes with improved separation performance of water/ethanol mixtures. *J. Membr. Sci.* 438, 105–111.



- Karbasi, S., Fekrat, F., Semnani, D., Razavi, S., Zargar, E.N., 2016. Evaluation of structural and mechanical properties of electrospun nano-micro hybrid of poly hydroxybutyrate-chitosan/silk scaffold for cartilage tissue engineering. *Adv. Biomed. Res.* 5, 180–188.
- Karri, V.V.S.R., Kuppusamy, G., Talluri, S.V., Mannemala, S.S., Kollipara, R., Wadhwani, A.D., et al., 2016. Curcumin loaded chitosan nanoparticles impregnated into collagen-alginate scaffolds for diabetic wound healing. *Int. J. Biol. Macromol.* 93, 1519–1529.
- Kaya, M., Akyuz, B., Bulut, E., Sargin, I., Eroglu, F., Tan, G., 2016. Chitosan nanofiber production from *Drosophila* by electrospinning. *Int. J. Biol. Macromol.* 92, 49–55.
- Kean, T., Thanou, M., 2011. Chitin and chitosan: sources, production and medical applications. *Renew. Resour. Funct. Polym. Biomater.*
- Kessler, M.W., Grande, D.A., 2008. Tissue engineering and cartilage. *Organogenesis* 4, 28–32.
- Khan, Y., Yaszemski, M.J., Mikos, A.G., Laurencin, C.T., 2008. Tissue engineering of bone: material and matrix considerations. *J. Bone Joint Surg.* 90, 36–42.
- Kim, Y.-D., Pofali, P., Park, T.-E., Singh, B., Cho, K., Maharjan, S., et al., 2016. Gene therapy for bone tissue engineering. *Tissue Eng. Regener. Med.* 13, 111–125.
- Kock, L., Van Donkelaar, C.C., Ito, K., 2012. Tissue engineering of functional articular cartilage: the current status. *Cell Tissue Res.* 347, 613–627.
- Kumar, M.N.R., 2000. A review of chitin and chitosan applications. *React. Funct. Polym.* 46, 1–27.
- Kumari, S., Singh, R.P., 2013. Glycolic acid functionalized chitosan–Au–Fe 3 O 4 hybrid nanoparticle based nanohybrid scaffold for drug delivery. *Int. J. Biol. Macromol.* 54, 244–249.
- Kuo, C.-Y., Chen, C.-H., Hsiao, C.-Y., Chen, J.-P., 2015. Incorporation of chitosan in biomimetic gelatin/chondroitin-6-sulfate/hyaluronan cryogel for cartilage tissue engineering. *Carbohydr. Polym.* 117, 722–730.
- Kwon, O.-J., Kang, E., Choi, J.-W., Kim, S.W., Yun, C.-O., 2013. Therapeutic targeting of chitosan–PEG–folate-complexed oncolytic adenovirus for active and systemic cancer gene therapy. *J. Control. Release* 169, 257–265.
- Langer, R., Tirrell, D.A., 2004. Designing materials for biology and medicine. *Nature* 428, 487–492.
- Lee, M.-H., Thomas, J.L., Chen, J.-Z., Jan, J.-S., Lin, H.-Y., 2016. Activation of tumor suppressor p53 gene expression by magnetic thymine-imprinted chitosan nanoparticles. *Chem. Commun.* 52, 2137–2140.
- Levengood, S.K.L., Zhang, M., 2014. Chitosan-based scaffolds for bone tissue engineering. *J. Mater. Chem. B* 2, 3161–3184.
- Li, K.C., Hu, Y.C., 2015. Cartilage tissue engineering: recent advances and perspectives from gene regulation/therapy. *Adv. Healthc. Mater.* 4, 948–968.
- Li, R., Hu, P., Ren, X., Worley, S., Huang, T., 2013. Antimicrobial N-halamine modified chitosan films. *Carbohydr. Polym.* 92, 534–539.
- Li, L., Wang, N., Jin, X., Deng, R., Nie, S., Sun, L., et al., 2014. Biodegradable and injectable in situ cross-linking chitosan-hyaluronic acid based hydrogels for postoperative adhesion prevention. *Biomaterials* 35, 3903–3917.
- Li, K., Xing, R., Liu, S., Li, P., 2016. Advances in preparation, analysis and biological activities of single chitooligosaccharides. *Carbohydr. Polym.* 139, 178–190.
- Liu, C., Bai, R., 2014. Recent advances in chitosan and its derivatives as adsorbents for removal of pollutants from water and wastewater. *Curr. Opin. Chem. Eng.* 4, 62–70.

- Liu, M., Zheng, H., Chen, J., Li, S., Huang, J., Zhou, C., 2016a. Chitosan-chitin nanocrystal composite scaffolds for tissue engineering. *Carbohydr. Polym.* 152, 832–840.
- Liu, X., Mo, Y., Liu, X., Guo, R., Zhang, Y., Xue, W., et al., 2016b. Synthesis, characterisation and preliminary investigation of the haemocompatibility of polyethyleneimine-grafted carboxymethyl chitosan for gene delivery. *Mater. Sci. Eng. C* 62, 173–182.
- Liu, J., Meng, C.-G., Liu, S., Kan, J., Jin, C.-H., 2017. Preparation and characterization of protocatechuic acid grafted chitosan films with antioxidant activity. *Food Hydrocol.* 63, 457–466.
- Logithkumar, R., Keshavnarayan, A., Dhivya, S., Chawla, A., Saravanan, S., Selvamurugan, N., 2016. A review of chitosan and its derivatives in bone tissue engineering. *Carbohydr. Polym.* 151, 172–188.
- Lu, B., Wang, T., Li, Z., Dai, F., Lv, L., Tang, F., et al., 2016. Healing of skin wounds with a chitosan–gelatin sponge loaded with tannins and platelet-rich plasma. *Int. J. Biol. Macromol.* 82, 884–891.
- Lu, Z., Gao, J., He, Q., Wu, J., Liang, D., Yang, H., et al., 2017. Enhanced antibacterial and wound healing activities of microporous chitosan-Ag/ZnO composite dressing. *Carbohydr. Polym.* 156, 460–469.
- Luo, Y., Wang, Q., 2013. Recent advances of chitosan and its derivatives for novel applications in food science. *J. Food Process. Beverag.* 1, 1–13.
- Luo, Y., Wang, Q., 2014. Recent development of chitosan-based polyelectrolyte complexes with natural polysaccharides for drug delivery. *Int. J. Biol. Macromol.* 64, 353–367.
- Ma, P.X., Zhang, R., 2001. Microtubular architecture of biodegradable polymer scaffolds. *J. Biomed. Mater. Res.* 56, 469–477.
- Ma, X., Guo, L., Ji, Q., Tan, Y., Xing, Y., Xia, Y., 2016. Physical hydrogels constructed on a macro-cross-linking cationic polysaccharide with tunable, excellent mechanical performance. *Polym. Chem.* 7, 26–30.
- Mahanta, A.K., Maiti, P., 2016. Chitin and chitosan nanocomposites for tissue engineering. *Chitin and Chitosan for Regenerative Medicine*. Springer.
- Mahanta, A.K., Mittal, V., Singh, N., Dash, D., Malik, S., Kumar, M., et al., 2015. Polyurethane-grafted chitosan as new biomaterials for controlled drug delivery. *Macromolecules* 48, 2654–2666.
- Mahmoud, A.A., Salama, A.H., 2016. Norfloxacin-loaded collagen/chitosan scaffolds for skin reconstruction: preparation, evaluation and in-vivo wound healing assessment. *Eur. J. Pharm. Sci.* 83, 155–165.
- Maksym, P.V., 2015. Chitosan as a hemostatic agent: current state. *Eur. J. Med.* 2, 24–33.
- Man, Z., Hu, X., Liu, Z., Huang, H., Meng, Q., Zhang, X., et al., 2016. Transplantation of allogenic chondrocytes with chitosan hydrogel-demineralized bone matrix hybrid scaffold to repair rabbit cartilage injury. *Biomaterials* 108, 157–167.
- Mansuri, S., Kesharwani, P., Jain, K., Tekade, R.K., Jain, N., 2016. Mucoadhesion: a promising approach in drug delivery system. *React. Funct. Polym.* 100, 151–172.
- Mao, J., Zhou, Y.-S., Wu, T., 2016. High-absorbing chitosan dressings for hemostasis and wound healing. *J. Clin. Rehabil. Tissue Eng. Res.* 20, 2391–2396.
- Martins, A.F., Facchi, S.P., Follmann, H.D., Pereira, A.G., Rubira, A.F., Muniz, E.C., 2014. Antimicrobial activity of chitosan derivatives containing N-quaternized moieties in its backbone: a review. *Int. J. Mole. Sci.* 15, 20800–20832.
- Masaali, E., Morshed, M., Nasr-Esfahani, M.H., Sadri, S., Hilderink, J., Van Apeldoorn, A., et al., 2013. Fabrication, characterization and cellular compatibility of poly

- (hydroxy alkanoate) composite nanofibrous scaffolds for nerve tissue engineering. *PLoS One* 8, e57157.
- Mcgrath, B., McCarthy, S., Kuhn, S., Wold, A., Stolten, M., Bennett, A., 2014. Biocompatible and bioabsorbable derivatized chitosan compositions. Google Patents.
- Min, B.-M., Lee, S.W., Lim, J.N., You, Y., Lee, T.S., Kang, P.H., et al., 2004. Chitin and chitosan nanofibers: electrospinning of chitin and deacetylation of chitin nanofibers. *Polymer* 45, 7137–7142.
- Mirahmadi, F., Tafazzoli-shadpour, M., Shokrgozar, M.A., Bonakdar, S., 2013. Enhanced mechanical properties of thermosensitive chitosan hydrogel by silk fibers for cartilage tissue engineering. *Mater. Sci. Eng. C* 33, 4786–4794.
- Mohapatra, S., Wang, C., 2013. Graphene hydrogel and method for using the same. Google Patents.
- Morgado, P.I., Miguel, S.P., Correia, I.J., Aguiar-Ricardo, A., 2017. Ibuprofen loaded PVA/chitosan membranes: a highly efficient strategy towards an improved skin wound healing. *Carbohydr. Polym.* 159, 136–145.
- Muthukumar, T., Aravinthan, A., Sharmila, J., Kim, N.S., Kim, J.-H., 2016. Collagen/chitosan porous bone tissue engineering composite scaffold incorporated with Ginseng compound K. *Carbohydr. Polym.* 152, 566–574.
- Muzzarelli, R.A., El Mehtedi, M., Bottegoni, C., Aquili, A., Gigante, A., 2015. Genipin-crosslinked chitosan gels and scaffolds for tissue engineering and regeneration of cartilage and bone. *Mar. Drugs* 13, 7314–7338.
- Nawrotek, K., Tylman, M., Rudnicka, K., Gatkowska, J., Wieczorek, M., 2016. Epineurium-mimicking chitosan conduits for peripheral nervous tissue engineering. *Carbohydr. Polym.* 152, 119–128.
- Nesic, A., Gordic, M., Onjia, A., DaVidovic, S., Miljkovic, M., Dimitrijevic-Brankovic, S., 2017. Chitosan-triclosan films for potential use as bio-antimicrobial bags in healthcare sector. *Mater. Lett.* 186, 368–371.
- Nie, J., Lu, W., Ma, J., Yang, L., Wang, Z., Qin, A., et al., 2015. Orientation in multi-layer chitosan hydrogel: morphology, mechanism, and design principle. *Sci. Rep.* 5, 1–7.
- Nwe, N., Furuie, T., Tamura, H., 2009. The mechanical and biological properties of chitosan scaffolds for tissue regeneration templates are significantly enhanced by chitosan from *Gongronella butleri*. *Materials* 2, 374–398.
- Ohkawa, K., Cha, D., Kim, H., Nishida, A., Yamamoto, H., 2004. Electrospinning of chitosan. *Macromol. Rapid Commun.* 25, 1600–1605.
- Ouerghemmi, S., Degoutin, S., Tabary, N., Cazaux, F., Maton, M., Gaucher, V., et al., 2016. Triclosan loaded electrospun nanofibers based on a cyclodextrin polymer and chitosan polyelectrolyte complex. *Int. J. Pharm.* 513, 483–495.
- Oyervides-Muñoz, E., Pollet, E., Ulrich, G., Sosa-Santillan, G., Avérous, L., 2017. Original method for synthesis of chitosan-based antimicrobial agent by quaternary ammonium grafting. *Carbohydr. Polym.* 157, 1922–1932.
- Pack, D.W., Hoffman, A.S., Pun, S., Stayton, P.S., 2005. Design and development of polymers for gene delivery. *Nat. Rev. Drug Discov.* 4, 581–593.
- Park, P.-J., Je, J.-Y., Jung, W.-K., Ahn, C.-B., Kim, S.-K., 2004. Anticoagulant activity of heterochitosans and their oligosaccharide sulfates. *Eur. Food Res. Technol.* 219, 529–533.
- Park, H., Choi, B., Hu, J., Lee, M., 2013. Injectable chitosan hyaluronic acid hydrogels for cartilage tissue engineering. *Acta Biomater.* 9, 4779–4786.

- Patrúlea, V., Ostafe, V., Borchard, G., Jordan, O., 2015. Chitosan as a starting material for wound healing applications. *Eur. J. Pharm. Biopharm.* 97, 417–426.
- Petrova, V., Chernyakov, D.D., Moskalenko, Y.E., Gasilova, E.R., Strelina, I.A., Okatova, O.V., et al., 2017. O, N-(2-sulfoethyl) chitosan: synthesis and properties of solutions and films. *Carbohydr. Polym.* 157, 866–874.
- Pillai, C., Paul, W., Sharma, C.P., 2009. Chitin and chitosan polymers: chemistry, solubility and fiber formation. *Progress Polym. Sci.* 34, 641–678.
- Radhakumary, C., Antonty, M., Sreenivasan, K., 2011. Drug loaded thermoresponsive and cytocompatible chitosan based hydrogel as a potential wound dressing. *Carbohydr. Polym.* 83, 705–713.
- Raftery, R., O'Brien, F.J., Cryan, S.-A., 2013. Chitosan for gene delivery and orthopedic tissue engineering applications. *Molecules* 18, 5611–5647.
- Raftery, R.M., Tierney, E.G., Curtin, C.M., Cryan, S.-A., O'Brien, F.J., 2015. Development of a gene-activated scaffold platform for tissue engineering applications using chitosan-pDNA nanoparticles on collagen-based scaffolds. *J. Control. Release* 210, 84–94.
- Ran, J., Hu, J., Sun, G., Chen, S., Jiang, P., Shen, X., et al., 2016. A novel chitosan-tussah silk fibroin/nano-hydroxyapatite composite bone scaffold platform with tunable mechanical strength in a wide range. *Int. J. Biol. Macromol.* 93, 87–97.
- Reed, J.D., Krueger, C.G., Madrigal-Carballo, S., 2014. Tannin-chitosan composites. Google Patents.
- Rezwan, K., Chen, Q., Blaker, J., Boccaccini, A.R., 2006. Biodegradable and bioactive porous polymer/inorganic composite scaffolds for bone tissue engineering. *Biomaterials* 27, 3413–3431.
- Ribeiro, L.N., Alcântara, A.C., Darder, M., Aranda, P., Araújo-Moreira, F.M., Ruiz-Hitzky, E., 2014. Pectin-coated chitosan–LDH bionanocomposite beads as potential systems for colon-targeted drug delivery. *Int. J. Pharm.* 463, 1–9.
- Roberts, G., 2013. *Langmuir-Blodgett Films*. Springer Science & Business Media.
- Rodríguez-Vázquez, M., Vega-Ruiz, B., Ramos-Zúñiga, R., Saldaña-Koppel, D.A., Quiñones-Olvera, L.F., 2015. Chitosan and its potential use as a scaffold for tissue engineering in regenerative medicine. *BioMed Res. Int.* 2015, 1–15.
- Sámamo-Valencia, C., Martínez-Castañón, G., Martínez-Gutiérrez, F., Ruiz, F., Toro-Vázquez, J., Morales-Rueda, J., et al., 2014. Characterization and biocompatibility of chitosan gels with silver and gold nanoparticles. *J. Nanomater.* 2014, 142.
- Sangsanoh, P., Supaphol, P., 2006. Stability improvement of electrospun chitosan nanofibrous membranes in neutral or weak basic aqueous solutions. *Biomacromolecules* 7, 2710–2714.
- Saravanan, S., Leena, R., Selvamurugan, N., 2016. Chitosan based biocomposite scaffolds for bone tissue engineering. *Int. J. Biol. Macromol.* 93, 1354–1365.
- Semnani, D., Naghashzargar, E., Hadianfar, M., Dehghan Manshadi, F., Mohammadi, S., Karbasi, S., et al., 2017. Evaluation of PCL/chitosan electrospun nanofibers for liver tissue engineering. *Int. J. Polym. Mater. Polym. Biomater.* 66, 149–157.
- Shahriarpanah, S., Nourmohammadi, J., Amoabediny, G., 2016. Fabrication and characterization of carboxylated starch-chitosan bioactive scaffold for bone regeneration. *Int. J. Biol. Macromol.* 93, 1069–1078.
- Shakir, M., Jolly, R., Khan, M.S., Rauf, A., Kazmi, S., 2016. Nano-hydroxyapatite/ $\beta$ -CD/chitosan nanocomposite for potential applications in bone tissue engineering. *Int. J. Biol. Macromol.* 93, 276–289.

- Silva, S.S., Luna, S.M., Gomes, M.E., Benesch, J., Pashkuleva, I., Mano, J.F., et al., 2008. Plasma surface modification of chitosan membranes: characterization and preliminary cell response studies. *Macromol. Biosci.* 8, 568–576.
- Sinha, M., Banik, R.M., Halder, C., Maiti, P., 2013. Development of ciprofloxacin hydrochloride loaded poly (ethylene glycol)/chitosan scaffold as wound dressing. *J. Porous Mater.* 20, 799–807.
- Sivashankari, P., Prabakaran, M., 2016. Prospects of chitosan-based scaffolds for growth factor release in tissue engineering. *Int. J. Biol. Macromol.* 93, 1382–1389.
- Skop, N.B., Calderon, F., Levison, S.W., Gandhi, C.D., Cho, C.H., 2013. Heparin cross-linked chitosan microspheres for the delivery of neural stem cells and growth factors for central nervous system repair. *Acta Biomater.* 9, 6834–6843.
- Smart, J.D., 2005. The basics and underlying mechanisms of mucoadhesion. *Adv. Drug Deliv. Rev.* 57, 1556–1568.
- Sogias, I.A., Williams, A.C., Khutoryanskiy, V.V., 2008. Why is chitosan mucoadhesive? *Biomacromolecules* 9, 1837–1842.
- Soltani, S., Ebrahimian-Hosseinabadi, M., Kharazi, A.Z., 2016. Chitosan/graphene and poly (D, L-lactic-co-glycolic acid)/graphene nano-composites for nerve tissue engineering. *Tissue Eng. Regen. Med.* 13, 684–690.
- Song, H.-F., Chen, A.-Z., Wang, S.-B., Kang, Y.-Q., Ye, S.-F., Liu, Y.-G., et al., 2014. Preparation of chitosan-based hemostatic sponges by supercritical fluid technology. *Materials* 7, 2459–2473.
- Stephen-Haynes, J., Gibson, E., Greenwood, M., 2014. Chitosan: a natural solution for wound healing. *J. Commun. Nurs.* 28, 48–53.
- Sudarshan, N., Hoover, D., Knorr, D., 1992. Antibacterial action of chitosan. *Food Biotechnol.* 6, 257–272.
- Sun, P., Huang, W., Jin, M., Wang, Q., Fan, B., Kang, L., et al., 2016. Chitosan-based nanoparticles for survivin targeted siRNA delivery in breast tumor therapy and preventing its metastasis. *Int. J. Nanomed.* 11, 4931.
- Sun, Z., Shi, C., Wang, X., Fang, Q., Huang, J., 2017. Synthesis, characterization, and antimicrobial activities of sulfonated chitosan. *Carbohydr. Polym.* 155, 321–328.
- Sundaram, M.N., Deepthi, S., Jayakumar, R., 2016. Chitosan-gelatin composite scaffolds in bone tissue engineering. *Chitin and Chitosan for Regenerative Medicine*. Springer.
- Svirshchevskaya, E., Zubareva, A., Boyko, A., Shustova, O., Grechikhina, M., Shagdarova, B.T., et al., 2016. Analysis of toxicity and biocompatibility of chitosan derivatives with different physico-chemical properties. *Appl. Biochem. Microbiol.* 52, 483–490.
- Takara, E.A., Marchese, J., Ochoa, N.A., 2015. NaOH treatment of chitosan films: impact on macromolecular structure and film properties. *Carbohydr. Polym.* 132, 25–30.
- Teotia, R.S., Kalita, D., Singh, A.K., Verma, S.K., Kadam, S.S., Bellare, J.R., 2015. Bifunctional polysulfone-chitosan composite hollow fiber membrane for bioartificial liver. *ACS Biomater. Sci. Eng.* 1, 372–381.
- Thorat, N., Otari, S., Patil, R., Bohara, R., Yadav, H., Koli, V., et al., 2014. Synthesis, characterization and biocompatibility of chitosan functionalized superparamagnetic nanoparticles for heat activated curing of cancer cells. *Dalton Trans.* 43, 17343–17351.
- Timashev, P., Bardakova, K., Minaev, N., Demina, T., Mishchenko, T., Mitroshina, E., et al., 2016. Compatibility of cells of the nervous system with structured biodegradable chitosan-based hydrogel matrices. *Appl. Biochem. Microbiol.* 52, 508–514.

- Tiwari, G., Tiwari, R., Sriwastawa, B., Bhati, L., Pandey, S., Pandey, P., et al., 2012. Drug delivery systems: an updated review. *Int. J. Pharm. Investig.* 2, 2.
- Tripathi, A., Melo, J.S., 2015. Preparation of a sponge-like biocomposite agarose–chitosan scaffold with primary hepatocytes for establishing an in vitro 3D liver tissue model. *RSC Adv.* 5, 30701–30710.
- Uswatta, S.P., Okeke, I.U., Jayasuriya, A.C., 2016. Injectable porous nano-hydroxyapatite/chitosan/tripolyphosphate scaffolds with improved compressive strength for bone regeneration. *Mater. Sci. Eng. C* 69, 505–512.
- Vakili, M., Rafatullah, M., Salamatina, B., Abdullah, A.Z., Ibrahim, M.H., Tan, K.B., et al., 2014. Application of chitosan and its derivatives as adsorbents for dye removal from water and wastewater: a review. *Carbohydr. Polym.* 113, 115–130.
- Vedakumari, W.S., Ayaz, N., Karthick, A.S., Senthil, R., Sastry, T.P., 2017. Quercetin impregnated chitosan–fibrin composite scaffolds as potential wound dressing materials—fabrication, characterization and in vivo analysis. *Eur. J. Pharm. Sci.* 97, 106–112.
- Venkatesan, J., Jayakumar, R., Mohandas, A., Bhatnagar, I., Kim, S.-K., 2014. Antimicrobial activity of chitosan-carbon nanotube hydrogels. *Materials* 7, 3946–3955.
- Wang, K., Kievit, F.M., Florczyk, S.J., Stephen, Z.R., Zhang, M., 2015. 3D porous chitosan–alginate scaffolds as an in vitro model for evaluating nanoparticle-mediated tumor targeting and gene delivery to prostate cancer. *Biomacromolecules* 16, 3362–3372.
- Wang, B., Hu, Q., Wan, T., Yang, F., Cui, L., Hu, S., et al., 2016a. Porous lactose-modified chitosan scaffold for liver tissue engineering: influence of galactose moieties on cell attachment and mechanical stability. *Int. J. Polym. Sci.* 2016, 1–8. Article ID 2862738.
- Wang, N., Xu, X., Li, H., Zhai, J., Yuan, L., Zhang, K., et al., 2016b. Preparation and application of a xanthate-modified thiourea chitosan sponge for the removal of Pb (2) from aqueous solutions. *Industr. Eng. Chem. Res.* 55, 4960–4968.
- Wang, Q., Chen, S., Chen, D., 2017. Preparation and characterization of chitosan based injectable hydrogels enhanced by chitin nano-whiskers. *J. Mech. Behav. Biomed. Mater.* 65, 466–477.
- Wedmore, I., Mcmanus, J.G., Pusateri, A.E., Holcomb, J.B., 2006. A special report on the chitosan-based hemostatic dressing: experience in current combat operations. *J. Trauma Acute Care Surg.* 60, 655–658.
- Wei, G., Ma, P.X., 2004. Structure and properties of nano-hydroxyapatite/polymer composite scaffolds for bone tissue engineering. *Biomaterials* 25, 4749–4757.
- Weir, M.D., Xu, H.H., 2010. Osteoblastic induction on calcium phosphate cement–chitosan constructs for bone tissue engineering. *J. Biomed. Mater. Res. Part A* 94, 223–233.
- Wrobel, S., Serra, S.C., Ribeiro-Samy, S., Sousa, N., Heimann, C., Barwig, C., et al., 2014. In vitro evaluation of cell-seeded chitosan films for peripheral nerve tissue engineering. *Tissue Eng. Part A* 20, 2339–2349.
- Xu, Y., Han, J., Lin, H., 2017. Fabrication and characterization of a self-crosslinking chitosan hydrogel under mild conditions without the use of strong bases. *Carbohydr. Polym.* 156, 372–379.
- Yan, J., Wu, T., Ding, Z., Li, X., 2016. Preparation and characterization of carbon nanotubes/chitosan composite foam with enhanced elastic property. *Carbohydr. Polym.* 136, 1288–1296.

- Yang, Y., Yang, S., Wang, Y., Yu, Z., Ao, H., Zhang, H., et al., 2016. Anti-infective efficacy, cytocompatibility and biocompatibility of a 3D-printed osteoconductive composite scaffold functionalized with quaternized chitosan. *Acta Biomater.* 46, 112–128.
- Yao, Q., Nooeaid, P., Roether, J.A., Dong, Y., Zhang, Q., Boccaccini, A.R., 2013. Bioglass®-based scaffolds incorporating polycaprolactone and chitosan coatings for controlled vancomycin delivery. *Ceram. Int.* 39, 7517–7522.
- Zawko, S., Schmidt, C., 2016. Dendritic macroporous hydrogels prepared by crystal templating. Google Patents.
- Zazakowny, K., Lewandowska-Łańcucka, J., Mastalska-Popławska, J., Kamiński, K., Kusior, A., Radecka, M., et al., 2016. Biopolymeric hydrogels – nanostructured TiO<sub>2</sub> hybrid materials as potential injectable scaffolds for bone regeneration. *Colloids Surf. B Biointerf.* 148, 607–614.
- Zhang, D., Zhou, W., Wei, B., Wang, X., Tang, R., Nie, J., et al., 2015. Carboxyl-modified poly (vinyl alcohol)-crosslinked chitosan hydrogel films for potential wound dressing. *Carbohydr. Polym.* 125, 189–199.
- Zo, S.M., Singh, D., Kumar, A., Cho, Y.W., Oh, T.H., Han, S.S., 2012. Chitosan-hydroxyapatite macroporous matrix for bone tissue engineering. *Curr. Sci. (Bangalore)* 103, 1438–1446.

# Hydroxyapatite: an inorganic ceramic for biomedical applications

Varun Saxena<sup>1</sup>, Ishani Shukla<sup>2</sup> and Lalit M. Pandey<sup>1</sup>

<sup>1</sup>*Department of Biosciences and Bioengineering, Indian Institute of Technology Guwahati, Guwahati, India* <sup>2</sup>*Department of Industrial & Management Engineering, Indian Institute of Technology Kanpur, Kanpur, India*

## 8.1 INTRODUCTION

Hydroxyapatite (HAp) is a calcium phosphate ceramic. Calcium HAp [HAp,  $\text{Ca}_{10}(\text{PO}_4)_6(\text{OH})_2$ , Ca:P molar ratio of 1.67] possesses chemical and mechanical similarities to the mineral component of the hard tissues such as bone, tooth, dentine, enamel, and calcified parts of tendons (Orlovskii et al., 2002) and owns good bioactivity, biodegradability, osteoconductivity, biological stability, and affinity at biological pH values (Shi et al., 2002). In the human body, it is found in carbonated apatite form with small calcium deficiency. Calcium HAp is insoluble at physiological pH (7.4) but is slightly soluble at acidic pH, that is, below 6.5 (Maitra, 2005). Apatite is a common term given to the metal phosphates, generally found in chloro ( $\text{Cl}^-$ ), fluoro ( $\text{F}^-$ ), and hydroxy ( $\text{OH}^-$ ) form. The term *apatite* is generated from the Greek word “apate,” which means “deceit.” The term was coined because of the varying colored appearance in different crystals owing to different elemental configurations with the basic formula  $\text{M}_{10}(\text{ZO}_4)_6\text{X}_2$ , where M represents a variety of minerals such as Ca, Mg, Fe, Cd, etc., and Z represents P, As, V, S, C, S, etc. X represents F, Cl, Br, OH, etc. (Suetsugu and Tateishi). The most common apatite found in the body is calcium HAp. Depending upon the Ca:P ratios, calcium phosphate encompasses variable phases, listed in Table 8.1.

HAp is the most extensively used bioceramic in prosthetic applications because of its similarity with the crystallography and the chemical composition of the human bone. The major advantage of HAp is the application based synthesis system and it can be synthesized in many forms such as dense ceramic (Zhou et al., 2015), powder (Kulpetchdara et al., 2016), coating material (Mahmood and Mohammed, 2016), and porous material (Uswatta et al., 2016) depending upon the application. The wide application of HAp has attracted researchers to use it as a delivery system for proteins, peptides, genes, and drugs (Paul and Sharma, 1999; Zhu et al., 2004; Kazemzadeh-Narbat et al., 2010; Yi et al., 2016), because



**Table 8.1** Variable Phases of HAp

S. No.	Ca/P Ratio	General Name	Formula
1	0.5	Monocalcium phosphate	$\text{Ca}(\text{H}_2\text{PO}_4)_2$
2	1.0	Dicalcium phosphate	$\text{CaHPO}_4$
3	1.33	Octacalcium phosphate	$\text{Ca}_8(\text{HPO}_4)_2(\text{PO}_4)_4$
4	1.5	Tricalcium phosphate	$\text{Ca}_3(\text{PO}_4)_2$
5	1.67	HAp	$\text{Ca}_{10}(\text{PO}_4)_6(\text{OH})_2$

of its excellent tailorable properties. Besides using HAp as a delivery vehicle for bioactive compounds, HAp is a promising ceramic for bone tissue engineering (Treccani et al., 2013; Gopi et al., 2014b), dental application (Lett et al., 2016; Pignatelli et al., 2016), and stem cell differentiation (Hoffman et al., 2016; Tohgi et al., 2016).

Musculoskeletal diseases such as osteoporosis, osteomyelitis (OM), osteonecrosis, arthritis, bone fracture, and bone tumor are the major problems prevalent these days. Due to a heavy rate of accidents and insufficient availability of treatment, the situation has given rise to a major hunt in the field for biomedical research. Bone tissue engineering is generally applied to cure serious damage to bone caused by various factors. Bone tissue engineering pacts with the bone regeneration strategies by overcoming the inherent biological, mechanical, and structural obstacles. Bone regeneration strategies include the approaches to engineer the bone, the cellular responses of bone cells to the engineered materials, and the effect of the engineering stratagem to osteogenic genes and proteins (Healy and Guldberg, 2007). Materials that are used in tissue engineering are termed as “biomaterials” and generally include metals and alloys, ceramics and glasses, polymers and composites. Metals and metal alloys have played a pivotal role in bone tissue engineering but their lower biological responses and corrosion frequency have been their major drawbacks. Ceramics are inorganic bioactive materials that get resorbed after supporting repair of the damaged tissue. Ceramics are used in joint replacement, bone repair, and augmentation (Davis, 2003). Among all the ceramics currently being used in biomedical engineering, calcium HAp is the most explored bioceramic for bone tissue engineering.

Development of nanotechnology has placed a major impact over material sciences. The discrete electronic energy level at nanorange provides enhanced properties such as higher surface-to-volume ratio and higher mechanical strength to the nanomaterial. Nanomaterials, due to their specific surface properties, are being researched for a vast level of biomedical and environmental applications. These applications include drug delivery (Hasan et al., 2017), nanoantibiotics (Saxena et al., 2018b), tissue engineering (Hasan et al., 2018a,b), 3D printing (Roy et al., 2018), biodiesel production (Sharma et al., 2018b), and environmental cleanup (Tiwari et al., 2017; Sharma et al., 2018a). Nano-HAp is widely used bioceramic material for biomedical applications because of its excellent

biocompatibility and osteoconductive properties (Andronescu et al., 2016). For tissue engineering, a scaffold must have high porosity for larger surface-to-volume ratio, specific surface properties to enable cell adhesion, mechanical integrity, and biocompatibility (Prakasam et al., 2015). HAp, at nanorange, typically 1–100 nm in size, possesses all these given properties and hence is vastly being analyzed in the form of scaffolds for orthopedic applications. The particle size, shape, and degree of crystallinity can be controlled through the sintering process. The final properties of a material directly depend on the synthesis methodology, initial grain size, agglomeration, and the sintering temperature and pressure. Nanoporous HAp is widely in use due to its high cargo loading capacity, in comparison to HAp nanoparticles (NPs) with fewer porosity. Their hollow core aids the loader pool, while nanoporous shell pedals the loading and release of the guest molecules (Yang et al., 2013).

Pure HAp (Ca:P = 1.67) is resistant to resorption after being implemented in the body and hence researchers have tried to use HAp as an inorganic matrix for various biomedical applications. Nano-HAp doped with heavy metals like zinc, silver, copper, etc., have shown better antimicrobial activity against various bacterial strains (Stanić et al., 2010; Jadalannagari et al., 2013; Tobaldi et al., 2016). Hence, to find the maximum similarity with the chemical and mechanical properties of bone together, researchers are still exploring doping HAp with various elements.

---

## 8.2 BASIC STRUCTURE OF CALCIUM HYDROXYAPATITE

The crystal structure of the synthetic material plays a pivotal role in basic properties such as solubility, bioactivity, and biocompatibility of the material. All these properties are tailorable according to the crystal structure of the material. For example carbonate substituted HAp is more bioactive than stoichiometric HAp (Redey et al., 1999). The native crystal structure of HAp remains in hexagonal space group  $P6_3/m$  with lattice parameter  $a = b = 9.432$  and  $c = 6.881$  and  $\gamma = 120$  degrees (Kay et al., 1964) but in case of stoichiometric HAp the space group remains in monoclinic  $P2_1/b$  form (Elliott et al., 1973). Generally both natural and synthetic HAp remains either defective or poorly crystalline, which leads to broad diffraction lines in X-ray diffraction (XRD). Hence, the slight structural difference between hexagonal and monoclinic structure cannot be distinguished properly by the XRD data. The study reveals that both the hexagonal and monoclinic structures satisfy the basic properties of HAp but energetically  $P6_3/m$  hexagonal structure is not favorable (Ma and Liu, 2009). (Haverty et al., 2005) revealed that HAp crystallizes in a mixture of 23%  $P2_1/b$  and 77%  $P2_1$  monoclinic phases (Leventouri, 2006). To explain their study they revealed that the hexagonal structure generally defines the nonstoichiometric HAp containing impurities of  $Cl^-$  and  $F^-$  ions. In chloro and fluoroapatite, the  $Cl^-$  or  $F^-$  ions lie

at the center of Ca triangles on mirror planes at  $z = 0.25$  and  $0.75$ . Array of  $\text{PO}_4^{3-}$  tetrahedra are held together by  $\text{Ca}^{2+}$  ion.  $\text{Ca}^{2+}$  ions occur at axes and are in accurately aligned columns. However, in the case of HAp this configuration is possible only if  $\text{OH}^-$  ion superpose each other at a distance of  $0.7 \text{ \AA}$ . Hence the hexagonal form of HAp can only be defined by the removal of mirror planes at  $z = 0.25$  and  $0.75$  giving rise to the hexagonal space group 173,  $\text{P6}_3$  symmetry (Haverty et al., 2005). Fig. 8.1 shows the crystal structure of HAp presenting the  $c$ -axis, which remains perpendicular to the  $a$ -axis lying at 120 degrees.

Human bone is a biphasic form of inorganic–organic matrix (calcium HAp–collagen). Human bone mineral is a nonstoichiometric nanocrystalline apatite with impurities in form of cosubstituted trace elements of  $\text{Na}^+$ ,  $\text{Mg}^{2+}$ ,  $\text{Zn}^{2+}$ ,  $\text{Sr}^{2+}$ ,  $\text{K}^+$ ,  $\text{F}^-$ ,  $\text{Cl}^-$ ,  $\text{CO}_3^{2-}$ , Si, etc. (Suetsugu and Tateishi). These impurities provide the inversed centers for the OH directions. In general the cations substitute the  $\text{Ca}^{2+}$  ion,  $\text{SiO}_4^{4-}$  replaces the  $\text{PO}_4$  tetrahedra and fluoride, and the chloride ion replaces the hydroxyl group in the basic crystal lattice (Lin et al., 2011). Thus, from various studies it can be concluded that the pure, synthetic, or

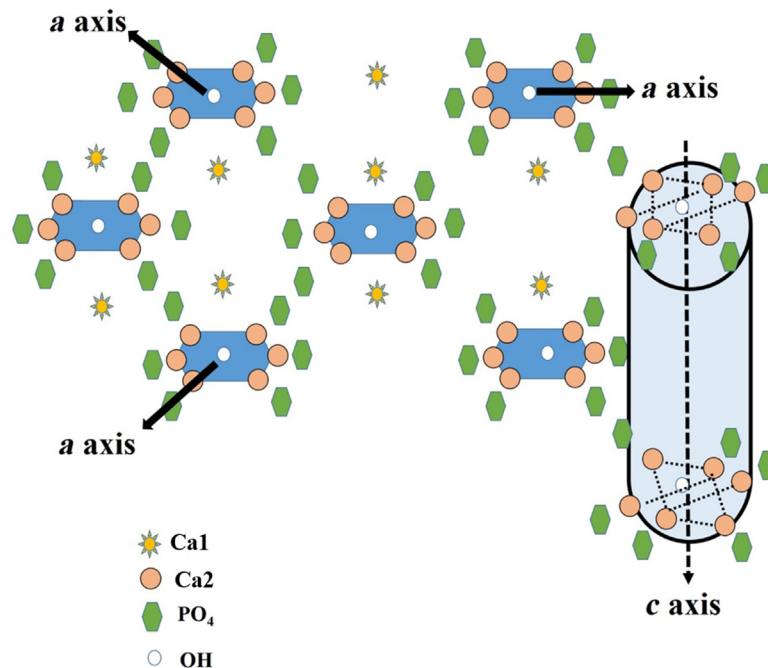


FIGURE 8.1

Crystal structure of HAp, the three  $a$ -axis at 120 degree angle, and the perpendicular  $c$ -axis.

**Table 8.2** Hexagonal and Monoclinic Crystal Structure of HAp

Properties	Hexagonal	Monoclinic
Space group symmetry	$P6_3/m$	$P2_1/b$
Lattice parameter	$a = b = 9.432$ , $c = 6.881$ Å, $\gamma = 120$ degrees	$a = 9.4214(8)$ Å, $b = 2a$ , $c = 6.8814(7)$ Å, $\gamma = 120$ degrees
Sintering temperature	25°C–100°C	Elevated temperature, 850°C
Details	Array of PO <sub>4</sub> tetrahedra held together by Ca ion. Ca ions occurs at axes and in accurately aligned columns.	Same as hexagon, only direction of OH group changes.

stoichiometric HAp remains in monoclinic form and on the other hand, the non-stoichiometric HAp or natural HAp remains in hexagonal form. A detailed comparison between hexagonal and monoclinic structure of HAp is given in Table 8.2. Although there is a very small difference between the hexagonal and the monoclinic geometry of the HAp particles, this difference exerts an effective impact over some physicochemical properties of the HAp such as compressive strength and porosity (Xue et al., 2016). Because of this dependence, the synthesis and effect of monoclinic HAp over biological activities is attracting the investigators more (Bystrov et al., 2013; Bystrov, 2015; Slepko and Demkov, 2015; Horiuchi et al., 2016).

Although the hexagonal geometry is centrosymmetric, but the monoclinic geometry of HAp is noncentrosymmetric and thus can encompass piezoelectric properties. Tofail et al. (2009) studied the piezoelectric nature of the sintered HAp using a direct quasistatic and an ultrasound measurement technique. However, they could not find the fix value of piezoelectric coefficient yet they reported the presence of piezoelectricity in HAp (Tofail et al., 2009). Later Bystrov et al. (2015) studied the piezoelectric properties of the ordered monoclinic HAp. Their study revealed that the ordered form of HAp possesses piezoelectricity with a piezoelectric coefficient  $\sim 15.7$  pm/V (Bystrov, 2015). This piezoelectricity of HAp resembles the natural bone and thus helps in the bone cell proliferation. Human osteoblast cells have shown enhanced growth and proliferation in the presence of ferroelectric materials (Vaněk et al., 2016). Because of this piezoelectricity of the material, the protein interaction with the material enhances. In general, the piezoelectric current modulates the voltage generated by bone stress, leading to the higher osteogenic activity. The piezoelectric response of bone tissue majorly senses the large tissue deformation and growth for the deposition. Although dry bone is considered to be piezoelectric, the piezoelectric property of the fully hydrated bone is still unclear (Rodriguez et al., 2016).

### 8.3 SYNTHESIS ROUTES OF HYDROXYAPATITE

During the past decades, diverse synthesis routes have been optimized to synthesize the nano-HAp with variable reaction processing conditions. Each method summarizes the different reaction parameters to synthesize the HAp in nanorange. Many of the researchers with variable levels of success have tried various approaches. These synthesis routes directly govern the basic and inherent properties of the HAp matrix. In the present chapter, we have tried to review all these methods. A brief detail of all these methods is as follows.

#### 8.3.1 PHYSICAL METHOD

Physical methods are generally known as the top down approach. In this method, an external force such as temperature or pressure is applied to initiate the reaction and it does not require a solvent in the synthesis. Hence they remain unaffected by the synthesis parameters and are generally used for bulk production. These methods lack control over the size and morphology of the synthesized materials. Physical methods can be classified into two major forms.

##### 8.3.1.1 *Solid state method*

In this method, high temperature range, that is, 500°C–1400°C, is applied to the raw materials such as calcium and phosphate precursors to initiate the reaction. The mechanism of the methods can be concluded as the solid diffusion of ions amongst the powdered raw materials. To synthesize the nano-HAp, the raw materials are first ball milled overnight. The calcium and phosphate resources are first mixed with additives such as hydrofluoric acid, binder such as PVA, and an organic vehicle such as acetone to form a slurry before milling. This slurry is then dried and compressed at elevated pressure, that is, 135 MPa, followed by sintering at >1250°C (Rao and Kannan, 2002; Pramanik et al., 2007; Ho et al., 2013).

##### 8.3.1.2 *Mechanochemical technique*

In this method the starting materials (calcium and phosphate precursor) are first weighed to coincide with the stoichiometric HAp and are sieved before use. These materials are then mixed in either water or acetone and are ball milled through zirconia balls. The samples are then dried and sintered at elevated temperature >1100°C. This method is purely dependent upon the mechanical force exerted by the zirconia balls at higher milling speed and generally gives a nano-sized HAp (Ebrahimi-Kahrizsangi et al., 2011; Fahami et al., 2016, 2011, 2012; Hattori et al., 2015; Bulina et al., 2016).

### 8.3.2 CHEMICAL METHODS

As described earlier, the lack of control over morphology and size leads to the need for wet methods or chemical methods. These methods are generally considered as the bottom up approaches. In these methods suitable calcium and phosphate precursors are mixed in molar stoichiometric ratios and are then allowed to react. Generally calcium nitrate and diammonium hydrogen phosphate are taken as calcium and phosphate precursors respectively. Various parameters govern the reaction process to control the size and morphology. Solution-based reactions can be accomplished in either water or in organic solvents. These reactions can be processed either at room temperature or at elevated temperature ranges. pH also plays a very important role in solvent-based methods. These chemical methods can be classified into the following subgroups.

#### 8.3.2.1 Chemical precipitation method

Among all the chemical methods, the conventional chemical method is the most abundant chemical route of synthesis of HAp. The mechanism involves the insolubility of HAp at higher pH range, generally  $>9$ . The typical process involved is the addition of one precursor dropwise to another at temperature ranging from room temperature to  $>65^{\circ}\text{C}$ , under constant stirring. After the process is over the pH is increased up to 11. Various pH ranges have been optimized. The process also involves the regular washing after synthesis to remove the byproducts, generally nitrates. The samples are then dried and calcinated at higher temperature, that is, at  $650^{\circ}\text{C}$  (Kakiage et al., 2015; Peng et al., 2015; Andrade et al., 2016; Barandehfard et al., 2016; Ramakrishnan et al., 2016).

#### 8.3.2.2 Sol–gel method

This method was the first method introduced as a chemical method to synthesize the nano-HAp. However this method is generally used for coating of HAp over other materials, rather than the conventional synthesis. This method is advantageous over chemical precipitation as it offers atomic/molecular level mixing of the reactants leading to the homogeneity and the nanosized resultant powder. The typical process involves the three-dimensional solution network by mixing inorganic alkoxides in either water or in organic solvents by a hydrolysis process followed by aging and gelation at room temperature. Gels are formed by dehydration process and the mesh like network is formed. After gelation, the samples are dried at higher temperature ( $80^{\circ}\text{C}$ ) and are sintered at variable temperature ( $500^{\circ}\text{C}$ – $700^{\circ}\text{C}$ ) to remove the organic residues (Hsieh et al., 2001; Kim and Kumta, 2004; Kuriakose et al., 2004; Chen et al., 2011; Asri et al., 2016).

#### 8.3.2.3 Hydrothermal/solvothermal method

Hydrothermal or solvothermal synthesis route is so called depending upon the solvent utilized during the synthesis process. In the hydrothermal process water is generally taken as the solvent whereas in the solvothermal process solvents other

than water, generally organic solvents, are used. In a typical process, the calcium and phosphate precursors are first mixed in a molar stoichiometric ratio of 1.67 Ca:P. The mixture is then stirred for about 30 minutes. The solution obtained is then transferred to a Teflon coated stainless steel hydrothermal chamber/autoclave and is then placed at elevated temperature at about 150°C. The reaction occurs at higher pressure and temperature. After 12 hours, the autoclave is allowed to cool down at room temperature and the powder obtained is then dried and calcinated at higher temperature (Sadat-Shojai et al., 2013; Wu et al., 2013; An et al., 2016; Sierra-Pallares et al., 2016; Zhou et al., 2017).

#### **8.3.2.4 Emulsion technique**

The emulsion technique provides an advantage over other wet methods in controlling the morphology of the synthesized materials. In a typical synthesis process, the surfactants are first mixed with the organic solvents at the critical micellar concentration (CMC) to form micelles. The calcium and phosphate precursor are then mixed at the molar stoichiometric ratio of 1.67 Ca:P, the solution obtained is stirred, and the pH of the solution is then set to >9. The precipitate thus obtained is then dried and calcinated at elevated temperature. At CMC the resultant HAp obtained remains spherical in structure. At surfactant concentration more than CMC the micelles tend to elongate thus changing the morphology of the resultant HAp. At very high surfactant concentration nanorods of HAp have been obtained (Wu et al., 2013; Bakhtiari et al., 2016; Ma et al., 2016; Wang et al., 2016a).

#### **8.3.2.5 Sonochemical technique**

In this process, in addition to the chemical method, an ultrasonic treatment is given to the synthesized solution after complete mixing. The typical process involved is the addition of one precursor dropwise to another at temperature ranging from room temperature to higher, that is, 65°C, under a constant stirring. After the process is over the pH is increased up to 11. The sample is then irradiated with ultrasonic waves for 30 minutes. These ultrasonic waves cause regular expansion and contraction in the solution and generate a local heat producing nanosized HAp (Brundavanam et al., 2015; Utara and Klinkaewnarong, 2015; Biswas et al., 2016; Bouyarmane et al., 2016).

### **8.3.3 BIOMIMETIC TECHNIQUES**

In this method the calcium and phosphate precursors, generally  $\text{CaCl}_2$  and  $\text{Na}_2\text{HPO}_4$ , are soaked in simulated body fluid (SBF) separately. These solutions are then mixed dropwise and are stirred for 24 hours. Thus obtained precipitate is then dried and calcinated at higher temperature (Tas 2000; Wang et al., 2002; Gopi et al., 2014a; Leena et al., 2016). In another method banana peels with pectin have also been used as a reducing agent for HAp for green synthesis (Wan et al., 2007). Bovine bone was also utilized as a source for HAp synthesis. In a typical process, the bovine bone was cleaned and washed with boiling water for

5–6 hours. After the removal of all possible organic materials such as proteins, lipids, tendons, and bone marrow the remaining bone material was dried at elevated temperature (80°C) followed by calcination at 650°C/950°C (Sobczak et al., 2009). To form nano-HAp, the dried samples were ball milled followed by ultrasonication before calcination at 800°C (Kusrini et al., 2012).

## 8.4 CHARACTERIZATIONS OF HYDROXYAPATITE

There are various possible ways to characterize the HAp to confirm the chemical formulation, crystallization, and functional groups involved in the molecular structure of the HAp. Briefly, these methods include the following.

### 8.4.1 X-RAY POWDER DIFFRACTION

XRD is the first level of characterization for any ceramic and inorganic material. It tells about the crystal structure, miller indices, phase, crystal purity, crystalline size, as well as the information about the grain boundary present in the inorganic crystal. The basic principle of XRD is the diffraction of the X-rays from the crystalline plane of the material at different angles. Bragg's law relates these diffraction patterns with the crystalline plane.

$$n\lambda = 2d\sin\theta$$

where  $\lambda$  is the wavelength of the X-ray,  $\theta$  is the angle of the diffracted ray, and  $d$  is the separation in the lattice points. The major peaks at  $2\theta = 22.8, 27.43, 29.03, 29.99, 33.01, 40, 47.29$ , and  $53.06$  degrees demonstrate the HAp crystal for (002), (102), (211), (202), (301), (130), (222), (303) planes, respectively (Ramakrishnan et al., 2016), which can be matched with the calcium hydrogen phosphate hydroxide (JCPDS data-base; Pattern number 74-0565).

### 8.4.2 RAMAN SPECTROSCOPY

Raman spectroscopy is based on inelastic scattering of monochromatic light from a laser source. It observes the vibrational, rotational, and other low-frequency modes in a system. When light waves interact with the polarized ellipsoid of a molecule, an oscillation dipole is induced, which consequently gives rise to a Raman band. In the Raman spectrum, variable bands arrive due to the symmetric stretching, vibrations caused by multiple bonds, and the vibrations resulted from heavy metals. Together all these vibrational modes provide strong Raman bands. In the Raman pattern a sharp peak at 960 per cm is generally observed that corresponds to the Raman shift of the phosphate group (Yilmaz and Evis, 2013).



### 8.4.3 FOURIER TRANSFORM INFRARED SPECTROSCOPY

The Fourier transform infrared spectroscopy (FTIR) analysis is utilized for the analysis of the functional groups attached to a material. This method includes the collection of interferogram of a sample by irradiating the infrared rays followed by a Fourier transform (FT) on the interferogram to obtain the spectrum. The most characteristic functional groups in the FTIR spectrum of HAp are  $\text{PO}_4^{3-}$ ,  $\text{HPO}_4^{2-}$ ,  $\text{OH}^-$ , and  $\text{CO}_3^{2-}$  (Berzina-Cimdina and Borodajenko, 2012). Carbonate functional groups are present in form of substitution. These functional groups are generally characterized by the absorption spectrum at various wavenumber ranges such as 3571 per cm for OH stretching and 633 per cm for O–H deformation. The phosphate groups shows absorption peaks at 470, 568, 602, 964, 1041, and 1093 per cm.  $\text{CO}_3^{2-}$  group shows absorption peaks between 870 and 880 per cm. Extensive absorption peaks for carbonate are present between 1460 and 1530 per cm. Among all these, asymmetric phosphate stretching peak is the characteristic peak of phosphate present in HAp present at 964 per cm (Arsad et al., 2011).

### 8.4.4 MECHANICAL CHARACTERIZATION OF HYDROXYAPATITE

The mechanical strength of the HAp can be measured using Vickers hardness using micro- universal testing machine and indentation toughness (Woodard et al., 2007). The general compressive strength of pure HAp remains 300–600 MPa with a Young's modulus ranging from 80 to 120 GPa and Vickers hardness 4.413–5.198 GPa (Silva et al., 2001). In general, the Vickers hardness is measured using a 200 gm load. In an experiment the maximum hardness was found to be 5.11 GPa, which was decreased with the increase in porosity (Song et al., 2011). In another study, the scaffold made up of HAp possesses  $34.4 \pm 2.2$  MPa compressive strength for microporous structure and  $27.4 \pm 4.2$  MPa for nonmicroporous structure (Woodard et al., 2007).

---

## 8.5 BIOACTIVITY OF HYDROXYAPATITE

The cellular integration of the cell and the molecular interaction in bone formation has been in studied for a long time. There are several signals that are passed to the stem cells to be differentiated into bone cells. Tissue-engineering researchers have studied HAp interaction with bone cells extensively. This section will focus on the differentiation and proliferation of osteoblast cells on the HAp.

The interaction between bone and the HAp (implant) depends on many complex reactions between biological macromolecules and the implant. The first level of interaction remains between the implant and the protein (Pandey and Pattanayek, 2011). The adsorption of protein may be either single, or competitive (Pandey and Pattanayek, 2013), and/or reversible protein adsorption (Pandey et al., 2013). The rate of cell interaction depends on the metabolic rate of host

cells and the bone density. The surface chemistry plays a crucial role in protein adsorption as well as protein aggregation (Pandey et al., 2012). The nanoporous or nanosized structure of implant increases the number of contact points between the implant surface and the host cells because of its high surface-to-volume ratio. In general, the RGD sequences (arginine, glycine, and aspartate) present on the host cell membrane are considered as the first line of contact at the material/cell interface. Ionic interaction between the host cell and the material surface takes place, which helps in adsorption and retention of the protein over the material surface. The changes in the resident ion concentration and presence of protein layer influence the cell behavior and responses to the engineered material. Extracellular matrix based materials show enhanced osteoblast attachment over its surface, which in turn process the cell signal for the proliferation of bone cells (Wen et al., 2016). Cells recognize the cell surface receptor over the material surface and prompt cellular responses. Such biomacromolecular interactions with the implanted material decide the selection and/or rejection of the material through the immune system. A recent study explains that the microstructure plays a very important role in the immune response in generation of the macrophage, responsible for inflammatory reaction. These microstructures regulate contact points available for interaction. It was reported that the immune response was higher for the plate-like structures than that of the needle like structure (Mestres et al., 2015). Alteration in the microstructure may also occur during the biological responses; hence, to inspect the effect of local surface structure over biological responses remains the major challenge for a tissue engineer.

### 8.5.1 CELLULAR MECHANISM AT BONE—MATERIAL INTERFACE

It is believed that at the bone—material interface a reprecipitation of the calcium and phosphate ion takes place, which subsequently forms the carbonate apatite at the interface. The apatite formation favors the ionic exchange between the bone cell and material. The exchange of ions fills the gap between the bone and the engineered material via formation of a matrix between bone cells and the engineered material. Thereafter, proteins get adsorbed at the junction point enhancing stem cell proliferation and differentiation into osteoblast cells chemotactically via increase in the calcium intake (Bertazzo et al., 2010).

Protein adsorption is a crucial stage in cell proliferation during the biological interaction of the material. Adsorption of protein, as discussed earlier in Section 8.5, takes place through the ionic interaction and hydrophobic interactions between the material surface and the body fluid. This ionic interaction depends upon the surface properties of the material. These properties include the topography, roughness, porosity, ionic dispersion, wettability, and grain boundaries. Due to the ion exchange process, the surface of the HAp material continuously revises and hence, the protein undergoes alteration in its 3D structure for proper alignment and conjugation; this phenomenon is called Vroman effect. The cellular attachment thereafter takes place with the help of these proteins, generally

integrin, which connects the cell membrane with the outer environment. The local environment such as pH plays a crucial role in this interaction. Under physiological concentration, ion concentration neutralizes the protein charge for proper cell proliferation. The interaction of integrin utilizes the RGD sequences for proper binding.

### 8.5.2 RESORPTION OF HYDROXYAPATITE

The resorption of HAp takes place because of the osteoclast, macrophage, and fibroblast activity during bone remodeling. Briefly, osteoblasts cells allow the activity of osteoclasts, that is, the removal of the dead cells simultaneously. Osteoclast cells generate tight junctions at the cellular boundary and polarize the actin filament, which in turns generates the ring structure comprising podosomes and integrin containing cytoskeletons. Finally, the proteolytic enzymes, largely Cathepsin K and acid, are secreted through the plasma membrane in contact with the engineered material, which degrades the HAp (Sammons, 2015). HAp degrades in the form of ions, which are consumed by the cells themselves for their various metabolic activities. As HAp comprised the mineral components of the bone, its degradation does not produce any harmful or toxic end product after the metabolic reaction. The resorption of HAp thus mineralizes the local environment and fulfills the ionic and mineral requirement.

---

## 8.6 ROLE OF ELEMENTAL DOPING IN HYDROXYAPATITE

The human bone mineral is a nonstoichiometric nanocrystalline apatite with impurities in the form of cosubstituted trace elements of Na, Mg, Zn, Sr, K, F, Cl, Si, etc. Here arrives the difference between the natural HAp (human bone) and the synthetic HAp. Synthetic HAp generally remains the pure form of HAp with low crystal defects. This is the reason the chemically synthesized HAp does not carry the exact similarity with the bone composition and mechanical strength together. Hence, to mimic the native bone structure, researchers have tried various elemental doping into the HAp matrix.

Substitution of ions in HAp deviates the lattice parameters and as a result, the crystal arrangement alters depending upon the additives and their occupied position. For example, at elevated  $\text{Sr}^{2+}$  concentration, the lattice parameters of the *a*- and *c*-axes of the apatite structure get elongated. The increase in the lattice dimensions and lattice volume indicates that strontium is incorporated in the HA structure (ionic radii:  $\text{Sr}^{2+} = 1.13 \text{ \AA}$ ,  $\text{Ca}^{2+} = 1.00 \text{ \AA}$ ) (Saint-Jean, Camire et al., 2005). The most common type of substitution is carbonated HAp; carbonated HAp is shown to have an improved bioactivity compared with pure HAp, leading to a greater solubility of the carbonated phase (Porter et al., 2005). Biological apatites are generally a mixture of two types: A and B. In A type carbonated

HAp,  $\text{CO}_3^{2-}$  ions substitute for  $\text{OH}^-$  ion and in B type carbonated ion  $\text{CO}_3^{2-}$  ions substitute for  $\text{PO}_4^{3-}$  ions. In both the cases the imbalanced charge changes the stoichiometry of the compound and generates the possibility of impurities in the crystal lattice (Uskokovic and Uskokovic, 2011). In addition, these metal ions play a crucial role in protein aggregation (Singh et al., 2017), which may alter the fate of an implant in vivo. Hence, many researchers have tried the doping of these elements in the HAp seeking more effective biological responses and properties with various degree of success. In this section, we shall summarize the effect of following elemental doping in HAp.

### 8.6.1 LITHIUM-DOPED HYDROXYAPATITE

Lithium has been utilized as a trace dopant in the HAp matrix. Although, doping of lithium decreases the solubility of HAp, it does not alter the native crystal structure of HAp. Gamma attenuation coefficient, which explores the penetration effect of gamma rays into a material, was increased with increase in the lithium concentration, which is an important parameter while using a material as an implant material (Badran et al., 2017). Hence, an increase in lithium ion concentration increases the mechanical strength HAp. The maximum value of gamma attenuation coefficient was 2.0 per cm. Li substituted HAp also altered the dielectric properties of HAp cement (HAC) and hence is highly recommended for bone and dental implant. Lower concentration of lithium is suggested for the patient who undergoes radiation examination with gamma rays (Wang et al., 2016f; Badran et al., 2017).

### 8.6.2 SELENIUM-DOPED HYDROXYAPATITE

Selenium, a carcinogenic element, also does not alter the crystal structure of HAp. Also, selenium deficiency can cause various illnesses, mainly cancer (Ames, 2001). Doping of Se into HAp matrix alters the charge distribution over the material surface and thus enhances the loading efficiency of the HAp for its usage as a drug delivery vehicle. An increase in loading efficiency from 34.1% to 41.7% was obtained after Se doping. Se-doped HAp has been utilized as a potential lysozyme delivery vehicle (Wang et al., 2016d). Beside this, the excellent antitumor activity of the Se-doped HAp was also examined (Wang et al., 2016e). The study revealed that 10% doping of Se into the HAp matrix was sufficient to degrade the osteosarcoma cells. The synthesized material was presumed to be a pH responsive material for anticancerous activity.

### 8.6.3 ALUMINUM-DOPED HYDROXYAPATITE

Aluminum is a trace element found in hard tissues and has been reported to be a disease inducer at elevated concentrations (Ali et al., 2016). Doping of Al into HAp decreases the size as well as crystallinity of HAp. It distorts the vicinity and

integrity of the crystal at the site of doping (Wang et al., 2016b), which consequently increases the calcium deficiency in the HAp crystal and thus the Ca/P ratio alters. It was reported that a lower concentration of Al, that is, 1 mg/mL of HAp crystal did not cause any cytotoxicity (Kolekar et al., 2016).

#### 8.6.4 ZIRCONIUM-DOPED HYDROXYAPATITE

Zirconium is generally utilized for its mechanical strength. The native of Zr into HAp crystal enhances the mechanical strength of the ceramic.  $Zr^{2+}$  replaces the  $Ca^{2+}$  ion from the lattice and thus does not alter the basic phase configuration of HAp (Silva et al., 2001). Although the intrinsic doping of Zr into HAp matrix enhances the mechanical property, osteogenicity remains very low. Hence, different kinds of research are going on to enhance the osteogenicity of Zr-doped HAp. Various researchers have tried to codope Zr with other elements such as Ca, Mg, Sr, Zn, etc. Ca-Zr-doped HAp showed enhanced osteogenic activity (Castkova et al., 2016). Other elements when codoped with Zr showed enhanced mechanical and biological properties and did not alter the basic phase configuration of HAp crystal. An increment in compressive strength of Zr-doped HAp was found to be 850 MPa, which was higher than that of pure HAp, that is, 300–600 MPa (Kaygili and Keser, 2016).

#### 8.6.5 SILVER-DOPED HYDROXYAPATITE

Silver NPs are well known antimicrobial agents. Ag NPs are found in trace concentration in the human body and are utilized as a nutrient element in hard and some soft tissues. Also, silver is used to stimulate the immune system in the body. Silver readily reacts with the body proteins, amino acids, and free anions (Lansdown, 2006). Silver composites have shown excellent antimicrobial activity (Stoica et al., 2015), and hence doping of Ag NPs generally results in the antimicrobial HAp matrix. Various authors have reported doping of Ag into HAp matrix with various applications (Ciobanu et al., 2011; Samani et al., 2013; Anjaneyulu et al., 2016; Huang et al., 2017). Doping of Ag into HAp matrix also enhances the mechanical strength of HAp ceramic without altering the phase behavior of HAp. Hence, HAp-doped with Ag is considered as a best fit scaffold material for orthopedic applications (Anjaneyulu et al., 2016). Also Ag-doped HAp has shown better corrosion resistance in presence of SBF (Mirzaee et al., 2016).

#### 8.6.6 MAGNESIUM-DOPED HYDROXYAPATITE

Magnesium is also found as the trace element in bone as well as other hard tissues, and hence is very useful for bone tissue engineering. In addition, Mg is also utilized in more than 300 metabolic reactions in human body. Mg also serves for normal neural function and supports in maintaining the immune system. Mg also serves in maintaining the blood glucose level and helps in the production of

protein. Doping of Mg into HAp matrix enhances the crystallinity as well as the mechanical strength of HAp. Lower concentration of Mg doping has shown no toxicity with enhanced mechanical strength from 38 to 72 MPa (Lala et al., 2017). In addition, Mg doping enhances the osteoblast activity with optimized degradability and thus enhances the bone growth (Lu et al., 2011).

### 8.6.7 MANGANESE-DOPED HYDROXYAPATITE

Manganese is the most important trace element found in the human body. It serves in various metabolic reactions inside the human body. Mn serves in bone formation, bone metabolism, and synthesis of various enzymes for building bones. Mn also possesses the antioxidant activity and serves in the removal of toxic materials. Hence, Mn doping in HAp has been a great research interest for tissue engineers. Mn doping enhances the thermal stability of HAp (Paluszkievicz et al., 2010), which helps in the enhancing the stability of HAp under oxidative stress.

### 8.6.8 IRON-DOPED HYDROXYAPATITE

Iron is an important trace material found in the human body. It serves in the formation of red blood cells. In addition, it is a major part of hemoglobin. It serves in transportation of oxygen from lungs to the rest of the body. Iron also helps in the conversion of energy from blood sugar. Besides this, iron serves in the normal functionality of nervous as well as the immune system and takes part in the formation of various metabolic enzymes. Iron based nanocomposites have been proven for their antibacterial properties (Bhushan et al., 2018; Negut et al., 2018) and hyperthermia applications (Raland and Borah, 2016; Raland et al., 2017). The doping of iron into HAp serves various functions and helps in many applications of HAp. Because of its natural magnetic properties, iron serves in magnetically targeting the HAp at the site of action and hence is very useful in targeted drug delivery through HAp (Lin et al., 2013a). In addition doping of iron also serves in making HAp suitable for hyperthermia application for cancer treatment (Tampieri et al., 2012). Fe-doped HAp has also been utilized for bone tissue engineering as it enhances the stability of HAp and also provides the dielectric properties to HAp, which is the native property of bones (Kaygili et al., 2014).

### 8.6.9 ZINC-DOPED HYDROXYAPATITE

Zinc is a native element found in the body. It is found in bone as well as other hard tissues. It plays a major role in the immune system and serves in cell division and cell growth. Zinc serves various metabolic as well as defense reactions of the human body and precisely works in wound healing and energy conversion. Zinc deficiency has been noticed in Alzheimer's and Parkinson's disease (Brender et al., 2010). In addition, zinc also act as an antidepressant (Nowak et al., 2005). Incorporation of zinc into HAp matrix takes place by the removal of

Ca ion from the lattice. An ion exchange method takes place during this process. But a very small amount of Zn is suitable for doping as a higher concentration >0.1% may alter the basic and native phase of HAp (Matsunaga et al., 2010). ZnO NPs are considered as antimicrobial agents, and hence doping of ZnO NPs into HAp serves in the utilization of HAp as antimicrobial agent with enhanced mechanical properties (Saha et al., 2010; Radulescu et al., 2016b; Saxena et al., 2018a,b). Fig. 8.2 summarizes the antibiotic resistance mechanism of microbes and the antimicrobial mechanism of ZnO NPs. ZnO NPs possesses three inherent mechanisms for antimicrobial action, that is, by reactive oxygen species (ROS) generation, by attack of Zn NPs to nucleus and protein and by the disruption of cell wall by Zn NPs, which differ from the mechanism of the resistance generation by the microbes, that is, efflux, drug modification, target modification, and enzyme deactivation. Hence, ZnO NPs are considered as the most suitable nanoantibiotic for antibiotic resistant bacteria.

#### 8.6.10 ANION-DOPED HYDROXYAPATITE

Doping of anions in HAp matrix stabilizes the HAp structure. Generally, fluoride, chloride, and carbonate are substituted in HAp matrix for various biomedical applications. Unlike cations, the anionic doping takes place by the removal of OH group present in HAp (Kannan et al., 2011). Carbonated HAp is considered as the second most abundant element found in bone apatite after calcium phosphate. In addition, carbonated HAp is considered more bioactive in terms of osteogenesis than pure and synthetic HAp (Redey et al., 1999). In the similar way, fluoridated HAp has shown better osteogenic activity than that of pure HAp. Fluorine is present in a trace amount in bone and is considered as the promoter for osteogenesis (Li et al., 2016b). Chlorine substitution provides thermal and electrical stability to the HAp (Nihmath and Ramesan, 2016).

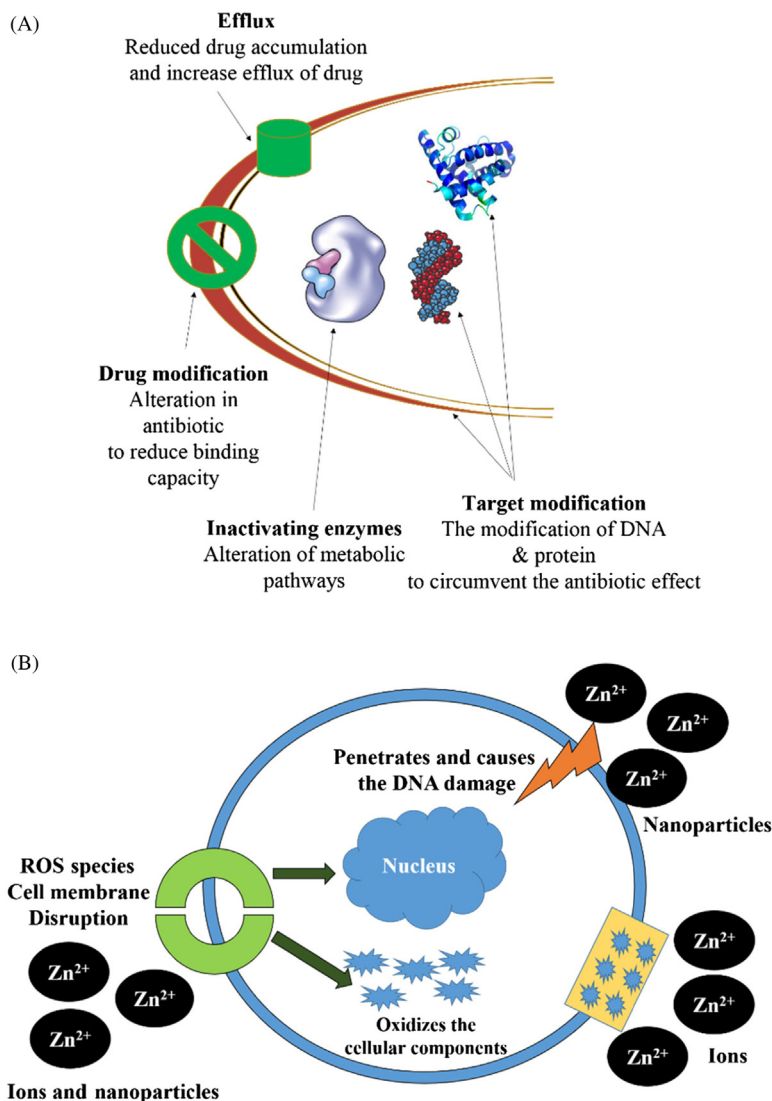
---

### 8.7 APPLICATIONS OF HYDROXYAPATITE

As discussed earlier, because of its excellent biocompatible properties, HAp is used in various biomedical applications with variable rate of success. In this section, we have summarized few of these applications with some recent examples. These applications include drug delivery, dental applications, treatment of OM, stem cell differentiation, and HAp as a coating material.

#### 8.7.1 HYDROXYAPATITE AS A DRUG DELIVERY VEHICLE FOR ANTIBIOTICS IN BONE INFECTION

NPs are majorly attentive for drug delivery applications for either systemic or local delivery of drugs. The long-term structural instability and instability at

**FIGURE 8.2**

(A) Antimicrobial resistance mechanism of microbes. (B) Antimicrobial activity of ZnO NPs.

higher concentration of various delivery vehicles limits their potential use. In addition, many of these drug delivery vehicles are susceptible to biodegradation, which limits their bioavailability and enduring applications.

Ceramic NPs, on the other hand, enjoy several advantages due to their unique properties compared with metallic and polymeric NPs. Firstly, ceramic NPs are



bioactive and undergo less biodegradation over long periods. This enables them to retain drugs for a long time, resulting in sustained drug delivery with diffusion-controlled release kinetics, that is, dependent on concentration gradient. Secondly, ceramic NPs do not swell or change porosity in aqueous environment and are more stable to pH and temperature changes unlike polymeric NPs. The above-mentioned reasons could be helpful to prevent burst release of drug through prolonged desorption, an issue mostly observed in polymeric based delivery systems. Thirdly and most importantly, carefully fabricated and engineered ceramic NPs may resemble the targeted tissue in terms of chemistry, crystalline structure, size and ratio of different constituents (e.g., Ca:P ratio in bone). This feature further adds on to the bioactivity of the materials making them highly biocompatible for drug delivery in such tissues. For localized treatments, the rate-controlled administration of therapeutic is desirable, which can be achieved by retaining the delivery vehicle at the site of action. HAp in this contrast has attracted the researchers because of its higher bioactivity and biocompatibility. [Table 8.3](#) summarizes a few examples of HAp and its composites as a potential drug delivery vehicle.

Application of HAp as a drug delivery vehicle has been an extensive research area because of its excellent biocompatible properties. Because of its mineral similarity with the bone, this material has extensively been examined as a potential drug delivery vehicle for the bone infection. In the early 1990s, [Itokazu et al. \(1994\)](#) suggested the use of porous HAp blocks for the effective delivery of arbekacin for the treatment of OM ([Itokazu et al., 1994](#)). Later, in 1997, the same group confirmed the role of their aminoglycoside antibiotic, arbekacin loaded porous HAp, in Wistar male rat model in vivo. With their conclusion, it was revealed that HAp is a very promising vehicle for the effective delivery of the antibiotics as they found the dual advantage of the HAp, loaded with the drug in the treatment of the infected bone. First, the antibiotic was able to affect the microbiome of the infectious area, and second, HAp stimulated the osteogenicity because of its integrity with the bone ([Itokazu et al., 1997](#)).

Various kinds of antibiotics have been loaded over the HAp matrix for the treatment of various kinds of bone infection. For example, [Yamashita et al. \(1998\)](#) investigated the calcium HAp ceramic implants impregnated with imipenem/cilastatin sodium, flomoxef sodium, piperacillin sodium, vancomycin hydrochloride, gentamicin sulfate, and cefmetazol sodium antibiotics. They treated various bacterial infected cells with the mentioned antibiotics. They found that much less or no amount of infection remained after treatment. The antibiotic-calcium HAp ceramic composites show variable positive functionality after implementation. Briefly, they control the infection, restore mechanical strength, encourage osteoconduction into their pores, and avoid the need of further surgery. Moving onto another example, [Joosten et al. \(2004\)](#) studied the HAC to deliver the gentamycin in the treatment of OM both in vivo and in vitro. They concluded that in HAC/gentamicin-treated animals, there was no growth after 7 days of culturing in BHI bouillon with no side effect of both gentamycin and HAC. The synergistic effect of both the antibiotic and the HAC cures the bone infection with

**Table 8.3** Examples of Drug Delivery Through HAp and Its Composites

S. No.	Material	Name of the drug	Release profile and effect of the drug	References
1	Porous HAp fibers	BSA as a model drug	Controlled release	<a href="#">Yi et al. (2016)</a>
2	HAp NPs	Methylprednisolone acetate	Initial burst and then slow release, treatment of rheumatoid arthritis	<a href="#">Jafari et al. (2016)</a>
3	Hollow HAp microspheres	Doxorubicin hydrochloride	Controlled release, anticancerous	<a href="#">Lai et al. (2016)</a>
4	HAp-MgFe <sub>2</sub> O <sub>4</sub> nanocomposite	Ibuprofen	Initial burst and then slow release, General pain killer	<a href="#">Foroughi et al. (2016)</a>
5	HAp nanocrystals	Kiteplatin	pH sensitive, overcomes cisplatin resistance	<a href="#">Lelli et al. (2016)</a>
6	Calcium carbonate-calcium phosphate	Sodium fusidate	Sustained release, OM treatment	<a href="#">Noukrati et al. (2016)</a>
7	Si-doped HAp/gelatine scaffolds	Vancomycin	First-order release kinetics, antibiotic	<a href="#">Martínez-Vázquez et al. (2015)</a>
8	Sodium alginate/chitosan/HAp nanocomposite	Doxorubicin	pH sensitive, liver cancer	<a href="#">Abou Taleb et al. (2015)</a>
9	HAp microsphere	Chlorhexidine	Sustained release, antimicrobial	<a href="#">Soriano-Souza et al. (2015)</a>
10	Micro/nanohybrid structured HAp	Icariin	Sustained release, femoral defect repair	<a href="#">Wu et al. (2015)</a>
11	HAp nanowhiskers	Terbinafine	Sustained release, antifungal, colon targeting drug	<a href="#">Cellet et al. (2015)</a>
12	Fe <sub>3</sub> O <sub>4</sub> /HAp composite	Doxorubicin	Controlled release, anticancerous	<a href="#">Gu et al. (2014)</a>
13	Fluorescent HAp nanocrystals	Alendronate	Initial burst and then slow release, bone treatment	<a href="#">Singh et al. (2014)</a>
14	Mesoporous magnetic (Fe <sub>3</sub> O <sub>4</sub> ) carbonated HAp microsphere	Gentamycin	Sustained release, antibiotic	<a href="#">Guo et al. (2014)</a>
15	Porous HAp/ Na(Y/Gd)F <sub>4</sub> :Yb <sup>3+</sup> ,Er <sup>3+</sup> composite	Indomethacin	High burst release, then slower release, antiinflammatory drug	<a href="#">Liu et al. (2014)</a>
16	Nano-HAp	Doxorubicin	Linear, faster for lower dose, anticancerous, liver cancer	<a href="#">Kundu et al. (2013)</a>
17	HAp/collagen hybrid gels	Paclitaxel	Controlled release, anticancerous, breast cancer	<a href="#">Watanabe et al. (2013)</a>
18	Strontium substituted HAp microsphere	Vancomycin	Initial burst and then slow release, antibiotic	<a href="#">Lin et al. (2013b)</a>
19	Hollow mesoporous HAp NPs	Doxorubicin	pH sensitive, anticancerous, breast cancer	<a href="#">Yang et al. (2013)</a>
20	Hollow microspheres of HAp	Ibuprofen	Initial burst and then slow release, antiinflammatory	<a href="#">Qi et al. (2013)</a>

low time duration in the healing process. HAp has shown better integrity with the drug adsorbed over its surface. Majorly, nano-HAp, porous HAp, and nanoporous HAp has been examined for its potential use in drug delivery application. All three mentioned forms of HAp show high surface-to-volume ratios, which plays a major role in the loading of effective amount of antibiotic over its surface. The high surface-to-volume ratio increases the number of contact points for the drug and thus increases the amount of the drug to be loaded.

Many researchers have utilized the HAp as an inorganic matrix and reinforced it with other organic and inorganic materials to form a stable composite of HAp to be utilized as a plausible drug delivery vehicle. [Marques et al. \(2016b\)](#) tried Sr-doped porous calcium phosphate granules loaded with levofloxacin (LEV). They designed the material with molar ratio of  $(\text{Ca}:\text{Sr}:\text{Mg})/\text{P} = 1.62$ . Porous pure and Sr and Mg/Sr-doped spherical granules of biphasic calcium phosphates. Sr-doped HAp showed the maximum biocompatibility and an effective antibiotic release profile that was suitable for the treatment of OM ([Marques et al., 2016a](#)). Comeau et al. also improved the structural nature of calcium polyphosphate (CPP) crystal with insertion of strontium (Sr) and investigated the release pattern of vancomycin from this modified bioactive glass. Their conclusion revealed that the doping of Sr might serve to both employ antibiotic release from the amorphous CPP matrix and bone regeneration ([Comeau and Filiaggi, 2016](#)). Similarly, [Marques et al. \(2016b\)](#) demonstrated the LEV adsorbed Sr and Mg-doped calcium phosphate powder. Their study revealed that physisorption took place to fix the LEV at the surface of the particles and their material was proven as a controlled drug release system ([Marques et al., 2016b](#)).

Another modification approach for the application of HAp as a drug delivery vehicle includes the compositing of HAp with polymeric matrix. Polymers due to their higher surface area are suitable for the drug loading in an effective amount. For example, [Son et al. \(2011\)](#) performed ionic immobilization of dexamethasone (DEX)-loaded poly (lactic-co-glycolic acid) (PLGA) microspheres on the HAp scaffold surfaces. The volume and quality of newly formed bone was found to be enhanced when the defects were filled with DEX-loaded HAp scaffold as compared with the HAp scaffold alone ([Son et al., 2011](#)). Similarly, [Sundaram and Rajendran \(2015\)](#) loaded ciprofloxacin over HAp-polycaprolactone (PCL) nanocomposite film for sustainable bone implants. They found that PCL film showed low disbanding rate with an initial weight loss. However, ciprofloxacin-loaded HAp-PCL films suffered a higher weight loss due to the burst release of ciprofloxacin. In addition, the newly synthesized composite films also observed higher water absorption rate with increase in the HAp concentration. The film underwent the controlled release of ciprofloxacin ([Sundaram and Rajendran, 2015](#)).

#### **8.7.1.1 Drug release kinetics**

There is a direct relation in the matrix degradation and the drug release. Various efforts have been implemented to correlate the matrix degradation with the drug

release. The rate of matrix degradation controls the release of the drug. [Dion et al. \(2005\)](#) investigated the release pattern of vancomycin through amorphous CPP and correlated the matrix degradation with antibiotic release. Three models primarily give the release of the drug. They are first-order kinetics, Gallagher–Corrigan model, and Higuchi models. All these drug release kinetic models describe the release of drug under various reaction conditions and local environment.

1. The first-order kinetics describes the release of the drug from the porous matrices. The first-order kinetics is generally given by the following formula:

$$f_t = f_{\max}(1 - e^{-k_1 t})$$

Where  $f_t$  is the fraction of drug released in  $t$  time,  $f_{\max}$  is maximum fraction of drug released during the process, and  $k_1$  is the first-order kinetic constant ( $\text{h}^{-1}$ ) ([Dash et al., 2010](#)).

2. The Gallagher–Corrigan model summarizes the two state model, which is very common to most of the drug delivery systems. Briefly, it includes a first burst release of the drug from the surface followed by a controlled release from the matrix degradation. It is given by the formula:

$$f_t = f_{\max}(1 - e^{-k_1 t}) + (f_{\max} - f_b) \cdot \frac{e^{k_2 t - k_2 t_{2\max}}}{1 + (e^{k_2 t - k_2 t_{2\max}})}$$

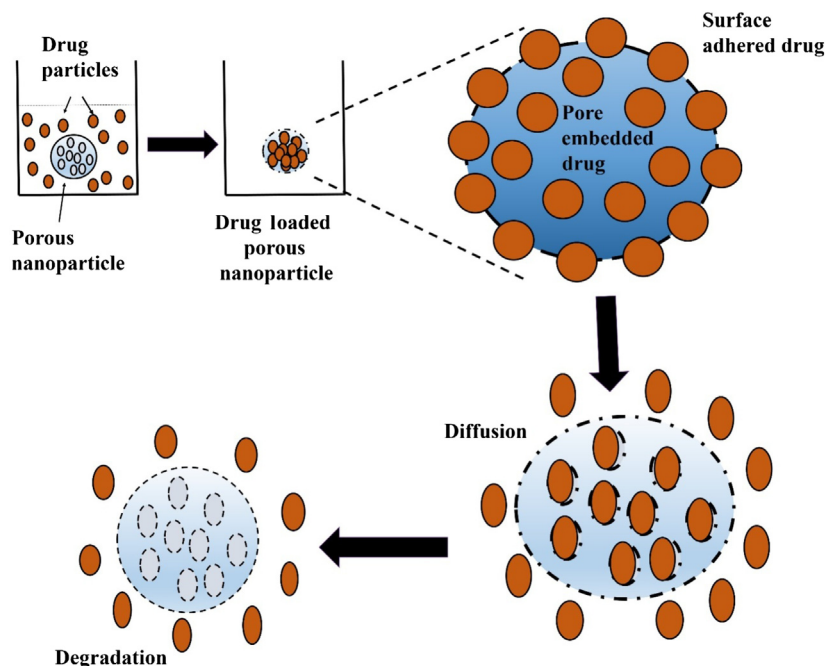
Where  $f_t$  is fraction of drug released in  $t$  time,  $f_{\max}$  is maximum fraction of drug released during process, and  $f_b$  is fraction of drug released during 1st stage the burst effect.  $k_1$  is the first-order kinetic constant ( $\text{h}^{-1}$ ) (1st stage of release),  $k_2$  is the kinetic constant for 2nd stage of release process matrix degradation, and  $t_{2\max}$  is the time to max drug release rate (h) ([Balcerzak and Mucha, 2010](#)).

3. The Higuchi model is used for the analysis of the drug release from a nonswollen matrix. The general description is given by the formula:

$$f_t = K_H \times t^{0.5}$$

where  $f_t$  is the fraction of drug released in  $t$  time and  $K_H$  is Higuchi dissolution constant ([Jarosz et al., 2016](#)).

The drug release profile from the HAp can be described by any or all of the given models. The most common model used to describe the drug release from the HAp matrix is Gallagher–Corrigan model. The mechanism of drug delivery using HAp matrix is represented in [Fig. 8.3](#). First, the drug adhered over the surface of the HAp matrix is released in a bulk amount and then the drug is released in a controlled fashion with the degradation of the HAp matrix.

**FIGURE 8.3**

Drug release mechanism from HAp Matrix.

## 8.7.2 HYDROXYAPATITE IN DENTAL APPLICATIONS

HAp is also a main component of teeth. Hence, usage of HAp is highly suggested for the restoration of enamel. For restoration of enamel, initial integration with enamel is required, which remains a major challenge in using HAp for enamel restoration. Hence, to synthesize the functionally graded material, HAp is doped or composited with various other elements for its usage in dentistry. There are various applications of HAp in dental science. In this section, we will review these applications in brief with a few recent examples.

### 8.7.2.1 Enamel restoration

Various strategies have been applied in using HAp for enamel restoration. Enamel is the outermost part of the tooth, the hardest tissue of the body and is most highly mineralized. The major mineralization of tooth enamel is covered by HAp. It protects the tooth from decay, local temperature, and chemicals. Hence, it is very important to protect the enamel covering of the dentine. Pain in tooth generally arises when the dentine is exposed to the external environment. This condition generally occurs because of the abrasion and erosion of the enamel. The situation is termed as dentin hypersensitivity. The erosion of the enamel occurs

because of extensive usage of acid drinks, tobacco chewing, and various environmental factors such as wear and shear. In the protection of enamel, saliva plays an important role by covering the enamel with shielding calcium and by reducing the local concentration of acids in diet. Enamel, once eroded, can cause severe damage to the tooth cells such as dentine. General signs of enamel erosion are sensitivity, discoloration, cracks, and cupping. Hence, the major focus of dentists remains to protect the enamel or to restore the enamel after erosion. Generally, fluoridated materials are used to reduce enamel demineralization. Fluoridated HAp has also been utilized to reduce the demineralization of enamel (Hill et al., 2015). Amelotin is the enamel protein that is confined at the interface of enamel and the apical surface of ameloblasts cells. It is expressed during the enamel maturation. Enamel formation takes place because of the biomineralization of carbonated HAp. Researchers have proved that this amelotin protein is responsible for the biomineralization process (Abbarin et al., 2015) and eventually produces enamel. Hence, HAp in enamel regeneration is strongly proposed for its vast and effective applications (Hontsu et al., 2011; Anastasiou et al., 2016; Wren, 2016).

#### **8.7.2.2 Dental fillers**

The demineralization of enamel can cause severe damages to tooth cells. Various approaches have been tried to overcome the demineralization of enamel. When demineralization occurs at a localized area and/or in case of severe damage of the tooth, fillers are utilized to provide the tooth cell a supporting environment for regeneration of enamel. In general, polymer based composites are used as a filler material for dental applications. Their fibrous structure increases the contact point for the cells to proliferate, and thus provides strength to the tooth. Lower mechanical strength, polymerization, shrinkage, and lower bonding with the enamel surface make the usage of polymers as dental fillers less desirable. In this respect, various approaches have been tried to overcome these obstacles. Similarity with the enamel structure and higher mechanical strength make HAp a very strong candidate for dental fillers. HAp, when used as a filler compound in nanorod morphology, showed better integration with enamel and was considered as a material to enhance the adhesive properties of dental materials (Sadat-Shojai et al., 2010). Various approaches are under investigation to enhance the mechanical strength of dental fillers at nanorange with optimal binding efficiency with enamel surface. In a recent study, fluoridated HAp was synthesized and utilized as dental filler. The tensile strength of 45.5 MPa was achieved by loading of 0.02% loading of fluoridated HAp. The study also confirmed that fluoride ions are released through the fluoridated HAp nanorods because of the biodegradable nature of HAp. These fluoride ions in presence of SBF cause biomineralization and subsequently prevent secondary caries (Taheri et al., 2015).

#### **8.7.2.3 Dental implants**

Another application of HAp in the dental industry is the use of HAp as a dental implant. Although all these applications serve in the same context of similarity in

chemical composition and mechanical strength with enamel, the usage of HAp material as dental implant is affected by various surface properties of HAp. The integration between the cells and material is strongly dependent on the surface chemistry and roughness of the implant material. In general, implants with higher roughness and wettability of surface or porous chemistry are suggested for implant application. HAp mixed with titanium nitride was used as covering material for polymer to enhance the mechanical strength and cellular integration (Boonyawan et al., 2016). HAp is generally used as a coating material for dental implants with better bone implant interaction and less peripheral bone loss. The coating process and thickness of HAp over the dental implant also affects the cell integrity and contact with the implant. Generally, thin layering of HAp is preferred to use HAp as a coating material. A thin HAp coating that was sputtered over the dental implant showed better cellular interaction than that of thick layering under periimplantitis condition (Madi et al., 2016). The application of HAp coating over the implant material depends on the morphology of implant as well as the site of action. Thickness of HAp and cortical layer play a crucial role in cellular integrity of implant with the cells. In 2000, Ong et al. reported that screw implant with HAp coating should be applied for anterior maxilla and posterior mandibles, because of the depth that remains higher than 10 mm and thinner cortical layer. In a similar way, at the posterior maxilla, the cortical layer remains ultrathin with lower density and hence HAp coated cylindrical implants are suggested (Ong and Chan, 2000).

### 8.7.3 HYDROXYAPATITE AND STEM CELL DIFFERENTIATION

In tissue regeneration, stem cells play an important role. A stem cell is a cell that has the ability of self-renewing, that is, they can form many of the cells like themselves. They have the power of healing by reconstructing the cells or the tissue. In the early stage of life, stem cells have a fast frequency and ability to form any kind of cells in the human body. At the embryonic stage, they remain in unprogrammed stage and subsequently are known as embryonic stem cells (ESCs). The ability of ESCs to be differentiated into any kind of cells makes it possible to form various organs and tissues such as kidney, liver, heart, lungs, skin, etc., generating a complete human body.

#### 8.7.3.1 *Types of stem cells*

There are various kinds of stem cells depending upon their functionality and specificity. Briefly they can be classified into the following.

##### 8.7.3.1.1 Embryonic stem cells

ESCs are pluripotent in nature, that is, they can be differentiated into any kind of cell in a fully developed body except that of placenta and umbilical cord. ESCs are important because of their usage as renewable resources in studying development and diseases.

#### 8.7.3.1.2 Adult stem cells

Adult stem cells are also considered as tissue specific stem cells. These cells are more specialized than ESCs. These stem cells can give rise to many kinds of cells at their host area. They are tissue specific in terms of their differentiation specificity, for example, hematopoietic stem cells can give rise to blood cells only and no other cell lines, osteoblasts can produce only bone cells, etc.

#### 8.7.3.1.3 Mesenchymal stem cells

These kinds of stem cells are also known as stromal cells. These stem cells can be differentiated into connective tissue surrounding organ and other tissues. Because of their native property of forming connective tissue, these stem cells are the most studied stem cells for bone tissue engineering.

### ***8.7.3.2 Hydroxyapatite interaction with stem cells***

Human bone marrow consists of a number of mesenchymal stem cells (MSCs). Various studies are ongoing in utilization of HAp as a differentiation microenvironment to produce osteoblast cells from MSCs. Two mRNA activities, alkaline phosphatase and bone Gla protein, are generally studied for the study of the differentiation activity of HAp. The cellular division and differentiation of MSCs into osteoblast cells is regulated through the calcium intake of the cells. An enhancement in the calcium intake of the stem cells enhances the cell division and various growth factors such as osteogenin promotes the differentiation of MSCs into bone cells. Various approaches in this field have been applied.

### ***8.7.3.3 Mechanism of osteoblast differentiation of mesenchymal stem cells in presence of hydroxyapatite***

When MSCs are cultured over HAp surfaces with proper cell culture medium the process starts with the cellular adhesion over the HAp surface because of the higher surface-to-volume ratio of the porous material and number of contact points, which subsequently increases the cell adhesion as discussed in [Section 8.5](#). After 2 weeks of culture, more cells adhere over the HAp surfaces and cells start to grow over the surfaces. The formation takes place in the 3rd and the 4th week of the cell culture. In detail, it has been found that on a preexisting bone surface lamellar bone is generally produced. HAp, because of its mineral similarity, provides a native bone-like environment to the growing MSCs causing the differentiation of MSCs into osteoblast cells. These osteoblast cells then rapidly divide to produce the mature bone cells ([Ohgushi et al., 1993](#)). Pure HAp possesses little stoichiometric difference with the bone structure, as HAp generally remains the pure form of HAp with low crystal defects. Indeed the human bone mineral is a nonstoichiometric nanocrystalline apatite with impurities given in [Section 8.6](#). This stoichiometric difference causes the various ranges of success when HAp is utilized as a differentiating scaffold for osteogenic differentiation.



Researchers are trying various combinations of HAp with other materials to overcome the obstacle of few but effective stoichiometric dissimilarity with bone.

PCL/HAp biphasic compound was utilized for the differentiation of MSCs into osteoblast cells for bone tissue engineering. In this study, it was revealed that dental pulp stem cells, MSCs, and adipose derived MSCs were able to be differentiated into osteoblast cells with variable level of differentiation. Dental pulp stem cells were least efficient for differentiation into osteoblast cells (Chuenjitkuntaworn et al., 2016). In a similar way, Sanaei-rad et al. (2016) revealed the role of nanofibrous scaffolds based on hybrid PLGA/gelatin coated with HAp for differentiation of MSCs into osteoblasts. They electrospun the PLGA/gelatin for structuring the scaffold. Their study explored that the nanofibrous structure helps in the differentiation of stem cells into specialized osteoblasts. In addition, the coating of HAp enhances the differentiation of stem cells (Sanaei-rad et al., 2016). Bioactive natural protein (silk)–Hap nanocarriers and HAp-doped alginate beads have also been studied to explore the differentiation of MSCs into osteoblast cells (Ding et al., 2016; Wang et al., 2016c). In their study they found the inconstant level of differentiation of MSCs into osteoblast cells with variable concentration of fillers. In both studies, it is mentioned that the composite had more differentiating ability than the native HAp matrix. The mechanism of this is still unrevealed but we suspect from all these studies that HAp helps in differentiation of stem cells to osteoblast cells by providing a native environment similar to that of bone. In all the studies fillers generally possess either nanosized or fibrous structure or polymeric structure. Hence, the morphology of the scaffold may play an important role in the differentiation of MSCs into osteoblast cells. In addition, the fibrous/nanosized structure provides more surface area for the cells to adhere over the surface of the scaffold. Hence, it can be concluded that higher surface area with the maximum chemical similarity with the natural bone makes HAp and its composites a potential tool for stem cell differentiation for bone tissue engineering.

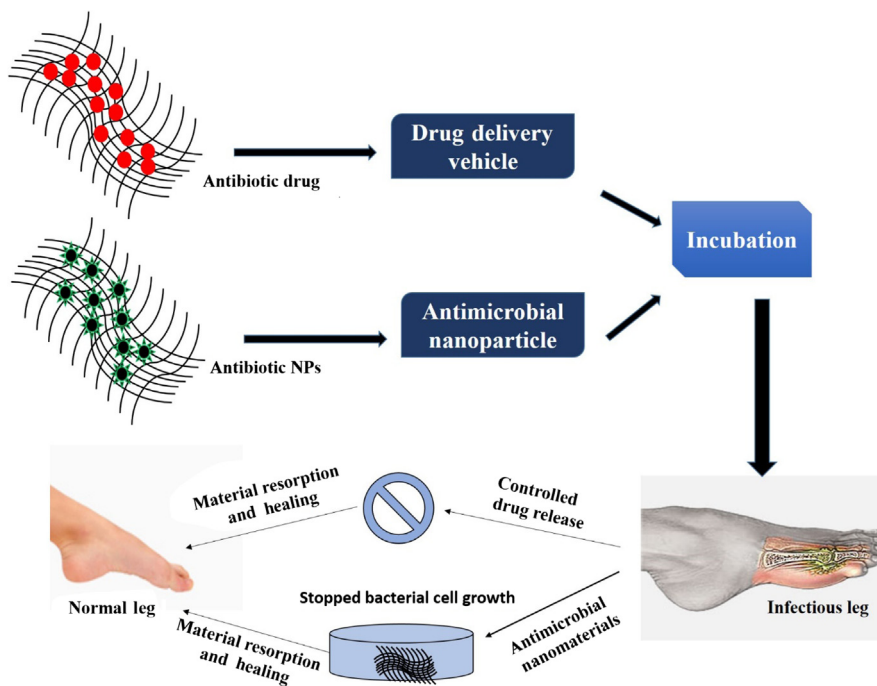
#### 8.7.4 HYDROXYAPATITE IN THE TREATMENT OF OSTEOMYELITIS

OM is an infection in bone by a microbial pathogen resulting in an inflammatory response that may lead to osteolysis, that is, bone demolition. Direct contamination through open fracture and infection through the bloodstream (hematogenic) are the two major routes of OM development. These infections sometimes may become acute leading to chronic susceptibility. The situation is clinically termed as OM. Multiple bone biopsies are required in the diagnosis and the treatment of the infected bone. The heterogeneity of the bone colonization sometimes results in false monotonous cultures. A bone biopsy is the gold standard for diagnosing OM. However, the invasive nature of this method results in rejection, especially for diabetic patients. In diabetic foot, OM generally results from a preexisting infected foot wound. There are two ways to diagnose diabetic foot OM, that is, the poor or no healing and/or palpated foot with a metal implant. The microbiome

of diabetic foot OM contains *Staphylococcus*, *Corynebacterium*, *Streptococcus*, and *Propionibacterium* species. They primarily consist of Gram-positive bacteria, especially *Staphylococcus aureus* and beta hemolytic streptococci (van Asten et al., 2015). HAp loaded with antibiotic drug or doped/conjugated with antimicrobial NPs have been under investigation for a long time for the treatment of OM. There is a dual advantage of using HAp for the antibiotic delivery and/or antimicrobial NP-doped HAp. First is the eradication of bone infection because of the antimicrobial action of drugs/NPs and second is the bone healing process guided by the HAp surface because of its chemical similarity and affinity with the bone cells (Jiang et al., 2011). Various examples of antibiotic delivery through HAp matrix have been explored, which we already discussed in the Section 8.5. Many NPs such as Ag, ZnO, Au, chitosan, fullerenes, and carbon nanotubes have shown their excellent antibacterial properties (Huh and Kwon, 2011). Among all these NPs ZnO NPs are successful candidates for potential antibacterial applications owing to their extensive growth inhibition, at low concentration and smaller particle size. ZnO NPs destroy the bacterial cell membrane by affecting the lipids and the protein, which eventually causes a leakage of intracellular contents resulting in the death of bacterial cell. ZnO NPs also generates the ROS  $O_2^-$ , which disrupt the cell wall of the bacteria. ZnO also produces  $Zn^{2+}$  ions, which penetrate the bacterial cells and oxidize the cellular components such as DNA and protein and eventually kill the bacteria (Sirelkhatim et al., 2015). Doping of silver, copper, zinc, and cobalt has been done in HAp matrix to attain antimicrobial activity for various bone infection treatments such as OM (Kim et al., 1998; Ajduković et al., 2016). Fig. 8.4 comprises the schematic of the OM treatment through HAp.

### 8.7.5 HYDROXYAPATITE AS COATING MATERIAL

Metallic implants are liable to compression, torsion, bending and possesses excellent mechanical strength. However, metallic implants are bioinert, that is, they cannot form chemical bonds with bone cells. In addition, they are highly susceptible to corrosion under hydrophilic/physiological environment. Metallic implants sometimes cause bacterial infection at the site of action, leading to the inflammatory and allergic conditions. Hence, to achieve bioactivity, to enhance the corrosion resistance, and to reduce the chances of bacterial infection, bioactive compounds are coated over the metallic alloys by various techniques such as plasma spray (ur Rahman et al., 2016), electrodeposition (Ionita et al., 2016), MAPLE technique (Rădulescu et al., 2016a), and hydrothermal coating (Prado da Silva et al., 2017). Recently, Bakhsheshi-Rad et al. (2016) coated the magnesium alloy with fluorine-doped HAp–PCL duplex to enhance the corrosion resistance as well as the mechanical strength. A high corrosion resistance ( $2.9 \times 10^3 \text{ k}\Omega \text{ cm}^2$ ) was achieved as a result of the coating. In addition, the duplex coating exhibited the compressive strength of 265 MPa, which was higher than that of noncoated alloy, that is, 175 MPa after dispersion in Kokubo solution, which represents the physiological condition (Bakhsheshi-Rad et al., 2016). In another study Dunne

**FIGURE 8.4**

Schematic of the OM treatment through Hap.

et al. studied the corrosion behavior of Mg alloy with coating of HAp under the influence of phosphate buffer saline (PBS) using hydrogen evolution technique, that is, comparison of 1 mL of  $H_2$  evolved per mg of Mg melted by corrosion. They found that EW62 (Mg–6%Nd–2%Y–0.5%Zr) alloy exhibits the best corrosion resistance after coating of HAp. The amount of  $H_2$  evolved per mg of Mg melting was least in this alloy with a value of 56 ml/cm<sup>2</sup> (Dunne et al., 2016). Besides corrosion resistance and enhanced mechanical strength, HAp coating over metallic implants have also been investigated for various other applications. For example, the osteogenic activity of the HAp coated Ti alloy was investigated by Ripamonti et al. (2012). In addition, various drug loaded HAp has been coated over metallic implants to reduce the chances of implant assisted bacterial infection (IABI). For example, gentamycin and vancomycin loaded HAp was coated over titanium alloy to reduce the biofilm production (Ionita et al., 2016; Thomas et al., 2016). As discussed in Section 8.7.4, HAp suffers with the poor loading efficiency for organic drugs. Hence, various approaches are under investigation to reduce the IABI using inorganic antibiotic. In this regard, Gambardella et al. (2016) suggested the magnetic HAp coating as a nanoantibiotic to reduce the IABI. In their

study they coated the magnetite/HAp thin film over silicon wafer substrate using HA/Magnetite (90:10 wt%) as template. They found the reduction in the number of bacteria after the incubation of 4 hours under the influence of an external magnetic field. Hence magnetic HAp can be used as a potential nanoantibiotic coating to reduce the chances of IABI (Gambardella et al., 2016). All these experiments prove HAp coating over metallic implants as a promising tool for their bioactivity, stability, and reduction of IABI.

---

## 8.8 CHALLENGES AND LIMITATIONS OF HYDROXYAPATITE

Besides innumerable biological and chemical properties, a few of drawbacks hinder the applications of HAp. The major drawback of synthetic HAp is its stoichiometric ratio, that is,  $\text{Ca:P} = 1.67$ . The synthetic HAp remains in its purest form, which provides it higher mechanical strength and other biogenic properties. Nevertheless, the natural/human bone remains in nonstoichiometric form as we discussed earlier in Section 8.6.4. Hence, no form of synthetic material possesses the exact physical, chemical, and mechanical similarity as bone. This remains the major challenge for the researchers, working for bone tissue engineering. Various combinations have been scrutinized to overcome these obstacles. Doping of nano-material not only provides the mechanical strength but also provides the closeness to the stoichiometric similarity with bone enhancing the osteogenic activity of the HAp. Doping of Zn is generally preferred, as it has shown the enhanced osteogenic activity of HAp (Ito et al., 2002).

For drug delivery applications the major challenge with HAp remains its poor drug loading efficiency. Most of the drugs that are effective against the microbiome remain hydrophobic in nature. HAp suffers with lower loading capacity with such drugs. Another challenge with HAp in drug delivery application is its lower degradation rate. The drug adsorbed at the surface of HAp is released in a burst manner. The second phase of drug release usually remains dependent on the degradation rate of HAp. However, slower rate of drug release is preferable in many situations, but long-term antibiotic at regular intervals may cause allergy and some severe side effects to the host cells at the local environment. Another challenge with HAp in drug delivery remains the target deficiency. This is the major reason that HAp is not utilized as a targeted drug delivery vehicle. Most of the ceramic materials lack in target efficiency because of their native physical and chemical properties, surface structure, and morphology. The last challenge in using HAp as a drug delivery vehicle is the lack of stimuli response. Thus, application of HAp remains constraint in controlled drug delivery applications. Hence, it is necessary for the researchers to overcome these obstacles. Many trials have been applied in this regard. To enhance the loading efficiency various approaches have been implemented. Many researchers have tried to blend HAp with polymeric matrix to enhance the total surface area as well as to enhance the number

of contact points for hydrophobic–hydrophobic interaction, which ultimately enhances the overall drug loading efficiency of the HAp. Also various approaches have been implemented to make the porous nano-HAp and/or nanoporous HAp to enhance the surface-to-volume ratio, which enhances the percentage of drug loading over HAp matrix (Son et al., 2011; Liu et al., 2016; Macha et al., 2016). To encounter the targeted drug delivery many researchers have tried to modulate the HAp surface through various targeting agents. For magnetically targeted drug delivery  $\text{Fe}_3\text{O}_4$  is doped into HAp matrix (Campodoni et al., 2016; Foroughi et al., 2016). In a similar way hyaluronic acid modified HAp surface was utilized to target the tumor cells for the local delivery of doxorubicin, an anticancerous drug (Xiong et al., 2016). HAp nanoporous structures are generally considered for pH sensitive drug release. pH sensitivity of the HAp depends on the pore size of the porous material (Lelli et al., 2016; Li et al., 2016a,b). Beside this, various other application dependent approaches have been implemented. For example, citrate modified HAp was utilized to enhance the pH responsivity (Verma et al., 2016) of HAp. In another experiment neodymium-doped HAp was prepared to produce a colon specific drug delivery system (Victor et al., 2016).

### 8.8.1 COMPLICATIONS OF HYDROXYAPATITE

Besides many positive qualities and properties, HAp has also shown various degree of complications. Though the level of complication has been low, still it cannot be neglected. HAp is generally used as bone cement. Though all the bone cements are of similar configuration, the small changes in their structure, the differences in the grain boundary, and their small dissimilarities with the bone at the implant area cause negative response to generate the immune response against the bone cement. For example, HAp implant showed lower level of complications (3%) when utilized as an orbital bone cement. Although the authors did not find any implant loss, small degree of rejection was concluded as the complication. Authors suggested that dextran wrapping may be an alternate to reduce these small complications to avoid using donor tissue (Oestreicher et al., 1997). In another example, small amounts of inflammatory cells were present when HAp was utilized as an implant coating for total hip arthroplasty (Bloebaum et al., 1994). Various other studies have been done to explore the complications of HAp. HAp was analyzed for secondary pediatric craniofacial reconstruction. It showed moderate degree of infection (range: 4 months to 4 years), after an average of 17.3 months of surgery. The authors concluded that HAp should not be utilized as a bone cement because of its high degree of infection. In a recent study, Ye et al. (2016) explored the contact rate of unfastened HAp orbital implants in enucleation surgery. Two ways were utilized to study the implant exposure rate. First was rectus end-to-end suturing (REES) closure and the second was rectus orthotopic suturing closure (ROSC). In their study, an average of 2% implant exposure was seen in REES and an average 9.6% implant exposure was found in ROSC. They explored that the vascularization of rectus muscle was the reason behind the

lower rate of implant exposure in REES, which was absent in ROSC leading to the higher rate of implant exposure (Ye et al., 2016).

---

## 8.9 CONCLUSION

HAp is a very cogent candidate for orthopedic applications. Among the tissue engineers, HAp remains the first material of choice for bone tissue engineering. Excluding these many applications of HAp, some major issues such as exact chemical and mechanical dissimilarity with bone, lower drug loading capacity, lower stimuli responsiveness and targeted deficiency have remained a challenge for bone treatment. Notwithstanding the fact that various trials listed in this chapter have been implemented to overcome these obstacles with variable range of success in vitro, the long-term efficacy of HAp is still questionable. Hence, for bone tissue engineering, we strongly recommend the use of antimicrobial metal and metal oxide–doped HAp, rather than antibiotic loaded HAp to avoid the complications of antibiotics and antibiotic resistance. Furthermore, we suggest the modification of HAp surface with various stimuli responsive functional group such as methylvinylether, spiropyran, nitroaromatic, imine, and acetyl group for temperature, light, hypoxia, and pH responsiveness respectively. Implant exposure is another drawback of HAp when used for long duration as discussed in Section 8.8.1. To overcome this, enfolding of HAp with various biodegradable polymers is suggested. Overall, HAp is a quintessential bioceramic for biomedical applications with the requirement of additional studies to revamp HAp and its properties for long-term in vivo applications.

---

## REFERENCES

- Abbarin, N., Miguel, S.S., Holcroft, J., Iwasaki, K., Ganss, B., 2015. The enamel protein amelotin is a promoter of hydroxyapatite mineralization. *J. Bone Mineral Res.* 30 (5), 775–785.
- Abou Taleb, M.F., Alkahtani, A., Mohamed, S.K., 2015. Radiation synthesis and characterization of sodium alginate/chitosan/hydroxyapatite nanocomposite hydrogels: a drug delivery system for liver cancer. *Polym. Bull.* 72 (4), 725–742.
- Ajduković, Z.R., Mihajilov-Krstev, T.M., Ignjatović, N.L., Stojanović, Z., Mladenović-Antić, S.B., Kocić, B.D., et al., 2016. In vitro evaluation of nanoscale hydroxyapatite-based bone reconstructive materials with antimicrobial properties. *J. Nanosci. Nanotechnol.* 16 (2), 1420–1428.
- Ali, A.A., Ahmed, H.I., Abu-Elfotuh, K., 2016. The potential effect of epigallocatechin-3-gallate alone or in combination with vitamin E and selenium on Alzheimer's disease induced by aluminum in rats. 1(2), 1–10.
- Ames, B.N., 2001. DNA damage from micronutrient deficiencies is likely to be a major cause of cancer. *Mutat. Res./Fundam. Molec. Mech. Mutagen.* 475 (1), 7–20.

- An, L., Li, W., Xu, Y., Zeng, D., Cheng, Y., Wang, G., 2016. Controlled additive-free hydrothermal synthesis and characterization of uniform hydroxyapatite nanobelts. *Ceram. Int.* 42 (2), 3104–3112.
- Anastasiou, A., Thomson, C., Hussain, S., Edwards, T., Strafford, S., Malinowski, M., et al., 2016. Sintering of calcium phosphates with a femtosecond pulsed laser for hard tissue engineering. *Mater. Design* 101, 346–354.
- Andrade, F.A.C., Vercik, L. Cd.O., Monteiro, F.J., Rigo, E.Cd.S., 2016. Preparation, characterization and antibacterial properties of silver nanoparticles–hydroxyapatite composites by a simple and eco-friendly method. *Ceram. Int.* 42 (2), 2271–2280.
- Andronesu, E., Grumezescu, A.M., Gușă, M.-I., Holban, A.M., Ilie, F.-C., Irimia, A., et al., 2016. Chapter 6—Nano-hydroxyapatite: novel approaches in biomedical applications. In: Grumezescu, A.M. (Ed.), *Nanobiomaterials in Hard Tissue Engineering*. William Andrew Publishing, pp. 189–213.
- Anjaneyulu, U., Priyadarshini, B., Grace, A.N., Vijayalakshmi, U., 2016. Fabrication and characterization of Ag doped hydroxyapatite-polyvinyl alcohol composite nanofibers and its in vitro biological evaluations for bone tissue engineering applications. *J. Sol-Gel Sci. Technol.* 18 (3), 1–12.
- Arasad, M.S., Lee, P.M., Hung, L.K., 2011. Synthesis and characterization of hydroxyapatite nanoparticles and  $\beta$ -TCP particles. In: *2nd International Conference on Biotechnology and Food Science*.
- Asri, R.I.M., Harun, W.S.W., Hassan, M.A., Ghani, S.A.C., Buyong, Z., 2016. A review of hydroxyapatite-based coating techniques: sol–gel and electrochemical depositions on biocompatible metals. *J. Mech. Behav. Biomed. Mater.* 57, 95–108.
- Badran, H., Yahia, I., Hamdy, M.S., Awwad, N., 2017. Lithium-doped hydroxyapatite nano-composites: synthesis, characterization, gamma attenuation coefficient and dielectric properties. *Radiat. Phys. Chem.* 130, 85–91.
- Bakhsheshi-Rad, H., Hamzah, E., Kasiri-Asgarani, M., Jabbarzare, S., Iqbal, N., Kadir, M.A., 2016. Deposition of nanostructured fluorine-doped hydroxyapatite–polycaprolactone duplex coating to enhance the mechanical properties and corrosion resistance of Mg alloy for biomedical applications. *Mater. Sci. Eng. C* 60, 526–537.
- Bakhtiari, L., Javadpour, J., Rezaie, H.R., Erfan, M., Mazinani, B., Aminian, A., 2016. Pore size control in the synthesis of hydroxyapatite nanoparticles: the effect of pore expander content and the synthesis temperature. *Ceram. Int.* 42 (9), 11259–11264.
- Balcerzak, J., Mucha, M., 2010. Analysis of model drug release kinetics from complex matrices of polylactide-chitosan. *Progress Chem. Appl. Chitin Derivat.* 15, 117–125.
- Barandehfard, F., Kianpour Rad, M., Hosseinnia, A., Khoshroo, K., Tahriri, M., Jazayeri, H.E., et al., 2016. The addition of synthesized hydroxyapatite and fluorapatite nanoparticles to a glass-ionomer cement for dental restoration and its effects on mechanical properties. *Ceram. Int.* 42 (15), 17866–17875.
- Bertazzo, S., Zambuzzi, W.F., Campos, D.D., Ogeda, T.L., Ferreira, C.V., Bertran, C.A., 2010. Hydroxyapatite surface solubility and effect on cell adhesion. *Colloids Surf. B Biointerf.* 78 (2), 177–184.
- Berzina-Cimdina, L., Borodajenko, N., 2012. *Research of Calcium Phosphates Using Fourier Transform Infrared Spectroscopy*. INTECH Open Access Publisher.



- Bhushan, M., Kumar, Y., Periyasamy, L., Viswanath, A.K., 2018. Antibacterial applications of  $\alpha$ -Fe<sub>2</sub>O<sub>3</sub>/Co<sub>3</sub>O<sub>4</sub> nanocomposites and study of their structural, optical, magnetic and cytotoxic characteristics. *Appl. Nanosci.* 8 (1–2), 137–153.
- Biswas, P., Sharma, A., Krishnan, M., Johnson, R., Mohan, M.K., Bose, S., 2016. Fabrication of MgAl<sub>2</sub>O<sub>4</sub> spinel scaffolds and sonochemical synthesis and deposition of hydroxyapatite nanorods. *J. Am. Ceram. Soc.* 99 (5), 1544–1549.
- Bloebaum, R.D., Beeks, D., Dorr, L.D., Savory, C.G., DuPont, J.A., Hofmann, A.A., 1994. Complications with hydroxyapatite participate separation in total hip arthroplasty. *Clin. Orthop. Relat. Res.* 298, 19–26.
- Boonyawan, D., Waruriya, P., Suttiat, K., 2016. Characterization of titanium nitride–hydroxyapatite on PEEK for dental implants by co-axis target magnetron sputtering. *Surface Coat. Technol.* 306 (Part A), 164–170.
- Bouyarmanc, H., Gouza, A., Masse, S., Saoiabi, S., Saoiabi, A., Coradin, T., et al., 2016. Nanoscale conversion of chlorapatite into hydroxyapatite using ultrasound irradiation. *Colloids Surf. A Physicochem. Eng. Aspects* 495, 187–192.
- Brender, J.R., Hartman, K., Nanga, R.P.R., Popovych, N., de la Salud Bea, R., Vivekanandan, S., et al., 2010. Role of zinc in human islet amyloid polypeptide aggregation. *J. Am. Chem. Soc.* 132 (26), 8973–8983.
- Brundavanam, S., Jai Poinern, G.E., Fawcett, D., 2015. Synthesis of a hydroxyapatite nanopowder via ultrasound irradiation from calcium hydroxide powders for potential biomedical applications. *Nanosci. Nanoeng.* 3 (1), 1–7.
- Bulina, N.V., Chaikina, M.V., Prosanov, I.Y., Gerasimov, K.B., Ishchenko, A.V., Dudina, D.V., 2016. Mechanochemical synthesis of SiO<sub>4</sub>—substituted hydroxyapatite, part III—thermal stability. *Eur. J. Inorgan. Chem.* 2016 (12), 1866–1874.
- Bystrov, V.S., 2015. Piezoelectricity in the ordered monoclinic hydroxyapatite. *Ferroelectrics* 475 (1), 148–153.
- Bystrov, V.S., Paramonova, E.V., Costa, M.E.V., Santos, C., Almeida, M., Kopyl, S., et al., 2013. A computational study of the properties and surface interactions of hydroxyapatite. *Ferroelectrics* 449 (1), 94–101.
- Campodoni, E., Adamiano, A., Dozio, S.M., Panseri, S., Montesi, M., Sprio, S., et al., 2016. Development of innovative hybrid and intrinsically magnetic nanobeads as a drug delivery system. *Nanomedicine* 11 (16), 2119–2130.
- Castkova, K., Hadraba, H., Matousek, A., Roupčova, P., Chlup, Z., Novotna, L., et al., 2016. Synthesis of Ca, Y-zirconia/hydroxyapatite nanoparticles and composites. *J. Eur. Ceram. Soc.* 36 (12), 2903–2912.
- Cellet, T.S.P., Pereira, G.M., Muniz, E.C., Silva, R., Rubira, A.F., 2015. Hydroxyapatite nanowhiskers embedded in chondroitin sulfate microspheres as colon targeted drug delivery systems. *J. Mater. Chem. B* 3 (33), 6837–6846.
- Chen, J., Wang, Y., Chen, X., Ren, L., Lai, C., He, W., et al., 2011. A simple sol-gel technique for synthesis of nanostructured hydroxyapatite, tricalcium phosphate and biphasic powders. *Mater. Lett.* 65 (12), 1923–1926.
- Chuenjitkuntaworn, B., Osathanon, T., Nowwarote, N., Supaphol, P., Pavasant, P., 2016. The efficacy of polycaprolactone/hydroxyapatite scaffold in combination with mesenchymal stem cells for bone tissue engineering. *J. Biomed. Mater. Res. Part A* 104 (1), 264–271.
- Ciobanu, C.S., Massuyeau, F., Constantin, L.V., Predoi, D., 2011. Structural and physical properties of antibacterial Ag-doped nano-hydroxyapatite synthesized at 100 °C. *Nanosci. Res. Lett.* 6 (1), 1.



- Comeau, P.A., Filiaggi, M.J., 2016. Structural analysis of  $x\text{SrO}-(50-x)\text{CaO}-50\text{P}_2\text{O}_5$  glasses with  $x = 0, 5$ , or 10 mol% for potential use in a local delivery system for osteomyelitis treatment. *Mater. Sci. Eng. C* 58, 639–647.
- Dash, S., Murthy, P.N., Nath, L., Chowdhury, P., 2010. Kinetic modeling on drug release from controlled drug delivery systems. *Acta Pol. Pharm.* 67 (3), 217–223.
- Davis, J., 2003. Overview of biomaterials and their use in medical devices, *Handbook of Materials for Medical Devices*, Illustrated ed. ASM International, Materials Park, OH, pp. 1–11.
- Ding, Z., Fan, Z., Huang, X., Bai, S., Song, D., Lu, Q., et al., 2016. Bioactive natural protein–hydroxyapatite nanocarriers for optimizing osteogenic differentiation of mesenchymal stem cells. *J. Mater. Chem. B* 4 (20), 3555–3561.
- Dion, A., Langman, M., Hall, G., Filiaggi, M., 2005. Vancomycin release behaviour from amorphous calcium polyphosphate matrices intended for osteomyelitis treatment. *Biomaterials* 26 (35), 7276–7285.
- Dunne, C.F., Levy, G.K., Hakimi, O., Aghion, E., Twomey, B., Stanton, K.T., 2016. Corrosion behaviour of biodegradable magnesium alloys with hydroxyapatite coatings. *Surface Coat. Technol.* 289, 37–44.
- Ebrahimi-Kahrizsangi, R., Nasiri-Tabrizi, B., Chami, A., 2011. Characterization of single-crystal fluorapatite nanoparticles synthesized via mechanochemical method. *Particuology* 9 (5), 537–544.
- Elliott, J.C., Mackie, P., Young, R., 1973. Monoclinic hydroxyapatite. *Science* 180 (4090), 1055–1057.
- Fahami, A., Ebrahimi-Kahrizsangi, R., Nasiri-Tabrizi, B., 2011. Mechanochemical synthesis of hydroxyapatite/titanium nanocomposite. *Solid State Sci.* 13 (1), 135–141.
- Fahami, A., Nasiri-Tabrizi, B., Ebrahimi-Kahrizsangi, R., 2012. Synthesis of calcium phosphate-based composite nanopowders by mechanochemical process and subsequent thermal treatment. *Ceram. Int.* 38 (8), 6729–6738.
- Fahami, A., Nasiri-Tabrizi, B., Beall, G.W., Basirun, W.J., 2016. Materials and product engineering structural insights of mechanically induced aluminum-doped hydroxyapatite nanoparticles by Rietveld refinement. *Chin. J. Chem. Eng.* 25 (2), 238–247.
- Foroughi, F., Hassanzadeh-Tabrizi, S., Bigham, A., 2016. In situ microemulsion synthesis of hydroxyapatite-MgFe<sub>2</sub>O<sub>4</sub> nanocomposite as a magnetic drug delivery system. *Mater. Sci. Eng. C* 68, 774–779.
- Gambardella, A., Bianchi, M., Kaciulis, S., Mezzi, A., Brucalè, M., Cavallini, M., et al., 2016. Magnetic hydroxyapatite coatings as a new tool in medicine: a scanning probe investigation. *Mater. Sci. Eng. C* 62, 444–449.
- Gopi, D., Kanimozhi, K., Bhuvaneshwari, N., Indira, J., Kavitha, L., 2014a. Novel banana peel pectin mediated green route for the synthesis of hydroxyapatite nanoparticles and their spectral characterization. *Spectrochim. Acta Part A Mole. Biomole. Spectrosc.* 118, 589–597.
- Gopi, D., Shinyjoy, E., Kavitha, L., 2014b. Synthesis and spectral characterization of silver/magnesium co-substituted hydroxyapatite for biomedical applications. *Spectrochim. Acta Part A Mole. Biomol. Spectrosc.* 127, 286–291.
- Gu, L., He, X., Wu, Z., 2014. Mesoporous Fe<sub>3</sub>O<sub>4</sub>/hydroxyapatite composite for targeted drug delivery. *Mater. Res. Bull.* 59, 65–68.
- Guo, Y.-P., Long, T., Tang, S., Guo, Y.-J., Zhu, Z.-A., 2014. Hydrothermal fabrication of magnetic mesoporous carbonated hydroxyapatite microspheres: biocompatibility,

- osteoinductivity, drug delivery property and bactericidal property. *J. Mater. Chem. B* 2 (19), 2899.
- Hasan, A., Waibhaw, G., Tiwari, S., Dharmalingam, K., Shukla, I., Pandey, L.M., 2017. Fabrication and characterization of chitosan, polyvinylpyrrolidone, and cellulose nanowhiskers nanocomposite films for wound healing drug delivery application. *J. Biomed. Mater. Res. Part A* 105 (9), 2391–2404.
- Hasan, A., Saxena, V., Pandey, L.M., 2018a. Surface functionalization of Ti6Al4V via self-assembled monolayers for improved protein adsorption and fibroblast adhesion. *Langmuir* 34 (11), 3494–3506.
- Hasan, A., Waibhaw, G., Saxena, V., Pandey, L.M., 2018b. Nano-biocomposite scaffolds of chitosan, carboxymethyl cellulose and silver nanoparticle modified cellulose nanowhiskers for bone tissue engineering applications. *Int. J. Biol. Macromol.* 111, 923–934.
- Hattori, Y., Mori, H., Chou, J., Otsuka, M., 2015. Mechanochemical synthesis of zinc-apatitic calcium phosphate and the controlled zinc release for bone tissue engineering. *Drug Dev. Industr. Pharm.* 42 (4), 1–7.
- Haverty, D., Tofail, S.A.M., Stanton, K.T., McMonagle, J.B., 2005. Structure and stability of hydroxyapatite: density functional calculation and Rietveld analysis. *Phys. Rev. B* 71 (9), 094103.
- Healy, K., Guldberg, R., 2007. Bone tissue engineering. *J. Musculosk. Neur. Interact.* 7 (4), 328.
- Hill, R.G., Gillam, D.G., Chen, X., 2015. The ability of a nano hydroxyapatite toothpaste and oral rinse containing fluoride to protect enamel during an acid challenge using 19F solid state NMR spectroscopy. *Mater. Lett.* 156, 69–71.
- Ho, W.-F., Hsu, H.-C., Hsu, S.-K., Hung, C.-W., Wu, S.-C., 2013. Calcium phosphate bioceramics synthesized from eggshell powders through a solid state reaction. *Ceram. Int.* 39 (6), 6467–6473.
- Hoffman, R.M., Kajiura, S., Cao, W., Liu, F., Amoh, Y., 2016. Cryopreservation of hair-follicle associated pluripotent (HAP) stem cells maintains differentiation and hair-growth potential. *Biobanking and Cryopreservation of Stem Cells*. Springer, pp. 191–198.
- Hontsu, S., Yoshikawa, K., Kato, N., Kawakami, Y., Hayami, T., Nishikawa, H., et al., 2011. Restoration and conservation of dental enamel using a flexible apatite sheet. *J. Austral. Ceram. Soc.* 47 (1), 11–13.
- Horiuchi, N., Wada, N., Nozaki, K., Nakamura, M., Nagai, A., Yamashita, K., 2016. Dielectric relaxation in monoclinic hydroxyapatite: observation of hydroxide ion dipoles. *J. Appl. Phys.* 119 (8), 084903.
- Hsieh, M.-F., Perng, L.-H., Chin, T.-S., Perng, H.-G., 2001. Phase purity of sol–gel-derived hydroxyapatite ceramic. *Biomaterials* 22 (19), 2601–2607.
- Huang, Y., Zhang, X., Zhang, H., Qiao, H., Zhang, X., Jia, T., et al., 2017. Fabrication of silver-and strontium-doped hydroxyapatite/TiO<sub>2</sub> nanotube bilayer coatings for enhancing bactericidal effect and osteoinductivity. *Ceram. Int.* 43 (1), 992–1007.
- Huh, A.J., Kwon, Y.J., 2011. “Nanoantibiotics”: a new paradigm for treating infectious diseases using nanomaterials in the antibiotics resistant era. *J. Control. Release* 156 (2), 128–145.

- Ionita, D., Bajenaru-Georgescu, D., Totea, G., Mazare, A., Schmuki, P., Demetrescu, I., 2016. Activity of vancomycin release from bioinspired coatings of hydroxyapatite or TiO<sub>2</sub> nanotubes. *Int. J. Pharm.* 296–302.
- Ito, A., Kawamura, H., Otsuka, M., Ikeuchi, M., Ohgushi, H., Ishikawa, K., et al., 2002. Zinc-releasing calcium phosphate for stimulating bone formation. *Mater. Sci. Eng. C* 22 (1), 21–25.
- Itokazu, M., Matsunaga, T., Kumazawa, S., Oka, M., 1994. Treatment of osteomyelitis by antibiotic impregnated porous hydroxyapatite block. *Clin. Mater.* 17 (4), 173–179.
- Itokazu, M., Ohno, T., Tanemori, T., Wada, E., Kato, N., Watanabe, K., 1997. Antibiotic-loaded hydroxyapatite blocks in the treatment of experimental osteomyelitis in rats. *J. Med. Microbiol.* 46 (9), 779–783.
- Jadalannagari, S., Deshmukh, K., Ramanan, S.R., Kowshik, M., 2013. Antimicrobial activity of hemocompatible silver doped hydroxyapatite nanoparticles synthesized by modified sol–gel technique. *Appl. Nanosci.* 4 (2), 133–141.
- Jafari, S., Maleki-Dizaji, N., Barar, J., Barzegar-Jalali, M., Rameshrad, M., Adibkia, K., 2016. Methylprednisolone acetate-loaded hydroxyapatite nanoparticles as a potential drug delivery system for treatment of rheumatoid arthritis: in vitro and in vivo evaluations. *Eur. J. Pharm. Sci.* 91, 225–235.
- Jarosz, M., Pawlik, A., Szuwarzyński, M., Jaskuła, M., Sulka, G.D., 2016. Nanoporous anodic titanium dioxide layers as potential drug delivery systems: drug release kinetics and mechanism. *Colloids Surf. B Biointerf.* 143, 447–454.
- Jiang, J.-L., Li, Y.-F., Fang, T.-L., Zhou, J., Li, X.-L., Wang, Y.-C., et al., 2011. Vancomycin-loaded nano-hydroxyapatite pellets to treat MRSA-induced chronic osteomyelitis with bone defect in rabbits. *Inflam. Res.* 61 (3), 207–215.
- Joosten, U., Joist, A., Frebel, T., Brandt, B., Diederichs, S., von Eiff, C., 2004. Evaluation of an in situ setting injectable calcium phosphate as a new carrier material for gentamicin in the treatment of chronic osteomyelitis: studies in vitro and in vivo. *Biomaterials* 25 (18), 4287–4295.
- Kakiage, M., Iwase, K., Kobayashi, H., 2015. Effect of citric acid addition on disaggregation of crystalline hydroxyapatite nanoparticles under calcium-rich conditions. *Mater. Lett.* 156, 39–41.
- Kannan, S., Vieira, S.I., Olhero, S.M., Torres, P.M.C., Pina, S., da Cruz e Silva, O.A.B., et al., 2011. Synthesis, mechanical and biological characterization of ionic doped carbonated hydroxyapatite/ $\beta$ -tricalcium phosphate mixtures. *Acta Biomater.* 7 (4), 1835–1843.
- Kay, M.I., Young, R., Posner, A., 1964. Crystal structure of hydroxyapatite. *Nature* 204.4963 (1964): 1050.
- Kaygili, O., Keser, S., 2016. Zr/Mg, Zr/Sr and Zr/Zn co-doped hydroxyapatites: synthesis and characterization. *Ceram. Int.* 42 (7), 9270–9273.
- Kaygili, O., Dorozhkin, S.V., Ates, T., Al-Ghamdi, A.A., Yakuphanoglu, F., 2014. Dielectric properties of Fe doped hydroxyapatite prepared by sol–gel method. *Ceram. Int.* 40 (7), 9395–9402.
- Kazemzadeh-Narbat, M., Kindrachuk, J., Duan, K., Jenssen, H., Hancock, R.E.W., Wang, R., 2010. Antimicrobial peptides on calcium phosphate-coated titanium for the prevention of implant-associated infections. *Biomaterials* 31 (36), 9519–9526.
- Kim, I.-S., Kumta, P.N., 2004. Sol–gel synthesis and characterization of nanostructured hydroxyapatite powder. *Mater. Sci. Eng. B* 111 (2–3), 232–236.

- Kim, T.N., Feng, Q.L., Kim, J.O., Wu, J., Wang, H., Chen, G.C., et al., 1998. Antimicrobial effects of metal ions ( $\text{Ag}^+$ ,  $\text{Cu}^{2+}$ ,  $\text{Zn}^{2+}$ ) in hydroxyapatite. *J. Mater. Sci. Mater. Med.* 9 (3), 129–134.
- Kolekar, T.V., Thorat, N.D., Yadav, H.M., Magalad, V.T., Shinde, M.A., Bandgar, S.S., et al., 2016. Nanocrystalline hydroxyapatite doped with aluminium: a potential carrier for biomedical applications. *Ceram. Int.* 42 (4), 5304–5311.
- Kulpetchdara, K., Limpichaipanit, A., Rujijanagul, G., Randorn, C., Chokethawai, K., 2016. Influence of the nano hydroxyapatite powder on thermally sprayed HA coatings onto stainless steel. *Surf. Coat. Technol.* 306, 181–186.
- Kundu, B., Ghosh, D., Sinha, M.K., Sen, P.S., Balla, V.K., Das, N., et al., 2013. Doxorubicin-intercalated nano-hydroxyapatite drug-delivery system for liver cancer: an animal model. *Ceram. Int.* 39 (8), 9557–9566.
- Kuriakose, T.A., Kalkura, S.N., Palanichamy, M., Arivuoli, D., Dierks, K., Bocelli, G., et al., 2004. Synthesis of stoichiometric nano crystalline hydroxyapatite by ethanol-based sol–gel technique at low temperature. *J. Crystal Growth* 263 (1–4), 517–523.
- Kusrini, E., Pudjiastuti, A.R., Astutiningsih, S., Harjanto, S., 2012. Preparation of hydroxyapatite from bovine bone by combination methods of ultrasonic and spray drying. In: *International Conference on Chemical, Bio-Chemical and Environmental Sciences (ICBEE'2012)*, Singapore.
- Lai, W., Chen, C., Ren, X., Lee, I.-S., Jiang, G., Kong, X., 2016. Hydrothermal fabrication of porous hollow hydroxyapatite microspheres for a drug delivery system. *Mater. Sci. Eng. C* 62, 166–172.
- Lala, S., Maity, T.N., Singha, M., Biswas, K., Pradhan, S.K., 2017. Effect of doping (Mg, Mn, Zn) on the microstructure and mechanical properties of spark plasma sintered hydroxyapatites synthesized by mechanical alloying. *Ceram. Int.* 43 (2), 2389–2397.
- Lansdown, A.B., 2006. Silver in health care: antimicrobial effects and safety in use. *Curr. Probl. Dermatol.* 33, 17–34.
- Leena, M., Rana, D., Webster, T.J., Ramalingam, M., 2016. Accelerated synthesis of biomimetic nano hydroxyapatite using simulated body fluid. *Mater. Chem. Phys.* 180, 166–172.
- Lelli, M., Roveri, N., Marzano, C., Hoeschele, J.D., Curci, A., Margiotta, N., et al., 2016. Hydroxyapatite nanocrystals as a smart, pH sensitive, delivery system for kiteplatin. *Dalton Trans.* 45 (33), 13187–13195.
- Lett, J.A., Sundareswari, M., Ravichandran, K., 2016. Porous hydroxyapatite scaffolds for orthopedic and dental applications-the role of binders. *Mater. Today Proc.* 3 (6), 1672–1677.
- Leventouri, T., 2006. Synthetic and biological hydroxyapatites: crystal structure questions. *Biomaterials* 27 (18), 3339–3342.
- Li, D., Huang, X., Wu, Y., Li, J., Cheng, W., He, J., et al., 2016a. Preparation of pH-responsive mesoporous hydroxyapatite nanoparticles for intracellular controlled release of an anticancer drug. *Biomater. Sci.* 4 (2), 272–280.
- Li, Z., Huang, B., Mai, S., Wu, X., Zhang, H., Qiao, W., et al., 2016b. Effects of fluoridation of porcine hydroxyapatite on osteoblastic activity of human MG63 cells. *Sci. Technol. Adv. Mater.* 16 (3), 035006.
- Lin, K., Zhang, M., Zhai, W., Qu, H., Chang, J., 2011. Fabrication and characterization of hydroxyapatite/wollastonite composite bioceramics with controllable properties for hard tissue repair. *J. Am. Ceram. Soc.* 94 (1), 99–105.

- Lin, K., Chen, L., Liu, P., Zou, Z., Zhang, M., Shen, Y., et al., 2013a. Hollow magnetic hydroxyapatite microspheres with hierarchically mesoporous microstructure for pH-responsive drug delivery. *Cryst. Eng. Comm.* 15 (15), 2999–3008.
- Lin, K., Liu, P., Wei, L., Zou, Z., Zhang, W., Qian, Y., et al., 2013b. Strontium substituted hydroxyapatite porous microspheres: Surfactant-free hydrothermal synthesis, enhanced biological response and sustained drug release. *Chem. Eng. J.* 222, 49–59.
- Liu, M., Liu, H., Sun, S., Li, X., Zhou, Y., Hou, Z., et al., 2014. Multifunctional hydroxyapatite/Na(Y/Gd)F<sub>4</sub>:Yb<sup>3+</sup> + Er<sup>3+</sup> + composite fibers for drug delivery and dual modal imaging. *Langmuir* 30 (4), 1176–1182.
- Liu, M., Jing, H., Bai, R., Wang, Y., 2016. Adsorption of icariin on nano-hydroxyapatite: isotherm, kinetics, PH, ionic strength and construction. *Nanomed. Nanotechnol. Biol. Med.* 12 (2), 478–479.
- Lu, J., Wei, J., Yan, Y., Li, H., Jia, J., Wei, S., et al., 2011. Preparation and preliminary cytocompatibility of magnesium doped apatite cement with degradability for bone regeneration. *J. Mater. Sci. Mater. Med.* 22 (3), 607–615.
- Ma, G., Liu, X.Y., 2009. Hydroxyapatite: hexagonal or monoclinic? *Cryst. Growth Des.* 9 (7), 2991–2994.
- Ma, X., Chen, Y., Qian, J., Yuan, Y., Liu, C., 2016. Controllable synthesis of spherical hydroxyapatite nanoparticles using inverse microemulsion method. *Mater. Chem. Phys.* 183, 220–229.
- Macha, I.J., Ben-Nissan, B., Santos, J., Cazalbou, S., Milthorpe, B., 2016. Hydroxyapatite/PLA biocomposite thin films for slow drug delivery of antibiotics for the treatment of bone and implant-related infections. *Key Eng. Mater.* 696, 271–276.
- Madi, M., Zakaria, O., Ichinose, S., Kasugai, S., 2016. Effect of induced periimplantitis on dental implants with and without ultrathin hydroxyapatite coating. *Implant Dentis.* 25 (1), 39–46.
- Mahmood, D.F., Mohammed, S.A., 2016. The effect of pores in dual nano hydroxyapatite coating on thermally oxidized commercial pure titanium: mechanical and histological evaluation. *J. Baghdad College Dentis.* 28 (1), 17–25.
- Maitra, A., 2005. Calcium phosphate nanoparticles: second-generation nonviral vectors in gene therapy. *Expert Rev. Molec. Diagnost.* 5 (6), 893–905.
- Marques, C.F., Lemos, A., Vieira, S.I., da Cruz e Silva, O.A.B., Bettencourt, A., Ferreira, J.M.F., 2016a. Antibiotic-loaded Sr-doped porous calcium phosphate granules as multifunctional bone grafts. *Ceram. Int.* 42 (2), 2706–2716.
- Marques, C.F., Matos, A.C., Ribeiro, I.A.C., Gonçalves, L.M., Bettencourt, A., Ferreira, J. M.F., 2016b. Insights on the properties of levofloxacin-adsorbed Sr- and Mg-doped calcium phosphate powders. *J. Mater. Sci. Mater. Med.* 27 (7), 123.
- Martínez-Vázquez, F.J., Cabañas, M.V., Paris, J.L., Lozano, D., Vallet-Regí, M., 2015. Fabrication of novel Si-doped hydroxyapatite/gelatine scaffolds by rapid prototyping for drug delivery and bone regeneration. *Acta Biomater.* 15, 200–209.
- Matsunaga, K., Murata, H., Mizoguchi, T., Nakahira, A., 2010. Mechanism of incorporation of zinc into hydroxyapatite. *Acta Biomater.* 6 (6), 2289–2293.
- Mestres, G., Espanol, M., Xia, W., Persson, C., Ginebra, M.-P., Ott, M.K., 2015. Inflammatory response to nano- and microstructured hydroxyapatite. *PLoS One* 10 (4), e0120381.

- Mirzaee, M., Vaezi, M., Palizdar, Y., 2016. Synthesis and characterization of silver doped hydroxyapatite nanocomposite coatings and evaluation of their antibacterial and corrosion resistance properties in simulated body fluid. *Mater. Sci. Eng. C* 69, 675–684.
- Negut, I., Grumezescu, V., Fica, A., Grumezescu, A.M., Holban, A.M., Popescu, R.C., et al., 2018. MAPLE deposition of *Nigella sativa* functionalized Fe<sub>3</sub>O<sub>4</sub> nanoparticles for antimicrobial coatings. *Appl. Surf. Sci.* 455, 513–521.
- Nihmath, A., Ramesan, M., 2016. Preparation, characterization, thermal, and electrical properties of chlorinated ethylene propylene diene monomer/hydroxyapatite nanocomposites. *Polym. Compos.* 39 (6), 2093–2100.
- Noukrati, H., Cazalbou, S., Demnati, I., Rey, C., Barroug, A., Combes, C., 2016. Injectability, microstructure and release properties of sodium fusidate-loaded apatitic cement as a local drug-delivery system. *Mater. Sci. Eng. C* 59, 177–184.
- Nowak, G., Szewczyk, B., Pilc, A., 2005. Zinc and depression. An update. *Pharmacol. Rep.* 57 (6), 713–718.
- Oestreicher, J.H., Liu, E., Berkowitz, M., 1997. Complications of hydroxyapatite orbital implants. *Ophthalmology* 104 (2), 324–329.
- Ohgushi, H., Dohi, Y., Tamai, S., Tabata, S., 1993. Osteogenic differentiation of marrow stromal stem cells in porous hydroxyapatite ceramics. *J. Biomed. Mater. Res.* 27 (11), 1401–1407.
- Ong, J.L., Chan, D.C.N., 2000. Hydroxyapatite and their use as coatings in dental implants: a review. *28 (5&6)*, 667–707.
- Orlovskii, V., Komlev, V., Barinov, S., 2002. Hydroxyapatite and hydroxyapatite-based ceramics. *Inorgan. Mater.* 38 (10), 973–984.
- Paluszkievicz, C., Ślósarczyk, A., Pijocha, D., Sitarz, M., Bućko, M., Zima, A., et al., 2010. Synthesis, structural properties and thermal stability of Mn-doped hydroxyapatite. *J. Mole. Struct.* 976 (1), 301–309.
- Pandey, L.M., Pattanayek, S.K., 2011. Hybrid surface from self-assembled layer and its effect on protein adsorption. *Appl. Surface Sci.* 257 (10), 4731–4737.
- Pandey, L.M., Le Denmat, S., Delabouglise, D., Bruckert, F., Pattanayek, S.K., Weidenhaupt, M., 2012. Surface chemistry at the nanometer scale influences insulin aggregation. *Colloids Surf. B Biointerf.* 100, 69–76.
- Pandey, L.M., Pattanayek, S.K., 2013. Properties of competitively adsorbed BSA and fibrinogen from their mixture on mixed and hybrid surfaces. *Appl. Surf. Sci.* 264, 832–837.
- Pandey, L.M., Pattanayek, S.K., Delabouglise, D., 2013. Properties of adsorbed bovine serum albumin and fibrinogen on self-assembled monolayers. *J. Phys. Chem. C* 117 (12), 6151–6160.
- Paul, W., Sharma, C., 1999. Development of porous spherical hydroxyapatite granules: application towards protein delivery. *J. Mater. Sci. Mater. Med.* 10 (7), 383–388.
- Peng, H., Wang, J., Lv, S., Wen, J., Chen, J.-F., 2015. Synthesis and characterization of hydroxyapatite nanoparticles prepared by a high-gravity precipitation method. *Ceram. Int.* 41 (10), 14340–14349.
- Pignatelli, I., Kumar, A., Shah, K., Balonis, M., Bauchy, M., Wu, B., et al., 2016. Vertical scanning interferometry: a new method to quantify re-/de-mineralization dynamics of dental enamel. *Dental Mater.* 32 (10), e251–e261.

- Porter, A., Patel, N., Brooks, R., Best, S., Rushton, N., Bonfield, W., 2005. Effect of carbonate substitution on the ultrastructural characteristics of hydroxyapatite implants. *J. Mater. Sci. Mater. Med.* 16 (10), 899–907.
- Prado da Silva, M.H., Navarro da Rocha, D., Moura, F.N., Costa, A.M., Louro, L.H.L., 2017. Adhesion characterization of zinc-substituted hydroxyapatite coatings. *Key Engineering Materials*. Trans Tech Publ.
- Prakasam, M., Locs, J., Salma-Ancane, K., Loca, D., Largeteau, A., Berzina-Cimdina, L., 2015. Fabrication, properties and applications of dense hydroxyapatite: a review. *J. Funct. Biomater.* 6 (4), 1099–1140.
- Pramanik, S., Agarwal, A.K., Rai, K.N., Garg, A., 2007. Development of high strength hydroxyapatite by solid-state-sintering process. *Ceram. Int.* 33 (3), 419–426.
- Qi, C., Zhu, Y.-J., Lu, B.-Q., Zhao, X.-Y., Zhao, J., Chen, F., et al., 2013. Hydroxyapatite hierarchically nanostructured porous hollow microspheres: rapid, sustainable microwave-hydrothermal synthesis by using creatine phosphate as an organic phosphorus source and application in drug delivery and protein adsorption. *Chem. Eur. J.* 19 (17), 5332–5341.
- Rădulescu, D., Grumezescu, V., Andronescu, E., Holban, A.M., Grumezescu, A.M., Socol, G., et al., 2016a. Biocompatible cephalosporin-hydroxyapatite-poly(lactic-co-glycolic acid)-coatings fabricated by MAPLE technique for the prevention of bone implant associated infections. *Appl. Surf. Sci.* 374, 387–396.
- Radulescu, M., Andronescu, E., Cirja, A., Holban, A.M., Mogoanta, L., Balseanu, T.-A., et al., 2016b. Antimicrobial coatings based on zinc oxide and orange oil for improved bioactive wound dressings and other applications. *Rom. J. Morphol. Embryol.* 57 (1), 107–114.
- Raland, R., Borah, J., 2016. Efficacy of heat generation in CTAB coated Mn doped ZnFe<sub>2</sub>O<sub>4</sub> nanoparticles for magnetic hyperthermia. *J. Phys. D Appl. Phys.* 50 (3), 035001.
- Raland, R., Saikia, D., Borgohain, C., Borah, J., 2017. Heating efficiency and correlation between the structural and magnetic properties of oleic acid coated MnFe<sub>2</sub>O<sub>4</sub> nanoparticles for magnetic hyperthermia application. *J. Phys. D Appl. Phys.* 50 (32), 325004.
- Ramakrishnan, P., Nagarajan, S., Thiruvengatam, V., Palanisami, T., Naidu, R., Mallavarapu, M., et al., 2016. Cation doped hydroxyapatite nanoparticles enhance strontium adsorption from aqueous system: a comparative study with and without calcination. *Appl. Clay Sci.* 134, 136–144.
- Rao, R.R., Kannan, T., 2002. Synthesis and sintering of hydroxyapatite–zirconia composites. *Mater. Sci. Eng. C* 20 (1), 187–193.
- Redey, S., Razzouk, S., Rey, C., Bernache-Assollant, D., Leroy, G., Nardin, M., et al., 1999. Osteoclast adhesion and activity on synthetic hydroxyapatite, carbonated hydroxyapatite, and natural calcium carbonate: relationship to surface energies. *J. Biomed. Mater. Res.* 45 (2), 140–147.
- Ripamonti, U., Roden, L.C., Renton, L.F., 2012. Osteoinductive hydroxyapatite-coated titanium implants. *Biomaterials* 33 (15), 3813–3823.
- Rodriguez, R., Rangel, D., Fonseca, G., Gonzalez, M., Vargas, S., 2016. Piezoelectric properties of synthetic hydroxyapatite-based organic-inorganic hydrated materials. *Resul. Phys.* 6, 925–932.
- Roy, A., Saxena, V., Pandey, L.M., 2018. 3D printing for cardiovascular tissue engineering: a review. *Mater. Technol.* 33 (6), 433–442.



- Sadat-Shojai, M., Atai, M., Nodehi, A., Khanlar, L.N., 2010. Hydroxyapatite nanorods as novel fillers for improving the properties of dental adhesives: synthesis and application. *Dental Mater.* 26 (5), 471–482.
- Sadat-Shojai, M., Khorasani, M.-T., Dinpanah-Khoshdargi, E., Jamshidi, A., 2013. Synthesis methods for nanosized hydroxyapatite with diverse structures. *Acta Biomater.* 9 (8), 7591–7621.
- Saha, N., Keskinbora, K., Suvaci, E., Basu, B., 2010. Sintering, microstructure, mechanical, and antimicrobial properties of HAp-ZnO biocomposites. *J. Biomed. Mater. Res. Part B Appl. Biomater.* 95 (2), 430–440.
- Saint-Jean, S.J., Camire, C.L., Nevsten, P., Hansen, S., Ginebra, M.P., 2005. Study of the reactivity and in vitro bioactivity of Sr-substituted alpha-TCP cements. *J. Mater. Sci. Mater. Med.* 16 (11), 993–1001.
- Samani, S., Hossainipour, S., Tamizifar, M., Rezaie, H., 2013. In vitro antibacterial evaluation of sol–gel-derived Zn-, Ag-, and (Zn + Ag)-doped hydroxyapatite coatings against methicillin-resistant *Staphylococcus aureus*. *J. Biomed. Mater. Res. Part A* 101 (1), 222–230.
- Sammons, R., 2015. 3 - Biological responses to hydroxyapatite A2—Mucalo, Michael. *Hydroxyapatite (Hap) for Biomedical Applications*. Woodhead Publishing, pp. 53–83.
- Sanaei-rad, P., Jafarzadeh Kashi, T.-s., Seyedjafari, E., Soleimani, M., 2016. Enhancement of stem cell differentiation to osteogenic lineage on hydroxyapatite-coated hybrid PLGA/gelatin nanofiber scaffolds. *Biologicals* 44 (6), 511–516.
- Saxena, V., Hasan, A., Pandey, L.M., 2018a. Effect of Zn/ZnO integration with hydroxyapatite: a review. *Mater. Technol.* 33 (2), 79–92.
- Saxena, V., Hasan, A., Sharma, S., Pandey, L.M., 2018b. Edible oil nanoemulsion: an organic nanoantibiotic as a potential biomolecule delivery vehicle. *Int. J. Polym. Mater. Polym. Biomater.* 67 (7), 410–419.
- Sharma, S., Hasan, A., Kumar, N., Pandey, L.M., 2018a. Removal of methylene blue dye from aqueous solution using immobilized *Agrobacterium fabrum* biomass along with iron oxide nanoparticles as biosorbent. *Environ. Sci. Pollut. Res.* 25 (22), 21605–21615.
- Sharma, S., Saxena, V., Baranwal, A., Chandra, P., Pandey, L.M., 2018b. Engineered nanoporous materials mediated heterogeneous catalysts and their implications in biodiesel production. *Mater. Sci. Energy Technol.* 1 (1), 11–21.
- Shi, D., Jiang, G., Bauer, J., 2002. The effect of structural characteristics on the in vitro bioactivity of hydroxyapatite. *J. Biomed. Mater. Res.* 63 (1), 71–78.
- Sierra-Pallares, J., Huddle, T., García-Serna, J., Alonso, E., Mato, F., Shvets, I., et al., 2016. Understanding bottom-up continuous hydrothermal synthesis of nanoparticles using empirical measurement and computational simulation. *NanoResearch* 9 (11), 3377–3387.
- Silva, V.V., Domingues, R.Z., Lameiras, F.S., 2001. Microstructural and mechanical study of zirconia-hydroxyapatite (ZH) composite ceramics for biomedical applications. *Compos. Sci. Technol.* 61 (2), 301–310.
- Singh, R.K., Kim, T.-H., Patel, K.D., Kim, J.-J., Kim, H.-W., 2014. Development of biocompatible apatite nanorod-based drug-delivery system with in situ fluorescence imaging capacity. *J. Mater. Chem. B* 2 (14), 2039.



- Singh, A., Datta, P., Pandey, L.M., 2017. Deciphering the mechanistic insight into the stoichiometric ratio dependent behavior of Cu (II) on BSA fibrillation. *Int. J. Biol. Macromol.* 97, 662–670.
- Sirelkhatim, A., Mahmud, S., Seeni, A., Kaus, N.H.M., Ann, L.C., Bakhori, S.K.M., et al., 2015. Review on zinc oxide nanoparticles: antibacterial activity and toxicity mechanism. *Nano-Micro Lett.* 7 (3), 219–242.
- Slepko, A., Demkov, A.A., 2015. Hydroxyapatite: vibrational spectra and monoclinic to hexagonal phase transition. *J. Appl. Phys.* 117 (7), 074701.
- Sobczak, A., Kowalski, Z., Wzorek, Z., 2009. Preparation of hydroxyapatite from animal bones. *Acta Bioeng. Biomech.* 11 (4), 23–28.
- Son, J.S., Appleford, M., Ong, J.L., Wenke, J.C., Kim, J.M., Choi, S.H., et al., 2011. Porous hydroxyapatite scaffold with three-dimensional localized drug delivery system using biodegradable microspheres. *J. Control. Release* 153 (2), 133–140.
- Song, J., Liu, Y., Zhang, Y., Jiao, L., 2011. Mechanical properties of hydroxyapatite ceramics sintered from powders with different morphologies. *Mater. Sci. Eng. A* 528 (16–17), 5421–5427.
- Soriano-Souza, C.A., Rossi, A.L., Mavropoulos, E., Hausen, M.A., Tanaka, M.N., Calasans-Maia, M.D., et al., 2015. Chlorhexidine-loaded hydroxyapatite microspheres as an antimicrobial delivery system and its effect on in vivo osteo-conductive properties. *J. Mater. Sci. Mater. Med.* 26, 166.
- Stanić, V., Dimitrijević, S., Antić-Stanković, J., Mitrić, M., Jokić, B., Plećaš, I.B., et al., 2010. Synthesis, characterization and antimicrobial activity of copper and zinc-doped hydroxyapatite nanopowders. *Appl. Surf. Sci.* 256 (20), 6083–6089.
- Stoica, P., Râpă, M., Chifiriuc, M.-C., Lungu, M., Tatia, R., Nîră, M.I., et al., 2015. Antifungal bionanocomposites based on poly (lactic acid) and silver nanoparticles for potential medical devices. *Roman. Biotechnol. Lett* 20, 10696–10707.
- Suetsugu, Y., Tateishi, T., 2011. *Implants and biomaterials (hydroxyapatite)*. National Institute of Material Science, Ibaraki, Japan.
- Sundaram, N.M., Rajendran, N., 2015. Biodegradation and cytotoxicity of ciprofloxacin-loaded hydroxyapatite-polycaprolactone nanocomposite film for sustainable bone implants. *Int. J. Nanomed.* 119, 119–127.
- Taheri, M.M., Abdul Kadir, M.R., Shokuhfar, T., Hamlekhan, A., Shirdar, M.R., Naghizadeh, F., 2015. Fluoridated hydroxyapatite nanorods as novel fillers for improving mechanical properties of dental composite: synthesis and application. *Mater. Design* 82, 119–125.
- Tampieri, A., D'Alessandro, T., Sandri, M., Sprio, S., Landi, E., Bertinetti, L., et al., 2012. Intrinsic magnetism and hyperthermia in bioactive Fe-doped hydroxyapatite. *Acta Biomater.* 8 (2), 843–851.
- Tas, A.C., 2000. Synthesis of biomimetic Ca-hydroxyapatite powders at 37 C in synthetic body fluids. *Biomaterials* 21 (14), 1429–1438.
- Thomas, M.B., Metoki, N., Mandler, D., Eliaz, N., 2016. In situ potentiostatic deposition of calcium phosphate with gentamicin-loaded chitosan nanoparticles on titanium alloy surfaces. *Electrochim. Acta.* 222, 355–360.
- Tiwari, S., Hasan, A., Pandey, L.M., 2017. A novel bio-sorbent comprising encapsulated *Agrobacterium fabrum* (SLAJ731) and iron oxide nanoparticles for removal of crude oil co-contaminant, lead Pb (II). *J. Environ. Chem. Eng.* 5 (1), 442–452.

- Tobaldi, D.M., Piccirillo, C., Rozman, N., Pullar, R.C., Seabra, M.P., Škapin, A.S., et al., 2016. Effects of Cu, Zn and Cu-Zn addition on the microstructure and antibacterial and photocatalytic functional properties of Cu-Zn modified TiO<sub>2</sub> nano-heterostructures. *J. Photochem. Photobiol. A Chem.* 330, 44–54.
- Tofail, S.A.M., Haverty, D., Cox, F., Erhart, J., Hána, P., Ryzhenko, V., 2009. Direct and ultrasonic measurements of macroscopic piezoelectricity in sintered hydroxyapatite. *J. Appl. Phys.* 105 (6), 064103.
- Tohgi, N., Obara, K., Yashiro, M., Hamada, Y., Arakawa, N., Mii, S., et al., 2016. Human hair-follicle associated pluripotent (hHAP) stem cells differentiate to cardiac-muscle cells. *Cell Cycle*. 16 (1), 95–99.
- Treccani, L., Klein, T.Y., Meder, F., Pardun, K., Rezwani, K., 2013. Functionalized ceramics for biomedical, biotechnological and environmental applications. *Acta Biomater.* 9 (7), 7115–7150.
- ur Rahman, Z., Shabib, I., Haider, W., 2016. Surface characterization and cytotoxicity analysis of plasma sprayed coatings on titanium alloys. *Mater. Sci. Eng. C* 67, 675–683.
- Uskokovic, V., Uskokovic, D.P., 2011. Nanosized hydroxyapatite and other calcium phosphates: chemistry of formation and application as drug and gene delivery agents. *J. Biomed. Mater. Res. B Appl. Biomater.* 96 (1), 152–191.
- Uswatta, S.P., Okeke, I.U., Jayasuriya, A.C., 2016. Injectable porous nano-hydroxyapatite/chitosan/tripolyphosphate scaffolds with improved compressive strength for bone regeneration. *Mater. Sci. Eng. C* 69, 505–512.
- Utara, S., Klinkaewnarong, J., 2015. Sonochemical synthesis of nano-hydroxyapatite using natural rubber latex as a templating agent. *Ceram. Int.* 41 (10), 14860–14867.
- van Asten, S.A.V., La Fontaine, J., Peters, E.J.G., Bhavan, K., Kim, P.J., Lavery, L.A., 2015. The microbiome of diabetic foot osteomyelitis. *Eur. J. Clin. Microbiol. Infect. Diseases* 35 (2), 293–298.
- Vaněk, P., Kolská, Z., Luxbacher, T., García, J.A.L., Lehocký, M., Vandrovcová, M., et al., 2016. Electrical activity of ferroelectric biomaterials and its effects on the adhesion, growth and enzymatic activity of human osteoblast-like cells. *J. Phys. D Appl. Phys.* 49 (17), 175403.
- Verma, G., Barick, K., Shetake, N.G., Pandey, B., Hassan, P., 2016. Citrate-functionalized hydroxyapatite nanoparticles for pH-responsive drug delivery. *RSC Adv.* 6 (81), 77968–77976.
- Victor, S.P., Paul, W., Vineeth, V., Komeri, R., Jayabalan, M., Sharma, C.P., 2016. Neodymium doped hydroxyapatite theranostic nanoplatforams for colon specific drug delivery applications. *Colloids Surf. B: Biointerf.* 145, 539–547.
- Wan, Y.Z., Huang, Y., Yuan, C.D., Raman, S., Zhu, Y., Jiang, H.J., et al., 2007. Biomimetic synthesis of hydroxyapatite/bacterial cellulose nanocomposites for biomedical applications. *Mater. Sci. Eng. C* 27 (4), 855–864.
- Wang, X., Li, Y., Wei, J., De Groot, K., 2002. Development of biomimetic nano-hydroxyapatite/poly (hexamethylene adipamide) composites. *Biomaterials* 23 (24), 4787–4791.
- Wang, A.-J., Paterson, T., Owen, R., Sherborne, C., Dugan, J., Li, J.-M., et al., 2016a. Photocurable high internal phase emulsions (HIPEs) containing hydroxyapatite for additive manufacture of tissue engineering scaffolds with multi-scale porosity. *Mater. Sci. Eng. C* 67, 51–58.

- Wang, M., Wang, L., Shi, C., Sun, T., Zeng, Y., Zhu, Y., 2016b. The crystal structure and chemical state of aluminum-doped hydroxyapatite by experimental and first principles calculation studies. *Phys. Chem. Chem. Phys.* 18 (31), 21789–21796.
- Wang, M.O., Bracaglia, L., Thompson, J.A., Fisher, J.P., 2016c. Hydroxyapatite-doped alginate beads as scaffolds for the osteoblastic differentiation of mesenchymal stem cells. *J. Biomed. Mater. Res. Part A* 104 (9), 2325–2333.
- Wang, Y., Hao, H., Zhang, S., 2016d. Lysozyme loading and release from Se doped hydroxyapatite nanoparticles. *Mater. Sci. Eng. C* 61, 545–552.
- Wang, Y., Wang, J., Hao, H., Cai, M., Wang, S., Ma, J., et al., 2016e. In vitro and in vivo mechanism of bone tumor inhibition by selenium-doped bone mineral nanoparticles. *ACS Nano* 10 (11), 9927–9937.
- Wang, Y., Yang, X., Gu, Z., Qin, H., Li, L., Liu, J., et al., 2016f. In vitro study on the degradation of lithium-doped hydroxyapatite for bone tissue engineering scaffold. *Mater. Sci. Eng. C* 66, 185–192.
- Watanabe, K., Nishio, Y., Makiura, R., Nakahira, A., Kojima, C., 2013. Paclitaxel-loaded hydroxyapatite/collagen hybrid gels as drug delivery systems for metastatic cancer cells. *Int. J. Pharm.* 446 (1–2), 81–86.
- Wen, C., Kang, H., Shih, Y.-R.V., Hwang, Y., Varghese, S., 2016. In vivo comparison of biomineralized scaffold-directed osteogenic differentiation of human embryonic and mesenchymal stem cells. *Drug Deliv. Translat. Res.* 6 (2), 121–131.
- Woodard, J.R., Hildore, A.J., Lan, S.K., Park, C., Morgan, A.W., Eurell, J.A.C., et al., 2007. The mechanical properties and osteoconductivity of hydroxyapatite bone scaffolds with multi-scale porosity. *Biomaterials* 28 (1), 45–54.
- Wren, A.W., 2016. Vitreous materials for dental restoration and reconstruction. *Biocompatible Glasses*. Springer, pp. 203–225.
- Wu, S.-C., Tsou, H.-K., Hsu, H.-C., Hsu, S.-K., Liou, S.-P., Ho, W.-F., 2013. A hydrothermal synthesis of eggshell and fruit waste extract to produce nanosized hydroxyapatite. *Ceram. Int.* 39 (7), 8183–8188.
- Wu, Y., Xia, L., Zhou, Y., Ma, W., Zhang, N., Chang, J., et al., 2015. Evaluation of osteogenesis and angiogenesis of icariin loaded on micro/nano hybrid structured hydroxyapatite granules as a local drug delivery system for femoral defect repair. *J. Mater. Chem. B* 3 (24), 4871–4883.
- Xiong, H., Du, S., Ni, J., Zhou, J., Yao, J., 2016. Mitochondria and nuclei dual-targeted heterogeneous hydroxyapatite nanoparticles for enhancing therapeutic efficacy of doxorubicin. *Biomaterials* 94, 70–83.
- Xue, B., Farghaly, A.A., Guo, Z., Zhao, P., Li, H., Zhou, C., et al., 2016. Monoclinic hydroxyapatite nanoplates hybrid composite with improved compressive strength, and porosity for bone defect repair: biomimetic synthesis and characterization. *J. Nanosci. Nanotechnol.* 16 (3), 2254–2263.
- Yamashita, Y., Uchida, A., Yamakawa, T., Shinto, Y., Araki, N., Kato, K., 1998. Treatment of chronic osteomyelitis using calcium hydroxyapatite ceramic implants impregnated with antibiotic. *Int. Orthop.* 22 (4), 247–251.
- Yang, Y.-H., Liu, C.-H., Liang, Y.-H., Lin, F.-H., Wu, K.C.W., 2013. Hollow mesoporous hydroxyapatite nanoparticles (hmHANPs) with enhanced drug loading and pH-responsive release properties for intracellular drug delivery. *J. Mater. Chem. B* 1 (19), 2447.

- Ye, J., Gao, Q., He, J.J., Gao, T., Ning, Q.Y., Xie, J.J., 2016. Exposure rate of unwrapped hydroxyapatite orbital implants in enucleation surgery. *Br. J. Ophthalmol.* 100 (6), 860–865.
- Yi, Z., Wang, K., Tian, J., Shu, Y., Yang, J., Xiao, W., et al., 2016. Hierarchical porous hydroxyapatite fibers with a hollow structure as drug delivery carriers. *Ceram. Int.* 42 (16), 19079–19085.
- Yilmaz, B., Evis, Z., 2013. Raman spectroscopy investigation of nano hydroxyapatite doped with yttrium and fluoride ions. *Spectrosc. Lett.* 47 (1), 24–29.
- Zhou, C., Deng, C., Chen, X., Zhao, X., Chen, Y., Fan, Y., et al., 2015. Mechanical and biological properties of the micro-/nano-grain functionally graded hydroxyapatite bioceramics for bone tissue engineering. *J. Mech. Behav. Biomed. Mater.* 48, 1–11.
- Zhou, H., Yang, M., Hou, S., Deng, L., 2017. Mesoporous hydroxyapatite nanoparticles hydrothermally synthesized in aqueous solution with hexametaphosphate and tea polyphenols. *Mater. Sci. Eng. C* 71, 439–445.
- Zhu, S., Huang, B., Zhou, K., Huang, S., Liu, F., Li, Y., et al., 2004. Hydroxyapatite nanoparticles as a novel gene carrier. *J. Nanopart. Res.* 6 (2), 307–311.

# Mechanical behavior of hydroxyapatite-based dental resin composites

# 9

F. Fabiano<sup>1</sup>, L. Calabrese<sup>2</sup> and E. Proverbio<sup>2</sup>

<sup>1</sup>Department of Biomedical Sciences, Dentistry and Morphological and Functional Imaging, University of Messina, Messina, Italy <sup>2</sup>Department of Engineering, University of Messina, Messina, Italy

## 9.1 INTRODUCTION

Limits affecting the long-term durability of resin composites in large stress-bearing restorations are today the main challenge faced by dental materials companies with consequent efforts to improve the mechanical and biological properties of these materials. To bypass the drawbacks present in commercial resin-based composite a balanced equilibrium between composite morphology, mechanical performances, and antimicrobial activity needs to be achieved.

A wide range of formulations have been tested to improve restorations with several inorganic particles fillers. In particular, the scientific community has worked on filler packing, optimization of filler content, and development of new innovative hybrid fillers (Liu et al., 2013a; Domingo et al., 2001; Zhang and Darvell, 2012a).

Calcium phosphates (CaPs), such as hydroxyapatite, amorphous calcium phosphates, or tetracalcium phosphate, were investigated as novel fillers to obtain a dental resin composite with mineral releasing property in comparison with bioinert inorganic particles filler (Corrêa et al., 2015; Domingo et al., 2003; Zhang and Darvell, 2012b). Hydroxyapatite  $[\text{Ca}_{10}(\text{PO}_4)_6(\text{OH})_2]$  represents, thanks to its good cation exchange rate with metals, a very promising active material for the release of antimicrobial molecule or ions (i.e., silver, copper, and zinc). In fact, secondary caries often occur due to restoration failure, mainly because of the higher capacity of resin composite materials to accumulate biofilm in comparison with other restorative materials, such as amalgam. In particular, ethylene glycol dimethacrylate (EGDMA) and triethylene glycol dimethacrylate (TEGDMA) have been shown to promote the attachment and proliferation of two different cariogenic strains such as *Lactobacillus acidophilus* and *Streptococcus sobrinus* (Gupta et al., 2012; Hansel et al., 1998; Khalichi et al., 2004).

Hydroxyapatite (HA) was introduced for first time in dentistry in 1975 by Nery et al. as filling material for intrabony defects. As the main biomineral

constituent in enamel and dentine, HA is liable for their hardness, mechanical properties, as well as excellent bioactivity and biocompatibility (Kantharia et al., 2014). For this reason, in the last 5 years hydroxyapatite whiskers (wHA) and nanofibers have been introduced as novel bioactive reinforcing fillers in dental restorations.

This filler is potentially able to increase the bonding strength between restoration and tooth with the formation of a stable Ca-P interlayer (Zhang et al., 2010). Considering that in commercial resin composite the main reason for stress-bearing posterior restorations failure is the brittle behavior of quartz particles, the use of hydroxyapatite filler (whiskers, nanorods, nanofibers, etc.) has demonstrated to provide larger load transfer and favor toughening mechanisms, in addition, increasing flexural modulus and fracture toughness of unfilled resins (Lezaja et al., 2013; Santos et al., 2002; Arcís et al., 2002).

wHA have been considered an optimal filler choice compared with the other reinforcing whiskers based on carbon, ceramic, glass, metal and polymer, which can cause cytotoxicity effects and are lacking in term of bioactivity.

In literature, a systematic analysis both of the mechanical and biocompatibility performances of different hydroxyapatite-based composites and different commercial composites formulated with nano- and microhybrid particle sizes still lacks. A miniflexural test (Calabrese et al., 2015) was employed to simulate clinically realistic specimen dimensions whereas the mesio-distal diameter of molars is about 11 mm and the cervico-incisal length of central incisors is around 13 mm. Furthermore, several overlapping irradiations [240 seconds ( $40 \text{ seconds} \times 3 \times 2$ )] are required as the exit window of all clinical light-cure units is smaller than 25 mm. This leads to specimens that are cured inhomogeneously. This phenomenon induces also a differential polymerization shrinkage in resin composites, thus causing residual stresses in proximity of the regions where the incomplete polymerization occurred.

This information is of primary interest to achieve a final consistency and specific formulation suitable for the optimal incorporation of wHA mixed with particulate fillers as well as to optimize the mechanical properties of the composite paste.

In addition, the easy functionalization of hydroxyapatite (HA) filler with metals such as silver, copper, and zinc represents the most promising pathway to obtain an antimicrobial release during time of active molecules or ions to avoid secondary caries activation (Kolmas et al., 2014).

---

## 9.2 DENTAL COMPOSITES

### 9.2.1 RESIN MATRIX FOR DENTAL COMPOSITES

In 1962 Bowen marked the route of conservative dentistry, differentiating and at the same time combining esthetic and functional needs in tooth restoration (Bowen et al., 1963). In fact, the concept of dental composites appeared in this

year with the introduction in dentistry of a molecule called bisphenol A glycerolate dimethacrylate (Bis-GMA). This allowed tridimensional elongation of the polymeric chains with consequent improvement in mechanical properties of the networks in comparison with acrylic resins thus preserving the tooth structure both from the mechanical and esthetic point of view.

Dental composites are made by three combined components:

1. An organic phase (matrix phase) is composed by a combined system of aromatic and aliphatic monomers mono-, di-, or trifunctionalized, other than photopolymerization initiators, accelerators, inhibitors, and dyes. In particular, the photoinitiation system is usually represented by a camphorquinone associated with a tertiary amine such as 4-n,n-dimethylamino-phenyl-ethanol. To stabilize the formulation during storage, hydroquinone monomethyl ether is added. Moreover, to avoid UV-light absorption on the amine prior to use, 2-hydroxy-4-methoxybenzophenone is also inserted (Cramer et al., 2011).
2. A filler phases or inorganic phase. The mechanical and physical properties of the final product depend on the inorganic filler typology and its percentage. This phase also influences optical, radiopacity, thermal, and shrinkage behavior of the dental composite.
3. An eventual interfacial phase based on a coupling agent. The organo-silane-based agent permits to enhance and promote the interaction between the inorganic filler and organic matrix by forming to one end (terminal) links between silane groups and SiO<sub>2</sub> group on the filler, while on the other end covalent bonds between methacrylate groups are formed (Ferracane, 2011).

Dimethacrylate monomers can form bonds with other molecules or structures until a maximum of four links, favoring the cross-linking process. Today Bis-GMA represents still the main component of resin composite, however due to its high viscosity the formulation of the matrix is modulated by the addition of viscosity controllers such as bisphenol A dimethacrylate (Bis-DMA), ethoxylated bisphenol A glycol dimethacrylate (Bis-EMA), TEGDMA, 2-hydroxyethyl methacrylate (HEMA), methyl methacrylate or urethane dimethacrylate (UDMA), and EGDMA (Hervás-García et al., 2006; Culbertson et al., 1997; Millich et al., 1998). The main reason is the presence on the aliphatic chains of Bis-GMA of hydroxyl groups (—OH), which brings strong hydrogen-based intermolecular links generating less flexible monomer nuclei, thus inhibiting chain mobility and preventing the homopolymer from achieving high degrees of conversion. With the addition of viscosity controllers with more flexible structure an increase in reactivity is typically observed and consequently the resin curing progresses to a higher degree of conversion (Ogliari et al., 2008).

In the dental market, the formulations usually preferred are based on Bis-GMA/TEGDMA monomer or on Bis-GMA/UDMA/TEGDMA, or Bis-GMA/UDMA/Bis-EMA polymers. The mixture choice defines the mechanical properties as well as viscosity, reactivity, water uptake, and swelling of the final composite (Tilbrook et al., 2000; Manhart et al., 2000).

Over time the increased esthetic demand by patients has led to the focus of the scientific community on improvement in resin-based composite, both in terms of durability and mechanical performance.

### 9.2.2 POLYMERIZATION PROCESS

Three phases in the cross-linking process can be identified: initiation, propagation, and termination.

The network cross-linking is mediated by a photopolymerization process with visible light, in particular the reaction of the light sensible component generates free radicals (initiation phase), which are able to open the double carbon bonds on the methacrylate groups permitting the activation of polymer chain reaction (Leprince et al., 2013).

At first a gel phase occurs that will determine the shrinkage stress of the final product and after this a glassy stage is predominant, where an increase in mechanical performances of the composite can be highlighted (Schmalz, 2009). The phases of propagation and termination are diffusion-dependent. In the termination phase the domains stop reacting when two radicals collide decreasing the polymer flow and the network growth. The propagation phase, instead, occurs when a polymeric radical and a mobile portion of methacrylate monomer react with consequent polymer chain growth via covalent bonds formation. During the gelification (Cramer et al., 2011), the radicals located on long polymer chains are restricted in mobility while small monomers can still diffuse through the network forming new initiation domains. Indeed, with a so-called autoacceleration mechanism the free radicals increase in parallel with the polymerization thus permitting the fast curing process of these materials (Anseth et al., 1995; Leprince et al., 2009). For this reason, the reaction is not dependent on the diffusion until a high rate of conversion is reached, which usually happens in the glassy stage of the cross-linking. After the network vitrification starts, the reaction slows down due to the increase in viscosity of the matrix until stopping the diffusion. This kinetic step, called also autodeceleration, is important because as a result the presence of residual unreacted methacrylates domains will determine both the postcure behavior of the resin-based composite as well as the different refractive index in the organic component (Leprince et al., 2010a; Lovell et al., 1999; Truffier-Boutry et al., 2006). The percentage of residual double bonds unreacted compared with the initial one in the final resin composite represents the indirect parameter with which to evaluate the degree of conversion of the matrix and thus the efficiency of polymerization.

Indeed, the final degree of conversion obtained will be never equal to 100%, but the maximum range possible will be anyway obtained during the irradiation step, around 35%–77% (Schmalz, 2009). The unreacted species, which remain entrapped in the lattice, are able to affect both the potential toxicity of the material and the physical properties.



### 9.2.3 FILLER TYPOLOGIES

A widely proposed classification of resin composite is based on grain size of the filler. In particular, dental composites can be differentiated and loaded with (1) macrofiller, with a size ranged between 1 and 100  $\mu\text{m}$ ; the mechanical performances of this composite are high but unfortunately the polish step is difficult as is maintaining a smooth surface; (2) microfiller, with a particle dimension of 0.04  $\mu\text{m}$ , the matrix is loaded with an higher percentage through the insertion of prepolymerized resin fillers in the formulate thus leading to a good compromise between polishability and mechanical performance; or (3) hybrid filler, which possesses different grain sizes ranging between 0.4 and 1  $\mu\text{m}$  and which is usually called universal composite; these show a good marginal integrity (Ferracane, 2011). Fig. 9.1 shows the classification of dental composites based on distribution of macro-, micro-, and nanofiller particles.

Another classification, which is a more clinical one, is based on the percentage of filler loaded in the organic phase (Hervás-García et al., 2006) and it is useful for clinical decision-making:

1. Hybrid composites, in which the inorganic filler is constituted by a percentage of 60% or more and the composition varies in particle size and chemistry (0.4–1  $\mu\text{m}$ ) plus colloidal silica of 0.04  $\mu\text{m}$ . This typology possesses the adaptability to be used in anterior and posterior dental sectors.
2. Flowable composites are characterized both by a low viscosity and filler content so they can be applied in lower stress-bearing restorations like those in cervical areas.
3. Condensable composites possess a high filler ratio; however this causes a decrease in handling process, and in esthetic cases, they are used with a condensation technique mainly in class II restorations where the reproducibility of the occlusal cuspidal anatomy is needed.

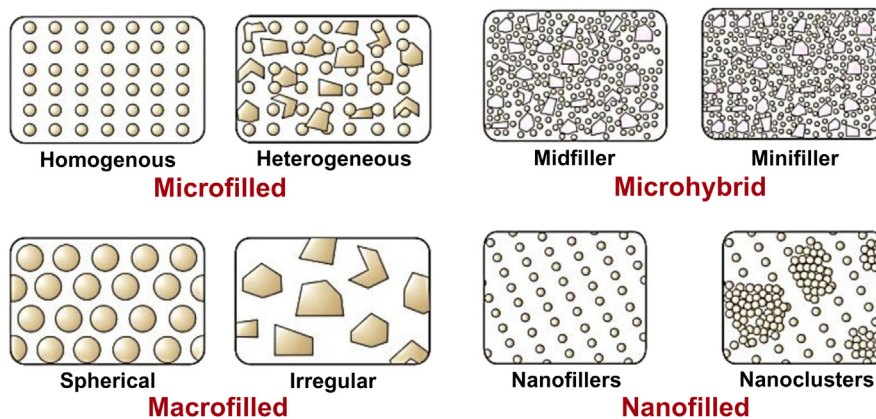


FIGURE 9.1

Classification of dental composites on the basis of particle size and structure (Khurshid et al., 2015).

Moreover, under the recently coined term *nanocomposites* it is possible to differentiate between nanohybrids and nanofilled composites. The nanohybrids are made by the combination between milled particles and nanofiller with a dimension of 40–50 nm. Nanofilled composites, on the other hand, can be divided in silica particle ranging between 20 and 75 nm and agglomerates of zirconia-silica and silica particles. The nanodimension results in a higher load capacity (around 79% in volume) in the matrix, which is greatly reduced and has better dispersion as well as enhanced interface area interactions of the composite constituents, thus limiting the polymerization shrinkage (Sachdeva et al., 2015).

Filler particle can be differentiated on the basis of chemical, morphological, and dimensional parameters. The most common inorganic particles used are silicon dioxide, boron silicates, and lithium aluminum silicate; often the quartz is partially substituted with strontium, titania, zinc, barium, aluminum, and/or zirconium. A simplified schematization of the main filler types and their elemental compositions is reported in Table 9.1.

The first filler usually used for dental restoration materials is silicon dioxide, termed silica (or quartz when it is in crystalline state). It can be considered the basis for other classes of fillers such as glass fillers or silicates. This material has been studied extensively including its synthesis and modifications, and is widely available at low cost (Habib et al., 2016). Different methods have been carried out to obtain silica filler, such as top-down technique, which however results in irregular shape morphology; or the bottom-up technique to obtain a functionalized filler, pyrogenic synthesis other than the Stober process, which produces monodispersed solid phases with an approximately standardized spherical shape in a range from 50 up to 2000 nm (Kim et al., 2007; Nozawa et al., 2005).

The alkaline glasses filler class is based on silicon dioxide including also fractions of alkaline oxides that integrate into the silica network. The introduction in the matrix of these alkaline oxides, such as barium oxide (BaO) and strontium oxide (SrO), permits to improve the wear resistance of dental composites during clinical function.

In recent years, in the organic–inorganic hybrids filler class, a different filler phase was proposed with the introduction of ORMOCER where a silane-modified polymer was proposed as silica nucleation center. By using this system, an increase in the wettability and a lower shrinkage were observed as well as improved adhesion to tooth hardness and compressive strength.

**Table 9.1** Main Filler Types and Their Elemental Compositions (Habib et al., 2016)

Filler Type	Examples	Chemical Composition
Oxides	Silica, alumina, titania, zirconia	$M_xO_y$
Alkaline silicate glass	Barium glass, strontium glass	$M_xO_ySiO_2$
Biomimetic filler	Hydroxyapatite	$Ca_5(PO_4)_3OH$
Organic–inorganic hybrids	ORMOCERS	$SiO_2$ -polymer

Another filler typology is represented by prepolymerized composite particles. In this class typology the filler is mixed with the unpolymerized resin before its incorporation in the matrix thus permitting the lowering of viscosity and the increase in the filler loading. Minor shrinkage and major fracture toughness are shown for this type of filler.

Porous filler was explored for silica, alumina, glasses, and so on. This filler typology has demonstrated better mechanical performance thanks to the improved interaction with the matrix and it was also suggested as a carrier to deliver bioactive molecules.

However, nowadays a remarkable attention is given to calcium-based fillers. Synthetic calcium phosphate materials are divided in two main groups: HA and amorphous calcium phosphate. Amorphous calcium phosphate-based composite has been largely studied. For these materials, although the bioactivity and the release properties were improved if compared with the glass-based composite, the mechanical properties and durability drastically decrease.

HA size and morphology affect significantly the mechanical properties of the resin composite, however, if compared with amorphous calcium phosphate, generally the mechanical performances shown are better. Spheroidal particles, whiskers, fibers, and urchin shapes have been synthesized and tested giving promising results for dental restoration thanks mainly to their high bioactive functionalization. Moreover, with the introduction of the nanocomposite concept, novel synthesis methods have been evaluated to obtain different morphologies and dimensions of calcium-based crystals. The reproduction of tooth structure with its natural HA, which ranged between 1 and 10 nm, is not well represented by using commercially available sizes and thus the integration as well as the adhesion of the synthetic composite with the natural component produce sometimes an unstable restoration (Jandt and Sigusch, 2009).

Nanocomposites have shown to have major polishability, optical, and esthetic characteristics, increased wear resistance, and good mechanical performance such as strength, flexural properties, and hardness in comparison with micro- or macroscale filler. The main failure cause of commercial composites, in fact, is due to the formation of cracks and their propagation in the regions between resin and filler; on the other hand, the use of nanoscale particles has marked the reduction of this phenomenon through the better interfacial interactions between the organic and inorganic phase as well as the reduction in the thermal expansion coefficients, low shrinkage, and increase in surface area. The range size varies from 5 to 100 nm of the single particle, otherwise agglomerates of multiples nanoparticles can reach 100 nm and more. The nanofiller is dispersed in a well compacted way in the matrix, permitting a uniform stress distribution during function along with a good abrasion resistance in contrast with the micrometric and hybrid fillers, which form defects in the surface and marginal leakage during time. The resulting surface, in fact, after the polish phase is smoother, preventing plaque retention and secondary caries occurrence (Moszner and Klapdohr, 2004).

Finally, filler dimension and morphology affect wear resistance and mechanical properties of resin-based composite, and thus are of fundamental importance to explore new proof of concepts in this field.

## 9.3 HA FILLER AS A NEW CHALLENGE FOR RESTORATIVE DENTISTRY

### 9.3.1 HYDROXYAPATITE CRYSTAL MORPHOLOGIES

During the past few decades, relevant research efforts were carried out to improve or optimize various synthesis approaches of bioceramics HA for biomedical applications, mainly in orthopedics and dentistry. Several methods were used to synthesize HA as in exemplum precipitation (Santos et al., 2004), sol–gel (Chai and Ben-Nissan, 1999; Choudhury and Agrawal, 2011), electrodeposition (Manso et al., 2000; Jamesh et al., 2012), conversion coating (Chen et al., 2011a; Su et al., 2012), or hydrothermal (Earl et al., 2006; Suchanek et al., 2015) techniques.

Shape, size, and surface area of HA particles are parameter sensitive to selected synthesis techniques and at the same time to the specific synthesis parameters developed in the research protocol (e.g., constituents, template, pH, temperature, etc.) (Nayak, 2010). The morphological nature of the bioceramic HA filler plays an important role on the biocompatibility and mechanical performance of the dental composite resin.

The simplest morphology of HA particles is the spheroidal shape. It was investigated as dental filler for several applications. The particle size and distribution have relevant effect on durability of the filler and with a correct mix design can improve the mechanical performances of the composite.

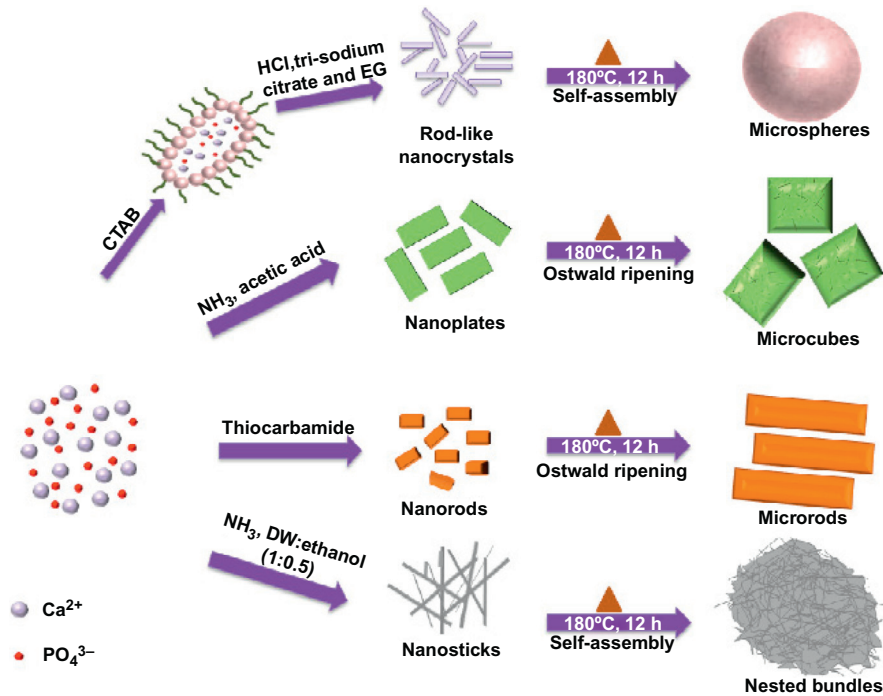
In this regard, to improve stability and physicomechanical properties of the dental composite resin, other shapes of HA (such as whiskers and nanofibers) could be considered as effective materials in the dentistry field. Analogously a new urchin-like hydroxyapatite (UHA), synthesized by microwave approach, was applied as a dental filler with promising results (Habib et al., 2016).

The growth mechanism of HA microstructures involves crystallization, Ostwald ripening, and self-assembly processes, which were supposed to be the specific channels for the formation of different morphologies (Mary et al., 2016). A schematization of growth processes of HA microstructures is reported in Fig. 9.2.

The future focus in this research field is the evolution of novel multiform morphologies of HA microstructures using a simple and versatile HA synthesis procedure. These synthesis strategies need to be able to build spheres, rods, plates, or whisker blocks by a suitable adjustment of pH, temperature, additives, and solvent without any further posttreatment of the filler.

#### 9.3.1.1 Spheroidal particles

An important parameter is related to the dimension of filler both in mechanical and biological performances of HA-based composite materials. Considering that

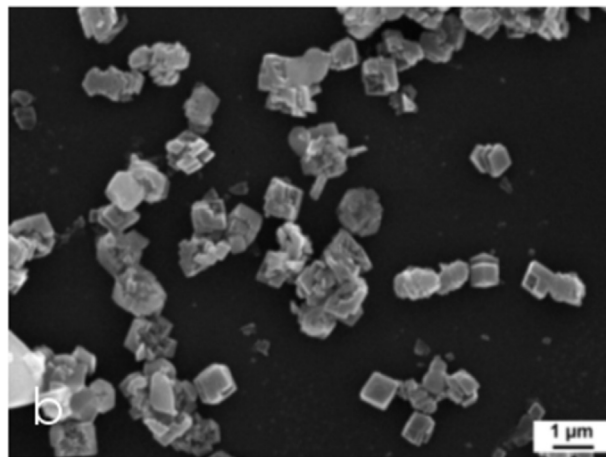
**FIGURE 9.2**

Schematic illustration of growth processes of HA microstructures (Mary et al., 2016).

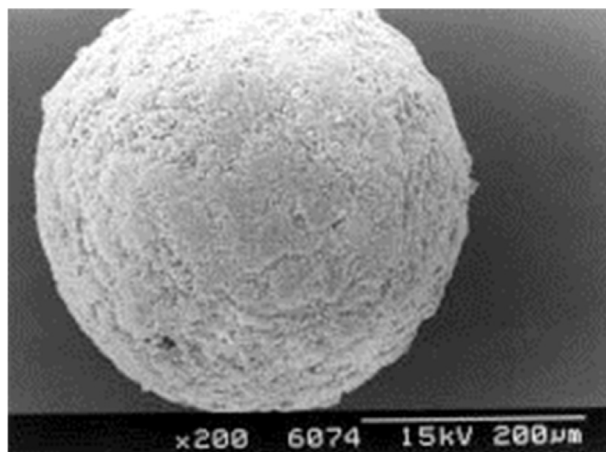
biological apatite in the calcified tissues has a nanometric dimension (Weiner and Wagner, 1998), HA with nanometric shape is often chosen as the optimal filler for composite pastes in dental research due to the chemical and phase affinity with dental enamel (Al-Sanabani et al., 2013). HA synthesis is reported in a great many literature references. The common morphology of particles is characterized by spheroidal cubic or microrod shape. The crystals do not present a preferential growth direction. In Fig. 9.3 an image of cubic shaped HA particles is shown.

The particles are usually in nanosize dimension to have a large surface area and increase the surface interaction for a good adhesion with resin matrix or for a future functionalization. With this purpose a possible improvement can be obtained by using HA particles with a porous spheroidal shape (Sopyan et al., 2007), usually high performing for applications in drug delivery functionality (Paul and Sharma, 1999; Komlev et al., 2002). Fig. 9.4 shows a micrograph of a HA porous sphere.

Nanodimensional and nanocrystalline forms of HA are able to reproduce both composition and dimensions of constituents of the calcified tissues. Thus, these fillers, thanks also their excellent biocompatibility, could be used efficiently as

**FIGURE 9.3**

SEM image of cubic HA crystals (Bogdanoviciene et al., 2010).

**FIGURE 9.4**

SEM image of a HA porous sphere (Paul and Sharma, 1999).

biomaterials in dental applications (Cai and Tang, 2008; Ginebra et al., 2004). Furthermore microsize HA can be also investigated, thanks to its better stability in water compared with nanosize HA. Further development of calcium orthophosphate-based biomaterials obviously will stand to benefit mostly from nanotechnology (Calabrese et al., 2015), which offers unique approaches to overcome shortcomings of many conventional materials (Dorozhkin, 2012).



### 9.3.1.2 Whiskers

HA particles can be considered whiskers if, despite the spheroidal shape, the crystal growth occurs in a preferential direction, obtaining a rod-like structure with a high aspect ratio (length/diameter). In particular whiskers can be considered high strength thread-like dislocation free crystals with the diameter of 1–10  $\mu\text{m}$  and the length to diameter ratio  $5 < l/d < 1000$  (Knyazev et al., 2012). The driving force of this type of filler is that HA whisker (coded usually HW or wHA) had a similar structure to enamel rods (Popowics et al., 2004), which would make it a promising filler to stimulate biocompatibility and reinforcing effects on bioceramics dental resin composite. Therefore, research activities focused on HA whiskers synthesis and/or application have received much attention in the last several years.

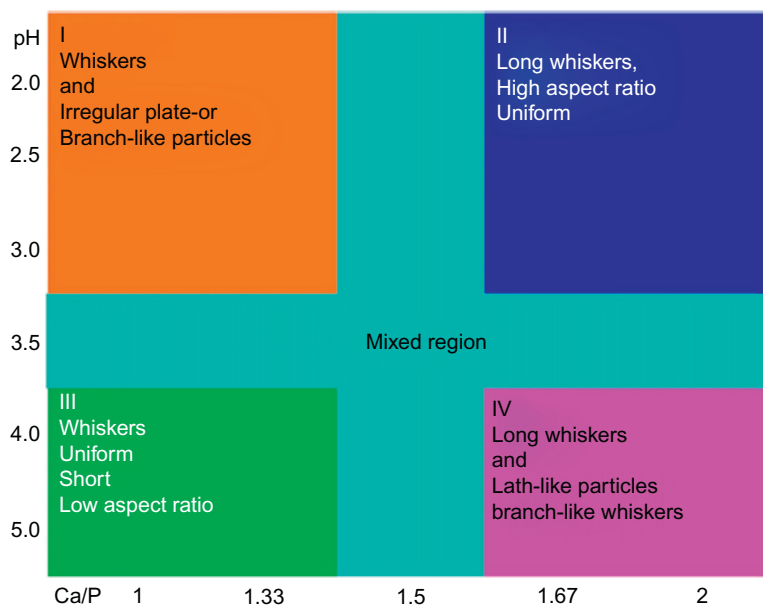
The first fibers or needle-shaped HA crystals were investigated around 1990 (Mortier et al., 1989; Nonami et al., 1989). However, the HWs have a relatively low crystallinity and a nonuniform shape. Then Yoshimura et al. succeeded in obtaining fine HA whiskers with high crystallinity and with homogeneous rod shapes by a hydrothermal method (Yoshimura and Suda, 1994; Yoshimura et al., 1994). Afterwards several articles proposed new synthesis improvements or approaches in HW production.

The preparation of well-defined HA crystals with specific shape controlled morphology was the aim of several recent research investigations (Neira et al., 2009). Nowadays several synthesis techniques to obtain HA whiskers can be identified such as hydrolysis of calcium phosphate precursors (Tas, 2007), chelate decomposition (Roeder et al., 2006), and homogeneous or hydrothermal homogeneous precipitation (Zhang et al., 2003; Zhang and Darvell, 2010). The latter method is usually used due to its efficient reaction rate. At the same time HW with homogenous morphology and high length/diameter aspect ratio can be obtained (Zhang and Darvell, 2011; Neira et al., 2008). This technique is based on the hydrolysis of an organic additive, which is commonly an amide used to control the solution pH and to modify the crystal growth.

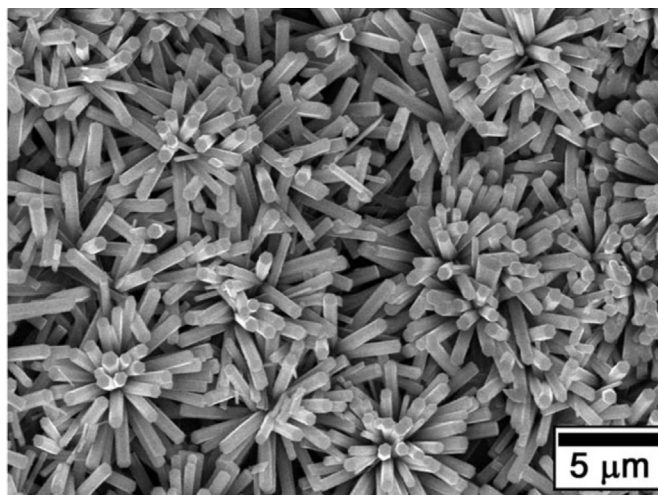
Neira et al. (2008) showed that gradual and greater increase of solution pH in the hydrothermal synthesis increases the crystallinity of wHA obtaining well-defined hexagonal single crystal morphology. Analogously in Zhang and Darvell (2011) the effects of several solution parameters were investigated, such as Ca concentration, Ca/P ratio, and pH. They showed that a transition from whiskers to plate-like structure could occur if an incorrect ratio of constituents is chosen during the synthesis procedure. A visual summary of dependence of whisker aspect ratio and morphology with pH and Ca/P content is reported in Fig. 9.5.

Analogously Neira et al. (2009) showed that particle morphology of the HA crystals can be controlled by urea and the Ca/P constituents concentration in the hydrothermal process.

Fig. 9.6 shows a SEM image of HA whiskers for a reference formulation. The particles reveal a clear elongated micrometer-sized morphology with a faceted

**FIGURE 9.5**

Morphology distribution of HA prepared using various pHs and iCa/Ps based on  $i[\text{Ca}] = 42 \text{ mmol/L}$  (Zhang and Darvell, 2011).

**FIGURE 9.6**

Whiskers morphology obtained with  $0.167 \text{ M Ca}^{2+}$ ,  $0.10 \text{ M PO}_4^{3-}$ ,  $0.50 \text{ M urea}$  in Neira et al. (2009).



hexagonal prism-like morphology, with a quite uniform size distribution. The whisker crystals are characterized by width of about 1.0–2.0  $\mu\text{m}$  and a length of about 5–10  $\mu\text{m}$ .

Confirming the relevant importance of this research aspect, recently [Mohammadi et al. \(2016\)](#) and [Goto and Sekino \(2016\)](#) proposed works to better understand it, proposing an optimal concentration of urea additive required for obtaining short fibers with whisker morphology and how urea concentration influences the HA morphology in the hydrothermal synthesis.

### 9.3.1.3 Fibers

In comparison with HA fillers characterized by low length/diameter aspect ratio fibers, HA filler is a preferred solution to reinforce the dental resin materials. Fibers are characterized by aspect ratio usually in the range of 200 and thus could provide much higher load transfer at the filler/matrix interphase, also improving toughness of the dental composite. They can also make composites with improved toughness. For this reason several research activities are focused on synthesis and incorporation of HA micro- and nanofibers for biomedical composite applications.

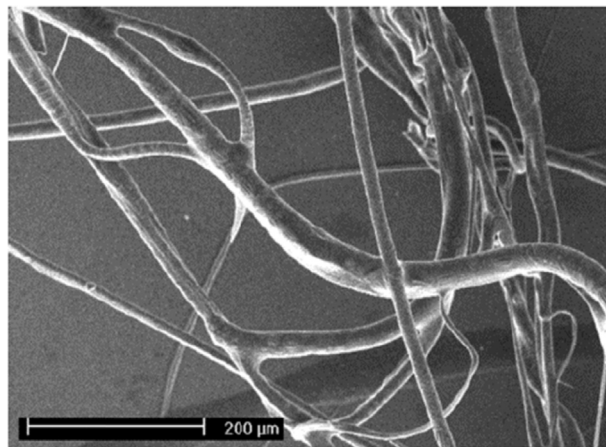
Recently, HA fibers were chosen as dental fillers with the purpose to develop new functional dental composite resins with enhanced mechanical and durability performance. In this regard, promising results can be observed in the literature ([Chen et al., 2011b, 2012](#); [Kasuga et al., 2000](#)).

Several synthesis techniques to obtain HA fibers were proposed in the literature. At first HA fibers were prepared by homogeneous precipitation method ([Kandori et al., 2005](#)), sol–gel growth method ([Kamiya et al., 1989](#); [Tanahashi et al., 1992](#)), and hydrothermal method ([Ito et al., 1996](#)). However, significant improvements were obtained by using electrospinning procedure for HA fibers synthesis ([Ramanan and Venkatesh, 2004](#); [Wu and Hench, 2004](#)). In particular [Wu and Hench \(2004\)](#) proposed an electrospinning approach to obtain HA fibers. The approach was to electrospin a polymeric slurry HA base with a polymer matrix. After the complete removal of the polymer by calcination, the surface of the HA fibers was rough and homogeneous. The pure HA fibers obtained by electrospinning are characterized by a very high length/diameter aspect. The morphology obtained in [Wu and Hench \(2004\)](#) is a length up to 10 mm and diameter about 10–30  $\mu\text{m}$ . The diameter of the HA grain size was about 1  $\mu\text{m}$  in the HA fibers. A SEM magnification of obtained HA fibers is reported in [Fig. 9.7](#).

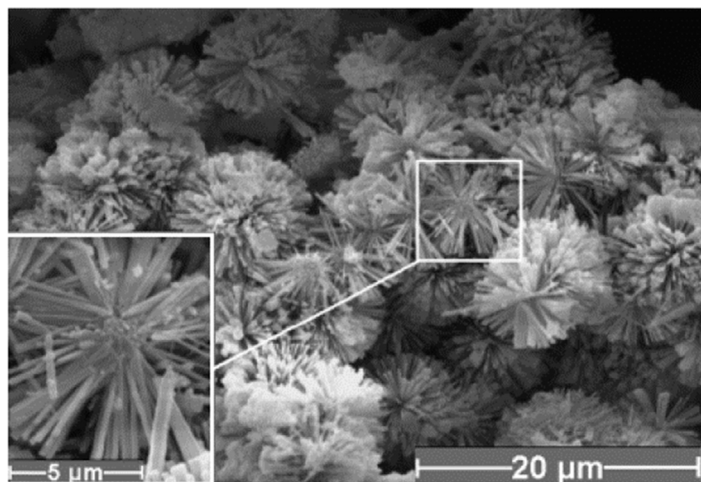
A valid alternative to electrospinning technique is the hydrothermal microwave-assisted method to significantly reduce the manufacturing times. Recently [Mendez-Lozano et al. \(2017\)](#) obtained HA nanofibers with diameters in the order of 450 nm and lengths of about 70  $\mu\text{m}$ , proposing a reaction time in the range 15–45 minutes by microwave source.

### 9.3.1.4 Urchin-like

Bioinspired by the retention capacity of sea urchin spines, a new dental resin composite can be obtained by incorporating in the resin matrix HA crystals

**FIGURE 9.7**

SEM image of HA fibers (Wu and Hench, 2004).

**FIGURE 9.8**

SEM image of SEM image showing urchin-like HA nanostructure (Lak et al., 2008).

having a morphology similar to the urchin (UHA). UHA is a bioceramic filler with a hierarchical structure with a globular appearance. Its morphology is constituted by rods extending radially from the center, like an urchin (Fig. 9.8).

The structure in the literature is also called a dandelion-like (Lak et al., 2008) or flower-like HA (Liu et al., 2004) nanostructure. Usually, this particular hierarchical structure is obtained using hydrothermal synthesis technique (Lak et al., 2008;

Liu et al., 2004; Yang et al., 2011). Changing preparation parameters (synthesis compounds, time, temperature, pH, etc.) makes it possible to control shape and dimension of the UHA nanostructure.

Yang et al. (2011) showed that by increasing aging time, a well interconnected, structured, and very compact urchin can be obtained. Based on their experimental research they indicated that at first growth center of assembly urchins takes place, and afterward the nanowhiskers continue to assemble and grow around the cores, forming the characteristic large and compact sphere structure.

At first, during the synthesis, a three-dimensional cluster of critical size is formed, which is able to act as nuclei for HA crystals germination and develop into a crystallite (Liu et al., 2004). In the second step all the nanorods are grown individually from a central spherical nucleus and no considerable aggregation occurs (Lak et al., 2008). The nanorods are grown from the core of the nanostructure and are densely aligned perpendicular to the surface of the core.

Liu et al. (2004) showed that the urchin-like structure can be obtained easily at alkaline solution. In hydrothermal synthesis with pH in the range  $7 < \text{pH} < 12$  an incomplete radial structure is obtained. Only some preferential radial direction of growth can be identified and a bowknot-like HA nanostructure is obtained (Fig. 9.9).

Thanks to its peculiar structure, which combines both globular and whisker facilities, UHA can be easily dispersed in the resin matrix compared with the conventional fiber-like HA. Furthermore, the radial ordered rods of UHA could increase the interlocking force between matrix and fillers facilitating strengthening of the composite resin. Thus, UHA could, therefore, increase significantly the mechanical performances of dental composite resin (Liu et al., 2014).

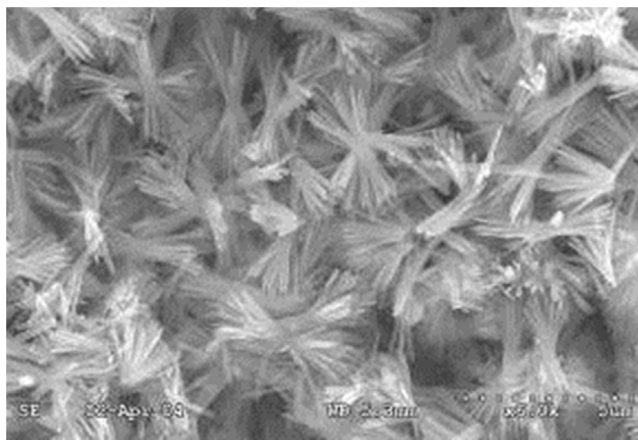


**FIGURE 9.9**

SEM image of SEM image showing bowknot-like HA nanostructure (Liu et al., 2004).

### 9.3.2 CHEMICOPHYSICAL PROPERTIES OF HA-BASED COMPOSITE

In the composite restorative field, an important issue is the definition of new specific techniques that can determine properties and functionalities of the dental composite resin to clarify the impact of HA filler addition on the biomaterial performances. In this regard, some chemicophysical properties are discussed, investigating also the common analytical techniques applied to help characterize dental composite materials.

### 9.3.3 DEGREE OF CONVERSION

The final success of dental restorations depends on many factors, such as the technique or the material used, but one of the most important is represented by the optimal curing degree of a visible light cross-linkable dental composite resin (Flury et al., 2012).

The most recent and widespread light curing is represented by light-emitting diode (LED) curing units that generate a light with a wavelength spectrum distribution between 400 and 500 nm. The wavelength peak of this light unit is at 460 nm, which also represents the absorption range of camphorquinone (Wiggins et al., 2004). As the lights had a higher irradiation in the region of the peak absorption of CQ, it was expected that these lights would be more effective than previously utilized quartz halogen tungsten lights and thus would be able to provide a greater depth of cure (Mills et al., 1999). Different direct and indirect techniques are available to assess the degree of conversion. For example, the use of Vickers and Knoop hardness tests are considered an indirect and accurate parameter that can be related with the level of curing of resin composites and thus the degree of conversion (Halvorson et al., 2003; Ferracane, 1985; Leprince et al., 2012). Furthermore the hardness is usually related to physical properties of resin composites such as mechanical strength, stiffness, and intraoral softening resistance (Uhl et al., 2003; Bonaccorsi et al., 2012).

According to ISO 4049, the scraping technique allows to experimentally determine the depth of cure and therefore the curing degree (or conversion degree) of the dental resins. The composite paste is filled into a cylindrical mold with thin glass slides covering both sides and cured using LED curing unit for 20 seconds. After removing uncured parts with ethanol the curing depth can be measured by simple micrometer. A procedure usually used to define depth of cure is based on top and bottom hardness measurements. In this procedure the approach is based on calculating the ratio of bottom/top hardness and giving an arbitrary minimum value for this ratio to identify an effective curing degree of the bottom surface. Values ranging from 0.80 to 0.85 have often been used (Flury et al., 2012). Specimens are considered to be adequately cured when the B/T ratio exceeds 80%. Furthermore, a B/T ratio of 80% corresponds to 90% of the maximum conversion possible at the top surface of a composite (Bouschlicher et al., 2004). Anyway, considering that a high degree of cure can be obtained on the surface of

restorations, even if a low intensity curing light is used for a short exposure time (Rueggeberg et al., 1993), therefore, this method usually overestimates the depth of cure compared with its calculation by Vickers hardness measurements along the sample cross-section.

Moreover, two other spectroscopic techniques are used to directly measure the polymerization efficiency, namely Fourier transform infrared spectroscopy (FTIR) and Raman spectroscopy.

FTIR detects the vibrations of chemical links; in fact, the material will absorb the infrared radiation generated. Consequently, the spectrometer identifies the infrared radiation on the tested sample and measures the wavelengths and the intensity absorbed on the composite. A spectrum is generated through a mathematical technique called Fourier transform. The absorption intensity at a well-defined wavelength identifies the presence of a specific chemical group responsible for the absorption (Ferracane and Greener, 1984). Concerning resin-based composite, the spectrum analyzed is related to the height peak at about 1637 per cm, which represents the stretching vibration of the double carbon bonds on the methacrylate groups before and after the cross-linking step. Moreover, aromatic carbon bonds with a characteristic peak at about 1608 per cm are recorded before and after polymerization. The degree of conversion for methacrylates-based composites is equal to:

$$DC(\%) = 1 - \frac{(A_{1637}/A_{1608})_{\text{polymer}}}{(A_{1637}/A_{1608})_{\text{monomer}}} \times 100$$

Therefore in the above equation the absorbance values both of aliphatic and aromatic carbon bonds of the cured polymer are divided for the absorbance values of the unpolymerized monomer (Liu et al., 2013a).

Raman spectroscopy also generates a spectrum of peaks by diffusion of the light through the polymeric matrix. The depth of cure, in addition, is mapped by microtechnique, which analyzes the wavelength at different points in the surface sample at high magnification (Pianelli et al., 1999).

Different parameters should be taken into account when considering the degree of conversion, such as the light typology, the distance of the tip from the specimen, the time, the thickness, and the composite formulation. This last can be varied mainly by changing the filler content or typology or its morphology other than its surface treatment. Liu et al. introduced a functional interfacial layer on the wHA surface based on poly(Bis-GMA) to enhance the interaction between matrix and filler surface area (Liu et al., 2013a). wHA with different graft ratio of poly (Bis-GMA) showed better incorporation mechanism in the resin matrix thanks to the similar molecular structure of the graft agent. Moreover, this innovative formulation permitted to obtain a lower volume shrinkage due to formation of a wide range of covalent and hydrogen bonds permitting the relaxation of internal stresses other than a better distribution. However, when compared with the simple wHA composite, the degree of conversion dropped significantly mainly because the activation of the photoinitiator system during light propagation was

shielded by the higher refractive index resulting from the sum of that of grafted poly(Bis-GMA) lamina to that of wHA.

Also Zhang et al. evaluated the successful incorporation and interaction both of wHA and nanoparticles (nHA) with the resin-based matrix. Assessing a significant increase of microhardness other than mechanical properties with (log) filler loading for both nHA and wHA, in particular for wHA, the values obtained were highly significant (Zhang and Darvell, 2012b).

However, it should be considered that usually the standard protocols used to analyze Vickers hardness (HV) provide specimens with a thickness of 2 mm, which can affect the degree of conversion and thus the final microhardness behavior (Domingo et al., 2001; Lezaja et al., 2013; Arcís et al., 2002).

In fact, favorable results have been obtained utilizing a 1-mm build-up technique in microhybrid resin composites, which permits a more homogeneous cross-linking layer in comparison with a thicker one, especially in this case where the presence of a radio-opaque filler such as HA can shield the light propagation. Additionally, a postcuring step of the superficial layer can minimize the mechanical discrepancies among the laminae in an incremental technique as the one suggested and thus provide a more homogeneous hardness distribution along the section. Indeed, microhardness differences between layers of the composite restorations can increase interlaminar stresses under masticatory conditions, leading to possible fracture of the bulk of restoration (Fabiano et al., 2014; David et al., 2007).

As previously described, the filler content can influence the mechanical and physicochemical properties, such as the degree of conversion of HA-based composites.

In this regard, Fig. 9.10 reports the changing in hardness (HV) distribution at varying HA nanoparticles' mass fractions in a conventional resin composite

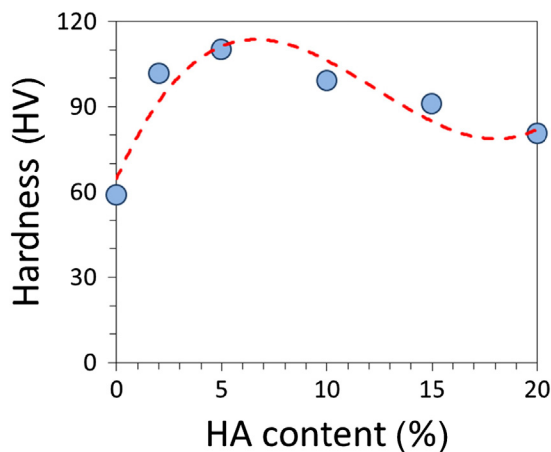


FIGURE 9.10

Vickers hardness resin composites at increasing HA content.

formulation, partially substituting the silica-based filler. Respectively, HA-5, HA10, HA-15, and HA-20 were tested. As reference the composite resin, not modified with HA filler, HA-0, is also reported.

The HA-0 sample shows a quite homogeneous distribution of hardness with values compatible with literature results for Kerr Herculite XRV samples (Jafarzadeh et al., 2015).

HA-based composites possess higher microhardness values in comparison to the control at 0% of HA. In fact, it can be observed a significant increase of HV from HA-0% to HA-5%.

Furthermore, the HV of HA-20% was lower, about 25%, than the HA-5% samples. The reason could be that with the increasing of HA mass fraction the shielding effect of the HA fillers becomes more prominent, reducing the degree of conversion of the matrix, consequently increasing the availability of uncured monomers and initiator, which causes a lowering in the mechanical properties (Leitune et al., 2013). This could have adverse effects on the stress distribution under loading conditions.

These results indicate the effective action of HA filler on the hardening of composite paste, in accordance with the considerations previously discussed. However a shielding effect of HA filler could be also identified. This phenomenon becomes important only at high HA filler contents, resulting in a slight stiffness reduction that can be related with a nonhomogeneous distribution of hardness along the thickness.

The degree of conversion has a substantial effect on final mechanical properties. In fact, during the curing, dental resin composites evolve from plastic viscous to a rubbery viscoelastic behavior up to a final elastic brittle stage. During this last stage, related to material vitrification, a large amount of shrinkage stress is generated due to residual stresses within incomplete polymerization areas, especially under overlapping irradiations. In fact, to compensate for the polymerization of the central region of the  $25 \times 2 \times 2$  rectangular specimen, the associated post-gel shrinkage stresses were accommodated by local deformation of partially irradiated contiguous zones. As the contiguous zones of the sample were irradiated, the curing shrinkage occurs, inducing on the overlapped zones interlaminar tensile stresses in the resin composite (Palin et al., 2005).

After the gelation, steric hindrance becomes relevant and the material acquires measurable elastic properties. In particular, the elastic modulus increases with increasing conversion degree of the resin up to its maximum value at the vitrification stage (Krämer et al., 2008). If the bottom layers of composite restoration resins are not suitably cured, its elastic modulus will be lower than that on the surface, thus increasing the material stress and strain under masticatory forces.

### 9.3.4 SHRINKAGE

The swelling effect as well as the durability in aggressive medium of the composite is dependent on the degree of cross-linking (Tamareselv and Rueggeberg, 1994;



Asmussen and Peutzfeldt, 2001; Benetti et al., 2009). This important parameter is indirectly assessed by the presence of a high glass transition temperature, which means the reduced diffusion and enhanced viscosity of the network. The glass transition temperature,  $T_g$ , can be measured by dynamic mechanical analysis and differential scanning calorimetry analysis. This last represents the demarcation line between gel and glassy phase, and it is around 47.5°C; above this threshold the polymer will return to the gel stage (Asmussen and Peutzfeldt, 2003a; Dewaele et al., 2009). Another indirect test foresees the immersion in a solvent (e.g., ethanol) and the variation detection of surface hardness rates before and after the softening process (Asmussen and Peutzfeldt, 2001, 2003b).

Cross-linking process in resin dental composites is based on a free-radical mechanism, which leads, during the light-curing activation, to dimensional shrinkage mainly in the polymeric matrix (Silikas et al., 2000). During the polymerization the van der Waals bonds in the monomer mixture are substituted by covalent bonds decreasing the distance of the molecule from 4 to 1.5 Å causing the volumetric shrinkage of the network, usually around 1% up to 6% (Loshaek and Fox, 1953; Tobolsky et al., 1948; Weinmann et al., 2005; Kleverlaan and Feilzer, 2005). This phase corresponds at the same time at the increase in elastic modulus and stiffness of the composite; if the material is inside a free-bonding container (structure), the stress relaxation can occur with enough time. This condition is not clinically applicable, in fact generally the composite is bonded by physicochemical methods to dental tissue thus reducing the plastic deformation of the material and maintaining high stress levels. For these reasons, the induced material deformation develops tensile stresses mainly distributed in the interface area between restoration and natural dental tissue (bonding area).

These internal stresses could compromise the effectiveness of the final restoration, weakening the marginal seal of the bonded restorations. The main side effects of restoration failure are discoloration, secondary caries infiltration, dentinal hypersensitivity, or fracture and crack propagation of the cavity walls with consequent cusp displacement (Causton et al., 1985; McCulloch and Smith, 1986; Meredith and Setchell, n.d.; Pearson and Hegarty, 1987). Microtomography is a recent tool available to analyze the correlation between shrinkage and gap formation of resin composites (Kakaboura et al., 2007). Another method to assess the volume shrinkage of the resin composites is the detection of the density before ( $\rho_{\text{monomer}}$ ) and after ( $\rho_{\text{polymer}}$ ) the cross-linking (Liu et al., 2013a). The equation used is equal to:

$$\Delta V\% = 100 \times \left( 1 - \frac{\rho_{\text{polymer}}}{\rho_{\text{monomer}}} \right)$$

Several attempts have been pursued to decrease the polymerization shrinkage, such as formulations changes or in photoinitiation system. This last, in fact, is strictly correlated with light-curing typologies and setup. The diversification in the formulation has concerned mainly the inorganic phase and its technology, but also the organic matrix was renewed with the introduction on the market of



products such as siloranes and ormocers (Schneider et al., 2010; Feilzer et al., 1995). Concerning the filler phase, Oduncu reported that the volume shrinkage decreases with the increase of HA filler content. In particular, by comparing HA/alumina and HA/zirconia composites the polymerization shrinkage ranged from 3.80% up to 6.04% (v/v). The lowest value was detected for the 70% (w/w) of HA/alumina; the main reason can be ascribed to lower density of alumina filler than the zirconia one.

Experimental results obtained by Liu et al. (2013b) concerning the polymerization shrinkage evolution of a resin composite at different ratios of HA/SiO<sub>2</sub> filler evidenced as the addition of nano-HAP particles decreased the shrinkage from about 3.25% to about 2.0%. The decrease of polymerization shrinkage mainly resulted from higher refractive index of HA, which influences the cross-linking process; since lower degree of conversion is reached with the increasing of mass ratio as a consequence the shrinkage decreases.

Similarly, Al-maamori et al. (2014) explained the linear shrinkage decrease at increasing content of micro-HA in a light-curing matrix considering that the higher inorganic content is associated with lower polymerization values, which are in direct relation with reduction of shrinkage and considering furthermore that the HA particles can act as obstacles to resin polymerization.

Considering the high free energy of HA nanoparticles filler it can be suggested that its use will permit a higher loading ratio and thus a lower volume shrinkage in the dental composite (Oduncu et al., 2010).

### 9.3.5 OPTICAL PROPERTIES

The optical properties are related to the specific composition of resin-based composite in terms of matrix but also of filler phases. Many factors influence the quality and the depth of cure, such as the thickness, the shade, and the molar absorptivity (Chen et al., 2007; Shortall, 2005; Leprince et al., 2011). Considering that the commercial formulation of matrix is pretty much consolidated, what can make the difference in light transmission is represented by the quantity, typology, and dimensions of filler. The light scattering can increase when the filler size is equal to half of the wavelength transmitted with consequent reduction of hardness and depth of cure; of course this last is not significant when the size of particles possess a dimension value far away from the wavelength of the cure light and therefore the light is directly transmitted as in the case of nanocomposites (Emami et al., 2005; dos Santos et al., 2008). Another important parameter is also represented by the refractive index of the filler utilized, in fact, where the gap between the index of matrix and that of the filler is higher, a lower polymerization occurs in the resin–filler interface (Howard et al., 2010). In commercial composite, generally this gap is lower considering that silica has a refractive index of 1.46, which is similar to that of Bis-GMA/TEGDMA mixture. On the other hand, the main drawback found in the use of HA filler is its higher refractive index in comparison to that of the polymeric matrix. In particular, the

refractive index of HA is 1.65, whereas that of conventional matrix is 1.5 (Habib et al., 2016). This optical characteristic can explain why it is possible to observe an increase in mechanical and physicochemical properties with addition of HA at low ratios, while at higher ratio the value patterns significantly decrease. In fact, in our previous study, a threshold of 20% of HA content and an optimal composite behavior at 5% of HA can be identified, where the refractive index of the filler does not affect the degree of conversion and thus the final performance. The organic phase composition represents, in addition, an important aspect. If photons are not absorbed by the right amount of photoinitiators or pigments or other compounds, they will be converted into heat, which can provide harmful effects on pulp tissue (Leprince et al., 2010b).

### 9.3.6 SORPTION/SOLUBILITY IN WATER

The water uptake and elution onto the polymeric network can affect the durability and stability of the resin composite, generating, for example, the hydrolysis of the coupling agent (silane) and by forming defect areas such as crack or filler–matrix debonding. In addition, it is generally reported as a diffusion-controlled process. By analyzing different composite formulations no differences in diffusion coefficients were found, leading to the conclusion that the principal pathway of water absorption is through the matrix, and in second instance by matrix–filler interface. However, this behavior is strictly related to other important parameters that can indirectly affect the cross-linking and thus cause an increase in water cluster absorption and formation, for example, degree of conversion and filler content.

Generally, the water uptake and the elution of the samples stored in water are obtained according the following equations:

$$\text{Water uptake(w/w)} = \frac{m_w - m_d}{m_0} \times 100$$

$$\text{Elution in water(w/w)} = \frac{m_0 - m_d}{m_0} \times 100$$

where  $m_0$  is the initial weight of the sample,  $m_w$  is the weight after reaching a constant pattern, and  $m_d$  is the weight after the dry step.

Several studies highlighted that the addition of HA reduces water uptake as well as elution primarily in the morphology of whiskers instead of nanosized particles. For example, the addition of silanized HA in dental cement demonstrated a low rate of water uptake; this assumption was also confirmed by Santos et al. (2002), who conducted an experimental campaign on silanized and unsilanized HA-based composite demonstrating the beneficial effect of filler surface treatment and the lower water equilibrium uptake, around 1.60%.

Analyzing Fig. 9.11, the water sorption of resin decreases with an increase in filler loading and HA silanization although the latter has no significant effect on the filler content. Very low content of nonfunctionalized HA filler (group B) does not have beneficial effect on water sorption.

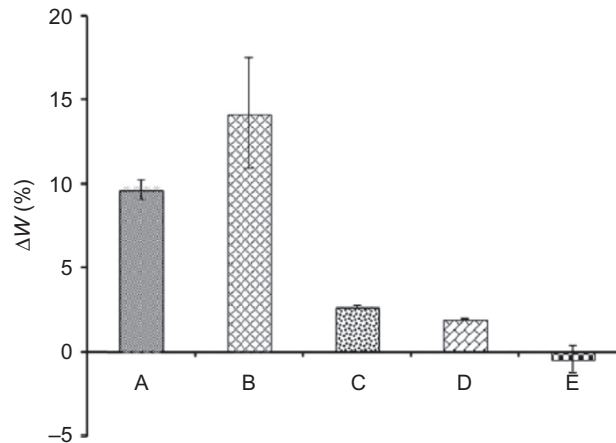


**FIGURE 9.11**

The weight % change of water adsorption for six test groups samples. Group A resin only; Group B resin + 10% nonsilanized HAP fillers; Group C resin + 30% nonsilanized HAP fillers; Group D resin + 10% silanized HAP fillers, Group E resin + 30% silanized HAP fillers (Lung et al., 2016).

Furthermore, some studies showed that the diffusion coefficients are not strictly related to HA mass fraction in the composite, while the equilibrium uptake decreased at increasing filler content (Domingo et al., 2001; Santos et al., 2002; Deb et al., 1995).

Anyway, it should be taken into account that differences between the water behavior can arise by the radio-opaque HA filler, which can lower the degree of conversion of the polymeric matrix.

A critical problem reported by Zhang and Darvell (2012b) for nanohydroxyapatite is the tendency to form inclusions, microvoids, and aggregates; these defects are not wet by the polymer and are not well dispersed, causing water infiltration. The same behavior was also found by Domingo et al. (2001), where the resulting data assessed that the water uptake and elution rates were increased in nanohydroxyapatite-based composite compared with microhydroxyapatite.

Indeed, composite materials do not follow the classic Fickian diffusion theory (Ritger and Peppas, 1987). After suspension in solution, in fact, water is absorbed by the methacrylates-based lattice and thus diffuses in the defects associated with nanofiller. The swelling phenomenon triggers the elution of unreacted compounds as well as HA filler. After this stage, intrinsic structural changes can be generated as well as pH solution increased. On the other hand, whisker morphology results in an optimal bonding interaction between filler and matrix, reducing water uptake and elution and demonstrating high stability and durability during aging. On the basis of the data analyzed, the use of nano-HA loading resin composite

should be avoided because of the high solubility in water, which limits their use in clinical conditions.

### 9.3.7 MECHANICAL PROPERTIES OF HA-BASED RESIN COMPOSITE FOR RESTORATIVE DENTISTRY

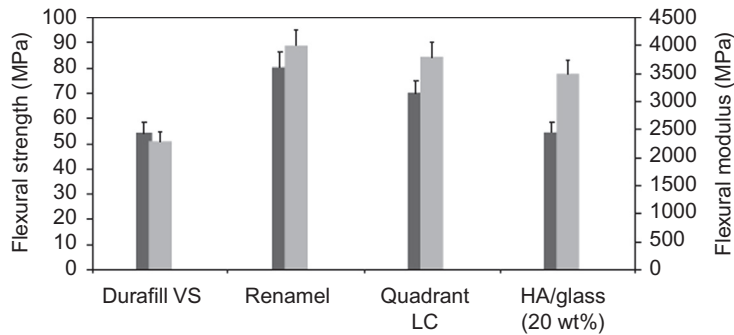
HA spheroidal particulate was investigated as dental filler in resin composite for dentistry applications. The size of HA particles had a significant effect on the mechanical properties of composites (Habib et al., 2016). The performance of resin composite with only HA particles as filler was studied to obtain a product with a high biocompatibility and bioactivity. Arcís et al. (2002) tried to increase knowledge in the use of HA as reinforcing filler in composite materials for dental restoration applications by analyzing their mechanical performance improvement, performing flexural and microhardness tests. The results showed that an increase of stiffness and hardness can be obtained by adding HA filler (in the range 40–60 wt %); a reduction of strength was also observed. Furthermore they also showed that diffusion of water through their HA composite resins affects the mechanical properties due to hygroscopic behavior of their nanoscopic HA filler. Consequently they confirmed that these materials in this form are not adequate for dental restoration due to deleterious degradation in wet conditions. In this regard, the use of an effective coupling agent could have beneficial effect on the composite formulation facilitating the self-adhesion to the mineral phase of dental tissue (Morra, 1993) stimulating also the interaction of resin matrix with HA filler.

Domingo et al. (2001) reported an extensive experimental campaign on 12 resin composite batches by using four different coupling agents. In their work, the hydrolytic stability of the composites was analyzed through their elution in water and water-uptake characteristics. For some of their studied dental composites, the values of the mechanical properties are closed to those of commercial materials. Their samples, characterized by 60 wt% of HA filler, evidenced modulus in the range 7–8 GPa. Most of the commercial dental composites are reinforced with up to 80–90 wt% of inorganic fillers (Lygre et al., 1999), evidencing elastic modulus ranging from 5 to 25 GPa (Willems et al., 1992). Furthermore the use of coupling agent (citrate, acrylate, methacrylate) on micro-HA particles induced relatively low elution-in-water and water uptake (2–3 wt% maximum), making these results clinically acceptable for restorative dentistry application.

From Calabrese et al. (2016), in Fig. 9.12 the comparison between three commercial dental restorative materials and a 20% HA/silica samples is reported.

The elastic modulus of HA filled composite is quite similar to commercial ones. Concerning strength performances, Renamel composite showed higher flexural strength (about 80 MPa) compared with the other ones. 20%HA/silica and Durafill VS samples showed the lowest one with a flexural strength with a mean value of about 55 MPa.

Similarly other research articles have shown the promising effect of addition of functionalized, usually silanized, HA particles in composite resins (Lung et al., 2016;

**FIGURE 9.12**

Flexural strength (dark gray) and elastic modulus (light gray) of four resin-based composites (Calabrese et al., 2016).

Pan et al., 2013); however the improvement of mechanical performance and reduction of water uptake are still needed.

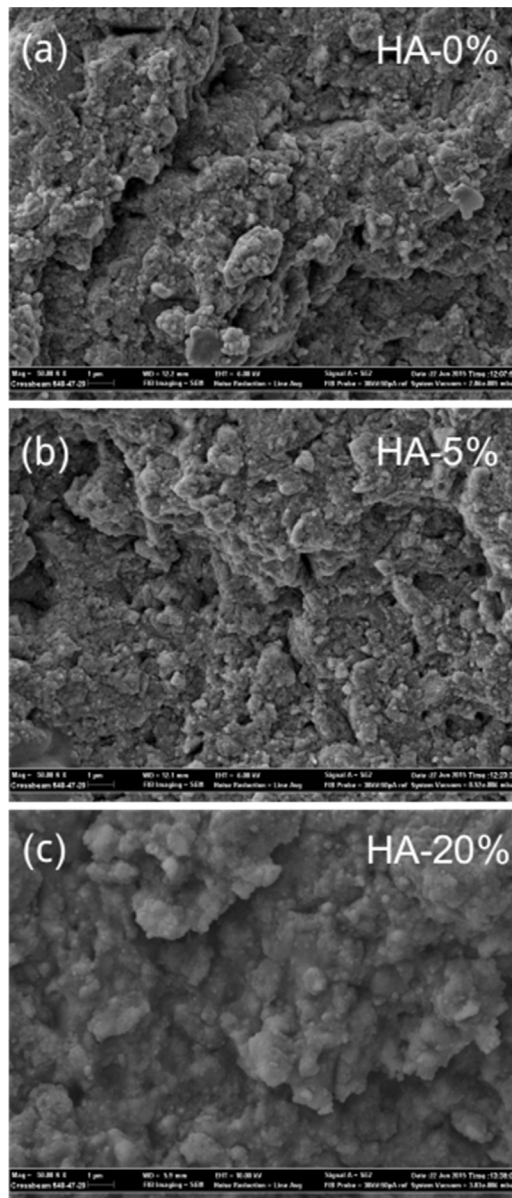
The percentage of silanized HA filler usually has a relevant effect on modulus, which increases progressively at increasing of HA content. However, usually the addition of HA filler does not induce significant effect on strength performance, although in some cases a decrease can be observed when the volume fraction of the filler exceeds a threshold value (Santos et al., 2001).

Conversely, Liu et al. (2013b) showed, in mixed silanized HAP/SiO<sub>2</sub> filler in Bis-GMA/TEGDMA resin, that the mechanical properties (e.g., elastic modulus and flexural and compressive strength) gradually decreased increasing the HAP filler content. In particular, dental composite reinforced with lower amount of silanized HA filler (HAP/SiO<sub>2</sub> around 0.25) was considered suitable for dental applications.

Fig. 9.13 shows SEM images of the fracture surface of three reference silica-based composite resins differing in HA amount. This analysis allows us to evaluate the morphology of the dental composites and to relate it to their mechanical behavior.

The morphology of composite with 5%wt of HA filler sample (HA-5%) is quite similar to the control (HA-0%), confirming the optimal mechanical affinity of resin/filler interaction at low amount in HA particles replaces the silica filler. Different consideration can be drawn for the specimens with higher content of HA. HA-20 sample has a porous surface characterized by some voids and cracks. This morphology indicates a poor adhesion between the filler and the polymer matrix. Due to the large volume content of filler in the composite material, the resin is not enough to wet the fillers and microdomains consisting of resin particles coated ceramic filler are created, increasing the risks of generations of defects (voids, air bubbles, debonding, etc.).

Filler reinforcing efficiency is strictly related to the resin/filler interfacial adhesion. At high HA content, an insufficient interaction between filler and matrix can

**FIGURE 9.13**

SEM images of HA/silica-based dental composite at different HA wt%. (a) Unfilled (b) 5% HA (c) 20% HA composite resins.

be obtained. This could generate areas with not wetted HA filler limiting also the HA filler packing, as confirmed by the presence of defected areas in HA-20 sample, despite an almost homogeneous surface in HA-0 and HA-5 samples.

A possible approach to enhance mechanical performances of HA-based composite resin is to use higher aspect ratio filler than conventional spheroidal HA one. Recently, great attention has been reported on the development and synthesis of apatite fillers at varying size, ratio, shape, and morphology to optimize its reinforcing action on composite materials. In this regard, other shapes of HA such as whiskers and nanofibers were of interest for composite resin development.

Addition of HA nanofibers (about 3 wt% pf HA on 57 wt% of glass filled composite) increased about 30% flexural strength of dental composites resin with 60% silica microparticle filler (Chen et al., 2011b). Analogously HA whiskers had increased flexural modulus, fracture toughness, and HV of unfilled resins (Zhang and Darvell, 2012a). It was evidenced that HA particles with high aspect ratio can act as effective reinforcing filler.

A couple of possible mechanisms of stress transfer between matrix and high aspect ratio HA filler were proposed in Calabrese et al. (2016). A first mechanism, called adhesive links, is related with the adhesive performance of resin with the particulate. The HA whiskers could act as stress bridges between two neighboring resin domains. The second one, the mechanical link, could be mainly due to friction between the randomly oriented HA whiskers that are in contact in the composite bulk. A graphical schematization is shown in Fig. 9.14.

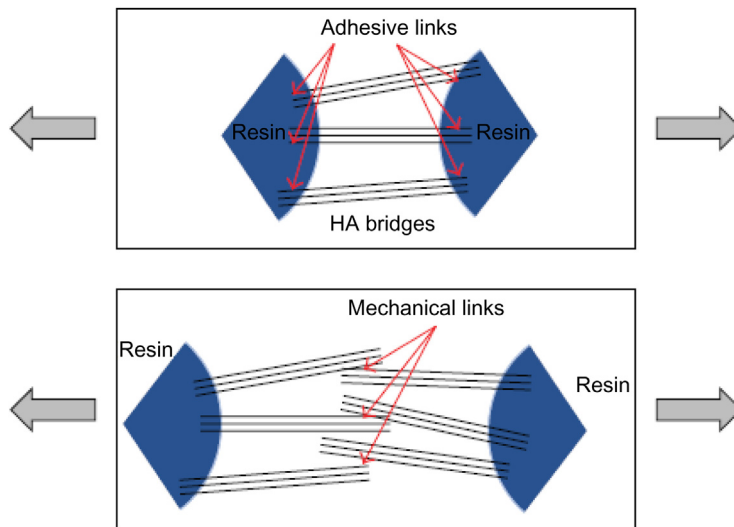


**FIGURE 9.14**

Mechanisms of stress transfer on HA whiskers based composite resins (Calabrese et al., 2016).

Adhesive links increase the stiffness better than the mechanical links. In the former, bridges of HA better resist the tensile stress applied despite the mechanical links (this structural configuration is characterized by a low mechanical resistance to shear). Anyway, the second one is relevant in multiaxial or complex load conditions.

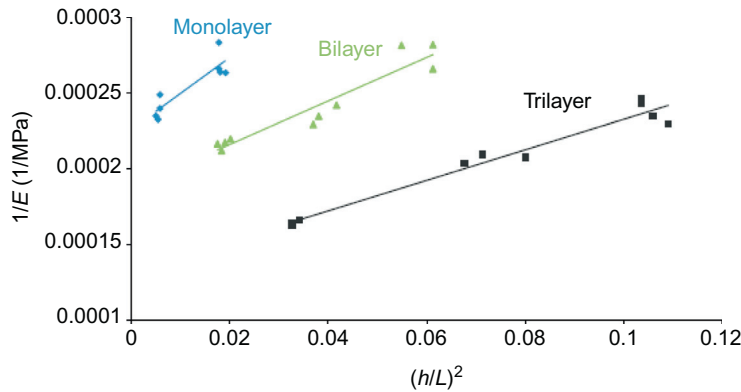
HA whisker based resin composite materials, thanks to their good dispersion and adhesion with the matrix, also showed the toughness of the composite material retarding crack propagation. Furthermore a large surface area of fillers increases the HA/matrix interfacial adhesion thus providing reduced both water uptake and elution in immersed conditions compared with conventional particulate filler (Zhang and Darvell, 2012a). However, water can still induce a surface degradation due to softening and progressive removal of surface polymeric matrix parts. The hydrolytic dissolution of the coupling agent could also facilitate the pulling-out of the HA filler micro- or nanoparticles (Söderholm et al., 1996). Furthermore absorbed water can swell and plasticize the resin, facilitating the resin degradation and the solvent or residual unreacted monomers extraction inducing the formation of preferential water diffusion pathways (Braden and Clarke, 1984; Braden, 1984). Moreover, water sorption reduces the hoop stress around the filler particles, which facilitates the plucking-out of filler particles (Domingo et al., 2003).

Recently, a novel UHA was prepared through microwave irradiation and was applied as a dental filler with very promising results.

The addition of UHA filler significantly improved the mechanical performance (strength, stiffness and microhardness). Furthermore, when used in combination with silica nanoparticles, UHA evidenced the optimal application inducing a significant increase of flexural strength, flexural modulus, and compressive strength respectively of 50%, 40%, and 13% (Liu et al., 2014).

Nevertheless the main disadvantage of HA particles as filler for restorative dentistry is its higher refractive index than resin matrix ( $n = 1.65$  vs  $1.5$  for the resin). The mismatch of refractive index influences the light scattering, decreasing monomer conversion and depth of cure (Ruyter and Oysaed, 1982). Anyway, by using a different light-cured organic phase and/or HA filler with specific crystal size and shape the optical and mechanical properties of HA-based composite resin could be optimized. Consequently the use of HA particles in dental restoration materials is still a fundamental and promising research area. Anyway, an effective cross-linking of the composite restorative resins is crucial to have optimal clinical and mechanical performances with high repeatability. Composite materials with low conversion rates could affect several important parameters such as mechanical performance, water solubility, biocompatibility, etc., limiting the composites' durability (Filho et al., 2008; Poggio et al., 2012). In this regard, the large prismatic specimens, as stated in ISO 4049, are not simple to prepare without flaws especially with compule packaging. At the same time, several overlapping irradiation steps are required considering that the curing window of all clinical light-lamp units is smaller than 25 mm. This leads to possible cross-linking inhomogeneity during curing on large shaped samples. Based on these considerations,



**FIGURE 9.15**

Trends comparison of  $1/E_f$  in terms of  $(h/L)^2$  for monolayer, bilayer, and trilayer composite samples.

fundamental parameters that influence the resin catalysis and consequently the mechanical properties of the composite resin are sample dimensions, curing time, and the chosen layering steps (Willems et al., 1992). For this reason a possible approach is to perform three-point flexural mechanical test of the composite materials at varying specimen dimensions to determine the real elastic modulus of the resin composite (Calabrese et al., 2015). Furthermore, to have information on the effect of geometry and curing procedure on mechanical performances, Calabrese et al. (2015) evaluated the effect of layering light-curing steps (up to three layers step) on the mechanical performances of the HA-based composite resin (Fig. 9.15).

The trilayer samples (black scatter points) evidenced the highest apparent elastic modulus,  $E$  (and conversely the lowest  $1/E$  ratio) in all span ranges ( $h/L$  ratio). For low layering steps (i.e., monolayer or bilayer steps), the apparent elastic modulus,  $E$ , progressively decreases. Each sample batch evidenced a quite linear trend on the plot. BY a linear interpolation, the elastic and shear stiffness of each specimens batches can be extrapolated, achieving an improved knowledge on the mechanical behavior of the composite paste. The results are summarized in Table 9.2.

**Table 9.2** Elastic and Shear Modulus of Multilayer Composite Resins Batches

	$E$ (MPa)	$G$ (MPa)
Monolayer	4416.1	497.7
Bilayer	5346.3	813.4
Trilayer	7591.8	1166.0

The shear modulus,  $G$ , observed on trilayer batch is about double the monolayer one. This behavior can be justified considering that a multilayer procedure could be able to achieve a better cohesion and shear strength, thus playing a relevant role on the limited formation of interlaminar and residual stresses, favoring consequently high and stable performances on composite samples.

The knowledge of the elastic and shear stiffness of the resin composites is relevant for their effective and suitable use in the restorative dentistry field. For dental application, in the oral cavity, the required composite dimensions are compatible with the MFT setup, where lower values of stiffness and strength than the IFT one were observed. Therefore, an unsuitable evaluation of these mechanical parameters can induce marginal breakdown or local fracture in the restorations. This aspect is significantly highlighted considering that Class I, II, and IV restorations are subjected to relevant stress-bearing where a high flexural strength is required to withstand biting forces without fracture. At the same time a high stiffness is necessary to maintain its shape under load (Calabrese et al., 2015).

### 9.3.8 BIOCOMPATIBILITY ISSUES

In the last few decades, the conversion from amalgam to resin composite was mainly due to the rising concerns on biocompatibility correlating to the leaching of mercury-based material. However, several studies have demonstrated that resin composites can also cause harmful effects on human health through unpolymerized monomers and inorganic components diffusion (e.g., residual unreacted compounds, impurities, additives, residual degradation products). These substances can be ingested or diffuse in the dental pulp or be inhaled both by patients as well as operators. In fact, the complete degree of conversion is impossible to reach with a maximum threshold of generally 70% after 24 hours. For this reason, the cytotoxic effect is more detected in this frame of time (Gupta et al., 2012).

The effect of composite compounds' release on adjacent dental tissues such as pulp or periodontium must be taken into account, and depends on different factors like the surface area in contact, the kinetic of release, the penetration in the dentinal tubules, dose dependence effect, and the possible accumulation in the pulp. For these reasons, as with all dental materials, commercial or innovative resin composite formulations must be tested according to ISO 10993-5 (1992, Biological Evaluation of Medical Devices-Part 5:Test for cytotoxicity—in vitro methods) to assess genotoxic, mutagenic, and estrogenic effects before commercialization (Geurtsen et al., 1998).

Also if in vitro tests do not reproduce the clinical conditions under which resin composites are subjected, few in vivo studies have been carried out to analyze the release of toxic substances for dental composites. Indeed, other than for passive hydrolysis the durability of the material is compromised also by mechanical swelling, water sorption, and chemical/enzymatic degradation, which enhance the release during aging of the unreacted components of the network. The instruments used for the detection of dissolved components are high performance liquid

chromatography and liquid/gas chromatography. In addition, mass spectrometry permits to analyze and quantify molecules through their ionization according to their mass/charge ratio usually by static or fluctuating magnetic fields. The most common procedure consists of aging in solution a standardized resin composite sample for a specific period of time, which can vary but in general is short (around 24 hours) (Van Landuyt et al., 2011).

The inorganic phase composition is important to limit the cytotoxic effect of resin composites. In fact, the right filler synthesis technology as well as morphologies can enhance the free energy of the surface improving the filler/matrix interactions and consequently permitting the increase in filler content in the final formulation. This last causes a lower monomer ratio in the final product, which is known to be the main toxic component. In fact, some studies provide a methacrylates release range between 1.5% and 5%; these concentrations are however still able to produce cytotoxic effects. Between the monomers commercially used, HEMA showed the highest release rate. This behavior was justified considering that the molecular weight and the dimensions are really low in comparison with the other organic components. The second monomer in terms of elution rate is the TEGDMA. On the other hand, several studies showed no UDMA detection in solution after aging samples for 24 hours. Moreover, Bis-GMA, due to its high molecular weight and dimensions as well as low solubility, is released in an insignificant amount. Between the monomers commercially available the Bis-GMA presents the maximum value in term of viscosity, which lowers the conversion degree of double bonds in the matrix, thus causing a higher release (elution rate) in the medium. This problem is limited by the use of low viscosity monomers (copolymer mixing) such TEGDMA or UDMA (Leprince et al., 2013).

A wide range of studies have focused on the total and partial substitution of the inorganic phase with calcium-based filler (Liu et al., 2013a; Domingo et al., 2001, 2003). The main reasons are the good interaction of this compound with dental tissues, the easy functionalization, and the well-known biocompatibility and bioactivity. Between them, HA-based composites have shown less cytotoxicity by preserving the mechanical properties and also providing a high cellular growth rate. In fact, an important characteristic that should be not underestimated is the demonstrated ability of HA-based composites to form a compact layer of apatite on the surface when suspended in body fluid solution, which marks the potential bioactivity of this type of material toward enamel/dentin when compared with inert inorganic filler.

Zhang et al. (2010) demonstrated how the biocompatibility of HA filler is related to its morphology. In particular, HA particles with dimensions of  $278 \pm 65$  nm in length tend to agglomerate highlighting defects as pores and voids, which represent the preferential pathway for water absorption in solution and swelling of the composite. This process generates surface deterioration, softening, and elution of the entrapped and unreacted components. The miscibility and dispersion of the different phases as well as reagents is of fundamental importance in guaranteeing the biocompatibility of the system by preventing the

leaching and elution of unreacted monomers. The presence of these last can be related to a nonhomogeneous cross-linking of the dimethacrylates network with consequent free radicals' availability to form microgel domains wetted by unreacted monomers. Multiple microgel domains will agglomerate in clusters with consequent formation of micropores between the clusters. If the immersion medium penetrates during clinical conditions (swelling phase) in the interstice between the polymeric chains, the unreacted components can leach from the lattice especially in the case of unreacted compounds stuck in the micropores.

On the other hand, wHA with dimensions of about  $116 \pm 23 \mu\text{m}$  in length permit a homogeneous dispersion and wettability of the filler in the organic matrix thus guaranteeing lower water uptake and elution ratios of the unreacted compounds, limiting the interaction of the solution with the surface. The data indicate that whisker morphology represents a better option for load dental composite guaranteeing high biocompatibility and proliferation of L929 cells, improving also the properties of the polymeric phase.

To assess the biocompatibility of these innovative formulations at increasing ratios of HA whiskers, the toxicity of these composites on immortalized human monocyte THP-1 cell line was evaluated.

The incubation of THP-1 cells with different concentrations of various composite powders for 48 hours caused a dose-dependent decrease in cell viability measured by MTT assay. In particular, the resin composites with highest HA content (80%–100%), at all concentrations, showed a cytotoxic effect on THP-1 cell culture, reducing cell viability up to 45% at the highest concentration in comparison to control cells. Composites with 40%–60% HA content were also cytotoxic. This main reason can be ascribed to the shielding effect of the HA fillers that, at high content, reduce the degree of conversion of the matrix, consequently increasing the availability of cytotoxic uncured monomers and amines (Kolmas et al., 2014). Among the HA composites, the HA-20 batch evidenced very low cytotoxic effects. The slight increase of cell growth rate above 100%, at this HA rate, is mainly due to the favoring effect of the filler on cell proliferation in the HA-20 design configuration. Until this range the bonds between micelles provide a good interaction at matrix/filler interface while, on the other hand, with the addition of 40–60 vol% (percolation threshold), wHA filler produces agglomerates that causes brittleness and shielding effects. After the data obtained thus far, it can be suggested that the HA implementation in the design of filler phase can be useful both in terms of biocompatibility as well as mechanical properties of the final resin composite under a percolation threshold of 20% in weight.

---

## 9.4 CONCLUDING REMARKS AND FUTURE TRENDS

Many national and international grants have been given in the last few decades to improve resin-based composite formulation. At the same time, dental material

companies have focused their attention on improvement of the photoinitiator system as well as on reducing both the toxicity and the pigmentation, and optimizing the interaction and absorption between initiator and light-curing unit (Leprince et al., 2013). However, no change of the main components was achieved and the main drawbacks responsible for composites failure have been not surpassed.

Nanomaterials have been widely used in recent years thanks to their high surface free energy, which permits to improve mechanical and physicochemical properties, stimulating significantly the research activity in material dentistry applications (Khurshid et al., 2015; Melo et al., 2013; Kovvuru et al., 2012). The successful implementation has not yet been achieved mainly because of the agglomeration tendency of the particles. For this reason, some interesting aspects should be explored such as the introduction by surface modification of charges on the nanoparticles to form dipole repulsion avoiding their tendency to aggregate. In addition, the use of the pearl mill technique should be optimized to be implemented in the synthesis technology process of composites. In this last, nanoceramic or metal fillers are milled with a suspension of nanoparticles agglomeration to break links already formed. In the field of nanomaterials for restorative dentistry different attempts have been made, such the addition of single-walled carbon nanotubes, and  $\text{TiO}_2$  and  $\text{Al}_2\text{O}_3$  nanoparticles as well as nanohydroxyapatite synthesis.

Other research fields have analyzed the incorporation of antibacterial molecules and remineralizing agents in resin-based composite; however they have not obtained a final material that is able to act as an “ionic pump” permitting, thus, the controlled and slow release over time. Dental amalgam was well known to possess an antimicrobial activity due to its silver release. On the other hand, the main reason of failure in resin composite is the occurrence of secondary caries mainly in the interface between natural tooth and restoration. Several issues have arisen in the introduction of antibacterial molecules such as the reduction of activity over time, a light shielding effect, as well as a decrease in mechanical properties. Different studies are present in the literature, where the incorporation of silver has been attempted. For example silver doped HA has been incorporated in resin-based composite to provide both efficient reinforcement and high antibacterial activity (Sodagar et al., 2016; Ai et al., 2017). Furthermore, antibacterial and mechanically strong nanocomposites were developed effectively incorporating a quaternary ammonium dimethacrylate, silver nanoparticles (Cheng et al., 2012). On the basis of the above considerations, it is clear how this research field is expected to grow even more in the near future.

In dentistry, as in medicine, smart materials as well as self-repairing materials still represent a utopia. In the future, it will be possible to possess a material able to release bioactive molecules, such as fluoride or antibiotics, under the command of particular stimuli, for example temperature, mechanical stress, pH change, magnetic field, and so on (Jones, 2004; Badami and Ahuja, 2014; Pérez et al., 2013).

The added value of the dental restoration composites could be improved by enhancing their service lives and adding self-repair capabilities. A possible approach to increase their durability and service life is to obturate the microcracks

formed during or after the composite solidification in the dental cavity (Huyang et al., 2016; Wu et al., 2016a). Furthermore an aspect that not should be avoided is to verify the durability of the functional dental composites. Consequently, the development of a dental HA composite with excellent self-healing efficacy even while being immersed in water is a crucial point that requires further validation. The purpose is to guarantee self-healing efficacy without evidence of performance decrease and material degradation during water aging (Wu et al., 2016b). The new self-healing composite may be a promising solution in dental applications field, yielding high durability and service life materials.

In addition, to the previous material classes another incoming field of study is represented by materials for tissue regeneration, such as the deposition of HA solution to enamel or enamel reconstruction through an amelogenin network (Lippert et al., 2004; Fan et al., 2007; Krishnan et al., 2016; Zeitz et al., 2016).

Anyway, the starting point leading to the future of tissue regeneration is represented by the realization of hierarchical HA-based scaffolds that possess biomineralization and biomimetic properties (Li et al., 2008; Si et al., 2016; Huang et al., 2015; Ciocca et al., 2015). The scaffold should be able to provide a multi-functionalized platform that guarantees the orientation as well as nucleation of HA filler (Palmer et al., 2008).

The field of dental composite materials continues to acquire relevant and stimulating advances in several aspects such as resin compounds, filler reinforcement and its functionalization, as well as synthesis and preparation techniques. The future both for research and clinical practice on HA-based composites is stimulating with exciting new developments that could be achieved. This involving research is furthermore devoted to finding solutions and improvements concretely and effectively implementable in the dental field, optimizing basic properties such as esthetic and functional restoration or oral hygiene.

---

## REFERENCES

- Ai, M., Du, Z., Zhu, S., Geng, H., Zhang, X., Cai, Q., et al., 2017. Composite resin reinforced with silver nanoparticles—laden hydroxyapatite nanowires for dental application. *Dent. Mater.* 33, 12–22. Available from: <https://doi.org/10.1016/j.dental.2016.09.038>.
- Al-maamori, M.H., Awad, S.H., Hussein, A.K., 2014. Mechanical properties and linear shrinkage of resins reinforced with micro hydroxyapatite for dental restoration. *Int. J. Curr. Eng. Technol.* 4, 2151–2154.
- Al-Sanabani, J.S., Madfa, A.A., Al-Sanabani, F.A., 2013. Application of calcium phosphate materials in dentistry. *Int. J. Biomater.* 2013, 876132. Available from: <https://doi.org/10.1155/2013/876132>.
- Anseth, K.S., Newman, S.M., Bowman, C.N., 1995. Polymeric dental composites: properties and reaction behavior of multimethacrylate dental restorations, *Biopolymers II*. *Advances in Polymer Science*, vol. 122. Springer, Berlin Heidelberg, pp. 177–217. Available from: [https://doi.org/10.1007/3540587888\\_16](https://doi.org/10.1007/3540587888_16).

- Arcís, R.W., López-Macipe, A., Toledano, M., Osorio, E., Rodríguez-Clemente, R., Murtra, J., et al., 2002. Mechanical properties of visible light-cured resins reinforced with hydroxyapatite for dental restoration. *Dent. Mater.* 18, 49–57. Available from: [https://doi.org/10.1016/S0109-5641\(01\)00019-7](https://doi.org/10.1016/S0109-5641(01)00019-7).
- Asmussen, E., Peutzfeldt, A., 2001. Influence of selected components on crosslink density in polymer structures. *Eur. J. Oral Sci.* 109, 282–285.
- Asmussen, E., Peutzfeldt, A., 2003a. Polymer structure of a light-cured resin composite in relation to distance from the surface. *Eur. J. Oral Sci.* 111, 277–279. Available from: <https://doi.org/10.1034/j.1600-0722.2003.00044.x>.
- Asmussen, E., Peutzfeldt, A., 2003b. Two-step curing: influence on conversion and softening of a dental polymer. *Dent. Mater.* 19, 466–470. Available from: [https://doi.org/10.1016/S0109-5641\(02\)00091-X](https://doi.org/10.1016/S0109-5641(02)00091-X).
- Badami, V., Ahuja, B., 2014. Biosmart materials: breaking new ground in dentistry. *Sci. World J.* 2014, 986912. Available from: <https://doi.org/10.1155/2014/986912>.
- Benetti, A.R., Asmussen, E., Munksgaard, E.C., Dewaele, M., Peutzfeldt, A., Leloup, G., et al., 2009. Softening and elution of monomers in ethanol. *Dent. Mater.* 25, 1007–1013. Available from: <https://doi.org/10.1016/j.dental.2009.01.104>.
- Bogdanoviciene, I., Tonsuaadu, K., Mikli, V., Grigoraviciute-Puroniene, I., Beganskiene, A., Kareiva, A., 2010. pH impact on the sol-gel preparation of calcium hydroxyapatite,  $\text{Ca}_{10}(\text{PO}_4)_6(\text{OH})_2$ , using a novel complexing agent, DCTA. *Open Chem.* 8, 1323–1330. Available from: <https://doi.org/10.2478/s11532-010-0113-0>.
- Bonaccorsi, L.M., Borsellino, C., Calabrese, L., Cordasco, G., Fabiano, F., Fabiano, V., et al., 2012. Performances evaluation of a bis-GMA resin-based composite for dental restoration. *Acta Med. Mediterr.* 28, 163–166.
- Bouschlicher, M.R., Rueggeberg, F.A., Wilson, B.M., 2004. Correlation of bottom-to-top surface microhardness and conversion ratios for a variety of resin composite compositions. *Oper. Dent.* 29, 698–704.
- Bowen, R.L., Paffenbarger, G.C., Schoonover, I.C., Souder, W., Skinner, E.W., Paffenbarger, G.C., et al., 1963. Properties of a silica-reinforced polymer for dental restorations. *J. Am. Dent. Assoc.* 66, 57–64. Available from: <https://doi.org/10.14219/JADA.ARCHIVE.1963.0010>.
- Braden, M., 1984. Water absorption characteristics of dental microfine composite filling materials. II. Experimental materials. *Biomaterials* 5, 373–375. Available from: [https://doi.org/10.1016/0142-9612\(84\)90039-5](https://doi.org/10.1016/0142-9612(84)90039-5).
- Braden, M., Clarke, R.L., 1984. Water absorption characteristics of dental microfine composite filling materials. I. Proprietary materials. *Biomaterials* 5, 369–372. Available from: [https://doi.org/10.1016/0142-9612\(84\)90038-3](https://doi.org/10.1016/0142-9612(84)90038-3).
- Cai, Y., Tang, R., 2008. Calcium phosphate nanoparticles in biomineralization and biomaterials. *J. Mater. Chem.* 18, 3775. Available from: <https://doi.org/10.1039/b805407j>.
- Calabrese, L., Fabiano, F., Bonaccorsi, L.M., Fabiano, V., Borsellino, C., 2015. Evaluation of the clinical impact of ISO 4049 in comparison with miniflexural test on mechanical performances of resin based composite. *Int. J. Biomater.* 2015, 149798. Available from: <https://doi.org/10.1155/2015/149798>.
- Calabrese, L., Fabiano, F., Currò, M., Borsellino, C., Bonaccorsi, L.M., Fabiano, V., et al., 2016. Hydroxyapatite whiskers based resin composite versus commercial dental composites: mechanical and biocompatibility characterization. *Adv. Mater. Sci. Eng.* 2016. Available from: <https://doi.org/10.1155/2016/2172365>.



- Causton, B.E., Miller, B., Sefton, J., 1985. The deformation of cusps by bonded posterior composite restorations: an in vitro study. *Br. Dent. J.* 159, 397–400.
- Chai, C.S., Ben-Nissan, B., 1999. Bioactive nanocrystalline sol-gel hydroxyapatite coatings. *J. Mater. Sci. Mater. Med.* 10, 465–469. Available from: <https://doi.org/10.1023/A:1008992807888>.
- Chen, Y.-C., Ferracane, J.L., Prahl, S.A., 2007. Quantum yield of conversion of the photoinitiator camphorquinone. *Dent. Mater.* 23, 655–664. Available from: <https://doi.org/10.1016/j.dental.2006.06.005>.
- Chen, X.B., Birbilis, N., Abbott, T.B., 2011a. A simple route towards a hydroxyapatite–Mg(OH)<sub>2</sub> conversion coating for magnesium. *Corros. Sci.* 53, 2263–2268. Available from: <https://doi.org/10.1016/j.corsci.2011.03.008>.
- Chen, L., Yu, Q., Wang, Y., Li, H., 2011b. BisGMA/TEGDMA dental composite containing high aspect-ratio hydroxyapatite nanofibers. *Dent. Mater.* 27, 1187–1195. Available from: <https://doi.org/10.1016/j.dental.2011.08.403>.
- Chen, L., Xu, C., Wang, Y., Shi, J., Yu, Q., Li, H., 2012. BisGMA/TEGDMA dental nanocomposites containing glyoxylic acid-modified high-aspect ratio hydroxyapatite nanofibers with enhanced dispersion. *Biomed. Mater.* 7, 45014. Available from: <https://doi.org/10.1088/1748-6041/7/4/045014>.
- Cheng, L., Weir, M.D., Xu, H.H.K., Antonucci, J.M., Kraigsley, A.M., Lin, N.J., et al., 2012. Antibacterial amorphous calcium phosphate nanocomposites with a quaternary ammonium dimethacrylate and silver nanoparticles. *Dent. Mater.* 28, 561–572. Available from: <https://doi.org/10.1016/j.dental.2012.01.005>.
- Choudhury, P., Agrawal, D.C., 2011. Sol–gel derived hydroxyapatite coatings on titanium substrates. *Surf. Coat. Technol.* 206, 360–365. Available from: <https://doi.org/10.1016/j.surfcoat.2011.07.031>.
- Ciocca, L., Lesci, I.G., Mezini, O., Parrilli, A., Ragazzini, S., Rinnovati, R., et al., 2015. Customized hybrid biomimetic hydroxyapatite scaffold for bone tissue regeneration. *J. Biomed. Mater. Res. Part B Appl. Biomater.* Available from: <https://doi.org/10.1002/jbm.b.33597>.
- Corrêa, J.M., Mori, M., Sanches, H.L., Da Cruz, A.D., Poiate, E., Poiate, I.A.V.P., 2015. Silver nanoparticles in dental biomaterials. *Int. J. Biomater.* 2015. Available from: <https://doi.org/10.1155/2015/485275>.
- Cramer, N.B., Stansbury, J.W., Bowman, C.N., 2011. Recent advances and developments in composite dental restorative materials. *J. Dent. Res.* 90, 402–416. Available from: <https://doi.org/10.1177/0022034510381263>.
- Culbertson, B.M., Wan, Q., Tong, Y., 1997. Preparation and evaluation of visible light-cured multi-methacrylates for dental composites. *J. Macromol. Sci.* 34, 2405–2421. Available from: <https://doi.org/10.1080/10601329708010056>.
- David, J.R., Gomes, O.M., Gomes, J.C., Loguercio, A.D., Reis, A., 2007. Effect of exposure time on curing efficiency of polymerizing units equipped with light-emitting diodes. *J. Oral Sci.* 49, 19–24. Available from: <https://doi.org/10.2334/josnusd.49.19>.
- Deb, S., Braden, M., Bonfield, W., 1995. Water absorption characteristics of modified hydroxyapatite bone cements. *Biomaterials* 16, 1095–1100. Available from: [https://doi.org/10.1016/0142-9612\(95\)98906-U](https://doi.org/10.1016/0142-9612(95)98906-U).
- Dewaele, M., Asmussen, E., Peutzfeldt, A., Munksgaard, E.C., Benetti, A.R., Finné, G., et al., 2009. Influence of curing protocol on selected properties of light-curing polymers: degree of conversion, volume contraction, elastic modulus, and glass transition temperature. *Dent. Mater.* 25, 1576–1584. Available from: <https://doi.org/10.1016/j.dental.2009.08.001>.



- Domingo, C., Arcís, R.W., López-Macipe, A., Osorio, R., Rodríguez-Clemente, R., Murtra, J., et al., 2001. Dental composites reinforced with hydroxyapatite: mechanical behavior and absorption/elution characteristics. *J. Biomed. Mater. Res.* 56, 297–305.
- Domingo, C., Arcís, R.W., Osorio, E., Osorio, R., Fanovich, M.A., Rodríguez-Clemente, R., et al., 2003. Hydrolytic stability of experimental hydroxyapatite-filled dental composite materials. *Dent. Mater.* 19, 478–486. Available from: [https://doi.org/10.1016/S0109-5641\(02\)00093-3](https://doi.org/10.1016/S0109-5641(02)00093-3).
- Dorozhkin, S.V., 2012. Nanodimensional and nanocrystalline calcium orthophosphates. *Am. J. Biomed. Eng.* 2, 48–97. Available from: <https://doi.org/10.5923/j.ajbe.20120203.01>.
- Earl, J.S., Wood, D.J., Milne, S.J., 2006. Hydrothermal synthesis of hydroxyapatite. *J. Phys. Conf. Ser.* 26, 268–271. Available from: <https://doi.org/10.1088/1742-6596/26/1/064>.
- Emami, N., Sjö Dahl, M., Söderholm, K.J.M., 2005. How filler properties, filler fraction, sample thickness and light source affect light attenuation in particulate filled resin composites. *Dent. Mater.* 21, 721–730. Available from: <https://doi.org/10.1016/j.dental.2005.01.002>.
- Fabiano, F., Borsellino, C., Bonaccorsi, L.M., Calabrese, L., Fabiano, V., Mavilia, G., 2014. Influence of irradiation exposure time on the depth cure of restorative resin composite. *AAPP Atti Della Accad. Peloritana Dei Pericolanti, Cl. Di Sci. Fis. Mat. E Nat.* 92. Available from: <https://doi.org/10.1478/AAPP.92S1A1>.
- Fan, Y.W., Sun, Z., Wang, R., Abbott, C., Moradian-Oldak, J., 2007. Enamel inspired nanocomposite fabrication through amelogenin supramolecular assembly. *Biomaterials* 28, 3034–3042. Available from: <https://doi.org/10.1016/j.biomaterials.2007.02.016>.
- Feilzer, A.J., Dooren, L.H., de Gee, A.J., Davidson, C.L., 1995. Influence of light intensity on polymerization shrinkage and integrity of restoration-cavity interface. *Eur. J. Oral Sci.* 103, 322–326.
- Ferracane, J.L., 1985. Correlation between hardness and degree of conversion during the setting reaction of unfilled dental restorative resins. *Dent. Mater.* 1, 11–14. Available from: [https://doi.org/10.1016/S0109-5641\(85\)80058-0](https://doi.org/10.1016/S0109-5641(85)80058-0).
- Ferracane, J.L., 2011. Resin composite—state of the art. *Dent. Mater.* 27, 29–38. Available from: <https://doi.org/10.1016/j.dental.2010.10.020>.
- Ferracane, J.L., Greener, E.H., 1984. Fourier transform infrared analysis of degree of polymerization in unfilled resins—methods comparison. *J. Dent. Res.* 63, 1093–1095. Available from: <https://doi.org/10.1177/00220345840630081901>.
- Filho, J.D.N., Poskus, L.T., Guimarães, J.G.A., Barcellos, A.A.L., Silva, E.M., 2008. Degree of conversion and plasticization of dimethacrylate-based polymeric matrices: influence of light-curing mode. *J. Oral Sci.* 50, 315–321. Available from: <https://doi.org/10.2334/josnusd.50.315>.
- Flury, S., Hayoz, S., Peutzfeldt, A., Hüsler, J., Lussi, A., 2012. Depth of cure of resin composites: is the ISO 4049 method suitable for bulk fill materials? *Dent. Mater.* 28, 521–528. Available from: <https://doi.org/10.1016/j.dental.2012.02.002>.
- Geurtsen, W., Lehmann, F., Spahl, W., Leyhausen, G., 1998. Cytotoxicity of 35 dental resin composite monomers/additives in permanent 3T3 and three human primary fibroblast cultures. *J. Biomed. Mater. Res.* 41, 474–480.
- Ginebra, M.P., Driessens, F.C.M., Planell, J.A., 2004. Effect of the particle size on the micro and nanostructural features of a calcium phosphate cement: a kinetic analysis. *Biomaterials* 25, 3453–3462. Available from: <https://doi.org/10.1016/j.biomaterials.2003.10.049>.

- Goto, T., Sekino, T., 2016. Synthesis of TiO<sub>2</sub> modified hydroxyapatite with various morphology by urea-assisted hydrothermal method. *Mater. Sci. Forum* 868, 28–32. Available from: <https://doi.org/10.4028/www.scientific.net/MSF.868.28>.
- Gupta, S.K., Saxena, P., Pant, V.A., Pant, A.B., 2012. Release and toxicity of dental resin composite. *Toxicol. Int.* 19, 225–234. Available from: <https://doi.org/10.4103/0971-6580.103652>.
- Habib, E., Wang, R., Wang, Y., Zhu, M., Zhu, X.X., 2016. Inorganic fillers for dental resin composites: present and future. *ACS Biomater. Sci. Eng.* 2, 1–11. Available from: <https://doi.org/10.1021/acsbiomaterials.5b00401>.
- Halvorson, R.H., Erickson, R.L., Davidson, C.L., 2003. The effect of filler and silane content on conversion of resin-based composite. *Dent. Mater.* 19, 327–333. Available from: [https://doi.org/10.1016/S0109-5641\(02\)00062-3](https://doi.org/10.1016/S0109-5641(02)00062-3).
- Hansel, C., Leyhausen, G., Mai, U.E., Geurtsen, W., 1998. Effects of various resin composite (co)monomers and extracts on two caries-associated micro-organisms in vitro. *J. Dent. Res.* 77, 60–67.
- Hervás-García, A., Martínez-Lozano, M.A., Cabanes-Vila, J., Barjau-Escribano, A., Fos-Galve, P., 2006. Composite resins. A review of the materials and clinical indications. *Med. Oral, Patol. Oral Y Cirugía Bucal.* 11, E215–20.
- Howard, B., Wilson, N.D., Newman, S.M., Pfeifer, C.S., Stansbury, J.W., 2010. Relationships between conversion, temperature and optical properties during composite photopolymerization. *Acta Biomater.* 6, 2053–2059. Available from: <https://doi.org/10.1016/j.actbio.2009.11.006>.
- Huang, Z., Cui, F., Feng, Q., Guo, X., 2015. Incorporation of strontium into hydroxyapatite via biomineralization of collagen fibrils. *Ceram. Int.* 41, 8773–8778. Available from: <https://doi.org/10.1016/j.ceramint.2015.03.102>.
- Huyang, G., Debertin, A.E., Sun, J., 2016. Design and development of self-healing dental composites. *Mater. Des.* 94, 295–302. Available from: <https://doi.org/10.1016/j.matdes.2016.01.046>.
- Ito, A., Nakamura, S., Aoki, H., Akao, M., Teraoka, K., Tsutsumi, S., et al., 1996. Hydrothermal growth of carbonate-containing hydroxyapatite single crystals. *J. Cryst. Growth* 163, 311–317. Available from: [https://doi.org/10.1016/0022-0248\(95\)00955-8](https://doi.org/10.1016/0022-0248(95)00955-8).
- Jafarzadeh, T.-S., Erfan, M., Behroozibakhsh, M., Fatemi, M., Masaali, R., Rezaei, Y., et al., 2015. Evaluation of polymerization efficacy in composite resins via FT-IR spectroscopy and vickers microhardness test. *J. Dent. Res. Dent. Clin. Dent. Prospects* 9, 226–232. Available from: <https://doi.org/10.15171/joddd.2015.041>.
- Jamesh, M., Kumar, S., Narayanan, T.S.N.S., 2012. Electrodeposition of hydroxyapatite coating on magnesium for biomedical applications. *J. Coat. Technol. Res.* 9, 495–502. Available from: <https://doi.org/10.1007/s11998-011-9382-6>.
- Jandt, K.D., Sigusch, B.W., 2009. Future perspectives of resin-based dental materials. *Dent. Mater.* 25, 1001–1006. Available from: <https://doi.org/10.1016/j.dental.2009.02.009>.
- Jones, R.A.L., 2004. Biomimetic polymers: tough and smart. *Nat. Mater.* 3, 209–210. Available from: <https://doi.org/10.1038/nmat1109>.
- Kakaboura, A., Rahiotis, C., Watts, D., Silikas, N., Eliades, G., 2007. 3D-marginal adaptation versus setting shrinkage in light-cured microhybrid resin composites. *Dent. Mater.* 23, 272–278. Available from: <https://doi.org/10.1016/j.dental.2006.01.020>.
- Kamiya, K., Yoko, T., Tanaka, K., Fujiyama, Y., 1989. Growth of fibrous hydroxyapatite in the gel system. *J. Mater. Sci.* 24, 827–832. Available from: <https://doi.org/10.1007/BF01148764>.

- Kandori, K., Horigami, N., Yasukawa, A., Ishikawa, T., 2005. Texture and formation mechanism of fibrous calcium hydroxyapatite particles prepared by decomposition of calcium-EDTA chelates. *J. Am. Ceram. Soc.* 80, 1157–1164. Available from: <https://doi.org/10.1111/j.1151-2916.1997.tb02958.x>.
- Kantharia, N., Naik, S., Apte, S., Kheur, M., Kheur, S., Kale, B., 2014. Nano-hydroxyapatite and its contemporary applications. *Bone* 34, 1–71.
- Kasuga, T., Ota, Y., Nogami, M., Abe, Y., 2000. Preparation and mechanical properties of polylactic acid composites containing hydroxyapatite fibers. *Biomaterials* 22, 19–23. Available from: [https://doi.org/10.1016/S0142-9612\(00\)00091-0](https://doi.org/10.1016/S0142-9612(00)00091-0).
- Khalichi, P., Cvitkovitch, D.G., Santerre, J.P., 2004. Effect of composite resin biodegradation products on oral streptococcal growth. *Biomaterials* 25, 5467–5472. Available from: <https://doi.org/10.1016/j.biomaterials.2003.12.056>.
- Khurshid, Z., Zafar, M., Qasim, S., Shahab, S., Naseem, M., AbuReqaiba, A., 2015. Advances in nanotechnology for restorative dentistry. *Materials (Basel)* 8, 717–731. Available from: <https://doi.org/10.3390/ma8020717>.
- Kim, J.W., Kim, L.U., Kim, C.K., 2007. Size control of silica nanoparticles and their surface treatment for fabrication of dental nanocomposites. *Biomacromolecules* 8, 215–222. Available from: <https://doi.org/10.1021/bm060560b>.
- Kleverlaan, C.J., Feilzer, A.J., 2005. Polymerization shrinkage and contraction stress of dental resin composites. *Dent. Mater.* 21, 1150–1157. Available from: <https://doi.org/10.1016/j.dental.2005.02.004>.
- Knyazev, A.V., Bulanov, E.N., Vlasova, E.V., 2012. Synthesis of hydroxyapatite whiskers. *Inorg. Mater. Appl. Res.* 3, 417–420. Available from: <https://doi.org/10.1134/S2075113312050073>.
- Kolmas, J., Groszyk, E., Kwiatkowska-Różycka, D., 2014. Substituted hydroxyapatites with antibacterial properties. *Biomed. Res. Int.* 2014, 178123. Available from: <https://doi.org/10.1155/2014/178123>.
- Komlev, V.S., Barinov, S.M., Koplik, E.V., 2002. A method to fabricate porous spherical hydroxyapatite granules intended for time-controlled drug release. *Biomaterials* 23, 3449–3454. Available from: [https://doi.org/10.1016/S0142-9612\(02\)00049-2](https://doi.org/10.1016/S0142-9612(02)00049-2).
- Kovvuru, S.K., Mahita, V.N., Manjunatha, B., Babu, B.S., 2012. Nanotechnology: the emerging science in dentistry. *J. Orofac. Res.* 2, 33–36.
- Krämer, N., Lohbauer, U., García-Godoy, F., Frankenberger, R., 2008. Light curing of resin-based composites in the LED era. *Am. J. Dent.* 21, 135–142.
- Krishnan, V., Bhatia, A., Varma, H., 2016. Development, characterization and comparison of two strontium doped nano hydroxyapatite molecules for enamel repair/regeneration. *Dent. Mater.* 32, 646–659. Available from: <https://doi.org/10.1016/j.dental.2016.02.002>.
- Lak, A., Mazloumi, M., Mohajerani, M., Kajbafvala, A., Zanganeh, S., Arami, H., et al., 2008. Self-assembly of dandelion-like hydroxyapatite nanostructures via hydrothermal method. *J. Am. Ceram. Soc.* 91, 3292–3297. Available from: <https://doi.org/10.1111/j.1551-2916.2008.02600.x>.
- Leitune, V.C.B., Collares, F.M., Trommer, R.M., Andrioli, D.G., Bergmann, C.P., Samuel, S. M.W., 2013. The addition of nanostructured hydroxyapatite to an experimental adhesive resin. *J. Dent.* 41, 321–327. Available from: <https://doi.org/10.1016/j.jdent.2013.01.001>.
- Leprince, J., Lamblin, G., Truffier-Boutry, D., Demoustier-Champagne, S., Devaux, J., Mestdagh, M., et al., 2009. Kinetic study of free radicals trapped in dental resins stored in different environments. *Acta Biomater.* 5, 2518–2524. Available from: <https://doi.org/10.1016/j.actbio.2009.04.034>.

- Leprince, J.G., Lamblin, G., Devaux, J., Dewaele, M., Mestdagh, M., Palin, W.M., et al., 2010a. Irradiation modes' impact on radical entrapment in photoactive resins. *J. Dent. Res.* 89, 1494–1498. Available from: <https://doi.org/10.1177/0022034510384624>.
- Leprince, J., Devaux, J., Mullier, T., Vreven, J., Leloup, G., 2010b. Pulpal-temperature rise and polymerization efficiency of LED curing lights. *Oper. Dent.* 35, 220–230. Available from: <https://doi.org/10.2341/09-203-L>.
- Leprince, J.G., Hadis, M., Shortall, A.C., Ferracane, J.L., Devaux, J., Leloup, G., et al., 2011. Photoinitiator type and applicability of exposure reciprocity law in filled and unfilled photoactive resins. *Dent. Mater.* 27, 157–164. Available from: <https://doi.org/10.1016/j.dental.2010.09.011>.
- Leprince, J.G., Leveque, P., Nysten, B., Gallez, B., Devaux, J., Leloup, G., 2012. New insight into the “depth of cure” of dimethacrylate-based dental composites. *Dent. Mater.* 28, 512–520. Available from: <https://doi.org/10.1016/j.dental.2011.12.004>.
- Leprince, J.G., Palin, W.M., Hadis, M.A., Devaux, J., Leloup, G., 2013. Progress in dimethacrylate-based dental composite technology and curing efficiency. In: *Dental Materials*, pp. 139–156. <https://doi.org/10.1016/j.dental.2012.11.005>.
- Lezaja, M., Veljovic, D.N., Jokic, B.M., Cvijovic-Alagic, I., Zrilic, M.M., Miletic, V., 2013. Effect of hydroxyapatite spheres, whiskers, and nanoparticles on mechanical properties of a model BisGMA/TEGDMA composite initially and after storage. *J. Biomed. Mater. Res. Part B Appl. Biomater.* 101, 1469–1476. Available from: <https://doi.org/10.1002/jbm.b.32967>.
- Li, L., Pan, H., Tao, J., Xu, X., Mao, C., Gu, X., et al., 2008. Repair of enamel by using hydroxyapatite nanoparticles as the building blocks. *J. Mater. Chem.* 18, 4079. Available from: <https://doi.org/10.1039/b806090h>.
- Lippert, F., Parker, D.M., Jandt, K.D., 2004. In vitro demineralization/remineralization cycles at human tooth enamel surfaces investigated by AFM and nanoindentation. *J. Colloid Interface Sci.* 280, 442–448. Available from: <https://doi.org/10.1016/j.jcis.2004.08.016>.
- Liu, J., Li, K., Wang, H., Zhu, M., Yan, H., 2004. Rapid formation of hydroxyapatite nanostructures by microwave irradiation. *Chem. Phys. Lett.* 396, 429–432. Available from: <https://doi.org/10.1016/j.cplett.2004.08.094>.
- Liu, F., Wang, R., Cheng, Y., Jiang, X., Zhang, Q., Zhu, M., 2013a. Polymer grafted hydroxyapatite whisker as a filler for dental composite resin with enhanced physical and mechanical properties. *Mater. Sci. Eng. C* 33, 4994–5000. Available from: <https://doi.org/10.1016/j.msec.2013.08.029>.
- Liu, F., Hu, J., Ruili, W., Yingying, P., Jiang, X., Zhu, M., 2013b. Effect of filler ratio on properties of nano-hydroxyapatite/SiO<sub>2</sub> based bioactive dental resin composites. *Mater. Sci. Forum.* 745–746, 466–472. Available from: <https://doi.org/10.4028/www.scientific.net/MSF.745-746.466>.
- Liu, F., Sun, B., Jiang, X., Aldeyab, S.S., Zhang, Q., Zhu, M., 2014. Mechanical properties of dental resin/composite containing urchin-like hydroxyapatite. *Dent. Mater.* 30, 1358–1368. Available from: <https://doi.org/10.1016/j.dental.2014.10.003>.
- Loshack, S., Fox, T.G., 1953. Cross-linked polymers. I. Factors influencing the efficiency of cross-linking in copolymers of methyl methacrylate and glycol dimethacrylates 1. *J. Am. Chem. Soc.* 75, 3544–3550. Available from: <https://doi.org/10.1021/ja01110a068>.
- Lovell, L.G., Stansbury, J.W., Syrpes, D.C., Bowman, C.N., 1999. Effects of composition and reactivity on the reaction kinetics of dimethacrylate/dimethacrylate copolymerizations. *Macromolecules* 32, 3913–3921. Available from: <https://doi.org/10.1021/ma990258d>.

- Lung, C.Y.K., Sarfraz, Z., Habib, A., Khan, A.S., Matinlinna, J.P., 2016. Effect of silanization of hydroxyapatite fillers on physical and mechanical properties of a bis-GMA based resin composite. *J. Mech. Behav. Biomed. Mater.* 54, 283–294. Available from: <https://doi.org/10.1016/j.jmbbm.2015.09.033>.
- Lygre, H., Hol, P.J., Solheim, E., Moe, G., 1999. Organic leachables from polymer-based dental filling materials. *Eur. J. Oral Sci.* 107, 378–383. Available from: <https://doi.org/10.1046/j.0909-8836.1999.eos107509.x>.
- Manhart, J., Kunzelmann, K.H., Chen, H.Y., Hickel, R., 2000. Mechanical properties of new composite restorative materials. *J. Biomed. Mater. Res.* 53, 353–361.
- Manso, M., Jiménez, C., Morant, C., Herrero, P., Martínez-Duart, J., 2000. Electrodeposition of hydroxyapatite coatings in basic conditions. *Biomaterials* 21, 1755–1761. Available from: [https://doi.org/10.1016/S0142-9612\(00\)00061-2](https://doi.org/10.1016/S0142-9612(00)00061-2).
- Mary, I.R., Sonia, S., Viji, S., Mangalaraj, D., Viswanathan, C., Ponpandian, N., 2016. Novel multiform morphologies of hydroxyapatite: synthesis and growth mechanism. *Appl. Surf. Sci.* 361, 25–32. Available from: <https://doi.org/10.1016/j.apsusc.2015.11.123>.
- McCulloch, A.J., Smith, B.G., 1986. In vitro studies of cuspal movement produced by adhesive restorative materials. *Br. Dent. J.* 161, 405–409.
- Melo, M.A.S., Guedes, S.F.F., Xu, H.H.K., Rodrigues, L.K.A., 2013. Nanotechnology-based restorative materials for dental caries management. *Trends Biotechnol.* 31, 459–467. Available from: <https://doi.org/10.1016/j.tibtech.2013.05.010>.
- Mendez-Lozano, N., Velazquez-Castillo, R., Rivera-Muñoz, E.M., Bucio-Galindo, L., Mondragon-Galicia, G., Manzano-Ramirez, A., et al., 2017. Crystal growth and structural analysis of hydroxyapatite nanofibers synthesized by the hydrothermal microwave-assisted method. *Ceram. Int.* 43, 451–457. Available from: <https://doi.org/10.1016/j.ceramint.2016.09.179>.
- Meredith, N., Setchell, D.J., n.d. In vitro measurement of cuspal strain and displacement in composite restored teeth. *J. Dent.* 25, 331–337.
- Millich, F., Jeang, L., Eick, J.D., Chappelow, C.C., Pinzino, C.S., 1998. Elements of light-cured epoxy-based dental polymer systems. *J. Dent. Res.* 77, 603–608. Available from: <https://doi.org/10.1177/00220345980770041301>.
- Mills, R.W., Jandt, K.D., Ashworth, S.H., 1999. Dental composite depth of cure with halogen and blue light emitting diode technology. *Br. Dent. J.* 186, 388–391. Available from: <https://doi.org/10.1038/sj.bdj.4800120a>.
- Mohammadi, Z., Sheikh-Mehdi Mesgar, A., Rasouli-Disfani, F., 2016. Preparation and characterization of single phase, biphasic and triphasic calcium phosphate whisker-like fibers by homogenous precipitation using urea. *Ceram. Int.* 42, 6955–6961. Available from: <https://doi.org/10.1016/j.ceramint.2016.01.081>.
- Morra, M., 1993. Acid-base properties of adhesive dental polymers. *Dent. Mater.* 9, 375–378. Available from: [https://doi.org/10.1016/0109-5641\(93\)90060-4](https://doi.org/10.1016/0109-5641(93)90060-4).
- Mortier, A., Lemaitre, J., Rodrique, L., Rouxhet, P.G., 1989. Synthesis and thermal behavior of well-crystallized calcium-deficient phosphate apatite. *J. Solid State Chem.* 78, 215–219. Available from: [https://doi.org/10.1016/0022-4596\(89\)90099-6](https://doi.org/10.1016/0022-4596(89)90099-6).
- Moszner, N., Klapdohr, S., 2004. Nanotechnology for dental composites. *Int. J. Nanotechnol.* 1, 130–156.
- Nayak, A.K., 2010. Hydroxyapatite synthesis methodologies: an overview. *Int. J. Chem. Tech. Res.* 2, 903–907.

- Neira, I.S., Guitián, F., Taniguchi, T., Watanabe, T., Yoshimura, M., 2008. Hydrothermal synthesis of hydroxyapatite whiskers with sharp faceted hexagonal morphology. *J. Mater. Sci.* 43, 2171–2178. Available from: <https://doi.org/10.1007/s10853-007-2032-9>.
- Neira, I.S., Kolen'ko, Y.V., Lebedev, O.I., Van Tendeloo, G., Gupta, H.S., Guitián, F., et al., 2009. An effective morphology control of hydroxyapatite crystals via hydrothermal synthesis. *Cryst. Growth Des.* 9, 466–474. Available from: <https://doi.org/10.1021/cg800738a>.
- Nonami, T., Griffith, A.A., Irwin, G.R., 1989. Study on diopside whiskers precipitation type hydroxyapatite. *MRS Proc.* 175, 71. Available from: <https://doi.org/10.1557/PROC-175-71>.
- Nozawa, K., Gailhanou, H., Raison, L., Panizza, P., Ushiki, H., Sellier, E., et al., 2005. Smart control of monodisperse stober silica particles: effect of reactant addition rate on growth process. *Langmuir* 21, 1516–1523. Available from: <https://doi.org/10.1021/la048569r>.
- Oduncu, B.S., Yucel, S., Aydin, I., Sener, I.D., Yamaner, G., 2010. Polymerisation shrinkage of light – cured hydroxyapatite (HA) – reinforced dental composites. *Int. J. Biomed. Eng. Technol.* 4, 130–135.
- Ogliari, F.A., Ely, C., Zanchi, C.H., Fortes, C.B.B., Samuel, S.M.W., Demarco, F.F., et al., 2008. Influence of chain extender length of aromatic dimethacrylates on polymer network development. *Dent. Mater.* 24, 165–171. Available from: <https://doi.org/10.1016/j.dental.2007.03.007>.
- Palin, W.M., Fleming, G.J.P., Marquis, P.M., 2005. The reliability of standardized flexure strength testing procedures for a light-activated resin-based composite. *Dent. Mater.* 21, 911–919. Available from: <https://doi.org/10.1016/j.dental.2005.01.005>.
- Palmer, L.C., Newcomb, C.J., Kaltz, S.R., Spoerke, E.D., Stupp, S.I., 2008. Biomimetic systems for hydroxyapatite mineralization inspired by bone and enamel. *Chem. Rev.* 108, 4754–4783. Available from: <https://doi.org/10.1021/cr8004422>.
- Pan, Y., Liu, F., Xu, D., Jiang, X., Yu, H., Zhu, M., 2013. Novel acrylic resin denture base with enhanced mechanical properties by the incorporation of PMMA-modified hydroxyapatite. *Prog. Nat. Sci. Mater. Int.* 23, 89–93. Available from: <https://doi.org/10.1016/j.pnsc.2013.01.016>.
- Paul, W., Sharma, C.P., 1999. Development of porous spherical hydroxyapatite granules: application towards protein delivery. *J. Mater. Sci. Mater. Med.* 10, 383–388. Available from: <https://doi.org/10.1023/A:1008918412198>.
- Pearson, G.J., Hegarty, S.M., 1987. Cusp movement in molar teeth using dentine adhesives and composite filling materials. *Biomaterials* 8, 473–476.
- Pérez, R.A., Won, J.-E., Knowles, J.C., Kim, H.-W., 2013. Naturally and synthetic smart composite biomaterials for tissue regeneration. *Adv. Drug Deliv. Rev.* 65, 471–496. Available from: <https://doi.org/10.1016/j.addr.2012.03.009>.
- Pianelli, C., Devaux, J., Bebelman, S., Leloup, G., 1999. The micro-Raman spectroscopy, a useful tool to determine the degree of conversion of light-activated composite resins. *J. Biomed. Mater. Res.* 48, 675–681.
- Poggio, C., Gaviati, S., Lombardini, M., Chiesa, M., 2012. Evaluation of Vickers hardness and depth of cure of six composite resins photo-activated with different polymerization modes. *J. Conserv. Dent.* 15, 237. Available from: <https://doi.org/10.4103/0972-0707.97946>.
- Popowics, T.E., Rensberger, J.M., Herring, S.W., Burke, F.J.T., Popowics, T.E., Rensberger, J.M., et al., 2004. Enamel microstructure and microstrain in the fracture of human and pig molar cusps. *Arch. Oral Biol.* 49, 595–605. Available from: <https://doi.org/10.1016/j.archoralbio.2004.01.016>.



- Ramanan, S.R., Venkatesh, R., 2004. A study of hydroxyapatite fibers prepared via sol-gel route. *Mater. Lett.* 58, 3320–3323. Available from: <https://doi.org/10.1016/j.matlet.2004.06.030>.
- Ritger, P.L., Peppas, N.A., 1987. A simple equation for description of solute release I. Fickian and non-Fickian release from non-swellable devices in the form of slabs, spheres, cylinders or discs. *J. Control. Release* 5, 23–36. Available from: [https://doi.org/10.1016/0168-3659\(87\)90034-4](https://doi.org/10.1016/0168-3659(87)90034-4).
- Roeder, R.K., Converse, G.L., Leng, H., Yue, W., 2006. Kinetic effects on hydroxyapatite whiskers synthesized by the chelate decomposition method. *J. Am. Ceram. Soc.* 2096–2104. Available from: <https://doi.org/10.1111/j.1551-2916.2006.01067.x>.
- Rueggeberg, F.A., Caughman, W.F., Curtis, J.W., Davis, H.C., 1993. Factors affecting cure at depths within light-activated resin composites. *Am. J. Dent.* 6, 91–95.
- Ruyter, I.E., Oysaet, H., 1982. Conversion in different depths of ultraviolet and visible light activated composite materials. *Acta Odontol. Scand.* 40, 179–192. Available from: <https://doi.org/10.3109/00016358209012726>.
- Sachdeva, S., Kapoor, P., Ak, T., Noor, R., 2015. Nano-composite dental resins: an overview. *Ann. Dent. Spec.* 3, 52–55.
- Santos, C., Luklinska, Z., Clarke, R., 2001. Hydroxyapatite as a filler for dental composite materials: mechanical properties and in vitro bioactivity of composites. *J. Mater.* 2, 565–573.
- Santos, C., Clarke, R.L., Braden, M., Guitian, F., Davy, K.W.M., 2002. Water absorption characteristics of dental composites incorporating hydroxyapatite filler. *Biomaterials* 23, 1897–1904. Available from: [https://doi.org/10.1016/S0142-9612\(01\)00331-3](https://doi.org/10.1016/S0142-9612(01)00331-3).
- Santos, M.H., De Oliveira, M., Souza, L.P.D.F., Mansur, H.S., Vasconcelos, W.L., 2004. Synthesis control and characterization of hydroxyapatite prepared by wet precipitation process. *Mater. Res.* 7, 625–630. Available from: <https://doi.org/10.1590/S1516-14392004000400017>.
- dos Santos, G.B., Alto, R.V.M., Filho, H.R.S., da Silva, E.M., Fellows, C.E., 2008. Light transmission on dental resin composites. *Dent. Mater.* 24, 571–576. Available from: <https://doi.org/10.1016/j.dental.2007.06.015>.
- Schmalz, G., 2009. Resin-based composites. *Biocompatibility of Dental Materials*. Springer, Berlin, Heidelberg, pp. 99–137. Available from: [https://doi.org/10.1007/978-3-540-77782-3\\_5](https://doi.org/10.1007/978-3-540-77782-3_5).
- Schneider, L.F.J., Cavalcante, L.M., Silikas, N., 2010. Shrinkage stresses generated during resin-composite applications: a review. *J. Dent. Biomech.* 2010. Available from: <https://doi.org/10.4061/2010/131630>.
- Shortall, A.C., 2005. How light source and product shade influence cure depth for a contemporary composite. *J. Oral Rehabil.* 32, 906–911. Available from: <https://doi.org/10.1111/j.1365-2842.2005.01523.x>.
- Si, J., Cui, Z., Wang, Q., Liu, Q., Liu, C., 2016. Biomimetic composite scaffolds based on mineralization of hydroxyapatite on electrospun poly( $\epsilon$ -caprolactone)/nanocellulose fibers. *Carbohydr. Polym.* 143, 270–278. Available from: <https://doi.org/10.1016/j.carbpol.2016.02.015>.
- Silikas, N., Eliades, G., Watts, D.C., 2000. Light intensity effects on resin-composite degree of conversion and shrinkage strain. *Dent. Mater.* 16, 292–296. Available from: [https://doi.org/10.1016/S0109-5641\(00\)00020-8](https://doi.org/10.1016/S0109-5641(00)00020-8).
- Sodagar, A., Akhavan, A., Hashemi, E., Arab, S., Pourhajibagher, M., Sodagar, K., et al., 2016. Evaluation of the antibacterial activity of a conventional orthodontic composite containing silver/hydroxyapatite nanoparticles. *Prog. Orthod.* 17, 40. Available from: <https://doi.org/10.1186/s40510-016-0153-x>.

- Söderholm, K.J., Mukherjee, R., Longmate, J., 1996. Filler leachability of composites stored in distilled water or artificial saliva. *J. Dent. Res.* 75, 1692–1699. Available from: <https://doi.org/10.1177/00220345960750091201>.
- Sopyan, I., Mel, M., Ramesh, S., Khalid, K.A., 2007. Porous hydroxyapatite for artificial bone applications. *Sci. Technol. Adv. Mater.* 8, 116–123. Available from: <https://doi.org/10.1016/j.stam.2006.11.017>.
- Su, Y., Li, G., Lian, J., 2012. A chemical conversion hydroxyapatite coating on AZ60 magnesium alloy and its electrochemical corrosion behaviour. *Int. J. Electrochem. Sci.* 7, 11497–11511.
- Suchanek, K., Bartkowiak, A., Gdowik, A., Perzanowski, M., Kąc, S., Szaraniec, B., et al., 2015. Crystalline hydroxyapatite coatings synthesized under hydrothermal conditions on modified titanium substrates. *Mater. Sci. Eng. C* 51, 57–63. Available from: <https://doi.org/10.1016/j.msec.2015.02.029>.
- Tamareseelvy, K., Rueggeberg, F.A., 1994. Dynamic mechanical analysis of two crosslinked copolymer systems. *Dent. Mater.* 10, 290–297. Available from: [https://doi.org/10.1016/0109-5641\(94\)90036-1](https://doi.org/10.1016/0109-5641(94)90036-1).
- Tanahashi, M., Kamiya, K., Suzuki, T., Nasu, H., 1992. Fibrous hydroxyapatite grown in the gel system: effects of pH of the solution on the growth rate and morphology. *J. Mater. Sci. Mater. Med.* 3, 48–53. Available from: <https://doi.org/10.1007/BF00702944>.
- Tas, A.C., 2007. Formation of calcium phosphate whiskers in hydrogen peroxide (H<sub>2</sub>O<sub>2</sub>) solutions at 90°C. *J. Am. Ceram. Soc.* 90, 2358–2362. Available from: <https://doi.org/10.1111/j.1551-2916.2007.01768.x>.
- Tilbrook, D.A., Clarke, R.L., Howle, N.E., Braden, M., 2000. Photocurable epoxy-polyol matrices for use in dental composites I. *Biomaterials* 21, 1743–1753. Available from: [https://doi.org/10.1016/S0142-9612\(00\)00059-4](https://doi.org/10.1016/S0142-9612(00)00059-4).
- Tobolsky, A.V., Leonard, F., Roeser, G.P., 1948. Use of polymerizable ring compounds in constant volume polymerizations. *J. Polym. Sci.* 3, 604–606. Available from: <https://doi.org/10.1002/pol.1948.120030415>.
- Truffier-Boutry, D., Demoustier-Champagne, S., Devaux, J., Biebuyck, J.J., Mestdagh, M., Larbanois, P., et al., 2006. A physico-chemical explanation of the post-polymerization shrinkage in dental resins. *Dent. Mater.* 22, 405–412. Available from: <https://doi.org/10.1016/j.dental.2005.04.030>.
- Uhl, A., Mills, R.W., Jandt, K.D., 2003. Photoinitiator dependent composite depth of cure and Knoop hardness with halogen and LED light curing units. *Biomaterials* 24, 1787–1795. Available from: [https://doi.org/10.1016/S0142-9612\(02\)00532-X](https://doi.org/10.1016/S0142-9612(02)00532-X).
- Van Landuyt, K.L., Nawrot, T., Geebelen, B., De Munck, J., Snauwaert, J., Yoshihara, K., et al., 2011. How much do resin-based dental materials release? A meta-analytical approach. *Dent. Mater.* 27, 723–747. Available from: <https://doi.org/10.1016/j.dental.2011.05.001>.
- Weiner, S., Wagner, H.D., 1998. The material bone: structure mechanical function relations. *Annu. Rev. Mater. Sci.* 28, 271–298. Available from: <https://doi.org/10.1146/annurev.matsci.28.1.271>.
- Weinmann, W., Thalacker, C., Guggenberger, R., 2005. Siloranes in dental composites. In: *Dental Materials*, pp. 68–74. <https://doi.org/10.1016/j.dental.2004.10.007>.
- Wiggins, K.M., Hartung, M., Althoff, O., Wastian, C., Mitra, S.B., 2004. Curing performance of a new-generation light-emitting diode dental curing unit. *J. Am. Dent. Assoc.* 135, 1471–1479. Available from: <https://doi.org/10.14219/jada.archive.2004.0059>.



- Willems, G., Lambrechts, P., Braem, M., Celis, J.P., Vanherle, G., 1992. A classification of dental composites according to their morphological and mechanical characteristics. *Dent. Mater.* 8, 310–319. Available from: [https://doi.org/10.1016/0109-5641\(92\)90106-M](https://doi.org/10.1016/0109-5641(92)90106-M).
- Wu, Y., Hench, L.L., 2004. Preparation of hydroxyapatite fibers by electrospinning technique. *Commun. Am. Ceram. Soc.* 1991, 1988–1991. Available from: <https://doi.org/10.1111/j.1151-2916.2004.tb06351.x>.
- Wu, J., Weir, M.D., Zhang, Q., Zhou, C., Melo, M.A.S., Xu, H.H.K., 2016a. Novel self-healing dental resin with microcapsules of polymerizable triethylene glycol dimethacrylate and N,N-dihydroxyethyl-p-toluidine. *Dent. Mater.* 32, 294–304. Available from: <https://doi.org/10.1016/j.dental.2015.11.014>.
- Wu, J., Weir, M.D., Melo, M.A.S., Strassler, H.E., Xu, H.H.K., 2016b. Effects of water-aging on self-healing dental composite containing microcapsules. *J. Dent.* 47, 86–93. Available from: <https://doi.org/10.1016/j.jdent.2016.01.008>.
- Yang, L., Liu, Q., Liang, T., Yin, J., Qin, L., Tang, Y., et al., 2011. Hydrothermal synthesis of hydroxyapatite urchins and its drug release property. *Adv. Mater. Res.* 311–313, 1681–1684. Available from: <https://doi.org/10.4028/www.scientific.net/AMR.311-313.1681>.
- Yoshimura, M., Suda, H., 1994. Hydrothermal processing of hydroxyapatite past present and future. *Hydroxyapatite and Related Materials*. CRC Press, Boca Raton, FL, pp. 45–72.
- Yoshimura, M., Suda, H., Okamoto, K., Ioku, K., 1994. Hydrothermal synthesis of biocompatible whiskers. *J. Mater. Sci.* 29, 3399–3402. Available from: <https://doi.org/10.1007/BF00352039>.
- Zeitz, C., Faidt, T., Grandthyll, S., Hähl, H., Thewes, N., Spengler, C., et al., 2016. Synthesis of hydroxyapatite substrates: bridging the gap between model surfaces and enamel. *ACS Appl. Mater. Interf.* 8, 25848–25855. Available from: <https://doi.org/10.1021/acsami.6b10089>.
- Zhang, H., Darvell, B.W., 2010. Constitution and morphology of hydroxyapatite whiskers prepared using amine additives. *J. Eur. Ceram. Soc.* 30, 2041–2048. Available from: <https://doi.org/10.1016/j.jeurceramsoc.2010.04.013>.
- Zhang, H., Darvell, B.W., 2011. Morphology and structural characteristics of hydroxyapatite whiskers: effect of the initial Ca concentration, Ca/P ratio and pH. *Acta Biomater.* 7, 2960–2968. Available from: <https://doi.org/10.1016/j.actbio.2011.03.020>.
- Zhang, H., Darvell, B.W., 2012a. Mechanical properties of hydroxyapatite whisker-reinforced bis-GMA-based resin composites. *Dent. Mater.* 28, 824–830. Available from: <https://doi.org/10.1016/j.dental.2012.04.030>.
- Zhang, H., Darvell, B.W., 2012b. Failure and behavior in water of hydroxyapatite whisker-reinforced bis-GMA-based resin composites. *J. Mech. Behav. Biomed. Mater.* 10, 39–47. Available from: <https://doi.org/10.1016/j.jmbbm.2012.02.021>.
- Zhang, H., Wang, Y., Yan, Y., Li, S., 2003. Precipitation of biocompatible hydroxyapatite whiskers from moderately acid solution. *Ceram. Int.* 29, 413–418. Available from: [https://doi.org/10.1016/S0272-8842\(02\)00153-0](https://doi.org/10.1016/S0272-8842(02)00153-0).
- Zhang, H., Zhang, M., Shen, Y., Pan, H., Zhang, K., Lu, W.W., 2010. Biocompatibility and bioactivity of hydroxyapatite whiskers reinforced bis-GMA based composites. In: 2010 3rd Int. Conf. Biomed. Eng. Informatics, IEEE, pp. 1640–1644. Available from: <https://doi.org/10.1109/BMEI.2010.5639603>.

Molecular study of  
simulated body fluid and  
temperature on  
polyurethane/graphene  
polymeric nanocomposites:  
calcium carbonate and  
polymethyl methacrylate  
using dynamics modeling  
by Monte Carlo for  
applications in bone  
regeneration

Juan-Ramón Campos-Cruz<sup>1</sup>, Norma-Aurea Rangel-Vázquez<sup>1</sup> and  
Ricardo Rangel-Vázquez<sup>2</sup>

<sup>1</sup>National Institute of Technology of Mexico/Aguascalientes Institute of Technology,  
Aguascalientes, Mexico <sup>2</sup>PCC, Haciendas Ave., Aguascalientes, Mexico

## 10.1 INTRODUCTION

### 10.1.1 POLYMERS

The polymeric materials are based on large molecules formed by covalent bonds and constituted by the union of many simple units (monomer). Monomers are the basic units for the formation of polymeric materials, and depending on how they are bonded they can give linear or nonlinear structures. Actually, the great utility of polymers is that they can synthesize the polymer that meets a series of properties that are needed (hardness, plasticity, density, etc.). The properties of any polymeric material are directly or indirectly bonded to its molecular structure. That is, they are a consequence of the structuring of the macromolecules that

constitute a specific material and, in many cases, are a reflection of the dynamic processes that are given at molecular scale (Alemán and Muñoz-Guerra, 2003).

### 10.1.1.1 Polyurethane

Polyurethanes (PUs) are synthesized from the exothermic reaction of molecules containing at least two isocyanate groups ( $\text{N}=\text{C}=\text{O}$ ) with molecules having active hydrogen atoms, the polyols being the most important because the structure contains between two and eight hydroxyl (OH) groups. The isocyanate group reacts with hydrogen atoms bound to more electronegative atoms than carbon. A relatively limited number of isocyanates and polyols are required to satisfy the requirements of both physical and chemical properties. The adequate use of different types of catalysts, surfactants, and other additives allows the synthesis of the suitable polymer. The chemical structure of PU is shown in Fig. 10.1.

According to the types of isocyanate (aromatic or aliphatic) and polyol (polyether or polyester), materials of different characteristics are obtained: flexible and rigid foams, thermosetting and thermoplastic elastomers, adhesives, coatings, sealants, fibers, inks, and material compounds (Quintero and Gómez, 2007).

#### 10.1.1.1.1 Polyurethane properties

PUs are block copolymers that are used as biomaterials because of their good biocompatibility and chemical and structural versatility, characteristics that make possible with a huge variety of properties. However, certain PUs are susceptible to hydrolytic and oxidative degradation under physiological conditions, a property that allows the development of temporary applications in regenerative medicine.

PUs are composed of soft segments that are grouped into soft domains with glass transition temperature below room temperature (viscous or gummy phase), and hard blocks or segments that form hard domains with a transition temperature



FIGURE 10.1

PU chemical structure in where, ● oxygen, ● carbon, ○ hydrogen, and ● nitrogen atoms, respectively.

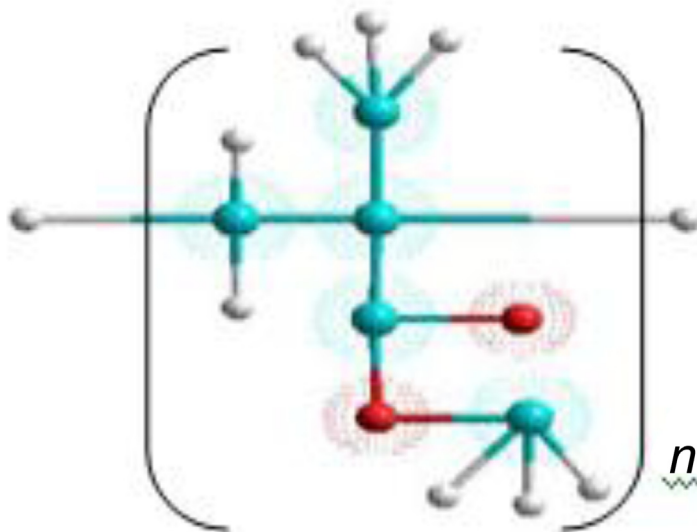
(glass or melting) above room temperature (glass phase). The soft segments (polyethers, polyesters, polyester ester, polycarbonates, or polysiloxanes) provide flexibility, while the hard segments (blocks with urethane, urea, amide, or aromatic rings) act as points of physical reversible cross-linking by crystallization and/or molecular association. The morphology of PU systems is a principal factor in the final properties of the materials.

The attraction forces between the soft segments are of the van der Waals type, whereas the hard segments interact mainly by hydrogen bond between urethane groups and  $\pi$  stacking between aromatic rings of adjacent chains generating that these interactions are directly related to the cohesive energy of the functional groups and also determine the microstructure, physicochemical properties, and mechanical behavior of PU. While permanent implantable devices require PUs with high biostability to avoid failure, synthetic tissue engineering extracellular matrices are temporary and bioresorbable polymers are required whose degradation products are reabsorbed *in vivo* by complete elimination by metabolic pathways without residual side effects (Caracciolo and Abraham, 2015).

#### 10.1.1.1.2 Polyurethane applications

PUs represent the most versatile materials for application in biomedical devices. To illustrate this variety, the following are some applications of PU systems more relevant in different biomedical fields:

- Cardiovascular surgery (mainly bistable PUs). Cardiac pacemaker insulation, cardiac assistance devices, total artificial heart, small diameter vascular grafts (less than 6 mm), membranes for pericardial and myocardial repair, intravenous and multilumen catheters, cardiac valves, intraaortic balloons, coating with antitumor agents.
- Reconstructive surgery. Materials for wounds and ulcers, tissue adhesives, breast implants.
- Orthopedic surgery and traumatology. Replacements for bone defect correction, bone regeneration, and for replacement of nucleus pulposus in intervertebral disc, injectable cements for the treatment of vertebral compression fractures with osteoporosis kyphoplasty, matrices for regeneration or replacement of menisci.
- Tissue engineering (mainly bioresorbable PUs). Artificial skin, membranes for the treatment of periodontitis, prostheses of the esophagus and trachea, nerve regeneration channels.
- Controlled release of bioactive agents. Functional PU coatings (hydrophilic, hydrophobic, antimicrobial, nonthrombogenic, lubricants, drug releasers, heparinized catheters).
- Applications in medical supplies. Encapsulation of membranes in hemodialysis filters, oxygenators and hemoconcentrators, coating of probes and gloves (Caracciolo and Abraham, 2015).

**FIGURE 10.2**

PMMA chemical structure in where, ● oxygen, ● carbon, and ○ hydrogen atoms, respectively.

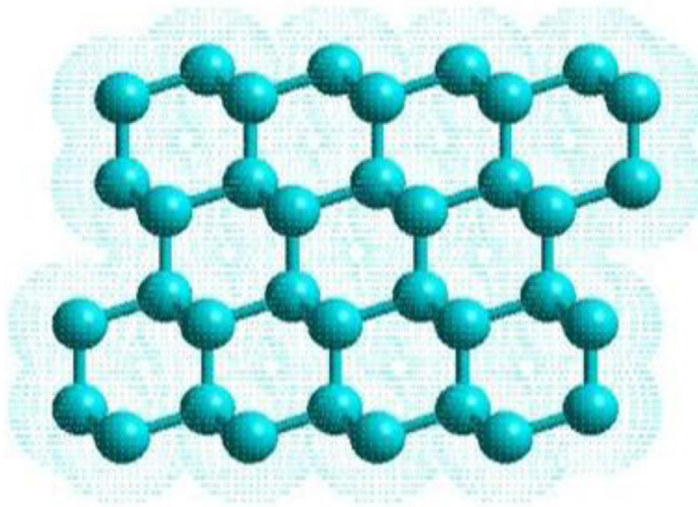
#### 10.1.1.2 Polymethyl methacrylate

Polymethyl methacrylate (PMMA) (see Fig. 10.2) is a hard, rigid, and transparent thermoplastic that has good resistance to weather conditions and is impact resistant. It is the most important material in the group of thermoplastics called acrylics (Cardona et al., 2011).

##### 10.1.1.2.1 Polymethyl methacrylate properties

PMMA is an amorphous polymer characterized by its transparency, tear strength, and elasticity. It is an isotropic material and significantly bioinert, is attacked only by mineral acids, but is resistant to alkalis, water, and most aqueous solutions of inorganic salts (Zivic et al., 2011). Also, PMMA is a tough thermoplastic, resistant, has excellent optical properties with high refractive index and good resistance to aging and the weather. It is a lightweight material with a density of  $1.19 \text{ kg/m}^3$ , and presents good mechanical resistance and stability. The transparency of this plastic is between 85% and 92%, a reason why it passes almost all the UV rays and its power of diffusion is almost null (Jaebelon, 2010).

PMMA is known as one of the most biocompatible polymers and is widely used in medical applications. It can usually be found in contact lenses and implantable ocular lenses due to the excellent optical properties, and in dialysis membranes, dentures, and maxillofacial prostheses. It also highlights its application as bone cement for prosthetic fixations as it is used as a fixation of the

**FIGURE 10.3**

Graphene structure.

prosthesis to the bone (Navarro et al., 2010). PMMA has been used as self-polymerizing bone cement in orthopedics since 1960 with the aim of fixing the orthopedic implants to the bones and transferring the mechanical loads of the implant to the bone (Zivic et al., 2011).

#### 10.1.1.3 Graphene

Graphene is a flat laminar structure in the form of a two-dimensional network with thickness of the order of one atom. The network is composed of densely packed carbon atoms with a bead-like conformation by covalent bonds that would be formed from the superposition of the  $sp^2$  hybrid bonds of the carbon atoms (Torres-Silva and López-Bonilla, 2011). Graphene can be visualized as a hexagonal network on an atomic scale, made up of carbon atoms with bonds of approximately 0.142 nm in length, as shown in Fig. 10.3 (Paul and Sharma, 2011). The structure of graphene is composed of two equivalent subnetworks of carbon atoms bonded together with sigma bonds. Each carbon atom in the network has a  $\pi$  orbital that contributes to a delocalized network of electrons (Zhu et al., 2010).

##### 10.1.1.3.1 Graphene properties

Graphene is a two-dimensional nanometric structure of strongly cohesive carbon atoms on a uniform, slightly flat, undulating surface. From this particular configuration or arrangement, its electronic, mechanical, and chemical properties (Liu et al., 2012) are obtained, including high thermal conductivity, high electrical

conductivity, high transparency, high mechanical resistance, inherent flexibility, and large specific surface area (Xue et al., 2012).

- Thermal conductivity. The thermal conductivity of graphene is dominated by phonons and has been measured at approximately 5000 W/mK; copper at room temperature has a thermal conductivity of 401 W/mK. Therefore the heat conduction of graphene is 10 times better than copper.
- Electrical conductivity. The conductivity of a two-dimensional sheet of material is given by  $\sigma = en\mu$ . The mobility is theoretically limited to  $\mu = 200,000 \text{ cm}^2/\text{Vs}$  by acoustic phonons at a carrier density of  $n = 10^{12}/\text{cm}^2$ . The resistivity of a 2D sheet, also called the resistance per square, is then  $31 \Omega$ . Using the thickness of the layer, a conductivity greater than  $0.96 \times 10^6/\Omega \text{ cm}$  is obtained for the graphene. This is somewhat higher than copper conductivity, which is  $0.60 \times 10^6/\Omega \text{ cm}$ .
- Density. The hexagonal unit of graphene contains two carbon atoms and has an area of  $0.052 \text{ nm}^2$ . Therefore its density can be calculated as  $0.77 \text{ mg/m}^2$ .
- Transparency. Graphene is almost transparent, absorbing only 2.3% of the light intensity, independently of the wavelength in the optical domain, with the result being that the suspended graphene does not present any color.
- Strength. Graphene has breaking strength of 42 N/m. A hypothetical steel film of the same thickness as graphene would have a tear strength of 0.084–0.40 N/m. Therefore, graphene is more than 100 times stronger than the stronger steel (Shekhawat and Ritchie, 2015).

Graphene has many properties. It is more transparent than plastic, but conducts heat and electricity better than any metal, is an elastic film, behaves like a waterproof membrane, and is chemically inert and stable, which is why it appears to be the ideal transparent electric conductor of the next generation. In the area of energy, graphene provides new solutions to current challenges related to the generation and storage of energy with nano-enhanced products. Graphene based systems are used for the production of photovoltaic energy, fuel cells, and energy storage (supercapacitors, batteries, and storage of hydrogen) (Ferrari et al., 2015).

#### 10.1.1.4 Calcium carbonate

Calcium carbonate (CC) ( $\text{CaCO}_3$ ) is found in crystalline state as calcite with hexagonal structure and aragonite of rhombohedral form. The CC is obtained from the limestone rocks through various methods such as grinding or calcium precipitation, obtaining lower levels of impurities with a homogeneous morphological structure.

##### 10.1.1.4.1 Calcium carbonate properties

CC nanoparticles are employed in a controlled release system due to slow biodegradation as well as the ease of encapsulating various drugs as bioactive proteins. With regard to cytotoxicity, it has been shown that bone cement synthesized from CC shows no effect on osteoprogenitor cells of the bone marrow. The CCs have



excellent properties of biocompatibility, osteoconductivity, and are reabsorbable in the organism producing a regeneration of bone tissue when they are used as biomedical cement (Maleki-Dizaj et al., 2015).

## 10.1.2 PROSTHESIS

Biomedical implants and prostheses are artificial replacements of original structural components of a biological system, such as the human body, that try to supplant the function of the original element. Depending on the use, these artificial replacements can be constructed of metallic, polymeric, ceramic materials, or combinations thereof. Once implanted in the organism, each of these materials is subject to specific degradation processes. The first requirement for implanting a material in the body is its biocompatibility, equivalent to the absence of organic rejection. The material must support the body environment without degrading to a point that conspires against the fulfillment of its functional objective (Nag and Banerjee, 2012).

### 10.1.2.1 Materials

The classification of the biomaterials is carried out according to the behavior when they are implanted or according to their chemical nature. Although several products may be combined in the design of a prosthesis, three major groups may be established depending on the chemical nature of the synthetic biomaterials: metals, ceramics, and polymers.

#### 10.1.2.1.1 Metals

Among the most used metals in the manufacture of prostheses are different kinds of stainless steels; alloys such as Co–Cr, Co–Cr–Mo, Co–Cr–Ni; as well as titanium and various alloys based on titanium, aluminum, and vanadium. Today, there is a variety of chemical compositions for stainless steel used in medicine; for example, type 302 (Fe/Cr<sub>18</sub>/Ni<sub>8</sub>) or 316 L type (Fe/Cr<sub>18</sub>/Ni<sub>10</sub>/Mo<sub>3</sub>), which in its composition incorporates molybdenum, which improves corrosion resistance. The introduction of titanium and its alloys (e.g., Ti<sub>6</sub>Al<sub>4</sub>V) has extended the field of application of metals.

#### 10.1.2.1.2 Ceramics

Although ceramics are attractive as biomaterials, they are mechanically weak; this phenomenon lies in the fact that they are chemically inert materials, do not usually trigger unwanted responses in the tissue in which they are implanted, and are not susceptible to microbial attack. They are very resistant to wear and generally behave as good thermal and electrical insulation. All these properties are advantageous for the development of bone prostheses. This term includes alumina (aluminum oxide), hydroxyapatite, calcium phosphates, such as [Ca<sub>3</sub>(PO<sub>4</sub>)<sub>2</sub>]<sub>3</sub>Ca(OH)<sub>2</sub>, different forms of carbon and so-called bioglass (whose composition is based in SiO<sub>2</sub>–CaO–Na<sub>2</sub>O–P<sub>2</sub>O<sub>5</sub>, and some containing MgO and K<sub>2</sub>O).



### 10.1.2.1.3 Polymers

A wide variety of polymers can be used as biomaterials because the physical properties and chemical stability of these depend on a set of variables such as the chemical composition of the polymer and the degree of cross-linking. One of the advantages they present is that they can be endowed with a wide variety of properties by the introduction of chemical additives, macromolecules, or second phases. The shape, the structure, the texture, the rigidity, and the flexibility are properties that can determine their use (Singh, 2011).

## 10.1.3 SIMULATED BODY FLUID

Simulated body fluid (SBF) of the human body is also known as Hanks' solution, which consists of a culture medium used in biomedical research for cell preservation. This fluid is constituted according to the composition shown in Table 10.1. SBF of the human body is a solution containing concentrations of ions analogous to those of human blood plasma. Its formulation has been reported and optimized by Kokubo et al., and is used as a culture medium for cell preservation, allowing prediction of the bioactivity of materials such as polymers (De-Souza et al., 2014).

## 10.1.4 COMPUTATIONAL CHEMISTRY

Computational chemistry is an area of chemistry that makes use of mathematical models to simulate the interactions between the atoms of substances and thus solve problems of a chemical nature (Leiva and Estrín, 2011). It is born from the need to understand important aspects that cannot be solved in a practical way, as it is to know intermediate states in reactions that are carried out quickly, to know the behavior of a material at very high temperatures that are very difficult to reach in a laboratory, or simply to calculate properties in systems of high cost. Thus, computational chemistry is an application of new computational technologies and mathematics to understand a chemical system.

Previously, theoretical chemistry explained chemical phenomena through classical physics, however, its research and development innovated to include

**Table 10.1** Components of the Hanks Solution or SBF

Reactive	g/L	Reactive	g/L
NaCl	8.00	MgCl <sub>2</sub> ·6H <sub>2</sub> O	0.10
KCl	0.40	Na <sub>2</sub> HPO <sub>4</sub> ·2H <sub>2</sub> O	0.06
NaHCO <sub>3</sub>	0.35	KH <sub>2</sub> PO <sub>4</sub>	0.06
Glucose	1.00	MgSO <sub>4</sub> ·7H <sub>2</sub> O	0.06
CaCl <sub>2</sub> ·2H <sub>2</sub> O	0.19		

quantum physics, which is based on Erwin Schrödinger's equations, including calculations and advanced mathematics that required the use of tools for resolution. But it was not until the early 1970s when quantum models were used to solve and calculate molecular properties. The results obtained through computational chemistry have led to its use not only in the basic aspects of theoretical chemistry, but also in fields such as pharmacology, molecular biology, and organic and inorganic chemistry, to name a few.

The last Nobel Prize for computational chemistry work reaffirms the importance of this area of science. This was awarded in 2013 to researchers Martin Karplus, Michael Levitt, and Arieh Warshel for the development of computational models for the description of complex chemical systems (Development of Multiscale Models for Complex Chemical Systems); these researchers adequately combined classical theories and quantum physics and chemistry for such research. Today's computational chemistry comprises areas of chemistry, biology, and physics coupled with computation, which allows for the investigation of atoms, molecules, and macromolecules through a computer system. This type of analysis is usually carried out when laboratory research is inappropriate, impractical, or impossible due to the extreme conditions of such experiments (high temperatures, vacuum conditions, etc.), or the high costs that are generated.

In general terms, it is a discipline that encompasses all aspects of chemistry research that benefit from the application of computers, including aspects such as molecular modeling, computational methods, computer-aided molecular design, chemical databases, organic synthesis design, the search of data on chemical bases, or control of equipment for chemical analysis. The main purpose of computational chemistry is to predict all kinds of molecular properties of chemical systems using physicochemistry, molecular physics, and quantum physics.

To be able to apply this, it is necessary to have basic knowledge of the fundamentals of theoretical methods, ability to critically analyze the results, ability to manage software, and access to hardware resources optimized for calculation. As already mentioned, computational chemistry encompasses a wide range of mathematical methods that can be divided into two broad categories (Valles-Sánchez et al., 2014).

#### 10.1.4.1 *Molecular mechanics*

Models of molecular mechanics (MM) or force fields (see Fig. 10.4) describe electronic energy as a parametric function of nuclear coordinates. The building blocks in the force field methods are atoms, that is, the electrons are not considered as individual particles. This means that the union information must be provided explicitly, rather than being the result of solving Schrödinger's equation. The quantum aspects of the nuclear movement are also neglected. That is, the dynamics of atoms are treated by classical mechanics, that is, Newton's second law.

For phenomena independent of time, the problem is reduced to calculating the energy in a given geometry. Often, the focus is on the search for stable molecule geometries and/or different conformations. The problem is then reduced to the

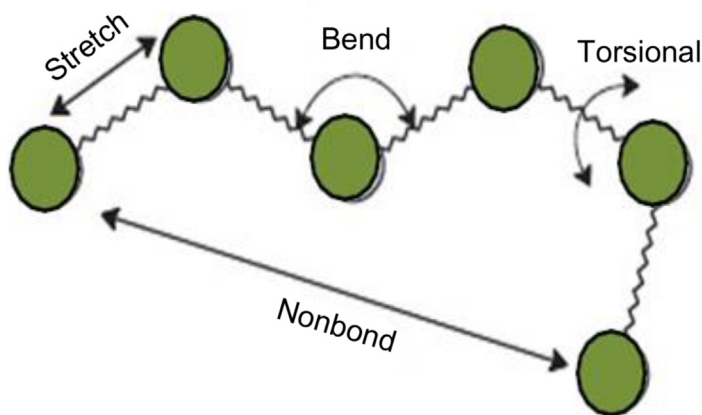
**FIGURE 10.4**

Illustration of the energy terms of the force field.

search for energy minima (and possibly also some first-order saddle points) on the potential energy surface. In these methods molecules are described by spheres and springs model, with atoms having different sizes and bonds having different bonding lengths and forces.

The basis of force field methods is the consideration that molecules tend to be composed of units that are structurally similar in different molecules. The image that molecules consisting of structural units (functional groups) behaving similarly in different molecules forms the very basis of organic chemistry (Jensen, 2007).

#### 10.1.4.2 Quantum mechanics

Quantum mechanics (QM) is the correct mathematical description of the behavior of electrons and therefore of chemistry. In theory, QM can accurately predict any property of an atom or molecule. In practice, the QM equations have only been solved exactly for one-electron systems. A large number of methods have been developed to approach the solution of multiple electron systems. Two formulations of the QM were developed by Schrödinger and Heisenberg. The following is the contribution of Schrödinger as it is the basis of almost all methods of computational chemistry. The time-independent Schrödinger equation can be written as presented in Eq. (10.1):

$$\hat{H}\psi = i\hbar \frac{\partial \psi}{\partial t} \quad (10.1)$$

The corresponding Hamiltonian operator is represented by Eq. (10.2) as shown:

$$H = -\sum_i \frac{1}{2} \nabla_i^2 - \sum_k \frac{1}{2M_k} \nabla_k^2 - \sum_i \sum_k \frac{Z_k}{r_{ik}} + \sum_{i < j} \frac{1}{r_{ij}} + \sum_{k < l} \frac{Z_k Z_l}{r_{kl}} \quad (10.2)$$

Where the first term is the sum of the kinetic energy of the  $i$ th electron; the second term is the sum of the kinetic energy of the  $k$ -order nucleus; the third term is the sum of the Coulomb interaction of the  $i$ th electron and the  $k$ th nucleus; the fourth term is the sum of the Coulomb interaction of the  $i$ th and  $j$ th electron of the electron; and the fifth term is the sum of the Coulomb interaction of the  $k$ th nucleus and the  $l$ th nucleus. The expression is written here in dimensionless form or atomic units.

A complete description of a system requires a solution of the Schrödinger equation, which includes both electronic and nuclear degrees of freedom. Since the nuclei are heavier than the electrons, then the electronic and nuclear coordinates are separated in Eq. (10.1). This is known as the Born–Oppenheimer approximation. The wave function is separated into the nuclear wave function and the electronic wave function. The electronic Schrödinger equation can be written as shown in Eq. (10.3).

$$\hat{H}_e \psi(R, r) = E_e \psi(R, r) \quad (10.3)$$

With:

$$\hat{H}_e = - \sum_i \frac{1}{2} \nabla_i^2 - \sum_i \sum_k \frac{Z_k}{r_{ik}} + \sum_{i < j} \frac{1}{r_{ij}} \quad (10.4)$$

To further reduce the method for solving the Schrödinger equation, it can be assumed that there is no interaction between the electrons in the system. Therefore, the Hamiltonian of the system is simplified to:

$$\hat{H} = \sum_i \hat{h}_i \quad (10.5)$$

where

$$\hat{h}_i = - \frac{1}{2} \nabla_i^2 - \sum_k \frac{Z_k}{r_{i,k}} \quad (10.6)$$

If the system falls under the weak coupling regime of electronic correlation, the problem of many bodies can be assigned to a single particle problem under an effective theory average field. Among the theoretical middle-field methods, the most popular method is based on the Hartree–Fock (HF) theory that uses the independent electron approach within the self-consistent field. The total wave function of a system of  $N$  electrons is constructed based on the assumption of independent movement of the electron. Because of Pauli’s exclusion principle, the wave function can be written through Slater’s determinant of the  $N$  orthonormal individual electron wave functions as shown in Eq. (10.7).

$$\psi_{SD} = \frac{1}{\sqrt{N!}} \begin{vmatrix} \chi_1(1) & \chi_2(1) & \cdots & \chi_N(1) \\ \chi_1(2) & \chi_2(2) & \cdots & \chi_N(2) \\ \vdots & \vdots & \ddots & \vdots \\ \chi_1(N) & \chi_2(N) & \cdots & \chi_N(N) \end{vmatrix} = |\chi_1 \chi_2 \chi_3 \cdots \chi_n\rangle \quad (10.7)$$

We can apply the Roothaan–Hall approximation for  $\varphi$ , and vary the  $c_{vi}$  coefficient to minimize the integral using the principle of energy variation, this leads to the determinant Eq. (10.8):

$$\sum_{i=1}^N (F_{\mu\nu} - \varepsilon_i S_{\mu\nu}) C_{vi} = 0 \quad (10.8)$$

Hence,

$$\begin{vmatrix} F_{11} - ES_{11} & F_{12} - ES_{12} & \cdots & F_{1N} - ES_{1N} \\ F_{21} - ES_{21} & F_{22} - ES_{22} & \cdots & F_{2N} - ES_{2N} \\ \vdots & \vdots & \ddots & \vdots \\ F_{N1} - ES_{N1} & F_{N2} - ES_{N2} & \cdots & F_{NN} - ES_{NN} \end{vmatrix} = 0 \quad (10.9)$$

$F_{\mu\nu}$  is represented by Eq. (10.10):

$$F_{\mu\nu} = \left\langle \mu \left| -\frac{1}{2} \nabla^2 \right| \nu \right\rangle - \sum_k Z_k \left\langle \mu \left| \frac{1}{r_k} \right| \nu \right\rangle + \sum_{\lambda\sigma} 2 \sum_{i=1}^{\text{occupied}} c_{\lambda i}^* c_{\sigma i} \left[ \left\langle \mu \nu \left| \frac{1}{r_{ij}} \right| \lambda \sigma \right\rangle - \frac{1}{2} \left\langle \mu \lambda \left| \frac{1}{r_{ij}} \right| \nu \sigma \right\rangle \right] \quad (10.10)$$

The HF method uses a single electronic wave function  $x$ , which assumes an electron moves independently in the average potential field. Therefore, the function of the electron correlation cannot be considered. Thus, the Slater determinant of the wave function used by the HF method satisfies the Pauli exclusion principle, and this part of the electron correlation is known as the interchange interaction. In general the electron correlation energy is defined as the difference between the “true” energy of the state and the energy of HF ( $E_{\text{corr}} = E - E_{\text{HF}}$ ).

#### 10.1.4.3 Monte Carlo

The Monte Carlo technique is a stochastic methodology in which the structural facts and the thermodynamic properties are obtained from averages. It tries to obtain a Boltzmann sampling of a system according to an algorithm that consists of generating random structures, evaluating its energy, and deciding from an appropriate criterion whether the new structure generated is accepted or discarded. The simplest Monte Carlo formalism is the Metropolis algorithm, in which the generation of new structures takes place at random, ensuring the microscopic reversibility of the system (Alemán and Muñoz-Guerra, 2003). This method starts from a given geometry, which is commonly a local minimum; new configurations are generated by adding a random perturbation to one or more atoms.

In Monte Carlo methods, the new geometry is accepted as the starting point for the next step if it is less energy than the current one. Otherwise, the Boltzmann factor  $e(-\Delta E/kT)$  is computed and compared with a random number between 0 and 1. If  $e(-\Delta E/kT)$  is less than this number, the new geometry is accepted; if not the next step is taken from the previous geometry. This generates a sequence of configurations from which geometries can be selected for further minimization. To have a reasonable acceptance ratio, however, the step size should be fairly small (Jensen, 2007).

## 10.1.5 MOLECULAR PROPERTIES

### 10.1.5.1 *Molecular energy*

Energy is one of the most useful concepts in science. Energy analysis can predict which molecular processes are likely to occur or which are not likely to occur.

All computational chemistry techniques define the energy in such a way that the system with the lowest energy is the most stable. Therefore, the search for the form of a molecule corresponds to the search for the form with the lowest energy. The amount of energy in a system is often divided into kinetic energy and potential energy. The kinetic energy can be separated in the movement of vibration, translation, and rotation. The potential energy can simply be expressed as Coulomb's law, or it can be divided into stretching and flexing energies of bonds, conformational energy, hydrogen bonds, and so on.

### 10.1.5.2 *Optimization geometry*

It is a technique of molecular modeling, whose objective is to obtain the conformation of lower energy. Given a potential energy function  $V$  that describes the curve of that energy and depends on one or more independent variables  $x_i$  (atomic coordinates), energy minimization is a nonlinear optimization problem in which we try to find the values of those variables that make the function have a minimum value, so that mathematically its derivative is equal to zero (Barnard, 2009).

### 10.1.5.3 *Quantitative structure–activity relationships properties*

Starting from basic chemical and physical theories, it is clear that there must be a connection between the structure of a molecule and its biological activity. It is also clear, however, that the connection is very complex, and it is highly unlikely that biological activity can never be completely predicted. Statistical methods are often used to correlate the molecular structure and properties of observed biological activity, hence quantitative structure–activity relationships (QSAR) thus provide a tool for predicting that novel modifications to compounds must be tested. A variety of molecular descriptors are included in a traditional QSAR study. Typically, these include a measure of lipophilicity (often taken as the partition coefficient between water and 1-octanol), the electron and steric substituent parameters (Hammett and Taft constants), and  $pK_{a/b}$  values for acidic and/or basic groups, molecular weight, IR frequencies, dipole moments, NMR chemical shifts, etc. have also been used (Jensen, 2007).

#### 10.1.5.3.1 Partition coefficient ( $\log P$ )

The partition coefficient is a parameter that measures the hydrophobicity of a molecule that affects the absorption, bioavailability, hydrophobic interactions between drug and receptor, metabolism, as well as toxicity (Andrés et al., 2015).

#### 10.1.5.4 Fourier-transform infrared spectroscopy

In infrared spectroscopy, the IR radiation is passed through a sample; part of the infrared radiation is absorbed by the sample and another part passes through it. The resulting spectrum represents molecular absorption and transmission, creating a molecular fingerprint of the sample. An infrared spectrum represents a fingerprint of the sample with absorption peaks corresponding to the frequencies of the vibrations between the bonds of the atoms that make up the material. Because each different material is a unique combination of atoms, there cannot be two compounds with exactly the same infrared spectrum (Barbes et al., 2014).

#### 10.1.5.5 Electrostatic potential maps

Electrostatics is the study of interactions between charges of the bodies. It is important for understanding the interactions of electrons, which are described by a wave function or electron density. Another very useful function is the electrostatic potential, which is a function that is defined at each point in the real three-dimensional space. If a charged particle is added to a system without disturbing it the energy of placing said particle at any point in space is the electrostatic potential moment of the charge of the particle.

The requirement that there is no movement of existing charges (electron density polarization) is described by stating that electrostatic potential is the energy of placing an infinitesimal point charge on the system (Young, 2001). Thus molecular electrostatic potential maps (MESP) are graphical representations of the electrostatic charges distributed in the molecules, that is to say, contour diagrams that by means of color variations symbolize the differences of electronic densities throughout the molecule.

---

## 10.2 METHODOLOGY

The calculation of the QSAR properties is done through the Compute menu located in the menu bar, in the drop-down window the QSAR Properties option is selected and the properties are calculated as the surface area, volume, mass, etc.

### 10.2.1 FOURIER-TRANSFORM INFRARED SPECTROSCOPY ANALYSIS

To perform the Fourier-transform infrared spectroscopy (FTIR) analysis, the menu bar is used to select the Compute option and then choose *Vibration, totation analysis option and then should apply the Vibration, totation analysis option*. When this is done, the message “Computing the force matrix” appears in the status line, followed by the percentage of progress. When the calculation ends the legend on the status line changes to, Calculating the vibrational spectrum. To obtain the infrared spectrum, select the Vibrational spectrum option located on the Compute menu of the menu bar.

### 10.2.2 ELECTROSTATIC POTENTIAL MAP

MESP is obtained from the menu bar and, from the Compute option, choose Plot Molecular Graphs, which opens the options window and from the top menu Molecular Properties is selected the property Electrostatic Potential with the 3D Mapped Isosurface modality, thus the MESP is shown as a three-dimensional contour. Subsequently the same window is changed to the Isosurface Rendering menu and the Translucent surface option is selected, so that the MESP can be viewed in a slightly transparent way and with it the structure of the molecule can be further observed and specifically detected in the areas of the molecule with greater or lesser electron density, that is, both nucleophilic and electrophilic zones. Finally, in this same window the Mapped Function Options menu is chosen from the option red to blue so that the colors of the MESP are red for electrophilic areas (susceptible to nucleophilic attacks), blue for nucleophilic zones (susceptible to electrophilic attacks), and green for neutral zones.

### 10.2.3 DETERMINATION OF THE EFFECT OF TEMPERATURE ON THE NANOCOMPOSITE

The effect of temperature (308.15K, 310.15K, and 313.15K) on the PU/G/PMMA and PU/G/CC nanocomposites was performed with the Monte Carlo simulation (see Fig. 10.5).

This tool was used from the Compute menu located in the menu bar, selecting the Monte Carlo alternative. This window specifies the temperature in degrees

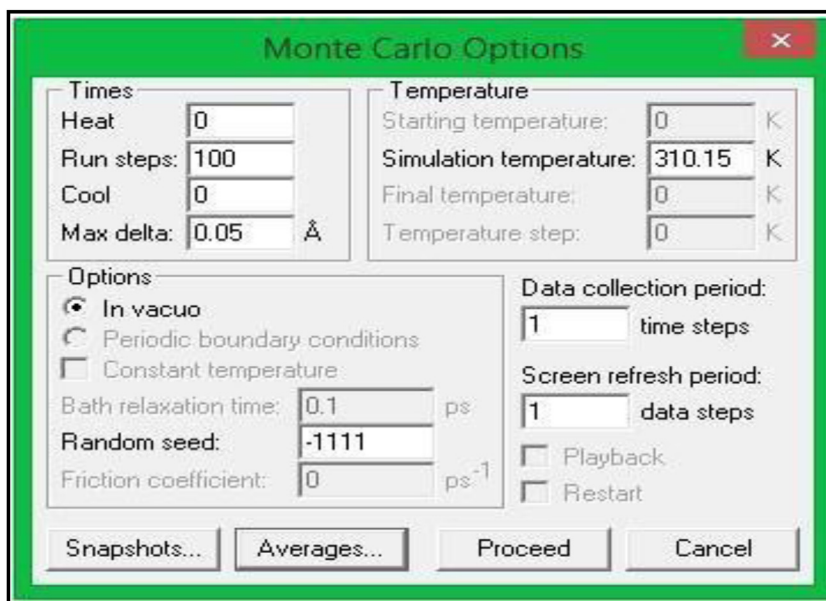


**FIGURE 10.5**

Monte Carlo options.



**Table 10.2** Hanks' Solution and Number of Molecules Calculated

Reactive	g/L	Number of Molecules	Reactive	g/L	Number of Molecules
NaCl	8.00	133	MgCl <sub>2</sub> ·6H <sub>2</sub> O	0.10	2
KCl	0.40	7	Na <sub>2</sub> HPO <sub>4</sub> ·2H <sub>2</sub> O	0.06	1
NaHCO <sub>3</sub>	0.35	6	KH <sub>2</sub> PO <sub>4</sub>	0.06	1
Glucose	1.00	17	MgSO <sub>4</sub> ·7H <sub>2</sub> O	0.06	1
CaCl <sub>2</sub> ·2H <sub>2</sub> O	0.19	3			

Kelvin at which the calculation will be performed, as well as the number of steps to be performed. Specifying this only selects the option Proceed, and thus starts the calculation. Once this is done, the MESP is calculated and the FTIR analysis is carried out.

## 10.2.4 SIMULATED BODY FLUID CHARACTERIZATION

The calculations of the SBF analysis were performed using MM with the AMBER model because the type of elements that make up the SBF are not parametrized for the semiempirical models of QM. Using the AMBER model the Gibbs free energy and optimization geometry was calculated, the FTIR was analyzed and the MESP was determined. The SBF composition was obtained by the Hanks solution as shown in [Table 10.2](#).

### 10.2.4.1 Determination of the effect of temperature and SBF on the nanocomposite

The molecular structure of the components of the Hanks solution and the PU/G/PMMA and PU/G/CC nanocomposite was analyzed by Monte Carlo simulation; free energy, FTIR, and MESP calculations were carried out to determine the effect of the temperature combination (308.15K, 310.15K, and 313.15K) and the SBF in the nanocomposites to find possible changes in these two systems and thus estimate the effect that FFS will have on the prosthesis.

## 10.3 RESULTS

### 10.3.1 POLYURETHANE/GRAPHENE/POLYMETHYL METHACRYLATE NANOCOMPOSITE

#### 10.3.1.1 Optimization geometry and partition coefficient

The calculations made with the Monte Carlo method determined the effect of the temperature in the nanocomposite in conjunction with the chemical composition

of the SBF were found the geometries shown in Fig. 10.6 for the temperatures of 308.15K, 310.15K, and 313.05K, which have Gibbs free energy ( $\Delta G$ ) of 1188.58, 1175.62, and 1187.84 Kcal/mol, respectively, and therefore, there is no spontaneous reaction between the SBF and the nanocomposite mainly because there is no formation of new hydrogen (Baena et al., 2004).

It was appreciated that the Gibbs free energy calculated at all three temperatures shows little variation between body temperature and the possible changes that could be experienced with respect to body temperature (310.15K) are 1.10% and 1.03% with respect to 308.15K and 313.15K, respectively, whereby the prosthesis has excellent thermodynamic stability.

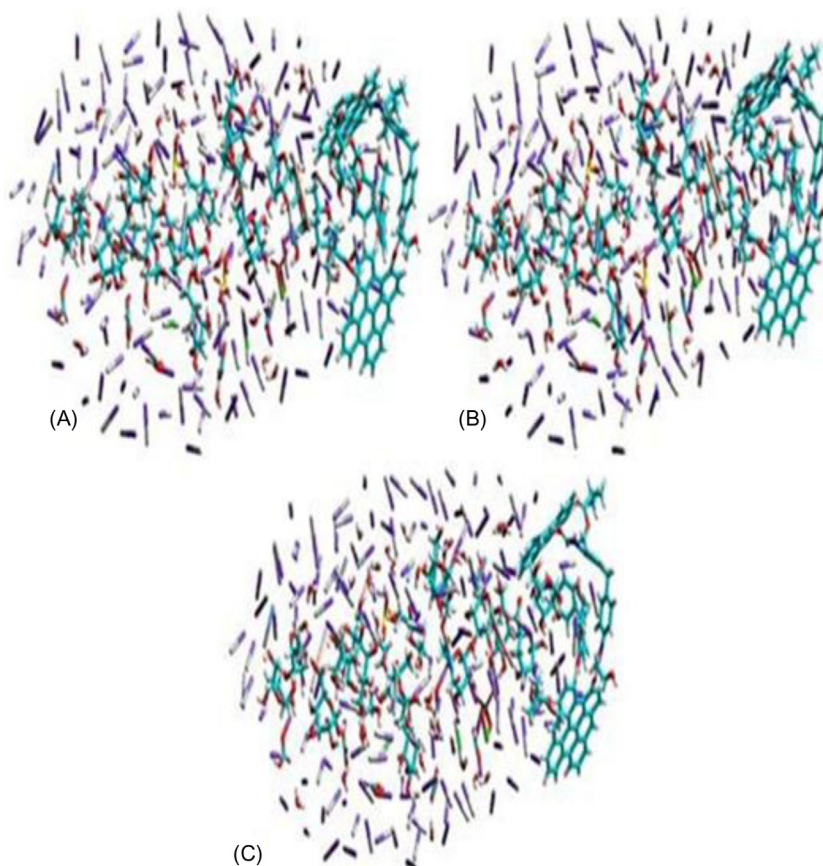


**FIGURE 10.6**

Optimized molecular geometry of the PU/G/PMMA nanocomposite in the presence of SBF at different temperatures: (A) 308.15K, (B) 310.15K, and (C) 313.15K, where hydrogen  $\circ$ , carbon  $\bullet$ , oxygen  $\bullet$ , sodium  $\bullet$ , chlorine  $\bullet$ , potassium  $\bullet$ , calcium  $\bullet$ , magnesium  $\bullet$ , phosphorus  $\bullet$ , sulfur  $\bullet$ , and nitrogen  $\bullet$ .

**Table 10.3**  $\Delta G$  and Log  $P$  Values of the PU/G/PMMA Nanocomposite in the Presence of SBF at Different Temperatures

Properties	Temperatures		
	35°C	37°C	40°C
$\Delta G$ (Kcal/mol)	1188.58	1175.62	1187.84
Log $P$	131.84	131.84	131.84

The three systems had a partition coefficient value of 131.84 as shown in Table 10.3 thus confirming the hydrophobic character, that is, the SBF would not have the ability to traverse the constituents of the nanocomposite and there would be no swelling by the rupture of intermolecular hydrogen bridges, and that would generate the hydrolysis of the unstable bonds causing the diminution of the mechanical, chemical, and physical properties (Comini et al., 2006). In addition, because of the chemical nature of the nanocomposite being a hydrocarbon chain, it is unable to form hydrogen bonds with water, that is, the introduction of any bond other than hydrogen into the water causes a disruption of the hydrogen bonding network between water molecules. Hence the hydrogen bonds are tangentially reoriented to the surface to minimize the disruption of the 3D hydrogen bonding of the water molecules and thus give rise to a cage-like structure in the water around the nonpolar surface; in this way the water molecules that form the cage restrict their mobility (Haselmeier et al., 1995).

### 10.3.1.2 Fourier-transform infrared spectroscopy

Table 10.4 shows the main frequencies in the infrared spectra of the PU/G/PMMA nanocomposite in the presence of SBF at different temperatures (308.15K, 310.15K, and 313.15K), where it is shown that there are no changes or displacements in the frequencies of the bonds of the chemical components of this system due to the rigidity of the graphene product of the hybridized orbital  $\sigma$ , which provides the structural and chemical stability by holding together the carbon atoms in the graphene and therefore the nanocomposite (Khenfouch et al., 2012).

Likewise, the vibrations of the cross-linking between the graphene and the PU in the range of 7896–7866 and 5308–4735  $\text{cm}^{-1}$  attributed to the symmetrical tension and the spinning bending of the OH bond. The PMMA uptake in the PU/G was observed between 7885–7852 and 5173–4870  $\text{cm}^{-1}$  corresponding to the symmetrical tension and shear flexion of the OH bond, respectively.

Minimal displacements are observed in the vibration frequencies, which do not influence the structure of the nanocomposite when in contact with the SBF and at the same time to thermal changes. This is due to the fact that the energy of the hydrogen bonds present in the nanocomposite is the main reason why they act as protectors of the structure and properties before temperature changes. As shown in Fig. 4.20, the molecules have covalent bonds resulting in the nanocomposite being insoluble in the SBF.

**Table 10.4** FTIR Analysis of the PU/G/PMMA Nanocomposite in the Presence of SBF at Different Temperatures

Bond	Molecule	Frequencies (cm <sup>-1</sup> )			Vibration
		Temperatures			
		35° C	37° C	40° C	
O—H	PU-Graphene	7889—7869	7896—7866	7895—7875	Symmetrical stretching
O—H	PMMA-graphene	7885—7852	7886—7880	7885—7884	Symmetrical stretching
O—H	H <sub>2</sub> O	5651—5534	5675—5535	5573—5537	Symmetrical and asymmetrical stretching
O—H	Glucose	5623—5574	5677—5578	5605—5577	Symmetrical stretching
O—H	PU	7011—7010	7011—7002	7011—7009	Symmetrical stretching
N—H	PU	6258—6249	6253—6250	6275—6245	Symmetrical stretching
C—H	Graphene	5909—5787	5895—5766	5873—5772	Symmetrical stretching
C—H	Glucose	5854—5589	5811—5586	5799—5614	Symmetrical and asymmetrical stretching
C—H	PMMA	5660—5403	5665—5408	5615—5443	Symmetrical and asymmetrical stretching
C—H	PU	5826—5501	5637—5483	5640—5497	Symmetrical and asymmetrical stretching
O—H	PU-graphene	5306—5209	5308—4735	5259—4613	Scissoring vibration
O—H	PMMA-graphene	5173—4935	5173—4922	5130—4870	Scissoring vibration
C—C	Graphene	3642—3197	3647—3233	3643—2882	Symmetrical and asymmetrical stretching
C=O	PU	3459—3395	3517—3511	3484—3440	Symmetrical stretching
C=O	PU	3459—3395	3517—3511	3484—3440	Symmetrical stretching
C—C	PU	3403—3267	3388—3258	3380—3215	Symmetrical stretching
C=O	NaHCO <sub>3</sub>	3239—3201	3228—3200	3235—3217	Symmetrical stretching
C—H	Glucose	3270—2848	3222—2912	3236—2918	Scissoring vibration
C=O	PMMA	3228	3222	3217—3209	Symmetrical stretching
C—C	Glucose	3164—2722	3175—2838	3146—2845	Symmetrical and asymmetrical stretching
C—H	Graphene	3114—2794	3069—2789	3094—2882	Scissoring vibration
N—H	PU	3112—2967	3087—3005	3297—3224	Scissoring vibration
N—C	PU	2375—2339	2363—2354	2385—2352	Symmetrical stretching
C—C	PU	3058—2908	3086—2981	3078—3051	Symmetrical stretching
C—C	PMMA	2954—2842	2992—2750	3038—2832	Symmetrical and asymmetrical stretching
C—O	Glucose	3018—2593	2986—2613	2941—2694	Symmetrical stretching
O—H	Glucose	2777—2314	2852—2355	2863—2278	Scissoring vibration
C—H	PU	2922—2384	2936—2343	2914—2345	Wagging and scissoring vibration

(Continued)

**Table 10.4** FTIR Analysis of the PU/G/PMMA Nanocomposite in the Presence of SBF at Different Temperatures *Continued*

Bond	Molecule	Frequencies (cm <sup>-1</sup> )			Vibration
		Temperatures			
		35°C	37°C	40°C	
C—O	PMMA	2842–2709	2860	2991–2832	Symmetrical stretching
C—H	PMMA	2955–2671	2855–2574	2916–2582	Wagging vibration
C—C	PU	2718–2083	2726–2080	2735–2102	Symmetrical stretching
C—C	Graphene	2695–469	2617–534	2724–456	Wagging and scissoring vibration
C=O	PU	2544–2497	2516–2476	2498–2443	Symmetrical stretching
O—H	PU	2490–2396	2447–2395	2594–2245	Scissoring vibration
S=O	MgSO <sub>4</sub>	2358	2344	2296	Symmetrical stretching
O—H	NaHCO <sub>3</sub>	2377	2330–2316	2278–2256	Scissoring vibration
C—O	PU	1953–1661	1943–1601	1908–1546	Symmetrical stretching
C—C	PMMA	1870–1659	1935–1663	1962–1697	Twisting vibration
C—C	PU	2128–1741	1928–1738	1967–1697	Twisting vibration
C—C	PU	1862, 1616–790	1884–1869, 1633–609	1888, 1631–733	Scissoring vibration
Na—O	NaHCO <sub>3</sub>	1894–1814	1905–1811	1989–1880	Symmetrical stretching
Na—O	Na <sub>2</sub> HPO <sub>4</sub>	1835	1899–1719	1861	Symmetrical stretching
C—O	PMMA	1837–1812	1857–1841	1864–1824	Symmetrical stretching
S—O	MgSO <sub>4</sub>	1891, 1670	1815, 1648	1913, 1506	Symmetrical and asymmetrical stretching
P—O	KH <sub>2</sub> PO <sub>4</sub>	1780–1756	1874–1750	1771–1750	Symmetrical and asymmetrical stretching
P—O	Na <sub>2</sub> HPO <sub>4</sub>	1777	1856	1751	Symmetrical stretching
C—C	Glucose	1642–361	1540–333	1546–379	Scissoring vibration
C—O	NaHCO <sub>3</sub>	1412	1483–1423	1574–1412	Symmetrical stretching
C—O	Glucose	1645–599	1540–598	1523–593	Scissoring vibration
C—N	PU	1527–1524	1503	1553	Wagging vibration
Ca—Cl	CaCl <sub>2</sub>	1519–1516	1519–1516	1518	Symmetrical stretching
Na—Cl	NaCl	1472–1454	1479–1451	1472–1454	Symmetrical stretching
C=O	PU	1475	1486	1439	Scissoring vibration
C=O	PMMA	1498–1482	1485–1463	1506–1357	Scissoring vibration
N—H	PU	1472–1134	1333–1088	1430–1025	Wagging vibration
C—O	NaHCO <sub>3</sub>	1399–1369	1423–1379	1375–1362	Symmetrical stretching
K—Cl	KCl	1267–1260	1291–1260	1270–1257	Symmetrical stretching
O—H	H <sub>2</sub> O	1227–1067	1223–1014	1234–1048	Wagging and scissoring vibration
C—O	PU	997–881	989–887	995–882	Scissoring vibration
Ca—Cl	CaCl <sub>2</sub>	924–919	921–920	928–921	Symmetrical stretching
Mg—Cl	MgCl <sub>2</sub>	919–915	919–913	916–915	Symmetrical stretching
C=O	NaHCO <sub>3</sub>	906–719	916–722	888–731	Scissoring vibration
C—O	NaHCO <sub>3</sub>	905–690	888–696	879–660	Scissoring vibration

(Continued)

**Table 10.4** FTIR Analysis of the PU/G/PMMA Nanocomposite in the Presence of SBF at Different Temperatures *Continued*

Bond	Molecule	Frequencies (cm <sup>-1</sup> )			Vibration
		Temperatures			
		35° C	37° C	40° C	
S—O	MgSO <sub>4</sub>	682, 611	682,627	735, 619	Wagging and scissoring vibration
P=O	Na <sub>2</sub> HPO <sub>4</sub>	630–578	698–667	698–596	Wagging vibration
S=O	MgSO <sub>4</sub>	576–450	548–351	579–468	Wagging and scissoring vibration
C—O	NaHCO <sub>3</sub>	515–415	718–503	640–429	Wagging vibration
Mg—Cl	MgCl <sub>2</sub>	422–390	492–426	475–413	Scissoring vibration
P—O	KH <sub>2</sub> PO <sub>4</sub>	379	388	467	Wagging vibration
P—O	Na <sub>2</sub> HPO <sub>4</sub>	387	454	471	Wagging vibration
Na—O	NaHCO <sub>3</sub>	556–335	462–348	432–353	Scissoring vibration
P=O	KH <sub>2</sub> PO <sub>4</sub>	486	652–647	621, 424	Scissoring vibration
Ca—Cl	CaCl <sub>2</sub>	338–303	385–355	412–349	Scissoring vibration

### 10.3.1.3 Electrostatic potential map

The distribution of electron density in real space represents a characteristic property of materials because it influences both the chemical bond and geometry, where structural stability is generated by the forces of attraction present between the electrons and nuclei.

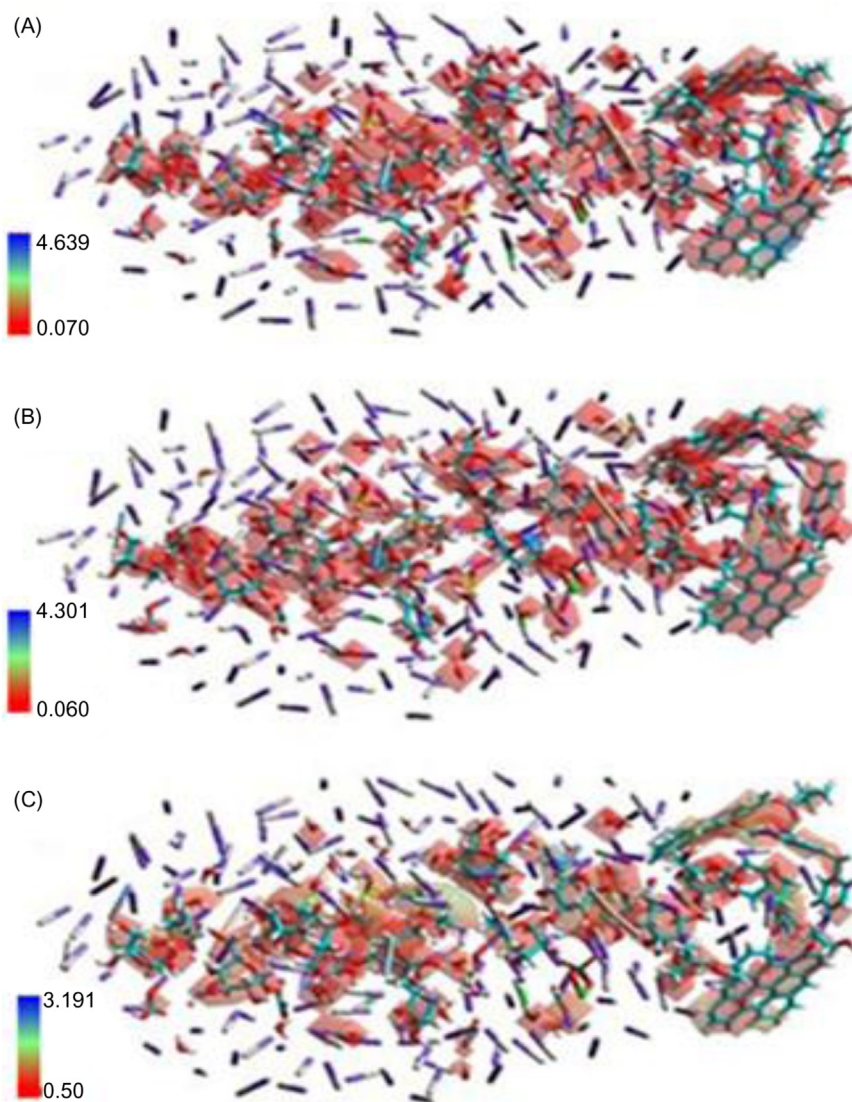
Fig. 10.7 shows the MESP of the nanocomposite at the corresponding analysis temperatures (308.15K, 310.15K, and 313.15K) where the graphene has an electronic distribution in the C—C bonds attributed to the covalent bond (Choi et al., 2010). These nucleophilic and electrophilic zones are mainly present in organic compounds such as glucose and nanocomposite formed by PU/G/PMMA. Fig. 10.7 shows how the electronic distribution in the three systems is presented in a similar way, presenting a red coloration that indicates that it is highly charged with electrons in the electrophilic zones. This behavior favors the property of the prosthesis as it will be suitable for the transport of electrical impulses through this composite material.

## 10.3.2 POLYURETHANE/GRAPHENE/CALCIUM CARBONATE NANOCOMPOSITE

### 10.3.2.1 Optimization geometry, minimum energy, and partition coefficient

Table 10.5 shows the Gibbs free energy with respect to the various temperatures where it is seen that at 308.15K the nanocomposite with CC presents a marked



**FIGURE 10.7**

MESP of the PU/G/PMMA nanocomposite in the presence of SBF at different temperatures: (A) 308.15K, (B) 310.15K, and (C) 313.15K, where hydrogen  $\circ$ , carbon  $\circ$ , oxygen  $\circ$ , sodium  $\circ$ , chlorine  $\circ$ , potassium  $\circ$ , calcium  $\circ$ , magnesium  $\circ$ , phosphorus  $\circ$ , sulfur  $\circ$ , and nitrogen  $\circ$ .

**Table 10.5**  $\Delta G$  and Log  $P$  Values of the PU/G/CC Nanocomposite in the Presence of SBF at Different Temperatures

Properties	Temperatures		
	35°C	37°C	40°C
$\Delta G$ (Kcal/mol)	98,970	12,486.70	12,636.60
Log $P$	129	129	129

change in comparison with the other temperatures; this is because the CC of the nanocomposite generates the formation of intermolecular bonds because the SBF is a solution that consists of salts then, the anions have at least one pair of free electrons that are used in the formation of a bond with the calcium that represents the most common metal ion, generating a greater presence of calcium on the surface of the nanocomposite (Kamal, 2014) producing a recrystallization (Hellrup, 2016) and increased the cross-link density (Sadeghi et al., 2014) (see Fig. 10.8) phenomenon called nucleation and is caused by the clustering of ions at the boundary of the nanocomposite with SBF (Xu et al., 2007). This effect represents a loss of 87.38% of the structural stability of the nanocomposite at 308.15K, however at 313.15K the decrease in properties is 1.186%.

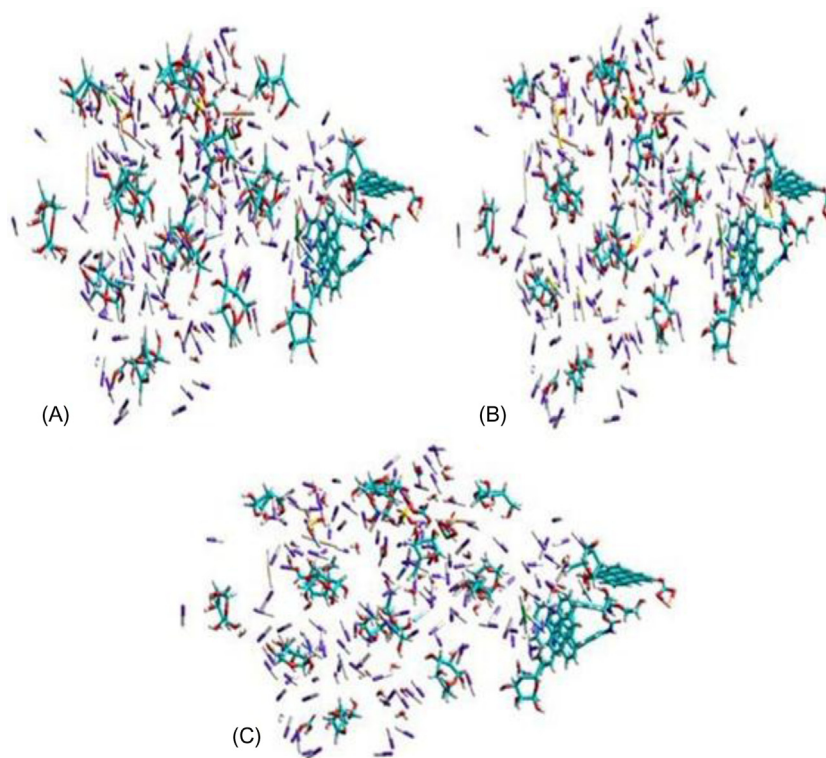
When comparing Tables 10.3 and 10.5 we see a significant variation in the Gibbs free energy that is attributed to nucleation. The log  $P$  obtained in the three temperatures shows a hydrophobic behavior, that is, it is verified that there will be a reaction of formation of a CC in the surface of the nanocomposite producing a loss in the thermodynamic stability (Aragón et al., 2011).

### 10.3.2.2 Fourier-transform infrared spectroscopy

Table 10.6 shows the PU/G/CC nanocomposite, the several FTIR regions in the presence of the blood fluid at different temperatures, and where the symmetrical vibrations of the OH and CH bonds corresponding to the  $\text{CaCO}_3$ ,  $\text{KH}_2\text{PO}_4$  and graphene are observed in the range of  $7919\text{--}7010\text{ cm}^{-1}$ , for the area between  $6322$  and  $6255\text{ cm}^{-1}$ . The symmetrical stretching vibrations of the amino group of the PU were observed. From  $6089$  to  $5475\text{ cm}^{-1}$  the vibrations were attributed to the symmetrical and asymmetrical stretching in addition to the CH-bonding of the graphene, glucose, and PU respectively. The OH bonds were determined from  $5489$  to  $4392\text{ cm}^{-1}$  and were assigned to the scissoring vibrations of the PU/graphene cross-linking,  $\text{CaCO}_3$ , and water (Adina et al., 2010). Adsorbed water band is relatively wide from  $4675$  to  $4392\text{ cm}^{-1}$  (Slosarczyk et al., 2010).

The glucose present in the SBF has the symmetrical and asymmetrical vibrations of the OH, CH bonds of the  $\text{CH}_3$ , and  $\text{CH}_2$  while the CC bond is between  $3862\text{--}3322$  and  $3316\text{--}3221\text{ cm}^{-1}$  (Adina et al., 2010; Mahabole et al., 2012) and the CH balance was observed between  $3364$  and  $3136\text{ cm}^{-1}$ . It can be seen that the symmetrical and asymmetrical vibrations of CC,  $\text{C}=\text{C}$ , and  $\text{C}=\text{O}$  of



**FIGURE 10.8**

Optimized molecular geometry of the PU/G/CC nanocomposite in the presence of SBF at different temperatures: (A) 308.15K, (B) 310.15K, and (C) 313.15K, where hydrogen  $\text{O}$ , carbon  $\text{C}$ , oxygen  $\text{O}$ , sodium  $\text{Na}$ , chlorine  $\text{Cl}$ , potassium  $\text{K}$ , calcium  $\text{Ca}$ , magnesium  $\text{Mg}$ , phosphorus  $\text{P}$ , sulfur  $\text{S}$ , and nitrogen  $\text{N}$ .

graphene and PU were determined between  $3389$  and  $3167\text{ cm}^{-1}$ . The principal peak of glucose was localized in the range of  $1401$ – $1325\text{ cm}^{-1}$  and it is characteristic for the CO stretch vibration, besides  $955$ – $813\text{ cm}^{-1}$  were observed in the endocyclic and exocyclic CO bonds (Adina et al., 2010). The OH and C=O vibrations of the sodium carbonates from the SBF were assigned in the  $3207$ – $3088\text{ cm}^{-1}$  region. The symmetrical vibration of the carbonyl group corresponding to the CC is located between  $3189$  and  $3112\text{ cm}^{-1}$ .

The scissoring flexions of glucose corresponded between  $3207$  and  $1982\text{ cm}^{-1}$  and were assigned to the CC, CH, and OH bonds, respectively. The sign between  $1938$  and  $1913\text{ cm}^{-1}$  corresponds to the C=O stretch of the carbonyl group present in the SBF (Sindhu et al., 2011). The bending vibration of the water molecules is at  $1794$ – $1773$ ,  $1254$ – $1230$ , and  $974$ – $874\text{ cm}^{-1}$  and the rocking band appears at  $845$ – $804$  and  $307$ – $282\text{ cm}^{-1}$  (Assaoudi et al., 2007). Between  $1246$

**Table 10.6** FTIR Analysis of the PU/G/CC Nanocomposite in the Presence of SBF at Different Temperatures

Bond	Molecule	Frequencies (cm <sup>-1</sup> )			Vibration
		Temperatures			
		35° C	37° C	40° C	
O—H	CaCO <sub>3</sub> , graphene	7886—7854	7915—7885	7919—7894	Symmetrical stretching
C—H	CaCO <sub>3</sub> , graphene	7887—7852	7890—7865	7892—7879	Symmetrical stretching
O—H	KH <sub>2</sub> PO <sub>4</sub>	7011—7010	7105—7098	7125—7104	Symmetrical stretching
N—H	PU	6258—6255	6315—6257	6322—6266	Symmetrical stretching
C—H	Graphene	5985—5761	6048—5847	6089—5913	Symmetrical stretching
C—H	Glucose	5854—5475	5934—5526	5944—5538	Symmetrical and asymmetrical stretching
C—H	PU	5813—5501	5902—5561	5911—5573	Symmetrical and asymmetrical stretching
C—H	PU	5651—5528	5767—5621	5789—5661	Rocking vibration
C—H	Glucose	5618—5475	5725—5509	5733—5518	Symmetrical and asymmetrical stretching
O—H	PU-graphene	5306—5209	5484—5372	5489—5377	Scissoring vibration
O—H	CaCO <sub>3</sub> , graphene	5251—4788	5349—4915	5351—4922	Scissoring vibration
O—H	Water	4522—4392	4633—4401	4675—4418	Scissoring vibration
O—H	CaCO <sub>3</sub> , graphene	7886—7854	7915—7885	7919—7894	Symmetrical stretching
C—H	Glucose	3762—3433, 3388—3374	3819—3405, 3401—3388	3862—3474, 3460—3409	Scissoring vibration
C—C	Glucose	3495—3358, 3348—3322	3507—3366, 3455—3397	3511—3380, 3466—3396	Symmetrical and asymmetrical stretching
C—C	Graphene	3514—3378, 3314—3298	3598—3407, 3389—3269	3613—3429, 3391—3277	Symmetrical and asymmetrical stretching
C=C	PU	3419, 3401, 3380—3337	3425—3399, 3391—3364	3461—3406, 3398—3356	Symmetrical stretching
O—H	Glucose	3351	3350	3354	Symmetrical stretching
C—C	PU	3350, 3283—3273	3371, 3296—3284	3389, 3309—3286	Symmetrical stretching
C—H	Glucose	3295—3281, 3263—3257	3305—3278, 3266—3260	3316—3279, 3291—3254	Symmetrical stretching
C—C	Graphene	3278, 3261— 3253	3306—3265	3386—3296	Symmetrical stretching

(Continued)

**Table 10.6** FTIR Analysis of the PU/G/CC Nanocomposite in the Presence of SBF at Different Temperatures *Continued*

Bond	Molecule	Frequencies (cm <sup>-1</sup> )			Vibration
		Temperatures			
		35°C	37°C	40°C	
C—C	Glucose	3276–3270, 3252, 3245, 3224–3221	3279–3270, 3250–3215	3306–3285, 3255–3224	Symmetrical and asymmetrical stretching
C=C	PU, graphene	3264, 3190	3279–3205	3306–3251	Symmetrical stretching
C=O	PU	3264	3271	3280	Symmetrical stretching
C—C	PU	3249–3236	3298–3266	3325–3274	Symmetrical stretching
C—H	Glucose	3238–3200, 3185, 3158, 3136–3136	3305–3255, 3209–3164, 3105	3364–3247, 3225–3155	Rocking vibration
C—C	Graphene	3218–3197, 3167	3285–3205, 3179	3366–3214	Rocking vibration
O—H	NaHCO <sub>3</sub>	3142	3149	3207	Rocking vibration
C=O	NaHCO <sub>3</sub>	3132–3088	3175–3106	3179–3118	Symmetrical stretching
C—H	Graphene	3129, 3093	3198–3105	3205–3123	Scissoring vibration
C—C	Glucose	3127–3107, 2892–2864	3166–3128, 2914–2880	3189–3274, 2926–2889	Symmetrical stretching
C=O	CaCO <sub>3</sub>	3122, 3112	3179, 3122	3189–3140	Symmetrical stretching
N—H	PU	3119–3060	3125–3074	3129–3083	Scissoring vibration
C—H	Glucose	3116, 3098–3097, 2949–2919, 2756, 2616, 2341	3169–3105, 2966–2833, 2655–2402	3207–3155, 3009–2866, 2674–2458	Scissoring vibration
C—C	PU	3090, 3060	3095–3104	3156–3111	Symmetrical stretching
C—C	Graphene	3040, 2809	3045, 2837	3059–2901	Symmetrical stretching
C—H	PU	3000	3009	3016	Symmetrical stretching
O—H	Glucose	2727, 2593–2533, 2480	2816, 2608–2513	2828, 2644–2527	Scissoring vibration
C—O	Glucose	2709–2649, 2430, 1982	2745–2619, 2506–2444, 2000	2789–2633, 2524–2461, 2009	Scissoring vibration
C—C	Graphene	2695–2095	2708–2211	2729–2216	Wagging and scissoring vibration
C=O	PU	2544–2497	2549–2528	2561–2547	Symmetrical stretching

(Continued)

**Table 10.6** FTIR Analysis of the PU/G/CC Nanocomposite in the Presence of SBF at Different Temperatures *Continued*

Bond	Molecule	Frequencies (cm <sup>-1</sup> )			Vibration
		Temperatures			
		35° C	37° C	40° C	
C–N	PU	2402	2416–2410	2444–2419	Symmetrical stretching
C–C	Glucose	2294–2202, 2064–2013, 1982–1974, 1964	2345–2214, 2107–2083, 1998–1979	2405–2219, 2163–2127, 2004–1985	Symmetrical stretching
C–H	Glucose	2064–2013, 1982–1974, 1964, 1957	2106–2066, 2008–1977, 1969–1960	2151–2074, 2129–2050, 2008–1965	Symmetrical stretching
C–H	Graphene	1976, 1946	1979–1963	1989–1966	Symmetrical stretching
C–O	PU	1975–1974	1998–1982	2008–1991	Symmetrical stretching
P=O	KH <sub>2</sub> PO <sub>4</sub>	1968	1974	1979	Symmetrical stretching
C–O	Glucose	1963–1962, 1957–1950, 1947	1968–1960, 1958–1949	1971–1964, 1960–1952	Symmetrical stretching
C–H	PU	1959	1960	1963	Twisting vibration
C–O	PU	1959	1960	1963	Twisting vibration
O–H	Glucose	1957–1950, 1947, 1796–1771	1960–1952, 1809–1785	1965–1659, 1864–1791	Twisting vibration
Mg–O	MgSO <sub>4</sub>	1948	1952	1963	Twisting vibration
C–C	Graphene	1946, 1913	1949–1925	1952–1937	Twisting vibration
C–C	Glucose	1920, 1855, 1796–1771	1928–1899, 1808–1786	1935–1906, 1855–1793	Twisting vibration
C–O	Glucose	1920, 1855, 1796–1771, 1755	1926–1849, 1800–1766, 1760	1934–1865, 1826–1784, 1772–1765	Twisting vibration
O–H	Grafeno-CaCO <sub>3</sub>	1913, 1754	1920–1889	1925–1891	Twisting vibration
C=O	NaHCO	1913–1873	1936–1896	1938–1903	Stretching
C–H	Graphene	1844, 1784, 1754	1859, 1790–1762	1864, 1794–1786	Stretching
C=O	CaCO <sub>3</sub>	1844, 1750	1857, 1763	1866, 1794	Stretching
Mg–Cl	MgCl <sub>2</sub>	1793	1816	1823	Stretching
O–H	Water	1773	1782	1794	Bending
C–H	Glucose	1768–1762, 1731	1779–1781, 1745–1733	1783–1769, 1752–1741	Bending
P=O	KH <sub>2</sub> PO <sub>4</sub>	1759	1765	1770	Bending
C–C	Graphene	1754, 1727, 1432	1750–1735	1752–1738	Bending
C–C	Glucose	1748–1736, 1731, 1423	1750–1742, 1734–1720	1754–1749, 1735–1729	Bending

(Continued)

**Table 10.6** FTIR Analysis of the PU/G/CC Nanocomposite in the Presence of SBF at Different Temperatures *Continued*

Bond	Molecule	Frequencies (cm <sup>-1</sup> )			Vibration
		Temperatures			
		35° C	37° C	40° C	
C–H	PU	1733–1727, 1626	1735–1729, 1655	1738–1732, 1678–1664	Bending
C–C	PU	1733	1735	1742	Stretching
C–H	PU-graphene	1727, 1529	1730, 1533–1537	1734, 1542	Stretching
OCH–NH	PU	1714	1719	1723	Stretching
Ca–O	CaCO <sub>3</sub>	1679–1626, 1405	1682–1655, 1432–1418	1695–1672, 1448–1420	Stretching
N–H	PU	1626–1529	1630–1554	1645–1571	Stretching
C–O	PU	1626–1529	1632–1583	1647–1597	Stretching
Na–Cl	NaCl	1458	1462	1473	Stretching
Na–Cl	NaCl	1456	1466	1482	Wagging vibration
C–O	Glucose	1423, 1349–1325	1435–1389, 1367–1345	1446–1401, 1388–1369	Stretching
C–C	Graphene	1405–1377, 1251	1432–1386, 1234–1241	1464–1405, 1307–1271	Stretching
O–H	PU-graphene	1405	1419	1424	Stretching
C–C	Glucose	1325–1213, 1205, 1182	1345–1289, 1264–1237	1394–1296, 1275–1241	Stretching
O–H	Glucose	1300–1213, 1205, 1198	1324–1284, 1231–1205	1344–1309, 1286–1231	Stretching
C–H	Glucose	1266–1213, 1205	1274–1214, 1216	1280–1247, 1233	Stretching
O–H	Water	1230	1247	1254	Bending
P–O	KH <sub>2</sub> PO <sub>4</sub>	1226	1238	1246	Stretching
C–C	PU	1223–1201, 1194, 1185	1246–1235, 1221–1193	1287–1255, 1249–1208	Stretching
C–N	PU	1223–1208, 1194–1172, 1105	1248–1236, 1209–1185, 1133–1119	1267–1249, 1236–1206, 1184–1067	Twisting vibration
C–O	PU	1208, 1194–1172, 1105	1237–1185, 1136–1119	1245–1979, 1145–1137	Twisting vibration
C–C	Graphene	1193–1185, 1172–1131, 1105–1046	1216–1173, 1154–1089, 1041–1030	1233–1191, 1158–1037	Stretching
C–H	Graphene	1193, 1105–1046	1231–1084, 1047–1029	1254–1168, 1103–1086	Twisting vibration
C–C	Glucose	1185–1164, 1124, 1077–1000, 986–949	1254–1209, 1191–1174, 1037–994, 963–950	1283–1247, 1162–1049, 1005–948	Stretching
Ca–O	CaCO <sub>3</sub>	1131, 1105–998	1161–1046, 1001–984	1193–1075, 1014–997	Stretching

(Continued)

**Table 10.6** FTIR Analysis of the PU/G/CC Nanocomposite in the Presence of SBF at Different Temperatures *Continued*

Bond	Molecule	Frequencies (cm <sup>-1</sup> )			Vibration
		Temperatures			
		35° C	37° C	40° C	
O—H	Glucose	1124, 1077–994, 949–945	1166–1108, 1049–1000, 987–954	1189–1153, 1097–1014, 1002–967	Stretching
C—C	PU	1105–1046, 954, 930	1184–1049, 1013–975	1208–1117, 1034–986	Stretching
C—C	Graphene	1003–998, 985–962, 954–901	1025–1008, 997–971, 960–924	1045–1019, 1003–981, 964–933	Stretching
C—O	NaHCO <sub>3</sub>	980, 922	1009–948	1025–967	Stretching
Ca—O	CaCO <sub>3</sub>	962, 954	983–967	985–972	Stretching
Mg—Cl	MgCl <sub>2</sub>	958	964	970	Stretching
O—H	Water	956, 935, 889, 874	968–941, 905–893	974–955, 933–917	Bending
C—O	Glucose	939–936, 822–813	945–933, 867–829	955–939, 894–841	Stretching
C—N	PU	930, 876, 867	941–894, 877–860	957–906, 884–870	Stretching
C—O	PU	930–884, 867–856,	935–887, 876–861	945–927, 891–873	Stretching
C—C	Glucose	929–924, 850–813	945–932, 877–822	967–942, 891–843	Stretching
Ca—Cl	CaCl <sub>2</sub>	919–913	933–927	945–937	Stretching
Na—O	NaHCO <sub>3</sub>	888–871	915–877	926–904	Scissoring vibration
N—H	PU	867–851	876–856	895–871	Scissoring vibration
Ca—O	NaHCO <sub>3</sub>	871	896	893	Scissoring vibration
P—O	NaHPO <sub>4</sub>	864	872	882	Scissoring vibration
O—H	NaHCO <sub>3</sub>	857	861	869	Scissoring vibration
C—C	PU	856–817, 743–714	858–847, 795–726	871–856, 809–764	Scissoring vibration
C—C	Graphene	851–817, 743–714	869–822, 795–728	894–836, 803–761	Scissoring vibration
C—O	NaHCO <sub>3</sub>	824–795, 743–714	856–808, 766–739	874–819, 794–766	Scissoring vibration
Ca—O	CaCO <sub>3</sub>	819–795, 743	823–817, 761–754	875–834, 792–766	Scissoring vibration
Na—O	NaHCO <sub>3</sub>	817–795, 743–714, 283, 274	839–801, 762–703, 296–282	845–795, 766–733, 345–312	Scissoring vibration
O—H	Water	804, 298	819–800, 325–311	845–827, 349–322	Rocking
C—C	Glucose	657, 523, 494–412, 384–329, 298, 278	715–586, 566–473, 411–394, 318–293	746–619, 607–582, 573–416, 368–341	Scissoring vibration

(Continued)

**Table 10.6** FTIR Analysis of the PU/G/CC Nanocomposite in the Presence of SBF at Different Temperatures *Continued*

Bond	Molecule	Frequencies (cm <sup>-1</sup> )			Vibration
		Temperatures			
		35° C	37° C	40° C	
Na—Cl	NaCl	301—300, 298—207	367—331, 309—275	375—361, 328—294	Stretching
P—O	KH <sub>2</sub> PO <sub>4</sub>	300—280	315—294	336—317	Wagging vibration
Mg—Cl	MgCl <sub>2</sub>	300—280	318—297	333—308	Scissoring vibration
Ca—Cl	CaCl <sub>2</sub>	300—280	306—283	319—291	Scissoring vibration
KCl	KCl	298—283, 219—207	301—299, 247—221	319—307, 268—249	Wagging vibration
O—H	Water	282	291—276	307—281	Wagging vibration
S—O	MgSO <sub>4</sub>	274—217	280—228	286—246	Wagging vibration

and 1226 cm<sup>-1</sup> was associated with stretching of the KH<sub>2</sub>PO<sub>4</sub> (Togkalidou et al., 2001). The CaO bond showed a double sign in the area of 1193–998 cm<sup>-1</sup> as well as a strong adsorption between 985 and 954 cm<sup>-1</sup> (Adina et al., 2010). PO bond from KH<sub>2</sub>PO<sub>4</sub> was localized between 336 and 280 cm<sup>-1</sup> (Słosarczyk et al., 2010). The intense IR absorption band, around 864–882 cm<sup>-1</sup>, was assigned to asymmetric P–O stretching from NaHPO<sub>4</sub>.

### 10.3.2.3 Electrostatic potential map

MESP shows electronic distributions of nuclei and electrons of a molecule and in Fig. 10.9 it is seen that the electrophilic charges (*red* color) were located in the CO, OH, and C=O bonds of glucose, water, PU, and CaCO<sub>3</sub> respectively, whereas the nucleophilic charges (*blue* color) corresponded to the CH and KH<sub>2</sub>PO<sub>4</sub> bonds. It is noted that the decrease in temperature increases the negative charge from 0.016 to 0.60 eV, which is attributed to the loss of structural stability of 87.38% as seen in the Gibbs free energy changes from Table 10.5.

## 10.4 CONCLUSIONS

The determination of the effect of the temperature change was established from the Monte Carlo simulation, from which the properties were calculated as Gibbs free energy, which practically did not change with respect to the energy calculated at room temperature, which indicates that despite these temperature changes the prosthesis will remain stable and will retain its structure and properties. Infrared spectra were also calculated at each of the temperatures observing insignificant changes in each of them; the same happened with the maps of electrostatic potential since they were very similar. Based on this, it was established that



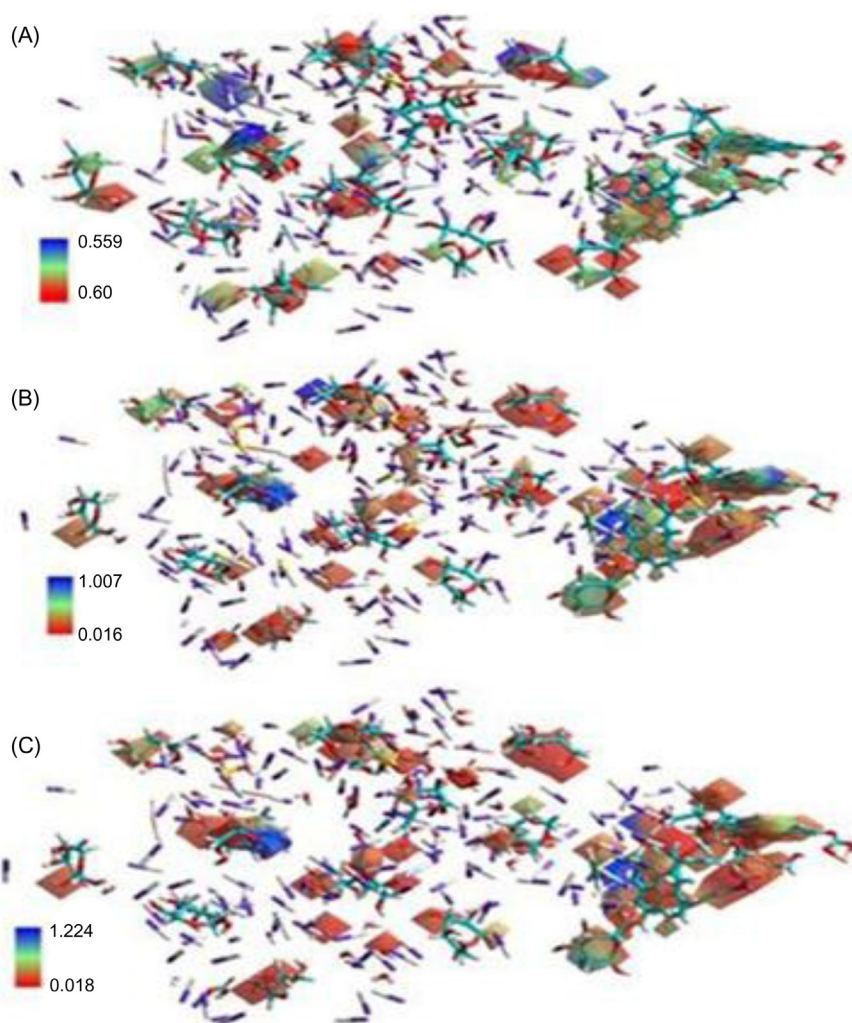


**FIGURE 10.9**

MESP of the PU/G/CC nanocomposite in the presence of SBF at different temperatures: (A) 308.15K, (B) 310.15K, and (C) 313.15K, where hydrogen  $\text{O}$ , carbon  $\text{C}$ , oxygen  $\text{O}$ , sodium  $\text{Na}$ , chlorine  $\text{Cl}$ , potassium  $\text{K}$ , calcium  $\text{Ca}$ , magnesium  $\text{Mg}$ , phosphorus  $\text{P}$ , sulfur  $\text{S}$ , and nitrogen  $\text{N}$ .

the change in body temperature would not affect the structure or properties of the PU/G/PMMA nanocomposite, which would form the prosthesis.

Regarding the PU/G/CC prosthesis, the same procedure was performed as with the PMMA nanocomposite. However, the results indicated that when replacing PMMA with CC, the prosthesis won't be adequate due to the decrease in



Gibbs free energy of 87.38% with a change from 310.15K to 308.15K, which means that there will be no thermodynamic stability. In addition, an increase in the molecular vibrations of the FTIR spectrum attributed to the van der Waals attractions and the formation of calcium on the surface of the nanocomposite was observed; this behavior was verified with the MESP when determining a greater zone of electrophilic attacks, which increase with the temperature change. Therefore, the prosthesis should be designed from the PU/G/PMMA nanocomposite.

## REFERENCES

- Adina, C., Florinela, F., Abdelmoumen, T., Carmen, S., 2010. Application Of FTIR spectroscopy for a rapid determination of some hydrolytic enzymes activity on sea buckthorn substrate. *Roman. Biotech. Let.* 15, 5738–5744.
- Alemán, C., Muñoz-Guerra, S., 2003. Aplicaciones de los métodos computacionales al estudio de la estructura y propiedades de polímeros. *Polímeros* 13, 250–264.
- Andrés, A., Rosés, M., Ràfols, C., Bosch, E., Espinosa, S., Segarra, V., et al., 2015. Setup and validation of shake-flask procedures for the determination of partition coefficients (logD) from low drug amounts. *Eur. J. Pharm. Sci.* 76, 181–191.
- Aragón, J., González, R., Fuentes, G., Palín, L., Croce, G., Viterbo, D., 2011. Development and characterization of a novel bioresorbable and bioactive biomaterial based on polyvinyl acetate, calcium carbonate and coralline hydroxyapatite. *Mat. Res.* 14, 25–30.
- Assaaoudi, H., Fang, Z., Butler, I.S., Ryan, D.H., Kozinski, J.A., 2007. Characterization of a new magnesium hydrogen orthophosphate salt,  $Mg_{3.5}H_2(PO_4)_3$ , synthesized in supercritical water. *Solid State Sci.* 9, 385–393.
- Baena, Y., Pinzón, J., Barbosa, H., Martínez, F., 2004. Estudio termodinámico de la transferencia de acetaminofén desde el agua hasta el octanol. *Braz. J. Pharm. Sci.* 40, 413–420.
- Barbes, L., Radulescu, C., Stîhi, C., 2014. ATR-FTIR spectroscopy characterisation of polymeric materials. *Roman. Rep. Phys.* 66, 765–777.
- Barnard, A.S., 2009. Computational strategies for predicting the potential risks associated with nanotechnology. *Nanoscale* 1, 89–95.
- Caracciolo, P.C., Abraham, G.A., 2015. Poliuretanos biomédicos: síntesis, propiedades, procesamiento y aplicaciones de Biomateriales aplicados al diseño de sistemas terapéuticos avanzados. *Universidade de Coimbra*, pp. 147–181.
- Cardona, L.R., Brousse, M., Mieres, M., Arias, S., Gutiérrez, E., 2011. Evaluación de la resistencia de un prototipo de placa de compresión dinámica (PCD) fabricada de poli-metilmetakrilato (PMMA) probada en fémur canino osteotomizado. *Rev. Med. Vet.* 21, 13–24.
- Choi, E.Y., Han, T.H., Hong, J., Kim, J.E., Lee, S.H., Kim, H.W., et al., 2010. Noncovalent functionalization of graphene with end-functional polymers. *J. Mater. Chem.* 1, 1–4.
- Comini, L.R., Nuñez, S.C., Arguello, G.A., Cabrera, J.L., 2006. Determinación del coeficiente de partición (log P) para derivados antraquinónicos aislados de *heterophyllaea pustulata* Hook. F. (Rubiáceas). *Acta Farm. Bonaerense.* 25, 252–255.

- De-Souza, M.G., Figueroa, Y., Ramírez, A.L., Prin, J.L., Guzmán, P.J., Otero, B., et al., 2014. Hidrogeles de poli(acrilamida): Evaluación de su comportamiento en fluido fisiológico simulado (SBF). *Rev. Iberoamer. Polím.* 15, 198–210.
- Ferrari, C., Bonaccorso, F., Novoselov, K.S., Roche, S., Boggild, P., 2015. Science and technology roadmap for graphene. *Nanoscale* 7, 4587–5062.
- Haselmeier, R., Holz, M., Marbach, W., Weingaertner, H., 1995. Water dynamics near a dissolved noble gas. *J. Phys. Chem.* 99, 2243–2246.
- Hellrup, J., 2016. Pharmaceutical Nanocomposites Structure–Mobility–Functionality Relationships in the Amorphous State. Universidad de UPPSALA, Sweden.
- Jaebon, T., 2010. Polymethylmethacrylate: properties and contemporary uses in orthopaedics. *J. Am. Acad. Orthop. Surg.* 18, 297–305.
- Jensen, F., 2007. Introduction to Computational Chemistry. WILEY, Denmark.
- Kamal, H., 2014. Structure and physical properties of silver borate bioactive glasses. *Res. J. Pharm. Biol. Chem. Sci.* 5, 822–832.
- Khenfouch, M., Baïtoul, M., Aarab, H., Maaza, M., 2012. Morphological, vibrational and thermal properties of confined graphene nanosheets in an individual polymeric nanochannel by electrospinning. *Graphene* 1, 15–20.
- Leiva, E., Estrín, D.A., 2011. Química computacional: Simulaciones matemáticas del comportamiento de átomos y moléculas. *Asociación Civil Ciencia Hoy, Ciencia Hoy* 21, 46–50.
- Lewars, E., 2011. Computational chemistry: introduction to the theory and applications of molecular and quantum mechanics. *An Outline of What Computational Chemistry Is All About*. Kluwer Academic Publishers, Canada, pp. 1–7.
- Liu, Y., Dong, X., Chen, P., 2012. Biological and chemical sensors based on graphene materials. *Chem. Soc. Rev.* 41, 2283–2307.
- Mahabole, M.P., Bahir, M.M., Kalyankar, N.V., Khairnar, R.S., 2012. Effect of incubation in simulated body fluid on dielectric and photoluminescence properties of nano-hydroxyapatite ceramic doped with strontium ions. *J. Biomed. Sci. Eng.* 5, 396–405.
- Maleki-Dizaj, S., Barzegar-Jalali, M., Hossein-Zarrintan, M., Adibkia, K., Lotfipour, F., 2015. Calcium carbonate nanoparticles: potential in bone and tooth disorders. *Pharm. Sci.* 20, 175–182.
- Nag, S., Banerjee, R., 2012. Fundamentals of medical implant materials, *ASM Handbook*, 23, pp. 1–17.
- Navarro, C.H., Nieto, V.M., García-Miranda, S., Lesso, R., Moreno, K.J., Louvier-Hernández, F., et al., 2010. Síntesis y caracterización de un recubrimiento de tipo PMMA-CaO. *Superficies y Vacío* 23, 31–35.
- Paul, W., Sharma, C.P., 2011. Blood compatibility and biomedical applications of graphene. *Trends Biomater. Artif. Organs.* 25, 91–94.
- Quintero, M.W., Gómez, J.R., 2007. Los Polimeros de poliuretano y la industria colombiana: una oportunidad para el aceite de palma. *Palmas* 28, 35–42.
- Sadeghi, H., Shakouri, Z., Shirazi, M.M.A., 2014. Evaluation of microstructure of natural rubber/nano-calcium carbonate nanocomposites by solvent transport properties. *J. Plast. Rubber Compos. Macromol. Eng.* 43, 177–186.
- Shekhawat, A., Ritchie, R.O., 2015. Toughness and strength of nanocrystalline graphene. *Nat. Commun.* 7, 1–8.
- Sindhu, R., Ammu, B., Binod, P., Deepthi, S.K., Ramachandran, K.B., Soccol, C.R., et al., 2011. Production and characterization of Poly-3-hydroxybutyrate from crude glycerol by *Bacillus sphaericus* NII 0838 and improving its thermal properties by blending with other polymers. *Braz. Arch. Biol. Technol.* 54, 783–794.

- Singh, A.V., 2011. Biopolymers in drug delivery: a review. *Newsletter* 1, 666–674.
- Slosarczyk, A., Paszkiewicz, Z., Zima, A., 2010. The effect of phosphate source on the sintering of carbonate substituted hydroxyapatite. *Ceram. Int.* 36, 577–582.
- Togkalidou, T., Fujiwara, M., Patel, S., Braatz, R.D., 2001. Solute concentration prediction using chemometrics and ATR-FTIR spectroscopy. *J. Cryst. Growth*. 231, 534–543.
- Torres-Silva, H., López-Bonilla, J., 2011. Aspectos quirales del grafeno. *Rev. Chilena Ing.* 19, 67–75.
- Valles-Sánchez, L., Rosales-Marines, L.E., Serrato-Villegas, L., 2014. Métodos y usos de la Química computacional. *Rev. Científica Univ. Autónoma Coahuila* 6, 17–21.
- Xu, A.W., Ma, Y., Colfen, H., 2007. Biomimetic mineralization. *J. Mater. Chem.* 17, 415–449.
- Xue, Y., Liu, J., Zhang, M., Dai, L., 2012. Graphene-based materials for energy. *MRS Bullet.* 37, 1265–1272.
- Young, D.C., 2001. *Computational Chemistry: A Practical Guide for Applying Techniques to Real-World Problems*. Wiley, New York.
- Zhu, Y., Murali, S., Cai, W., Li, X., Suk, J.W., Potts, J.R., 2010. Graphene and graphene oxide: synthesis, properties. *Adv. Mater.* 20, 1–19.
- Zivic, F., Babic, M., Favaro, G., Cauni, M., Grujovic, N., Mitrovic, S., 2011. Microindentation of polymethyl methacrylate (PMMA) based bone cement. *Tribol. Industr.* 3, 146–152.

# New insights into nanohydroxyapatite/chitosan nanocomposites for bone tissue regeneration

# 11

**Gabriela Ruphuay<sup>1,2</sup>, Jose Carlos Lopes<sup>1</sup>, Madalena Maria Dias<sup>1</sup> and Maria Filomena Barreiro<sup>2,3</sup>**

<sup>1</sup>Laboratory of Separation and Reaction Engineering - Laboratory of Catalysis and Materials (LSRE-LCM), Faculty of Engineering, University of Porto, Porto, Portugal <sup>2</sup>Laboratory of Separation and Reaction Engineering - Laboratory of Catalysis and Materials (LSRE-LCM), Bragança Polytechnic Institute, Bragança, Portugal <sup>3</sup>Centro de Investigação de Montanha (CIMO), Instituto Politécnico de Bragança, Campus de Santa Apolónia, Bragança, Portugal

## 11.1 INTRODUCTION

A great interest has been given to synthetic and stoichiometric hydroxyapatite (HAp) as a biomaterial due to its similarity with the mineral phase found in hard tissues (Levengood and Zhang, 2014). It possesses exceptional biocompatibility (Chen et al., 2007) and bioactivity (Hossein Fathi et al., 2009; Fathi et al., 2008) with respect to bone cells and surrounding tissues, which makes it a suitable material for the replacement of small parts of bone, filling of cavities in dentistry, and coating of metallic implants (Ferraz et al., 2004). Additionally, this bioceramic has a high capacity of ad- and absorption, making it an excellent candidate for drug delivery applications, such as long-acting drugs for anticancer treatment of bone tumors (Itokazu et al., 1998; Bose and Tarafder, 2012).

Bones are not only the frame that supports the human body, allowing its mobility and protecting it against injury, but also the storehouse for minerals that are essential for the functioning of other life-sustaining systems in the body. For these reasons, healthy bones are critically important for the overall health and quality of life. Unfortunately, bone is the most frequently transplanted tissue after blood transfusions. The clinical need to replace, restore, or regenerate bone tissue comprises the fields of dental, maxillofacial, orthopedic, spinal, and cranial surgery, being osteoporosis the most important cause of fracture in the elderly (Brydone et al., 2010; Campana et al., 2014; Services, U.S.D.o.H.a.H., 2004).

As a matter of fact, the International Osteoporosis Foundation reported in 2010 an estimation of 3.5 million new fractures in the European Union caused by osteoporosis, representing an economic burden of approximately 37 billion EUR (Svedbom et al., 2013).

Medical solutions for bone repair and regeneration are still a major challenge. Even though they present serious drawbacks, biologically derived bone grafts have been implanted for many years, as temporary or permanent prostheses, and are still today available in the market at great scale. Due to the numerous disadvantages of biological grafts, current efforts are focused on the development of manmade materials that, in comparison with orthodox treatments, have great potential to improve the regeneration of bone or its replacement when damaged, with the advantage that they are easily available and might be processed and modified to suit specific needs (Brydone et al., 2010; Bose et al., 2012). In this context, the development of HAp-based nanocomposite materials is very promising not only in terms of market opportunities, but also due to the contribution they could impart to regenerative medicine, particularly for hard tissue regeneration.

The first attempt to produce an implantable polymer/Ca-P composite was carried out in 1981 and consisted in the development of HAp/polyethylene formulations by pioneer Prof. William Bonfield and his colleagues (Bonfield et al., 1981). Ever since, many studies have been conducted in this field, including the use of FDA-approved, synthetic-biodegradable polymers such as poly(L-lactic acid) (PLA; Wei and Ma, 2004), poly(glycolic acid) (PGA; Agrawal et al., 1995), and their copolymers (PLGA), with applications as drug carriers, bone fixation screws, plates, resorbable sutures, among others (Agrawal and Ray, 2001; Dorozhkin, 2011).

More recently, the incorporation of nanohydroxyapatite (n-HAp) into natural polymers is recognized as one of the most viable approaches to produce materials mimicking natural bone. Besides the expected biodegradability, natural polymers can be biologically active promoting better interactions with cells and, therefore, excellent cell adhesion and growth (O'Brien, 2011). In particular, the combination of n-HAp with chitosan (CS) has been of great interest for the production of nonload-bearing bone grafts, given the advantageous properties of CS that allows the manufacturing of nanohydroxyapatite/CS (n-HAp/CS) materials with improved properties. Among other features, CS promotes osteoblasts adhesion and proliferation, possesses antimicrobial properties, and can be processed using mild conditions and shaped into different forms (Costa-Pinto et al., 2011). However, besides the many studies proving its suitability for tissue regeneration, n-HAp/CS materials have not yet reached the market at great scale.

This chapter is a compilation of fundamentals in bone tissue engineering, focusing on the recent advances on the use of HAp and CS as biomaterials for bone regeneration, and progresses in what concerns the fabrication of HAp/CS nanocomposite materials.

## 11.2 OVERVIEW OF BONE BIOLOGY

Natural bone is a complex hybrid material with extracellular matrix (ECM) composed of approximately 60%–70% of an inorganic mineral, precipitated onto 20%–30% of an organic matrix, and a small portion of water (Levengood and Zhang, 2014; Amit et al., 2006). Structurally, it is highly organized in a hierarchical manner, from the nano- to the macroscale, as shown in Fig. 11.1. At the nanoscale, the mineral phase consists of calcium phosphate, plate-like nanocrystals, of 2–6 nm thickness, 30–50 nm width, and 60–100 nm length, chemically and structurally very similar to synthetic n-HAp (Levengood and Zhang, 2014; Amit et al., 2006) (see Table 11.1).

At the microscale, bone can be divided in two categories based on density: cortical and cancellous bone. Cortical or compact tissue is very dense, with a porosity of 3%–5%, and forms the outer layer of bone, providing support and protection. The less-dense inner part is constituted by cancellous bone, also known as trabecular or spongy-like bone; it is highly porous, with 30%–90% porosity, and contains the bone marrow (Levengood and Zhang, 2014; Bose and Tarafder, 2012; Costa-Pinto et al., 2011; Burr and Allen, 2013). Together, the cortical and trabecular tissues form the skeletal element of bone. However, bone is also a very dynamic tissue that constantly experiences modeling and remodeling processes as a consequence of mechanical and metabolic changes.

Five primary cells dictate bone formation and remodeling: mesenchymal stem cells (MSCs), osteoblasts, osteocytes, osteoclasts, and bone lining cells. MSCs are found in the bone marrow and in the periosteum, the fibrous layer on the outside surface of bone. They are multipotent stromal cells that can differentiate into osteoblasts, the single-nuclei cells in charge of bone matrix protein secretion and bone mineralization. After completing their main function of synthesizing bone matrix, osteoblasts undergo three different transformations: they remain entrapped in bone as osteocytes, they flatten into bone lining cells, and the remnants suffer apoptosis.

Osteocytes are the most abundant cells present in bone, representing more than 90% of cells within the bone matrix and surfaces, and their main function is the coordination of osteoblasts and osteoclasts functions in response to mechanical and hormonal signals. Bone lining cells are relatively inactive forms of osteoblasts whose function is to cover the inactive surface of bone; they may recover the ability to synthesize bone matrix and participate in the regulation of calcium exchanges. Finally, osteoclasts are the cells responsible for the resorption of mineralized bone. All these cells work together in a balanced way to maintain the integrity of healthy bone, as well as to regenerate bone that has suffered trauma or disease. In the last case, when the defect size is critical, bone grafts are necessary to assist bone healing (Levengood and Zhang, 2014; Costa-Pinto et al., 2011; Burr and Allen, 2013).

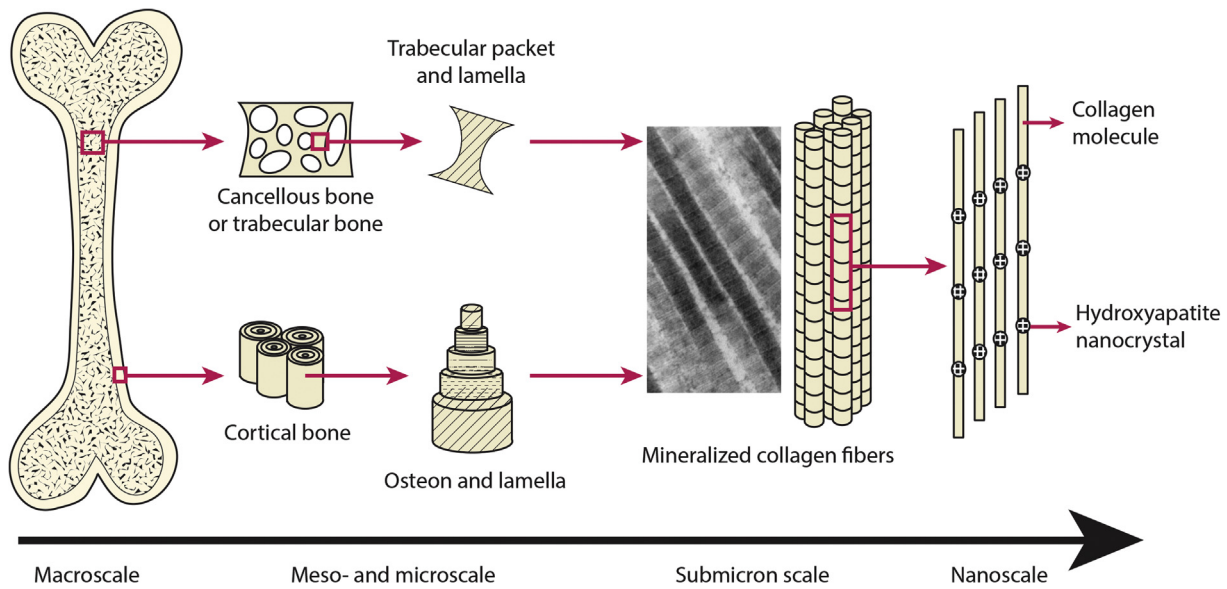


**FIGURE 11.1**

Hierarchical organization of bone.

**Table 11.1** Typical Composition of the Inorganic Phase of Adult Human Calcified Tissues and Hydroxyapatite

Composition	Enamel	Dentin	Bone	Hydroxyapatite
Calcium (wt.%)	36.5	35.1	34.8	39.6
Phosphorus (as P) (wt.%)	17.7	16.9	15.2	18.5
Ca/P (molar ratio)	1.63	1.61	1.71	1.67
Sodium (wt.%)	0.5	0.6	0.9	—
Magnesium (wt.%)	0.44	1.23	0.72	—
Potassium (wt.%)	0.08	0.05	0.03	—
Carbonate (as $\text{CO}_3^{2-}$ ) (wt.%)	3.5	5.6	7.4	—
Fluoride (wt.%)	0.01	0.06	0.03	—
Chloride (wt.%)	0.30	0.01	0.13	—
Pyrophosphate (as $\text{P}_2\text{O}_7^{4-}$ ) (wt.%)	0.022	0.10	0.07	—
Total inorganic (wt.%)	97	70	65	—
Total organic (wt.%)	1.5	20	25	—
Water (wt.%)	1.5	10	10	—

Adapted from Bose, S., Tarafder, S., 2012. Calcium phosphate ceramic systems in growth factor and drug delivery for bone tissue engineering: a review. *Acta Biomater.*, 8 (4), 1401–1421.

## 11.3 THE IDEAL BONE GRAFT

Considering the compositional, structural, mechanical, and biological complexity of natural bone, the design of an ideal bone graft is not an easy task. The requirements for a graft intended to mimic all features of bone are numerous and diverse, however, there are a few key factors that must be fulfilled.

Based on O'Brien (2011), they can be summarized in terms of biocompatibility, biodegradability, mechanical properties, structural requirements, and manufacturing technology.

### 11.3.1 BIOCOMPATIBILITY

An indispensable requirement of bone grafts is biocompatibility. This term can be defined as the ability of a material to support normal cellular activity, including molecular signaling systems, without causing any systemic or local effects to the host tissue (Bose et al., 2012). Therefore, the graft should be *osteoconductive*, that is, it should promote cell adhesion on its surface and migration within its pores, cell proliferation, and formation of ECM. In addition, *osteoinductive* properties are necessary, that is, the bone substitute must induce the formation of new bone through the reclusion of progenitor cells and biomolecular signaling (Bose et al., 2012; Ricciardi and Bostrom, 2013). Along with osteoconductive and osteoinductive properties, products of bone graft degradation should be nontoxic and easily excreted by metabolic pathways (Liu and Ma, 2004).



### 11.3.2 BIODEGRADABILITY

The main objective of a bone graft is to assist tissue regeneration by providing a bridge that will fill critical size bone defects in such a way that it allows the body's own cells to replace, over time, the implanted substitute. Therefore, grafts should degrade in vivo, in a controlled manner, and ideally at a rate that closely matches the one of formation of the new tissue in the implantation site (Bose et al., 2012; O'Brien, 2011; Rodrigues et al., 2013).

### 11.3.3 MECHANICAL PROPERTIES

One of the main challenges in bone tissue engineering is, still today, to achieve an adequate balance between mechanical properties and structural requirements, such as high porosity. The bone substitute should be able to support mechanical stresses in the implantation site from the moment of grafting throughout the whole remodeling process, which leads to a further challenge considering that healing times vary with age; tissue of a younger individual normally requires less time to heal than that of the elderly. In addition, the graft should be able to resist surgical handling during the implantation process (O'Brien, 2011).

### 11.3.4 STRUCTURAL REQUIREMENTS

The structural features of the bone substitute are critical since they can affect both its mechanical properties and its capacity to promote *osteogenesis*, the formation of bone tissue. Bone grafts can be cortical, cancellous, or a combination of both each one with different mechanical and structural properties, which can be used in different applications depending on the surgical requirements. Cortical bone grafts are less frequently used and they are often applied onlay, that is, the graft is applied or laid on the surface of the tissue, to provide structural support and strength. Cancellous bone grafts, on the other hand, lack mechanical strength but are characterized for inducing osteogenesis. This type of bone substitute is commonly implanted in nonunion fractures, maxillofacial and dental defects, spinal fusion, and other small defects (Oryan et al., 2014). Typically, cancellous bone grafts take the form of 3D-porous scaffolds, and the ability to promote adequate osteogenesis greatly depends on its architecture. Scaffolds should be highly porous, to guarantee cellular penetration, and their pores should be interconnected, both to allow the diffusion of nutrients to cells as well as the exit of waste and degradation products out of the scaffold (O'Brien, 2011).

### 11.3.5 MANUFACTURING TECHNOLOGY

Last but not least, clinical and commercial viability are key factors to consider when engineering bone grafts. The manufacturing process should be cost effective

and easily scalable from laboratorial to industrial production. Additionally, it is important to consider the clinician's point of view, since they are the ones ultimately using the product. For example, they typically prefer a bone graft that can be easily adapted into different shapes and an off-the shelf product ready to be implanted; the fewer extra surgical procedures prior to implantation, the better (O'Brien, 2011).

---

## 11.4 OVERVIEW OF COMMERCIALY AVAILABLE BONE GRAFTS

Solutions for bone repair include the use of materials that, if not autologous, are either of natural or synthetic origin. Biological or natural bone grafts are those obtained from either human or animal origin; thus, autogenous, allogeneous, and xenogeneous grafts are all within this classification (Kolk et al., 2012). Synthetic grafts, also known as alloplastic grafts, include the use of polymers but mainly ceramic-based materials such as HAp, calcium sulfate, and bioactive glass (Kolk et al., 2012; Kumar et al., 2013). There is also the alternative of using composite and hybrid materials, commonly consisting in the combination of ceramic-based materials with polymers.

Autogenous grafts are obtained from nonessential bones of the same individual receiving the graft. They fulfill all primordial properties for bone regeneration as they are osteoconductive, osteoinductive, and they carry osteogenic cells and growth factors without the risk of transmitting immune or infective diseases. Nevertheless, due to the requirement of a surgical donor site, this type of graft can lead to postoperative pain, blood loss or hematomas, possibility of infection and esthetic deformity, among other complications (Campana et al., 2014).

Bone grafts obtained from another individual of the same species are called allogenic; they are harvested from cadavers, making them readily available in different shapes and sizes. Allografts are also osteoinductive and osteoconductive but not osteogenic, since they lack viable cells. They can be acquired from bone banks unprocessed and frozen, thus including all growth factors and normal ultrastructure. Otherwise, their processing includes steps such as defatting, removing the bone marrow, and commonly freeze-drying, which changes the graft's mechanical properties, making them less resistant. Finally, they have to be sterilized before use. This type of graft overcomes the limitations presented by autografts, but presents some limitations such as high cost, risk of rejection and, additionally, concerns related to disease transmission in spite of undergoing sterilization (Zimmermann and Moghaddam, 2011).

The term *xenograft* refers to bone substitutes acquired from a species other than human, frequently bovine bone tissue. Usually, all organic material is

removed from the animal tissue by a high temperature treatment, followed by a chemical procedure with a strong base, such as NaOH, to obtain a porous HAp material. Xenogenic materials are readily available and show adequate absorption characteristics; however, they exhibit the same disadvantages as allografts, with additional risk of transmission of zoonoses, allergenic response, and a more likely rejection of the graft (Oryan et al., 2014). In addition to ceramic-based xenografts, another readily available biological graft is the so-called demineralized bone matrix (DBM). It is obtained mainly from human, bovine, or equine bone tissue through decalcification and sterilization, resulting in a sponge-like collagen material (Kolk et al., 2012; Zimmermann and Moghaddam, 2011). Some commercially natural bone substitute materials are listed in Table 11.2.

With regard to synthetic materials, ceramic-based grafts are the most commonly used, especially based on HAp and  $\beta$ -tricalcium phosphate ( $\beta$ -TCP), due to the advantages they present in what concerns osteoconductivity, long shelf life, unlimited supply, and absence of risk of disease or virus infection. In addition, they can be produced with different shapes, porosity and composition; commercially they are usually sold as granules, injectable pastes, and cements, among other forms (Zimmermann and Moghaddam, 2011; Dorozhkin, 2010). As for the disadvantages of these alloplastic grafts, the synthesis of HAp and  $\beta$ -TCP with the desired characteristics (Ca/P ratio, crystallinity and morphology, etc.) can be challenging and, despite its hardness and porosity, they are brittle, limiting their applications (Zimmermann and Moghaddam, 2011).

In efforts to improve the overall properties of ceramic materials, they have been combined with other components, mainly polymers, to produce composite and hybrid materials. Many scientists use these terms interchangeably and there is still no clear borderline between them. For the purposes of this work, the terms are used according to IUPAC definitions (McNaught and McNaught, 2014); therefore, a composite is a material constituted by two or more components comprising multiple, different nongaseous phases such that at least one of which is a continuous phase. The term *hybrid* refers to a material composed by an intimate mixture of organic or inorganic components, or both in which normally the components interpenetrate at scales less than 1  $\mu\text{m}$ .

A number of biodegradable polymers, both synthetic and natural, have been used in combination with ceramic materials, including PLA, PGA, PLGA, collagen, alginate, and CS, among others. In this context, the combination with collagen has been widely studied and currently the market offers a variety of ceramic/collagen products. CS-based products, on the other hand, besides the many studies proving its suitability for tissue regeneration, have not yet reached the market at great scale. A list of some commercially available calcium phosphate-based alloplastic composites and hybrid grafts is shown in Table 11.3.

**Table 11.2** List of Some Commercially Available Biological Grafts

Company	Product Name	Composition/Source	Form	References
Ace Surgical Supply Co., Inc.	Nu-Oss	Both mineral phase and DBM derived from bovine tissue	Granules and blocks	<a href="#">Ace Surgical Supply Co., Inc. (2016)</a>
	AlloOss	Both mineral phase and DBM derived from human tissue	Particles, blocks and putty	
AlloSource	AlloFuse	Derived from DBM of human tissue	Gel, paste, and putty	<a href="#">AlloSource TM (2016)</a>
	AlloFuse Plus	Derived from DBM and ground cancellous bone of human tissue	Paste and putty	
Biomet3i Botiss Dental GmbH	Endobon	Derived from mineral phase of bovine bone	Granules	<a href="#">Biomet3i TM (2016)</a>
	Cerabone	Derived from mineral phase of bovine bone	Granules and blocks	<a href="#">Botiss Dental GmbH (2016)</a>
	Maxgraft	Derived from cancellous and cortical bone of human tissue	Granules and blocks	
D-bone DePuy Synthes	D-bone	Derived from mineral phase of bovine bone	Granules	<a href="#">D-bone (2016)</a>
	Allograft Bone Chips and Blocks	Derived from cancellous and cortical bone of human tissue	Chips and blocks	<a href="#">DePuy Synthes TM (2016)</a>
	DBX Material	Derived from DBM of human tissue in sodium hyaluronate carrier	Putty and strip	
Exactech	Optecure	Derived from DBM of human tissue and a hydrogel carrier provided separately	Dry mix kit (powder with hydrogel)	<a href="#">Exactech (2016)</a>
	Optecure + ccc	Cortical cancellous chips derived from human tissue	Chips (1–3 mm)	
Geistlich Pharma	Geistlich Bio-Oss	Derived from mineral phase of bovine bone	Granules	<a href="#">Geistlich Pharma (2016)</a>
	Geistlich Bio-Oss Collagen	90% Geistlich Bio-Oss (granules) and 10% porcine collagen	Scaffold	
Ost-Developpement	Laddec	Derived from mineral phase of bovine bone	Chips and blocks	<a href="#">Ost-Developpement (2016)</a>
	Lubboc	Derived from mineral phase of bovine bone	Chips, grafts and blocks	

*(Continued)*

**Table 11.2** List of Some Commercially Available Biological Grafts *Continued*

Company	Product Name	Composition/Source	Form	References
Osteohealth	Equimatrix	Derived from mineral phase of equine bone	Granules	<a href="#">Osteohealth (2016)</a>
	OSSIF-i sem	Both mineral phase and DBM derived from human tissue	Particles, sponge strip and filler	
SigmaGraft Biomaterials	Optimatrix	Derived from DBM of porcine tissue	Membrane	<a href="#">SigmaGraft Biomaterials (2016)</a> <a href="#">Tecross (2016)</a>
	InterOss	Derived from mineral phase of bovine bone	Granules	
Tecross	Tecross mp3 and Tecross putty	Derived from mineral phase of equine bone and additional collagen gel	Prehydrated bone mix, putty	
	Tecross Gen-Oss and Tecross Chips	Derived from mineral phase of equine bone	Granules and chips	

**Table 11.3** List of Some Commercially Available Alloplastic and Composites Grafts

Company	Product Name	Composition	Form	References
Artoss GmbH	NanoBone	HAp (76% for granules, 61% for blocks and putty) and silicon dioxide (24% granules and 39% blocks and putty)	Granules, blocks, and putty	<a href="#">Artoss GmbH (2016)</a>
Baxter	Actifuse	Silicate substituted calcium phosphate	Granules and scaffolds	<a href="#">Baxter (2016)</a>
Berkeley Advanced Biomaterials Inc.	Bi-Ostetic	Tricalcium phosphate and HAp	Granules, blocks, and cylinders	<a href="#">Berkeley Advanced Biomaterials Inc. (2016)</a>
	Bi-Ostetic Foam	Type I bovine collagen, tricalcium phosphate and HAp	Foam	
Biocomposites Ltd.	geneX	$\beta$ -TCP and calcium sulfate	Putty	<a href="#">Biocomposites Ltd. (2016)</a>
	Allogran-R	$\beta$ -TCP	Granules	
Ceramed	NeoBone	75% HAp and 25% TCP	Granules, blocks, and wedges	<a href="#">Ceramed (2016)</a>
	NeoCement	Solid phase: tetracalcium phosphate and TCP. Liquid phase: citric acid, CS and apyrogenic water.	Cement (to be mixed before use)	
	k-IBS	Calcium phosphate granules and CS	Injectable gel	
	n-IBS	100% HAp nanoparticles	Injectable	
Curasan	Cerasorb M	>99% $\beta$ -TCP	Granules	<a href="#">Curasan (2016)</a>
Sunstar Degradable Solutions AG	Guidor <i>easy-graft</i>	$\beta$ -TCP granules coated with PLGA, mixed with BioLinker ( <i>N</i> -methyl-2-pyrrolidone liquid activator)	Granules	<a href="#">Sunstar Degradable Solutions AG (2016)</a>
DePuy Synthes	chronOS	100% $\beta$ -TCP	Granules and scaffolds	<a href="#">DePuy Synthes TM (2016)</a>
	Norian	Carbonated apatite and polylactide/glycolide copolymer fibers	Injectable and fast-set putty	
Exactech	OpteMx	60% HAp and 40% $\beta$ -TCP	Granules and scaffolds	<a href="#">Exactech (2016)</a>

(Continued)

**Table 11.3** List of Some Commercially Available Alloplastic and Composites Grafts *Continued*

Company	Product Name	Composition	Form	References
Fluidinova	nanoXIM-HAp100	100% HAp nanoparticles in pure water at concentrations 15.0 and 30.0 wt.%	Paste	<a href="#">Fluidinova (2016)</a>
	nanoXIM-HAp200	100% HAp nanoparticles agglomerates	Powder	
	nanoXIM-TCP200	100% Ca-deficient HAp nanoparticles agglomerates with 90% $\beta$ -TCP phase purity	Powder	
Heraeus Kulzer GmbH	Ostim	100% HAp nanoparticles suspended aqueous phase at concentrations 35.0 wt.%	Paste	<a href="#">Heraeus Kulzer GmbH (2016)</a>
Hoya Technosurgical Corporation	Apaceram	HAp	Particles and scaffolds	<a href="#">Hoya Technosurgical Corporation (2016)</a>
Impladent Ltd.	Osteogen	Calcium apatite (nonspecified)	Powder	<a href="#">Impladent Ltd. (2016)</a>
Kerr	Bioplant	Calcium hydroxide and biodegradable polymer (nonspecified)	Spherical beads	<a href="#">Kerr TM (2016)</a>
Stryker GmbH & Co.	HydroSet Injectable	<i>Powder:</i> Di-, tri-, and tetracalcium phosphate. <i>Liquid:</i> Sodium phosphate, polyvinyl-pyrrolidone and water	Paste (to be mixed before use)	<a href="#">Stryker GmbH &amp; Co. (2016)</a>
	BoneSave	80% TCP and 20% HAp	Granules	
	BoneSource	HAp	Cement	
	Vitoss	$\beta$ -TCP and bioactive glass (nonspecified)	Scaffold	
Teknimed S.A.S.	BBTrauma			
Zimmer Biomet	Cementek	Calcium apatite (nonspecified) powder plus separate aqueous solution	Injectable (to be mixed before use)	<a href="#">Teknimed S.A.S. (2016)</a>
	Calcitite	100% HAp	Granules	<a href="#">Zimmer Biomet TM (2016)</a>
	IngeniOs	100% HAp or 100% $\beta$ -TCP	Particles	

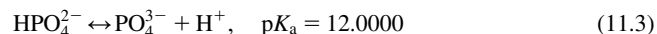
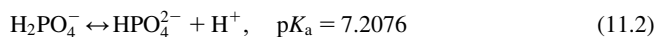
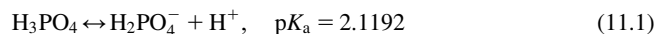
## 11.5 HYDROXYAPATITE AS A BIOMATERIAL FOR BONE REGENERATION

HAp is a member of a large isomorphous series of minerals called *apatites*, which means “deceivers” in Greek, a name given due to their diversity of form and color. Apatites can be found in nature mainly in mineral deposits and in mammals bones and teeth (Park, 2009). The apatite profusely found in sedimentary rocks is essentially carbonate fluoroapatite, whereas the one found in bones and teeth is very similar, in terms of crystallography and chemical composition, to HAp (Park, 2009; Kantharia et al., 2014).

The stoichiometry of HAp is represented by the formula  $\text{Ca}_{10}(\text{PO}_4)_6(\text{OH})_2$ ; it is a double salt of TCP and calcium hydroxide with a Ca/P ratio of 1.67. Deviations from Ca/P stoichiometric ratio can lead to phase impurities in HAp, such as TCP or CaO, that may affect biological responses (Mucalo, 2015). At physiological temperature and pH ranging from 4 to 12, it is considered the most stable and less soluble calcium phosphate of all (Mucalo, 2015; Koutsopoulos, 2001). However, the solubility of HAp, which is partly responsible for vital properties such as biocompatibility and bioactivity, depends on several factors; thus, the study of its dissolution mechanisms and rate is a topic of great interest.

The solubility rate of HAp depends on shape, crystal size, porosity, crystallinity, and crystallite size. In general, it is soluble in acidic solutions, insoluble in alkaline ones and slightly soluble in distilled water, which increases with the addition of electrolytes. Therefore, solubility varies depending on the surrounding environment; for example, in physiological environments it is affected by the presence of amino acids, proteins, enzymes, and other organic compounds.

Barbucci (2002) explains the solubility equilibrium dynamics of calcium phosphates in wet and biological environments, starting from the influence of their chemical nature on the solubility product value. Phosphate-containing compounds in solution are ruled by the following equilibria:

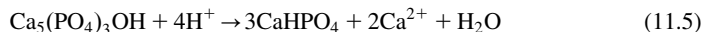


These equations show that in a very acidic solution,  $\text{H}_2\text{PO}_4^-$  species are predominant, near neutrality  $\text{HPO}_4^{2-}$  is favored, and  $\text{PO}_4^{3-}$  species are dominant in basic solutions. Consequently, in the presence of  $\text{Ca}^{2+}$  the precipitation of HAp is favored in a basic environment; thus, with the contribution of the  $\text{OH}^-$  groups, its solubility product ( $K_{\text{SP}}$ ) is:

$$K_{\text{SP}} = [\text{Ca}^{2+}]^5 [\text{PO}_4^{3-}]^3 [\text{OH}^-] \quad (11.4)$$



Then, in acidic conditions, below pH values of 4.3–4.8, HAp becomes very slowly soluble and undergoes the following transformation as a result of the decrease in  $\text{OH}^-$  concentration and the presence of  $\text{H}^+$ :



Chemical composition and crystallinity of HAp are two of the main factors directly influencing biological responses. HAp can be found in two different crystal forms: hexagonal and monoclinic. The hexagonal structure is most frequently found, with  $P6_3/m$  space group and lattice parameters of  $a = b = 9.432$ ,  $c = 6.881$ , and  $\gamma = 120$  degrees. In this structure, tetrahedral  $\text{PO}_4$  groups are held together by interspersed Ca ions. The Ca ions are arranged in two distinct sites, the so-called Ca(I) are accurately aligned in columns, and the Ca(II) are organized in equilateral triangles centered on the screw axis. Finally, the hydroxide groups (OH) are found on the screw axes arranged in a column (see Fig. 11.2) (Ma and Liu, 2009).

The atomic arrangement in HAp structure is directly related with its properties, and thus with its potential biomedical applications. In aqueous media, HAp presents different net charges in its crystal planes;  $a$  and  $b$  planes are positively charged, while charges in  $c$  plane, are negative. Therefore, it is expected that  $a$  and  $b$  planes tend to attract acidic groups of proteins, whereas the  $c$  planes attract basic groups of proteins (Mucalo, 2015; Kandori et al., 2009; Uskoković and Uskoković, 2011). Moreover, morphology of HAp particles has an effect on their

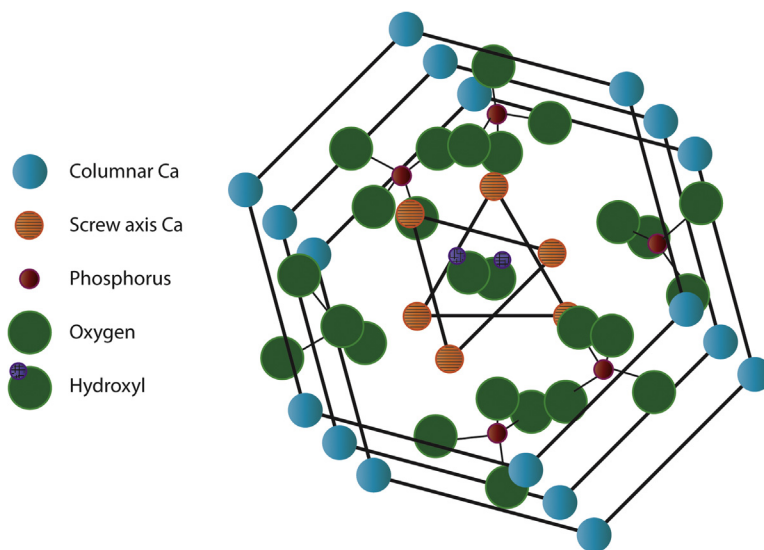


**FIGURE 11.2**

Schematic representation of hexagonal HAp.

net charge; due to the elongation of HAp particles along the *c*-axis in their typical rod-like morphology, it is believed that the net charge of the particles would be shifted positive, giving a higher specificity of adsorption onto negatively charged proteins (Uskoković and Uskoković, 2011); nevertheless, this is influenced by the pH of the aqueous medium, which, at the same time, influences the dissolution mechanism and rate of HAp, as previously explained.

Dissolution mechanism and rate of HAp are, to a great extent, responsible for HAp's well known osseointegration and bioactivity properties, where *osseointegration* refers to the ability to bind to the bone, whereas *bioactivity* is the ability of a material to induce a specific biological activity such as forming Ca-containing minerals. It has been proposed that these two remarkable properties are due to a mechanism that happens at the HAp–tissue interface after implantation, starting by the dissolution of HAp (Mucalo, 2015; Bertazzo et al., 2010; Ducheyne and Qiu, 1999). Following dissolution, the supersaturated solution at the interface causes the reprecipitation of calcium and phosphate ions, with the formation of carbonate apatite (Ducheyne et al., 1993). At this point, an exchange of ions between the HAp implant and the host bone starts, promoting both bone bonding through the deposition of the ions on the collagenous matrix, and the adsorption of the host bone proteins to HAp surface (Mucalo, 2015; Bertazzo et al., 2010; Ducheyne and Qiu, 1999). Finally, attracted by the high concentration of phosphate and calcium ions, MSCs migrate to the implant surface, differentiate into osteoblasts, and start producing new bone (Ducheyne and Qiu, 1999). An illustration of this mechanism is shown in Fig. 11.3.

Besides chemical composition, crystallinity, and morphology, particle size is another key property that affects biological responses to HAp-containing grafts and, thus, its performance throughout the mechanism described above. In its nanometric form, nanohydroxyapatite has been proven to be more advantageous to the conventional micrometric sized HAp in what concerns the promotion of osteoblast adhesion, differentiation and proliferation, osseointegration, and deposition of Ca-containing minerals on its surface (Supova, 2009; Webster et al., 2000).

Cells are sensitive to the topography of an implant, both at micro- and nanoscale, since it influences factors affecting protein adsorption; among them, surface chemistry, roughness, and surface-free energy (Rouahi et al., 2006; dos Santos et al., 2009). Thanks to their increased surface area and higher percentages of atoms at the surface, nanoscale materials have higher surface energy, wettability, and surface reactivity when compared with conventional sized materials (Gleiter, 1995; Sato and Webster, 2004), which is translated into increased numbers of grain boundaries, to which proteins preferentially adsorb. As a result, grafts containing HAp in its nanometric form have shown enhanced osteoblast adhesion and function, decrease fibroblast adhesion, and enhanced bone remodeling (Tran and Webster, 2009; Yang et al., 2011).

Finally, when it comes to biomedical applications, biodegradation of materials into nontoxic products is highly desirable. In this sense, HAp is an appropriate

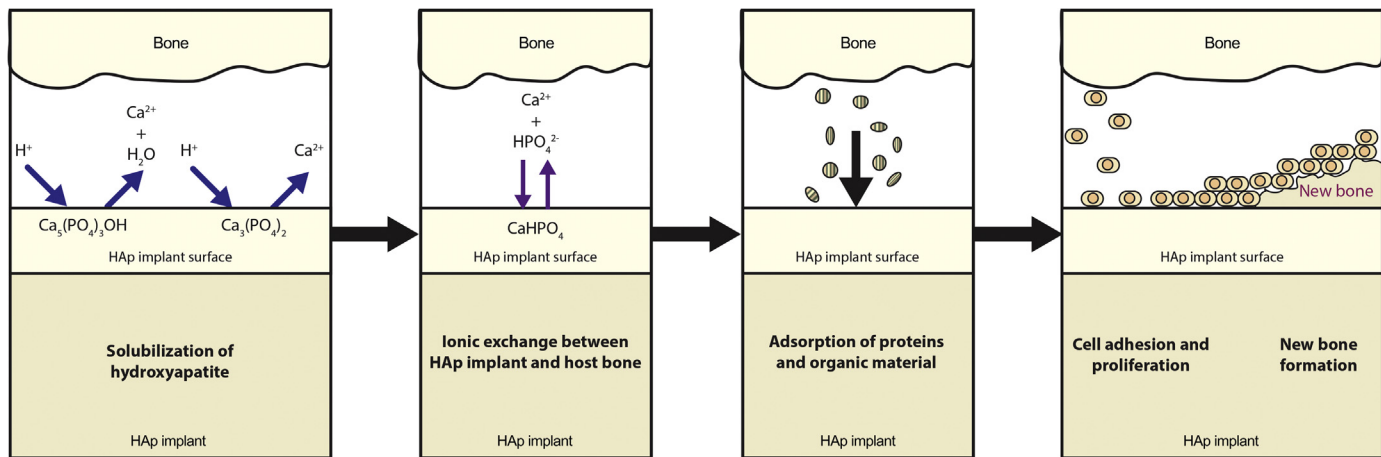


**FIGURE 11.3**

Schematic diagram representing the proposed mechanism that occurs at the surface of HAp after implantation.

ceramic material, not only for bone regeneration applications but also as a drug delivery system. Its degradation products are  $\text{Ca}^{2+}$  and  $\text{PO}_4^{3-}$  ions that already naturally occur in the body, since they are found in the bloodstream at relatively high concentrations (1–5 mM) (Bose and Tarafder, 2012).

---

## 11.6 CHITOSAN AS A BIOMATERIAL FOR BONE REGENERATION

CS is the main derivative of natural polymer chitin, the second most abundant natural polysaccharide on Earth, estimated to be produced almost as much as cellulose, with an annual production assessed to be over  $10^5$  tons worldwide (Zikakis, 2012; Ravi Kumar, 2000). Chitin is a white, inelastic, hard, nitrogenous polysaccharide found in the exoskeleton and in the internal structure of invertebrates, mainly in crustacean shells but also in some microorganisms, yeast, and fungi (Hamid et al., 2013). The use of chitin-based and chitin-derived biomaterials is growing particularly for applications requiring the biodegradability property.

The high nitrogen content gives unique properties to chitin and CS, making them of commercial interest (Georgieva et al., 2012). CS is obtained from the partial deacetylation of chitin, typically by chemical hydrolysis under strong alkaline conditions or by enzymatic hydrolysis under the action of particular enzymes such as chitin deacetylase (Croisier and Jérôme, 2013). Therefore, CS is characterized mainly by its degree of deacetylation (DD); to be considered CS DD should be at least 50% (Costa-Pinto et al., 2011). Structures of both natural polymers are shown in Fig. 11.4.

CS is a linear polymer of (1→4)-linked 2-amino-2-deoxy- $\beta$ -D-glucopyranose characterized mainly by a DD usually ranging from 50% to 95%, and molecular weight, which can vary from 50 kDa to more than 1000 kDa depending on its source and preparation method (Costa-Pinto et al., 2011; Di Martino et al., 2005; Domb and Kumar, 2011). It is a semicrystalline compound, with crystallinity dependent on its DD, and soluble in aqueous acidic solutions, where its solubility is mostly dependent on the protonation of amino groups (Costa-Pinto et al., 2011), which facilitates its processability, in opposition to some currently used materials in biomedical applications (Ravi Kumar, 2000).

CS presents a wide list of desirable properties for bone regeneration and controlled drug delivery, namely biocompatibility (Bavariya et al., 2014; Shin et al., 2005); mucoadhesiveness (He et al., 1998; Lehr et al., 1992); hydrophilic character, which promotes osteoblast adhesion and proliferation (Seol et al., 2004); wound healing properties (Azad et al., 2004; Ueno et al., 1999); and nontoxic biodegradation products (Croisier and Jérôme, 2013; Di Martino et al., 2005). Most of these properties are caused mainly by its cationic nature. This polymer contains

in its main backbone primary amino groups that become positively charged in acidic medium, as shown in Fig. 11.5 (Samal et al., 2012).

With a  $pK_a$  around 6.0–6.5 (Samal et al., 2012; Dash et al., 2011), it is both reactive and soluble as a function of pH, presenting solubility in the majority of organic acidic solutions including formic, acetic, tartaric, and citric acid

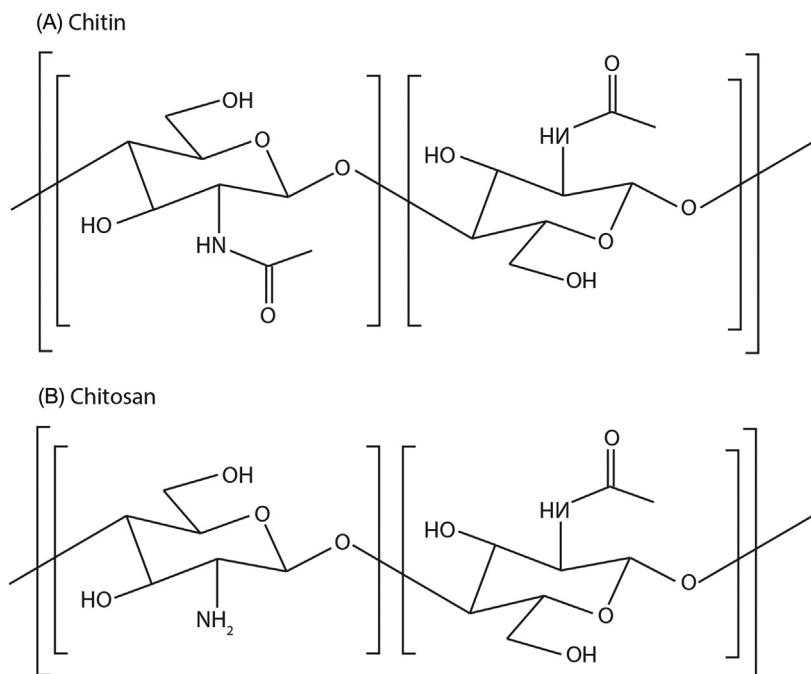


**FIGURE 11.4**

Structure of (A) chitin and (B) CS.

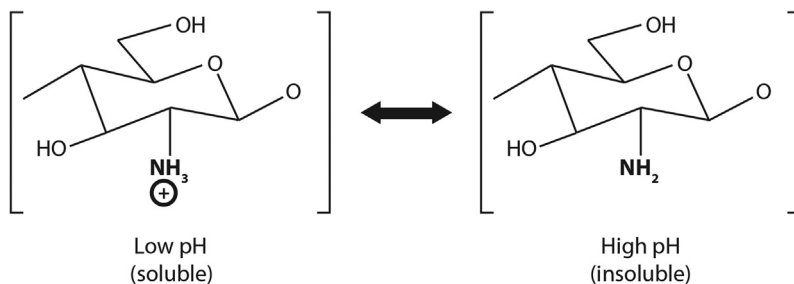


**FIGURE 11.5**

Cationic nature of CS.

(Nagpal et al., 2010). Thus, at low pH, the amino groups are protonated and render CS a cationic polyelectrolyte. This polyelectrolyte property has been employed to generate multilayer films or capsules using layer-by-layer assembly (Berth et al., 2002; Picart et al., 2005). Otherwise, at high pH the amines are deprotonated and CS changes from a soluble cationic polyelectrolyte to an insoluble polymer.

A notable effect of CS's polyelectrolyte behavior is the improved adhesion and proliferation of cells in the surface of CS-containing materials, caused by the electrostatic interaction of the positively charged CS with the negatively charged glycosaminoglycans (GAG), proteoglycans, and other negatively charged molecules. GAG and proteoglycans are noncollagenous ECM proteins that regulate and direct the construction and maintenance of the ECM (Burr and Allen, 2013). Given that both cytokines and growth factors bond to GAG, the formation of CS-GAG complexes in a bone graft is beneficial because they can promote the retention and concentration of these desirable substances on its surface (Di Martino et al., 2005; Kim et al., 2008).

In swollen state, CS acts as a natural bioadhesive, an ability that has been of special interest for drug delivery applications (Costa-Pinto et al., 2011; Şenel and McClure, 2004; Bertram and Bodmeier, 2006). The mucoadhesive property of CS is caused by its electrostatic interaction between positively charged CS and negatively charged residues, namely sialic acid, on mucosal surfaces (Croisier and Jérôme, 2013). Another feature of CS attributed to electrostatic interactions is its capacity to induce hemostasis, which has been related to interactions of positive charges of CS with negatively charged red blood cell membranes (Croisier and Jérôme, 2013; Rao and Sharma, 1997; Ong et al., 2008).

The antimicrobial activity of CS, a fundamental property in wound healing processes, has been widely studied (Ong et al., 2008; Altioek et al., 2010; Saravanan et al., 2011; Shi et al., 2006). In what regards orthopedic implants, bacterial infection is a major concern due to the severe consequences it can lead to, such as implant failure, hospitalization, and sometimes even mortality of the patient (Saravanan et al., 2011). Mechanisms explaining antibacterial and antifungal activity of CS are more complex. The first mechanism proposes that the high affinity of cationic groups of CS toward the anionic components in microorganisms' cell wall, such as Gram-negative lipopolysaccharide and cell surface proteins, alters the cells' permeability preventing the mass transport of essential materials across the cell wall. The second mechanism proposes the inhibition of the microbial RNA synthesis due to the bonding of protonated amino groups of CS with the cell DNA (Croisier and Jérôme, 2013; Domb and Kumar, 2011; Kong et al., 2010).

Another important property of CS is its biodegradability. A wide range of biomedical applications, including matrices for controlled drug release, resorbable devices such as bone cements, and scaffolds for tissue engineering, require the controlled degradation of the biomaterials over time to let the natural

tissue develop and completely replace the foreign element (Reis et al., 2008). CS's biodegradability takes place by lysozyme action, an abundant enzyme found in the human body, through the degradation into small glycomino chains, with degradation rate being inversely related to the DD. Regarding the biocompatibility of the degradation products, it has been reported that these products undergo a quick elimination by the kidney, thus avoiding accumulation in the body (Costa-Pinto et al., 2011; Reis et al., 2008).

In addition to all the above-mentioned desirable properties, including the solubility of CS in aqueous acidic medium that allows its processing under mild conditions (Levengood and Zhang, 2014; Croisier and Jérôme, 2013) together with CS's ability to be shaped into different forms such as porous scaffolds (Araujo et al., 2014; Ji et al., 2011; Siddiqui et al., 2015), fibers (Aklog et al., 2015; Albanna et al., 2013), sponges (Seol et al., 2004), and microparticles (Custódio et al., 2015; Obaidat et al., 2015; Shen et al., 2014), are advantageous features for tissue engineering applications (Costa-Pinto et al., 2011). Another advantage is its availability in large quantities and at adequate commercial grades (Bansal et al., 2011).

---

## 11.7 HYDROXYAPATITE/CHITOSAN NANOCOMPOSITE MATERIALS

The combination of n-HAp with CS has been of special interest for biomedical applications, particularly for bone regeneration. HAp by itself is highly brittle, whereas CS, despite its capacity to promote osteogenic cells' attachment and proliferation, it does not induce the deposition of bone minerals on its own. Therefore, when combining both components, HAp provides the required bioactivity while CS adds elasticity to the final material, resulting in a great candidate for nonload-bearing bone graft applications (Levengood and Zhang, 2014; Dorozhkin, 2011). However, even though combining HAp and CS can be advantageous, the production of such hybrid system still faces several challenges.

The final properties of any hybrid inorganic–organic system are affected by several important aspects that must be considered. A hybrid material consists of at least two phases separated by an interface, in which one of the phases is usually inorganic, consisting of filler particles, dispersed in the second phase, a polymeric matrix. The filler's shape and size, properties and volume percentage, the matrix properties such as molecular weight, the dispersion stability of the filler in the polymeric matrix, and the interactions in the filler/matrix interface are some of the main factors influencing the properties of the hybrid (Supova, 2009). Furthermore, in the case of hybrid materials for biomedical applications, biocompatibility, degradation rate, and nontoxicity must be considered as previously discussed.

From a chemical point of view, there are several ways to incorporate inorganic particles (fillers) into organic polymers, depending on the interactions between the constituents, either strong, weak, or without any chemical interactions between them. Strong interactions can be covalent, coordination type, and ionic bonds, whereas van der Waals, hydrogen bonds, and hydrophilic–hydrophobic are considered weak interactions. Inorganic–organic hybrid materials can be classified based on such interactions and the different arrangements of the polymer chains relative to the inorganic nanoparticles. In this regard, Kickelbick (2003) proposed four different types of arrangements, as shown in Fig. 11.6.

The first arrangement (Fig. 11.6A) takes place when, in the absence of strong interactions, the inorganic particles are dispersed in the organic matrix such that, depending on the functionalities of the components, the inorganic units undergo weak cross-linking through physical interactions with the polymer or, the

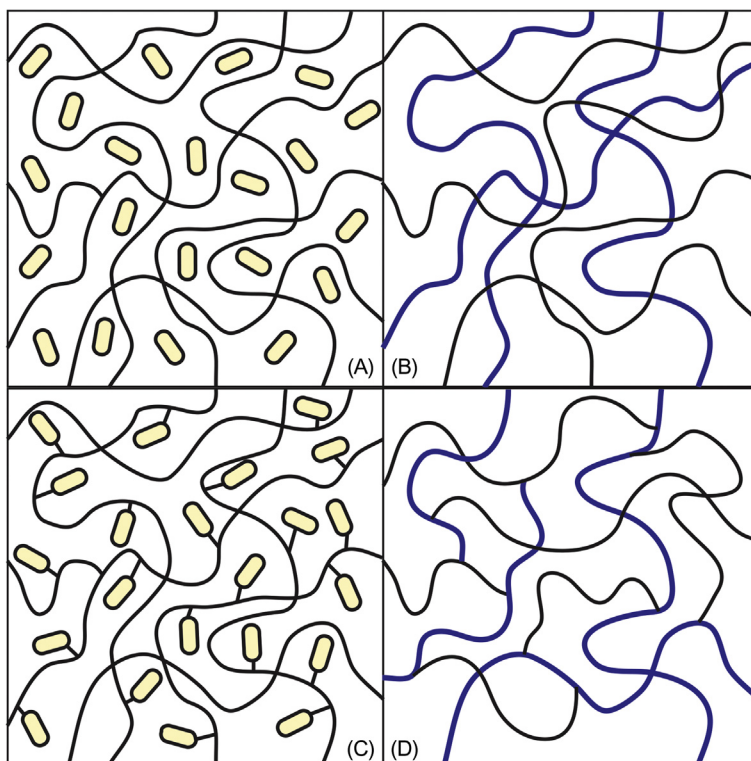


**FIGURE 11.6**

Schematic representation of different types of inorganic–organic hybrid materials based on polymeric chain arrangements relative to the inorganic particles: (A) inorganic particles embedded into the organic polymer; (B) IPNs; (C) inorganic particles chemically bound to the polymer backbone; and (D) dual inorganic–organic hybrid polymer.



inorganic particles are entrapped in a cross-linked polymeric matrix (Kickelbick, 2007). Interpenetrating polymer networks (IPNs) consist of a polymer comprising two or more networks that are, on a molecular scale, partially or totally interlaced but not covalently bound (Fig. 11.6B). In the case of inorganic–organic IPNs, formed for example by sol–gel reactions, one of the networks is formed by the inorganic component, and they can be processed either simultaneously or sequentially (Alemán et al., 2007). Finally, the hybrids can be produced by discrete (Fig. 11.6C) or interconnected (Fig. 11.6D) inorganic particles attached to the polymer backbone by covalent bonds (Kickelbick, 2003, 2007).

The chemical nature of CS makes it a versatile polymer as it can be either chemically or physically cross-linked. Chemical cross-linking is irreversible since a polymeric network is formed by covalent bonds, requiring the assistance of a cross-linking agent such as glutaraldehyde or genipin. Physical cross-linking, on the other hand, is reversible since linkage occurs through van der Waals forces, ionic attractions, hydrogen bonding, or hydrophobic interactions (Reis et al., 2008; Berger et al., 2004). Considering this, the incorporation of HAp nanoparticles into a CS matrix can be done following several techniques as described in the next section.

With advances in technology, various methods for producing HAp/CS nanocomposite materials have been reported, following both chemical and physical paths. In general, the production of HAp/CS materials requires a first stage of dispersion preparation, in which HAp and CS are combined to produce the base material that, in a second stage, is shaped into the final form. Thus, the second stage consists of the fixation of the structure—into microparticles, granules, scaffolds, cements, etc.—carried out by inducing phase separation and the elimination of the solvent. Afterward, the produced nanocomposites usually have to be subjected to purification and sterilization processes, since their potential applications are within the biomedical field. One of the key issues in these sequential procedures is to guarantee that none of the stages compromises, among other desirable properties, the morphological and architectural features of the final envisaged forms (scaffolds, powders, etc.) to ensure a suitable environment for cell attachment and proliferation. Fig. 11.7 shows schematically the stages used for the HAp/CS nanocomposite materials.

The dispersion preparation is a key stage of the productive process. Here the HAp is incorporated into the CS matrix. This step can be done in a number of ways; among all the methods reported, *in situ* coprecipitation and simple mixing are the most popular ones (Levengood and Zhang, 2014; Venkatesan and Kim, 2014).

In the so-called *in situ* coprecipitation the synthesis of HAp is carried out in the presence of CS in neutral or basic environment ( $\text{pH} \geq 7$ ), therefore, causing the precipitation of CS along with HAp simultaneously (Yamaguchi et al., 2001; Chen et al., 2002; Danilchenko et al., 2011). Yamaguchi et al. (2001) developed a methodology that consisted of dripping CS in  $\text{H}_3\text{PO}_4$  solution on a calcium hydroxide suspension. Homogeneous incorporation of HAp into the CS matrix has been reported using this process, however, the fact that the formation of HAp

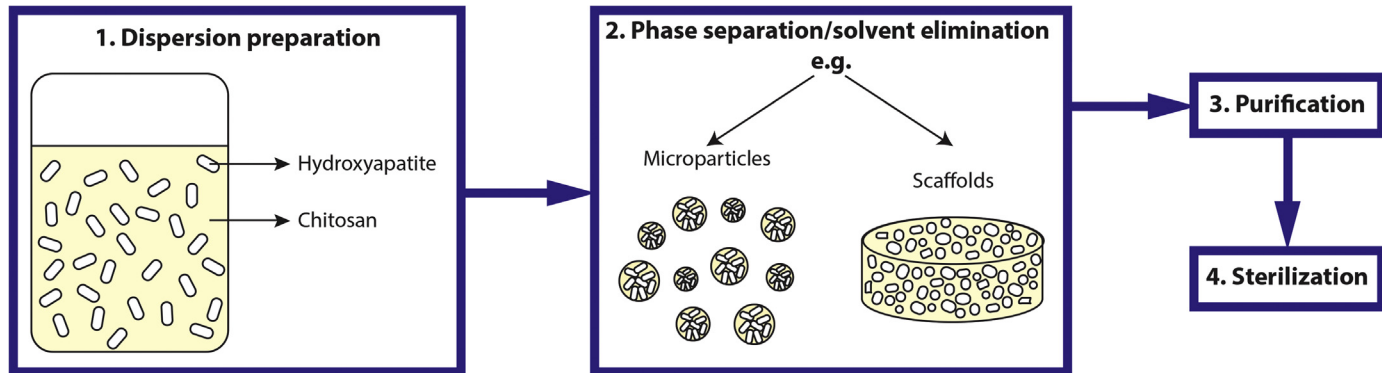


**FIGURE 11.7**

Schematic representation of the stages used for the HAp/CS nanocomposite materials.

occurs in the presence of CS can hinder the synthesis of high purity HAp and the achievement of the desired morphology.

An alternative method consists of physically mixing previously synthesized HAp particles, usually in powder form or ultrasonically dispersed in water, into a CS solution. Typically, this technique, also called *simple mixing* method, is carried out at lab-scale, by mixing both components in a vessel using a magnetic stirrer, resulting in final nanocomposite materials with quite favorable physicochemical and biological properties (Kim et al., 2009; Thein-Han and Misra, 2009; Zhao et al., 2002). This is a simple and straightforward technique that can also be advantageous in terms of reproducibility relative to the coprecipitation method; nevertheless it can lead to nonhomogeneous dispersions at a microscopic level due to the difficulty in controlling the mixing between the two dissimilar phases that can undergo phase separation (Supova, 2009; Peniche et al., 2010) and, therefore, originate final materials with weaker mechanical properties when compared with other methods (Hu et al., 2004; Chen et al., 2011).

An important parameter to consider when preparing n-HAp/CS hybrid dispersions is the pH, especially if HAp has to be introduced into an acidic environment that can influence its solubility, chemistry, and phase stability (Ito et al., 1996). When the method of physically mixing both components is used, HAp is often introduced in an acidic CS solution, resulting in dispersions with pH typically around 4, potentially causing the dissolution of HAp (Wilson and Hull, 2008). To the best of our knowledge, Wilson and Hull (2008) is the only report where HAp surface chemistry was studied after aging nanophase HAp particles in 0–2.5 wt.% CS acetate solutions for 30 days. After incorporation of HAp into CS solution, the HAp/CS mixtures had a pH around 4–5. The authors reported changes in HAp surface chemistry, colloid stability, and chemical composition after long-term aging of HAp in CS acetate gel solutions. Such changes were attributed to solubility effects, since HAp becomes slowly soluble at pH values lower than 5. It was also found that CS strongly adsorbs to HAp particles and improves colloid stability.

Following the dispersion preparation, the separation/solvent elimination stage involves the structural fixation of the n-HAp/CS nanocomposite material in its final form (e.g., microparticles, granules, pastes, scaffolds, cements, etc.), for which a number of methods can be used. The main techniques used for the production of microparticles and scaffolds, two of the most attractive structural forms of n-HAp/CS nanocomposites, are described in the next sections.

---

## 11.8 PREPARATION OF HYDROXYAPATITE/CHITOSAN MICROPARTICLES

The combination of HAp with CS for bone tissue engineering applications is typically directed to the production of porous scaffolds; nonetheless, advances in

science and technology have led to the development of particulate materials. The use of microparticles in tissue engineering and regenerative medicine can be very beneficial from a functional point of view; these are very versatile structures that, thanks to their reduced size, can be used as injectable systems, shaped into a solid substrate with increased surface area capable to promote chemical and biological reactions, or even be embedded into nanocomposite scaffolds for controlled release of bioactive substances (Oliveira and Mano, 2011; Silva et al., 2007a,b). In this context, the development of a particulate system containing n-HAp in a micrometer-sized matrix is advantageous; this approach allows HAp's superior properties at the nanoscale to be preserved in the form of microparticles that are easier to handle (Okuyama et al., 2006).

Emulsification is one of the most common methods used in the pharmaceutical industry for the production of microparticles. This method is based on the formation of an emulsion consisting of the n-HAp/CS dispersed into a nonmiscible phase. The presence of CS, which acts as a hydrogel precursor, allows the formation of the microparticles by hardening according to its sol–gel mechanism (Gasperini et al., 2014). Ding et al. (2012) produced HAp/CS composite microspheres by a water-in-oil (W/O) emulsion method such that HAp was precipitated in situ. For that,  $\text{Ca}(\text{NO}_3)_2$  was added to a CS solution and the mixture was emulsified in vegetable oil. Afterward, a phosphate source ( $\text{Na}_2\text{HPO}_4$ ) was added to the emulsion, followed by the addition of cross-linking agent glutaraldehyde and NaOH to induce the precipitation of the HAp within the CS matrix. As final product, the authors obtained 10- $\mu\text{m}$  HAp/CS composite microspheres with n-HAp particles homogeneously distributed in the CS. In addition, authors reported that the produced n-HAp was poorly crystalline and contained carbonate ions. Li et al. (2010) also produced HAp/CS composite particles by emulsification. In this case, the authors used a multiple water-oil-water emulsion method in which a mixture of  $\text{Ca}(\text{NO}_3)_2 \cdot 4\text{H}_2\text{O}$ , CS and  $(\text{NH}_4)_2\text{HPO}_4$  solutions were used as outer and inner aqueous phases respectively. Thus, the precipitation of HAp was carried out in situ and glutaraldehyde was used as cross-linking agent to finally produce the particles. Authors reported the production of core–shell HAp/CS composite nanospheres with 100- to 200-nm diameter.

Another appealing method for the production of n-HAp/CS microparticles is by spray drying. Among the existing techniques, spray drying is a promising technology for the manufacturing of microparticles with controllable size and morphology (Nandiyanto and Okuyama, 2011). It is a process widely used as a microencapsulation/stabilization technique in the food (Dias et al., 2015; Ribeiro et al., 2015) and pharmaceutical (Sollohub and Cal, 2010; Song et al., 2015) industries. Easy industrialization, cost-effectiveness, and continuous production are attractive features of this technique; however, special care must be taken with heat-sensitive materials, since prolonged contact with high temperatures can cause product degradation (Lima et al., 2012). This method is based on the drying of atomized droplets of a previously prepared solution or emulsion/dispersion using a cocurrent stream of hot gas.

Production of HAp/CS microparticles by spray drying was reported by Başargan et al. (2015) (Burr and Allen, 2013). In the approach used by the authors, a HAp/CS-slurry using the coprecipitation method ( $\text{pH} \geq 9.0$ ) was prepared, followed by spray drying. The effect of inlet temperatures ( $120^\circ\text{C}$  and  $160^\circ\text{C}$ ) and different HAp/CS weight ratios was studied. Spherical microparticles of mean size  $4\text{--}6\text{ }\mu\text{m}$  were produced, and an increase in the surface area with the addition of CS, as well as with the increase of inlet temperature, were observed. However, the FTIR analysis suggested the substitution of carbonate in the apatite structures, compromising the purity of HAp. Thermal degradation studies were not reported.

More recently, Ruphuy et al. (2016) produced n-HAp/CS composite microparticles by spray drying, using a standard nozzle of  $0.7\text{ mm}$  of diameter, and inlet temperature of  $170^\circ\text{C}$  and feed rate of approximately  $4.5\text{ mL/min}$  as operating conditions. The produced n-HAp/CS nanocomposite microparticles contained highly pure, nanometric HAp ( $50\text{ nm}$ ). The work studies the effect of pH and the presence of salts on the final microparticles' size and morphology. For that, n-HAp/CS nanodispersions were firstly prepared by simple mixing method at two different pH values, above ( $\text{pH} 7$ ) and below ( $\text{pH} 5.5$ ) CS  $\text{pK}_a$  ( $6.5$ ). The presence of salts was analyzed by preparing the nanocomposites with and without KCl. It was concluded that different types of spray-dried microparticles are produced depending on the pH at which the initial nanodispersions are produced; the microparticles produced at lower pH ( $\text{pH} 5.5$ ) were preferred over the particles produced at higher pH, which required an extra step in the production process and had a high tendency to form large agglomerates. Relative to the presence of KCl, it was determined that it has no beneficial effect on the stability of the precursor nanodispersions and its presence could hinder cells' metabolism by creating a hypertonic environment. In addition, it was proved that CS was not degraded during the spray drying process at the conditions used since no differences were observed when comparing the thermogravimetric (TG) plots of the spray-dried microparticles with TG plots of analogous of freeze-dried samples. Fig. 11.8 shows the SEM images of the obtained microparticles.

Besides W/O emulsion (Ding et al., 2012) and spray drying (Ruphuy et al., 2016; Başargan and Nasün-Saygılı, 2015), other methods that have been exploited to produce n-HAp/CS microparticles are supercritical assisted atomization (Reverchon and Adami, 2013), spray coagulation (Granja et al., 2004), and electro-spray coagulation (Chen et al., 2015). In the supercritical assisted atomization method, a supercritical fluid (commonly supercritical  $\text{CO}_2$ ) acts as a nonsolvent for the composite such that, when the n-HAp/CS composite dispersion is sprayed in the supercritical fluid, CS precipitates (Oliveira and Mano, 2011). Coagulation processes are based on polyelectrolytes ability to cross-link and form hydrogels; thus, in spray coagulation, the n-HAp/CS composite dispersion is sprayed into a bath solution under stirring, which contains a solution that promotes the hardening/gelation of CS (usually NaOH solution) (Dias et al., 2015; Lima et al., 2012). Lastly, electro-spraying consists of applying an electric

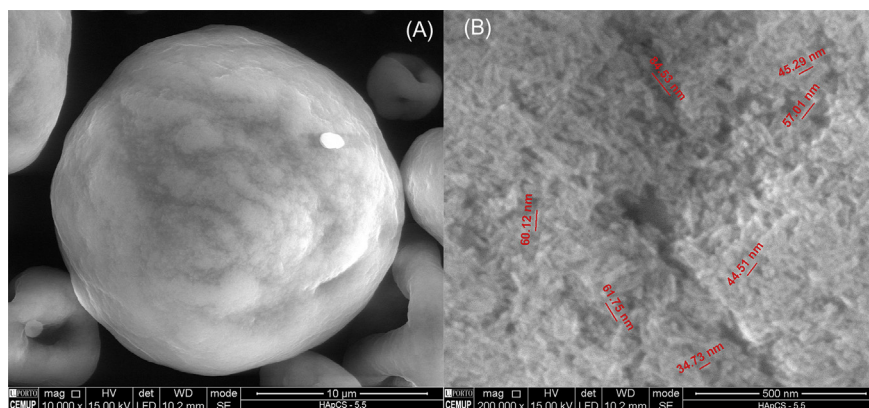


**FIGURE 11.8**

SEM images of the microparticles obtained by spray drying at lower pH (pH 5.5): (A) 10,000 × magnification showing one whole microparticle and (B) 200,000 × magnification showing the HAP nanoparticles at microparticle surface.

field to the composite dispersion extruded from a syringe. The high voltage potential applied makes the dispersion form a jet that, under specific parameters, allows the formation of the microparticles (Oliveira and Mano, 2011).

## 11.9 PREPARATION OF HYDROXYAPATITE/CHITOSAN SCAFFOLDS

The most typical structure produced for bone regeneration is *scaffold*. Taking advantage of the remarkable ability of bone self-regeneration, the idea behind a scaffold is to act as 3D template that once implanted in the bone defect, allows cell migration, adhesion, proliferation and eventually, the formation of new bone tissue. Considering this, microstructure is a key factor to be evaluated when producing scaffolds for bone regeneration. A combination of adequate pore sizes and interconnectivity is needed to allow the motion of cells throughout the scaffolds, as well as of the required nutrients and metabolites for cells' survival and proliferation (O'Brien, 2011). Several studies have been conducted regarding the relationship between pore size and cell activity, showing that both pores  $>100\ \mu\text{m}$  and pores  $<50\ \mu\text{m}$ , are important (Bose et al., 2012). Macropores ( $>100\ \mu\text{m}$ ) allow angiogenesis and contribute to nutrient and waste transport, whereas pores  $<50\ \mu\text{m}$  can improve osteointegration and generate cell anchoring sites (Agrawal and Ray, 2001; Lan Levensgood et al., 2010; Polak et al., 2011; Woodard et al., 2007; Klenke et al., 2008). Despite the advances achieved today, the production of the ideal bone scaffold still remains a challenge, mainly in what concerns the accomplishing of a balance between microstructure (high porosity with ideal pore

sizes) and mechanical properties (sufficient compression strength for a particular application).

The most frequently used technique to prepare n-HAp/CS scaffolds is freeze-drying. This is a simple procedure in which phase separation is induced by the formation of ice crystals upon freezing, followed by the elimination of the solvent by the sublimation of the ice crystals, producing the final nanocomposite 3D-porous structure (Levengood and Zhang, 2014; Costa-Pinto et al., 2011). Many authors using this technique obtained n-HAp/CS based nanocomposite scaffolds with desirable high porosity and interconnected pores (Thein-Han and Misra, 2009; Zhao et al., 2002; Kong et al., 2005, 2006; Oliveira et al., 2006; Jiang et al., 2008; Sultana et al., 2015). This technique, however, exhibits some limitations. Its major drawback is, probably, the formation of a surface skin caused by the collapse of the porous structure at the scaffold–air interface due to the interfacial tension generated during solvent evaporation (Levengood and Zhang, 2014). To avoid this phenomenon, temperature control must be rigorous such that an adequately low temperature is guaranteed to support the interfacial tension (Costa-Pinto et al., 2011). In addition, mechanical properties of these structures produced by freeze-drying are very limited, even if the scaffold is subjected to cross-linking of the CS (Costa-Pinto et al., 2011).

Zhang et al. (2015) recently studied the influence of the freeze-drying process on the final properties of HAp/CS nanocomposite scaffolds. For that, HAp/CS nanodispersions were prepared by simply mixing HAp nanoparticles in a CS solution. After dispersing the HAp particles by ultrasonication, the mixture was poured in cylindrical molds and subjected to different freezing methods (e.g., rapid cooling method was achieved using liquid nitrogen, whereas slow cooling method was carried out by placing samples in the freezer at  $-40^{\circ}\text{C}$  for 24 hours). The authors concluded that the prefreezing method has a great influence on the morphology and mechanical properties of the HAp/CS nanocomposite scaffolds. The scaffolds obtained by the slow cooling method exhibited both higher porosity and compression strength, comparatively with the ones obtained using the rapid cooling method.

Other popular phase separation/solvent elimination techniques to produce n-HAp/CS scaffolds are particulate leaching (Oliveira and Mano, 2011; Silva et al., 2007a), gas foaming (Silva et al., 2007b), and freeze-gelation (Okuyama et al., 2006). Particulate leaching is a multistep process, in which a porogen agent, such as salts, sugars, paraffin or gelatin, is mixed with the HAp/CS dispersion; next, the dispersion is subjected to freeze-drying, and finally, the porogen agent is leached out by immersion of the scaffold into a solvent solution, generating a final scaffold with two levels of porosity (one produced from the freeze-drying process and another one due to the porogen agent) (Levengood and Zhang, 2014). In gas foaming the formation of a porous structure is induced by the nucleation and growth of gas bubbles within the nanocomposite matrix by using a chemical foaming agent, which can leave unwanted contaminations, or a subcritical or



supercritical gas, for example, nitrogen or carbon dioxide, as blowing agents (Duarte et al., 2009a). Finally, in freeze-gelation pore formation occurs by freezing the nanocomposite dispersion followed by phase separation due the formation of solvent ice crystals. Then, the frozen scaffold is immersed, under freezing conditions, in a gelation solution bath, usually a mixture of NaOH and ethanol, thus inducing gelation and solvent exchange simultaneously. The final HAp/CS nanocomposite scaffold is obtained by air-drying (Rogina et al., 2015; Mu et al., 2010).

In most cases, the obtained n-HAp/CS nanocomposite material still presents residual substances left from the used process. The residual substances are reagents in excess, namely bases (e.g., NaOH) when the synthesis of HAp is carried out during the coprecipitation method or acids (e.g., acetic acid), which are used to solubilize the CS in the case of the simple mixing method. Thus, a purification/neutralization step is necessary to eliminate these residual substances that can compromise the material properties (cause structure disruption, or even inhibit cell growth and proliferation). The presence, for example, of residual acetic acid can cause scaffold disruption due to CS dissolution in acidic aqueous medium (Costa-Pinto et al., 2011). Additionally, to promote cell survival and proliferation, the culture environment must fulfill some fundamental physiological requirements, both in terms of composition and pH (Davis, 2011), which can be affected by the presence of acid and/or alkaline impurities.

Typically, purification/neutralization of n-HAp/CS scaffolds prepared by freeze-drying from dispersions obtained by the simple mixing method, which contain residual acetic acid remaining from CS solubilization, is carried out by immersion in an alkaline medium, washing with ultrapure water, and drying (usually through another freeze-drying step) (Levengood and Zhang, 2014; Thein-Han and Misra, 2009; Kong et al., 2005, 2006; Jiang et al., 2008; He et al., 2011). This neutralization process to remove the residual acetic acid is time consuming and can lead to low purity materials (i.e., materials with residual salts remaining from the used alkaline solution), as well as to materials with compromised structural integrity; the second freeze-drying step applied to the already formed scaffold can damage the porous structure. In fact, it has been reported that CS-based scaffolds undergo shrinkage and distortion after neutralization with NaOH solutions (Madihally and Matthew, 1999; Seda Tıǧlı et al., 2007).

---

## 11.10 HYDROXYAPATITE/CHITOSAN NANOCOMPOSITE MATERIALS STERILIZATION

As with any medical device that is implanted in the human body, n-HAp/CS nanocomposite materials produced for biomedical applications must be subjected to sterilization. The term *sterilization* refers to a procedure, either chemical or physical, whose purpose is to destroy all microbial life, including highly resistant



bacterial endospores (Rao and Sharma, 1995). Typical sterilization techniques include saturated water steam (autoclave), dry heat, ethylene oxide (EtO), and gamma irradiation. These techniques act either physically or chemically, and have proven to be effective eliminating microorganisms, however, they can induce changes in the macromolecular structure of polymeric materials by chain scission, oxidation, hydrolysis, and depolymerization, depending on the polymer's nature and the used sterilization technique (Juan et al., 2012). Studies conducted on CS-based materials have shown that these common sterilization techniques may cause irreversible modification in CS structure and function (Szymańska and Winnicka, 2015).

Therefore, when designing n-HAp/CS nanocomposite materials, sterilization is an important procedure to consider. Given that CS is a thermosensitive material, common sterilization techniques, such as dry heat and steam, are not appropriate since they can cause thermal degradation of the material. Jarry et al. (2001) studied the effects of steam sterilization on CS-based gels by autoclaving samples at 121°C for different times ranging from 0 to 60 minutes. Results from this study showed the degradation of CS after time periods as short as 10 minutes of autoclaving; the samples exhibited 30% decrease in molecular weight, three- to fivefold reduction in dynamic viscosity, and the mechanical properties of the CS-based gels, at 37°C, were significantly weakened. Likewise, Lim et al. (1999) analyzed the effects of heat treatment (dry heat and saturated steam) on the physical properties of CS. Temperatures from 60°C to 160°C were tested for time periods ranging from 0.5 to 4 hours. The samples experienced a change in color and lower water affinity (decreased aqueous solubility), which was attributed to heat-induced reactions involving the NH<sub>2</sub> groups, the formation of cross-links and chain rearrangements. Authors pointed out the need to further analyze if the colored samples have adverse effects on biocompatibility.

EtO and gamma irradiation, on the other hand, can affect CS chemical properties. The use of EtO risks the deposition of toxic residues on the materials surfaces and high-energy gamma irradiation can cause material degradation as well (Checinska et al., 2011). França et al. (2013) reported chemical changes on CS surface after exposure to EtO sterilization independently of its DD, which were attributed to oxidation of the amine groups. The experiments were conducted by exposing CS, in the form of powder, to EtO sterilization (30% EtO and 70% CO<sub>2</sub>) during 8 hours at 40°C and 40%–50% relative humidity. Furthermore, Marreco et al. (2004) reported a decreased in tensile strength of CS membranes after sterilization with EtO under the same conditions (30% EtO and 70% CO<sub>2</sub> for 8 hours at 40°C, and 40%–50% relative humidity). In this study, different sterilization methods were applied to CS membranes and the effects on morphological, mechanical properties, and cytotoxicity analyzed. Relative to gamma irradiation, Lim et al. (1998) conducted studies on CS films by irradiating samples with different doses, up to 25 kGy, at 0.73 kGy/h dose rate. Results showed that molecular weight of CS decreased considerably along with an increase in DD, with dependency on the gamma-irradiation dose.

Additionally, after irradiation exposure, water sorption capacity of the samples also decreased.

In this context, the use of supercritical CO<sub>2</sub> (scCO<sub>2</sub>) as an innovative sterilization technique has recently emerged (Checinska et al., 2011; Dillow et al., 2000; Hemmer et al., 2007; Kamihira et al., 1987; White et al., 2006; Zani et al., 2013; Zhang et al., 2006a,b) with high potentiality to sterilize n-HAp/CS composite materials. Supercritical CO<sub>2</sub> gathers a large amount of advantages that make it attractive for this particular application; it is an environmentally benign, nontoxic, nonflammable, noncorrosive, readily available, and inexpensive solvent (Duarte et al., 2009b; Quirk et al., 2004). This supercritical fluid has been well known for its outstanding solvent capacities due to its high diffusivity; it has been widely used in the food industry as an extraction medium, but also for processing pharmaceuticals due to its low critical temperature (Duarte et al., 2009a). Ruphuy et al. (2018) produced n-HAp/CS scaffolds using a scCO<sub>2</sub> assisted process in which scCO<sub>2</sub> was used for both purification and sterilization of the scaffolds in one single step. The overall process consisted of three simple stages: first, the preparation of the n-HAp/CS nanodispersions, followed by the structural fixation of the scaffolds by freeze-drying, and finally, the scCO<sub>2</sub> extraction. The latter was carried out in batch mode at a constant pressure of 8.0 MPa, and different extraction parameters were tested, namely temperatures of 40°C and 75°C and the number of cycles. It was determined that, by subjecting the scaffolds to the best-achieved conditions (two cycles at  $T = 75^{\circ}\text{C}$  and  $P = 8.0\text{ MPa}$ ) it was possible to remove 80% of the residual acetic acid. Furthermore, results from the microbiological assay showed no microbial growth on the scaffolds produced under such conditions (proving that the scaffolds were sterile), and the *in vitro* tests showed that the scaffolds were cytocompatible and osteoconductive. Finally, even when further studies are needed to validate scCO<sub>2</sub> extraction as an sterilization technique, the authors were able to produce scaffolds with desirable interconnected porous structure, fast swelling, and adequate pore sizes, using a process that allows the microstructural preservation of the scaffolds in contradistinction to other conventional methods.

---

## 11.11 CONCLUSIONS

HAp is an outstanding material exhibiting highly desirable properties for biomedical applications, mostly for bone regeneration, due to its similarity with the bone mineral phase. It has been combined with several polymers aiming at producing materials with improved properties. Particularly, its combination with CS has been of great interest for the production of nonload-bearing bone grafts, given the possibility to generate materials mimicking bone composition and with improved

properties, namely in what concerns elasticity. In addition, CS provides a wide list of interesting properties: it promotes osteoblasts' adhesion and proliferation, possesses antimicrobial properties, and it can be processed using mild conditions and can be shaped into different forms, to name some.

Commercially available products for bone regeneration still consist, to a great extent, of biological grafts, either from human or animal sources. However, these grafts present extensive drawbacks, namely, high cost, risk of rejection, risk of diseases and zoonoses transmission, allergenic responses, etc. In what concerns synthetic materials, the market offers a variety of calcium phosphate-based products, alone or combined with other components, mainly collagen. In the performed survey, only one company commercializing calcium phosphate-based products containing CS was found, showing that, besides the many studies proving its suitability for tissue regeneration, HAp/CS nanocomposite materials have not yet made the leap from the laboratory to the market.

Relative to the production of n-HAp/CS nanocomposite materials envisaging biomedical applications, a sequence of productive steps must be followed. Generally, the process starts with the dispersion preparation, in which n-HAp is incorporated into the CS solution. The second stage involves a phase separation/solvent elimination process in which the final structural form (e.g., microparticles or scaffolds) is fixed. Finally, as their potential applications are within the biomedical field, the produced nanocomposite materials have to be subjected to purification and sterilization processes.

The preparation of n-HAp/CS nanocomposite dispersions requires the introduction of HAp into an aqueous environment that can influence its solubility, surface chemistry, and phase stability, affecting, simultaneously, the HAp-nanoparticles/CS-matrix interface interactions and, therefore, the material's final properties. The phase separation/solvent elimination stage determines important structural features of the final product, such as pore size and interconnectivity, particle size, and morphology, and can dictate the need for subsequent purification processes. Purification is a fundamental procedure that can be time consuming, ineffective, and change the properties of the obtained n-HAp/CS nanocomposites.

Most common methods available today for sterilization can cause thermal degradation or deposition of toxic residues on the material's surface. In this context, supercritical CO<sub>2</sub> gathers a large amount of advantages, emerging as a technique with high potentiality to sterilize n-HAp/CS composite materials, without causing structural disruption or compromising the physicochemical and mechanical properties of final composite materials.

Finally, the overall process has an important influence in the final product in terms of efficiency, costs, reproducibility, properties, and versatility. It is of utmost importance from a clinical point of view to have ready-to-use products without requiring extra steps prior to use, and materials that can be easily adapted into different shapes.

## REFERENCES

- Ace Surgical Supply Co., Inc., Available from: <<http://www.acesurgical.com/bone-grafting.html>> (accessed 24.03.16.).
- Agrawal, C., Ray, R.B., 2001. Biodegradable polymeric scaffolds for musculoskeletal tissue engineering. *J. Biomed. Mater. Res.* 55 (2), 141–150.
- Agrawal, C.M., Niederauer, G.G., Athanasiou, K.A., 1995. Fabrication and characterization of PLA-PGA orthopedic implants. *Tiss. Eng.* 1 (3), 241–252.
- Aklog, Y.F., et al., 2015. Preparation of chitosan nanofibers from completely deacetylated chitosan powder by a downsizing process. *Int. J. Biol. Macromol.* 72, 1191–1195.
- Albanna, M.Z., et al., 2013. Chitosan fibers with improved biological and mechanical properties for tissue engineering applications. *J. Mech. Behav. Biomed. Mater.* 20, 217–226.
- Alemán, J., et al., 2007. Definitions of terms relating to the structure and processing of sols, gels, networks, and inorganic-organic hybrid materials (IUPAC Recommendations 2007). *Pure Appl. Chem.* 79 (10), 1801–1829.
- AlloSource TM, Available from: <<http://www.allosource.org>> (accessed 24.03.16.).
- Altioek, D., Altioek, E., Tihminlioglu, F., 2010. Physical, antibacterial and antioxidant properties of chitosan films incorporated with thyme oil for potential wound healing applications. *J. Mater. Sci. Mater. Med.* 21 (7), 2227–2236.
- Amit, S.M., Xinfeng, S., Antonios, G.M., 2006. Nanocomposite scaffolds for tissue engineering. In: Bronzino, J.D. (Ed.), *Tissue Engineering and Artificial Organs*. CRC Press, pp. 40-1–40-11.
- Araujo, J.V., et al., 2014. Novel porous scaffolds of pH responsive chitosan/carrageenan-based polyelectrolyte complexes for tissue engineering. *J. Biomed. Mater. Res. A* 102 (12), 4415–4426.
- Artoss GmbH, Available from: <<http://www.artoss.com/dental/produkte.html?L=1>> (accessed 28.03.16.).
- Azad, A.K., et al., 2004. Chitosan membrane as a wound-healing dressing: characterization and clinical application. *J. Biomed. Mater. Res. Part B Appl. Biomater.* 69B (2), 216–222.
- Bansal, V., et al., 2011. Applications of chitosan and chitosan derivatives in drug delivery. *Adv. Biol. Res.* 5 (1), 28–37.
- Barbucci, R., 2002. *Integrated Biomaterials Science*. Springer Science & Business Media.
- Başargan, T., Nasün-Saygılı, G., 2015. Spray dried mesoporous hydroxyapatite-chitosan biocomposites. *Polym. Plast. Technol. Eng.* 54 (11), 1172–1183.
- Bavariya, A.J., et al., 2014. Evaluation of biocompatibility and degradation of chitosan nanofiber membrane cross-linked with genipin. *J. Biomed. Mater. Res. Part B Appl. Biomater.* 102 (5), 1084–1092.
- Baxter, Available from: <[http://www.baxterbiosurgery.com/us/products/actifuse//formulations/actifuse\\_mis.html](http://www.baxterbiosurgery.com/us/products/actifuse//formulations/actifuse_mis.html)> (accessed 28.03.16.).
- Berger, J., et al., 2004. Structure and interactions in covalently and ionically crosslinked chitosan hydrogels for biomedical applications. *Eur. J. Pharm. Biopharm.* 57 (1), 19–34.
- Berkeley Advanced Biomaterials Inc., Available from: <<http://www.ostetic.com/products.html>> (accessed 28.03.16.).

- Bertazzo, S., et al., 2010. Hydroxyapatite surface solubility and effect on cell adhesion. *Colloids Surf. B Biointerfaces* 78 (2), 177–184.
- Berth, G., et al., 2002. Polyelectrolyte complexes and layer-by-layer capsules from chitosan/chitosan sulfate. *Biomacromolecules* 3 (3), 579–590.
- Bertram, U., Bodmeier, R., 2006. In situ gelling, bioadhesive nasal inserts for extended drug delivery: in vitro characterization of a new nasal dosage form. *Eur. J. Pharm. Sci.* 27 (1), 62–71.
- Biocomposites Ltd., Available from: <<http://www.biocomposites.com/our-products/>> (accessed 28.03.16.).
- Biomet3i TM, Available from: <<http://www.biomet3i.com/index.cfm?cty = US&lang = EN>> (accessed 24.03.16.).
- Bonfield, W., et al., 1981. Hydroxyapatite reinforced polyethylene—a mechanically compatible implant material for bone replacement. *Biomaterials* 2 (3), 185–186.
- Bose, S., Tarafder, S., 2012. Calcium phosphate ceramic systems in growth factor and drug delivery for bone tissue engineering: a review. *Acta Biomater.* 8 (4), 1401–1421.
- Bose, S., Roy, M., Bandyopadhyay, A., 2012. Recent advances in bone tissue engineering scaffolds. *Trends Biotechnol.* 30 (10), 546–554.
- Botiss Dental GmbH, Available from: <<https://www.botiss.com/en/>> (accessed 24.03.16.).
- Brydone, A., Meek, D., MacLaine, S., 2010. Bone grafting, orthopaedic biomaterials, and the clinical need for bone engineering. *Proc. Inst. Mech. Eng. H* 224 (12), 1329–1343.
- Burr, D.B., Allen, M.R., 2013. *Basic and Applied Bone Biology*. Elsevier Science.
- Campana, V., et al., 2014. Bone substitutes in orthopaedic surgery: from basic science to clinical practice. *J. Mater. Sci. Mater. Med.* 25 (10), 2445–2461.
- Ceramed, Available from: <[www.ceramed.pt](http://www.ceramed.pt)> (accessed 28.03.16.).
- Checinska, A., et al., 2011. Sterilization of biological pathogens using supercritical fluid carbon dioxide containing water and hydrogen peroxide. *J. Microbiol. Methods* 87 (1), 70–75.
- Chen, F., Wang, Z.-C., Lin, C.-J., 2002. Preparation and characterization of nano-sized hydroxyapatite particles and hydroxyapatite/chitosan nano-composite for use in biomedical materials. *Mater. Lett.* 57 (4), 858–861.
- Chen, F., et al., 2007. Biocompatibility of electrophoretical deposition of nanostructured hydroxyapatite coating on roughen titanium surface: in vitro evaluation using mesenchymal stem cells. *J. Biomed. Mater. Res. Part B Appl. Biomater.* 82B (1), 183–191.
- Chen, J., et al., 2011. Effects of in situ and physical mixing on mechanical and bioactive behaviors of nano hydroxyapatite–chitosan scaffolds. *J. Biomater. Sci. Polym. Ed.* 22 (15), 2097–2106.
- Chen, J., et al., 2015. Preparation of chitosan/nano hydroxyapatite organic–inorganic hybrid microspheres for bone repair. *Colloids Surf. B Biointerfaces* 134, 401–407.
- Costa-Pinto, A.R., Reis, R.L., Neves, N.M., 2011. Scaffolds based bone tissue engineering: the role of chitosan. *Tissue. Eng. Part. B Rev.* 17 (5), 331–347.
- Croisier, F., Jérôme, C., 2013. Chitosan-based biomaterials for tissue engineering. *Eur. Polym. J.* 49 (4), 780–792.
- Curasan, Available from: <<http://www.curasan.de/en/portfolio-item/cerasorb-m-granulate-dental/#toggle-id-2>> (accessed 28.03.16.).
- Custódio, C.A., et al., 2015. Cell selective chitosan microparticles as injectable cell carriers for tissue regeneration. *Biomaterials* 43, 23–31.

- Danilchenko, S.N., et al., 2011. Characterization and in vivo evaluation of chitosan-hydroxyapatite bone scaffolds made by one step coprecipitation method. *J. Biomed. Mater. Res. A* 96A (4), 639–647.
- Dash, M., et al., 2011. Chitosan—a versatile semi-synthetic polymer in biomedical applications. *Prog. Polym. Sci.* 36 (8), 981–1014.
- Davis, J.M., 2011. *Animal Cell Culture: Essential Methods*. Wiley.
- D-bone, Available from: <<http://dbonegraft.com>> (accessed 24.03.16.).
- DePuy Synthes TM, Available from: <<http://emea.depuyssynthes.com/hcp/biomaterials>> (accessed 24.03.16.).
- Dias, M.I., Ferreira, I.C.F.R., Barreiro, M.F., 2015. Microencapsulation of bioactives for food applications. *Food Funct.* 6 (4), 1035–1052.
- Dillow, A.K., et al., 2000. Supercritical fluid sterilization method. Google Patents.
- Di Martino, A., Sittering, M., Risbud, M.V., 2005. Chitosan: a versatile biopolymer for orthopaedic tissue-engineering. *Biomaterials* 26 (30), 5983–5990.
- Ding, C.-C., Teng, S.-H., Pan, H., 2012. In-situ generation of chitosan/hydroxyapatite composite microspheres for biomedical application. *Mater. Lett.* 79, 72–74.
- Domb, A.J., Kumar, N., 2011. *Biodegradable Polymers in Clinical Use and Clinical Development*. John Wiley & Sons.
- Dorozhkin, S.V., 2010. Calcium orthophosphates as bioceramics: state of the art. *J. Funct. Biomater.* 1 (1), 22.
- Dorozhkin, S.V., 2011. Biocomposites and hybrid biomaterials based on calcium orthophosphates. *Biomater* 1 (1), 3–56.
- Duarte, A.R.C., Mano, J., Reis, R., 2009a. Supercritical fluids in biomedical and tissue engineering applications: a review. *Int. Mater. Rev.* 54 (4), 214–222.
- Duarte, A.R.C., Mano, J.F., Reis, R.L., 2009b. Perspectives on: supercritical fluid technology for 3d tissue engineering scaffold applications. *J. Bioact. Compat. Polym.* 24 (4), 385–400.
- Ducheyne, P., Qiu, Q., 1999. Bioactive ceramics: the effect of surface reactivity on bone formation and bone cell function. *Biomaterials* 20 (23–24), 2287–2303.
- Ducheyne, P., Radin, S., King, L., 1993. The effect of calcium phosphate ceramic composition and structure on in vitro behavior. I. Dissolution. *J. Biomed. Mater. Res.* 27 (1), 25–34.
- Exactech, Available from: <<https://www.exac.com/products/biologics/>> (accessed 24.03.16.).
- Fathi, M., Hanifi, A., Mortazavi, V., 2008. Preparation and bioactivity evaluation of bone-like hydroxyapatite nanopowder. *J. Mater. Process. Technol.* 202 (1), 536–542.
- Ferraz, M., Monteiro, F., Manuel, C., 2004. Hydroxyapatite nanoparticles: a review of preparation methodologies. *J. Appl. Biomater. Biomech.* 2 (2), 74–80.
- Fluidinova, Available from: <<http://www.fluidinova.com>> (accessed 28.03.16.).
- França, R., et al., 2013. The effect of ethylene oxide sterilization on the surface chemistry and in vitro cytotoxicity of several kinds of chitosan. *J. Biomed. Mater. Res. Part B Appl. Biomater.* 101 (8), 1444–1455.
- Gasperini, L., Mano, J.F., Reis, R.L., 2014. Natural polymers for the microencapsulation of cells. *J. R. Soc. Interface* 11 (100).
- Geistlich Pharma, Available from: <<http://www.geistlich-pharma.com/en/>> (accessed 24.03.16.).
- Georgieva, V., Zvezdova, D., Vlaev, L., 2012. Non-isothermal kinetics of thermal degradation of chitosan. *Chem. Cent. J.* 6, 81.

- Gleiter, H., 1995. Nanostructured materials: state of the art and perspectives. *Nanostruct. Mater.* 6 (1–4), 3–14.
- Granja, P., et al., 2004. *Preparation and characterization of injectable chitosan-hydroxyapatite microspheres*. Key Engineering Materials. Trans Tech Publ.
- Hamid, R., et al., 2013. Chitinases: an update. *J. Pharm. Bioall. Sci.* 5 (1), 21–29.
- He, P., Davis, S.S., Illum, L., 1998. In vitro evaluation of the mucoadhesive properties of chitosan microspheres. *Int. J. Pharm.* 166 (1), 75–88.
- He, Q., et al., 2011. Preparation of chitosan films using different neutralizing solutions to improve endothelial cell compatibility. *J. Mater. Sci. Mater. Med.* 22 (12), 2791–2802.
- Hemmer, J.D., et al., 2007. Sterilization of bacterial spores by using supercritical carbon dioxide and hydrogen peroxide. *J. Biomed. Mater. Res. Part B Appl. Biomater.* 80B (2), 511–518.
- Heraeus Kulzer GmbH, Available from: <[http://heraeus-kulzer.com/en/int/dentist/products\\_from\\_a\\_to\\_z/ostim\\_1/ostim.aspx](http://heraeus-kulzer.com/en/int/dentist/products_from_a_to_z/ostim_1/ostim.aspx)> (accessed 28.03.16.).
- Hossein Fathi, M., Mortazavi, V., Roohani Esfahani, S.I., 2009. Bioactivity evaluation of synthetic nanocrystalline hydroxyapatite. *Dent. Res. J.* 5 (2), 81–87.
- Hoya Technosurgical Corporation, Available from: <[http://www.hoyatechnosurgical.co.jp/pentax/newceramics\\_e.php](http://www.hoyatechnosurgical.co.jp/pentax/newceramics_e.php)> (accessed 28.03.16.).
- Hu, Q., et al., 2004. Preparation and characterization of biodegradable chitosan/hydroxyapatite nanocomposite rods via in situ hybridization: a potential material as internal fixation of bone fracture. *Biomaterials* 25 (5), 779–785.
- Impladent Ltd., Available from: <<http://www.impladentltd.com/OsteoGen-p/200.htm>> (accessed 28.03.16.).
- Ito, M., et al., 1996. In vitro properties of a chitosan-bonded bone-filling paste: studies on solubility of calcium phosphate compounds. *J. Biomed. Mater. Res.* 32 (1), 95–98.
- Itokazu, M., et al., 1998. Development of porous apatite ceramic for local delivery of chemotherapeutic agents. *J. Biomed. Mater. Res.* 39 (4), 536–538.
- Jary, C., et al., 2001. Effects of steam sterilization on thermogelling chitosan-based gels. *J. Biomed. Mater. Res.* 58 (1), 127–135.
- Ji, C., et al., 2011. Fabrication of porous chitosan scaffolds for soft tissue engineering using dense gas CO<sub>2</sub>. *Acta Biomater.* 7 (4), 1653–1664.
- Jiang, L., et al., 2008. Preparation and properties of nano-hydroxyapatite/chitosan/carboxymethyl cellulose composite scaffold. *Carbohydr. Polym.* 74 (3), 680–684.
- Juan, A.S., et al., 2012. Degradation of chitosan-based materials after different sterilization treatments. *IOP Conf. Ser. Mater. Sci. Eng.* 31 (1), 012007.
- Kamihira, M., Taniguchi, M., Kobayashi, T., 1987. Sterilization of microorganisms with supercritical carbon dioxide. *Agric. Biol. Chem.* 51 (2), 407–412.
- Kandori, K., et al., 2009. Synthesis of positively charged calcium hydroxyapatite nanocrystals and their adsorption behavior of proteins. *Colloids Surf. B Biointerfaces* 73 (1), 140–145.
- Kantharia, N., et al., 2014. Nano-hydroxyapatite and its contemporary applications. *Bone* 34 (15.2), 1.71.
- Kerr TM, Available from: <<https://www.kerrdental.com/kerr-restoratives/bioplant-dental-bone-grafting-material>> (accessed 28.03.16.).
- Kickelbick, G., 2003. Concepts for the incorporation of inorganic building blocks into organic polymers on a nanoscale. *Prog. Polym. Sci.* 28 (1), 83–114.

- Kickelbick, G., 2007. Introduction to hybrid materials. Hybrid Materials. Wiley-VCH Verlag GmbH & Co. KGaA, pp. 1–48.
- Kim, I.-Y., et al., 2008. Chitosan and its derivatives for tissue engineering applications. *Biotechnol. Adv.* 26 (1), 1–21.
- Kim, S.-H., et al., 2009. Preparation of high flexible composite film of hydroxyapatite and chitosan. *Polym. Bull.* 62 (1), 111–118.
- Klenke, F.M., et al., 2008. Impact of pore size on the vascularization and osseointegration of ceramic bone substitutes in vivo. *J. Biomed. Mater. Res. A* 85A (3), 777–786.
- Kolk, A., et al., 2012. Current trends and future perspectives of bone substitute materials – from space holders to innovative biomaterials. *J. Craniomaxillofac. Surg.* 40 (8), 706–718.
- Kong, L., et al., 2005. Preparation and characterization of nano-hydroxyapatite/chitosan composite scaffolds. *J. Biomed. Mater. Res. A* 75A (2), 275–282.
- Kong, L., et al., 2006. A study on the bioactivity of chitosan/nano-hydroxyapatite composite scaffolds for bone tissue engineering. *Eur. Polym. J.* 42 (12), 3171–3179.
- Kong, M., et al., 2010. Antimicrobial properties of chitosan and mode of action: a state of the art review. *Int. J. Food Microbiol.* 144 (1), 51–63.
- Koutsopoulos, S., 2001. Kinetic study on the crystal growth of hydroxyapatite. *Langmuir* 17 (26), 8092–8097.
- Kumar, P., Vinitha, B., Fathima, G., 2013. Bone grafts in dentistry. *J. Pharm. Bioallied Sci.* 5 (Suppl 1), S125–S127.
- Lan Levengood, S.K., et al., 2010. The effect of BMP-2 on micro- and macroscale osteointegration of biphasic calcium phosphate scaffolds with multiscale porosity. *Acta Biomater.* 6 (8), 3283–3291.
- Lehr, C.-M., et al., 1992. In vitro evaluation of mucoadhesive properties of chitosan and some other natural polymers. *Int. J. Pharm.* 78 (1), 43–48.
- Levengood, S.K.L., Zhang, M., 2014. Chitosan-based scaffolds for bone tissue engineering. *J. Mater. Chem. B* 2, 3161.
- Li, X., et al., 2010. Synthesis and characterization of core-shell hydroxyapatite/chitosan biocomposite nanospheres. *J. Wuhan Univ. Technol. Mater. Sci. Ed.* 25 (2), 252–256.
- Lim, L.-Y., Khor, E., Koo, O., 1998.  $\gamma$  Irradiation of chitosan. *J. Biomed. Mater. Res.* 43 (3), 282–290.
- Lim, L.-Y., Khor, E., Ling, C.-E., 1999. Effects of dry heat and saturated steam on the physical properties of chitosan. *J. Biomed. Mater. Res.* 48 (2), 111–116.
- Lima, A.C., Sher, P., Mano, J.F., 2012. Production methodologies of polymeric and hydrogel particles for drug delivery applications. *Expert. Opin. Drug. Deliv.* 9 (2), 231–248.
- Liu, X., Ma, P.X., 2004. Polymeric scaffolds for bone tissue engineering. *Ann. Biomed. Eng.* 32 (3), 477–486.
- Ma, G., Liu, X.Y., 2009. Hydroxyapatite: hexagonal or monoclinic? *Cryst. Growth Des.* 9 (7), 2991–2994.
- Madihally, S.V., Matthew, H.W.T., 1999. Porous chitosan scaffolds for tissue engineering. *Biomaterials* 20 (12), 1133–1142.
- Marreco, P.R., et al., 2004. Effects of different sterilization methods on the morphology, mechanical properties, and cytotoxicity of chitosan membranes used as wound dressings. *J. Biomed. Mater. Res. Part B Appl. Biomater.* 71B (2), 268–277.



- McNaught, A.D., McNaught, A.D., 2014. *Compendium of Chemical Terminology* (Gold Book, Version 2.3.3). Blackwell Science Oxford.
- Mu, C., et al., 2010. Fabrication of microporous membranes by a feasible freeze method. *J. Memb. Sci.* 361 (1–2), 15–21.
- Mucalo, M., 2015. *Hydroxyapatite (HAp) for Biomedical Applications*. Elsevier Science.
- Nagpal, K., Singh, S.K., Mishra, D.N., 2010. Chitosan nanoparticles: a promising system in novel drug delivery. *Chem. Pharm. Bull. (Tokyo)* 58 (11), 1423–1430.
- Nandiyanto, A.B.D., Okuyama, K., 2011. Progress in developing spray-drying methods for the production of controlled morphology particles: from the nanometer to submicrometer size ranges. *Adv. Powder Technol.* 22 (1), 1–19.
- Obaidat, R., et al., 2015. Drying using supercritical fluid technology as a potential method for preparation of chitosan aerogel microparticles. *AAPS PharmSciTech.* 1–10.
- O'Brien, F.J., 2011. Biomaterials & scaffolds for tissue engineering. *Mater. Today* 14 (3), 88–95.
- Okuyama, K., et al., 2006. Preparation of functional nanostructured particles by spray drying. *Adv. Powder Technol.* 17 (6), 587–611.
- Oliveira, M.B., Mano, J.F., 2011. Polymer-based microparticles in tissue engineering and regenerative medicine. *Biotechnol. Prog.* 27 (4), 897–912.
- Oliveira, J.M., et al., 2006. Novel hydroxyapatite/chitosan bilayered scaffold for osteochondral tissue-engineering applications: scaffold design and its performance when seeded with goat bone marrow stromal cells. *Biomaterials* 27 (36), 6123–6137.
- Ong, S.-Y., et al., 2008. Development of a chitosan-based wound dressing with improved hemostatic and antimicrobial properties. *Biomaterials* 29 (32), 4323–4332.
- Oryan, A., et al., 2014. Bone regenerative medicine: classic options, novel strategies, and future directions. *J. Orthop. Surg.* 9 (1), 1–27.
- Ost-Developpement, Available from: <<http://www.ost-developpement.com>> (accessed 24.03.16.).
- Osteohealth, Available from: <<http://www.ostehealth.com/Products.aspx>> (accessed 24.03.16.).
- Park, J., 2009. *Bioceramics: Properties, Characterizations, and Applications*. Springer, New York.
- Peniche, C., et al., 2010. Chitosan/hydroxyapatite-based composites. *Bioteecnología Aplicada* 27, 202–210.
- Picart, C., et al., 2005. Controlled degradability of polysaccharide multilayer films in vitro and in vivo. *Adv. Funct. Mater.* 15 (11), 1771–1780.
- Polak, S.J., et al., 2011. Analysis of the roles of microporosity and BMP-2 on multiple measures of bone regeneration and healing in calcium phosphate scaffolds. *Acta Biomater.* 7 (4), 1760–1771.
- Quirk, R.A., et al., 2004. Supercritical fluid technologies and tissue engineering scaffolds. *Curr. Opin. Solid State Mater. Sci.* 8 (3–4), 313–321.
- Rao, S.B., Sharma, C.P., 1995. Sterilization of chitosan: implications. *J. Biomater. Appl.* 10 (2), 136–143.
- Rao, S.B., Sharma, C.P., 1997. Use of chitosan as a biomaterial: studies on its safety and hemostatic potential. *J. Biomed. Mater. Res.* 34 (1), 21–28.
- Ravi Kumar, M.N.V., 2000. A review of chitin and chitosan applications. *React. Funct. Polym.* 46 (1), 1–27.
- Reis, R.L., et al., 2008. *Natural-Based Polymers for Biomedical Applications*. Elsevier.

- Reverchon, E., Adami, R., 2013. Supercritical assisted atomization to produce nanostructured chitosan-hydroxyapatite microparticles for biomedical application. *Powder Technol.* 246 (0), 441–447.
- Ribeiro, A., et al., 2015. Spray-drying microencapsulation of synergistic antioxidant mushroom extracts and their use as functional food ingredients. *Food Chem.* 188 (0), 612–618.
- Ricciardi, B.F., Bostrom, M.P., 2013. Bone graft substitutes: claims and credibility. *Semin. Arthropl.* 24 (2), 119–123.
- Rodrigues, S.C., et al., 2013. Preparation and characterization of collagen-nanohydroxyapatite biocomposite scaffolds by cryogelation method for bone tissue engineering applications. *J. Biomed. Mater. Res. A* 101A (4), 1080–1094.
- Rogina, A., et al., 2015. Effect of in situ formed hydroxyapatite on microstructure of freeze-gelled chitosan-based biocomposite scaffolds. *Eur. Polym. J.* 68, 278–287.
- Rouahi, M., et al., 2006. Physico-chemical characteristics and protein adsorption potential of hydroxyapatite particles: influence on in vitro biocompatibility of ceramics after sintering. *Colloids Surf. B Biointerfaces* 47 (1), 10–19.
- Ruphuy, G., et al., 2016. Spray drying as a viable process to produce nano-hydroxyapatite/chitosan (n-HAp/CS) hybrid microparticles mimicking bone composition. *Adv. Powder Technol.* 27 (2), 575–583.
- Ruphuy, G., et al., 2018. Supercritical CO<sub>2</sub> assisted process for the production of high-purity and sterile nano-hydroxyapatite/chitosan hybrid scaffolds. *J. Biomed. Mater. Res. Part B Appl. Biomater.* 106 (3), 965–975.
- Samal, S.K., et al., 2012. Cationic polymers and their therapeutic potential. *Chem. Soc. Rev.* 41 (21), 7147–7194.
- dos Santos, E.A., et al., 2009. Chemical and topographical influence of hydroxyapatite and  $\beta$ -tricalcium phosphate surfaces on human osteoblastic cell behavior. *J. Biomed. Mater. Res. A* 89A (2), 510–520.
- Saravanan, S., et al., 2011. Preparation, characterization and antimicrobial activity of a biocomposite scaffold containing chitosan/nano-hydroxyapatite/nano-silver for bone tissue engineering. *Int. J. Biol. Macromol.* 49 (2), 188–193.
- Sato, M., Webster, T.J., 2004. Nanobiotechnology: implications for the future of nanotechnology in orthopedic applications. *Expert. Rev. Med. Dev.* 1 (1), 105–114.
- Seda Tıǧlı, R., Karakeçili, A., Gümüşderelioğlu, M., 2007. In vitro characterization of chitosan scaffolds: influence of composition and deacetylation degree. *J. Mater. Sci. Mater. Med.* 18 (9), 1665–1674.
- Şenel, S., McClure, S.J., 2004. Potential applications of chitosan in veterinary medicine. *Adv. Drug Deliv. Rev.* 56 (10), 1467–1480.
- Seol, Y.-J., et al., 2004. Chitosan sponges as tissue engineering scaffolds for bone formation. *Biotechnol. Lett.* 26 (13), 1037–1041.
- Services, U.S.D.o.H.a.H., 2004. The frequency of bone disease. Bone Health and Osteoporosis: A Report of the Surgeon General. U.S. Department of Health and Human Services, Office of the Surgeon General.
- Shen, Y.-B., et al., 2014. Preparation of chitosan microparticles with diverse molecular weights using supercritical fluid assisted atomization introduced by hydrodynamic cavitation mixer. *Powder Technol.* 254, 416–424.
- Shi, Z., et al., 2006. Antibacterial and mechanical properties of bone cement impregnated with chitosan nanoparticles. *Biomaterials* 27 (11), 2440–2449.

- Shin, S.-Y., et al., 2005. Biological evaluation of chitosan nanofiber membrane for guided bone regeneration. *J. Periodontol.* 76 (10), 1778–1784.
- Siddiqui, N., Pramanik, K., Jabbari, E., 2015. Osteogenic differentiation of human mesenchymal stem cells in freeze-gelled chitosan/nano  $\beta$ -tricalcium phosphate porous scaffolds crosslinked with genipin. *Mater. Sci. Eng. C* 54, 76–83.
- SigmaGraft Biomaterials, Available from: <<http://sigmagraft.com/inteross>> (accessed 24.03.16.).
- Silva, G., et al., 2007a. Materials in particulate form for tissue engineering. 2. Applications in bone. *J. Tissue. Eng. Regen. Med.* 1 (2), 97–109.
- Silva, G., Ducheyne, P., Reis, R., 2007b. Materials in particulate form for tissue engineering. 1. Basic concepts. *J. Tissue. Eng. Regen. Med.* 1 (1), 4–24.
- Sollohub, K., Cal, K., 2010. Spray drying technique: II. Current applications in pharmaceutical technology. *J. Pharm. Sci.* 99 (2), 587–597.
- Song, Y., et al., 2015. Synthesis and sustained-release property of drug-loaded chitosan microspheres by spray drying technique. *Am. J. Macromol. Sci.* 2 (1), 1–10.
- Stryker GmbH & Co., Available from: <<http://www.stryker.com/emea/Products/Orthopaedics/BoneSubstitutes/index.htm>> (accessed 28.03.16.).
- Sultana, N., et al., 2015. Chitosan-based nanocomposite scaffolds for tissue engineering applications. *Mater. Manuf. Processes* 30 (3), 273–278.
- Sunstar Degradable Solutions AG, Available from: <<http://us.guidor.com>> (accessed 28.03.16.).
- Supova, M., 2009. Problem of hydroxyapatite dispersion in polymer matrices: a review. *J. Mater. Sci. Mater. Med.* 20 (6), 1201–1213.
- Svedbom, A., et al., 2013. Osteoporosis in the European Union: a compendium of country-specific reports. *Arch. Osteoporos.* 8 (1–2), 1–218.
- Szymańska, E., Winnicka, K., 2015. Stability of chitosan—a challenge for pharmaceutical and biomedical applications. *Mar. Drugs* 13 (4), 1819.
- Tecnoss, Available from: <<http://www.tecnoss.com/product.html>> (accessed 24.03.16.).
- Teknimed S.A.S., Available from: <<http://www.teknimed.com/products-portfolio/products/orthopaedic-trauma-cmf/bone-substitutes/cementek/>> (accessed 28.03.16.).
- Thein-Han, W.W., Misra, R.D.K., 2009. Biomimetic chitosan–nanohydroxyapatite composite scaffolds for bone tissue engineering. *Acta Biomater.* 5 (4), 1182–1197.
- Tran, N., Webster, T.J., 2009. Nanotechnology for bone materials. *Wiley Interdisc. Rev. Nanomed. Nanobiotechnol.* 1 (3), 336–351.
- Ueno, H., et al., 1999. Accelerating effects of chitosan for healing at early phase of experimental open wound in dogs. *Biomaterials* 20 (15), 1407–1414.
- Uskoković, V., Uskoković, D.P., 2011. Nanosized hydroxyapatite and other calcium phosphates: chemistry of formation and application as drug and gene delivery agents. *J. Biomed. Mater. Res. Part B Appl. Biomater.* 96B (1), 152–191.
- Venkatesan, J., Kim, S.-K., 2014. Nano-hydroxyapatite composite biomaterials for bone tissue engineering—a review. *J. Biomed. Nanotechnol.* 10 (10), 3124–3140.
- Webster, T.J., et al., 2000. Enhanced functions of osteoblasts on nanophase ceramics. *Biomaterials* 21 (17), 1803–1810.
- Wei, G., Ma, P.X., 2004. Structure and properties of nano-hydroxyapatite/polymer composite scaffolds for bone tissue engineering. *Biomaterials* 25 (19), 4749–4757.
- White, A., Burns, D., Christensen, T.W., 2006. Effective terminal sterilization using supercritical carbon dioxide. *J. Biotechnol.* 123 (4), 504–515.

- Wilson, O.C., Hull, J.R., 2008. Surface modification of nanophase hydroxyapatite with chitosan. *Mater. Sci. Eng. C Biomim. Supramol. Syst.* 28 (3), 434–437.
- Woodard, J.R., et al., 2007. The mechanical properties and osteoconductivity of hydroxyapatite bone scaffolds with multi-scale porosity. *Biomaterials* 28 (1), 45–54.
- Yamaguchi, I., et al., 2001. Preparation and microstructure analysis of chitosan/hydroxyapatite nanocomposites. *J. Biomed. Mater. Res.* 55 (1), 20–27.
- Yang, L., Zhang, L., Webster, T.J., 2011. Nanobiomaterials: state of the art and future trends. *Adv. Eng. Mater.* 13 (6), B197–B217.
- Zani, F., et al., 2013. Sterilization of corticosteroids for ocular and pulmonary delivery with supercritical carbon dioxide. *Int. J. Pharm.* 450 (1–2), 218–224.
- Zhang, J., et al., 2006a. Sterilizing *Bacillus pumilus* spores using supercritical carbon dioxide. *J. Microbiol. Methods* 66 (3), 479–485.
- Zhang, J., et al., 2006b. Sterilization using high-pressure carbon dioxide. *J. Supercrit. Fluids* 38 (3), 354–372.
- Zhang, X., et al., 2015. The effect of the prefrozen process on properties of a chitosan/hydroxyapatite/poly(methyl methacrylate) composite prepared by freeze drying method used for bone tissue engineering. *RSC Adv.* 5 (97), 79679–79686.
- Zhao, F., et al., 2002. Preparation and histological evaluation of biomimetic three-dimensional hydroxyapatite/chitosan-gelatin network composite scaffolds. *Biomaterials* 23 (15), 3227–3234.
- Zikakis, J., 2012. *Chitin, Chitosan, and Related Enzymes*. Elsevier Science.
- Zimmer Biomet TM, Available from: <[http://www.zimmerdental.com/Products/Regenerative/rg\\_BoneGraftOverview.aspx](http://www.zimmerdental.com/Products/Regenerative/rg_BoneGraftOverview.aspx)> (accessed 28.03.16.).
- Zimmermann, G., Moghaddam, A., 2011. Allograft bone matrix versus synthetic bone graft substitutes. *Injury* 42 (Supplement 2), S16–S21.

# Production of polymer–bioactive glass nanocomposites for bone repair and substitution

# 12

**Helena P. Felgueiras and M. Teresa P. Amorim**

*Centre for Textile Science and Technology (2C2T), Department of Textile Engineering,  
University of Minho, Campus of Azurém, Guimarães, Portugal*

## 12.1 INTRODUCTION

An ideal synthetic bone graft is a porous material that can act as a temporary 3D-scaffold to support and promote bone growth. Its functions and performance should mimic that of porous cancellous bone (autograft) by stimulating the adhesion, proliferation, and differentiation mechanisms that are inherent to the structural complexity of natural tissues (Fillingham and Jacobs, 2016; Boyan et al., 1996). In face of the complexity that characterizes the human body, the requirements for scaffold materials for tissue engineering applications are many and very challenging. They should (1) be biocompatible and bioactive to promote osteogenesis and osteointegration; (2) bond to the host bone without inducing an inflammatory response, immunogenicity, or cytotoxicity; (3) possess interconnected porous structure that allows vascularization, bone ingrowth, and cell and fluids migration; (4) be flexible in terms of shape and size (fit the defect); (5) degrade at a specific rate and eventually be remodeled by osteoclast action; (6) display mechanical performance similar to the local host tissue; (7) be cost-effective for mass production purposes; and, finally, (8) be able to be sterilized and meet the requirements for clinical use (Jones, 2013; Hench and Kokubo, 2016).

Since their discovery in the 1970s by Hench, bioactive glasses (BGs) have been the subject of intense investigation as biomaterials for bone tissue repair and replacement (Hench, 2006; Hench et al., 1971). Their atomic structure allows BG to bind with the host tissues at a chemical level, and the gradual release of their ions into the surrounding media promotes the formation of a carbonate hydroxyapatite-like (HAC) layer on its surface, which increases their biocompatibility and osteointegration abilities (Hench, 1991; Jones et al., 2006; Hench and Paschall, 1973). Despite the impressive bioactivity revealed by the many BGs, these glasses cannot fulfill all the criteria for bone regeneration. Their low

fracture toughness and mechanical strength, especially in a porous form, limit their clinical application. As a result, BG cannot be used alone in applications where significant stress or cyclic load-bearing demands are applied (Roohani-Esfahani et al., 2011; Jones, 2013). To overcome these challenges, composites that incorporate BG in biopolymer matrices have been designed and investigated. The goal is not only to improve the scaffold mechanical properties, while maintaining the polymer flexibility and capacity to deform under load, but also to create a better environment for cell attachment and growth (Ding et al., 2016; Rezwani et al., 2006).

In this chapter, we introduced and categorized the different types of BG, highlighted some of the most common polymers used as matrices for composite production applied in bone tissue regeneration, and depicted the techniques used in the production of BG composites.

---

## 12.2 BIOACTIVE GLASS

Discovered in 1969 by Hench et al., BGs were first characterized as “materials that elicit specific biological responses that result in the bond between the tissues and the material” (Hench, 2006; Hench et al., 1971). Since then, they have been extensively studied for medical applications, namely as bone graft substitutes. BGs are amorphous and biologically active glasses with osteostimulative properties. They are composed of calcium and phosphate in a proportion that is similar to the bone hydroxyapatite, which accounts for its biocompatibility (Kaur et al., 2014). BG can react with physiological fluids to form tenacious bonds to bone through the formation of bone-like hydroxyapatite layers (Kaur et al., 2014). When implanted in living tissue, effective biological interactions and fixation of bone tissue with the material surface occurs, inducing specific intracellular and extracellular responses that ultimately stimulate rapid bone formation (Hench, 1991, 2006; Hench et al., 1971).

Many functional BGs have been developed over the years with proven capacity to maintain growth of osteoblasts (Hattar et al., 2002), fibroblasts (Alcaide et al., 2010), and chondroblasts (Bal et al., 2010) and to increase bone formation. The osteoactivity of each glass correlates with the solubility and composition of the glass (Penttinen, 2011). In Table 12.1 a list of the most common BG and respective composition is provided. Depending on chemical elements present, BG can be classified in silicate-based ( $\text{SiO}_2$ ), phosphate-based ( $\text{P}_2\text{O}_5$ ), and borate-based ( $\text{B}_2\text{O}_3$ , less common).

### 12.2.1 SILICATE-BASED BIOACTIVE GLASS

Since its discovery nearly 40 years ago, the now designated 45S5 or Bioglass (commercial name), which possesses unique bone-bonding properties, has been

extensively researched for biomedical applications (Hench et al., 1971; Hench, 1991). 45S5 is capable of forming a HAC layer on its surface when in contact with bodily fluids. Hench et al. has described a sequence of five reactions that precede the formation of a HAC layer (Table 12.2) (Hench, 1991). This layer resembles in composition the mineral portion of bone and is responsible for the BG bone-bonding abilities (Hoppe et al., 2011). Indeed, it attracts and promotes the adsorption of growth factors, which is quickly followed by attachment, proliferation, and differentiation of osteoprogenitor cells. Osteoblasts are then

**Table 12.1** Composition of the Most Common BG (Rahaman et al., 2011; Hoppe et al., 2011)

Bioactive Glass	Na <sub>2</sub> O	K <sub>2</sub> O	MgO	CaO	SiO <sub>2</sub>	P <sub>2</sub> O <sub>5</sub>	B <sub>2</sub> O <sub>3</sub>
Bioglass or 45S5	24.5	0	0	24.5	45.0	6.0	0
S520	21.0	7.0	0	18.0	52.0	2.0	0
6P53B	10.3	2.8	10.2	18.0	52.7	6.0	0
13–93	6.0	12.0	5.0	20.0	53	4.0	0
13–93B1	5.8	11.7	4.9	19.5	34.4	3.8	19.9
13–93B3	5.5	11.1	4.6	18.5	0	3.7	56.6
58S	0	0	0	32.6	58.2	9.1	0
60S	0	0	0	38.4	59.9	1.7	0
70S30C	0	0	0	28.6	71.4	0	0
77S	0	0	0	16.0	80.0	4.0	0
P <sub>50</sub> C <sub>35</sub> N <sub>15</sub>	9.3	0	0	19.7	0	71.0	0

**Table 12.2** Sequence of Events Preceding the Formation of a HAC Layer on the BG's Surface (Hench, 1991)

Stage 1	Rapid exchange of cations such as Na <sup>+</sup> or Ca <sup>2+</sup> with H <sup>+</sup> or H <sub>3</sub> O <sup>+</sup> from solution, leading to the hydrolysis of the silica groups and the creation of silanol (Si–OH) groups on the glass surface. pH increases due to consumption of H <sup>+</sup> .
Stage 2	Loss of soluble silica in the form of Si(OH) <sub>4</sub> to the solution and continued formation of Si–OH groups on the glass surface. Concentration of Si increases in solution.
Stage 3	Condensation and polymerization of an amorphous SiO <sub>2</sub> -rich layer on the surface of the glass depleted of Na <sup>+</sup> and Ca <sub>2</sub> <sup>+</sup> ions.
Stage 4	Migration of Ca <sub>2</sub> <sup>+</sup> and PO <sub>4</sub> <sup>3–</sup> ions from the glass through the SiO <sub>2</sub> layer and from the solution to the surface, forming CaO–PO <sub>4</sub> <sup>3–</sup> clusters on the top of the SiO <sub>2</sub> -rich layer. Growth of an amorphous calcium phosphate (CaP) layer.
Stage 5	Crystallization of the amorphous CaP by incorporation of OH <sup>–</sup> and CO <sub>3</sub> <sup>2–</sup> anions from the solution, resulting in the formation of a HAC layer.

responsible for the formation of the extracellular matrix, which mineralizes to form a nanocrystalline mineral and collagen on the surface of the BG (Hench and Polak, 2002; Ducheyne and Qiu, 1999). While these changes are taking place, the BG undergoes degradation and conversion.

The ionic dissolution products of silicon based BG have been shown to change the intracellular ionic concentrations and as a result to mediate cell metabolism (Fig. 12.1) (Ducheyne and Qiu, 1999; Jell and Stevens, 2006). By adding 45S5 to the culture medium the concentration of Ca in osteoblasts increases and so does the amount of ATP generated (Silver et al., 2001). Dissolution products of 45S5 are capable of upregulating (up to fivefold) gene expression in osteoblast-like cells, including cell metabolism, proliferation and cell–cell or matrix–cell adhesion (Xynos et al., 2001). They have also been described as upregulators of osteogenic markers such as bone sialoprotein or alkaline phosphatase, and as instigators of collagen type I formation and cell differentiation (Jell et al., 2008; Effah Kaufmann et al., 2000). Similar results have been acquired with other BGs (i.e., 13–93, 58S, 77S, etc.).

It has become clear that successful clinical application of scaffolds in bone tissue engineering highly depends on a functional vascularized network that is in

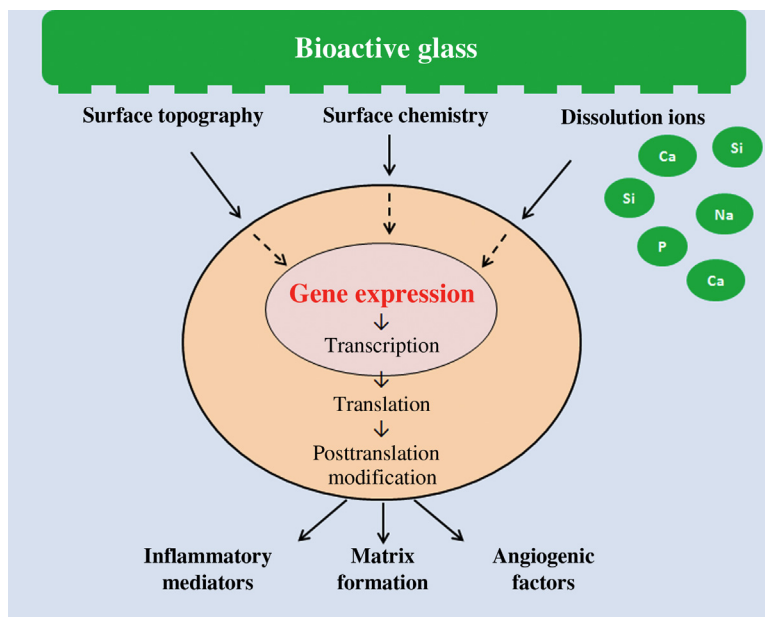


**FIGURE 12.1**

Gene expression mechanisms activated by BG.

*Adapted from Jell, G., Stevens, M.M., 2006. Gene activation by bioactive glasses. J. Mater. Sci. Mater. Med.*

*17, 997–1002.*



perfect harmony with the tissue regeneration rate. A strong porous structure that degrades at the same rate as the tissue is formed is desirable (Kaur et al., 2014). 45S5 is considered the BG gold standard; yet, there are restrictions to its processing in the form of porous 3D scaffolds. 45S5 has limited ability to sinter by viscous flow above its glass transition temperature ( $T_g$ ), and the narrow window between  $T_g$  and the onset of crystallization, raises severe difficulties in sintering the particles into a dense network, thus resulting in weak structures (Chen et al., 2006). In addition, 45S5 degrades very slowly, which makes it difficult to match the degradation rate of the scaffold with the rate of tissue formation (Huang et al., 2006). To overcome these limitations, BGs have been designed based on the 45S5 composition. The 13–93 is the most common example. Aside from the elements composing 45S5, it possesses traces of  $K_2O$  and  $MgO$  that provide the required stability to undergo viscous flow sintering and form 3D scaffolds without crystallization. Analyses of cell response did not detect differences in behavior between the 45S5 and the 13–93 BG (Brown et al., 2008).

### 12.2.2 PHOSPHATE-BASED BIOACTIVE GLASS

Phosphate-based BG is mostly used as bone filling materials and in the fabrication of scaffolds for bone tissue engineering. Its chemical similarities with the inorganic phase of bone, which increases its affinity and compatibility, make the BG from this class very desirable in bone substitution (Lakhkar et al., 2013). Yet, it is the BG's high solubility and variety of compositions that confers additional potential as resorbable materials, and that most affects cell behavior. Cell response varies according to the glasses' ionic dissolution rate; however, there is no universal predictable behavioral rule (Ahmed et al., 2004b,c; Khan et al., 2014). It has been shown that BGs with high dissolution rates inhibit osteoblastic cell growth and bone antigen expression, while BGs with low dissolution rates upregulate the osteoblasts proliferation and expression of bone sialoprotein, osteonectin, and fibronectin genes (Salih et al., 2000). The opposite has been reported as well (Skelton et al., 2007). To better control/predict the cell response and thus stabilize the glass network and degradation rate of the phosphate-based glasses, different oxides have been used as additives, for example,  $TiO_2$ ,  $B_2O_3$ ,  $ZnO$ ,  $MgO$ ,  $CuO$ , etc. (Navarro et al., 2003; Saranti et al., 2006; Ahmed et al., 2004a; Neel et al., 2005; Shu et al., 2010).

### 12.2.3 BORATE-BASED BIOACTIVE GLASS

Borate-based BGs are a more recent class of BGs. These have gained much interest due to their fast degradation rate that allows the formation of a more complete HAC layer than, for instance, 45S5 or 13–93 (Fu et al., 2010). Borate BG can be used as substrate for drug release in the treatment of bone infections and has been shown to support cell proliferation and differentiation in vitro

(Marion et al., 2005; Fu et al., 2009; Liu et al., 2010). It should be pointed out, however, that the release of borate ions represents a great limitation to its use in *in vitro* cultures, due to the ions' toxicity (Brown et al., 2009). Unexpectedly, *in vivo* reports have been more favorable with no cell toxicity being detected while using these BGs to support new tissue infiltration (Zhang et al., 2010). The greatest advantage of using borate-based BG is the ease of manufacture and the ability to control the composition and, thus, the degradation rate to match bone regeneration.

#### 12.2.4 FABRICATION OF BIOACTIVE GLASS SCAFFOLDS

The greatest advantage of preparing scaffolds using BG is the possibility to control the chemical composition and, consequently, the degradation rate. The scaffold's structure and chemistry can be tailored by changing the composition or processing conditions (Jones, 2013). Thus, scaffolds can be prepared with variable degradation rates that can both match the bone ingrowth and the remodeling. By optimizing the composition, processing, and sintering conditions, BG scaffolds can be produced with characteristics comparable to human trabecular and cortical bones (Gorustovich et al., 2009; Hoppe et al., 2011).

BGs were initially obtained via melting at high temperatures. Later, the sol–gel technique was defined as most suitable since it required lower processing temperatures and the resulting BG possessed increased bioactivity. Sol–gel process is a chemistry-based synthesis technique in which a solution containing the elemental precursors undergoes gelation reactions at room temperature to form a gel. The gel, formed of a wet inorganic network, is then subjected to aging processes to increase its strength, drying to remove the liquid byproduct, and sintering to form a porous 3D architecture (Brinker and Scherer, 2013; Valliant and Jones, 2011). Aside from requiring lower temperatures than the melting process, the sol–gel-derived BGs also possess an inherent nanoporosity and higher specific surface area, which works as a stimulant factor for cell response (Lei et al., 2010). This nanoporous architecture mimics more closely the hierarchical structure of natural tissues (Martin et al., 2012). The high surface area stimulates sol–gel-derived scaffolds to degrade and to create faster a HCA layer than melt-derived scaffolds. However, they can only be used in defects where low stress demands are applied since they have low resistance strength (Jones et al., 2006).

Aside from sol–gel, which is the most common method, there are other techniques used in the production of BG scaffolds. For instance, scaffolds can be prepared by thermal bonding of particles or fibers in a mold with the desired size and shape. A porogen, that is, sodium chloride, is mixed with the BG particles to increase the pore size and porosity of the scaffolds. Once the scaffolds are formed, the porogen is removed by leaching or decomposition (Kaur, 2017). This is a simple and straightforward method to produce scaffolds of regular porosity, however with low pore interconnectivity (Deliormanli and Rahaman, 2012).

Another possibility is to use the polymer foam replication method. Here, a synthetic or natural foam is immersed in a BG suspension to obtain a uniform coating. After drying, the polymer template and organic binders are burned at 300°C–600°C, and the glass struts are densified by sintering at 600°C–1000°C, depending on the glass composition and particle size (Fu et al., 2011a). The resulting scaffold displays a microstructure similar to dry human trabecular bone, with a highly porous architecture and interconnected porosity, however with low resistance strength (Xia and Chang, 2010).

#### 12.2.4.1 Mechanical Properties

Most reports have established the BG scaffolds mechanical response to compression loading or elastic modulus for selected deformation rates to be very low. Yet, at specific compositions and microstructures, the BG porous scaffolds may be prepared with compressive strengths similar to the human cortical bone. Fu et al. have shown that by emulating nature's design by direct-ink-write assembling of glass scaffolds with a periodic pattern, and controlled sintering of the filaments into anisotropic constructs similar to biological materials, porous BG scaffolds with a compressive strength (136 MPa) comparable to that of cortical bone (100–150 MPa) and a porosity (60%) comparable to that of trabecular bone can be produced (Fu et al., 2011b; Keaveny and Hayes, 1993). The microstructure of the scaffold has a strong effect on its resistance strength. Indeed, for the same porosity, scaffolds with an oriented pore architecture show far higher compressive strength than scaffolds with a random or isotropic pore architecture. Lui et al. produced 13–93 BG scaffolds by unidirectional freezing of camphene-based suspensions on a cold substrate, followed by thermal annealing to increase the pore diameter and orient their location. They found that the compressive strength along the pore orientation direction was 2–3 times the value obtained in the direction perpendicular to the pore orientation direction and, thus, revealed the potential of 13–93 BG scaffolds for the repair of large defects in load-bearing bones (Liu et al., 2011).

In addition to high strength and elastic modulus, scaffolds that are implanted in load-bearing bone defects and are subjected to cyclic stress should also possess good fracture toughness and reliability. The intrinsic brittleness or low resistance to crack propagation that is characteristic of ceramics and glasses are major limitations to the use of BG scaffolds in bone repair. Because of their low fracture toughness, ceramics and glass are very sensitive to the presence of small defects or cracks particularly under compressive loads. Once again, the organization and distribution of the porous along the scaffold architecture may overcome these limitations (Fu et al., 2011b; Liu et al., 2011). Very little research has however been dedicated to the study of the reliability or probability of failure of brittle materials. This is likely that due to the amount of samples necessary for this kind of studies and the precision in sample dimension, geometry, and testing conditions that are required may discourage researchers from pursuing further this line of investigation (Fu et al., 2011a).

### 12.3 NATURAL AND SYNTHETIC POLYMER–BIOACTIVE GLASS COMPOSITES

Despite the impressive bioactivity revealed by the many BG, the low fracture toughness and mechanical strength displayed, especially in a porous form, limits the BG clinical application. BG cannot be used alone in applications where significant stress or cyclic load-bearing demands are applied. Most porous BG scaffolds exhibit very low compressive and tensile strength, fracture toughness, and elastic modulus, when compared with cortical and cancellous bone (Fu et al., 2011a). Thus, the development of composites that incorporate BG in biopolymer matrices, represents an interesting approach, not only to improve the scaffold mechanical properties, while maintaining the polymer flexibility and capacity to deform under load, but also to create a better environment for cell attachment and growth (Ding et al., 2016; Rezwan et al., 2006).

The combination of biopolymers and inorganic fillers to develop tissue engineering scaffolds has been investigated for the last 20 years. Inorganic fillers are commonly added to the polymer matrices in the form of particles or fibers. Its size determines the effective mechanical properties of the composite, since depending on the BG microstructure different interactions between filler and matrix may be promoted (Koo, 2006). It has been shown that nanoscaled degradable fillers, like BG, aside from improving the implant biological performance can also increase its alkalinity, which can protect to a great extent the acidic degradation of some polymers, for example, polylactic acid (PLA) (Vollenweider et al., 2007). The nanoparticles' high specific surface area-to-volume ratio contributes to the scaffold superior protein and cell adhesion, since it increases the general bioactivity, in addition to mimicking more closely the structure of natural bone, which contains nanoscaled hydroxyapatite crystals combined with collagen (Webster et al., 1999; Boccaccini et al., 2010).

Natural and synthetic polymers have been used to produce BG composites with desirable properties for bone substitution. Natural polymers, which derive from renewable resources, are widely used in regenerative medicine because of their intrinsically bioactive and biodegradable properties and similarity to the extracellular matrix (Huang and Fu, 2010; Zhong et al., 2010). Among the many polysaccharides, polymeric carbohydrate molecules composed of long chains of monosaccharide units bound together by glycosidic bonds, like chitin, chitosan, hyaluronic acid, alginates, etc., possess the most desirable properties. It has been reported that scaffolds synthesized of chitin-BG by lyophilization technique exhibit adequate swelling and degradation as well as improved bioactivity, revealed by the increased deposition of apatite on the surface of the composite (Peter et al., 2010; Sowmya et al., 2011). Also, nanocomposite films based on chitosan blends with BG nanoparticles have been established as appropriate to develop guided tissue regeneration, as they stimulate osteoblasts' response towards cell differentiation and mineralization (Luz, 2012). Using the layer-by-layer approach, a chitosan-BG

composite has been produced with a homogeneous distribution of the BG nanoparticles along the multilayered surfaces. Chitosan provided the viscoelastic properties, while the BG provided bioactivity for the organic–inorganic structure. In vitro studies indicated that the multilayers induced the formation of apatite, a marker of bioactive behavior (Couto et al., 2009).

Synthetic polymers can be produced under controlled conditions and therefore exhibit predictable and reproducible mechanical and physical properties. They can also be synthesized without impurities reducing the risks of toxicity, immunogenicity, and infection, as they are formed of monomeric units of well-known and simple structure (Tian et al., 2012). Table 12.3 summarizes the properties of the synthetic polymers most commonly used as polymeric matrices for BG composite production: PLA, poly(glycolic acid) (PGA), poly(lactic-co-glycolic acid) (PLGA), poly( $\epsilon$ -caprolactone) (PCL), and poly(3-hydroxybutyrate) (P3HB).

The biodegradable poly- $\alpha$ -hydroxy esters, members of the aliphatic polyester family, PLA, PGA, and PLGA, have been used clinically for many years. Their inherent chemical properties allow fast hydrolytic degradation, being the resultant monomers easily removed by natural pathways (Mano et al., 2004). The degradation rate is affected by the polymers molecular weight, polydispersity, chemical composition and structure, processing parameters, environmental conditions, size, morphology (i.e., porosity), chain orientation, additives, hydrophilicity, etc. (Okamoto and John, 2013). Because, PLA, PGA, and PLGA degrade so quickly scaffolds may fail prematurely and their ionic products may not be removed at the same rate, resulting in strong inflammatory responses. The combination of these polymers with BG has proven to be very successful. Porous scaffolds of PLA and BG nanoparticles have been prepared by thermally induced phase-separation process and the results showed an improvement of the scaffold's

**Table 12.3** Physical Properties of Some of the Synthetic Polymers Used as Polymer Matrices in Scaffold Production

Polymer	Melting Point $T_m$ (°C)	Glass Transition Point $T_g$ (°C)	Biodegradation Time (months)	Tensile Strength (MPa)
PLA	180–220	60–65	> 24	Film/disk: 8–50 Fiber: 870–2300
PGA	225–230	35–40	6–12	Fiber: 340–920
PLGA	Amorphous	45–55	Adjustable 1–12	41–55
PCL	58	–72	>24	–
P3HB	175	2	–	35–45

Adapted from Rezwan, K., Chen, Q., Blaker, J., Boccaccini, A.R., 2006. Biodegradable and bioactive porous polymer/inorganic composite scaffolds for bone tissue engineering. *Biomaterials* 27, 3413–3431.

mechanical properties (Hong et al., 2008). Similar observations were made by Liu et al. by using solvent evaporation technique to combine low molecular weight PLA with sol–gel-derived BG nanoparticles. They reported that the mechanical properties were enhanced and the roughness of fractured surfaces decreased with the addition of BG. Besides, the composites were shown to be bioactive by forming a HAC layer once in contact with physiological fluids, and to instigate cell proliferation above nonmodified scaffolds (Liu et al., 2008, 2009).

PCL is bioresorbable and biocompatible, and has been applied in tissue regeneration for many years. Because PCL is degraded by hydrolysis of its ester linkages in physiological conditions, like PLA, PGA, and PLGA, and its biocompatibility efficacy has been extensively proved, the FDA has approved a number of medical devices made of PCL (Zahedi et al., 2012; Yoshimoto et al., 2003). PCL, also a member of the aliphatic polyester family, has a great advantage over the previously numbered polymers as it can take several years to degrade in vivo. Composite scaffolds of mesoporous BG and PCL have been produced by solvent casting–particulate leaching (SCPL) method, and their structure and properties characterized. By incorporating BG, the composite’s hydrophilicity was improved and the formation of a dense and continuous layer of apatite was instigated (Li et al., 2008). The biological and mechanical properties of a BG–PCL composite scaffold generated using sol–gel precursors via the electrospinning method revealed great levels of alkaline phosphatase activity and enhanced biocompatibility and bioactivity. The results from in vivo animal experiments established the potential of BG–PCL composite scaffolds as bone regenerative materials (Fig. 12.2) (Jo et al., 2009).

P3HB belongs to the biodegradable polyhydroxyalkanoate family and, because of its biocompatibility (Zhijiang et al., 2012), has been applied in the manufacture of many biomedical devices (Hazer et al., 2012). P3HB has demonstrated remarkable abilities to stimulate consistently favorable bone tissue responses, including instigating the formation of highly organized new bone structures, without inducing undesirable chronic inflammatory reactions, even after long periods of implantation (Misra et al., 2010b). Studies have been conducted to determine the relevance of BG in the P3HB scaffolds. Misra et al. compared the effects of introducing micro- and nanoscale BG particles on the thermal, mechanical, and microstructural properties of BG–P3HB composites produced by solvent casting. Composites with nanoscale BG were determined to be more stiff and its nanoscale topography was altered. As a result, protein adsorption increased and so did its bioactivity and water adsorption (Misra et al., 2008). Cytocompatibility studies (cell proliferation, cell attachment, alkaline phosphatase activity, and osteocalcin production) using human MG63 osteoblast-like cells showed these composite scaffolds to be suitable for cell attachment, proliferation, and differentiation (Misra et al., 2009). Following this line of investigation, in vivo testing were later performed using highly porous P3HB foams supplemented with nanoscale and microscale BG. Foams were implanted in rats as subcutaneous implants. After 1 week of implantation neither toxic nor foreign body responses

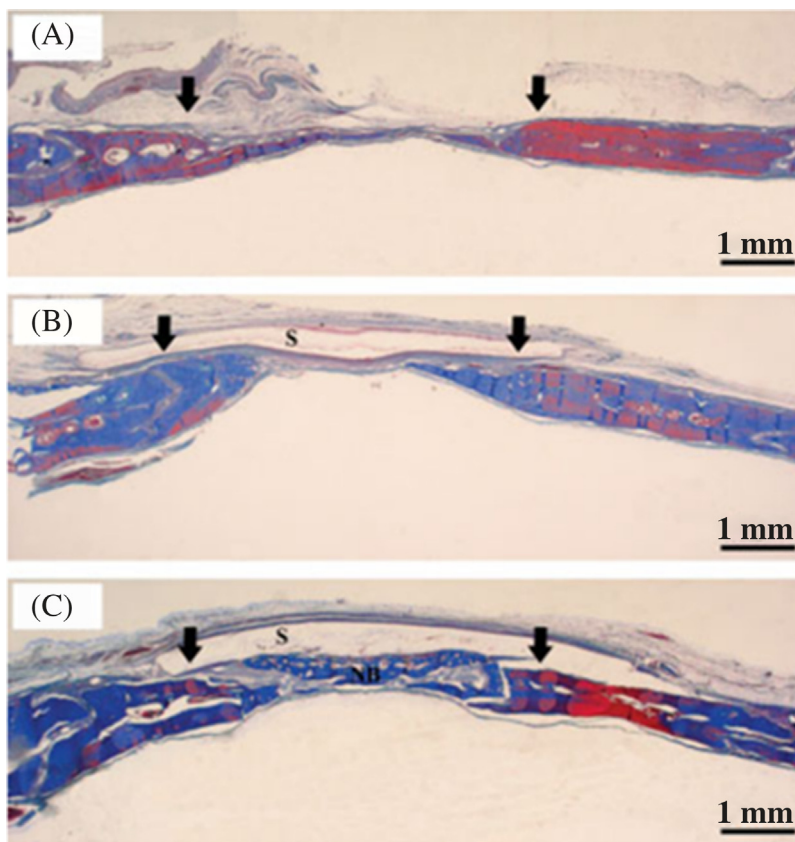


**FIGURE 12.2**

Optical micrographs of the stained bone tissues 3 weeks after membrane implantation: (A) empty defect, (B) pure PCL, (C) PCL-BG composite (arrows, defect margins; NB, new bone; S, sample) (Jo et al., 2009).

were observed. In addition to showing bioactivity and biocompatibility, the composite foams also displayed bactericidal properties, which were tested on the growth of *Staphylococcus aureus* (Fig. 12.3) (Misra et al., 2010a).

## 12.4 COMPOSITE PRODUCTION TECHNIQUES

Sol-gel technique has been defined as most suitable to produce BG with increased bioactivity (Jones, 2013). Yet, combining BG with biopolymers to improve both the mechanical and biological properties of the implantable materials can be accomplished with other techniques or combination



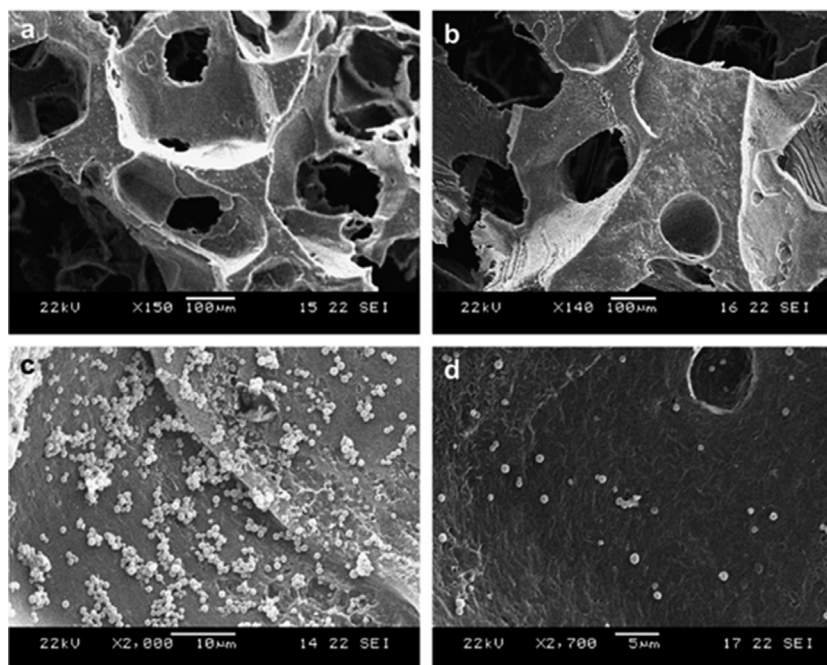


**FIGURE 12.3**

SEM micrographs of *S. aureus* attachment after 48 h on (A, C) P3HB foams and (B, D) P3HB-BG composite foams. A decrease in *S. aureus* bacteria on the surface of the P3HB-BG composite is evident (D) in comparison to single P3HB (C) (Misra et al., 2010a).

of techniques. Electrospinning, emulsification-solvent evaporation process for microsphere production, solvent casting, freeze-drying, and 3D printing are some of the most commonly used techniques, with the greatest potential for the biomedical field. Within these techniques we can find examples of composites in which both organic and inorganic phases interact, generating strong covalent bonds, or cases where multilayer structures are developed. Depending on the technique, scaffolds with different architectures and mechanical properties can be attained.

### 12.4.1 ELECTROSPINNING

Electrospinning is an old technique, dating back almost 120 years (Zeleny, 1914). However, it was only after the 1980s that the electrospinning technique regained interest. It is capable of consistently producing fibers in the submicron range with extremely high surface-to-volume ratio, tunable porosity, and malleability to conform over a wide variety of sizes and shapes, and allows to control the fibers



composition to achieve desired properties and functionality (Abrigo et al., 2014; Liang et al., 2007; Huang and Chang, 2003; Hunley and Long, 2008; Lannutti et al., 2007; Coelho et al., 2017). It is a simple and straightforward method, in which a polymer solution is pumped at constant rate by a syringe connected to a high DC voltage source. Electrospinning is based on the principle that strong mutual electrical repulsive forces overcome weaker forces of surface tension in the charged polymer liquid (Agarwal et al., 2013; Felgueiras et al., 2017a,b). The resultant electrospun fibers' diameter, morphology, and fiber orientation in a scaffold are defined by the equipment operating conditions, solution properties, and surrounding environment (Bhardwaj and Kundu, 2010).

The simplicity of the electrospinning technique allows for natural and synthetic polymers to be used in a single or multipolymer blend manner. Indeed, organic–inorganic composites and hybrid fibers are being developed combining the physical and mechanical performance with the material's biological properties. Biopolymer–BG suspensions have also been tested with the goal of integrating the brittle and inorganic phase of BG with the elastic and bioinert organic phase of the biopolymers. At the moment, there are two strategies to accomplish this. The first is to associate BG particles with the polymer solution with and without surfactants in an ultrasonic bath. Electrospun scaffolds of BG–PCL composite have been produced using this approach. It was seen that the bioactivity and the cells' alkaline phosphatase activity is significantly enhanced with the addition of the BG nanoparticles (Kouhi et al., 2013). Also the tensile strength of the fibrous scaffold can be improved (Lin et al., 2012a). The other approach combines the BG with the polymer in a hybrid solution. Here, the organic and inorganic phases interact on a molecular level. Single phase electrospun organic–inorganic scaffolds are thus produced. Chemical characterization revealed that only natural origin polymers, which possess multiple functional groups, can covalently bind to BG, while the synthetic could only accomplish this through weak hydrogen bonding (Allo et al., 2010). To overcome this, Gao et al. have proposed the use of a coupling agent, the 3-glycidoxypopyltrimethoxysilane (GPTMS), to prepare BG-gelatin hybrid scaffolds. The GPTMS agent provided the basis that led to the formation of a covalent bond between the organic and inorganic elements, which resulted in a significant enhancement of the tensile strength and elongation properties of the scaffold (Gao et al., 2013). It should be highlighted though that coupling agents are not always required for processing of synthetic polymers and BG in the form of hybrids, as there are ways to overcome the limitations of this combination. For instance, Kim et al. prepared a BG–PLA composite in which the electrospun fibers were sintered at 700°C, cut, and immersed in a PLA/THF solution followed by thermal compression at 130°C, to obtain a homogeneous dense scaffold. The resultant composite revealed great bioactivity, promoted the osteoblast-like cell attachment and growth, and increased the secretion of collagen proteins and the alkaline phosphatase activity (Kim et al., 2008).

### 12.4.2 MICROSPHERES

Nowadays, a variety of techniques can be used to prepared microspheres. Yet, the most common remains the emulsification-solvent evaporation process. Here, a polymer solution made in a volatile organic solvent is emulsified by agitation to obtain an oil/water emulsion that can be stabilized as droplets. Once the emulsion is stabilized, agitation is maintained and the solvent evaporates after diffusing through the continuous phase, resulting in solid microspheres. In the end, the microspheres are collected by filtration or centrifugation, washed, and dried (Watts et al., 1989; Hwisa et al., 2013). Depending on the nature of the polymer, application of the final product, and required degradation rate other techniques may be used, for example, coacervation, spray drying, milling, and supercritical fluid techniques (Kulshreshtha et al., 2010). During microsphere fabrication, BG particles can be incorporated or dispersed along the surface to increase the bioactivity of the polymer, accelerate the healing process by enhancing osteogenic and antiogenic phenomena, and to control the degradation rate.

Mesoporous and nonmesoporous BG were incorporated into alginate microspheres, a biocompatible, natural origin polymer. Dexamethasone-loading and release ability was tested in phosphate buffered saline solution, which was found to be enhanced in the presence of BG (Wu et al., 2010a). Alendronate sodium has been incorporated into poly(lactide-co-caprolactone)-BG composite microspheres produced by oil-in-water emulsion solvent evaporation method with successful results. Data determined these microspheres to be bioactive, noncytotoxic, and capable of promoting cell adhesion. Also, this releasing strategy was established as more efficient than oral administration (Mondal et al., 2012). The mechanical performance and capacity to produce a HAC layer on the surface of spherically shaped and small-sized microspheres, prepared of PCL and different concentrations of BG, have also been tested. It was seen that with increasing amounts of BG the microspheres' elastic modulus also increased. BG enhanced the hydrophilicity of PCL, which led to a higher water adsorption and faster degradation rate. The composite microspheres with the highest amount of BG stimulated vigorously the growth of apatite and with it its bioactivity (Lei et al., 2012).

### 12.4.3 SOLVENT CASTING—PARTICULATE LEACHING

SCPL is a simple, straightforward, and cost-effective method to produce composite polymeric scaffolds. Briefly, a polymer is dissolved in an organic solvent and particles with specific sizes and shapes are added to the solution. The mixture is shaped according to the recipient where the solution is poured or prepared. Once the solvent evaporates, a structure of composite material is attained. The composite material is then placed in a bath to dissolve the particles, leaving behind a porous structure (Farè, 2012; Lin et al., 2012b).

The simplicity of the method and the ability to control the porosity of the resulting structure allows its use in different research fields. However, since the

porous morphology is usually cubic-like, equiaxed, or spherical, and full interconnectivity is unlikely to be achieved, there are some limitations to its actual application (Bencherif et al., 2013). Single and multipolymer blends with and without inorganic fillers or particles like BG have been explored for porous scaffold fabrication in tissue engineering. Composite scaffolds of mesoporous and nonmesoporous BG and PCL were prepared using SCPL and their structure and properties characterized. Incorporation of BG increased the composite hydrophilicity and the ability to form a dense and continuous layer of apatite on the scaffolds' surface. The highly enhanced bioactivity of the PCL-BG composites was attributed to the ordered channels and BG particles high surface-to-volume ratio, which accelerated the ion exchange during incubation (Li et al., 2008). In another study, 45S5 powders were incorporated into a poly(3-hydroxybutyrate-co-3-hydroxyhexanoate) (PHBV) matrix to produce scaffolds by SCPL and in vitro and in vivo testing were conducted. Results showed that aside from increasing the hydrophilicity and compressive strength of the composite, the BG supplement also promoted chondrocyte's penetration length, thickness of cartilage-like tissue of in vivo constructs, and the mechanical strength of the formed cartilage tissue (Wu et al., 2013).

#### 12.4.4 FREEZE-DRYING

Freeze-drying belongs to the family of the thermally induced phase-separation techniques and was first described in the 1980s. In recent years, this technique has been used to produce highly porous scaffolds with interconnected and tailored architecture. The overall scaffold porosity and mechanical properties can be tailored by adjusting the conditions of processing and solution (Kane and Roeder, 2012).

This technique is based on the principle of dehydration. Briefly, a solution consisting of a solvent, polymer, and inorganic particles is subjected to rapid gelation causing the solids to be displaced into the interstitial spaces between ice crystals. Once the solution is fully frozen, the freeze-drying process begins and the materials are subjected to a cycle of temperatures ranging between 20°C and 80°C, that are applied for different periods of time. At the end, the suspension is sublimated under vacuum conditions (Qian and Zhang, 2011).

BG nanoparticles can be incorporated into the solution to reinforce the biological properties of the scaffolds (Maquet et al., 2004). Although this technique can be used as a single method, it usually occurs in combination with other techniques (Wu et al., 2010b). Gelatin-BG hybrid scaffolds produced by a combination of sol-gel, freeze-drying and particulate leaching processes are a successful example of that. By using sol-gel the amorphous BG were uniformly distributed into the gelatin matrix, acting as a reinforcing phase. A hierarchical pore structure with round micropores and nanopores was generated from the particulate leaching and freeze-drying processes, respectively. The hybrid scaffolds were established as more favorable for cell adhesion, proliferation, and osteogenic differentiation

than the pure gelatin scaffolds. Moreover, gene expression was highly promoted by BG addition (Qu and Liu, 2013).

### 12.4.5 3D PRINTING

3D printing technique is one of the most recent innovations introduced to the biomedical field to produce scaffolds of controllable architecture. This technique incorporates ink-jet technology to precisely place successive layers of powder or sheet material to build a 3D model from a series of cross-sectional layers. Once the model is complete, the unfused excess material is removed by compressed air or manually brushed (Rengier et al., 2010; Lipson and Kurman, 2013). Zhao et al.'s work gives us an excellent example of the use of polymer–BG composite scaffolds produced by 3D printing. Mesoporous BG and PHBV were combined at different concentrations, and their biological performance followed. Reports described these composite scaffolds as highly biocompatible, with enhanced bioactive and osteogenic properties, including fast apatite-forming ability. They were also seen to promote mesenchymal stem cells adhesion, proliferation, alkaline phosphatase activity, and bone-related gene expression. Data from *in vivo* testing revealed these composite scaffolds to exhibit a controlled degradation rate and their potential to stabilize the pH environment with increasing PHBV ratios. The capacity of PHBV-BG scaffolds to stimulate bone regeneration was also established (Zhao et al., 2014).

---

## 12.5 CONCLUSIONS

Many *in vitro*, *in vivo*, and clinical studies have shown BGs to perform above other bioceramic particles but not as well as autograft bone. The main reasons behind this are the fact that BG particles cannot be made into porous scaffolds without crystallizing during sintering, and the low mechanical performance of BG, which includes low fracture toughness and mechanical strength especially in a porous form. The first issue is being successfully overcome by using new compositions that can be sintered without crystallizing, and by applying new techniques to produce micro- and nanostructured BG scaffolds. Yet, these porous scaffolds can only be used in sites where there is little to no stress/load-bearing demand. It is here that the combination of biopolymers with BG comes as an advantage.

In the past 20 years various combinations of biopolymers and inorganic fillers were developed in the form of tissue engineering scaffolds for biomedical applications. BG, aside from improving the polymeric implant biological performance, due to its high specific surface area-to-volume ratio that contributes to the scaffold superior protein and cell adhesion, can also increase its alkalinity, which can protect at great extent the acidic degradation of some polymers. Conventional

composites do not seem to be able to mimic the hierarchical structure of bone. The greatest advantage of the polymer–BG composites are their ability to mimic closely the structure of natural bone, which contains nanoscale hydroxyapatite crystals (similar chemical composition of BG) combined with collagen, a natural polymer. There are many polymers that have been successfully combined with BG and their results have inspired researchers to investigate new applications of BG in biomedical engineering. Yet, their clinical effectiveness still requires further testing and proper validation. Nonetheless, the great potential of these micro- and nanostructures processed with biopolymers and inorganic fillers should be highlighted. In the future, it is expected these new composites will become more sophisticated, widening their areas of application.

---

## ACKNOWLEDGMENTS

This work is supported by national funds from FCT—Foundation for Science and Technology within the scope of the project UID/CTM/00264/2013, and by FEDER funds through the COMPETE 2020—*Programa Operacional Competitividade e Internacionalização* (POCI) with the reference project POCI-01-0145-FEDER-007136. Authors also acknowledge FCT, FEDER and POCI for funding the project PEPTEx with reference POCI-01-0145-FEDER-028074.

---

## REFERENCES

- Abrigo, M., McArthur, S.L., Kingshott, P., 2014. Electrospun nanofibers as dressings for chronic wound care: advances, challenges, and future prospects. *Macromol. Biosci.* 14, 772–792.
- Agarwal, S., Greiner, A., Wendorff, J.H., 2013. Functional materials by electrospinning of polymers. *Progress Polym. Sci.* 38, 963–991.
- Ahmed, I., Collins, C., Lewis, M., Olsen, I., Knowles, J., 2004a. Processing, characterisation and biocompatibility of iron-phosphate glass fibres for tissue engineering. *Biomaterials* 25, 3223–3232.
- Ahmed, I., Lewis, M., Olsen, I., Knowles, J., 2004b. Phosphate glasses for tissue engineering: part 1. Processing and characterisation of a ternary-based P2O5–CaO–Na2O glass system. *Biomaterials* 25, 491–499.
- Ahmed, I., Lewis, M., Olsen, I., Knowles, J., 2004c. Phosphate glasses for tissue engineering: part 2. Processing and characterisation of a ternary-based P2O5–CaO–Na2O glass fibre system. *Biomaterials* 25, 501–507.
- Alcaide, M., Portolés, P., López-Noriega, A., Arcos, D., Vallet-Regí, M., Portoles, M., 2010. Interaction of an ordered mesoporous bioactive glass with osteoblasts, fibroblasts and lymphocytes, demonstrating its biocompatibility as a potential bone graft material. *Acta Biomater.* 6, 892–899.
- Allo, B.A., Rizkalla, A.S., Mequanint, K., 2010. Synthesis and electrospinning of  $\epsilon$ -polycaprolactone-bioactive glass hybrid biomaterials via a sol–gel process. *Langmuir* 26, 18340–18348.

- Bal, B.S., Rahaman, M.N., Jayabalan, P., Kuroki, K., Cockrell, M.K., Yao, J.Q., et al., 2010. In vivo outcomes of tissue-engineered osteochondral grafts. *J. Biomed. Mater. Res. Part B Appl. Biomater.* 93, 164–174.
- Bencherif, S.A., Braschler, T.M., Renaud, P., 2013. Advances in the design of macroporous polymer scaffolds for potential applications in dentistry. *J. Periodont. Implant Sci.* 43, 251–261.
- Bhardwaj, N., Kundu, S.C., 2010. Electrospinning: a fascinating fiber fabrication technique. *Biotechnol. Adv.* 28, 325–347.
- Boccaccini, A.R., Erol, M., Stark, W.J., Mohn, D., Hong, Z., Mano, J.F., 2010. Polymer/bioactive glass nanocomposites for biomedical applications: a review. *Compos. Sci. Technol.* 70, 1764–1776.
- Boyan, B.D., Hummert, T.W., Dean, D.D., Schwartz, Z., 1996. Role of material surfaces in regulating bone and cartilage cell response. *Biomaterials* 17, 137–146.
- Brinker, C.J., Scherer, G.W., 2013. *Sol-Gel Science: The Physics and Chemistry of Sol-Gel Processing*. Academic Press.
- Brown, R.F., Day, D.E., Day, T.E., Jung, S., Rahaman, M.N., Fu, Q., 2008. Growth and differentiation of osteoblastic cells on 13–93 bioactive glass fibers and scaffolds. *Acta Biomater.* 4, 387–396.
- Brown, R.F., Rahaman, M.N., Dwilewicz, A.B., Huang, W., Day, D.E., Li, Y., et al., 2009. Effect of borate glass composition on its conversion to hydroxyapatite and on the proliferation of MC3T3-E1 cells. *J. Biomed. Mater. Res. Part A* 88, 392–400.
- Chen, Q.Z., Thompson, I.D., Boccaccini, A.R., 2006. 45S5 Bioglass®-derived glass–ceramic scaffolds for bone tissue engineering. *Biomaterials* 27, 2414–2425.
- Coelho, D., Sampaio, A., Silva, C.J., Felgueiras, H.P., Amorim, M.T.P., Zille, A., 2017. Antibacterial electrospun poly(vinyl alcohol)/enzymatic synthesized poly(catechol) nanofibrous midlayer membrane for ultrafiltration. *Appl. Mater. Sci. Interfaces* 9, 33107–33118.
- Couto, D.S., Alves, N.M., Mano, J.F., 2009. Nanostructured multilayer coatings combining chitosan with bioactive glass nanoparticles. *J. Nanosci. Nanotechnol.* 9, 1741–1748.
- Deliormanli, A.M., Rahaman, M.N., 2012. Direct-write assembly of silicate and borate bioactive glass scaffolds for bone repair. *J. Eur. Ceram. Soc.* 32, 3637–3646.
- Ding, Y., Souza, M.T., Li, W., Schubert, D.W., Boccaccini, A.R., Roether, J.A., 2016. Bioactive glass-biopolymer composites for applications in tissue engineering. *Handbook Bioceram. Biocompos.* 1, 325–356.
- Ducheyne, P., Qiu, Q., 1999. Bioactive ceramics: the effect of surface reactivity on bone formation and bone cell function. *Biomaterials* 20, 2287–2303.
- Effah Kaufmann, E., Ducheyne, P., Shapiro, I., 2000. Evaluation of osteoblast response to porous bioactive glass (45S5) substrates by RT-PCR analysis. *Tissue Eng.* 6, 19–28.
- Farè, S., 2012. Preparation and characterization of shape memory polymer scaffolds via solvent casting/particulate leaching. *J. Appl. Biomater.* 10, 119–126.
- Felgueiras, H.P., Amorim, M.T., 2017a. Functionalization of electrospun polymeric wound dressings with antimicrobial peptides: types, applications and immobilization processes (review). *Colloids Surf. B* 156, 133–148.
- Felgueiras, H.P., Amorim, M.T., 2017b. Electrospun polymeric dressings with tuned collagen type I and antimicrobial peptides activities for enhanced wound healing. *IOP Conf. Ser.: Mater. Sci. Eng.* 254, 062004.
- Fillingham, Y., Jacobs, J., 2016. Bone grafts and their substitutes. *Bone Joint J.* 98, 6–9.

- Fu, H., Fu, Q., Zhou, N., Huang, W., Rahaman, M.N., Wang, D., et al., 2009. In vitro evaluation of borate-based bioactive glass scaffolds prepared by a polymer foam replication method. *Mater. Sci. Eng. C* 29, 2275–2281.
- Fu, Q., Rahaman, M.N., Fu, H., Liu, X., 2010. Silicate, borosilicate, and borate bioactive glass scaffolds with controllable degradation rate for bone tissue engineering applications. I. Preparation and in vitro degradation. *J. Biomed. Mater. Res. Part A* 95, 164–171.
- Fu, Q., Saiz, E., Rahaman, M.N., Tomsia, A.P., 2011a. Bioactive glass scaffolds for bone tissue engineering: state of the art and future perspectives. *Mater. Sci. Eng. C* 31, 1245–1256.
- Fu, Q., Saiz, E., Tomsia, A.P., 2011b. Bioinspired strong and highly porous glass scaffolds. *Adv. Funct. Mater.* 21, 1058–1063.
- Gao, C., Gao, Q., Li, Y., Rahaman, M.N., Teramoto, A., Abe, K., 2013. In vitro evaluation of electrospun gelatin-bioactive glass hybrid scaffolds for bone regeneration. *J. Appl. Polym. Sci.* 127, 2588–2599.
- Gorustovich, A.A., Roether, J.A., Boccaccini, A.R., 2009. Effect of bioactive glasses on angiogenesis: a review of in vitro and in vivo evidences. *Tissue Eng. Part B Rev.* 16, 199–207.
- Hattar, S., Berdal, A., Asselin, A., Loty, S., Greenspan, D., Sautier, J., 2002. Behaviour of moderately differentiated osteoblast-like cells cultured in contact with bioactive glasses. *Eur. Cell. Mater.* 4, 61–69.
- Hazer, D.B., Kılıçay, E., Hazer, B., 2012. Poly (3-hydroxyalkanoate)s: diversification and biomedical applications: a state of the art review. *Mater. Sci. Eng. C* 32, 637–647.
- Hench, L.L., 1991. Bioceramics: from concept to clinic. *J. Am. Ceram. Soc.* 74, 1487–1510.
- Hench, L.L., 2006. The story of Bioglass®. *J. Mater. Sci. Mater. Med.* 17, 967–978.
- Hench, L., Kokubo, T., 2016. Properties of bioactive glasses and glass-ceramics. *Handbook of Biomaterial Properties*. Springer.
- Hench, L.L., Paschall, H., 1973. Direct chemical bond of bioactive glass-ceramic materials to bone and muscle. *J. Biomed. Mater. Res.* 7, 25–42.
- Hench, L.L., Polak, J.M., 2002. Third-generation biomedical materials. *Science* 295, 1014–1017.
- Hench, L.L., Splinter, R.J., Allen, W., Greenlee, T., 1971. Bonding mechanisms at the interface of ceramic prosthetic materials. *J. Biomed. Mater. Res.* 5, 117–141.
- Hong, Z., Reis, R.L., Mano, J.F., 2008. Preparation and in vitro characterization of scaffolds of poly (L-lactic acid) containing bioactive glass ceramic nanoparticles. *Acta Biomater.* 4, 1297–1306.
- Hoppe, A., Güldal, N.S., Boccaccini, A.R., 2011. A review of the biological response to ionic dissolution products from bioactive glasses and glass-ceramics. *Biomaterials* 32, 2757–2774.
- Huang, C.-F., Chang, F.-C., 2003. Comparison of hydrogen bonding interaction between PMMA/PMAA blends and PMMA-co-PMAA copolymers. *Polymer* 44, 2965–2974.
- Huang, S., Fu, X., 2010. Naturally derived materials-based cell and drug delivery systems in skin regeneration. *J. Control. Release* 142, 149–159.
- Huang, W., Day, D.E., Kittiratanapiboon, K., Rahaman, M.N., 2006. Kinetics and mechanisms of the conversion of silicate (45S5), borate, and borosilicate glasses to hydroxyapatite in dilute phosphate solutions. *J. Mater. Sci. Mater. Med.* 17, 583–596.



- Hunley, M.T., Long, T.E., 2008. Electrospinning functional nanoscale fibers: a perspective for the future. *Polym. Int.* 57, 385–389.
- Hwisa, N., Katakam, P., Chandu, B., Adiki, S., 2013. Solvent evaporation techniques as promising advancement in microencapsulation. *Vedic Res. Int. Biol. Med. Chem.* 1, 8–22.
- Jell, G., Stevens, M.M., 2006. Gene activation by bioactive glasses. *J. Mater. Sci. Mater. Med.* 17, 997–1002.
- Jell, G., Notingher, I., Tsigkou, O., Notingher, P., Polak, J., Hench, L., et al., 2008. Bioactive glass-induced osteoblast differentiation: a noninvasive spectroscopic study. *J. Biomed. Mater. Res. Part A* 86, 31–40.
- Jo, J.H., Lee, E.J., Shin, D.S., Kim, H.E., Kim, H.W., Koh, Y.H., et al., 2009. In vitro/ in vivo biocompatibility and mechanical properties of bioactive glass nanofiber and poly ( $\epsilon$ -caprolactone) composite materials. *J. Biomed. Mater. Res. Part B Appl. Biomater.* 91, 213–220.
- Jones, J.R., 2013. Review of bioactive glass: from Hench to hybrids. *Acta Biomater.* 9, 4457–4486.
- Jones, J.R., Ehrenfried, L.M., Hench, L.L., 2006. Optimising bioactive glass scaffolds for bone tissue engineering. *Biomaterials* 27, 964–973.
- Kane, R.J., Roeder, R.K., 2012. Effects of hydroxyapatite reinforcement on the architecture and mechanical properties of freeze-dried collagen scaffolds. *J. Mech. Behav. Biomed. Mater.* 7, 41–49.
- Kaur, G., 2017. *Bioactive Glasses: Potential Biomaterials for Future Therapy*. Springer.
- Kaur, G., Pandey, O.P., Singh, K., Homa, D., Scott, B., Pickrell, G., 2014. A review of bioactive glasses: their structure, properties, fabrication and apatite formation. *J. Biomed. Mater. Res. Part A* 102, 254–274.
- Keaveny, T.M., Hayes, W.C., 1993. Mechanical properties of cortical and trabecular bone. *Bone* 7, 285–344.
- Khan, A.F., Saleem, M., Afzal, A., Ali, A., Khan, A., Khan, A.R., 2014. Bioactive behavior of silicon substituted calcium phosphate based bioceramics for bone regeneration. *Mater. Sci. Eng. C* 35, 245–252.
- Kim, H.W., Lee, H.H., Chun, G.S., 2008. Bioactivity and osteoblast responses of novel biomedical nanocomposites of bioactive glass nanofiber filled poly (lactic acid). *J. Biomed. Mater. Res. Part A* 85, 651–663.
- Koo, J.H., 2006. *Polymer Nanocomposites*. McGraw-Hill Professional Pub.
- Kouhi, M., Morshed, M., Varshosaz, J., Fathi, M.H., 2013. Poly ( $\epsilon$ -caprolactone) incorporated bioactive glass nanoparticles and simvastatin nanocomposite nanofibers: preparation, characterization and in vitro drug release for bone regeneration applications. *Chem. Eng. J.* 228, 1057–1065.
- Kulshreshtha, A.K., Singh, O.N., Wall, G.M., 2010. *Pharmaceutical suspensions. From Formulation Development to Manufacturing*. Springer, New York.
- Lakhkar, N.J., Lee, I.-H., Kim, H.-W., Salih, V., Wall, I.B., Knowles, J.C., 2013. Bone formation controlled by biologically relevant inorganic ions: role and controlled delivery from phosphate-based glasses. *Adv. Drug Deliv. Rev.* 65, 405–420.
- Lannutti, J., Reneker, D., Ma, T., Tomasko, D., Farson, D., 2007. Electrospinning for tissue engineering scaffolds. *Mater. Sci. Eng. C* 27, 504–509.
- Lei, B., Chen, X., Wang, Y., Zhao, N., Du, C., Fang, L., 2010. Surface nanoscale patterning of bioactive glass to support cellular growth and differentiation. *J. Biomed. Mater. Res. Part A* 94, 1091–1099.



- Lei, B., Shin, K.H., Noh, D.Y., Koh, Y.H., Choi, W.Y., Kim, H.E., 2012. Bioactive glass microspheres as reinforcement for improving the mechanical properties and biological performance of poly ( $\epsilon$ -caprolactone) polymer for bone tissue regeneration. *J. Biomed. Mater. Res. Part B Appl. Biomater.* 100, 967–975.
- Li, X., Shi, J., Dong, X., Zhang, L., Zeng, H., 2008. A mesoporous bioactive glass/polycaprolactone composite scaffold and its bioactivity behavior. *J. Biomed. Mater. Res. Part A* 84, 84–91.
- Liang, D., Hsiao, B.S., Chu, B., 2007. Functional electrospun nanofibrous scaffolds for biomedical applications. *Adv. Drug Deliv. Rev.* 59, 1392–1412.
- Lin, H.-M., Lin, Y.-H., Hsu, F.-Y., 2012a. Preparation and characterization of mesoporous bioactive glass/polycaprolactone nanofibrous matrix for bone tissues engineering. *J. Mater. Sci. Mater. Med.* 23, 2619–2630.
- Lin, W., Li, Q., Zhu, T., 2012b. Study of solvent casting/particulate leaching technique membranes in pervaporation for dehydration of caprolactam. *J. Industr. Eng. Chem.* 18, 941–947.
- Lipson, H., Kurman, M., 2013. *Fabricated: The New World of 3D Printing*. John Wiley & Sons.
- Liu, A., Hong, Z., Zhuang, X., Chen, X., Cui, Y., Liu, Y., et al., 2008. Surface modification of bioactive glass nanoparticles and the mechanical and biological properties of poly (L-lactide) composites. *Acta Biomater.* 4, 1005–1015.
- Liu, A.-X., Wei, J.-C., Chen, X.-S., Jing, X.-B., Cui, Y., Liu, Y., 2009. Novel composites of poly (l-lactide) and surface modified bioactive  $\text{SiO}_2$ - $\text{CaO}$ - $\text{P}_2\text{O}_5$  gel nanoparticles: mechanical and biological properties. *Chin. J. Polym. Sci.* 27, 415–426.
- Liu, X., Xie, Z., Zhang, C., Pan, H., Rahaman, M.N., Zhang, X., et al., 2010. Bioactive borate glass scaffolds: in vitro and in vivo evaluation for use as a drug delivery system in the treatment of bone infection. *J. Mater. Sci. Mater. Med.* 21, 575–582.
- Liu, X., Rahaman, M.N., Fu, Q., 2011. Oriented bioactive glass (13-93) scaffolds with controllable pore size by unidirectional freezing of camphene-based suspensions: microstructure and mechanical response. *Acta Biomater.* 7, 406–416.
- Luz, G.M., 2012. Chitosan/bioactive glass nanoparticles composites for biomedical applications. *Biomed. Mater.* 7, 054104.
- Mano, J.F., Sousa, R.A., Boesel, L.F., Neves, N.M., Reis, R.L., 2004. Bioinert, biodegradable and injectable polymeric matrix composites for hard tissue replacement: state of the art and recent developments. *Compos. Sci. Technol.* 64, 789–817.
- Maquet, V., Boccaccini, A.R., Pravata, L., Notingher, I., Jérôme, R., 2004. Porous poly ( $\alpha$ -hydroxyacid)/Bioglass® composite scaffolds for bone tissue engineering. I: Preparation and in vitro characterisation. *Biomaterials* 25, 4185–4194.
- Marion, N.W., Liang, W., Liang, W., Reilly, G.C., Day, D.E., Rahaman, M.N., et al., 2005. Borate glass supports the in vitro osteogenic differentiation of human mesenchymal stem cells. *Mech. Adv. Mater. Struct.* 12, 239–246.
- Martin, R.A., Yue, S., Hanna, J.V., Lee, P., Newport, R.J., Smith, M.E., et al., 2012. Characterizing the hierarchical structures of bioactive sol–gel silicate glass and hybrid scaffolds for bone regeneration. *Philos. Trans. R. Soc. A* 370, 1422–1443.
- Misra, S.K., Mohn, D., Brunner, T.J., Stark, W.J., Philip, S.E., Roy, I., et al., 2008. Comparison of nanoscale and microscale bioactive glass on the properties of P (3HB)/Bioglass® composites. *Biomaterials* 29, 1750–1761.

- Misra, S.K., Ansari, T., Mohn, D., Valappil, S.P., Brunner, T.J., Stark, W.J., et al., 2009. Effect of nanoparticulate bioactive glass particles on bioactivity and cytocompatibility of poly (3-hydroxybutyrate) composites. *J. R. Soc. Interface* 7 (44), 453–465. rsif20090255.
- Misra, S.K., Ansari, T.I., Valappil, S.P., Mohn, D., Philip, S.E., Stark, W.J., et al., 2010a. Poly (3-hydroxybutyrate) multifunctional composite scaffolds for tissue engineering applications. *Biomaterials* 31, 2806–2815.
- Misra, S.K., Ohashi, F., Valappil, S.P., Knowles, J.C., Roy, I., Silva, S.R.P., et al., 2010b. Characterization of carbon nanotube (MWCNT) containing P (3HB)/bioactive glass composites for tissue engineering applications. *Acta Biomater.* 6, 735–742.
- Mondal, T., Sunny, M., Khastgir, D., Varma, H., Ramesh, P., 2012. Poly (L-lactide-co- $\epsilon$ -caprolactone) microspheres laden with bioactive glass-ceramic and alendronate sodium as bone regenerative scaffolds. *Mater. Sci. Eng. C* 32, 697–706.
- Navarro, M., Ginebra, M.P., Planell, J.A., 2003. Cellular response to calcium phosphate glasses with controlled solubility. *J. Biomed. Mater. Res. Part A* 67, 1009–1015.
- Neel, E.A., Ahmed, I., Pratten, J., Nazhat, S., Knowles, J., 2005. Characterisation of anti-bacterial copper releasing degradable phosphate glass fibres. *Biomaterials* 26, 2247–2254.
- Okamoto, M., John, B., 2013. Synthetic biopolymer nanocomposites for tissue engineering scaffolds. *Progress Polym. Sci.* 38, 1487–1503.
- Penttinen, R., 2011. Cell interaction with bioactive glasses and ceramics. *Bioact. Glasses Mater. Proper Appl.* 53, 145–180.
- Peter, M., Binulal, N., Soumya, S., Nair, S., Furuike, T., Tamura, H., et al., 2010. Nanocomposite scaffolds of bioactive glass ceramic nanoparticles disseminated chitosan matrix for tissue engineering applications. *Carbohydr. Polym.* 79, 284–289.
- Qian, L., Zhang, H., 2011. Controlled freezing and freeze drying: a versatile route for porous and micro-/nano-structured materials. *J. Chem. Technol. Biotechnol.* 86, 172–184.
- Qu, T., Liu, X., 2013. Nano-structured gelatin/bioactive glass hybrid scaffolds for the enhancement of odontogenic differentiation of human dental pulp stem cells. *J. Mater. Chem. B* 1, 4764–4772.
- Rahaman, M.N., Day, D.E., Bal, B.S., Fu, Q., Jung, S.B., Bonewald, L.F., et al., 2011. Bioactive glass in tissue engineering. *Acta Biomater.* 7, 2355–2373.
- Rengier, F., Mehndiratta, A., Von Tengg-Kobligh, H., Zechmann, C.M., Unterhinninghofen, R., Kauczor, H.-U., et al., 2010. 3D printing based on imaging data: review of medical applications. *Int. J. Comput. Assist. Radiol. Surg.* 5, 335–341.
- Rezwani, K., Chen, Q., Blaker, J., Boccaccini, A.R., 2006. Biodegradable and bioactive porous polymer/inorganic composite scaffolds for bone tissue engineering. *Biomaterials* 27, 3413–3431.
- Roohani-Esfahani, S., Nouri-Khorasani, S., Lu, Z., Appleyard, R., Zreiqat, H., 2011. Effects of bioactive glass nanoparticles on the mechanical and biological behavior of composite coated scaffolds. *Acta Biomater.* 7, 1307–1318.
- Salih, V., Franks, K., James, M., Hastings, G., Knowles, J., Olsen, I., 2000. Development of soluble glasses for biomedical use Part II: The biological response of human osteoblast cell lines to phosphate-based soluble glasses. *J. Mater. Sci. Mater. Med.* 11, 615–620.

- Saranti, A., Koutselas, I., Karakassides, M., 2006. Bioactive glasses in the system CaO–B<sub>2</sub>O<sub>3</sub>–P<sub>2</sub>O<sub>5</sub>: preparation, structural study and in vitro evaluation. *J. Non-Crystal. Solids* 352, 390–398.
- Shu, C., Wenjuan, Z., Xu, G., Wei, Z., Wei, J., Dongmei, W., 2010. Dissolution behavior and bioactivity study of glass ceramic scaffolds in the system of CaO–P<sub>2</sub>O<sub>5</sub>–NaO–ZnO prepared by sol–gel technique. *Mater. Sci. Eng. C* 30, 105–111.
- Silver, I.A., Deas, J., Erecińska, M., 2001. Interactions of bioactive glasses with osteoblasts in vitro: effects of 45S5 Bioglass®, and 58S and 77S bioactive glasses on metabolism, intracellular ion concentrations and cell viability. *Biomaterials* 22, 175–185.
- Skelton, K., Glenn, J., Clarke, S., Georgiou, G., Valappil, S., Knowles, J., et al., 2007. Effect of ternary phosphate-based glass compositions on osteoblast and osteoblast-like proliferation, differentiation and death in vitro. *Acta Biomater.* 3, 563–572.
- Sowmya, S., Kumar, P.S., Chennazhi, K., Nair, S., Tamura, H., Rangasamy, J., 2011. Biocompatible  $\beta$ -chitin hydrogel/nanobioactive glass ceramic nanocomposite scaffolds for periodontal bone regeneration. *Artif. Organs* 25, 1–11.
- Tian, H., Tang, Z., Zhuang, X., Chen, X., Jing, X., 2012. Biodegradable synthetic polymers: preparation, functionalization and biomedical application. *Progress Polym. Sci.* 37, 237–280.
- Valliant, E.M., Jones, J.R., 2011. Softening bioactive glass for bone regeneration: sol–gel hybrid materials. *Soft Matter* 7, 5083–5095.
- Vollenweider, M., Brunner, T.J., Knecht, S., Grass, R.N., Zehnder, M., Imfeld, T., et al., 2007. Remineralization of human dentin using ultrafine bioactive glass particles. *Acta Biomater.* 3, 936–943.
- Watts, P., Davies, M., Melia, C., 1989. Microencapsulation using emulsification/solvent evaporation: an overview of techniques and applications. *Crit. Rev. Therap. Drug Carrier Syst.* 7, 235–259.
- Webster, T.J., Siegel, R.W., Bizios, R., 1999. Osteoblast adhesion on nanophase ceramics. *Biomaterials* 20, 1221–1227.
- Wu, C., Zhu, Y., Chang, J., Zhang, Y., Xiao, Y., 2010a. Bioactive inorganic-materials/alginate composite microspheres with controllable drug-delivery ability. *J. Biomed. Mater. Res. Part B Appl. Biomater.* 94, 32–43.
- Wu, X., Liu, Y., Li, X., Wen, P., Zhang, Y., Long, Y., et al., 2010b. Preparation of aligned porous gelatin scaffolds by unidirectional freeze-drying method. *Acta Biomater.* 6, 1167–1177.
- Wu, J., Xue, K., Li, H., Sun, J., Liu, K., 2013. Improvement of PHBV scaffolds with bio-glass for cartilage tissue engineering. *PLoS One* 8, e71563.
- Xia, W., Chang, J., 2010. Bioactive glass scaffold with similar structure and mechanical properties of cancellous bone. *J. Biomed. Mater. Res. Part B Appl. Biomater.* 95, 449–455.
- Xynos, I.D., Edgar, A.J., Buttery, L.D., Hench, L.L., Polak, J.M., 2001. Gene-expression profiling of human osteoblasts following treatment with the ionic products of Bioglass® 45S5 dissolution. *J. Biomed. Mater. Res.* 55, 151–157.
- Yoshimoto, H., Shin, Y., Terai, H., Vacanti, J., 2003. A biodegradable nanofiber scaffold by electrospinning and its potential for bone tissue engineering. *Biomaterials* 24, 2077–2082.

- Zahedi, P., Karami, Z., Rezaeian, I., Jafari, S.H., Mahdaviani, P., Abdolghaffari, A.H., et al., 2012. Preparation and performance evaluation of tetracycline hydrochloride loaded wound dressing mats based on electrospun nanofibrous poly (lactic acid)/poly ( $\epsilon$ -caprolactone) blends. *J. Appl. Polym. Sci.* 124, 4174–4183.
- Zeleny, J., 1914. The electrical discharge from liquid points, and a hydrostatic method of measuring the electric intensity at their surfaces. *Phys. Rev.* 3, 69.
- Zhang, X., Jia, W., Gu, Y., Xiao, W., Liu, X., Wang, D., et al., 2010. Teicoplanin-loaded borate bioactive glass implants for treating chronic bone infection in a rabbit tibia osteomyelitis model. *Biomaterials* 31, 5865–5874.
- Zhao, S., Zhu, M., Zhang, J., Zhang, Y., Liu, Z., Zhu, Y., et al., 2014. Three dimensionally printed mesoporous bioactive glass and poly (3-hydroxybutyrate-co-3-hydroxyhexanoate) composite scaffolds for bone regeneration. *J. Mater. Chem. B* 2, 6106–6118.
- Zhijiang, C., Chengwei, H., Guang, Y., 2012. Poly (3-hydroxybutyrate-co-4-hydroxybutyrate)/bacterial cellulose composite porous scaffold: preparation, characterization and biocompatibility evaluation. *Carbohydr. Polym.* 87, 1073–1080.
- Zhong, S., Zhang, Y., Lim, C., 2010. Tissue scaffolds for skin wound healing and dermal reconstruction. *Wiley Interdiscipl. Rev. Nanomed. Nanobiotechnol.* 2, 510–525.

# Bioactive glass–based composites in bone tissue engineering: synthesis, processing, and cellular responses

# 13

Anuj Kumar<sup>1,2</sup> and Sung Soo Han<sup>1,2</sup>

<sup>1</sup>*School of Chemical Engineering, Yeungnam University, Gyeongsan, South Korea* <sup>2</sup>*Department of Nano, Medical and Polymer Materials, Yeungnam University, Gyeongsan, South Korea*

## 13.1 INTRODUCTION

Bioactive glasses (BGs) were discovered 45 years ago and have widely been used for clinical purposes (e.g., orthopedics and dentistry) since the 1980s. From the initial use of BGs as bioactive materials for bone filling materials and dental implants, their biomedical use has been expanded in a broad spectrum of therapeutic and tissue engineering applications (Baino et al., 2016a). However, in this chapter, the use of BGs only in the engineering of bone tissues is described. In this chapter, we describe how BGs-based composite scaffolds have widely been applied in the regeneration of bone tissues. We first highlight the bone structure as natural composite, concept of bone tissue engineering, BGs for bone tissue engineering and their composition, types, properties, and their cell response towards bone cells during regeneration of bone tissues. The synthesis of BGs, surface modifications, processing and their recent applications in bone tissue engineering are also discussed. Finally, major challenges and future perspectives in bone tissue engineering are briefly discussed.

### 13.1.1 BONE: A NATURAL COMPOSITE

Bone itself is considered as a natural composite and is composed of outer cortical bone and inner trabecular bone. In the bone structure, cortical bone is organized longitudinally (not as concentrically) along the trabeculae, while trabecular bone possesses various lamellar arrangements (Fratzl and Weinkamer, 2007; Vaz et al., 2011). The mechanical properties of the natural bone vary based on its structure and composition, which comprises the component's arrangements and bonding arrangements between collagen (Col) fibers and matrix (Fratzl and Weinkamer,

2007; Gibson and Ashby, 1999). The structure of bone can be understood in the following ways (Vaz et al., 2011):

1. cortical and trabecular bone (microstructural level),
2. Harversian systems, osteons, and trabeculae (microstructural point of view level),
3. intrinsic lamellae structure (submicrostructure level),
4. arrangements of type-I Col-fibrils and mineral phases (nanoscale level), and
5. molecular structure of components (molecular level).

For the macrostructural view, a femur can be considered to observe distinct parts of the bone as trabecular (spongy or cancellous) areas protected by a cortical (or compact) shielding. Cortical bone has porosity around 6%, while trabecular bone is highly porous structure and has porosity around 80% (Gibson and Ashby, 1999; Gibson, 2005; Fratzl and Weinkamer, 2007). Both distinct parts have almost the same composition elementally. The structure of cortical bone has concentric layers around a blood vessel (osteons or Haversian systems) and trabecular has a cellular structure composed of an interconnected network of rods and plates forming an open-cell foam structure (Gibson and Ashby, 1999; Gibson, 2005). The walls of the cell foam structure are restricted by trabeculae of thickness around 200  $\mu\text{m}$  (Fratzl and Weinkamer, 2007), which are surrounded by bone marrow (BM) and living cells. The cortical bone has Young's modulus values ranging from 10 to 20 GPa, while trabecular bone has stiffness values ranging between 0.3 and 3 GPa (Fung, 1993). Bone is a complex but made of a hierarchical ordered structure (as shown in Fig. 13.1), in which calcium phosphate crystals

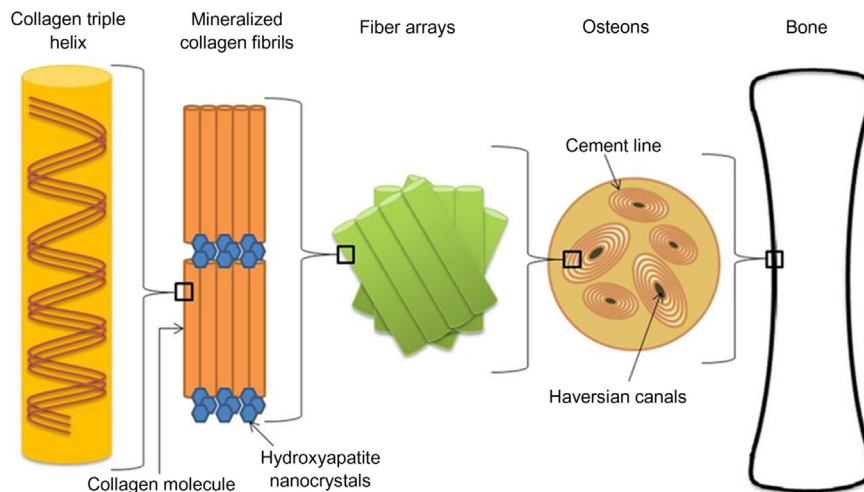


**FIGURE 13.1**

Hierarchical ordered structure of the bone (Kuttappan et al., 2016).

[carbonated apatite:  $\text{Ca}_5(\text{PO}_4, \text{CO}_3)_3(\text{OH})$ ] incorporated into type-I Col-fibers as protein (Fratzl et al., 2004; Park and Lakes, 1992). In dry bone, carbonated apatite comprises almost two-thirds of the total bone weight and the rest is organic material (i.e., Col) including other non-Col lipids and proteins (Fratzl and Weinkamer, 2007).

In this composite system, Col provides the capacity to bone for absorbing energy (i.e., to the toughness) and inorganic phase provides the stiffness to the bone tissues (Viguet-Carrin et al., 2006). Due to the staggered nature, orientation, length, and varying gap zones (site for nucleation of the calcium crystals) between Col molecules, it may result in different mechanical responses in the arrangement of Col-fibrils. Therefore, Col molecular arrangement, molecular packing, and crosslinking are the main factors responsible for the bone properties (Fratzl et al., 2004; Fratzl and Weinkamer, 2007; Viguet-Carrin et al., 2006; Buehler, 2006; Vaz et al., 2011). In this way, mineralized Col-fibrils have higher strength, stiffness, and energy until failure compared with the fibrils of pure Col (Buehler, 2007). Col has higher toughness (but not high stiffness) and shows a modulus value of 1.24 GPa, while carbonated apatite crystals are very strong and stiff (but not very tough) and show a modulus value of 165 GPa. The bone as natural composite combines both types of properties as stiffness and toughness from organic and inorganic phases (Vaz et al., 2011).

### 13.1.2 BONE TISSUE ENGINEERING

Bone defects due to the bone tissue damage either by aging, disease, sport-related injuries, or traumatic accidents are major concerns in the healthcare systems. The options for the treatment of bone defects are centered mainly on remodeling of the damaged bone tissues (Shadjou and Hasanzadeh, 2015). For this purpose, one of commonly employed strategies is to surgically implant suitable bone substitute into the area of damaged bone or bone-grafting by using natural and synthetic material (Sethuraman et al., 2010, 2011). But these conventional strategies show many complications such as morbidity of donor site, immunogenicity, donor availability, and mismatch in mechanical properties of bone substitute and native bone followed by the formation of fibrous capsule (Li and Wang, 2008; Nandi et al., 2010). In the last decades, cell-based therapies and tissue engineering have shown as potential alternatives to these conventional strategies. The engineering of damaged bone tissues involves the three main factors as scaffolding system, cells, and growth factors for successful regeneration of bone tissues by mimicking the microenvironment of the native bone tissues. This area of engineered bone tissues is collectively called “bone tissue engineering” (Shadjou and Hasanzadeh, 2015).

#### 13.1.2.1 Requirements for bone implant materials

The bone tissue engineering field is always searching for alternative bone substitutes that ideally eliminate the previous clinical issues in used treatment options

such as limited availability, donor-site morbidity, immune rejection, and transfer of pathogens (O’Keefe and Mao, 2011). Therefore, the key requirements for bone implant materials can be classified as (1) biocompatible porous scaffold, (2) osteogenic cells, (3) growth factors (morphogenic signals) that help to monitor osteogenic cells to phenotypically desirable type, and (4) sufficient vascularization for meeting proper nutrient supply and clearance needs for growing tissues (Shadjou and Hasanzadeh, 2015). However, for successful bone tissue regeneration, BGs-based scaffold in detail should have the following desired parameters for functioning as a suitable bone material (Kaur et al., 2014; Hutmacher, 2001; Karageorgiou and Kaplan, 2005; Levenberg, and Langer, 2004):

1. Biocompatibility (nontoxic and promote cell attachment/proliferation).
2. Crystalline phases (due to heat treatment) must not induce any cytotoxic effect or detrimental effect on bioactive process inside the cell/tissue bioconstruct.
3. No inflammatory response and cytotoxicity or immunogenicity behavior while degrading into nontoxic byproducts.
4. Desired mechanical performance to withstand any kind of strain or pressure during handling and tissue engineering procedure (comparable to the natural bone tissue).
5. Good apatite forming ability (bone-like material).
6. Controllable interconnected porosity supporting vascularization for directing cells to grow within the desired physical architecture (typical porosity:  $\sim 90\%$  and  $\geq 100\ \mu\text{m}$ ).
7. 3D microenvironment similar to natural bone tissue.
8. Finally, cost-effective for commercialization while maintaining desired features.

### 13.1.3 BIOACTIVE GLASSES FOR BONE TISSUE ENGINEERING

The bone regeneration mainly relies on the composition and microstructure of the bone scaffolds. For load-bearing bone tissues, several types of organic–inorganic-based scaffolding systems have been fabricated (Kumar et al., 2014, 2016, 2017a), but show some inferior properties [lack of biodegradation of hydroxyapatite (HA) in the body] that limit the use of bioceramics, for example, HA as inorganic phase (Zhou and Lee, 2011). In this context, BGs have shown great potential as promising inorganic components in the bone tissue engineering applications because of their molecular-level interactions for improving the mechanical properties, ability to form bone-like material (apatite) similar to HA, controlled degradation, and upregulation of the gene expression that control osteogenesis compared with bioceramics (Rahaman et al., 2011; Lei et al., 2012). Therefore, polymer/BGs composite has attracted great attention as a new of family bioactive materials that possibly mimic the features of natural bone tissue, demonstrating improved bone formation (Mishra et al., 2009; Hench et al., 2014).



## 13.2 BIOACTIVE GLASSES: COMPOSITION AND PROPERTIES

### 13.2.1 TYPE OF BIOACTIVE GLASSES

Glasses are typically brittle, optically transparent (often), act as amorphous solids without long-range order, and consist of the same building blocks with different pattern. Actually, glasses are essentially super-stiff liquids, where atoms are arranged randomly, more closely to that of liquid (Kingery et al., 1976; Shelby, 2005), and show time-dependent glass transformations over a temperature range. Based on their compositional aspects, BGs can be categorized in the following ways.

#### 13.2.1.1 Silicate-bioactive glasses

Silica-bioactive glasses have mostly basic tetrahedral shape ( $\text{SiO}_4$ )<sup>4-</sup> with varying connectivity via 1D, 2D, and 3D arrangements in both glassy and crystalline phases. Additionally, by preventing the close-packing of anion layers each O-anion is coordinated by two Si-cations, resulting in relatively open structures (Kingery et al., 1976; Shelby, 2005). Silica-bioactive glasses (e.g., 45S5 or 13-93) have widely been applied in bone tissue engineering because of their support for osteoblastic cell (e.g., MC3T3-E1) proliferation and differentiation in vitro (Fu et al., 2008).

#### 13.2.1.2 Borate/borosilicate-bioactive glasses

Borate/borosilicate-bioactive glasses have been manipulated with relative proportions of  $\text{B}_2\text{O}_3$  to obtain desired bioactive properties. Borate/borosilicate glasses (BSGs) are very reactive and more rapidly and completely to apatite than that of their silica counterparts (Yao et al., 2007; Huang et al., 2006). The conversion mechanism via borate-rich layer is similar to silicate-bioactive glass (Hench, 1998) and also the sintering behavior is more controlled compared with silicate-bioactive glasses (Liang et al., 2008). Boron as a trace element is needed for bone health (Uysal et al., 2009) and thus borate/borosilicate-bioactive glasses support in vitro cell proliferation and differentiation, while in vivo they enhance tissue infiltration (Marion et al., 2005). However,  $(\text{BO}_3)_3^-$  ions have been associated with toxicity depending on certain compositions and culture conditions (Yao et al., 2007; Huang et al., 2006). Borate/borosilicate-bioactive glasses (e.g., 13-93B2) have shown microstructure nearly identical to trabecular bone (Fu et al., 2008).

#### 13.2.1.3 Phosphate-bioactive glasses

Phosphate-bioactive glasses have a phosphate  $(\text{PO}_4)$ <sup>3-</sup> tetrahedron structural unit that is asymmetric in nature, where  $\text{P}_2\text{O}_5$  acts as a network former oxide. This asymmetry is responsible for low chemical durability, indicating ease hydration of P-O-P bonds (Gao et al., 2004) and the dissolution rate of phosphate-bioactive glasses is manipulated by incorporating appropriate metal oxides (e.g.,  $\text{TiO}_2$ ,

CuO, NiO, MnO, and  $\text{Fe}_2\text{O}_3$ ) to the glass composition (Neel et al., 2005a,b, 2007; Ahmed et al., 2004). Phosphate-bioactive glasses (e.g.,  $\text{Na}_2\text{O}$ -CaO-SrO- $\text{P}_2\text{O}_5$ ) have shown good physical and structural characterization as bone material (Neel et al., 2009) and regulated good metabolic activity and proliferation followed by differentiation of Bone Marrow Stromal Cells (BMSCs) (Vitale-Brovarone et al., 2008a).

#### 13.2.1.4 Doped-bioactive glasses

Doped-bioactive glasses (DBGs) are known as modified glass compositions using dopants or additional additives making it bioactive, bioresorbable, and/or biodegradable (Navarro et al., 2004). BGs have broadly been functionalized by using doping elements, such as Al, Cu, Zn, Fe, Cr, In, Ba, Sr, and Y (Branda et al., 2002; Hoppe et al., 2011; Wang et al., 2011; Singh et al., 2009). DBGs compositions doped with Ag showed good antibacterial properties, while maintaining their bioactive nature (Bellantone et al., 2002). Further, other oxides such as  $\text{Na}_2\text{O}$ ,  $\text{K}_2\text{O}$ , CaO, and MgO are beneficial to adjust the pH of the surroundings and CuO, ZnO, AgO, and  $\text{TiO}_2$  in addition to  $\text{SiO}_2$ ,  $\text{B}_2\text{O}_3$ , and  $\text{P}_2\text{O}_5$  facilitate the release of proper ions that can communicate antibacterial effect to the biomaterial.  $\text{Al}_2\text{O}_3$  is useful in improving the mechanical properties of the BGs, whereas Zn and Mg are well known to impart a stimulatory effect on osteoblastic cell proliferation, differentiation, and apatite forming ability (Yamaguchi, 1998; Saboori et al., 2009). In addition, Sr-doped BGs can stimulate osteogenesis and accelerate bone healing, while reducing bone resorption (Wong et al., 2004) and Y- and Cr-based BGs exhibited good apatite formation ability (Singh et al., 2009).

#### 13.2.1.5 Metallic-bioactive glasses

The bulk metallic glasses (BMGs) have unique properties such as superior mechanical strength, high fracture toughness, high elastic strain limit, and lower Young's modulus and are biodegradable without evolving hydrogel (Wang et al., 2004). BMGs show superior properties compared with conventional biomaterials (Horton and Parsell, 2003) and the main disadvantage of BMGs is the incorporation of nickel (Ni) that causes an allergic response and possibly behaves as a carcinogenic element (McGregor et al., 2000). Therefore, several studies have been performed for developing Ni-free BMGs (Liu et al., 2010; Zberg et al., 2009).

### 13.2.2 RESPONSE OF BIOACTIVE GLASSES TO CELLS

BGs have been tested for many mammalian species and no evidence of cytotoxicity was observed (Weinstein et al., 1980; Stanley et al., 1976). However, the composition of the BGs has a remarkable effect on its capability to support in vitro proliferation and differentiation of osteoblastic cells. Silica ( $\text{Si}^{4+}$ ) shows stimulatory effects on osteoblastic cells when its releasing level is between 0.1 and 100 ppm (Xynos et al., 2001). Sodium ( $\text{Na}^+$ ) does not reveal any significant

physiological effects except degradation and controlling release of other constituent ions (Wilson et al., 1981). Further, strontium ( $\text{Sr}^{2+}$ ) having concentration range between 8.7 and 87.6 ppm showed stimulatory effects on cells, while  $\text{Zn}^{2+}$  showed cytotoxic effects above 6.5 ppm concentration of  $\text{Zn}^{2+}$  (Murphy et al., 2009; Aina et al., 2007). The inclusion of  $\text{Zn}^{2+}$  more than 5% into BGs showed cytotoxic responses on human osteoblastic cells and oxidative damage was observed in case of endothelial, retinal, and peripheral blood lymphocytes (Wood, and Osborne, 2003; Del Río and Vélez-Pardo, 2004; Tang et al., 2001). Silicate-bioactive glasses (45S5 or 13-93)—based discs or porous scaffolds showed good in vitro osteoblastic cell proliferation and differentiation (Brown et al., 2008a; Fu et al., 2008), whereas borate-/borosilicate-bioactive glasses exhibited remarkably a lower ability to support in vitro osteoblastic cell proliferation and differentiation (Fu et al., 2010d; Brown et al., 2008b). This is possibly because of the fast degradation rate of the borate-based bioactive glasses and toxicity due to the release of the boron into the culture medium. Also, borate-based bioactive glasses subjected to lead the higher pH value of the culture medium (Rahaman et al., 2011). Therefore, the compositions of BGs must be developed having optimum concentrations of the elements for proper action of dissolution products.

### 13.2.3 ANTIBACTERIAL EFFECT OF BIOACTIVE GLASSES

It is well known that BGs-based scaffold itself show some certain antibacterial/antimicrobial activity due to the pH increase caused by the release of silicon ( $\text{Si}^{4+}$ ) and calcium ( $\text{Ca}^{2+}$ ) ions during dissolution (Stoor et al., 1998; Salinas and Vallet-Regí, 2016). Therefore, by looking at this benefit, it can be improved further during prosthesis infections with the incorporation of the elements having declared antibacterial activity such as silver ( $\text{Ag}^+$ ), zinc ( $\text{Zn}^{2+}$ ) or gallium ( $\text{Ga}^{3+}$ ) (El-Kady et al., 2012; Boyd et al., 2009; Ross-Gillespie et al., 2014; Nicolini et al., 2015; Salinas and Vallet-Regí, 2016). For example, Salinas and Vallet-Regí (2016) prepared mesoporous bioactive glass (MBG) scaffolds using rapid prototyping (RP) processing by involving 80% $\text{SiO}_2$ –15% $\text{CaO}$ –5% $\text{P}_2\text{O}_5$  mol% glass having revisited substitutions up to 3.5% of  $\text{Ce}_2\text{O}_3$  or  $\text{Ga}_2\text{O}_3$  or 7.0%  $\text{ZnO}$ . In this study, the incorporation of therapeutically active metallic ions slightly decreased the textural properties, inherent mesoporous order, and in vitro bioactive response in fluids mimicking human blood plasma.  $\text{Ga}^{3+}$  cause to behave as intermediate ions between network formers and network modifiers, and develop bacterial resistance differing from that of antibiotics or antimicrobial peptides. In addition, fast deposition of bone-like (apatite) layer can slow down or hinder the liberation of the specific biomolecules involving with the mesopores or even the release of the ions involving with antibacterial or other purposes (details shown in Fig. 13.2). Further, the incorporation of 4%  $\text{ZnO}$  in the MBG scaffolds drastically increased this antibacterial effect against *Staphylococcus aureus* (Sánchez-Salcedo et al., 2014). However,  $\text{Ga}^{3+}$  did not show antibacterial activity because  $\text{Ga}^{3+}$  ions were scarcely released from the MBG network. In addition, good osteoblast

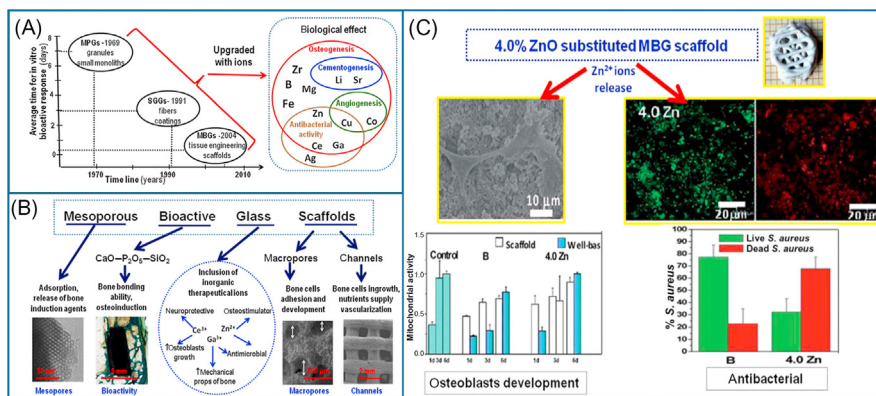


FIGURE 13.2

(A) Timeline of discovering of the three BGs families and approximate time required for apatite forming ability in SBF. (B) The required features of MBG scaffolds for bone tissue engineering, including extra properties coming from the incorporations of inorganic ions ( $\text{Ce}^{3+}$ ,  $\text{Ga}^{3+}$ , and  $\text{Zn}^{2+}$  ions). (C) In vitro cytocompatibility study in osteoblastic cells (left) and in vitro antibacterial effect against *S. aureus* (right) of MBG scaffolds having 4 mol% of ZnO (Sánchez-Salcedo et al., 2014).

development was observed when investigated in both the well base and in extracts of the culture medium after soaking Zn-scaffolds for 1, 3, and 6 days. As high as 7% ZnO reinforced MBG scaffold was not found biocompatible indicating critical point of concentration (Salinas and Vallet-Regí, 2016).

## 13.3 SYNTHESIS OF BIOACTIVE GLASSES

BG nanoparticles (BGNPs) are starting material as inorganic phase for the fabrication of the porous scaffolds for bone tissue engineering applications. Several studies have widely been reported for the synthesis of BGNPs. In this section, four major methods are discussed to prepare BGNPs as follows:

### 13.3.1 SOL–GEL METHOD

As a typical liquid phase synthesis method, sol–gel method involves the use of metal–organic precursors and converts them to inorganic materials either in water or in an organic solvent (Brinker and Scherer, 1990). A gel is formed after hydrolysis (acid/base) and polycondensation reactions and is further subject to calcination at  $600^{\circ}\text{C}$ – $700^{\circ}\text{C}$  to form BGNPs. In this method, tetraethyl orthosilicate, calcium nitrate, and triethylphosphate as typical precursors are utilized (Brinker and Scherer, 1990; Veerapandian and Yun, 2009). This method has shown a great

potential and versatility for the production of a variety of BGNPs. However, this method shows some limitations in terms of composition, remaining residual organic solvent (usually removed by calcination), the fact that it is time-consuming, and yields batch-to-batch variations (Boccaccini et al., 2010).

### 13.3.2 MICROEMULSION METHOD

This method is a thermodynamically stable, transparent, isotropic dispersion of the aqueous droplets of the two immiscible liquids (e.g., water and oil) stabilized by surfactant at the water/oil interface (Arriagada and Osseo-Asare, 1999). In this case, these aqueous droplets (usually ranging from 5 to 20 nm in diameter) (Lim et al., 1996) act as a micro/nanoreactor in which reactants collide and react with each other. Therefore, this method is beneficial to prepare nanosized particles composed of organic and inorganic components with minimum agglomeration. However, the main disadvantages of this method are low production yield and the use of a large amount of surfactant and oil phases (Lim et al., 1996; Bose and Saha 2003; Zhao et al., 2005; Boccaccini et al., 2010).

### 13.3.3 FLAME-SPRAY METHOD

Flame-spray method involves the use of organic liquid precursors loaded with metals and in this process, the liquid precursor is dispersed by oxygen over a nozzle thereby forming a spray that is ignited. While the spray is burning, organic content of the liquid precursor completely combusts finally to water ( $H_2O$ ) and carbon dioxide ( $CO_2$ ) and the metal constituents oxidize to nanoparticles (Stark et al., 2003; Brunner et al., 2006, 2009; Loher et al., 2005; Boccaccini et al., 2010).

### 13.3.4 LASER-SPINNING METHOD

Laser-spinning method has been developed to produce glass micro/nanofibers (Quintero et al., 2007). This method involves a quick heating and melting of the precursor material (small volume) up to high temperatures using high laser power. Then, at the same time, a supersonic jet is injected into the molten volume for blowing this molten material (Quintero et al., 2007, 2009a) followed by quick stretching and cooling by supersonic gas jet (Quintero et al., 2009b). By using this method, long fibers with extraordinary high aspect ratio and amorphous nature can be produced (Quintero et al., 2009a,b; Boccaccini et al., 2010).

---

## 13.4 SURFACE MODIFICATION OF BIOACTIVE GLASSES

For the desired biological performance, the surface of BGNPs can be modified by using different types of materials such as lactic acid, silane coupling, metallic

ions (e.g., B, Mg, Zn, Ag, Zr, Ti), and biomolecules (e.g., gentamicin and dexamethasone) (Boccaccini et al., 2010; Rabiee et al., 2015; Baino et al., 2016b). For example, Chen et al. (2009) investigated the surface modification of the BGs using lactic acid as hydrolysis promoter in the sol–gel process and obtained the decreased size of the BGNPs. The results showed nanoscaled surface morphology with high roughness and significantly improved the in vitro bioactivity (Chen et al., 2009). In another study, the silane coupling agent covalently grafted onto surface of BGNPs to improve their dispensability and cell proliferation was performed, which obtained the dispersed BGNPs ranging from 20 to 70 nm (Chen et al., 2008). Further, the increase in Ag concentration increased the structural densification and crystallization of Ag in BGNPs while it decreased the HA crystallization (Delben et al., 2009), and induced the antimicrobial effect into BGNPs (El-Kady et al., 2012). Tang et al. (2016) developed a trimodal (macro/micro/nanoporous) BG scaffolds loaded with a recombinant human bone morphogenetic protein-2 (BMP-2) that facilitated excellent in vitro cell attachment, proliferation, and osteogenesis (Tang et al., 2016). In another way, BGNPs have been used for coating other materials (e.g., HA) to obtain better mechanical performance and high bioactivity in a single biomaterial (Esfahani et al., 2008).

---

## 13.5 PROCESSING OF BIOACTIVE GLASSES–BASED SCAFFOLDS

For bone tissue regeneration, generally highly interconnected porous scaffolds with a mean diameter of 100  $\mu\text{m}$  (or greater) and open porosity above 50% have been considered to be the minimum requirements to facilitate tissue ingrowth and functioning of porous scaffolds (Sittinger et al., 2004; Kaur et al., 2014). For the processing of BGs-based scaffolds, various fabrication techniques such as mainly melt-derived process, sol–gel process, polymer-foam replication, freeze-casting, and RP have been performed.

### 13.5.1 MELT-DERIVED PROCESSING

This melt-derived process involves the formation of scaffolds by melting (thermally) to bond a loose and random packing of glass particles or short fibers into a mold with the desired geometry (Bellucci et al., 2010; Baino et al., 2009; Haimi et al., 2009; Vitale-Brovarone et al., 2008b). In addition, porogens have also been mixed and fused with the BGs particles to create and increase the pore size and porosity of the scaffolds and porogens can be removed by decomposition or leaching, but prior to the sintering process. However, the main disadvantage of this process is the poor pore interconnectivity within the scaffold at low loading of the porogens (Fu et al., 2011).

### 13.5.2 SOL–GEL PROCESSING

The sol–gel process involves the foaming of a sol by the incorporation of a surfactant and further condensation and gelation reactions to prepare the sol–gel system (Jones et al., 2004, 2006; Rainer et al., 2008). Then this sol–gel system is subjected to aging to strengthen the gel network, then the removal of liquid byproduct by drying followed by sintering to prepare 3D porous scaffolds. It results in a hierarchical pore architecture having interconnected mesopores (2–50 nm) that are inherent to the sol–gel process and macropores (10–500  $\mu\text{m}$ ) that resulted from the foaming process. As-obtained hierarchical pore architecture is very beneficial to stimulate the cell response to scaffold by mimicking more closely the hierarchical structure of natural tissues under a physiological environment. In this case, sol–gel derived scaffolds with high surface area (100–200  $\text{m}^2/\text{g}$ ) due to having mesopores in the glass network degrade and convert faster to bone-like material compared with melt-derived scaffolds with same composition. The sol–gel derived scaffolds show low strength (0.3–2.3 MPa) (Jones et al., 2006) and are suitable in low-load bone defects only.

### 13.5.3 POLYMER-FOAM REPLICATION

Polymer-foam replication mainly involves two steps: (1) the initial immersion of natural or synthetic polymeric foam in a ceramic suspension to coat a uniform layer on the foam struts, which is then dried; and (2) through careful heat treatment (typically between 300°C and 600°C) followed by glass struts are densified by the sintering at 600°C–1000°C depending on the composition and glass particle size. This process can produce the scaffold with the microstructure similar to the dry trabecular bone. The main advantage of this process is to produce highly interconnected and open porous scaffolds (porosity range: 40%–95%), but limited to the low load-bearing bone tissue engineering due to its lower mechanical strength of the prepared scaffolds. Silicate-, borate-, and borosilicate-based BGs scaffolds have widely been prepared by using this process (Chen et al., 2006; Vitale-Brovarone et al., 2007; Fu et al., 2011).

### 13.5.4 FREEZE-CASTING AND FREEZE-DRYING PROCESS

This process involves the rapid freezing of stable colloidal suspension of the particles in the mold followed by the sublimation (freeze-drying) of the frozen-solvent under vacuum. Further, porous scaffolds subject to sintering for removing the fine pores between the walls of the macropores and improve the mechanical properties of the scaffolds. In addition, oriented microstructure that is beneficial for higher mechanical strength of the porous scaffolds can be obtained by using directional freezing of the suspensions (Wegst et al., 2010; Fu et al., 2010a; Deville et al., 2006). However, these oriented scaffolds typically have lamellar microstructure (ranging from 10 to 40  $\mu\text{m}$ ) that are too small to support tissue



ingrowth. Additionally, it was observed that a columnar microstructure (changed from lamellar microstructure) with pore diameter 100–150  $\mu\text{m}$  has been prepared by adding organic solvent (e.g., 1,4-dioxane). Moreover, as-obtained oriented scaffolds showed good in vitro cell proliferation and differentiation and in vivo tissue infiltration (Fu et al., 2010b,c,d).

### 13.5.5 ELECTROSPINNING PROCESS

Electrospinning process involves the formation of nanofiber (e.g., nanofibrous mat) from the composite solution (e.g., polymer and BGs). In brief, as-prepared composite solution is loaded into a syringe and then electrospun onto a metal collector injected under a high DC voltage at a desired distance and speed. Finally, the electrospun mess (or nanofibrous mat) is peeled off and stored (Noh et al., 2010). This process is a simple and versatile process and produces the nanofibrous structure that mimics the features of native ECM and improves the bone cell migration, orientation, attachment, and proliferation (Xu et al., 2004; Hsu et al., 2015).

### 13.5.6 RAPID PROTOTYPING PROCESS

RP process involves layer-by-layer deposition of the material with fine detailing from a computer aided design file. By using this process, the architecture of the scaffolds can be controlled and optimized to obtain the desired mechanical performance, accelerated regeneration of bone tissues with monitoring bone formation with the anatomic cortical-trabecular structure (Hollister, 2005). Various RP processes such as 3D printing, ink-jet printing fused deposition modeling, selective laser sintering, stereolithography, and robocasting have been used for the fabrication of scaffolds from predesigned architecture (Hollister, 2005).

---

## 13.6 COMPOSITES FOR BONE TISSUE ENGINEERING APPLICATIONS

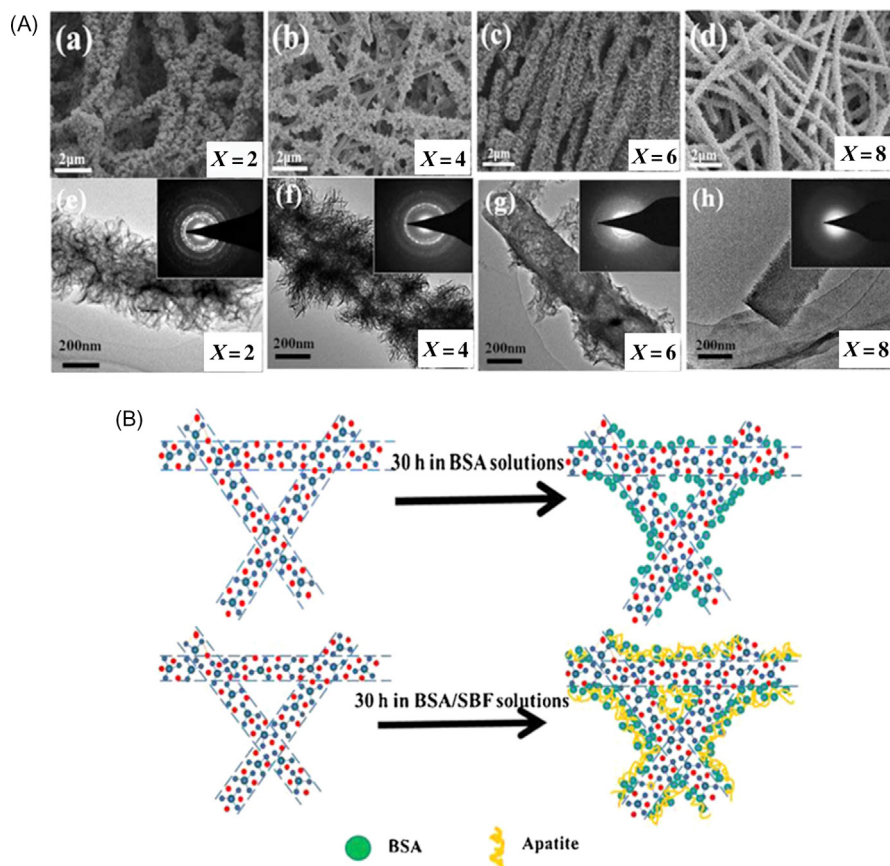
### 13.6.1 BIOACTIVE GLASSES–BASED COMPOSITE SCAFFOLDS

In general, HA degrades minimally while tricalcium phosphates show poor ability of Ca/P formation both in vitro and in vivo, although they are degradable. To overcome this problem, a biodegradable, bioactive, and mesoporous scaffold by coating HA-based scaffold with a nanocrystalline BG-layer followed by sintering at different temperatures was developed. BS1 scaffolds (sintered at 800°C with a 2 hours holding time) exhibited remarkable bioactivity and degradability simultaneously. The Ca/P forming capacity and rate of degradation of BS1 scaffolds was considerably decreased due to the formation of a nanocrystalline phase ( $\text{Si}_2\text{PO}_7$ ) during the sintering process, but improved their mechanical performances (Emadi et al., 2010). The low mechanical properties of calcium phosphate cements



(CPCs) is the major concern for stress bearing locations or defects in bone tissue engineering. For this, mechanical performance of CPCs was improved by reinforcing BG fibers (BGFs) (Nezafati et al., 2011) and HA-like crystals formed with oriented plate-like morphology on the surface of CPCs-BGFs (15 vol%) and good cell attachment, proliferation, and alkaline phosphate (ALP) activity were observed (Nezafati et al., 2013). Also, calcium hydroxide ( $\text{Ca}(\text{OH})_2$ )-based BG showed higher surface properties (surface area:  $100 \text{ m}^2/\text{g}$ ), spherical morphology and crystalline phases (apatite and wollastonite) after sintering at lower temperature than conventional temperature, better hardness ( $2.16 \pm 0.46 \text{ GPa}$  at  $980^\circ\text{C}$ ), and better MG-63 cell attachment and proliferation compared with calcium nitrate tetrahydrate [ $\text{Ca}(\text{NO}_3)_2$ ]-based BG (Shah et al., 2016). In addition, BGNPs (spherical shape and 30–60 nm in diameter) showed apatite forming ability in 7 days of simulated body fluid (SBF) incubation, an improvement in osteoblast cells proliferation and higher level of RUNX2 gene expression compared with HA and Si-HA nanoparticles (Fan et al., 2014). In another study, by increasing water/TEOS ratio (X ratio) from 2 to 8, Si–O–Si network in electrospun BGFs was remarkably improved and tunable and sustained protein release was successfully achieved with a designed protein loading process by using solution of SBF/bovine serum albumin (BSA) mixture. The kinetics of protein release presents a more controlled and sustained manner with the decreased X ratio (from 8 to 2) that is mainly attributed to the “anchoring” effect of crystalline HA-like mineral layers formed at the fiber surface (as shown in Fig. 13.3) (Li et al., 2014).

Zeimaran et al. (2016) prepared rod-like BGs having composition  $58\text{SiO}_2\text{--}33\text{CaO--}9\text{P}_2\text{O}_5$  (wt%) in different hydrothermal conditions ( $200^\circ\text{C}$  and  $220^\circ\text{C}$ ). The results showed the reduction in diameter of rods from microscale to nanoscale when temperature increased from  $200^\circ\text{C}$  to  $220^\circ\text{C}$  while improving crystallinity. Additionally, BGs nanorods showed higher bioactivity compared with BGs microrods (Zeimaran et al., 2016). In addition, the nanoporous structure in BG improved their bioactivity remarkably (accelerated deposition of HA-like layer as well as promoted the proliferation of BMSCs) (Ma et al., 2013). Miguez-Pacheco et al. (2016) prepared lithium (Li)-incorporated 45S5 BGs (Li-BGs) having  $\text{Na}_2\text{O}$  substituted by  $\text{Li}_2\text{O}$  with various amounts (2.5, 5.0, and 10.0 wt%  $\text{Li}_2\text{O}$ ) by using foam-replication method for the possible improvement in stimulation of osteoblast cell activity. The results showed good formation of HA-like (apatite) layer on the surface of Li-BGs when incubated in SBF and the formulations with 2.5 and 5.0 wt% of  $\text{Li}_2\text{O}$  content, in terms of Li-ions release, were only within the therapeutic range ( $<8.3 \text{ ppm}$ ) (Miguez-Pacheco et al., 2016). In addition, Li-ions were found to be released from BGNPs through diffusion-controlled process and both drugs as 5-FU or vancomycin were found to release beyond 32 days by a diffusion-controlled process (El-Kady et al., 2016). Bellucci et al. (2010) prepared compact and highly porous structure by using salt particles and potassium-based BG that could be sintered relatively at low temperature (i.e.,  $750^\circ\text{C}$ ). The obtained scaffold showed high porosity (70%–80%) and an appreciable mechanical performance (Young's modulus: 3.4–3.7 MPa) (Bellucci et al., 2010).

**FIGURE 13.3**

(A) SEM (a–d) and TEM (e–h) images of BGFs with different  $X$  ratio after immersion in SBF for 30 h. Inset: SAED patterns for the corresponding samples. (B) Schematic representation of BSA loading in BSA solution and BSA/SBF mixture solution (Li et al., 2014).

Li et al. (2015) prepared rod-like MBGs with controlled shapes and high specific surface areas using cetyltrimethylammonium bromide (CTAB) as templating agent. The controlling of dynamic process by shaping of the samples (spherical to short rod-like to long rod-like structures) was observed as the CTAB concentration was increased (Li et al., 2015). MBG ( $\text{SiO}_2\text{--CaO--P}_2\text{O}_5$ ) nanospheres (MBGNPs) synthesized by using mixed Pluronic P123 and CTAB under neutral condition showed uniform spherical morphology having diameters around 100 and 3.7 nm sized mesopores. Also, MBGNPs showed excellent HA-like (apatite) formation ability and much faster degradation rate compared with pure silica-nanoparticles. Additionally, MBGNPs exhibited good drug storage/release property for dexamethasone drug (Min et al., 2016). Wei et al. (2011) synthesized

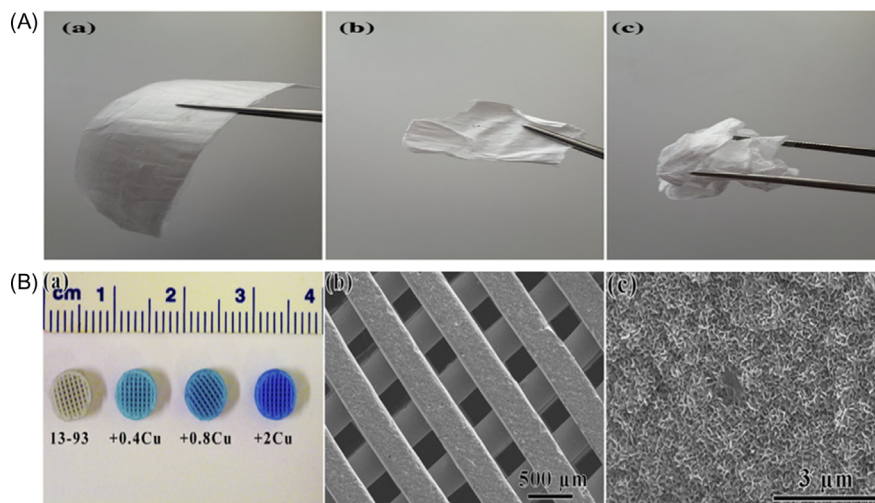
MBG materials with tunable macropores ranging from 0.6 to 200  $\mu\text{m}$  by using a nonionic block-copolymer surfactant and polystyrene (PS) or polyester fibers as mesostructure directing agent and macropore templates, respectively. The use of PS spherical templates produced macro-MBG materials with a uniform macropore size of 600 nm, while the use of polyester fibers produced tubular-MBG materials with tubular channels having diameter ranging between 8 and 200  $\mu\text{m}$  (adjusted by the diameters of polyester fibers). However, both materials have uniform mesopores of 5 nm in diameter (Wei et al., 2011). Oxidative stress has been identified as a vital pathological factor for inducing bone osteoporosis, which is responsible for low bone density and alters bone quality and facilitates bone fractures. For this,  $\text{Sr}^{2+}$  as antioxidant has been used in BGs for inducing osteoblast activity by stimulating bone formation and reducing bone resorption by restraining osteoclasts. Sr-BG improved cells proliferation and showed an antioxidative defense against reactive oxygen species. When tested in vitro, the proliferation of the cells significantly increased by 120% at SaOS-2 and 127% at EAhy926, and when tested in vivo, superoxide dismutase, glutathione peroxidase, and catalase were increased significantly in Sr-BG treated rats compared with other control groups, while a significant decrease was observed in thiobarbituric acid reactive substances (Jebahi et al., 2012). In another study,  $\text{Sr}^{2+}$  was partially substituted as SrO for  $\text{SiO}_2$  in  $\text{Na}_2\text{O}-\text{CaO}-\text{SrO}-\text{P}_2\text{O}_5-\text{SiO}_2$  by taking advantage of  $\text{Sr}^{2+}$ , which reduces bone resorption and stimulates regeneration of bone. The elastic modulus of BG was increased with increasing SrO for  $\text{SiO}_2$  and showed significant improvement in bioactivity and human osteosarcoma U2-OS cell viability and proliferation compared with BG without  $\text{Sr}^{2+}$ . The obtained BG can be more beneficial and potential biomaterials for bone regeneration compared with  $\text{Sr}^{2+}$  substitution for CaO in BG (Arepalli et al., 2016). Further, MBG with excellent osteogenic properties by incorporating ionic cobalt ( $\text{Co}^{2+}$ ), as chemical inducer of hypoxia-inducible factor (HIF)-1 $\alpha$  that induces hypoxia-like response, was developed. The incorporation of low amounts of  $\text{Co}^{2+}$  (<5%) into MBG scaffolds did not show significant cytotoxicity, while it enhanced vascular endothelial growth factor (VEGF) secretion, HIF-1 $\alpha$  expression, and bone-related gene expression of BMSCs significantly by supporting cells' attachment and proliferation in MBG scaffolds. In fact, the sustained release of ampicillin from  $\text{Co}^{2+}$  incorporated MBG scaffolds provides antibacterial properties (Wu et al., 2012). The potential effect of  $\text{Co}^{2+}$  and  $\text{Sr}^{2+}$  on increasing osteogenic activity of  $\text{Co}^{2+}/\text{Sr}^{2+}$  incorporated melt-derived BG was investigated. The results showed good deposition of HA-like (apatite) layer on the BG samples incubated in SBF for 3, 7, and 14 days and promoted in vitro osteogenic activity of human osteosarcoma cells significantly without any cytotoxicity (Kargozar et al., 2016). Further, the combined release of  $\text{Si}^{4+}$  and  $\text{Ca}^{2+}$  by BG improved the osteoblast biomineralization via upregulation of osteocalcin (OCN) expression as osteogenic marker and the release of  $\text{Mg}^{2+}$  delays such improvement. When ionic products of BG (experimental 6P53-b and commercial 45S5) treated with osteoblast cells (MC3T3-E1), gene expressions, including OCN and its upstream transcription

factors, growth factors, and signaling proteins were enhanced in both 6P53-b and 45S5 glass conditioned mediums. The enhanced mineral formation by this upregulation was observed by 45S5 glass conditioned mediums after 20 days and by 45S5/6P53-b ( $\text{Si}^{4+} + \text{Ca}^{2+} + \text{Mg}^{2+}$ ) conditioned mediums after 30 days. When treated with cells, 45S5 conditioned mediums showed slightly elevated levels of mineral content within ECM compared with 6P53-b conditioned mediums after 30 days, whereas control test showed no mineral content. It was observed that ions released from both 45S5 and 6P53-b BG upregulated OCN expression and biomineralization whereas  $\text{Mg}^{2+}$  released from 6P53-b downregulated OCN expression and delayed osteoblast biomineralization (Tousi et al., 2013). A radiopaque MBG (as MBGZ-7) was prepared by incorporating zirconium propoxide as precursor. The results showed good radiopaque level in MBGZ-7 and showed good deposition of HA-like crystals on its surface after 7 days of SBF incubation. It is expected to be used as a promising dispersed phase in composite materials for minimally invasive surgery procedures (i.e., injectable bone cements) (Tallia et al., 2014). Wu et al. (2013) prepared multifunctional copper (Cu)-containing MBGs (Cu-MBG) scaffolds with interconnective large pores (several 100  $\mu\text{m}$ ) as well as well-ordered mesopore channels ( $\sim 5$  nm) for combining angiogenesis capacity, osteostimulation, and antibacterial properties for regenerating damaged or lost bone tissues. Both Cu-MBG scaffolds and their ionic extracts could stimulate HIF-1 $\alpha$  and VEGF expression, and promoted significantly osteogenic differentiation of hBMSs by improving their gene expression [ALP, osteopontin, and OCN] for BMSCs. In addition, sustained release of ibuprofen was observed in Cu-MBG scaffolds and inhibited the bacterial viability significantly (Wu et al., 2013). In another study, titanium (Ti) reinforced phosphate-based glass showed desired cytocompatible surface, by supporting initial cell attachment, sustained cell viability, and increased cell proliferation similar to or significantly higher than Thermanox. Moreover, the obtained Ti-incorporated glasses regulated osteoblastic cell differentiation (osteoblast phenotype gene transcription and upregulated ALP and OCN expression) and the use of osteogenic media did not show any significant effect on ALP activity and OCN expression (Neel et al., 2014). Goel et al. (2012) designed a series of alkali-free BGs and developed the glass system  $\text{CaO}-\text{MgO}-\text{SiO}_2-\text{P}_2\text{O}_5-\text{CaF}_2$  along the diopside ( $\text{CaMgSi}_2\text{O}_6$ )-fluorapatite ( $\text{Ca}_5(\text{PO}_4)_3\text{F}$ )-tricalcium phosphate ( $3\text{CaOP}_2\text{O}_5$ ). Some of the glasses showed formation of HA on their surface within 1–12 hours of SBF incubation. The sintered but amorphous glass powder compacts showed good biological properties in terms of adherence and proliferation of tissue cells and the glass compositions enhanced the osteogenic differentiation of mesenchymal stem cells (MSCs) as assessed by the ALP activity (Goel et al., 2012). Five BG compositions in the  $\text{SiO}_2-\text{P}_2\text{O}_5-\text{CaO}-\text{Na}_2\text{O}-\text{CaF}_2$  system with varying amount of  $\text{CaF}_2$  from 0 to 32 mol% and 45S5 Bioglass were also evaluated for their apatite forming ability in serum-free and serum-containing cell culture media up to 7 days. In this study, low concentration of  $\text{F}^-$  ions showed enhanced formation of apatite, while higher  $\text{F}^-$  ions concentration facilitated formation of fluorite and calcite.

The presence of serum proteins delayed apatite precipitation for all compositions and 45S5 Bioglass only formed amorphous calcium phosphates while it has considerably higher phosphate content and higher  $\text{Ca}^{2+}$  and  $\text{PO}_4^{3-}$  ions in solutions (Shah et al., 2015). Leonardi et al. (2010) synthesized a novel bioresorbable  $\text{P}_2\text{O}_5\text{--SiO}_2\text{--CaO--MgO--Na}_2\text{O--K}_2\text{O}$  glass ceramic phosphate-based material (GC-ICEL). The solubility of GC-ICEL in different aqueous media (water, Tris-HCl, and acellular SBF) was investigated and results showed a continuous preferential dissolution of the  $\text{Na}_2\text{Mg}(\text{PO}_4)_3$  phase and residual amorphous phase in all the chosen media. The immersion of GC-ICEL in SBF showed the precipitation of a continuous layer of HA (apatite). For biocompatibility test of GC-ICEL, the stimulation of human bone marrow-derived stromal cells (hMSCs) differentiation over proliferation was observed. In addition, higher expression of bone-related genes in cells cultured on GC-ICEL compared with cells on TCPS confirms the bioactivity of this glass ceramic that might have a stimulatory effect on osteogenesis (Leonardi et al., 2010). Yazdanpanah et al. (2012) prepared nanocrystalline forsterite (NF) incorporated BG and the incorporation of NF showed improvement in the toughness of the BG matrix without deteriorating its intrinsic properties such as biomineralization behavior (Yazdanpanah et al., 2012) and further, NF (20–50 nm) reinforced 58S BG nanocomposite powders were synthesized in situ for the treatment of oral bone defect and showed high in vitro biocompatibility (cell viability) compared with control groups and good in vitro bioactivity when incubated in SBF (Saqaei et al., 2015). MBG nanofibers (MBGNFs) prepared by using sol-gel/electrospinning technique showed highly ordered one-dimensional channels in a hexagonally packed mesostructure and better drug-loading efficiency with reduction in burst release of gentamicin sulfate for prolonged release over 10 days. In addition, the bone-like apatite minerals formation was observed on the surface of MBGNFs and it provided a suitable environment for cellular attachment and proliferation, differentiation, and mineralization of MG-63 osteoblast-like cells. As bone graft using a rat calvarial defect model, the results showed good biodegradability and improved bone regeneration (Hsu et al., 2015). In another study, silicate-based 13-93 BGFs by involving poly (vinyl alcohol) (PVA) were prepared using sol-gel/electrospinning technique. After calcination at  $625^\circ\text{C}$ , the amorphous glass fibers with  $464 \pm 95$  nm (average diameter) were prepared successfully (as shown in Fig. 13.4A) and the deposition of Ca/P (HA-like materials) in SBF incubation showed a strong dependency on the concentration of the fibers (after 7 days at 0.5 mg/mL and after 30 days at 1 mg/mL). The results also showed good osteoblast cells response to the BGFs (Deliormanli, 2015).

Electrospun submicron-bioactive glass tubes prepared by sol-gel/coaxial electrospinning techniques showed a faster induction of HA-like mineral formation on both the outer and inner surfaces in SBF compared with solid fibers, where it was only on their surfaces. However, the proliferation rate of mouse preosteoblastic MC3T3-E1 cells on BG tubes and solid fibers was comparable. In addition, these structures showed delayed release behavior when loaded with a model protein drug, BSA, and



**FIGURE 13.4**

(A) Digital images of the 13-93 BG nonwoven mats before (a) and after calcination at 650°C (b and c) (Delormani, 2015). (B) (a) Digital image of as-fabricated four scaffolds prepared by robocasting and composed of 13-93 BG doped with 0, 0.4, 0.8, and 2.0 wt% CuO; (b) SEM image of a 13-93 BG scaffold doped with 0.8 wt% CuO; (c) SEM image of the surface of a glass filament (0.8 wt% CuO) after immersion of scaffold in SBF at 37°C for 7 days (Lin et al., 2016a).

the bioactivity of released lysozyme from tubes can be as high as 90.09% (Xie et al., 2012). In another study, the mechanical behavior was compared between BG granules incorporated graft layers and morselized cancellous bone allograft in various volume mixtures under clinically relevant conditions, because of osteoconductive and unique antibacterial properties. The graft layers were tested mechanically and results showed that true strains decreased absolutely, while aggregate modulus increased with increased BG content from 116 to 653 MPa. In addition, porosity decreased from 66% (allograft) to 15% (BG). BG granules are less porous and difficult to handle, while allograft subsides and creeps. A BG:allograft (1:1) volume mixture shows promise as the best graft biomaterial in load-bearing defects (Hulsen et al., 2016). Rodriguez et al. (2016) prepared Ti-containing glass series (one silica-based and one borate-based).  $\text{Ti}^{4+}$  was added at the expense of silicon dioxide ( $\text{SiO}_2$ ) for the silica-based series whereas at the expense of boron oxide ( $\text{B}_2\text{O}_3$ ) for the borate-based series. Amorphous structures were obtained for silica-based glass at 15 mol%  $\text{TiO}_2$  and borate-based glasses at 0 and 5 mol%. The obtained glass series degrade in situ and release ions at the implantation site. As per thermal analysis, borate-based glasses showed more suitability for coating metallic implants compared with their silica-based counterparts (Rodriguez et al., 2016). Strong porous 13-93 BG scaffolds with an oriented microstructure of columnar pores showed mostly

osteoconductive bone regeneration and normalized, increased from 37% (at 12 weeks) to 55% (at 24 weeks), whereas control sample showed bone regeneration from 25% (at 12 weeks) to 46% (at 24 weeks) when evaluated *in vivo* using a rat calvarial defect model. In addition, brittle mechanical property of the obtained scaffolds changed significantly to an elasto-plastic property *in vivo* at both time of implantations (Liu et al., 2013). In other study, for load-bearing bone regeneration, 3D silicate (13-93) and borate (13-93B3) BG scaffolds prepared by robotic deposition of organic solvent-based suspensions (inks) exhibited grid-like microstructure having 50% porosity and  $420 \pm 30$  nm pore width. Further, 13-93BG scaffolds showed a compressive strength of  $142 \pm 20$  MPa (comparable to the strength of human cortical bone) while 13-93B3 BG scaffolds showed a compressive strength of  $65 \pm 11$  MPa, which is far higher than that of trabecular. In addition, borate 13-93B3 BG scaffolds produced HA-like material faster than the silicate 13-93 BG scaffolds and showed a sharp decrease in strength with the incubation time in SBF (Deliormanli and Rahaman, 2012).

In another study, scaffolds composed of a physical mixture of silicate 13-93 and borate 13-93B3 BGFs were prepared by thermally bonding short glass fibers. The silicate 13-93 glass only scaffolds showed a better cell proliferation capacity and ALP of osteogenic MLOA5 cells compared with scaffolds having borate 13-93B3 glass fibers. The amount of new bone formation in the scaffolds having 13-93 glass fibers was significantly higher compared with scaffolds having 13-93B3 glass fibers after 12 weeks. The HA-like material was partially formed in case of 13-93 glass fibers and fully formed HA-like material with tubular morphology (Gu et al., 2013). Bellucci et al. (2014) developed four-oxide BGs with special compositions (derived from 45S5 Bioglass) that are characterized by a high amount of CaO (45.6 mol%) and by a partial or complete substitution of sodium oxide ( $\text{Na}_2\text{O}$ ) and/or potassium oxide ( $\text{K}_2\text{O}$ ) with 4.6 mol% in total. In particular, the glass composition with the highest potassium content did not show any sensible crystallization behavior. In addition, the samples showed excellent properties such as apatite forming ability and pH variation induced in the solution. Further, all samples and their ionic extracts did not show negative effects in the murine fibroblast (BALB/3T3) cell viability (Bellucci et al., 2014). In another study, two different amounts of manganese oxide ( $\text{MnO}$ ) were introduced into a glass system ( $\text{SiO}_2\text{--P}_2\text{O}_5\text{--CaO--MgO--Na}_2\text{O--K}_2\text{O}$ ) by using melt and quenching technique. Slightly delayed reactivity kinetics of Mn-doped glasses was observed compared with glass used as control, while maintaining a good degree of bioactivity and fluctuating trends during bioactivity process probably due to a reprecipitation of Mn compounds. In addition, Mn-doped glasses [ $\leq 50 \mu\text{g}/\text{cm}^2$  ( $\mu\text{g}$  of glass powder/ $\text{cm}^2$  of cell monolayer)] did not show cytotoxic effects on human MG-63 osteoblast cells cultured up to 5 days and showed good cell proliferation and spreading on Mn-doped glasses and mostly can promote the ALP expression and some BMPs (Miola et al., 2014). A borosilicate BG (BBG; designed 13-93B1) scaffolds having composition  $6\text{Na}_2\text{O--8K}_2\text{O--8MgO--22CaO--18B}_2\text{O}_3\text{--36SiO}_2\text{--2P}_2\text{O}_5$  (mol%) prepared by a foam-replication method showed a partial conversion of the glass to a porous HA-like material composed of

fine needle-like particles for 30 days of SBF incubation. Eight weeks postimplantation in noncritical sized defects (femoral head of rabbits), scaffolds were converted partially to HA-like material and integrated well with newly formed bone. Further, when loaded with platelet-rich plasma, regeneration of bone was supported by the scaffolds in segmental defects in the diaphysis of rabbit radii (Gu et al., 2014). Ojansivu et al. (2015) investigated that the ionic extracts from three experimental glasses (1-06, 2-06, and 3-06) and from a commercial glass (S53P4) alone are sufficient to induce osteogenic differentiation of human adipose stem cells or not. The results showed good cell viability in all the glass ionic extracts throughout the culturing period (14 days). The mineralization was excessive in osteogenic medium ionic extracts while there was a decrease in cell amount compared with the control. In addition, OCN production and Col Type-I accumulation in ECM increased consistently at 13 days of culture period. Out of four medium extracts, 2-06 and 3-06–based medium extracts induced the best osteogenic response. Moreover, ALP activity was not promoted by the medium extracts, regardless of the improved mineral formation (Ojansivu et al., 2015). The combination of mesoporous silica-based nanoparticles (MSNs) and bioactive factors could be a promising hybrid bone substitution. For this, bone-forming peptide (BFP), which is derived from BMP-7, was incorporated into the MSNs for a slow-release system for the delivery of osteogenic factor. In this case, small osteogenic peptide was encapsulated successfully in the mesopores and had no influence on mesoporous structure of MSNs. In addition, peptide-laden MSNs showed higher MG-63 cell proliferation, spreading, and ALP activity compared with MSNs without peptide encapsulation, indicating good *in vitro* cytocompatibility. In parallel, improved osteodifferentiation of hMSCs under the stimulation of peptide-laden MSNs was observed and confirmed that BFP released from MSNs could remarkably promote osteogenic differentiation of hMSCs, especially at 500 g/mL of peptide-laden MSNs (Luo et al., 2015). Previously, bioactive silicate glass (13-93) scaffolds having uniform grid-like microstructure were prepared and showed a compressive strength comparable to human cortical bone but having much lower flexural strength, but 13-93 scaffolds having a porosity gradient (a less porous outer region and a more porous inner region) showed a higher compressive strength ( $88 \pm 20$  MPa) and higher flexural strength ( $34 \pm 5$  MPa) compared with the value for uniform grid-like microstructure (compressive strength:  $72 \pm 10$  MPa and flexural strength:  $15 \pm 5$  MPa), respectively. Upon implantation for 12 weeks in rat calvarial defects, new bone infiltration through pore space of scaffolds with porosity gradient was similar to that for the uniform grid-like scaffolds and showed better mimicking to the microstructure of human long bone (Xiao et al., 2016). For improved tissue healing, inorganic ions release from a designed system could be an alternative strategy for using growth factors. Thus, the bioactive silicate (13-93) glass scaffolds doped with varying concentration of  $\text{Cu}^{2+}$  ions (0–2.0 wt% CuO) were fabricated in a grid-like microstructure by robotic deposition (as shown in Fig. 13.4B). Cu-doped scaffolds showed dose-dependent release of  $\text{Cu}^{2+}$  ions into SBF medium (*in vitro*) and partially converted to HA-like material. Further, the proliferation and ALP activity of osteoblastic

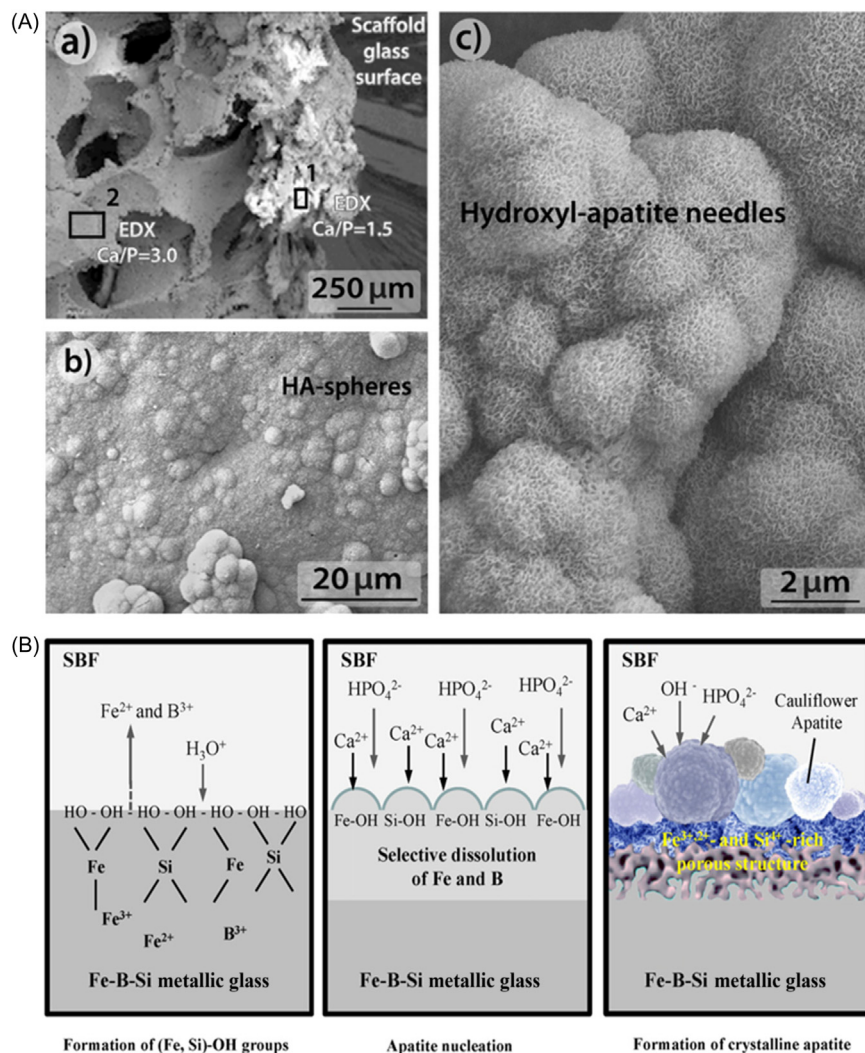


MC3T3-E1 cells cultured on the Cu-doped scaffolds were not affected by 0.4 and 0.8 wt% of CuO, but reduced significantly by 2.0 wt% of CuO. Similar behavior was observed for Cu-doped scaffolds when implanted for 6 weeks in rat calvarial defects. Also, the area of new blood vessels within the fibrous tissue (infiltrated scaffold) was increased with CuO content and was higher significantly higher in case of 2.0 wt% of CuO in the scaffolds. Additionally, the loading of BMP-2 (1  $\mu\text{g}/\text{defect}$ ) into scaffolds improved bone infiltration significantly, but reduced fibrous tissue formation in the scaffolds (Lin et al., 2016a).

Bioactive oxynitride glasses ( $\text{SiO}_2\text{—CaO—Na}_2\text{O—Si}_3\text{N}_4$  system) prepared by the introduction of nitrogen (N) into silicate network showed that N is substituted for oxygen and formation of  $[\text{SiO}_3\text{N}]$  tetrahedral and Q4 units having extra bridging of anions at the expense of Q3 units. The increase in N content increased glass transition temperature, hardness, fracture resistance, and Young's modulus due to extra crosslinking of the glass network. In these glasses, the substitution of  $\text{CaF}_2$  for CaO resulted in a decrease in glass transition temperature. Thus, these glass systems can be melted at lower temperatures, whereas fluorine facilitates higher solubility of N and no effect on the significant increase in the mechanical performance induced by N substitution. In addition, the level of bioactivity of these glass systems can be manipulated by varying N content (Bachar et al., 2016). Orgaz et al. (2016) developed melt-derived hierarchically interconnected porous scaffolds by using ICIE16 glass (as prepared by Wu et al., 2011) and BSG of composition 73.48  $\text{SiO}_2\text{—}11.35 \text{ B}_2\text{O}_3\text{—}15.11 \text{ Na}_2\text{O}$  (wt%) via the combination of gel-casting and foam-replication method. Further, the obtained ICIE16/BSG composite scaffolds were functionalized by a nitridation process with hot gas  $\text{N}_2/\text{ammonia}$  for 2 hours at  $550^\circ\text{C}$  for improving its interaction with biological systems. The results showed good mechanically stable composite scaffolds. Additionally, there was improved HA-like (apatite) forming ability (as shown in Fig. 13.5A) and cell proliferation and differentiation in vitro on nitrided scaffolds (ICIE16/BSG-NITRI) compared with nonnitrided scaffolds (Orgaz et al., 2016).

Recently, Qin et al. (2016) developed  $\text{Fe—B—Si}$  ( $\text{Fe}_{0.75}\text{B}_{0.15}\text{Si}_{0.1}$ ) $_{100-x}\text{Nb}_x$  ( $x = 0, 1, \text{ and } 3$  atomic%) metallic glasses without using allergic/toxic elements that showed excellent formation of bone-like (apatite) material in SBF. Additionally, in in vitro SBF incubation of samples not only apatite formation occurs but also facilitates progressive formation of the underlying alloy material. Moreover, the alloy material just beneath the apatite layer consisting of a hierarchical macro-/nano-porous structure *via* selective dissolution of the active F and B components on the surface and fast formation of  $\text{Fe—OH}$  or  $\text{Nb—OH}$  and  $\text{Si—OH}$  groups, and successively combine with  $\text{Ca}^{2+}$  and  $(\text{PO}_4)^{3-}$  ions when immersed in SBF for 3 or 9 days (the mechanism is shown in Fig. 13.5B) (Qin et al., 2016).

For in vivo long-term duration bone regeneration, three types of implant scaffolds, that is, untreated, phosphate solution treated, and BMP-2-loaded silicate 13-93 glass scaffolds, were used in rat calvarial defects for 6, 12, and 24 weeks postimplantation. Compared with untreated 13-93 glass scaffolds, treated scaffolds improved regeneration of bone for 6 weeks, but not for 12 or 24 weeks. BMP-2-loaded

**FIGURE 13.5**

(A) SEM images of the ICIE16/BSG-NITRI scaffold after SBF immersion for 7 days: (a) A partially broken scaffold showing an external- and inner-porous surface along with Ca/P ratio by using EDX analysis, (b) Panoramic view of surface of scaffold indicating typical HA-spheres, and (c) shows how they are formed-up needle-like crystals of HA at higher magnification ([Orgaz et al., 2016](#)). (B) Schematic illustration of the process of the apatite formation on the surface of Fe–B–Si in SBF ([Qin et al., 2016](#)).

scaffolds exhibited significantly better regeneration of bone for all three implantation time periods, and had almost infiltrated the lamellar bone completely within 12 weeks, while apatite (bone-like) forming ability was not significantly different at 24 weeks (30%–33%) for the three types of scaffolds. The area and number of blood vessels in new bone, infiltrated in BMP-2-loaded scaffolds at postimplantation of 6 and 12 weeks, were remarkably higher than those for untreated and treated scaffolds, but there was no difference for 24 weeks postimplantation (Lin et al., 2016b).

### 13.6.2 NATURAL POLYMER/BIOACTIVE GLASSES—BASED COMPOSITE SCAFFOLDS

Col-based hydrogels show poor physicochemical and mechanical stability that further limit their potential use in hard tissue engineering applications because of the substantial shrinkage during cell culture. Therefore, the incorporation of MBGNPs can improve the mechanical stability, ionic releasing for bone cells, and apatite forming ability. In addition, amine-functionalized MBGNPs may enable the physicochemical stability of the Col-hydrogels. For this, El-Fiqi et al. (2013) prepared aminated-MBGNPs reinforced Col-hydrogels (Col-MBGNPs) and the effect of MBGNPs content as well as its aminated surface on the properties of nanocomposite hydrogels was observed.

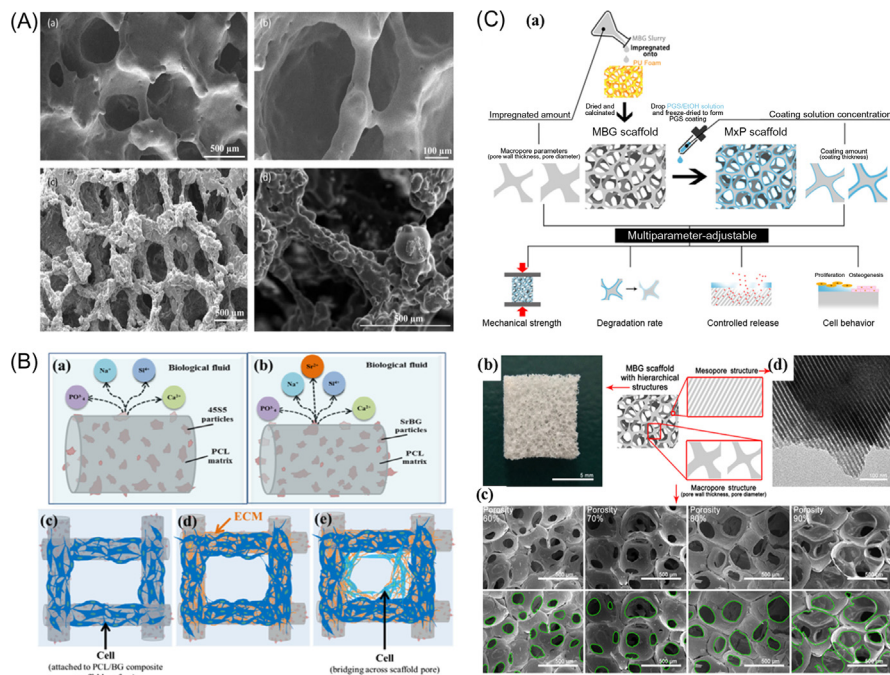
In this case, the hydrolytic/enzymatic degradation of the hydrogels was found to decrease, while mechanical properties of the hydrogels were improved significantly due to the incorporation of MBGNPs and its aminated surface. In addition, the prevention of hydrogel shrinkage was observed when cultured with MSCs (El-Fiqi et al., 2013). For the promotion of sufficient vascularization of tissue-engineered bioconstructs, one approach was used to focus on the cellular HIF-1 $\alpha$  course of action that respond hypoxia (low-oxygen concentration) and resulted in the activation of different pro-angiogenic genes as well as VEGF. Co<sup>2+</sup> ions are well known for artificial stabilization of HIF-1 $\alpha$  transcription factor to mimic hypoxia. Thus, Quinlan et al. (2015) prepared Co<sup>2+</sup> ions (110  $\mu$ m)-incorporated BG/Col glycosaminoglycan (BG/CGAG) scaffolds with BG particles of 38 and 100  $\mu$ m. The incorporation of BG particles improved the compressive modulus of the scaffolds, by maintaining their high porosity (>97%). In addition, the incorporation of Co<sup>2+</sup> into BG/CGAG scaffolds improved the production and expression of VEGF in endothelial cells. Moreover, all BG/CGAG scaffolds irrespective of the particle size showed the ability of good osteoblast cell proliferation and osteogenesis (Quinlan et al., 2015). Peter et al. (2010a) prepared chitosan (Chit)-based scaffolds reinforced with BG ceramic nanoparticles (nBGC: 100 nm). The results showed homogeneous distribution of nBGC within Chit matrix with interconnected macroporous microstructure (pore size: 150–300  $\mu$ m), adequate swelling and degradation behavior, and apatite forming ability of the obtained scaffolds. In addition, no toxicity was observed while attaching and proliferating cells on the scaffolds (Peter et al., 2010a). Further, Chit-based scaffolds

reinforced with varying amount of BGNPs ( $64\text{SiO}_2\cdot 28\text{CaO}\cdot 8\text{P}_2\text{O}_5$ ; 20 nm size) prepared by freeze-casting/freeze-drying method showed unidirectional microstructure of scaffolds with homogenous distribution of BGNPs among Chit matrix, indicating proper interfacial bonding between Chit and BGNPs. The values of compressive strength and modulus were increased from 0.034 to 0.419 MPa and 0.41 to 10.77 MPa, respectively, with the increased amount of BGNPs (from 0 to 50 wt%). The increase of BGNPs content increased the weight loss amount (in vitro degradation) and apatite forming ability was observed in all compositions, especially best for 30 wt% BGNPs (Pourhaghgouy et al., 2016). Cui et al. (2016) prepared injectable cement made of Chit solution and borate-BG particles and investigated bioactivity and setting mechanism with varying solid-to-liquid (SL) ratios. With increased SL ratio (from 1.0 to 2.5 g/mL), the injectability and initial setting-time (via sol–gel transition) were decreased from  $97\% \pm 1\%$  to  $84\% \pm 10\%$  and  $16.9 \pm 0.9$  to  $3.0 \pm 0.5$  minutes, respectively, whereas compressive strength increased from  $8 \pm 2$  to  $31 \pm 2$  MPa. In addition, the obtained cement maintained its cohesiveness in a vigorously stirred aqueous system and showed good deposition of HA-like material when incubated in SBF (Cui et al., 2016). In another study, Mozafari et al. (2010) prepared BGNPs incorporated cross-linked gelatin (Gel) macroporous scaffolds by using solvent-casting followed by freeze-drying/lamination method. The results showed evenly distributed BGNPs within cross-linked gel matrices with 3D interconnected microstructures (pore size: 200–500  $\mu\text{m}$  and porosity: 72%–86%) and Young's modulus similar to the natural spongy bone. In addition, in vitro cytotoxicity test showed good osteoblastic SaOD-2 cell attachment, migration, and penetration to the pores of the nanocomposite scaffolds (Mozafari et al., 2010). Further, a sponge-like composite scaffold of BG (70S30C: 70%  $\text{SiO}_2$ , 30%  $\text{CaO}$ ) and porcine gel was prepared and the results showed highly porous and interconnected structure of the obtained scaffolds. The rate and onset of HA-like (apatite) nucleation was observed comparable to that of BG. Modification of dehydrothermal process parameters induced varying degrees of crosslinking, suitable degradation behavior for specific application. Further, the use of genipin to support crosslinking by dehydrothermal process provided means of modifying degradability. Composite scaffolds showed good in vitro cytocompatibility with human dental pulp stem cells (HDPSCs) by confirming osteogenic differentiation of HDPSCs as well as ECM deposition via positive ALP staining and immunohistochemistry (Nadeem et al., 2013). Further, BGNPs reinforced Chit-Col injectable nanohybrid hydrogels showed thermosensitive response for gelation at approximately  $37^\circ\text{C}$  (body temperature). The incorporation of Col and BGNPs increased mechanical performance (after gelation), where the incorporation of 2 wt% BGNPs increased 39% of matrix stiffness compared with pure Chit hydrogels and further increased 95% of matrix stiffness by incorporating Col in the hydrogel system. In cytotoxicity and cell viability tests, no toxic effect on human osteosarcoma cells and kidney human embryo cell line (HEK 293T) was observed by the prepared hydrogels. Moreover, all hydrogel samples showed proper viscous behavior, allowing

gelation relatively in a short-time period (approximately 4 minutes) when injected by a syringe needle for demonstration (Moreira et al., 2016). Sharifi et al. (2016) prepared three types of composite scaffolds as Gel/Col hydrogel, Gel/Col/45S5 BGFs (150–450 nm) composite and Cu-doped composite scaffolds cross-linked with genipin as cross-linker by freeze-drying and electrospinning methods. The obtained scaffolds were highly porous having approximately 70–200  $\mu\text{m}$  pore diameters. In addition, cytocompatibility test revealed that  $\text{Cu}^{2+}$  containing composite scaffolds had better osteoblastic (SaOS-2) cell attachment and growth compared with other Cu-free composite scaffolds (Sharifi et al., 2016). By taking advantages of Chit and gel, scaffolds composed of Chit, gel, and nBGC showed macroporous structure of the scaffolds with pore size ranging from 150 to 300  $\mu\text{m}$  and the incorporation of nBGC decreased the swelling and degradation behavior of the scaffolds, whereas protein absorption increased. Also, higher amount of HA-like material deposited on scaffolds and increased with the time of incubation in SBF. The obtained composite scaffolds showed better cell attachment and spreading compared with Chit/gel scaffolds (Peter et al., 2010b). In another study, new boron-containing BG-based scaffolds coated with alginate (Alg) cross-linked by  $\text{Cu}^{2+}$  ions were synthesized. In this case, porous scaffolds were prepared by foam-replica method using the developed BG (65 $\text{SiO}_2$ :18.4 $\text{Na}_2\text{O}$ :0.1 $\text{MgO}$ :1.5 $\text{B}_2\text{O}_3$  as wt%) and coated with Alg by dipping method. The results showed that Alg was attached effectively on the surface of fabricated scaffolds with a homogeneous coating and retained amorphous structure after sintering process (as shown in Fig. 13.6A). The Alg coating improved the bioactivity and mechanical properties of the scaffolds as well as controlled release  $\text{Cu}^{2+}$  ions (Erol et al., 2012).

Gellan gum spongy-like hydrogels with 50 wt% BG showed a Young's modulus of 1.9 MPa in the dry state and 1.2 MPa in the wet state (hydrogel). However, these values are still below the required value for load-bearing applications and lower than the value obtained and reported for sintered BG having moderate porosity and BG having hydrophobic biopolymers. The obtained hydrogels showed the ability of apatite formation in SBF and good cell response (cell attachment and spreading) and cell viability when cultured with human adipose derived stem cells (Gantar et al., 2014). In another study, silk fibroin scaffolds reinforced with spray-dried MBG particles [SD-MBG:  $\text{SiO}_2$ –CaO (80/20 mol%)] showed highly interconnected porous structure and improved mechanical performance (compressive strength:  $0.9 \pm 0.2$  MPa and elastic modulus:  $6.9 \pm 1.0$  MPa) compared with pure silk-based scaffolds (compressive strength:  $0.5 \pm 0.05$  MPa and elastic modulus:  $1.1 \pm 0.2$  MPa). In addition, good apatite forming ability and good cytocompatibility and a good ALP activity towards human mesenchymal stromal cells was observed (Chandrasekaran et al., 2016). In another study, Kumar et al. (2017c) prepared xanthan gum (XG)/BG hybrid scaffolds reinforced with cellulose nanocrystals (CNCs). In this case, XG is an exo-polysaccharide and shows water-solubility and excellent biocompatibility. An aqueous solution of XG shows only weak “gel-like” behavior in the presence of suitable amount of



**FIGURE 13.6**

(A) SEM images showing pore (a) and strut microstructures (b) of the scaffold at 650°C for 4 h and Alg-coated scaffold (sample 10S) at low (c) and high (d) magnification (Erol et al., 2012). (B) Schematic representation of the dissolution of 45S5 BG (a) or Sr-BG particles (b) embedded within a PCL matrix when exposed to biological fluid and progress of cell growth on a composite having BG particles (c–e), indicating early phase of cell culture (c), cell proliferation, and secreting of ECM (d), and bridging of cell sheets (cells and ECM) across the pores of the scaffold (Poh et al., 2016). (C) (a) Schematic representation of designing and fabrication of MxP scaffold. MxP scaffolds were prepared by dropping PGS solution followed by freeze-drying and MBG scaffold was prepared by a modified cotemplating process (F127/PU), (b) digital image of the MBG scaffold, (c) SEM images of MBG scaffold having porosities ranging 60%–90%, and (d) TEM image of MBG scaffold showing mesoporous structure (Lin et al., 2015).

inorganic salt due to its double-helix conformation as microgel (Kumar et al., 2018; Geremia and Rinaudo, 2005; Le and Turgeon, 2013; Rao et al., 2016). The mechanical stability of this weak gel-like behavior was improved by the incorporation of silica-based BG followed by CNCs. The results showed highly porous structure of the hybrid scaffold-network with tunable and improved mechanical properties and good in vitro cytocompatibility with MC3T3-E1 preosteoblast cells (Kumar et al., 2017c).

### 13.6.3 SYNTHETIC POLYMER/BIOACTIVE GLASSES—BASED COMPOSITE SCAFFOLDS

Fernandes et al. (2016) prepared 10 wt%  $\text{Sr}^{2+}$ /BBG reinforced PLA membrane scaffolds by using electrospinning technique. Membrane scaffolds with smooth and uniform nanofibers were observed, while in vitro degradability and water uptake capacity were improved with a continuous release of cations. In addition, the results showed enhanced mechanical properties and promoted in vitro differentiation of BM-MSCs after incorporation of Sr-BBG glass particles (Fernandes et al., 2016).

In poly(L-lactide) (PLA)/BGNPs (100 nm) nanocomposite scaffolds, the increase in glass content decreased water absorption, while weight loss (in PBS) and cumulative ion concentrations released from composite scaffolds increased. Additionally, in vitro apatite forming ability in SBF was found to increase with the increase of BGNPs (El-Kady et al., 2010). Macro/mesoporous BG/PLA nanofibers (uniform size: 350 nm) prepared using nonionic copolymer poly(ethylene glycol)-block-poly(propylene glycol)-block-poly(polyethylene glycol) (P123) as template for mesoporous structure (5 nm) and macroporous structure (10  $\mu\text{m}$ ) structure derived from the overlapping of the nanofibers showed controlled release of drug and fats apatite forming ability (Han et al., 2014). Dziadek et al. (2015) prepared BG microparticles (12 and 21 vol%) reinforced polycaprolactone (PCL) composite films. In this case, two gel-derived  $\text{SiO}_2$ –CaO– $\text{P}_2\text{O}_5$  glass systems differing in  $\text{SiO}_2$  and CaO contents were used as S2: 80 $\text{SiO}_2$ –16CaO–4 $\text{P}_2\text{O}_5$  and A2: 40 $\text{SiO}_2$ –54CaO–6 $\text{P}_2\text{O}_5$ . Surfaces of PCL/BG film were denoted as GS and AS based on the exposure to Petri dish and gas phase, respectively. The incorporation of BG into PCL matrix improved the hydrophilicity of GS surfaces and hydrophobicity of the AS surfaces. In addition, significant improvement in Young's modulus [from 0.38 GPa (pure PCL) to 0.90 GPa (12A2-PCL) and 1.31 GPa (21A2-PCL)] was observed depending on higher amount of BG microparticles (Dziadek et al., 2015). Poh et al. (2016) prepared 50 wt% 45S5 Bioglass or  $\text{Sr}^{2+}$ -substituted BG particles (Sr-BG) reinforced PCL-based composite scaffolds by using additive manufacturing technique and compared the properties with separately prepared PCL (control) and PCL/CaP-coated scaffolds. The incorporation of 50 wt% BG particles decreased the compressive Young's modulus of the scaffold, while Ca/P-coated scaffold had a negligible effect on the porosity and compressive Young's modulus of the scaffold. Also, composite scaffolds showed good in vitro apatite forming ability on their surface. In addition, all composite scaffolds showed good BMSCs attachment and proliferation. However, in nonosteogenic media, only PCL/CaP-coated, PCL/5045S5 and PCL/50Sr-BG scaffolds showed an upregulation of osteogenic gene expression (as shown in Fig. 13.6B). In addition, the rate of cell attachment, proliferation, and osteogenic gene expression was improved for all types of scaffolds under a dynamic culture environment. When implanted subcutaneously into nude rats, host tissue infiltrated well into the composite scaffolds, but no mature bone formation was found in any type of scaffold group (Poh et al., 2016).

The incorporation of BGNPs particles improved absorption and degradation behavior, and mechanical performance of the PCL-based scaffolds. In addition, PCL/BGNPs (30 wt%) scaffold showed significantly improved in vitro apatite forming ability and cellular response compared with pure PCL scaffold (Lei et al., 2013). Further, PCL and zein-coated 45S5 BG scaffolds showed the significant improvement in the compressive strength of the scaffolds. Both uncoated and PCL/zein-coated 45S5 BG scaffolds showed good bone-like (apatite) deposition on the surface after 14 days of SBF immersion as well as improved biological activity of the BG scaffolds. In addition, the incorporation of zein accelerated the degradation rate of the coating in the investigated time period. The PCL/zein-coated 45S5 BG scaffolds revealed a potential controlled drug-release system with tetracycline hydrochloride for in situ drug-release in bone tissue engineering applications (Fereshteh et al., 2015a,b). In this study,  $\text{Sr}^{2+}$  or  $\text{Cu}^{2+}$  doped BG particles were incorporated into Gel/PCL nanofibrous scaffolds by using electro-spinning technique. The results showed improved in vitro bioactivity and the release of therapeutic ions was observed to have the range of 5.4–10.1 and 0.34–1.87 mg/g of the scaffolds for  $\text{Sr}^{2+}$  and  $\text{Cu}^{2+}$  ions, respectively. However, the concentration of  $\text{Sr}^{2+}$  and  $\text{Cu}^{2+}$  ions in the BG further can be increased for improving osteogenic, angiogenic and antibacterial potential of the nanofibrous scaffolds (Gonen et al., 2016). Killion et al. (2013) prepared poly(ethylene glycol dimethyl acrylate) (PEGDMA) scaffolds reinforced with BG particles (from 0 to 20 wt%) and showed improved biomechanical properties and in vitro apatite forming ability of the composite scaffolds compared with pure PEGDMA scaffolds (Killion et al., 2013). Haaparanta et al. (2015) prepared highly porous poly(lactic-co-glycolic acid) (PLGA)/BG composite scaffolds by combining 3D fibrous BG mess skeleton (porous) with highly porous PLGA. The results showed the highly porous and superior pore structure with dimensional stability during hydrolysis compared with pure PLGA scaffolds (Haaparanta et al., 2015). Lin et al. (2015) prepared a series of multiparameter-adjustable MBG scaffolds coated with uncross-linked poly(glycerol sebacate) (PGS) by a simple adsorption and lyophilization process. The coating of PGS onto MBG scaffolds successfully improved the toughness and adjustable mechanical strength covering the range of trabecular bone (2–12 MPa). The mechanical performance, degradation rate, controlled release behavior, and cell response of the composite scaffolds could be manipulated in a broad range by controlling the ratio of the sponge volume and impregnated slurry amount, and concentration of PGS solution (as shown in Fig. 13.6C(a)). The digital and SEM images as well as TEM image of mesoporous structure of MBG scaffold is shown in Fig. 13.6C(b–d). A multilevel degradation rate of the composite scaffold and controlled release rate of protein from mesopores could be achieved. In addition, the coating of PGS promoted the cell attachment and proliferation in a dose-dependent manner, without affecting osteogenic induction capacity of the MBG (Lin et al., 2015).

Chen et al. (2015a,b) prepared crack-free polydimethylsiloxane (PDMS) modified BGNPs (MBGNPs)-poly(ethylene glycol) (PEG) (PDMS-MBGNPs-PEG)



hybrid monoliths and investigated the effect of molecular weight of PEG on the properties of hybrid monoliths. The incorporation of low-molecular-weight PEG can prevent the crack formation significantly and speed up the gelation of the hybrid monoliths. However, the increase in molecular weight of PEG can change microstructure (surface) of the hybrid monoliths from porous to smooth surface. In addition, hybrid monoliths having low-molecular-weight PEG showed high apatite forming ability, while hybrid monoliths having high-molecular-weight PEG showed negligible ability of apatite deposition in the SBF. Moreover, PDMS-MBG-NPs-PEG 600 hybrid monolith showed high compressive strength and modulus ( $32 \pm 3$  and  $153 \pm 11$  MPa) and good osteoblastic MC3T3-E1 cell attachment and proliferation (Chen et al., 2015a,b). Hesaraki (2016) prepared a strong and bone cement by using a ternary ( $\text{SiO}_2\text{--CaO--P}_2\text{O}_5$ ) BG particles and a photocurable resin composed of hydroxyethyl methacrylate and poly(acrylic/maleic acid). This cure composite system showed a compressive strength around 95 MPa but reduced to around 20 MPa when soaked in SBF for 30 days. In addition, composite systems showed good in vitro apatite forming ability and good calvarium-derived newborn rat osteoblast cell attachment and proliferation (Hesaraki, 2016).

#### 13.6.4 MIXED NATURAL AND SYNTHETIC POLYMERS/BIOACTIVE GLASSES—BASED COMPOSITE SCAFFOLDS

Pon-On et al. (2014) prepared porous scaffolds with varying weight ratios (0.5/1, 1/1, and 2/1) of PVA-BG (15Ca:80Si:5 P) and Chit-Col by using three mechanical freeze-thaw cycles followed by freeze-drying method. The obtained PVA-BG/Chit-Col (1/1) composite scaffolds showed highest compressive modulus (214.64 MPa), while all composite scaffolds showed apatite forming ability after 7 days of SBF immersion. In addition, good UMR-106 cell attachment and proliferation was observed on the surface of the composite scaffolds and ALP activity was found to increase with increased culture time. Moreover, 81.14% of BSA loading and controlled releasing from composite scaffolds (especially with 1/1 weight ratio) was observed for over 4 weeks (Pon-On et al., 2014). Kumar et al. (2017b) prepared CNC reinforced PVA/silica glass hybrid scaffolds and a significant improvement in mechanical performance and MC3T3-E1 cell attachment and proliferation in vitro was observed (Kumar et al., 2017b).

Yazdimamaghani et al. (2015) prepared  $\text{Mg}^{2+}$  scaffolds coated with a multi-layer made of PCL and Gel reinforced with BG particles. For comparison, uncoated  $\text{Mg}^{2+}$  scaffolds and  $\text{Mg}^{2+}$  scaffolds coated with only PCL-BG were also prepared and analyzed. In this study, the coating of  $\text{Mg}^{2+}$  scaffolds with polymeric layer significantly improved the biodegradability. In addition,  $\text{Mg}^{2+}$  scaffolds coated with PCL showed better apatite forming ability by the deposition of bioactive minerals in cauliflower-like structure on the surface of the scaffolds.  $\text{Mg}^{2+}$  scaffold and  $\text{Mg}^{2+}$  scaffold coated with PCL-BG were fully degraded after

3 and 7 days, while around 87% of Mg-scaffold coated with PCL-BG and Gel-BG remained after 14 days (Yazdimamaghani et al., 2015). Nazemi et al. (2015) prepared two Chit-BG scaffolds with and without PLGA-NPs and investigated the effect of incorporating PLGA-NPs on a drug-release behavior of a scaffold. The results indicated that the swelling behavior of the scaffolds slightly decreased, while mechanical properties of the scaffolds increased due to the incorporation of PLGA-NPs. In addition, the incorporation of NPs did not affect the microstructure of the scaffold (Nazemi et al., 2015). Fan et al. (2016) prepared BGNPs/graphene nanosheets (BGNPs/GNS) scaffolds by using sol–gel/mold-compressing strategies. The results showed densely anchored BGNPs (average diameter: 28.75 nm) on both sides of GNS and scaffold with mass ratio 10 of BGNPs/GNS) exhibited better biocompatibility and higher osteointegration ability with surrounding tissues compared with other scaffolds. In addition, the incorporation of GNS significantly improved the hardness and Young's modulus of BG-based scaffolds (Fan et al., 2016). Kumar et al. (2017d) prepared PASG/CN hybrid hydrogels composed of polyacrylamide (PAAm), sodium alginate (SA), BG, and CNCs, where the amount of CNCs was varied from 2.5 to 10.0 wt%. As-prepared PASG/CN hybrid hydrogels exhibited highly porous structure, good in vitro bioactivity (apatite forming ability), and tunable and enhanced mechanical properties (strength and stiffness) in both dry and wet states compared with PASG hybrid hydrogel only. In addition, PASG/CN hybrid hydrogels showed better in vitro cytocompatibility with MC3T3-E1 preosteoblast cells in terms of qualitative (cell attachment via FESEM) and quantitative (proliferation via MTT assay) analyses. However, in vitro hydrophilicity and degradability of PASG/CN hybrid hydrogels were observed to be reduced compared with PASG hybrid hydrogel only (Kumar et al., 2017d).

---

### 13.7 CONCLUSION, MAJOR CHALLENGES, AND FUTURE PERSPECTIVE

The bone tissue engineering field is rapidly growing and searching for alternative treatment options to mimic more closely the architecture of the native bone tissues under a 3D micro/nanoenvironment (physiological) for successful regeneration of bone tissues. Several types of fabrication strategies have widely been established to fabricate bone scaffolds, but their applicability for successful regeneration of the bone tissues and commercialization are limited. Therefore, one of the major challenges in regeneration of bone tissues is to fabricate the scaffold having desired microstructural, mechanical, and biological performance for proper cellularization, controlled vascularization, and mineralization (bone formation) of the scaffolds. Actually, bone tissue is complex and, we need more understanding of the long-term in vivo behavior of the composite scaffolds, particularly degradation, ion-release kinetics, cellularization, and vascularization through the porous

system (Gerhardt and Boccaccini, 2010; Boccaccini et al., 2010; Shadjou and Hasanzadeh, 2015; Kumar and Han, 2016). Therefore, BGs are excellent candidates as inorganic phase for use in the fabrication of bone scaffolds and future directions will turn towards continuous research to find the most cost-effective strategies for commercial tissue-engineered bone (Shadjou and Hasanzadeh, 2015).

---

## ACKNOWLEDGMENTS

Authors would like to thank the authors whose research work and review articles have been cited in this book chapter. The writing of this book chapter was fully supported by the Basic Science Research Program through the National Research Foundation of Korea (NRF) funded by the Ministry of Education, Science and Technology (Grant No. 2017R1D1A3B03036276).

---

## REFERENCES

- Ahmed, I., Collins, C.A., Lewis, M.P., Olsen, I., Knowles, J.C., 2004. Processing, characterization and biocompatibility of iron-phosphate glass fibres for tissue engineering. *Biomaterials* 25, 3223–3232.
- Aina, V., Perardi, A., Bergandi, L., Malavasi, G., Menabue, L., Morterra, C., et al., 2007. Cytotoxicity of zinc-containing bioactive glasses in contact with human osteoblasts. *Chem. Biol. Interact.* 167, 207–218.
- Arepalli, S.K., Tripathi, H., Hira, S.K., Manna, P.P., Pyare, R., Singh, S.P., 2016. Enhanced bioactivity, biocompatibility and mechanical behavior of strontium substituted bioactive glasses. *Mater. Sci. Eng. C* 69, 108–116.
- Arriagada, F.J., Osseo-Asare, K., 1999. Synthesis of nanosize silica in a nonionic water-in-oil microemulsion: effects of the water/surfactant molar ratio and ammonia concentration. *J. Colloid Interface Sci.* 211, 210–220.
- Bachar, A., Mercier, C., Tricoteaux, A., Leriche, A., Follet, C., Hampshire, S., 2016. Bioactive oxynitride glasses: synthesis, structure and properties. *J. Eur. Ceram. Soc.* 36, 2869–2881.
- Baino, F., Verné, E., Vitale-Brovarone, C., 2009. 3-D high-strength glass–ceramic scaffolds containing fluoroapatite for load-bearing bone portions replacement. *Mater. Sci. Eng. C* 29, 2055–2062.
- Baino, F., Fiorilli, S., Vitale-Brovarone, C., 2016a. Bioactive glass-based materials with hierarchical porosity for medical applications: review of recent advances. *Acta Biomater.* 42, 18–32.
- Baino, F., Novajra, G., Miguez-Pacheco, V., Boccaccini, A.R., Vitale-Brovarone, C., 2016b. Bioactive glasses: special applications outside the skeletal system. *J. Non-Cryst. Solids* 432, 15–30.
- Bellantone, M., Williams, H.D., Hench, L.L., 2002. Broad-spectrum bactericidal activity of Ag<sub>2</sub>O-doped bioactive glass. *Antimicrob. Agents Chemother.* 46, 1940–1945.

- Bellucci, D., Cannillo, V., Ciardelli, G., Gentile, P., Sola, A., 2010. Potassium based bioactive glass for bone tissue engineering. *Ceram. Int.* 36, 2449–2453.
- Bellucci, D., Sola, A., Salvatori, R., Anesi, A., Chiarini, L., Cannillo, V., 2014. Sol–gel derived bioactive glasses with low tendency to crystallize: synthesis, post-sintering bioactivity and possible application for the production of porous scaffolds. *Mater. Sci. Eng. C* 43, 573–586.
- Boccaccini, A.R., Erol, M., Stark, W.J., Mohn, D., Hong, Z., Mano, J.F., 2010. Polymer/bioactive glass nanocomposites for biomedical applications: a review. *Compos. Sci. Technol.* 70, 1764–1776.
- Bose, S., Saha, S.K., 2003. Synthesis and characterization of hydroxyapatite nanopowders by emulsion technique. *Chem. Mater.* 15, 4464–4469.
- Boyd, D., Carroll, G., Towler, M.R., Freeman, C., Farthing, P., Brook, I.M., 2009. Preliminary investigation of novel bone graft substitutes based on strontium–calcium–zinc–silicate glasses. *J. Mater. Sci. Mater. Med.* 20, 413–420.
- Branda, F., Arcobello-Varlese, F., Costantini, A., Luciani, G., 2002. Effect of the substitution of  $M_2O_3$  ( $M = La, Y, In, Ga, Al$ ) for  $CaO$  on the bioactivity of  $2.5CaO \cdot 2SiO_2$  glass. *Biomaterials* 23, 711–716.
- Brinker, C.J., Scherer, G.W., 1990. *Sol-Gel Science: The Physics and Chemistry of Sol-Gel Processing*. Academic Press Inc., Boston, MA.
- Brown, R.F., Day, D.E., Day, T.E., Jung, S., Rahaman, M.N., Fu, Q., 2008a. Growth and differentiation of osteoblastic cells on 13–93 bioactive glass fibers and scaffolds. *Acta Biomater.* 4, 387–396.
- Brown, R.F., Dwilewicz, A.B., Huang, W.H., Li, Y., Rahaman, M.N., Bal, B.S., et al., 2008b. Conversion of borate glass to hydroxyapatite and its effect on proliferation of MC3T3-E1 cells. *J. Biomed. Mater. Res. Part A* 88A, 392–400.
- Brunner, T.J., Grass, R.N., Stark, W.J., 2006. Glass and bioglass nanopowders by flame synthesis. *Chem. Comm* 13, 1384–1386.
- Brunner, T.J., Stark, W.J., Boccaccini, A.R., 2009. Nanoscale bioactive silicate glasses in biomedical applications. In: Challa, S.S., Kumar, R. (Eds.), *Nanomaterials for the Life Sciences. Nanostructured Oxides*, vol. 2. WileyVCH GmbH & Co. KGaA, Weinheim, pp. 203–220.
- Buehler, M., 2006. Nature design tough collagen: explaining the nanostructure of collagen fibrils. *Proc. Natl Acad. Sci. USA* 103, 12285–12290.
- Buehler, M., 2007. Molecular nanomechanics of nascent bone: fibrillar toughening by mineralization. *Nanotechnology* 18, 295102.
- Chandrasekaran, A., Novajra, G., Carmagnola, I., Gentile, P., Fiorilli, S., Miola, M., et al., 2016. Physico-chemical and biological studies on three-dimensional porous silk/spray-dried mesoporous bioactive glass scaffolds. *Ceram. Int.* 42, 13761–13772.
- Chen, Q.Z., Thompson, I.D., Boccaccini, A.R., 2006. 45S5 Bioglass®-derived glass–ceramic scaffolds for bone tissue engineering. *Biomaterials* 27, 2414–2425.
- Chen, X., Guo, C., Zhao, N., 2008. Preparation and characterization of the sol–gel nanobioactive glasses modified by the coupling agent gamma-aminopropyltriethoxysilane. *Appl. Surf. Sci.* 255, 466–468.
- Chen, X., Lei, B., Wang, Y., Zhao, N., 2009. Morphological control and *in vitro* bioactivity of nanoscale bioactive glasses. *J. Non-Cryst. Solids* 355, 791–796.
- Chen, J., Du, Y., Que, W., Xing, Y., Chen, X., Lei, B., 2015a. Crack-free polydimethylsiloxane–bioactive glass–poly (ethylene glycol) hybrid monoliths with controlled biomineralization activity and mechanical property for bone tissue regeneration. *Colloids Surf. B* 136, 126–133.

- Chen, J., Que, W., Xing, Y., Lei, B., 2015b. Highly bioactive polysiloxane modified bioactive glass-poly (ethylene glycol) hybrids monoliths with controlled surface structure for bone tissue regeneration. *Appl. Surf. Sci.* 332, 542–548.
- Cui, X., Zhang, Y., Wang, H., Gu, Y., Li, L., Zhou, J., et al., 2016. An injectable borate bioactive glass cement for bone repair: preparation, bioactivity and setting mechanism. *J. Non-Cryst. Solids*. 432, 150–157.
- Delben, J.R.J., Pimentel, O.M., Coelho, M.B., Candelario, P.D., Furini, L.N., dos Santos, F.A., et al., 2009. Synthesis and thermal properties of nanoparticles of bioactive glasses containing silver. *J. Therm. Anal. Calorim.* 97, 433–436.
- Deliormanlı, A.M., 2015. Preparation, *in vitro* mineralization and osteoblast cell response of electrospun 13–93 bioactive glass nanofibers. *Mater. Sci. Eng. C* 53, 262–271.
- Deliormanlı, A.M., Rahaman, M.N., 2012. Direct-write assembly of silicate and borate bioactive glass scaffolds for bone repair. *J. Eur. Ceram. Soc.* 32, 3637–3646.
- Del Río, M.J., Vélez-Pardo, C., 2004. Transition metal-induced apoptosis in lymphocytes via hydroxyl radical generation, mitochondria dysfunction, and caspase-3 activation: an *in vitro* model for neurodegeneration. *Arch. Med. Res.* 35, 185–193.
- Deville, S., Saiz, E., Tomsia, A.P., 2006. Freeze casting of hydroxyapatite scaffolds for bone tissue engineering. *Biomaterials* 27, 5480–5489.
- Dziadek, M., Menaszek, E., Zagajczuk, B., Pawlik, J., Cholewa-Kowalska, K., 2015. New generation poly ( $\epsilon$ -caprolactone)/gel-derived bioactive glass composites for bone tissue engineering: part I. Material properties. *Mater. Sci. Eng. C* 56, 9–21.
- El-Fiqi, A., Lee, J.H., Lee, E.J., Kim, H.W., 2013. Collagen hydrogels incorporated with surface-aminated mesoporous nanobioactive glass: improvement of physicochemical stability and mechanical properties is effective for hard tissue engineering. *Acta Biomater.* 9, 9508–9521.
- El-Kady, A.M., Ali, A.F., Farag, M.M., 2010. Development, characterization, and *in vitro* bioactivity studies of sol–gel bioactive glass/poly (L-lactide) nanocomposite scaffolds. *Mater. Sci. Eng. C* 30, 120–131.
- El-Kady, A.M., Ali, A.F., Rizk, R.A., Ahmed, M.M., 2012. Synthesis, characterization and microbiological response of silver doped bioactive glass nanoparticles. *Ceram. Int.* 38, 177–188.
- El-Kady, A.M., Farag, M.M., El-Rashedi, A.M., 2016. Bioactive glass nanoparticles designed for multiple deliveries of lithium ions and drugs: curative and restorative bone treatment. *Eur. J. Pharm. Sci.* 91, 243–250.
- Emadi, R., Tavangarian, F., Esfahani, S.R., 2010. Biodegradable and bioactive properties of a novel bone scaffold coated with nanocrystalline bioactive glass for bone tissue engineering. *Mater. Lett.* 64, 1528–1531.
- Erol, M.M., Mouriño, V., Newby, P., Chatzistavrou, X., Roether, J.A., Hupa, L., et al., 2012. Copper-releasing, boron-containing bioactive glass-based scaffolds coated with alginate for bone tissue engineering. *Acta Biomater.* 8, 792–801.
- Esfahani, S.R., Tavangarian, F., Emadi, R., 2008. Nanostructured bioactive glass coating on porous hydroxyapatite scaffold for strength enhancement. *Mater. Lett.* 62, 3428–3430.
- Fan, J.P., Kalia, P., Di Silvio, L., Huang, J., 2014. *In vitro* response of human osteoblasts to multi-step sol–gel derived bioactive glass nanoparticles for bone tissue engineering. *Mater. Sci. Eng. C* 36, 206–214.
- Fan, Z., Wang, J., Liu, F., Nie, Y., Ren, L., Liu, B., 2016. A new composite scaffold of bioactive glass nanoparticles/graphene: synchronous improvements of cytocompatibility and mechanical property. *Colloids Surf. B* 145, 438–446.

- Fereshteh, Z., Nooeaid, P., Fathi, M., Bagri, A., Boccaccini, A.R., 2015a. The effect of coating type on mechanical properties and controlled drug release of PCL/zein coated 45S5 bioactive glass scaffolds for bone tissue engineering. *Mater. Sci. Eng. C* 54, 50–60.
- Fereshteh, Z., Nooeaid, P., Fathi, M., Bagri, A., Boccaccini, A.R., 2015b. Mechanical properties and drug release behavior of PCL/zein coated 45S5 bioactive glass scaffolds for bone tissue engineering application. *Data Brief* 4, 524–528.
- Fernandes, J.S., Gentile, P., Martins, M., Neves, N.M., Miller, C., Crawford, A., et al., 2016. Reinforcement of poly-L-lactic acid electrospun membranes with strontium borosilicate bioactive glasses for bone tissue engineering. *Acta Biomater.* 44, 168–177.
- Fratzl, P., Weinkamer, R., 2007. Nature's hierarchical materials. *Prog. Mater. Sci.* 52, 1263–1334.
- Fratzl, P., Gupta, H., Paschalis, E., Roshger, P., 2004. Structure and mechanical quality of the collagen-mineral nano-composite in bone. *J. Mater. Chem.* 14, 2115–2123.
- Fu, Q., Rahaman, M.N., Bal, B.S., Brown, R.F., Day, D.E., 2008. Mechanical and *in vitro* performance of 13–93 bioactive glass scaffolds prepared by a polymer foam replication technique. *Acta Biomater.* 4, 1854–1864.
- Fu, Q., Rahaman, M.N., Bal, B.S., Brown, R.F., 2010a. Preparation and *in vitro* evaluation of bioactive glass (13–93) scaffolds with oriented microstructures for repair and regeneration of load-bearing bones. *J. Biomed. Mater. Res. Part A* 93, 1380–1390.
- Fu, Q., Rahaman, M.N., Bal, B.S., Kuroki, K., Brown, R.F., 2010b. *In vivo* evaluation of 13–93 bioactive glass scaffolds with trabecular and oriented microstructures in a subcutaneous rat implantation model. *J. Biomed. Mater. Res. Part A* 95, 235–244.
- Fu, Q., Rahaman, M.N., Fu, H., Liu, X., 2010c. Silicate, borosilicate, and borate bioactive glass scaffolds with controllable degradation rate for bone tissue engineering applications. I. Preparation and *in vitro* degradation. *J. Biomed. Mater. Res. Part A* 95, 164–171.
- Fu, Q., Rahaman, M.N., Bal, B.S., Bonewald, L.F., Kuroki, K., Brown, R.F., 2010d. Silicate, borosilicate, and borate bioactive glass scaffolds with controllable degradation rate for bone tissue engineering applications. II. *In vitro* and *in vivo* biological evaluation. *J. Biomed. Mater. Res. Part A* 95, 172–179.
- Fu, Q., Saiz, E., Rahaman, M.N., Tomsia, A.P., 2011. Bioactive glass scaffolds for bone tissue engineering: state of the art and future perspectives. *Mater. Sci. Eng. C* 31, 1245–1256.
- Fung, Y., 1993. *Biomechanics: Mechanical Properties of Living Tissues*, second ed. Springer Verlag, New York.
- Gantar, A., da Silva, L.P., Oliveira, J.M., Marques, A.P., Correlo, V.M., Novak, S., et al., 2014. Nanoparticulate bioactive-glass-reinforced gellan-gum hydrogels for bone-tissue engineering. *Mater. Sci. Eng. C* 43, 27–36.
- Gao, H., Tan, T., Wang, D., 2004. Dissolution mechanism and release kinetics of phosphate controlled release glasses in aqueous medium. *J. Control. Release* 96, 29–36.
- Geremia, R., Rinaudo, M., 2005. In: Dumitriu, S. (Ed.), *Polysaccharides: Structural Diversity and Functional Versatility*, vol. 15. Marcel Dekker, New York, pp. 411–430.
- Gerhardt, L.C., Boccaccini, A.R., 2010. Bioactive glass and glass-ceramic scaffolds for bone tissue engineering. *Materials* 3, 3867–3910.
- Gibson, L., 2005. *Biomechanics of cellular solids*. *J. Biomech.* 38, 377–399.
- Gibson, L., Ashby, M., 1999. *Cellular Solids, Structure and Properties*, second ed. Cambridge University Press, Cambridge.

- Goel, A., Kapoor, S., Rajagopal, R.R., Pascual, M.J., Kim, H.W., Ferreira, J.M., 2012. Alkali-free bioactive glasses for bone tissue engineering: a preliminary investigation. *Acta Biomater.* 8, 361–372.
- Gonen, S.O., Taygun, M.E., Küçükbayrak, S., 2016. Fabrication of bioactive glass containing nanocomposite fiber mats for bone tissue engineering applications. *Compos. Struct.* 138, 96–106.
- Gu, Y., Huang, W., Rahaman, M.N., Day, D.E., 2013. Bone regeneration in rat calvarial defects implanted with fibrous scaffolds composed of a mixture of silicate and borate bioactive glasses. *Acta Biomater.* 9, 9126–9136.
- Gu, Y., Wang, G., Zhang, X., Zhang, Y., Zhang, C., Liu, X., et al., 2014. Biodegradable borosilicate bioactive glass scaffolds with a trabecular microstructure for bone repair. *Mater. Sci. Eng. C* 36, 294–300.
- Haaparanta, A.M., Uppstu, P., Hannula, M., Ellä, V., Rosling, A., Kellomäki, M., 2015. Improved dimensional stability with bioactive glass fibre skeleton in poly (lactide-co-glycolide) porous scaffolds for tissue engineering. *Mater. Sci. Eng. C* 56, 457–466.
- Haimi, S., Gorianc, G., Moimas, L., Lindroos, B., Huhtala, H., Rätty, S., et al., 2009. Characterization of zinc-releasing three-dimensional bioactive glass scaffolds and their effect on human adipose stem cell proliferation and osteogenic differentiation. *Acta Biomater.* 5, 3122–3131.
- Han, X., Wang, D., Chen, X., Lin, H., Qu, F., 2014. One-pot synthesis of macro-mesoporous bioactive glasses/polylactic acid for bone tissue engineering. *Mater. Sci. Eng. C* 43, 367–374.
- Hench, L.L., 1998. Bioactive materials: the potential for tissue regeneration. *J. Biomed. Mater. Res. Part A* 41, 511–518.
- Hench, L.L., Roki, N., Fenn, M.B., 2014. Bioactive glasses: importance of structure and properties in bone regeneration. *J. Mol. Struct.* 1073, 24–30.
- Hesaraki, S., 2016. Photocurable bioactive bone cement based on hydroxyethyl methacrylate-poly (acrylic/maleic) acid resin and mesoporous sol gel-derived bioactive glass. *Mater. Sci. Eng. C* 63, 535–545.
- Hollister, S.J., 2005. Porous scaffold design for tissue engineering. *Nat. Mater.* 4, 518–524.
- Hoppe, A., Güldal, N.S., Boccaccini, A.R., 2011. A review of the biological response to ionic dissolution products from bioactive glasses and glass-ceramics. *Biomaterials* 32, 2757–2774.
- Horton, J.A., Parsell, D.E., 2003. Biomedical potential of a zirconium-based bulk metallic glass. *Mater. Res. Soc. Symp. Proc.* 754, CC1.5.1.
- Hsu, F.Y., Weng, R.C., Lin, H.M., Lin, Y.H., Lu, M.R., Yu, J.L., et al., 2015. A biomimetic extracellular matrix composed of mesoporous bioactive glass as a bone graft material. *Micropor. Mesopor. Mater.* 212, 56–65.
- Huang, W., Day, D.E., Kittiratanapiboon, K., Rahaman, M.N., 2006. Kinetics and mechanisms of the conversion of silicate (45S5), borate, and borosilicate glasses to hydroxyapatite in dilute phosphate solutions. *J. Mater. Sci. Mater. Med.* 17, 583–596.
- Hulsen, D.J.W., Geurts, J., van Gestel, N.A.P., van Rietbergen, B., Arts, J.J., 2016. Mechanical behaviour of Bioactive Glass granules and morselized cancellous bone allograft in load bearing defects. *J. Biomech.* 49, 1121–1127.
- Hutmacher, D.W., 2001. Scaffold design and fabrication technologies for engineering tissues—state of the art and future perspectives. *J. Biomater. Sci. Polym. Ed.* 12, 107–124.



- Jebahi, S., Oudadesse, H., El Feki, H., Rebai, T., Keskes, H., Pellen, P., et al., 2012. Antioxidative/oxidative effects of strontium-doped bioactive glass as bone graft. *In vivo* assays in ovariectomised rats. *J. Appl. Biomed.* 10, 195–209.
- Jones, J.R., Ahir, S., Hench, L.L., 2004. Large-scale production of 3D bioactive glass macroporous scaffolds for tissue engineering. *J. Sol-Gel Sci. Technol.* 29, 179–188.
- Jones, J.R., Ehrenfried, L.M., Hench, L.L., 2006. Optimising bioactive glass scaffolds for bone tissue engineering. *Biomaterials* 27, 964–973.
- Karageorgiou, V., Kaplan, D., 2005. Porosity of 3D biomaterial scaffolds and osteogenesis. *Biomaterials* 26, 5474–5491.
- Kargozar, S., Lotfibakhshaiesh, N., Ai, J., Samadikuchaksaraie, A., Hill, R.G., Shah, P.A., et al., 2016. Synthesis, physico-chemical and biological characterization of strontium and cobalt substituted bioactive glasses for bone tissue engineering. *J. Non-Cryst. Solids* 449, 133–140.
- Kaur, G., Pandey, O.P., Singh, K., Homa, D., Scott, B., Pickrell, G., 2014. A review of bioactive glasses: their structure, properties, fabrication and apatite formation. *J. Biomed. Mater. Res. Part A* 102, 254–274.
- Killion, J.A., Kehoe, S., Geever, L.M., Devine, D.M., Sheehan, E., Boyd, D., et al., 2013. Hydrogel/bioactive glass composites for bone regeneration applications: synthesis and characterisation. *Mater. Sci. Eng. C* 33, 4203–4212.
- Kingery, W.D., Bowen, H.K., Uhlmann, D.R., 1976. *Introduction to Ceramics*, second ed. John Wiley and Sons, New York.
- Kumar, A., Han, S.S., 2016. Emergence of bioprinting in tissue engineering: a mini review. *Adv. Tissue Eng. Regen. Med.* 1, 00013. Available from: <https://doi.org/10.15406/atroa.2016.01.00013>.
- Kumar, A., Negi, Y.S., Choudhary, V., Bhardwaj, N.K., 2014. Microstructural and mechanical properties of porous biocomposite scaffolds based on polyvinyl alcohol, nano-hydroxyapatite and cellulose nanocrystals. *Cellulose* 21, 3409–3426.
- Kumar, A., Negi, Y.S., Choudhary, V., Bhardwaj, N.K., 2016. Fabrication of poly (vinyl alcohol)/ovalbumin/cellulose nanocrystals/nanohydroxyapatite based biocomposite scaffolds. *Int. J. Polym. Mater. Polym. Biomater.* 65, 191–201.
- Kumar, A., Rao, K.M., Haider, A., Han, S.S., Son, T.W., Kim, J.H., et al., 2017a. Fabrication and characterization of multicomponent polysaccharide/nano-hydroxyapatite composite scaffolds. *Polym. Plast. Technol. Eng.* 56, 983–991.
- Kumar, A., Negi, Y.S., Choudhary, V., Bhardwaj, N.K., Han, S.S., 2017b. Morphological, mechanical and in vitro cytocompatibility analysis of poly (vinyl alcohol)-silica glass hybrid scaffolds reinforced with cellulose nanocrystals. *Int. J. Polym. Anal. Ch.* 2, 139–151.
- Kumar, A., Rao, K.M., Kwon, S.E., Lee, Y.N., Han, S.S., 2017c. Xanthan gum/bioactive silica glass hybrid scaffolds reinforced with cellulose nanocrystals: morphological, mechanical and in vitro cytocompatibility study. *Mater. Lett.* 193, 274–278.
- Kumar, A., Rao, K.M., Han, S.S., 2017d. Synthesis of mechanically stiff and bioactive hybrid hydrogels for bone tissue engineering applications. *Chem. Eng. J.* 317, 119–131.
- Kumar, A., Rao, K.M., Han, S.S., 2018. Application of xanthan gum as polysaccharide in tissue engineering: a review. *Carbohydr. Polym.* 180, 128–144.
- Kuttappan, S., Mathew, D., Nair, M.B., 2016. Biomimetic composite scaffolds containing bioceramics and collagen/gelatin for bone tissue engineering—a mini review. *Int. J. Biol. Macromol.* 93, 1390–1401.



- Le, X.T., Turgeon, S.L., 2013. Rheological and structural study of electrostatic cross-linked xanthan gum hydrogels induced by  $\beta$ -lactoglobulin. *Soft Matter* 9, 3063–3073.
- Lei, B., Shin, K.H., Noh, D.Y., Jo, I.H., Koh, Y.H., Choi, W.Y., et al., 2012. Nanofibrous gelatin–silica hybrid scaffolds mimicking the native extracellular matrix (ECM) using thermally induced phase separation. *J. Mater. Chem.* 22, 14133–14140.
- Lei, B., Shin, K.H., Noh, D.Y., Jo, I.H., Koh, Y.H., Kim, H.E., et al., 2013. Sol–gel derived nanoscale bioactive glass (NBG) particles reinforced poly ( $\epsilon$ -caprolactone) composites for bone tissue engineering. *Mater. Sci. Eng. C* 33, 1102–1108.
- Leonardi, E., Ciapetti, G., Baldini, N., Novajra, G., Verné, E., Baino, F., et al., 2010. Response of human bone marrow stromal cells to a resorbable  $P_2O_5$ – $SiO_2$ – $CaO$ – $MgO$ – $Na_2O$ – $K_2O$  phosphate glass ceramic for tissue engineering applications. *Acta Biomater.* 6, 598–606.
- Levenberg, S., Langer, R., 2004. Advances in tissue engineering. *Curr. Top. Dev. Biol.* 61, 113–134.
- Li, J., Wang, H.L., 2008. Common implant-related advanced bone grafting complications: classification, etiology, and management. *Implant Dent.* 17, 389–401.
- Li, Y., Li, B., Xu, G., Ahmad, Z., Ren, Z., Dong, Y., et al., 2014. A feasible approach toward bioactive glass nanofibers with tunable protein release kinetics for bone scaffolds. *Colloids Surf. B* 122, 785–791.
- Li, Y., Chen, X., Ning, C., Yuan, B., Hu, Q., 2015. Facile synthesis of mesoporous bioactive glasses with controlled shapes. *Mater. Lett.* 161, 605–608.
- Liang, W., Rahaman, M.N., Day, D.E., Marion, N.W., Riley, G.C., Mao, J.J., 2008. Bioactive borate glass scaffold for bone tissue engineering. *J. Non-Cryst. Solids* 354, 1690–1696.
- Lim, G.K., Wang, J., Ng, S.C., Gan, L.M., 1996. Processing of fine hydroxyapatite powders via an inverse microemulsion route. *Mater. Lett.* 28, 431–436.
- Lin, D., Yang, K., Tang, W., Liu, Y., Yuan, Y., Liu, C., 2015. A poly (glycerol sebacate)-coated mesoporous bioactive glass scaffold with adjustable mechanical strength, degradation rate, controlled-release and cell behavior for bone tissue engineering. *Colloids Surf. B* 131, 1–11.
- Lin, Y., Xiao, W., Bal, B.S., Rahaman, M.N., 2016a. Effect of copper-doped silicate 13–93 bioactive glass scaffolds on the response of MC3T3-E1 cells *in vitro* and on bone regeneration and angiogenesis in rat calvarial defects *in vivo*. *Mater. Sci. Eng. C* 67, 440–452.
- Lin, Y., Xiao, W., Liu, X., Bal, B.S., Bonewald, L.F., Rahaman, M.N., 2016b. Long-term bone regeneration, mineralization and angiogenesis in rat calvarial defects implanted with strong porous bioactive glass (13–93) scaffolds. *J. Non-Cryst. Solids* 432, 120–129.
- Liu, L., Chan, K.C., Yu, Y., Chen, Q., 2010. Bio-activation of Ni-free Zr-based bulk metallic glass by surface modification. *Intermetallics* 18, 1978–1982.
- Liu, X., Rahaman, M.N., Fu, Q., 2013. Bone regeneration in strong porous bioactive glass (13-93) scaffolds with an oriented microstructure implanted in rat calvarial defects. *Acta Biomater.* 9, 4889–4898.
- Loher, S., Stark, W.J., Maciejewski, M., Baiker, A., Pratsinis, S.E., Reichardt, D., et al., 2005. Fluoro-apatite and calcium phosphate nanoparticles by flame synthesis. *Chem. Mater.* 17, 36–42.
- Luo, Z., Deng, Y., Zhang, R., Wang, M., Bai, Y., Zhao, Q., et al., 2015. Peptide-laden mesoporous silica nanoparticles with promoted bioactivity and osteo-differentiation ability for bone tissue engineering. *Colloids Surf. B* 131, 73–82.

- Ma, Z., Ji, H., Hu, X., Teng, Y., Zhao, G., Mo, L., et al., 2013. Investigation of bioactivity and cell effects of nano-porous sol-gel derived bioactive glass film. *Appl. Surf. Sci.* 284, 738–744.
- Marion, N.W., Liang, W., Liang, W., Reilly, G.C., Day, D.E., Rahaman, M.N., et al., 2005. Borate glass supports the *in vitro* osteogenic differentiation of human mesenchymal stem cells. *Mech. Adv. Mater. Struct.* 12, 239–246.
- McGregor, D.B., Baan, R.A., Partensky, C., Rice, J.M., Wilbourn, J.D., 2000. Evaluation of the carcinogenic risks to humans associated with surgical implants and other foreign bodies—a report of an IARC Monographs Programme Meeting. *Eur. J. Cancer* 36, 307–313.
- Miguez-Pacheco, V., Büttner, T., Maçon, A.L.B., Jones, J.R., Fey, T., de Ligny, D., et al., 2016. Development and characterization of lithium-releasing silicate bioactive glasses and their scaffolds for bone repair. *J. Non-Cryst. Solids* 432, 65–72.
- Min, Z., Huixue, W., Yujie, Z., Lixin, J., Hai, H., Yufang, Z., 2016. Synthesis of monodispersed mesoporous bioactive glass nanospheres for bone repair. *Mater. Lett.* 171, 259–262.
- Miola, M., Brovarone, C.V., Maina, G., Rossi, F., Bergandi, L., Ghigo, D., et al., 2014. *In vitro* study of manganese-doped bioactive glasses for bone regeneration. *Mater. Sci. Eng. C* 38, 107–118.
- Mishra, R., Basu, B., Kumar, A., 2009. Physical and cytocompatibility properties of bioactive glass–polyvinyl alcohol–sodium alginate biocomposite foams prepared via sol–gel processing for trabecular bone regeneration. *J. Mater. Sci. Mater. Med.* 20, 2493–2500.
- Moreira, C.D., Carvalho, S.M., Mansur, H.S., Pereira, M.M., 2016. Thermogelling chitosan–collagen–bioactive glass nanoparticle hybrids as potential injectable systems for tissue engineering. *Mater. Sci. Eng. C* 58, 1207–1216.
- Mozafari, M., Moztarzadeh, F., Rabiee, M., Azami, M., Maleknia, S., Tahriri, M., et al., 2010. Development of macroporous nanocomposite scaffolds of gelatin/bioactive glass prepared through layer solvent casting combined with lamination technique for bone tissue engineering. *Ceram. Int.* 36, 2431–2439.
- Murphy, S., Boyd, D., Moane, S., Bennett, M., 2009. The effect of composition on ion release from Ca–Sr–Na–Zn–Si glass bone grafts. *J. Mater. Sci. Mater. Med.* 20, 2207–2214.
- Nadeem, D., Kiamehr, M., Yang, X., Su, B., 2013. Fabrication and *in vitro* evaluation of a sponge-like bioactive-glass/gelatin composite scaffold for bone tissue engineering. *Mater. Sci. Eng. C* 33, 2669–2678.
- Nandi, S.K., Roy, S., Mukherjee, P., Kundu, B., De, D.K., Basu, D., 2010. Orthopaedic applications of bone graft & graft substitutes: a review. *Indian J. Med. Res.* 132, 15–30.
- Navarro, M., del Valle, S., Martínez, S., Zeppetelli, S., Ambrosio, L., Planell, J.A., et al., 2004. New macroporous calcium phosphate glass ceramic for guided bone regeneration. *Biomaterials* 25, 4233–4241.
- Nazemi, K., Azadpour, P., Moztarzadeh, F., Urbanska, A.M., Mozafari, M., 2015. Tissue-engineered chitosan/bioactive glass bone scaffolds integrated with PLGA nanoparticles: a therapeutic design for on-demand drug delivery. *Mater. Lett.* 138, 16–20.
- Neel, E.A.A., Ahmed, I., Blaker, J.J., Bismarck, A., Boccaccini, A.R., Lewis, M.P., et al., 2005a. Effect of iron on the surface, degradation and ion release properties of phosphate-based glass fibres. *Acta Biomater.* 1, 553–563.

- Neel, E.A.A., Ahmed, I., Pratten, J., Nazhat, S.N., Knowles, J.C., 2005b. Characterisation of antibacterial copper releasing degradable phosphate glass fibres. *Biomaterials* 26, 2247–2254.
- Neel, E.A.A., Mizoguchi, T., Ito, M., Bitar, M., Salih, V., Knowles, J.C., 2007. *In vitro* bioactivity and gene expression by cells cultured on titanium dioxide doped phosphate-based glasses. *Biomaterials* 28, 2967–2977.
- Neel, E.A.A., Chrzanowski, W., Pickup, D.M., O'Dell, L.A., Mordan, N.J., Newport, R.J., et al., 2009. Structure and properties of strontium-doped phosphate-based glasses. *J. R. Soc. Interface* 6, 435–446.
- Neel, E.A.A., Chrzanowski, W., Knowles, J.C., 2014. Biological performance of titania containing phosphate-based glasses for bone tissue engineering applications. *Mater. Sci. Eng. C* 35, 307–313.
- Nezafati, N., Moztarzadeh, F., Hesarak, S., Mozafari, M., 2011. Synergistically reinforcement of a self-setting calcium phosphate cement with bioactive glass fibers. *Ceram. Int.* 37, 927–934.
- Nezafati, N., Moztarzadeh, F., Hesarak, S., Moztarzadeh, Z., Mozafari, M., 2013. Biological response of a recently developed nanocomposite based on calcium phosphate cement and sol–gel derived bioactive glass fibers as substitution of bone tissues. *Ceram. Int.* 39, 289–297.
- Nicolini, V., Gambuzzi, E., Malavasi, G., Menabue, L., Menziani, M.C., Lusvardi, G., et al., 2015. Evidence of catalase mimetic activity in  $Ce^{3+}/Ce^{4+}$  doped bioactive glasses. *J. Phys. Chem. B* 119, 4009–4019.
- Noh, K.T., Lee, H.Y., Shin, U.S., Kim, H.W., 2010. Composite nanofiber of bioactive glass nanofiller incorporated poly (lactic acid) for bone regeneration. *Mater. Lett.* 64, 802–805.
- Ojansivu, M., Vanhatupa, S., Björkvik, L., Häkkinen, H., Kellomäki, M., Autio, R., et al., 2015. Bioactive glass ions as strong enhancers of osteogenic differentiation in human adipose stem cells. *Acta Biomater.* 21, 190–203.
- O'Keefe, R.J., Mao, J., 2011. Bone tissue engineering and regeneration: from discovery to the clinic—an overview. *Tissue Eng. Part B: Rev* 17, 389–392.
- Orgaz, F., Dzika, A., Szycht, O., Amat, D., Barba, F., Becerra, J., et al., 2016. Surface nitridation improves bone cell response to melt-derived bioactive silicate/borosilicate glass composite scaffolds. *Acta Biomater.* 29, 424–434.
- Park, J., Lakes, R., 1992. *Biomaterials: An Introduction*, second ed. Plenum Press, New York.
- Peter, M., Binulal, N.S., Soumya, S., Nair, S.V., Furuike, T., Tamura, H., et al., 2010a. Nanocomposite scaffolds of bioactive glass ceramic nanoparticles disseminated chitosan matrix for tissue engineering applications. *Carbohydr. Polym.* 79, 284–289.
- Peter, M., Binulal, N.S., Nair, S.V., Selvamurugan, N., Tamura, H., Jayakumar, R., 2010b. Novel biodegradable chitosan–gelatin/nano-bioactive glass ceramic composite scaffolds for alveolar bone tissue engineering. *Chem. Eng. J.* 158, 353–361.
- Poh, P.S., Huttmacher, D.W., Holzapfel, B.M., Solanki, A.K., Stevens, M.M., Woodruff, M. A., 2016. *In vitro* and *in vivo* bone formation potential of surface calcium phosphate-coated polycaprolactone and polycaprolactone/bioactive glass composite scaffolds. *Acta Biomater.* 30, 319–333.
- Pon-On, W., Charoenphandhu, N., Teerapornpuntakit, J., Thongbunchoo, J., Krishnamra, N., Tang, I.M., 2014. Mechanical properties, biological activity and protein controlled release by poly (vinyl alcohol)—bioglass/chitosan–collagen composite scaffolds: a bone tissue engineering applications. *Mater. Sci. Eng. C* 38, 63–72.

- Pourhaghgouy, M., Zamanian, A., Shahrezaee, M., Masouleh, M.P., 2016. Physicochemical properties and bioactivity of freeze-cast chitosan nanocomposite scaffolds reinforced with bioactive glass. *Mater. Sci. Eng. C* 58, 180–186.
- Qin, C., Hu, Q., Li, Y., Wang, Z., Zhao, W., Louzguine-Luzgin, D.V., et al., 2016. Novel bioactive Fe-based metallic glasses with excellent apatite-forming ability. *Mater. Sci. Eng. C* 69, 513–521.
- Quinlan, E., Partap, S., Azevedo, M.M., Jell, G., Stevens, M.M., O'Brien, F.J., 2015. Hypoxia-mimicking bioactive glass/collagen glycosaminoglycan composite scaffolds to enhance angiogenesis and bone repair. *Biomaterials* 52, 358–366.
- Quintero, F., Mann, A.B., Pou, J., Lusquiños, F., Riveiro, A., 2007. Rapid production of ultralong amorphous ceramic nanofibers by laser spinning. *Appl. Phys. Lett.* 90, 153109.
- Quintero, F., Dieste, O., Pou, J., Lusquiños, F., Riveiro, A., 2009a. On the conditions to produce micro-and nanofibres by laser spinning. *J. Phys. D Appl. Phys.* 42, 065501.
- Quintero, F., Pou, J., Comesaña, R., Lusquiños, F., Riveiro, A., Mann, A.B., et al., 2009b. Laser spinning of bioactive glass nanofibers. *Adv. Funct. Mater.* 19, 3084–3090.
- Rabiee, S.M., Nazparvar, N., Azizian, M., Vashae, D., Tayebi, L., 2015. Effect of ion substitution on properties of bioactive glasses: a review. *Ceram. Int.* 41, 7241–7251.
- Rahaman, M.N., Day, D.E., Bal, B.S., Fu, Q., Jung, S.B., Bonewald, L.F., et al., 2011. Bioactive glass in tissue engineering. *Acta Biomater.* 7, 2355–2373.
- Rainer, A., Giannitelli, S.M., Abbruzzese, F., Traversa, E., Licoccia, S., Trombetta, M., 2008. Fabrication of bioactive glass–ceramic foams mimicking human bone portions for regenerative medicine. *Acta Biomater.* 4, 362–369.
- Rao, K.M., Kumar, A., Haider, A., Han, S.S., 2016. Polysaccharides based antibacterial polyelectrolyte hydrogels with silver nanoparticles. *Mater. Lett.* 184, 189–192.
- Rodriguez, O., Curran, D.J., Papini, M., Placek, L.M., Wren, A.W., Schemitsch, E.H., et al., 2016. Characterization of silica-based and borate-based, titanium-containing bioactive glasses for coating metallic implants. *J. Non-Cryst. Solids* 433, 95–102.
- Ross-Gillespie, A., Weigert, M., Brown, S.P., Kümmerli, R., 2014. Gallium-mediated siderophore quenching as an evolutionarily robust antibacterial treatment. *Evol. Med. Public Health* 2014, 18–29.
- Saboori, A., Sheikhi, M., Moztaazadeh, F., Rabiee, M., Hesarakhi, S., Tahriri, M., et al., 2009. Sol-gel preparation, characterisation and *in vitro* bioactivity of Mg containing bioactive glass. *Adv. Appl. Ceram.* 108, 155–161.
- Salinas, A.J., Vallet-Regí, M., 2016. Glasses in bone regeneration: a multiscale issue. *J. Non-Cryst. Solids* 432, 9–14.
- Sánchez-Salcedo, S., Shruti, S., Salinas, A.J., Malavasi, G., Menabue, L., Vallet-Regí, M., 2014. *In vitro* antibacterial capacity and cytocompatibility of SiO<sub>2</sub>–CaO–P<sub>2</sub>O<sub>5</sub> meso-macroporous glass scaffolds enriched with ZnO. *J. Mater. Chem. B* 2, 4836–4847.
- Saqaei, M., Fathi, M., Edris, H., Mortazavi, V., 2015. Preparation and biocompatibility evaluation of bioactive glass–forsterite nanocomposite powder for oral bone defects treatment applications. *Mater. Sci. Eng. C* 56, 409–416.
- Sethuraman, S., Nair, L.S., El-Amin, S., Nguyen, M.T., Singh, A., Krogman, N., et al., 2010. Mechanical properties and osteocompatibility of novel biodegradable alanine based polyphosphazenes: side group effects. *Acta Biomater.* 6, 1931–1937.
- Sethuraman, S., Nair, L.S., El-Amin, S., Nguyen, M.T., Singh, A., Greish, Y.E., et al., 2011. Development and characterization of biodegradable nanocomposite injectables for orthopaedic applications based on polyphosphazenes. *J. Biomater. Sci. Polym. Ed.* 22, 733–752.

- Shadjou, N., Hasanzadeh, M., 2015. Bone tissue engineering using silica-based mesoporous nanobiomaterials: recent progress. *Mater. Sci. Eng. C* 55, 401–409.
- Shah, F.A., Brauer, D.S., Hill, R.G., Hing, K.A., 2015. Apatite formation of bioactive glasses is enhanced by low additions of fluoride but delayed in the presence of serum proteins. *Mater. Lett.* 153, 143–147.
- Shah, A.T., Batool, M., Chaudhry, A.A., Iqbal, F., Javaid, A., Zahid, S., et al., 2016. Effect of calcium hydroxide on mechanical strength and biological properties of bioactive glass. *J. Mech. Behav. Biomed. Mater.* 61, 617–626.
- Sharifi, E., Azami, M., Kajbafzadeh, A.M., Moztarzadeh, F., Faridi-Majidi, R., Shamousi, A., et al., 2016. Preparation of a biomimetic composite scaffold from gelatin/collagen and bioactive glass fibers for bone tissue engineering. *Mater. Sci. Eng. C* 59, 533–541.
- Shelby, J.E., 2005. *Introduction to Glass Science and Technology*, second ed. The Royal Society of Chemistry, Cambridge.
- Singh, K., Bala, I., Kumar, V., 2009. Structural, optical and bioactive properties of calcium borosilicate glasses. *Ceram. Int.* 35, 3401–3406.
- Sittinger, M., Hutmacher, D.W., Risbud, M.V., 2004. Current strategies for cell delivery in cartilage and bone regeneration. *Curr. Opin. Biotechnol.* 15, 411–418.
- Stanley, H.R., Hench, L., Going, R., Bennett, C., Chellemi, S.J., King, C., et al., 1976. The implantation of natural tooth form bioglasses in baboons: a preliminary report. *Oral Surg. Oral Med. Oral Pathol.* 42, 339–356.
- Stark, W.J., Mädler, L., Maciejewski, M., Pratsinis, S.E., Baiker, A., 2003. Flame synthesis of nanocrystalline ceria–zirconia: effect of carrier liquid. *Chem. Commun.* 5, 588–589.
- Stoor, P., Söderling, E., Salonen, J.L., 1998. Antibacterial effects of a bioactive glass paste on oral microorganisms. *Acta Odontol. Scand.* 56, 161–165.
- Tallia, F., Gallo, M., Pontiroli, L., Bairo, F., Fiorilli, S., Onida, B., et al., 2014. Zirconia-containing radiopaque mesoporous bioactive glasses. *Mater. Lett.* 130, 281–284.
- Tang, Z.L., Wasserloos, K., Croix, C.M.S., Pitt, B.R., 2001. Role of zinc in pulmonary endothelial cell response to oxidative stress. *Am. J. Physiol. Lung Cell. Mol. Physiol.* 281, L243–L249.
- Tang, W., Lin, D., Yu, Y., Niu, H., Guo, H., Yuan, Y., et al., 2016. Bioinspired trimodal macro/micro/nano-porous scaffolds loading rhBMP-2 for complete regeneration of critical size bone defect. *Acta Biomater.* 32, 309–323.
- Tousi, N.S., Velten, M.F., Bishop, T.J., Leong, K.K., Barkhordar, N.S., Marshall, G.W., et al., 2013. Combinatorial effect of  $\text{Si}^{4+}$ ,  $\text{Ca}^{2+}$ , and  $\text{Mg}^{2+}$  released from bioactive glasses on osteoblast osteocalcin expression and biomineralization. *Mater. Sci. Eng. C* 33, 2757–2765.
- Uysal, T., Ustidal, A., Sonmez, M.F., Ozturk, F., 2009. Stimulation of bone formation by dietary boron in an orthopedically expanded suture in rabbits. *Angle Orthod.* 79, 984–990.
- Vaz, M.F., Canhão, H., Fonseca, J.E., 2011. *Bone: A Composite Natural Material*. INTECH Open Access Publisher.
- Veerapandian, M., Yun, K., 2009. The state of the art in biomaterials as nanobiopharmaceuticals. *Dig. J. Nanomater. Bios.* 4, 243–262.
- Viguet-Carrin, S., Garnero, P., Delmas, P., 2006. The role of collagen in bone strength. *Osteoporos. Int.* 17, 319–336.
- Vitale-Brovarone, C., Verne, E., Robiglio, L., Appendino, P., Bassi, F., Martinasso, G., et al., 2007. Development of glass–ceramic scaffolds for bone tissue engineering: characterisation, proliferation of human osteoblasts and nodule formation. *Acta Biomater.* 3, 199–208.

- Vitale-Brovarone, C., Verne, E., Baino, F., Ciapetti, G., Leonardi, E., Baldini, N., 2008a. Bioresorbable phosphate scaffolds for bone regeneration. *Key Eng. Mater.* 361, 241–244.
- Vitale-Brovarone, C., Verné, E., Robiglio, L., Martinasso, G., Canuto, R.A., Muzio, G., 2008b. Biocompatible glass–ceramic materials for bone substitution. *J. Mater. Sci. Mater. Med.* 19, 471–478.
- Wang, W.H., Dong, C., Shek, C.H., 2004. Bulk metallic glasses. *Mater. Sci. Eng. R* 44, 45–89.
- Wang, X., Li, X., Ito, A., Sogo, Y., 2011. Synthesis and characterization of hierarchically macroporous and mesoporous  $\text{CaO-MO-SiO}_2\text{-P}_2\text{O}_5$  ( $\text{M} = \text{Mg, Zn, Sr}$ ) bioactive glass scaffolds. *Acta Biomater.* 7, 3638–3644.
- Wegst, U.G., Schecter, M., Donius, A.E., Hunger, P.M., 2010. Biomaterials by freeze casting. *Philos. Trans. A Math. Phys. Eng. Sci.* 368, 2099–2121.
- Wei, G., Yan, X., Yi, J., Zhao, L., Zhou, L., Wang, Y., et al., 2011. Synthesis and in-vitro bioactivity of mesoporous bioactive glasses with tunable macropores. *Micropor. Mesopor. Mater.* 143, 157–165.
- Weinstein, A.M., Klawitter, J.J., Cook, S.D., 1980. Implant-bone interface characteristics of bioglass dental implants. *J. Biomed. Mater. Res.* 14, 23–29.
- Wilson, J., Pigott, G.H., Schoen, F.J., Hench, L.L., 1981. Toxicology and biocompatibility of bioglasses. *J. Biomed. Mater. Res. Part A* 15, 805–817.
- Wong, C.T., Chen, Q.Z., Lu, W.W., Leong, J.C.Y., Chan, W.K., Cheung, K.M.C., et al., 2004. Ultrastructural study of mineralization of a strontium-containing hydroxyapatite (Sr-HA) cement *in vivo*. *J. Biomed. Mater. Res. Part A* 70, 428–435.
- Wood, J.P., Osborne, N.N., 2003. Zinc and energy requirements in induction of oxidative stress to retinal pigmented epithelial cells. *Neurochem. Res* 28, 1525–1533.
- Wu, Z.Y., Hill, R.G., Yue, S., Nightingale, D., Lee, P.D., Jones, J.R., 2011. Melt-derived bioactive glass scaffolds produced by a gel-cast foaming technique. *Acta Biomater.* 7, 1807–1816.
- Wu, C., Zhou, Y., Fan, W., Han, P., Chang, J., Yuen, J., et al., 2012. Hypoxia-mimicking mesoporous bioactive glass scaffolds with controllable cobalt ion release for bone tissue engineering. *Biomaterials* 33, 2076–2085.
- Wu, C., Zhou, Y., Xu, M., Han, P., Chen, L., Chang, J., et al., 2013. Copper-containing mesoporous bioactive glass scaffolds with multifunctional properties of angiogenesis capacity, osteostimulation and antibacterial activity. *Biomaterials* 34, 422–433.
- Xiao, W., Zaem, M.A., Bal, B.S., Rahaman, M.N., 2016. Creation of bioactive glass (13–93) scaffolds for structural bone repair using a combined finite element modeling and rapid prototyping approach. *Mater. Sci. Eng. C* 68, 651–662.
- Xie, J., Blough, E.R., Wang, C.H., 2012. Submicron bioactive glass tubes for bone tissue engineering. *Acta Biomater.* 8, 811–819.
- Xu, C.Y., Inai, R., Kotaki, M., Ramakrishna, S., 2004. Aligned biodegradable nanofibrous structure: a potential scaffold for blood vessel engineering. *Biomaterials* 25, 877–886.
- Xynos, I.D., Edgar, A.J., Buttery, L.D., Hench, L.L., Polak, J.M., 2001. Gene-expression profiling of human osteoblasts following treatment with the ionic products of Bioglass® 45S5 dissolution. *J. Biomed. Mater. Res. Part A* 55, 151–157.
- Yamaguchi, M., 1998. Role of zinc in bone formation and bone resorption. *J. Trace Elem. Exp. Med.* 11, 119–135.
- Yao, A., Wang, D., Huang, W., Fu, Q., Rahaman, M.N., Day, D.E., 2007. *In vitro* bioactive characteristics of borate-based glasses with controllable degradation behavior. *J. Am. Ceram. Soc.* 90, 303–306.

- Yazdanpanah, A., Kamalian, R., Moztarzadeh, F., Mozafari, M., Ravarian, R., Tayebi, L., 2012. Enhancement of fracture toughness in bioactive glass-based nanocomposites with nanocrystalline forsterite as advanced biomaterials for bone tissue engineering applications. *Ceram. Int.* 38, 5007–5014.
- Yazdimamaghani, M., Razavi, M., Vashaei, D., Pothineni, V.R., Rajadas, J., Tayebi, L., 2015. Significant degradability enhancement in multilayer coating of polycaprolactone-bioactive glass/gelatin-bioactive glass on magnesium scaffold for tissue engineering applications. *Appl. Surf. Sci.* 338, 137–145.
- Zberg, B., Uggowitzer, P.J., Löffler, J.F., 2009. MgZnCa glasses without clinically observable hydrogen evolution for biodegradable implants. *Nat. Mater.* 8, 887–891.
- Zeimaran, E., Pourshahrestani, S., Shirazi, S.F.S., Pingguan-Murphy, B., Kadri, N.A., Towler, M.R., 2016. Hydrothermal synthesis and characterisation of bioactive glass-ceramic nanorods. *J. Non-Cryst. Solids* 443, 118–124.
- Zhao, N.R., Wang, Y.J., Chen, X.F., Yang, Y.X., Wei, K., Wu, G., 2005. Preparation of bioactive nanoparticles in the system CaO–P<sub>2</sub>O<sub>5</sub>–SiO<sub>2</sub> using microemulsions. *Key Eng. Mater.* 288–289, 179–182.
- Zhou, H., Lee, J., 2011. Nanoscale hydroxyapatite particles for bone tissue engineering. *Acta Biomater.* 7, 2769–2781.

# Mechanical and wear properties of nano titanium based dental composite resin

# 14

**Rajul Vivek<sup>1</sup>, Ashish Kumar<sup>2</sup>, Thakur Prasad Chaturvedi<sup>1</sup> and Rajiv Prakash<sup>2</sup>**

<sup>1</sup>*Faculty of Dental Science, Institute of Medical Sciences, Banaras Hindu University, Varanasi, India* <sup>2</sup>*School of Materials Science and Technology, Indian Institute of Technology (Banaras Hindu University), Varanasi, India*

## 14.1 INTRODUCTION

Dental health has become more significant recently due to many diseases directly related to the oral cavity like cardiovascular, neurological, and respiratory diseases, many medical conditions, etc. In this respect, particularly polymeric restorative materials have received meticulous attention among numerous researchers, whose their aim has been to replace or restore missing or decayed tooth structure satisfying esthetic and functional needs at ambient conditions. In general, natural appearance; low cost with good shelf life; absence of odor, taste, or toxicants; resistance to water or bacterial growth; good mechanical strength; and good thermal conductivity are the main requirements for denture materials (McCabe and Walls, 2013; Marghalani, 2016; Sideridou et al., 2011; Kirmanidou et al., 2016). Particularly the prostheses made from resin based polymeric materials are most common because of their fair ability to mold at ordinary conditions with tremendous esthetic emergence and suitable physical properties in most clinical conditions (Bouillaguet et al., 2002; Jandt and Sigusch, 2009; Ferracane, 2013; Leprince et al., 2013; Swain et al., 2016).

To date, polymethyl methacrylate (PMMA) alone, modified PMMA, polyamide, polyethylene terephthalate (PET), etc. have been used as potential matrix for denture preparations. But polyamides still disqualify the criteria of standard PMMA due to poor modulus (Ucar et al., 2012). On the other hand, PET has lower toughness, lower fracture resistance, and poor color stability to PMMA (Takabayashi, 2010; Hamanaka et al., 2011). Therefore, these two materials are still under clinical trial for their biocompatibility and mechanical properties.

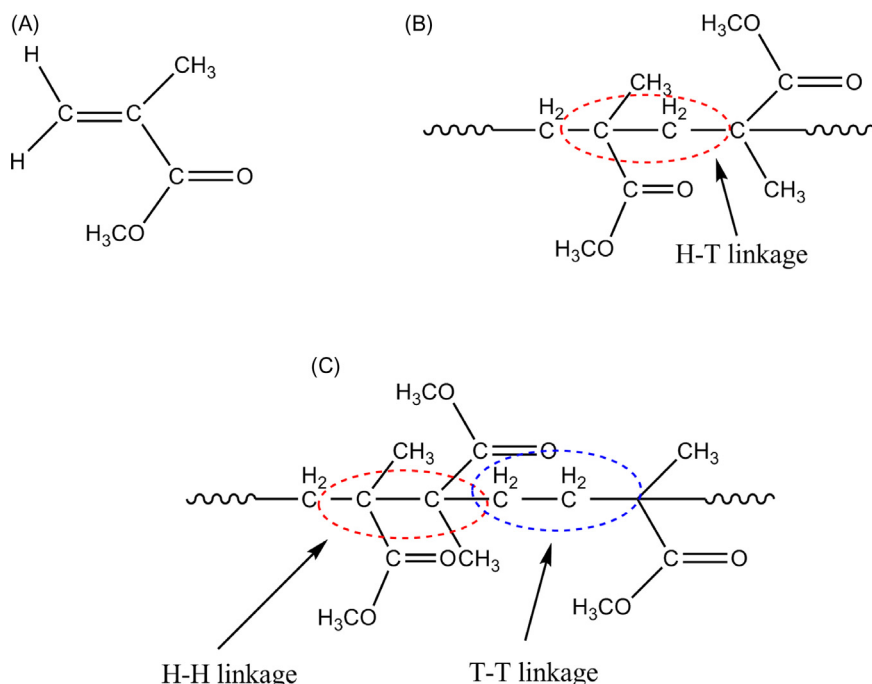


During the last few years, various polymeric PMMA resin matrixes (alone or in modified form) as powder along with polymerizable monomer are being used due to the matching of appropriate criteria for dentistry materials (see Section 1.1 for details). These include PMMA alone, polyethyl methacrylate (PEMA), polycarbonate, mixture of PEMA and diethyl phthalate, etc. as powder and ethylene glycol dimethacrylate, mixture of MMA and 1,4-butanediolmethacrylate, urathene ethylene dimethacrylate, butyl methacrylate, etc. as monomer (Mutluay et al., 2005). These materials consist of prominent drawbacks like swollen layers of variable thicknesses when coming in contact with a solvent used or monomer used, which usually diffuses into the polymer. The phenomenon of diffusion frequently depends on exposure time, temperature of the solvent, type of the solvent/monomer used, structure of polymer, and their glass transition temperature. This problem is due to the formation of composite materials. But this type of composite, especially in mandibular molars and premolars teeth, still has inadequate success due to deficient materials' properties. For example, low wear resistance resulting in a loss of tooth anatomy under disturbed occlusion, fracture within the body of the restorations and margins, and marginal leakage due to polymerization shrinkage are often considered as the common causes of failure especially in mandibular molar tooth composite restorations (Dupriez et al., 2015; Miculescu et al., 2015; Libeck et al., 2016). So these drawbacks have been rectified by introduction of some foreign materials like metals (silver, titanium, gold), metal oxide (Yttrium stabilized zirconia) or fibers along with use of appropriate coupling agents. The alteration of filler (by decreasing filler size and increasing filler content) in the matrix is one of the ways to improve mechanical and wear properties (De Souza, 2015).

### 14.1.1 POLYMETHYLMETHACRYLATES: A PROMINENT DENTURE MATRIX

PMMA is a homopolymer formed by polymerization of methyl methacrylate molecule as its repeating unit (as shown in Fig. 14.1). It is basically optically transparent and scratch resistant in nature. Due to the presence of a methyl group, it is not closely packed in its polymeric state. That is why it is noncrystalline. It has been reported that sterically hindered head-to-head or tail-to-tail adduct is less favored over head-to-tail adduct (Ali et al., 2015). Further on the basis of tacticity (a stereochemistry of adjacent chiral centers), there are three types of product possible in head-to-tail adduct, namely, *atactic*, *syndiotactic*, and *isotactic* (as shown in Fig. 14.2). Radical polymerization moderately favors *syndiotactic* head-to-tail adduct via lesser hindered radical intermediate (Ferguson and Ovenall, 1987), while stereo-complex adduct has been formed when polymerization is carried out in presence of Grignard type's of catalysts (Miyamoto and Inagaki, 1970).

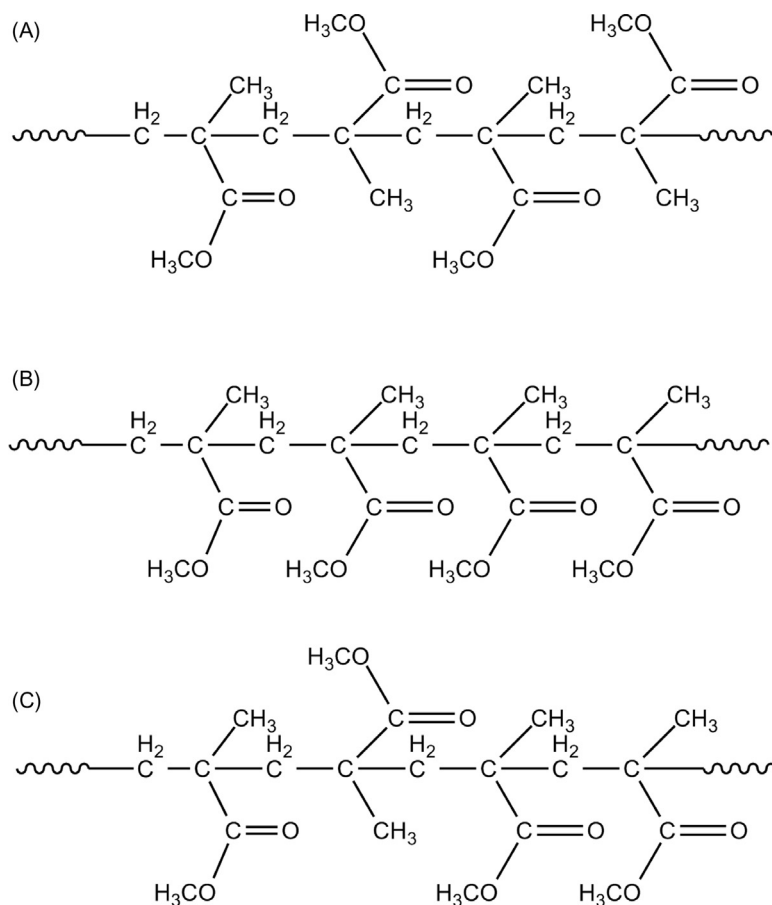
Dental acrylic materials consist of a solid component, traditionally called "powder," (PMMA, or its modified form) and a liquid component, traditionally

**FIGURE 14.1**

Chemical structure of (A) methyl methacrylate monomer, (B) head-to-tail (H-T) polymerized PMMA, and (C) head-to-head (H-H) or tail-to-tail (T-T) polymerized PMMA.

called “monomer,” (methyl methacrylate, or its modified form), and are one of the most frequently used dental applications. This is due to their low cost, acceptable esthetics, good processability, and stability in the oral environment. The most common uses of this material are fabrication of denture base, border seal of cavities, and provisional crowns. The powder contains usually reaction initiator moiety that is capable of polymerizing liquid monomers and changed into solid mass followed by different physical and chemical stages of polymerization under given conditions. Physical stages involve sandy, sticky, doughy, rubbery, and stiff stages while chemical stages involve induction, propagation, chain transfer, and termination as shown in Fig. 14.3.

It has been believed that alone PMMA undergoes flexural fatigue due to formation of stress concentration around the microcracks and then its propagation along the cracks, developed from continuous application of small forces and its repetitive nature. This type of fracture is most likely due to accidental dropping of denture materials by the patients. At the same time PMMA exhibits shrinkage properties upon thermal curing. Researchers have attempted to change his behavior by modifications of PMMA with SBR grafting or blending with other polymers like vinyl acrylics, light-activated urethane dimethacrylate, polyamides,

**FIGURE 14.2**

Conformation of various (H-T) polymerized PMMAs in (A) syndiotactic, (B) isotactic, and (C) atactic form.

epoxy resins, polystyrene, polyethylene (PE) and polycarbonate, and nylon (Alhareb et al., 2015; Durkan et al., 2013; Ladizesky et al., 1993; Tanoue et al., 2005; Borges et al., 2015). However flexural strength of as-modified materials was not much as better than PMMA itself. So incorporation of fillers is another choice to modify its mechanical and thermal properties and biocompatibility under clinical environment.

### 14.1.2 NANOFILLERS

The restorative materials that are biocompatible to oral mucosa, and have excellent physical properties (sufficient impact strength, good flexural strength and

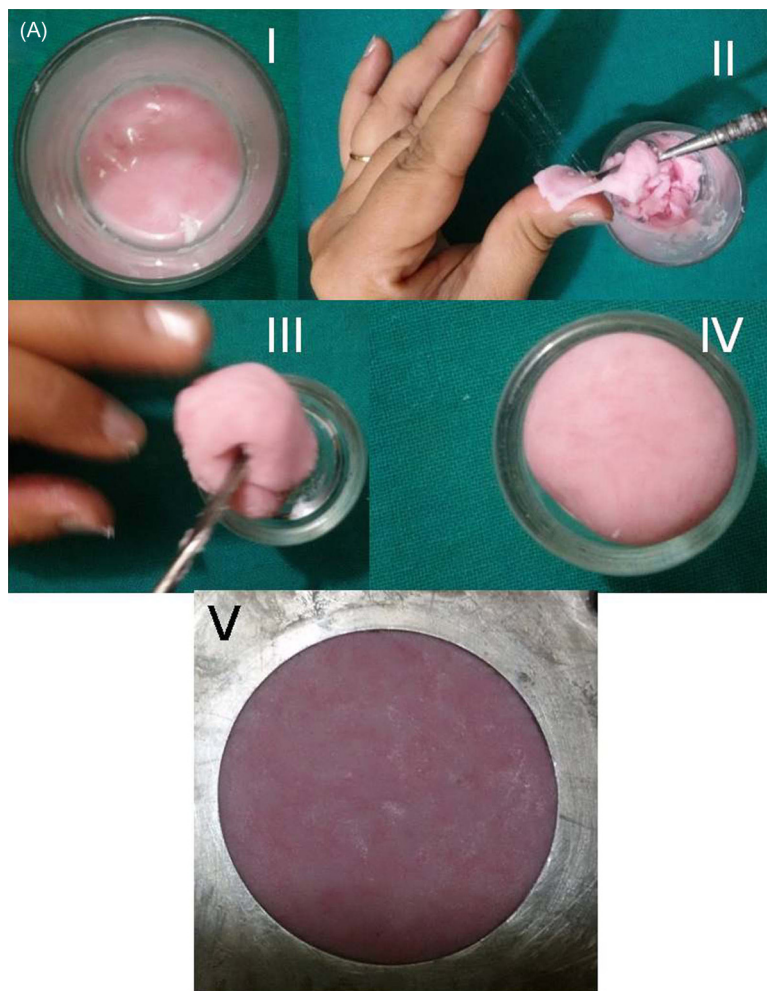


**FIGURE 14.3**

Various (A) physical and (B) chemical changes during polymerization of liquid using powder.

hardness), excellent esthetics, and good dimensional accuracy are considered as ideal for dental application. Here, except mechanical properties, PMMA fulfills all the criteria to succeed under clinical service. Therefore various strategies have been reported to date to improve the mechanical properties. This includes basically either advancement of an alternative material to PMMA or chemical manipulation of PMMA or even addition of filler to PMMA. However addition of filler is much better than other strategies to get the multifunctional properties of as-developed denture material.

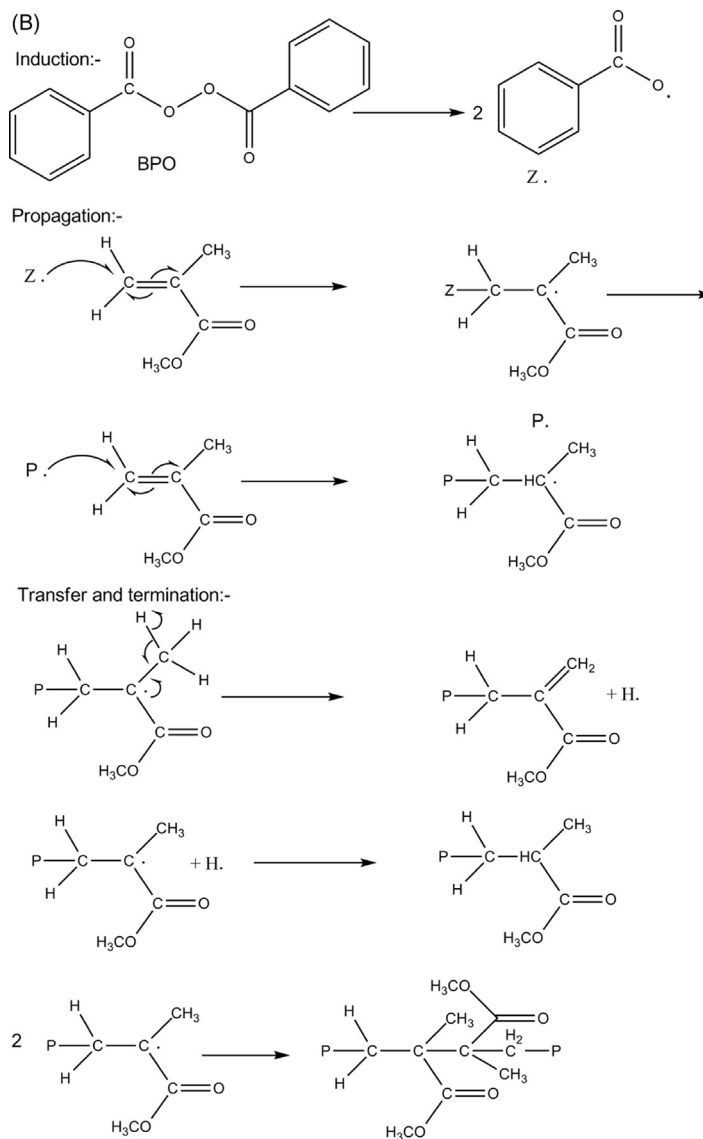


FIGURE 14.3

(Continued).

#### 14.1.2.1 Metal and metal oxide filler

It is without doubt that the mechanical strengths and thermal properties have been significantly improved by incorporation of metals or their alloys in wire or powder form and metal oxides. Actually the main purpose of adding these fillers is to

improve thermal properties and to decrease the curing shrinkage. Salts of gold, silver, platinum, copper, and palladium are used as filler in PMMA matrix to change the mechanical and color change properties (Nam, 2014; Nandish et al., 2016; Jagger et al., 1999). Herein, the authors observed increase in the bending deflection with the addition of silver and platinum, and decreased with the addition of palladium. Similarly, Vickers hardness increased with the addition of palladium and the color differences increased with increasing thermal treatment temperature (Aoyagi et al., 2015). These behavioral changes may be due to poor bonding between the metallic surface and resin matrix. Therefore coupling agents are used to solve bonding problems between filler and matrix. For example in PMMA/ZrO<sub>2</sub>–Al<sub>2</sub>O<sub>3</sub>–SiO<sub>2</sub> system composite, chitosan, and trimethoxy(propyl) silane are used individually as coupling agents to improve the hardness of resulting composite as  $18.75 \pm 2.05$  VHN and  $19.43 \pm 1.89$  VHN, respectively (Hasratningsih et al., 2016). However, it has been observed that hardness and bending strength of PMMA based composite is not good enough to achieve the best quality denture material. Various physiological and mechanical factors like attrition, abrasion, disturbed occlusion, fatigue, impact, etc. might be involved in a denture fracture. Among them, flexural fatigue and impact are most common failure mechanisms of PMMA based composite denture material. Extensive studies have been carried out yet to improve the flexural strength of PMMA with the addition of some filler of different shape and size or some modification in its processability; although, few improvements in their results are observed, which are limited in a certain extent to the some mechanical properties at the cost of other properties like biocompatibility.

#### 14.1.2.2 Fiber filler

Synthetic as well as natural fibers have been and are being used alone or in bundles as reinforcing agents in the composites. Synthetic fibers like carbon fiber, glass fiber, nylon, PE, PVA fiber, etc. create harsh environmental and health hazard problems for the workers employed in the preparation of their corresponding composites (Wang et al., 2014; Zhang and Matinlinna, 2012; Khan et al., 2015; Bocalon et al., 2016; John et al., 2015; Borges et al., 2015). The main drawbacks of carbon and aramid fiber are their difficulty in finishing and polishing, complicated surface treatment (in case of PE), and unpleasant emergence, which limit their usage as filler and thus the need for glass fiber. However, except for its excellent esthetic appearance, glass fiber possesses poor wettability in PMMA matrix and bad impact resistance. Therefore, prior to composite formation, a number of works have been reported based on modification of glass fiber surface to reduce the aforesaid issues.

Incorporation of natural fibers obtained from plants, crops, animals, or other sources and natural ceramics like seashells is one of the alternatives to reduce the issue of mechanical strength. Apart from this, natural fiber is considered as economic, nonhazardous, noncarcinogenic, renewable, and biodegradable in nature. A major goal of natural fiber based composite is to alleviate the need to use expensive artificial fibers that are dependent on nonrenewable sources.

### 14.1.3 RECENT SCENARIO OF NANOFILLER-BASED POLYMETHYL METHACRYLATE COMPOSITE FOR DENTIST

#### 14.1.3.1 Mechanical properties

To achieve all of the required properties in a single material, modification in materials are required. For example fibers and/or metal and their oxides are being incorporated to increase the mechanical and thermal properties of PMMA. Of the number of experimental advances to date, it has been reported that the addition of metal nanoparticles to PMMA matrix results in an increase in the surface hydrophobicity and reduction of the adherence to biomolecules (Cobb et al., 2000). Many metals (e.g., silver, cobalt chromium etc.), metal alloys (e.g., Ag–Au–Pd, Ni–Cr, Co–Cr, Ti–6Al–4V, Au–Ag–Pt, etc.) and metal oxides (e.g., aluminum dioxide, zinc oxide, zirconia, titania, etc.) have been used in experiments to improve the mechanical properties of PMMA (Gates et al., 1993; Kern and Thompson, 1994). However the concept of use of coupling agent has been incorporated to improve the debonding properties between filler and PMMA matrix.

Recently, extensive work is being done on biomolecules incorporated in polymer reinforced PMMA as a biocomposite to fulfill the biocompatibility criterion. For example PLA reinforced PMMA-hydroxyapatite composite is able to sustain human gingival fibroblast cells' growth suggesting its excellent biocompatibility (Radha et al., 2017).

A recent literature survey related to mechanical properties based on filler reinforced PMMA dental composite is tabulated in Table 14.1. On the basis of this table, it can be seen that a number of works have been done using ceramic and glass filler based PMMA composites towards the modification of mechanical properties. However, few works have been reported for the mechanical properties based on nanometals incorporated PMMA composite.

#### 14.1.3.2 Wear properties

Wear is the progressive loss in material or its surface caused by relative mechanical or chemical action. This includes erosion, abrasion, attrition, etc. Particularly in dentistry, intensive work has been conducted to build up an understanding towards wear resistance in a successful design and a choice of restorative dental materials. The methods that are most commonly used to study the tribological behavior of restorative materials are ball-on-disc, block-on-disc, and pin-on-disc, as shown schematically in Fig. 14.4.

Generally, in resin composites, wear process depends on distribution of filler, size of filler, and filler–matrix interaction (Zeng et al., 2005). For example, well-distributed fine particles (nanosized) protect the softer resin from abrasion and hence have good wear resistance (Zeng et al., 2005). Moreover poor interaction between filler and matrix causes plucking out of filler from matrix (Lambrechts et al., 2006). Fragile filler can pulled out from the surface of the resin composite and causes fast abrasion (Lambrechts et al., 2006), while wear resistance of

**Table 14.1** Mechanical Test Results of Denture Composites from Common Matrix and Fillers

Matrix Used	Filler Used	Flexural Strength (in Mpa)	Hardness (in kgfmm <sup>-2</sup> )	Fracture Toughness (in Mpam <sup>1/2</sup> )	Flexural Modulus (in GPa)	Tensile Modulus (in GPa)	References
<b>A. Metal and metal oxide filler</b>							
PMMA/MMA	Ag	92.27	—	—	—	—	(Han et al., 2015)
TEGDMA/bis-GMA	Ag supports hydroxylapatite	132.0	—	—	6.6	—	(Ai et al., 2017)
<b>B. Ceramic filler</b>							
PMMA/EGDMA	BaTiO <sub>3</sub>	98 Mpa	22.84	—	2.75	2.42	(Nidal et al., 2016)
TEGDMA/bis-GMA	Silica	125	—	—	21.8	—	(Rezvani et al., 2016)
TEGDMA/bis-GMA	SiO <sub>2</sub>	128	—	—	3.75	—	(Wang et al., 2016a,b)
UDMA/ bis-EMA	ZrO <sub>2</sub> -SiO <sub>2</sub> -YbF <sub>3</sub>	119.0	—	2.4	12.6	—	(Bijelic-Donova et al., 2016)
PMMA/MMA/EGDMA	Al <sub>2</sub> O <sub>3</sub> /YSZ	—	—	2.58	—	—	(Alhareb et al., 2015)
TEGDMA/bis-GMA	Barium glass + colloidal silica filler	153.3	—	2.2	13.7	—	(Tsujimoto et al., 2016)
PMMA/MMA	Nanoclay	652.0	—	—	23	—	(Mortazavi et al., 2012)
TEGDMA/bis-GMA	TiO <sub>2</sub>	—	—	1.8	—	—	(Dafar et al., 2016)

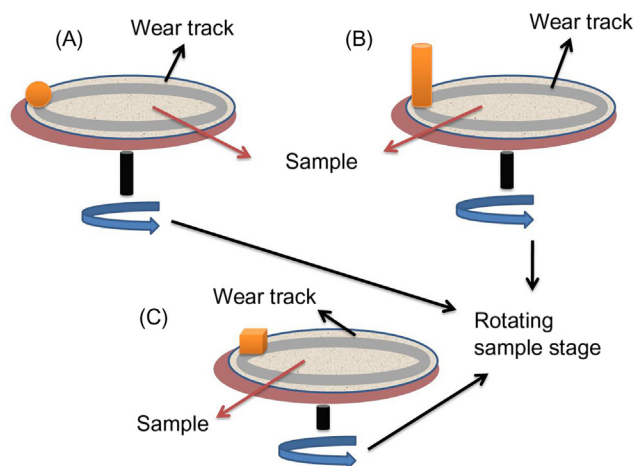
(Continued)



**Table 14.1** Mechanical Test Results of Denture Composites from Common Matrix and Fillers *Continued*

Matrix Used	Filler Used	Flexural Strength (in Mpa)	Hardness (in kgfmm <sup>-2</sup> )	Fracture Toughness (in Mpam <sup>1/2</sup> )	Flexural Modulus (in GPa)	Tensile Modulus (in GPa)	References
<b>C. Synthetic fiber</b>							
Polypropylene	Glass fiber	217.6	—	—	7.42	—	(Nagakura et al., 2017)
PMMA/bis-GMA	Glass fiber	155.0	—	4.7	3.9	—	(Lassila et al., 2016)
PMMA/bis-GMA	Glass fiber	108.0	—	2.75	—	—	(Bocalon et al., 2016)
TEGDMA/bis-GMA	E-glass fiber	259.91	—	—	—	—	(Fonseca et al., 2016)
MMA/bis-GMA	ZrO <sub>2</sub> fiber	—	26.99;	2.31	—	—	(Wang et al., 2016a,b)
PMMA/MMA	E-glass fiber	167.33	—	—	—	—	(Mathew et al., 2014)
<b>D. Natural fiber</b>							
PMMA	Oil palm fiber	95.60	—	—	5.40	—	(John et al., 2015)
PMMA/MMA	Seashell filler	—	25.12	—	—	—	(Karthick et al., 2014)

Abbreviations: MMA = Methyl methacrylate, TEGDMA = Triethylene glycol dimethacrylate, bis GMA = 2,2-bis[4-(2-hydroxy-3-methacryloxyprop-1-oxy)phenyl] propane, UDMA = urethane dimethacrylate.

**FIGURE 14.4**

Schematic representation of different wear mode based on (A) ball-on-disc, (B) pin-on-disc, and (C) block-on-disc.

composite decreases with increase in volume percentage of filler (Wang et al., 2003). On the other hand, the composition of polymeric matrix also plays an important role in the wear rate. For example, UEDMA/TEGDMA combination exhibits higher wear resistance than TEGDMA/bis-GMA (Lambrechts et al., 2006). It has been believed that denture resins are softer than tooth enamel and as such are too susceptible to abrasion when contacted to counter surfaces in presence of dentifrices like toothpaste or other cleaning agents (Ghazal et al., 2008). The toothpaste can accelerate the process of abrasion and depends on the properties of abrasive particles present in the composition of the paste. Therefore a cycle of wear is already well recognized in other applications like teeth materials, but has received relatively little attention in metal incorporated resin matrix denture materials. Recently, sliding wear resistance test has been performed on composition of various barium glass and colloidal silica filler in TEGDMA/bis-GMA matrix and observed higher resistance from wear with low filler content (Souza et al., 2016).

In the literature survey, we observed that there is a large amount of research work based on incorporation of various types of fillers like polymeric, metallic, nonmetallic, etc. that has been done to improve several materials' properties and clinical durability. However, long-term clinical durability and proper thermal conductivity are still a challenge for researchers. In this chapter we present our part of the research work that is based on tensile properties, thermal stability, and wear properties of as-prepared nano Ti/PMMA composite denture material.

---

## 14.2 EXPERIMENTAL

### 14.2.1 MATERIALS

DPI heat cured veined acrylic resin containing nylon fiber reinforced PMMA resin powder was purchased from Dental Product India, India. Titanium (Ti) powder (size = 50 nm) was purchased from SRL, India.

### 14.2.2 PREPARATION OF TI/POLYMETHYL METHACRYLATE COMPOSITE

Various nano Ti/nylon fiber reinforced PMMA composites were prepared by simple mixing of powder containing nano Ti (0.25%, 0.50%, 0.75%, and 1.00% by weight) and liquid in 2:1 weight ratio and followed by curing of resulting mixture in water bath for 40 minutes at 100°C. After that, all composites were preserved for further studies.

### 14.2.3 CHARACTERIZATION

Uniaxial tensile testing of as-prepared composites is carried out on Instron 3369 tensile machine, United States @1.5 mm/minute at room temperature using ASTM standard (D-638, type IV) dog bone sample (gauge length = 33.0 mm, thickness = 3.0 mm, and width = 6.0 mm). The entire dog bone sample is casted in their sandy stage. Morphological analysis of fractured area is analyzed by scanning electron microscope (SEM), Ziess, EVO18 Research, Germany. Prior to SEM analysis, a thin coating of Au–Pd alloy is deposited over the sample to dissipate the exposed electrons. Thermal analysis is done on Mettler Toledo (TGA/DTA STARe system, Switzerland) from 30°C to 800°C at the heating rate of 10°C/minute in N<sub>2</sub> gas environment. Wear tests are performed on Universal Tribometer, Rtech instruments, United States.

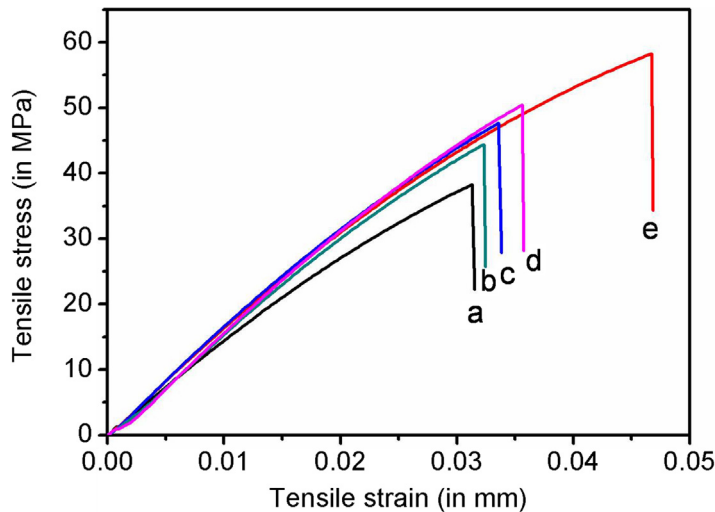
---

## 14.3 RESULTS AND DISCUSSION

### 14.3.1 MECHANICAL ANALYSIS

#### 14.3.1.1 Tensile test

The typical strain–stress of all samples is shown in [Fig. 14.5](#). From this graph, it is evident that the strain to failure property of Ti/PMMA composite is higher than pure PMMA and gradually increases with increase in nano Ti weight percent. The tensile parameters of pure PMMA and all as-prepared composites are shown in [Table 14.2](#). From this table it can be seen that the tensile strength of material has increased by 65% by incorporation of 1% nano Ti particles compared with pure PMMA.

**FIGURE 14.5**

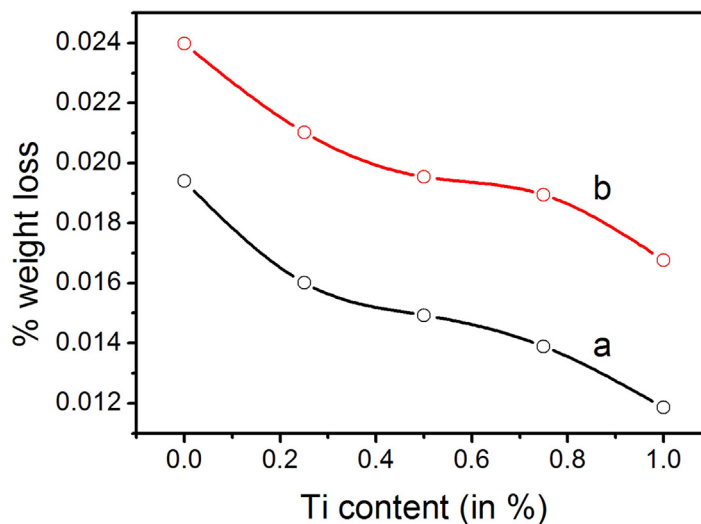
Strain–stress curve of pure PMMA (a) and various 0.25%–1.00% Ti/PMMA composites (b–e).

**Table 14.2** Tensile Test Parameters of Pure PMMA and Various Ti/PMMA Composites

Sample	Modulus (MPa)	Maximum Load (N)	Tensile Strength (in MPa)	Energy at Break (in J)
Pure PMMA	1488.55426	689.16623	38.287	0.38908
0.25% Ti/PMMA	1617.72319	798.92045	44.384	0.45430
0.50% Ti/PMMA	1651.26721	893.81365	49.656	0.57333
0.75% Ti/PMMA	1673.75264	908.70066	50.483	0.56609
1.00% Ti/PMMA	1691.34677	1049.05060	58.280	0.92128

### 14.3.1.2 Wear test

Good wear resistance characteristics of dental materials are very important because poor wear resistance may cause occlusion disharmony. Therefore, to check the wear resistance of our as-synthesized composite in presence of commercial toothpaste, a circular composite specimen of diameter = 6.0 cm was attrited with commercially available steel ball (diameter = 10.0 mm) mounted to machine. Thus this assembly gives a model of pin-on-disc type attrition. The tribological responses are carried out against force = 12 N and 15 N at 300 rpm for 600 seconds, which is considered as average value for brushing over dentistry region. The relative weight loss of different composites at two different forces is shown in Fig. 14.6. Except the larger loss at higher applied force, the trend of

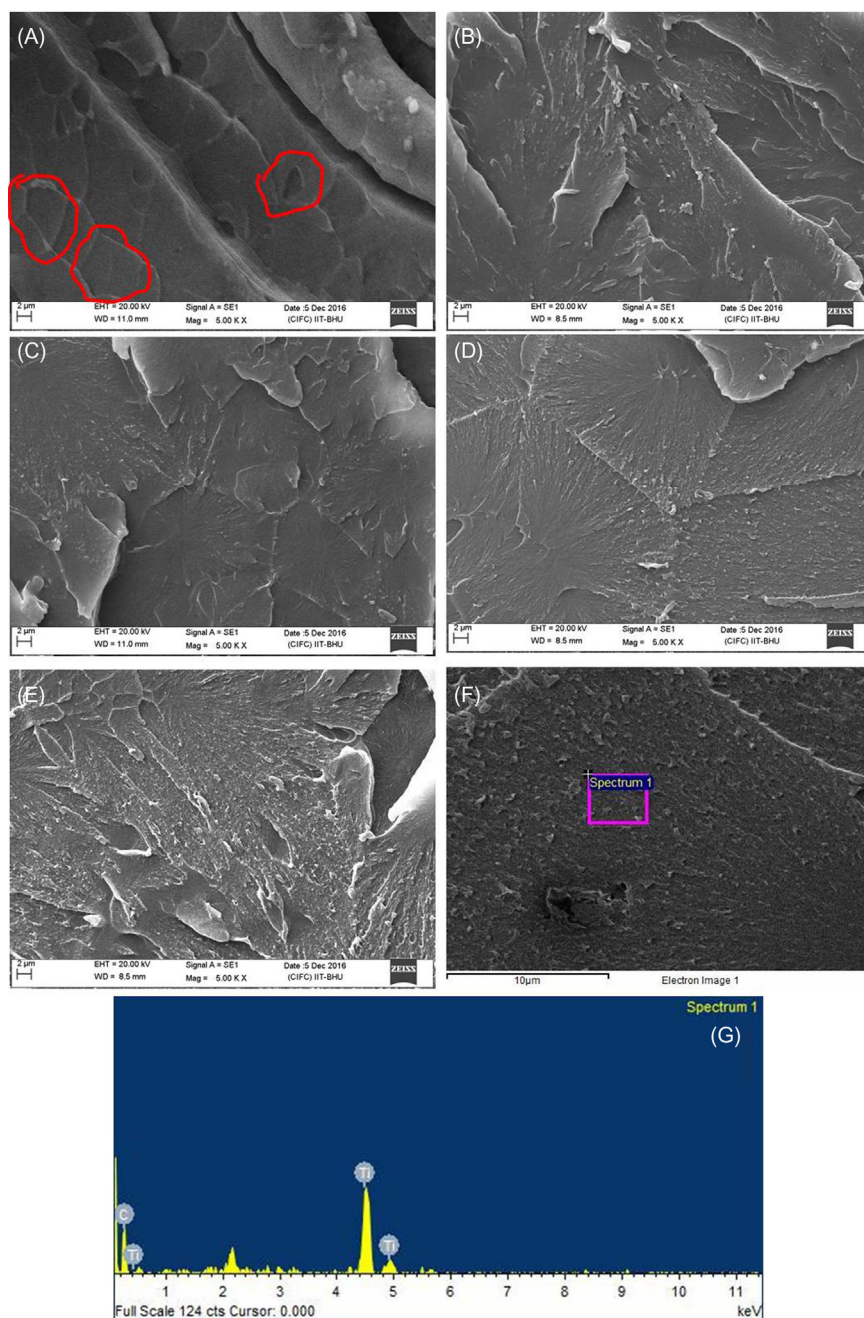
**FIGURE 14.6**

% Weight loss in materials on application of (a) 12 N and (b) 15 N force.

relative weight loss is almost the same in either case of applied force. Therefore it can be concluded that the wear resistance of as-prepared material increases with increase in Ti content.

### 14.3.2 MORPHOLOGICAL ANALYSIS

After the tensile test, microstructural analysis of fractured surface of pure PMMA and its various composites were performed by SEM (as shown in Fig. 14.7A–E) to study the failure mode of the samples. Fig. 14.7A shows failure mechanism of pure PMMA is highly brittle failure mode with crazing due to microvoids (as shown by red ovals). However, the introduction of nano Ti in PMMA matrix associated with better absorbing energy results in localized shear yielding. One can observe the directional particle pinning of the microcracks leaving behind a tail-like structure that latter collides with available voids and causes failure of the material (Ash et al., 2000). However, upon gradual addition of nanofiller, microvoids are diminished gradually and the particle pinning mechanism mainly dominates over the voids. That is why the tensile strength is expected to increase upon increase in filler. The involvement of nano Ti particles in the tail-like structure was confirmed by EDX as indicated by the pink square area in Fig. 14.6f,g. The EDX spectrum exhibits characteristic X-ray produced corresponding to  $L_{\alpha}$ ,  $K_{\alpha}$ , and  $K_{\beta}$  at 0.42, 4.50, and 4.85 keV, respectively (Rokosz et al., 2016).

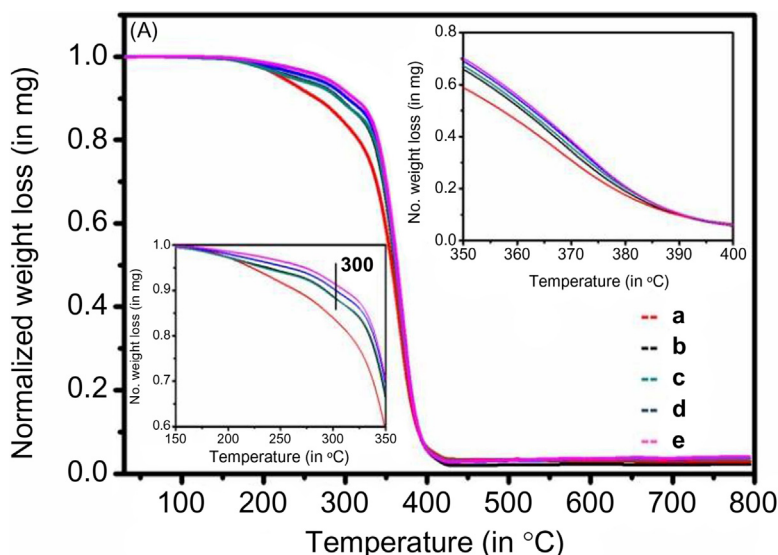
**FIGURE 14.7**

SEM image for fractured portion of pure PMMA (A), 0.25–1.00% Ti/PMMA composite (B–E) at similar magnifications and EDX of 1.00% Ti/PMMA composite (F and G).

### 14.3.3 THERMAL ANALYSIS

The influence of nano Ti incorporation in PMMA matrix was examined by TGA/DTA analysis and their respective curves are shown in Fig. 14.8. Fig. 14.8A shows the TGA curves for pure PMMA and its nanocomposites formed by nano Ti incorporation. The thermal decomposition of pure PMMA and its nanocomposites proceed in single stage in the temperature range from 280°C to 420°C due to scission of the main chain (Demir et al., 2006; Laachachi et al., 2009). Apart from this, except pure PMMA, all nanocomposites exhibit another weak peak at 300°C due to structural changes to the vicinity of nano Ti (see Fig. 14.8B for more details). The presence of nano Ti in PMMA matrix did not amend the complete degradation mechanism but did improve the thermal resistance. It means that extent of crosslinking in the matrix is almost the same even after nano Ti incorporation. To quantify the thermal resistance, and total loss, onset thermal decomposition ( $T_{\text{onset}}$ ), temperature at 50% weight loss ( $T_{50}$ ) and % residue at 800°C are calculated and summarized in Table 14.3.

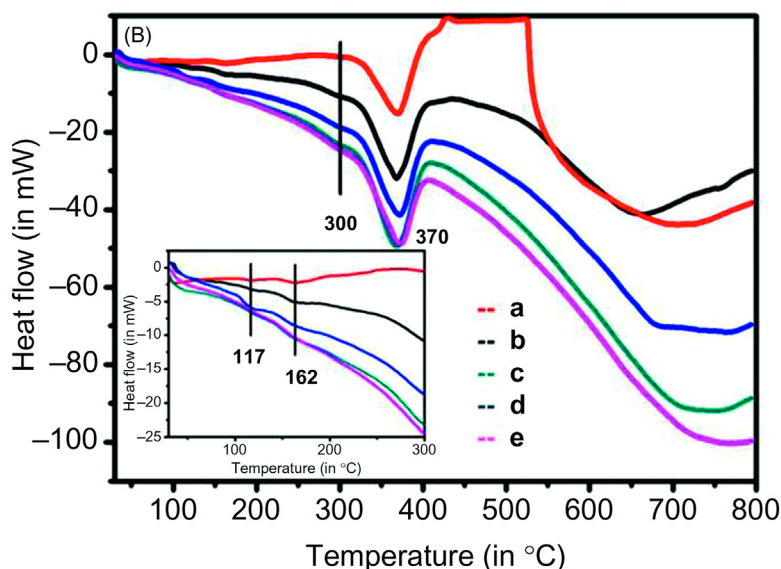
Fig. 14.8B shows DTA thermograms of pure PMMA and its composites. The important parameters derived from the study are shown in Table 14.3. In general, PMMA exhibits two endothermic peaks: one weak peak at lower temperature for  $T_g$  (transition from glassy to rubbery phase) and another strong peak at higher



**FIGURE 14.8**

(A) TGA curve and (B) DTA of (a) bare PMMA matrix, (b) 0.25% Ti/PMMA composite, (c) 0.50% Ti-PMMA composite, (d) 0.75% Ti-PMMA composite, and (e) 1.00% Ti-PMMA composite. Inset of figure shows zoomed view of similar curves to present various thermal changes.



**FIGURE 14.8**

(Continued).

**Table 14.3** Thermal Parameters of Pure PMMA and Different Ti/PMMA Composites

Sample	$T_{\text{onset}}$ (in °C)	$T_{50}$ (in °C)	% Residue at 800°C	$T_{g1}$ (in °C)	$T_{g2}$ (in °C)	$T_{g3}$ (in °C)
PMMA	332.13	357.0	2.1	117.0	162.0	—
0.25% Ti/PMMA	333.48	361.0	2.9	117.0	162.5	300.0
0.50% Ti/PMMA	334.02	362.1	3.52	116.82	162.0	300.0
0.75% Ti/PMMA	337.12	363.3	3.64	117.43	162.0	300.0
1.00% Ti/PMMA	338.17	364.0	3.92	117.0	161.7	300.0

temperature for complete decomposition of polymer chain. Usually, these exothermic peaks depend on the molecular weight and tacticity of the polymer. For example, the  $T_g$  peak for bulk isotactic form is  $\sim 60^\circ\text{C}$  and for bulk syndiotactic form is  $\sim 150^\circ\text{C}$ . However for bulk atactic having approximately 60% syndiotactic, the  $T_g$  value lies between  $110^\circ\text{C}$  and  $115^\circ\text{C}$  (Roth et al., 2006). In our case, we observed two  $T_g$ s (say  $T_{g1}$  and  $T_{g2}$ ) in pure PMMA and all composite materials (as shown in the inset of Fig. 14.8B). The  $T_{g1}$  peak observed at  $117^\circ\text{C}$  is corresponding to the bulk atactic conformer and while the  $T_{g2}$  peak at  $162^\circ\text{C}$  is corresponding to the bulk syndiotactic conformer. This mixture of different conformations in as-synthesized PMMAs results from the reaction of powder



(contains PMMA and reaction initiator) and liquid (contains MMA monomer). Apart from these, except pure PMMA, we observed one extra peak ( $T_{g3}$ ) at 300°C in all nano Ti/PMMA composites. This is due to the modification in local polymer structure to the vicinity of nano Ti that restricts the free movement of polymer chain. That is why it gives new  $T_g$  at higher temperature like another nanoparticle incorporated in PMMA matrix. However, those regions (within the polymer matrix) which are far from the nanoparticle, retains their polymer structure and gives  $T_g$ s peak at 117°C and 162°C (Singhal et al., 2013).

---

## 14.4 CONCLUSION

PMMA and its modified forms are regarded as a more prominent matrix for denture materials than epoxy resin, polycarbonates, or polyamides. However, polymerization shrinkage, which causes failure of prepared dentures, is one of the major problems for PMMA based materials. Therefore incorporation of additives like nanofillers is a better choice to achieve materials with multifunctional properties. Nano Ti/PMMA composite dentures are synthesized successfully at their sandy stage and studied for their mechanical, wear, and thermal properties. We observed 65% improvement in tensile strength of modified composite denture compared with its pure PMMA material by loading of 1% nano Ti. This is due to structural changes of PMMA to the vicinity of Ti. At the same time generation of a tail-like structure due to the presence of Ti in PMMA matrix is the main cause of failure of modified composite upon uniaxial tensile loading. Similarly, the wear resistance property also increases with increase in Ti contents. We observe approximately six times lower material loss compared with pure PMMA, while loading of only 1% Ti (by weight) in pure PMMA matrix. The complete thermal degradation of modified composite is observed to be similar to that of pure PMMA. However, prior to complete degradation, as-prepared composites exhibit new  $T_g$ s at 300°C due to structural changes near the particles.

---

## ACKNOWLEDGMENTS

Authors are thankful to Professor-in-charge, Central Instrument Facility, Indian Institute of Technology (Banaras Hindu University), Varanasi, India for consistent help in mechanical testing.

---

## REFERENCES

- Ai, M., Du, Z., Zhu, S., Geng, H., Zhang, X., Cai, Q., Yang, X., et al., 2017. Composite resin reinforced with silver nanoparticles—laden hydroxyapatite nanowires for dental application. *Dent. Mater.* 33, 12–22.

- Alhareb, A.O., Akil, H.M., Ahmad, Z.A., 2015. Mechanical properties of PMMA denture base reinforced by nitrile rubber particles with  $\text{Al}_2\text{O}_3/\text{YSZ}$  fillers. *Proc. Manufact.* 2, 301–306.
- Ali, U., Karim, K.J.B.A., Buang, N.A., 2015. A review of the properties and applications of poly (methyl methacrylate)(PMMA). *Polym. Rev.* 55, 678–705.
- Aoyagi, Y., Miyasaka, T., Ando, N., 2015. Application of noble metal clusters to PMMA resin and influence of mechanical properties and colour. *Dent. Mater. J.* 34, 781–788.
- Ash, B.J., Stone, J., Rogers, D.F., Schadler, L.S., Siegel, R.W., Benicewicz, B.C., et al., 2000. Investigation into the thermal and mechanical behavior of PMMA/alumina nanocomposites, *MRS Proceedings*, 661. Cambridge University Press, pp. KK2–KK10.
- Bijelic-Donova, J., Garoushi, S., Lassila, L.V., Keulemans, F., Vallittu, P.K., 2016. Mechanical and structural characterization of discontinuous fiber-reinforced dental resin composite. *J. Dent.* 52, 70–78.
- Bocalon, A.C.E., Mita, D., Narimya, I., Shouha, P., Xavier, T.A., Braga, R.R., 2016. Replacement of glass particles by multidirectional short glass fibers in experimental composites: effects on degree of conversion, mechanical properties and polymerization shrinkage. *Dent. Mater.* 32, e204–e210.
- Borges, A.L., Muenchow, E.A., de Oliveira Souza, A.C., Yoshida, T., Vallittu, P.K., Bottino, M.C., 2015. Effect of random/aligned nylon-6/MWCNT fibers on dental resin composite reinforcement. *J. Mech. Behav. Biomed. Mater.* 48, 134–144.
- Bouillaguet, S., Shaw, L., Gonzalez, L., Wataha, J.C., Krejci, I., 2002. Long-term cytotoxicity of resin-based dental restorative materials. *J. Oral Rehabil.* 29, 7–13.
- Cobb, D.S., Vargas, M.A., Fridrich, T.A., Bouschlicher, M.R., 2000. Metal surface treatment: characterization and effect on composite-to-metal bond strength. *Operat. Dentis.* 25, 427–433.
- Dafar, M.O., Grol, M.W., Canham, P.B., Dixon, S.J., Rizkalla, A.S., 2016. Reinforcement of flowable dental composites with titanium dioxide nanotubes. *Dent. Mater.* 32, 817–826.
- De Souza, G.M., 2015. Nanoparticles in restorative materials. *Nanotechnology in Endodontics*. Springer International Publishing, Switzerland, pp. 139–171.
- Demir, M.M., Memesa, M., Castignolles, P., Wegner, G., 2006. PMMA/zinc oxide nanocomposites prepared by in-situ bulk polymerization. *Macromol. Rapid Commun.* 27, 763–770.
- Dupriez, N.D., von Koeckritz, A.K., Kunzelmann, K.H., 2015. A comparative study of sliding wear of nonmetallic dental restorative materials with emphasis on micromechanical wear mechanisms. *J. Biomed. Mater. Res. Part B Appl. Biomater.* 103, 925–934.
- Durkan, R., Ayaz, E.A., Bagis, B., Gurbuz, A., Ozturk, N., Korkmaz, F.M., 2013. Comparative effects of denture cleansers on physical properties of polyamide and polymethyl methacrylate base polymers. *Dent. Mater. J.* 32, 367–375.
- Ferguson, R.C., Ovenall, D.W., 1987. High resolution NMR analysis of the stereochemistry of poly (methyl methacrylate). *Macromolecules* 20, 1245–1248.
- Ferracane, J.L., 2013. Resin-based composite performance: are there some things we can't predict? *Dent. Mater.* 29, 51–58.
- Fonseca, R.B., de Almeida, L.N., Mendes, G.A.M., Kasuya, A.V.B., Favarao, I.N., de Paula, M.S., 2016. Effect of short glass fiber/filler particle proportion on flexural and diametral tensile strength of a novel fiber-reinforced composite. *J. Prosth. Res.* 60, 47–53.

- Gates, W.D., Diaz-Arnold, A.M., Aquilino, S.A., Ryther, J.S., 1993. Comparison of the adhesive strength of a BIS-GMA cement to tin-plated and non-tin-plated alloys. *J. Prosth. Dent.* 69, 12–16.
- Ghazal, M., Yang, B., Ludwig, K., Kern, M., 2008. Two-body wear of resin and ceramic denture teeth in comparison to human enamel. *Dent. Mater.* 24, 502–507.
- Hamanaka, I., Takashaki, Y., Shimizu, H., 2011. Mechanical properties of injection moulded thermoplastic denture base resins. *Acta Odontol. Scand.* 1 (69), 75–79.
- Han, Z., Zhy, B., Chen, R., Huang, Z., Zhu, C., Zhang, X., 2015. Effect of silver-supported materials on the mechanical and antibacterial properties of reinforced acrylic resin composites. *Mater. Design.* 65, 1245–1252.
- Hasratiningsih, Z., Cahyanto, A., Takarini, V., Karline, E., Djustiana, N., Febrida, R., et al., 2016. Basic properties of PMMA reinforced using ceramic particles of  $ZrO_2$ - $Al_2O_3$ - $SiO_2$  coated with two types of coupling agents. *Key Eng. Mater.* 696, 93–98.
- Jagger, D.C., Harrison, A., Jandt, K.D., 1999. The reinforcement of dentures. *J. Oral Rehabil.* 26, 185–194.
- Jandt, K.D., Sigusch, B.W., 2009. Future perspectives of resin-based dental materials. *Dent. Mater.* 25, 1001–1006.
- John, J., Mani, S.A., Palaniswamy, K., Ramanathan, A., Razak, A.A.A., 2015. Flexural properties of poly(methyl methacrylate) resin reinforced with oil palm empty fruit bunch fibers: a preliminary finding. *J. Prosth.* 24, 233–238.
- Karthick, R., Sirisha, P., Sankar, M.R., 2014. Mechanical and tribological properties of PMMA-sea shell based biocomposite for dental application. *Proc. Mater. Sci.* 6, 1989–2000.
- Kern, M., Thompson, V.P., 1994. Influence of prolonged thermal cycling and water storage on the tensile bond strength of composite to NiCr alloy. *Dent. Mater.* 10, 19–25.
- Khan, A.S., Azam, M.T., Khan, M., Mian, S.A., Rehman, I.U., 2015. An update on glass fiber dental restorative composites: a systematic review. *Mater. Sci. Eng. C* 47, 26–39.
- Kirmanidou, Y., Sidira, M., Drosou, M.E., Bennani, V., Bakopoulou, A., Tsouknidas, A., et al., 2016. New Ti-alloys and surface modifications to improve the mechanical properties and the biological response to orthopedic and dental implants: a review. *BioMed Res. Int.* 2016, 1–21.
- Laachachi, A., Ferriol, M., Cochez, M., Cuesta, J.M.L., Ruch, D., 2009. A comparison of the role of boehmite (AlOOH) and alumina ( $Al_2O_3$ ) in the thermal stability and flammability of poly (methyl methacrylate). *Polym. Degrad. Stabil.* 94, 1373–1378.
- Ladizesky, N.H., Cheng, Y.Y., Chow, T.W., Ward, I.M., 1993. Acrylic resin reinforced with chopped high performance polyethylene fiber-properties and denture construction. *Dent. Mater.* 9, 128–135.
- Lambrechts, P., Goovaerts, K., Bharadwaj, D., De Munck, J., Bergmans, L., Peumans, M., et al., 2006. Degradation of tooth structure and restorative materials: a review. *Wear* 261, 980–986.
- Lassila, L., Garoushi, S., Vallittu, P.K., Sailyoja, E., 2016. Mechanical properties of fiber reinforced restorative composite with two distinguished fiber length distribution. *J. Med. Behav. Biomed. Mater.* 60, 331–338.
- Leprince, J.G., Palin, W.M., Hadis, M.A., Devaux, J., Leloup, G., 2013. Progress in dimethacrylate-based dental composite technology and curing efficiency. *Dent. Mater.* 29, 139–156.

- Libeck, W., Elsayed, A., Freitag-Wolf, S., Kern, M., 2016. Reducing the effect of polymerization shrinkage of temporary fixed dental prostheses by using different materials and fabrication techniques. *Dent. Mater.* 32, 1464–1471.
- Marghalani, H.Y., 2016. Resin-based dental composite materials. In: *Handbook of Bioceramics and Biocomposites*. Springer International Publishing, Switzerland, pp. 357–405.
- Mathew, M., Shenoy, K., Ravishankar, K.S., 2014. Flexural strength of E-glass-reinforced PMMA. *Int. J. Exp. Dent. Sci.* 3, 24–28.
- McCabe, J.F., Walls, A.W. (Eds.), 2013. *Applied Dental Materials*. ninth ed. John Wiley & Sons.
- Miculescu, F., Ciocan, L.T., Miculescu, M., Berbecaru, A., Oliva, J., Comaneanu, R.M., 2015. Failure analysis of dental prosthesis. *Hand Book of Bioceramics and Biocomposites*. Springer International Publishing, Switzerland, pp. 1–30.
- Miyamoto, T., Inagaki, H., 1970. The stereocomplex formation in PMMA and stereospecific polymerization of its monomer. *Polym. J.* 1, 46–54.
- Mortazavi, V., Atai, M., Fathi, M., Keshavarzi, S., Khalighinejad, N., Badrian, H., 2012. The effect of nanoclay filler loading on the flexural strength of fiberreinforced composites. *Dent. Res. J.* 9, 273–280.
- Mutluay, M.M., Ruyter, I.E., Nat, R., Philos, Dr, 2005. Evaluation of adhesion of chaiside hard relining materials to denture base polymers. *J. Prosth. Dentis.* 94, 445–452.
- Nagakura, M., Nishiyama, N., 2017. Fabrication and physical properties of glass fiber reinforced thermoplastics for non-metal clasp dentures. *J. Biomed. Mater. Res. B*, 105, 2254–2260.
- Nam, K.Y., 2014. Characterization and bacterial anti-adherent effect on modified PMMA denture acrylic resin containing platinum nanoparticles. *J. Adv. Prosth.* 6, 207–214.
- Nandish, B., Rijesh, M., Prabhu, S., 2016. Fabrication of hair and copper fiber reinforced polymethyl methacrylate (PMMA) composites and evaluation of their mechanical properties, thermal conductivity and color stability for dental applications. *Trends Biomater. Artif. Organs* 30 (1), 8–12.
- Nidal, W.E., Saied, H.M., Azlan, A., Zainal, A.M.I., 2016. Evaluation of the mechanical and radiopacity properties of poly(methyl methacrylate)/barium titanate-denture base composites. *Polym. Polym. Compos.* 24, 365–373.
- Radha, G., Balakumar, S., Venkatesan, B., Vellaichamy, E., 2017. A novel nanohydroxyapatite–PMMA hybrid scaffolds adopted by conjugated thermal induced phase separation (TIPS) and wet-chemical approach: analysis of its mechanical and biological properties. *Mater. Sci. Eng. C* 75, 221–228. Available from: <https://doi.org/10.1016/j.msec.2016.11.098>.
- Rezvani, M.B., Atai, M., Hamze, F., Hajrezai, R., 2016. The effect of silica nanoparticles on the mechanical properties of fiber-reinforced composite resins. *J. Dent. Res. Dent. Clin. Dent. Prospects* 10, 112–117.
- Rokosz, K., Hryniewicz, T., Matýsek, D., Raaen, S., Valíček, J., Dudek, Ł., et al., 2016. SEM, EDS and XPS analysis of the coatings obtained on titanium after plasma electrolytic oxidation in electrolytes containing copper nitrate. *Materials* 9, 318–329.
- Roth, C.B., Pound, A., Kamp, S.W., Murray, C.A., Dutcher, J.R., 2006. Molecular-weight dependence of the glass transition temperature of freely-standing poly (methyl methacrylate) films. *Eur. Phys. J. E* 20, 441–448.

- Sideridou, I.D., Karabela, M.M., Vouvoudi, E.C., 2011. Physical properties of current dental nanohybrid and nanofill light-cured resin composites. *Dent. Mater.* 27, 598–607.
- Singhal, A., Dubey, K.A., Bhardwaj, Y.K., Jain, D., Choudhury, S., Tyagi, A.K., 2013. UV-shielding transparent PMMA/ $\text{In}_2\text{O}_3$  nanocomposite films based on  $\text{In}_2\text{O}_3$  nanoparticles. *RSC Adv.* 3, 20913–20921.
- Souza, J.C., Bentes, A.C., Reis, K., Gavinha, S., Buciumeanu, M., Henriques, B., et al., 2016. Abrasive and sliding wear of resin composites for dental restorations. *Tribol. Int.* 102, 154–160.
- Swain, M.V., Coldea, A., Bilkhair, A., Guess, P.C., 2016. Interpenetrating network ceramic-resin composite dental restorative materials. *Dent. Mater.* 32, 34–42.
- Takabayashi, Y., 2010. Characteristics of denture thermoplastic resins for non metal clasp dentures. *Dent. Mater. J.* 29, 353–361.
- Tanoue, N., Nagano, K., Matsumura, H., 2005. Use of a light-polymerized composite removable partial denture base for a patient hypersensitive to poly (methyl methacrylate), polysulfone, and polycarbonate: a clinical report. *J. Prosth. Dent.* 93, 17–20.
- Tsujimoto, A., Barkmeier, W.W., Takamizawa, T., Watanabe, H., Johnson, W.W., Latta, M.A., et al., 2016. Relationship between mechanical properties and bond durability of short fiber-reinforced resin composite with universal adhesive. *Eur. J. Oral Sci.* 124 (5), 480–489.
- Ucar, Y., Akova, T., Aysan, I., 2012. Mechanical properties of polyamide versus different PMMA denture base materials. *J. Prosth.* 21, 173–176.
- Wang, L., D'Alpino, P.H.P., Lopes, L.G., Pereira, J.C., 2003. Mechanical properties of dental restorative materials: relative contribution of laboratory tests. *J. Appl. Oral Sci.* 11, 162–167.
- Wang, R., Tao, J., Yu, B., Dai, L., 2014. Characterization of multiwalled carbon nanotube-polymethyl methacrylate composite resins as denture base materials. *J. Prosth. Dent.* 111 (4), 318–326.
- Wang, T., Tsoi, J.K.H., Matinlinna, J.P., 2016a. A novel zirconia fibre-reinforced resin composite for dental use. *J. Mech. Behav. Biomed.* 53, 151–160.
- Wang, X., Cai, Q., Zhang, X., Wei, Y., Xu, M., Yang, X., et al., 2016b. Improved performance of Bis-GMA/TEGDMA dental composites by net-like structures formed from  $\text{SiO}_2$  nanofiber fillers. *Mater. Sci. Eng. C* 59, 464–470.
- Zeng, J., Sato, Y., Ohkubo, C., Hosoi, T., 2005. In vitro wear resistance of three types of composite resin denture teeth. *J. Prosth. Dent.* 94, 453–457.
- Zhang, M., Matinlinna, J.P., 2012. E-Glass fiber reinforced composites in dental applications. *Silicon* 4, 73–78.

# In vitro and in vivo technologies: an up to date overview in tissue engineering

# 15

**Roxana C. Popescu<sup>1,2</sup>, Ecaterina Andronescu<sup>2</sup> and Alexandru Mihai Grumezescu<sup>2</sup>**

*<sup>1</sup>Department of Life and Environmental Physics, “Horia Hulubei” National Institute for Physics and Nuclear Engineering, Magurele, Romania <sup>2</sup>Department of Oxide Materials and Nanomaterials, Faculty of Applied Chemistry and Materials Science, Politehnica University of Bucharest, Bucharest, Romania*

## 15.1 INTRODUCTION

When referring to tumor microenvironment we not only speak about the cancer cells, but about all cells in the environment where the tumor exists, such as, immune cells, fibroblasts, stem cells, inflammatory cells, endothelial cells in the blood vessels surrounding the area, lymphocytes, but also about the signaling molecules and extracellular matrix (ECM) that gives the 3D architecture of the tumor. The spatial organization of tumor facilitates in vivo similar cell–cell interaction and similar penetration and flows (Zanoni et al., 2016).

Referring to the circulatory properties of the tumor area, we must emphasize the enhanced permeability and retention effect, but also the hypoxia. The first one refers to the fact that the tumor has an increased blood flow, due to increased vascularization, accompanied by an abnormal architecture of the blood vessels, which leads to extensive permeation of biomolecules in tumor area (Greish, 2010; Richardson, 2012). The majority of chemical therapeutic approaches nowadays are based on this effect, however, even if there is a higher probability for the active substance to be passively transported and retained in the tumor, the lack of selectivity is one high disadvantage that is desired to be overcome.

Considering the second above-mentioned property, hypoxia refers to the lower oxygen level encountered in the solid tumors, compared with normal tissues. This is a result of improper vascularization of the malignant tissue, but also of the rapid consumption of the provided oxygen, as the cancerous cells have higher

metabolic and proliferation rates (Eales et al., 2016; Muz et al., 2015; Brown, 2007).

Taking into account the architecture of the tumor tissue, there are three different areas that differ by means of proliferation and morphology of the cells: (1) the outer layer, which is the proliferating area; here can also be encountered non-differentiated tumor cells like cancer stem cells, as in case of glioblastoma; (2) the inner layer, which is composed of viable but nonproliferating cells; and (3) the necrotic core. This difference in behavior of the cells arises mainly from their access to nutrients and oxygen and the possibility of nutrient and waste gradients (Fig. 15.1).

Compared with conventional in vitro 2D models, 3D models have several advantages coming from the fact that the tumor cells are similarly organized as in vivo models: thus, protein expression, gene expression, protein gradients, cell signaling, migration of cells, and drug response are similar to the responses in living beings.

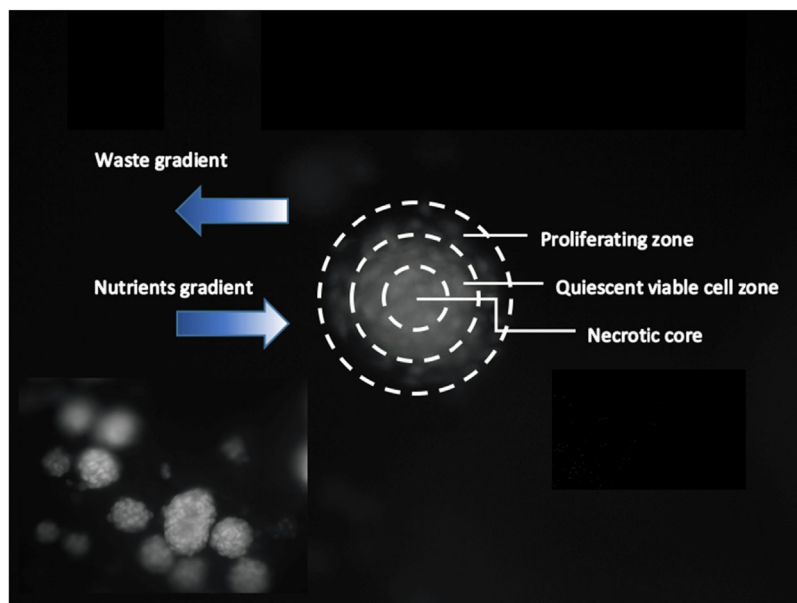


**FIGURE 15.1**

Fluorescence microscopy images of HepG2 hepatocarcinoma spheroids obtained using drop hanging method. Schematic representation of 3D tumor cell cultures properties and architecture.

*Adapted from Edmondson, R., Broglie, J. J., Adcock, A. F., & Yang, L., Three-dimensional cell culture systems and their applications in drug discovery and cell-based biosensors. Assay and drug development technologies, 12(4), 2014, 207–218.*

Even though in vitro tissue engineering technologies for development of tumor models have been employed to replace in vivo studies in cancer biology and drug discovery research, both models are very important at the moment, as no in vitro model can currently fulfill the whole complexity of the living organism. However, considering tissue engineering technologies, both in vitro and in vivo approaches start from the same principles and bases. For in vivo use, the previously obtained ex vivo models are transplanted into animal models. This chapter will discuss the latest methods and approaches for both in vitro and in vivo tissue engineering modeling of tumors.

---

## 15.2 IN VITRO TISSUE ENGINEERING TECHNOLOGIES FOR CANCER RESEARCH

### 15.2.1 3D CELL CULTURES

One of the most common alternative methods used to obtain in vitro tumor models is represented by the use of 3D cell cultures. Also known as multicellular tumor spheroids, 3D cell cultures are basically aggregates of cells that form spontaneously or due to external mechanical and/or chemical factors and offer ex vivo the same conditions as in the tumor microenvironment (architecture, oxygen and nutrients flows, etc.).

Currently, researchers prefer to use 3D tumor cell cultures in their studies instead of 2D models, for several reasons such as (1) more realistic drug response; (2) phenotypic heterogeneity of the culture; (3) the gene expression and cell behavior is closer to reality; (4) facilitates a more realistic tumor microenvironment ([Sigma-Aldrich](#)). This technology not only offers a model that is closer to in vivo, but has moreover the advantages of higher reproducibility, control of parameters, and better ethical consents.

There are several parameters that influence the response of tumor spheroids to therapeutic approaches, such as the oxygen tension, compactness, apoptosis inhibition, damage repair, and permeability of the tumor ([Zanoni et al., 2016](#)).

Compared with in vivo approaches, in vitro tissue engineered tumor models have the great advantage that they do not only provide architectonically and compositionally similar conditions to animal models, but they assure higher reproducibility, as one can control parameters like cell types, size of the tumor, its chemistry, architecture, mechanical properties, the bioresorption and dynamic flow ([Ricci C and Danti, 2013](#)). This has great implications in the outcomes of research experiments concerning biological mechanisms of cancer or testing of new drug candidates.

The currently available methods for the in vitro development of 3D cell cultures can be categorized into two main approaches: (1) liquid methods and (2) methods that use scaffolds.



### 15.2.1.1 Liquid methods

The most encountered and inexpensive methods used to obtain 3D cell cultures must be liquid methods, because they mostly require the main tumor cell population, appropriate culture medium, and a nonadherent cell culture vessel. Among the liquid methods used to obtain tumor spheroids one can recall:

1. The static suspension method, which was mainly destined to isolate neural stem cells from rats and supposes the use of serum-free medium in a low adhesion space. To create a microenvironment that prevents the attachment of tumor cells, several approaches have been used, such as low adhesion coatings with agar ([Abe-Fukasawa et al., 2018](#); [Yuhua et al., 1977](#)), poly ethylene glycol ([Schmitt et al., 2015](#)), etc. However, the resulting spheroids are quite inhomogeneous by means of dimension (20  $\mu\text{m}$ –1 mm).
2. The drop hanging method starts from making a tumor cell suspension with a high cell concentration per 10–20  $\mu\text{L}$  (the volume of a liquid drop). Drops from this cell culture are placed on a culture plate, which is then inverted to allow the gathering of the tumor cells on the tip of the drop. The method has a high reproducibility, although manipulating the spheroids is difficult (changing the culture medium, adding the treatment, etc.).
3. A spinner bioreactor is basically a vessel with an impeller that stirs the cell suspension and prevents the segregation of the tumor cells and thus their attachment. The stirring movement allows a better circulation of the oxygen and nutrients in the culture environment, however, it can cause mechanical damage to the cells. More recently, some methods involving the microencapsulation of the spheroids have been developed, which allow the protection of the cells ([Serra et al., 2011](#); [Tabata et al., 2014](#)). The method has a high reproducibility, production yield, and results in the formation of a population of dimensionally homogenous tumor spheroids.
4. The magnetic levitation method is far from being a conventional way of obtaining 3D tumor cell cultures. It is based on incubation of the cells with magnetic nanoparticles, which can be then lifted and kept floating in the culture medium by placing a permanent magnet on the top of the vessel. Moreover, the functionalizing/incorporation of magnetic nanoparticles leads to the aggregation and sticking of the cells together, eventually forming the spheroid architecture. By specific functionalizing ([Wen et al., 2017](#); [Huang et al., 2017](#)) this may allow the selection of certain populations of tumor cells and then the formation of the 3D spheroids from these isolates.

### 15.2.1.2 Scaffolds

Scaffolds are commonly used in tissue engineering applications and have the ability to facilitate the cells' attachment, growth, proliferation, and differentiation. The architecture and chemistry of the scaffolds simulates better the in vivo conditions, offering a biomimetic environment for the growth and development of the tissue. In case of 3D tumor cell cultures, the support scaffold must simulate the

properties of the ECM in the origin tissue, by means of morphology, composition, and mechanical behavior.

Among the materials used for scaffold development in 3D cell culture approaches, we recall: (1) naturally derived materials, like collagen, gelatin, hyaluronic acid, fibrinogen, alginate or silk, respectively; (2) synthetic materials, such as poly(ethylene) glycol, poly methyl methacrylate, poly lactic co glycolic acid, polyglycolide, polycaprolactone, etc.

Not particularly a scaffold-based method for obtaining 3D tumor cell cultures, the gel embedding method (Sun et al., 2018; Caliari and Burdick, 2016; Andersen et al., 2015) supposes the use of a hydrogel as substrate for the tumor cell culture; the gel's properties (hydrophilic character, softness, etc.) provide biomimetic conditions for cell–cell interaction and result in the tumor cells organizing into spheroids. Classical materials are collagen, alginate, ECM, etc.

Sheikholeslam et al. (2018) has recently developed a hydrogel for the micro-encapsulation and sustained growth of embryonic fibroblasts and respectively lung cancer cells. The self-assembly system composed of EFK8 peptide–single wall carbon nanotubes led to the formation of tumor-like spheroids with accelerated cell growth. Extracellular proteins and carbohydrate-based hydrogels were successfully used for the growth of primary human breast epithelial cells, which showed healthy in vivo like behavior (Sokol et al., 2016). This can be extended to the obtaining of tumor phenotype expressing cells.

Hamdi et al. (2015) used collagen scaffolds to obtain human 3D chondrosarcoma cell models for radiobiology studies. The group studied the effects of 2 Gy low versus high LET radiation on these models, in comparison to 2D cultures. Results showed that the metabolism of the cells in 3D culture is completely changed and delays in the gamma-H<sub>2</sub>A<sub>x</sub> induction might occur; moreover, high-LET radiation determines higher and long-lasting gamma-H<sub>2</sub>A<sub>x</sub> than low-LET in 3D cultures.

Scaffolds made of porous polylactic acid functionalized with collagen type I hydrogel successfully showed the ability to simulate the peritoneal metastasis process (De Jaeghere et al., 2018). The resulted materials were coseeded with cancer-associated fibroblasts, endothelial cells, macrophages, and cancer cells (ovarian cancer and colon cancer). The fused deposition modeling technique was used to print a 3D layered scaffold with controlled architecture and pore dimension; to perform the coating, the resulted materials were plasma-activated and immersed in a gel solution.

Rijal et al. (2017) studied the potential of poly(lactide-co-glycolide)-poly(ε-caprolactone) (PLGA-PCL)–based scaffolds, hydrogel respectively porous, for the growth and development of breast cancer cells, as potential systems for drug monitoring. The results showed that the porous scaffolds have better potential in sustaining the growth of breast cancer cells, compared with hydrogel systems. PCL based scaffolds with a mean pore diameter of 250–400 μm were developed by Balachander G et al. (Balachander) as a model for the study of breast cancer metastasis. Campbell et al. (2017) has also used an ice-templating technique to

seed breast cancer cells in cross-linked collagen scaffolds with highly controllable porous architecture for migration studies.

Chitosan/collagen/alginate fibrous scaffolds (Wang et al., 2016) were used to culture 3D breast cancer cells that exhibited epithelial mesenchymal transition phenotype, with implications in metastasis and drug resistance. The scaffolds were obtained using a spray-spinning method. Collagen–chitosan porous scaffolds have also been reported by Mahmoudzadeh and Mohammadpour (2016) as favorable for obtaining and sustaining 3D tumor cell cultures.

Chen et al. (2018) used collagen scaffolds to study the satellite formation in head and neck squamous cell carcinoma. For the same purpose, Young et al. (2018) have developed a platform based on 3D cocultures to simulate the micro-environment in head and neck cancer. The system is based on the infiltration of cancer-associated fibroblasts in a fibrous scaffold, which is then rolled to obtain a layered structure. The radiation resistance character was evaluated using this system.

Collagen scaffolds containing glycosaminoglycan or nanohydroxyapatite were proved to be suitable for the development of an in vitro 3D neuroblastoma model (Curtin et al., 2018); the resistance properties of the cell model were evaluated in comparison with 2D models and in vivo models. The resistance to cisplatin treatment was comparable to the in vivo model and moreover, the system proved to have applicability for miRNA-based gene delivery validation.

3D electrospun PCL scaffolds (Fong et al., 2013) were proved to be suitable for the development of a 3D Ewing sarcoma model similar to human tissues considering morphology, cells growth kinetics, protein expression, and resistance to drug treatment. Guiro et al. (2015) also evaluated the behavior of breast cancer cells cultured on poly( $\epsilon$ -caprolactone) scaffolds with aligned or random fiber disposal structure. The collagen fibers in the ECM of the resulted tumor tissue showed to be oriented by the scaffold's architecture; highly resistant breast cancer cells were obtained and cultured on the scaffolds and the protein expression was studied; results showed that both architecture are valid models for the development of breast cancer cell models. Similarly, Palomeras et al. (2016) used poly( $\epsilon$ -caprolactone) scaffolds for the culture and study of cancer stem cells in breast tumor models.

Tumor progression and its dynamics are very complex processes, which not only imply the migration of the cells, but also their transforming process.

The biology of cancer stem cells has recently been one of the hot topics in cancer research (Loureiro et al., 2017; Yoon, 2012; Medema, 2013). However, it has been proved that they express the best phenotype when cultured in 3D scaffold that mimics the in vivo architecture of the tumor tissues. For this, Wang et al. (2018) have cultured glioma cells in scaffolds made of porous chitosan, respectively of chitosan–hyaluronic acid. Compared with 2D cultures of the same cell lines, the 3D cultures allowed development of tumor spheroids and, moreover, they exhibited a high expression of cancer stem cells biomarkers. Smart poly(*N*-isopropylarylamide-*co*-Jeffamine M-1000 acryl-amide) scaffolds

(Heffernan et al., 2017) proved not only to be suitable for glioblastoma tumor spheroid formation, which expressed high stem-like phenotype, but they showed the ability to maintain the glioblastoma stem cells' multipotency and the self-renewal ability. Guiro et al. (2015) obtained scaffolds made of PCL fibers randomly placed to form a 3D structure similar to the ECM. These were colonized with resistant breast cancer cells, leading to an in vivo like behavior of the tumor cells: decrease in apoptosis and increase in stem-like markers, which showed to be an appropriate in vitro system for the study of the tumor microenvironment.

Angeloni et al. (2017) developed an in vitro 3D model that simulated the breast cancer metastasis in bone; the system uses a polyurethane scaffold, which mimics perfectly the architecture of the bone and is able to sustain the growth and differentiation of human adipose derived stem cells into osteoblast cells; these were further cocultured with breast cancer derived tumor-initiating cells. The formation of tumor aggregates could be observed after 3 weeks of coculture.

Polystyrene scaffolds were used for the culture of primary lymphoma cells in coculture with neonatal stromal cells, showing increased proliferation rates compared with the 2D models (Caicedo-Carvajal et al., 2011).

The use of decellularized parts or even whole organs in tissue engineering has been seen as a promising solution in solving the shortage of organ donors (Wang et al., 2017). This technique supposes the use of an ECM matrix coming from the targeted organ, which is free of cells or DNA and is cultivated with healthy cells that are able to proliferate and differentiate, to form a functional organ. The classical process mainly supposes the use of different detergent solution to "wash" the organ's native scaffold from everything that might contain the genetic material of the donor.

Guller et al. (2015) have been studying the possibility of using acellular organs from animals as scaffolds in the tissue engineering of tumors. These were obtained using an immersion–agitation method. The scaffolds showed high biocompatibility after implantation, independent of their organ of origin and favored the in vivo colonization with cells featuring specific cancerous character.

Rijal and Li (2017) have used decellularized breast tissue from mice containing collagen, glycoproteins, proteoglycans, etc., and have processed it into either hydrogels either highly porous scaffolds. Both normal and cancerous epithelial breast cancer cells were cultured on the scaffolds and their growth was monitored in comparison to polymeric PLGA and/or PCL scaffolds.

Decellularized intestinal scaffolds originally from porcine jejunum were used as growth support for Caco2 colon cancer cells, respectively, SW480 malignant human colon cancer cells cultured alone or in coculture with primary fibroblasts, to obtain an in vitro model to simulate the metastase colorectal cancer (Nietzer et al., 2016).

Besides the high biocompatibility of ECM-free scaffolds, the process of decellularization often implies a weakening of the structure and may compromise the scaffold integrity. In this regard Lü et al. (2018) have used a methylene blue-mediated photooxidation process to enhance the stiffness of such scaffolds by means of cross-linking. The process did not affect the integrity of the component

proteins and polypeptides and showed success in the culturing of breast cancer cells, hepatocarcinoma cells, and lung carcinoma cells. Moreover, the systems were also suitable for in vivo cell tumor invasion and growth promotion.

Rijal and Li (2017) have fabricated a tissue matrix scaffold using decellularized native ECM, having tissue-like architecture and resilience. The scaffolds showed to be suitable for coculture of cancerous and stromal cells.

Nowadays, there is a high offer for commercial 3D cell culture kits from different producers, which are easy and ready to use, offering highly reproducible results. Along with their cell culture kits, a lot of newly improved assay kits have been developed or adapted so that they are suitable for 3D models [Trypan Blue exclusion test, WST-1 cell viability assay, cell trackers, transfection kits, etc.]. Table 15.1 presents some commercially available kits based on scaffolds for 3D cell cultures.

**Table 15.1** Some Examples of Commercial Kits for 3D Tumor Cell Models That Use Scaffolds

Scaffold Category	Name and Company	Particularities	Reference
Basement Membrane Matrix (BME, animal-based), Alginate Hydrogel (plant-based), proprietary BioVision's Duo-Matrix and dry Scaffold (natural polymers, animal-free)  Collagen type I and patented absorbers	BioVision	Microplate containing 3D scaffolds; standardized and adaptable high-throughput method; ready to use complete kit.	BioVision
	RAFT 3D cell culture kit, Lonza	Microplate containing scaffolds; adaptable; easy to use; complex coculture models or barrier models including air-lift models can be made using cell culture inserts; versatile and applicable to many cell lines	Lonza
Collagen matrix	3D Collagen Culture kit, Merck	Applicability in cell angiogenesis, migration, apoptosis, proliferation, and tissue formation in a 3D collagen matrix; viable cells can be removed from the matrix for further analysis	Merckmillipore

(Continued)

**Table 15.1** Some Examples of Commercial Kits for 3D Tumor Cell Models That Use Scaffolds *Continued*

Scaffold Category	Name and Company	Particularities	Reference
Alginate bioscaffold	AlgiMatrix 3D cell culture system, ThermoFisher	Animal free lyophilized bioscaffold	<a href="#">ThermoFisher</a>
Synthetic cross-linked 3D hydrogel; human ECM; synthesized ECM containing Chemically synthesized HyStem (thiolated Hyaluronic acid), Extralink (thiol-reactive crosslinker), and degassed water and biologically purified Gelin-S (denatured collagen); synthesized hydrogel	HydroMatrix Peptide Hydrogel, MaxGel Human ECM, Hystem Stem Cell Culture, TrueGel3D hydrogels platform Sigma	Highly resemble in vivo environments, lot-to-lot consistency, high viability and proliferation for different types of cells, suitable for stem cell research	<a href="#">Sigma-Aldrich</a>
MatriGel	IncuCyte S3 3D multi-tumor spheroids assay, Essen Bioscience	System for 3D tumor spheroid generation and real time measurements; reproducible data	<a href="#">IncuCyte</a>
Natural ECM, basement membrane extracts, proteins	Cultrex 3D cell culture, Amsbio	Improved reproducibility, improved mechanical properties	<a href="#">Amsbio</a>
Alginate hydrogel, basement membrane extract, collagen III, collagen IV (human recombinant), vitronectin	3D cell culture matrix, Promokine	Standardized, user friendly, adaptable kits	<a href="#">Promocell</a>

Moreover, there are many other patented commercially available scaffolds that can be used to adapt a 3D cell culture assay to the needs. Some examples ([Goral et al., 2014](#)) are (1) hydrogel scaffolds (Matrigel, Tisseel, Qgel, ECMgel, Corgel BioHydrogel, and Nano Dox), (2) bioceramic scaffolds (BoneSource, Calcibon, ChronOS, Eurobone, HydroSet, Norian SRS, Ostim, MIIG X3 and Cortoss), etc.

### 15.2.2 BIOPRINTING

3D printing starts from a 3D complex geometry model built using a computer-aided design software and a printing device that deposits the material layer by layer, to form the desired structure. Bioprinting uses the same principles as

conventional 3D printing, but it moreover uses living cells, ECM components, different proteins or biochemical factors, naturally derived materials, as printing substrate. Of course, there are the less nonconventional two-step biofabrication processes (Polley et al., 2017; Trachtenberg et al., 2018; Choi et al., 2017; Wei et al., 2016) that suppose the obtaining of the 3D scaffold using a bioprinting technique, followed by the seeding and culturing of the cells.

Some advantages of bioprinting are (1) complex 3D architectures may be easily obtained at industrial scale; (2) they contain the living cells from the beginning and do not need an additional step to culture the cells; (3) efficiency and low cost; (4) high reproducibility, as the process is conducted through a computerized system. Considering the one step methods, there are some limitations to take into account, which include repeatability, cell number and dispersion, scalability, and spatial control (Knowlton et al., 2015).

There are three types of bioprinting technologies at the moment:

1. Inkjet bioprinting, which uses droplets of “bioinks,” which are basically biomaterials and encapsulated cells; the droplets are generated directly at the printing head, by means of a heater or a piezoelectric actuator.
2. The microextrusion method is based on the continuous extrusion of the “bioink” from the printing head, which is enabled continuously using pneumatic or mechanical forces.
3. Laser guided bioprinting uses a laser that is directed to the cell suspension and determines the entrapment of the cells into a substrate, due to differences in refractive indices.
4. Laser induced bioprinting starts from depositing a cell containing hydrogel underneath a laser absorbing layer, which acts as donor film; the laser induces a pressure that causes the formation of vapor bubbles.
5. Classical stereolithography has been adapted to bioprinting, as cells have been included in photoreactive materials and then curing using light has been done.
6. Digital micromirror projection is a new technology that uses a digital micromirror that reflects the UV light in a certain spatial pattern onto a macromere solution, which is photopolymerizable and contains a cell suspension.

Considering the study of complex implication of cancer stem cells in tumor models such as glioma, Xingliang et al. (2016) have proposed a 3D bioprinted glioma stem cell model, which uses as bioink a mix of cells, gelatin, alginate, and fibrinogen, resulting in a porous hydrogel that closely resembles the ECM. The viability of the cells was above 80% after printing and they showed high proliferation potential, characteristics of stem cells, differentiation and vascularization potential, verified through the expression of specific biomarkers. The same group (Dai et al., 2017) used a “custom-made coaxial extrusion 3D bioprinting system” to obtain an in vitro fibrillar brain tumor model; the resulting tissue not only showed high viability and proliferative activity of the component cells, but also good tumor–stromal interactions that were verified through genetic engineering,



using a recombinase gene for the transfection of the component cells. The expression of the recombinant fluorescent protein was better observed in the 3D model, compared with 2D models. 3D jet writing ([Jordahl et al., 2018](#)) is a similar technology for the fabrication of porous fibrillar structures to be used as models in different biomedical applications, including cancer biology. [Lee et al. \(2015\)](#) has also developed a 3D bioprinted model for brain cancer study (glioblastoma multiforme).

Also a bioink made of gelatin, alginate, and fibrinogen was used for the printing of a 3D cervical cancer structure ([Yu et al., 2014](#)). Results of the evaluation showed excellent viability after printing and proliferation rates of the cervical cancer cells inside the resulted structure; moreover, the cells formed spheroid structures, while protein expression measurements emphasized a high expression of matrix metalloproteinase; moreover, the chemoresistance was higher compared with 2D cell cultures.

[Sears et al. \(Patent\)](#) have developed a 3D bioprinted pancreatic tumor tissue model with a multilayered structure and a biomimetic microenvironment comprised of pancreatic stellate cells and endothelial cells forming the stromal microenvironment, respectively pancreatic cancer cells surrounded by the stromal area.

The two step biofabrication process is usually considered to be a 3D bioprinting technique, as they mostly use biologically derived materials for fabrication. [De Jaeghere et al. \(2018\)](#) have obtained layered polylactic acid scaffolds functionalized with type I collagen hydrogel to obtain an in vitro model for peritoneal metastases. A breast cancer metastasis in bone model ([Zhu et al., 2016](#)) was obtained using 3D bioprinting using a bioink made of hydrogel and nanohydroxyapatite; the resulting layered structure was then seeded with breast cancer cells cocultured with bone marrow mesenchymal stem cells.

The 3D printing market is rapidly growing at the moment, as there is a lot of potential to be exploited and, thus, new companies are continuously emerging. In bioprinting, companies as Organovo, which is worth at the moment over \$200 million, use 3D printing technologies to obtain functional tissues for medical research, surgical or therapeutic applications (Kay). Organovo ([Organovo](#)) is known for the ExVivire human liver and kidney tissues models with applications in toxicology and preclinical drug testing. Other examples are Cyfuse ([Cyfusebio](#)), which specializes in regenerative medicine; Aspect Biosystems ([AspectBiosystems](#)) is known for the 3DBioring Contractile Tissue Platform, which simulates the contraction and relaxation of human muscle; TeVido Biodevices ([Tevidobiodevices](#)) makes parts of the body to be used in reconstructive and cosmetic surgeries (e.g., nipples using the patient's own melanocytes). Other companies are Advanced Solutions Life Sciences ([LifeSciences](#)), Tissue Regeneration Systems (TRS), nScrypt ([nScrypt](#)), and EnvisionTEC ([EnvisionTEC](#)), which produces printers and technologies for various biomedical applications.

In cancer biology companies such as DigiLab ([Digilab](#)), N3D Biosciences ([n3DBiosciences](#)), CELLINK ([CELLINK](#)), and Regenovo ([Regenovo](#)) have



launched technologies that are suitable for tumor tissue development. N3D Biosciences uses bioprinting technologies in combination with magnetic levitation to create complex 3D biomimetic tissue structures, and also to implement contractile movements to the organoids (n3DBiosciences). Organovo has also been working for the development of a 3D human breast cancer model with applications in the study of targeted therapeutics; the model is based on breast cancer cells and a stromal microenvironment at the exterior of the spheroids (King). Recently, CTIBiotech and Microlight 3D, in collaboration with The Materials and Physical Engineering Laboratory and Jean Kuntzmann Laboratory in Grenoble have launched 3D-OncoCHIP, which is a platform that produces tumor spheroids using 3D bioprinting technologies (Webmaster).

### 15.2.3 MICROCHIPS AND MICROFLUIDICS

Bioreactors are closed systems that offer the proper environment for different biological processes to occur in strictly controlled conditions. These assure parameters like sterility, temperature, pressure, flow, etc. (Smith et al., 2018). Macroscale bioreactors can be static (normal plates, flasks, or other appropriate cell culture vessels) or dynamic (like stirring, rotary, hollow-fiber, or perfusion). However, microfluidic bioreactors have lately grown in interest, as they are actively contributing to the development of lab-on-a-chip or organ-on-a-chip approaches (Xu et al., 2018; Osaki et al., 2018; Wang et al., 2015b). This technology has the advantage of enabling a precise real time control of the flow parameters and, moreover, because it uses a limited smaller number of cell population, it provides an easier way to follow their response to signaling molecules (Sun et al., 2010), metabolic or physical gradients (Schwarz et al., 2016; Walsh et al., 2009), drug response (Pandya et al., 2017; Tang et al., 2017), or nanoparticles (Farokhzad et al., 2005; Ozelikkale et al., 2017a) response. Looking at a smaller scale can make easier the process of studying cancer cell population kinetics, tumor progression, angiogenesis process, invasion, metastasis, etc.

Considering the principle of tumor spheroids formation, there are two main categories: (1) emulsion-based techniques, in which cell suspension is either made in oil or cells encapsulated in a hydrogel (single emulsion techniques); these become double emulsions technique when culture medium is introduced as main phase; (2) microwells-like structures, which are designed as microscaled cell culture well arrays and are used for the generation and growth of highly accurate tumor spheroids.

Kwak et al. (2018) used a microfluidic system to generate tumor spheroids from cancer cells encapsulated and cultured in microdroplets with high generation yield and low range of dimensions. The method uses a droplet based biochip that generates cells encapsulated into a droplet; these are then incubated statically, during 24 hours, to allow the compact spheroid formation, the following 14 days the incubation being done with stirring, so that the formation of 2D monolayer

and sticking between the spheroids is prevented. The resulted 3D cultures are suitable for the study of anticancer drug resistance.

Similarly, Wang et al. (2015a) developed a tumor tissue microarray using a microfluidic chip, by combining both emulsion-based and microwells techniques: MCF-7 breast cancer cells were cultures in hydrogel scaffold droplets inside microwells. The resulting tumor spheroids were evaluated by means of immuno-histochemical staining for E-cadherin and Vinculin, showing a tissue structure similar to the glandular tube; also, the cell proliferation and pH were monitored.

Chen et al. (2015) developed a PDMS-based microwell array covered with PVA to be used in the in situ evaluation of multicellular tumor spheroids' susceptibility to different drugs. The platform not only allows the growth of the spheroids and the drug treatment, but also real time evaluation using live–dead fluorescence stain and cytotoxicity information (based on MTS assay and signal transduction pathway analysis). An open-access microchip array made by several layers of PDMS and polycarbonate was obtained using a soft lithography protocol (Lin et al., 2018): one layer is a nanoporous membrane in between a layer of cell culture chambers and one layer of media reservoir. The membrane has two roles: it works as a liquid flow stop enabling not only gas change and allowing the automatic cell's distribution in the chambers, but also mimics the endothelial layer, as it allows the media exchange by means of a diffusion process.

Microscale bioreactors allow the development of smart tools with high ability of parameters control. One recent example is given by Ross and Pompano (2018), which developed a lab-on-a-chip system for the study of cytokine secretion and signaling. The system allows the monitoring of the proteins diffusion in the tissue ex vivo, with high ability of quantifying cytokines from different classes like tumor necrosis factor alpha, interferon gamma, and interleukin-2 in live lymph node tissues.

The vascularization of microtissues by means of developing vascularized microfluidic tumor-on-a-chip models not only enables the interchange of nutrients and gases and assures the waste elimination in in vitro 3D tumor tissues, but also mimics better the in vivo tumor microenvironment, considering the signaling pathways from the vasculature and also the delivery of the therapeutic platforms (Osaki et al., 2018).

Boussommier-Calleja et al. (2018) used a microfluidic system that simulates a vascularized 3D tumor tissue to study its interaction with monocytes. This model has made possible the monitoring and evaluation of monocytes behavior from migration into the extravascular microenvironment to differentiation into macrophages. The results show that the motility of the inflammatory monocytes is based on actomyosin motility; moreover, they reduce the extravasation of cancer cells, which might mean reduced metastasis ability. After differentiation into macrophage-like cells their influence on the cancer cells migration is reduced. The system has been previously used for the study of early metastasis (Chen et al., 2017), being able to simulate steps like early metastatic seeding, transendothelial migration, early micrometastasis formation. The chip is based on a

microvascular network formed over 4–5 days and is suitable for pharmacological studies and confocal microscopy tracking.

Also considering the circulatory properties of the tumor tissue, [Ozcelikkale et al. \(2017b\)](#) has developed a microfluidic system (tumor on a chip T-MOC) that is useful in drug delivery studies and is able to simulate phenomena such as interstitial flow, plasma clearance, and transport of the drug inside the tumor. 3D breast cancer cell cultures were grown in the T-MOC and treated with doxorubicin, respectively, hyaluronic acid nanoparticles. The difference in size influenced the tumor culture penetration ability. Compared with 2D cultures, the 3D cultures showed a high expression of CD44, which is correlated with an increased drug resistance.

[Pandya et al. \(2017\)](#) developed a platform based on microfluidics and electrical sensing that detects the changes in impedance magnitude related to cancer cells treated with an inflow of chemotherapeutic drugs. The impedance magnitude gives information on the resistance of cancer cells to treatment.

---

### 15.3 IN VIVO TISSUE ENGINEERING TECHNOLOGIES FOR CANCER RESEARCH

The urge for developing in vitro 3D cell culture models comes from the need and desire to reduce the number of animals used in experiments and testing or to find models that reproduce so well the conditions in the living body, that the animals use would be totally unnecessary. However, at the moment there are no models able to simulate by all means the complexity of the living organisms, so in vivo preclinical testing is still necessary.

Considering the study of cancer biology and testing of chemotherapeutic drugs, in vivo tumor model animals are still used. Most commonly used animal models are ([Al, 2014](#)): (1) mice models (BALB/c, C57BL/6, Kunming, C3H), (2) rat models (Swiss albino, Wistar), (3) swine models, (4) zebrafish, (5) *Daphnia magna*, (6) chick embryo chorioallantoic membrane, etc.

Traditionally, in vivo cancer models are obtained by transplanting experimental tumors to animals, which include intravenous implantation (in cases of leukemia), subcutaneous implantation (in case of solid tumors) ([Kruczynski and Hill, 2002](#)), and intracranial implantation (in case of brain tumors). More recently, genetically modified animals, which are able to spontaneously develop cancer, have been obtained. In case of in vivo tumor models, the animals act as “living incubators” ([Sigma-Aldrich](#)). Metastasis tumor models are mostly obtained when high metastatic tumor cells are implanted in the organ of origin, intravenously or intracranially. Usually these cells are marked with a tracker that helps identify their exact position over time.

Among perfusable cancer models, macroscale models might be the only ones with applicability in in vitro models. While microfluidic tumor models are great

candidates for modeling characteristics of tumorigenesis like intracellular communication, metastasis, and drug resistance (Fong et al., 2014), considering in vivo approaches, bioreactors are better by means of overcoming the diffusional limitation of the microscaled models.

Ingram et al. (2010) has stated that single cell type tumor spheroids are less successful considering control of growth and development in vivo, as they do not model the stromal–epithelial interactions. For this, the group has used a bioreactor to produce 3D models composed of both stromal and malignant epithelial cells, which not only mimic architectonically the tumor, but also resemble the microlesions. The method is highly reproducible and has a high production yield, resulting between 100 and 600 particle tumors similar in diameter size.

Other example is in vitro 3D chondrosarcoma cell models can be used as xenografts to be transplanted in nude mice (Ollitrault et al., 2014). Also, patient derived xenografts, which are implanted in animals are the closest model to human (Colella et al., 2018), however these are limited by means of representativeness and prediction ability in human cancer.

Suzuki et al. (2014) used temperature responsive poly(*N*-isopropyl acryl amide) plates cultured with cancer cell lines to obtain cell sheets that were then transplanted to mice. These showed to form tumors with higher volume compared with tumors resulting from the injection of simple cell suspensions.

Rijal and Li (2017) used their decellularized breast tumor tissue to grow cancerous cells ex vivo and implant afterwards the 3D cultures in mice. This not only results in a successful development of the tumor tissue (compared with the classical subcutaneous implantation of the cells), but also accelerates the process of obtaining ready to use tumor animal models. Similarly, Guller et al. (2015) have used acellular organ scaffolds that were successfully in vivo colonized with tumor cells.

Zanoni et al. (2016) developed a method to analyze and correlate the morphology of large tumor spheroids obtained by liquid methods and their response to therapy, as variances in dimension and shape might correlate to totally different responses. The method is based on using MATLAB-based software, which analyzes some morphological parameters of the tumor spheroid (like volume and shape) that may induce variability in treatment response; these were used to pre-select tumor spheroids similar in morphology, which helped for the validation of a robust cytotoxicity assay.

---

## 15.4 CONCLUSIONS AND PERSPECTIVES

In the actual context, there is a need for developing and implementing standardized alternative methods to animal testing, in fields like cancer research and drug testing. Considering this field, a promising solution has been given by in vitro 3D tumor cell cultures.

Currently there are quite a few commercially available technologies based on liquid methods that use scaffolds or both approaches. Almost all big companies specializing in cell cultures and molecular biology offer laboratory vessels, scaffolds, and substances or whole kits for 3D cell culturing. Moreover, a lot of start-ups are offering solutions for more complex models, which imply different processes like circulation, cell signaling, etc.

At the moment microfluidic devices and bioprinting are the up-trending technologies on this market. Microscale bioreactors have the ability of higher control of the process parameters, and are easily to manipulate and monitor; also, phenomena like circulation through blood vessels and migration of cells can be easily simulated. On the other hand, bioprinting offers the advantage of high control of the structure's architecture, resulting in highly biomimetic and functional materials.

However, despite all these advances, there is no model that can fully replace the complexity of the living organism. The development of in vitro 3D tumor models is still a highly emerging field and there is still room for a lot of improvement.

---

## ACKNOWLEDGMENTS

This work was supported by a grant from the Romanian National Authority for Scientific Research and Innovation, UEFISCDI, project number 45PCCDI/2018-PN-III-P1-1.2-PCCDI-2017-0749-Nanostructuri bioactive pentru strategii terapeutice inovatoare.

---

## REFERENCES

- Abe-Fukasawa, N., Otsuka, K., Aihara, A., Itasaki, N., Nishino, T., 2018. Novel 3D liquid cell culture method for anchorage-independent cell growth, cell imaging and automated drugscreening. *Sci. Reports* 8, 3627.
- Al, P.R.C.E., 2014. *Rom. J. Morphol. Embryol.* 55, 1013–1101.
- Amsbio, Cultrex® 3D Cell Culture, <http://www.amsbio.com/cultrex.aspx>, accessed on 14.01.2019.
- Andersen, T., Auk-Emblem, P., Dornish, M., 2015. 3D cell culture in alginate hydrogels. *Microarrays (Basel)* 4, 133–161.
- Angeloni, V., Contessi, N., De marco, C., Bertoldi, S., Tanzi, M.C., Daidone, M.G., et al., 2017. Polyurethane foam scaffold as in vitro model for breast cancer bone metastasis. *Acta Biomater.* 63, 306–316.
- Aspectbiosystems, <https://www.aspectbiosystems.com>, accessed on 14.01.2019.
- Balachander, G., Balaji, S.A., Rangarajan, A., Chatterjee, K., 2016. Study of breast cancer metastasis in vitro using a 3D tissue scaffold. *Front. Bioeng. Biotechnol.* Available from: <https://doi.org/10.3389/conf.FBIOE.2016.01.00913> Conference Abstract: 10th World Biomaterials Congress.

- BioVision, 3D Cell Culture Ready-to-Use Scaffold Complete Kit, <https://www.biovision.com/3d-cell-culture-ready-to-use-scaffold-complete-kit.html> accessed on 14.01.2019.
- Boussommier-Calleja, A., Atiyas, Y., Haase, K., Headley, M., Lewis, C., Kamm, R.D., 2018. The effects of monocytes on tumor cell extravasation in a 3D vascularized microfluidic model. *Biomaterials*. Available from: <https://doi.org/10.1016/j.biomaterials.2018.03.005>.
- Brown, J.M., 2007. Tumor hypoxia in cancer therapy. *Methods Enzymol.* 435, 297–321.
- Caicedo-Carvajal, C.E., Liu, Q., Remache, Y., Goy, A., Suh, K.S., 2011. Cancer tissue engineering: a novel 3D polystyrene scaffold for in vitro isolation and amplification of lymphoma cancer cells from heterogeneous cell mixtures. *J. Tissue Eng.* 2011, 362326.
- Caliari, S.R., Burdick, J.A., 2016. A practical guide to hydrogels for cell culture. *Nat. Methods* 13, 405–414.
- Campbell, J.J., Husmann, A., Hume, R.D., Watson, C.J., Cameron, R.E., 2017. Development of three-dimensional collagen scaffolds with controlled architecture for cell migration studies using breast cancer cell lines. *Biomaterials* 114, 34–43.
- CTIBIOTEK and CELLINK BIO X 3D, <https://cellink.com/cellink-signs-collaboration-agreement-ctibiotek-bioprinting-patient-specific-cancer-tumors/> accessed on 14.01.2019.
- Chen, Y., Gao, D., Liu, H., Lin, S., Jiang, Y., 2015. Drug cytotoxicity and signaling pathway analysis with three-dimensional tumor spheroids in a microwell-based microfluidic chip for drug screening. *Anal. Chim. Acta* 898, 85–92.
- Chen, M.B., Whisler, J.A., Frose, J., Yu, C., Shin, Y., Kamm, R.D., 2017. On-chip human microvasculature assay for visualization and quantification of tumor cell extravasation dynamics. *Nat. Protoc.* 12, 865–880.
- Chen, C.-N., Chen, Y.-T., Yang, T.-L., 2018. Application of three-dimensional collagen scaffolds to recapitulate and monitor the dynamics of epithelial-mesenchymal transition during tumor satellite formation of head and neck cancer. *Biomaterials* 154, 134–146.
- Choi, Y.J., Yi, H.G., Kim, S.W., Cho, D.W., 2017. 3D cell printed tissue analogues: a new platform for theranostics. *Theranostics* 7, 3118–3137.
- Colella, G., Fazioli, F., Gallo, M., De chiara, A., Apice, G., Ruosi, C., et al., 2018. Sarcoma spheroids and organoids-promising tools in the era of personalized medicine. *Int. J. Mol. Sci.* 19, 1–15.
- Curtin, C., Nolan, J.C., Conlon, R., Deneweth, L., Gallagher, C., Tan, Y.J., et al., 2018. A physiologically relevant 3D collagen-based scaffold–neuroblastoma cell system exhibits chemosensitivity similar to orthotopic xenograft models. *Acta Biomater.* 70, 84–97.
- Cyfusebio, <https://www.cyfusebio.com/en/> accessed on 14.01.2019.
- Dai, X., Liu, L., Ouyang, J., Li, X., Zhang, X., Lan, Q., et al., 2017. Coaxial 3D bioprinting of self-assembled multicellular heterogeneous tumor fibers. *Sci. Reports* 7, 1457.
- De jaeghere, E., De vlieghe, E., Van hoorick, J., Van vlierberghe, S., Wagemans, G., Pieters, L., et al., 2018. Heterocellular 3D scaffolds as biomimetic to recapitulate the tumor microenvironment of peritoneal metastases in vitro and in vivo. *Biomaterials* 158, 95–105.
- Digilab, <http://www.digilabglobal.com>, accessed on 14.01.2019.
- Eales, K.L., Hollinshead, K.E., Tennant, D.A., 2016. Hypoxia and metabolic adaptation of cancer cells. *Oncogenesis* 5, e190.
- EnvisionTEC, <https://envisiontec.com>, accessed on 14.01.2019.
- Farokhzad, O.C., Khademhosseini, A., Jon, S., Hermmann, A., Cheng, J., Chin, C., et al., 2005. Microfluidic system for studying the interaction of nanoparticles and microparticles with cells. *Anal. Chem.* 77, 5453–5459.

- Fong, E.L.S., Lamhamedi-Cherradi, S.-E., Burdett, E., Ramamoorthy, V., Lazar, A.J., Kasper, F.K., et al., 2013. Modeling Ewing sarcoma tumors in vitro with 3D scaffolds. *Proc. Natl. Acad. Sci.* 110, 6500.
- Fong, E.L., Santoro, M., Farach-Carson, M.C., Kasper, F.K., Mikos, A.G., 2014. Tissue engineering perfusable cancer models. *Curr. Opin. Chem. Eng.* 3, 112–117.
- Goral, V.N., Au, S.H., Faris, R.A., Yuen, P.K., 2014. Microstructured multi-well plate for three-dimensional packed cell seeding and hepatocyte cell culture. *Biomicrofluidics* 8, 046502-046502.
- Greish, K., 2010. Enhanced permeability and retention (EPR) effect for anticancer nanomedicine drug targeting. *Methods Mol. Biol.* 624, 25–37.
- Guirro, K., Patel, S.A., Greco, S.J., Rameshwar, P., Arinzeh, T.L., 2015. Investigating breast cancer cell behavior using tissue engineering scaffolds. *PLoS One* 10, e0118724.
- Guller, A., Trusova, I., Petersen, E., Shekhter, A., Kurkov, A., Qian, Y., et al., 2015. Acellular organ scaffolds for tumor tissue engineering, *Proceedings volume 9668, “Micro + Nano Materials, Devices, and Applications”*, 96684G of the SPIE Conference “Micro + Nano Materials, Devices and Applications”, Sydney, New South Wales, Australia, 2015.
- Hamdi, D.H., Barbieri, S., Chevalier, F., Groetz, J.-E., Legendre, F., Demoor, M., et al., 2015. In vitro engineering of human 3D chondrosarcoma: a preclinical model relevant for investigations of radiation quality impact. *BMC Cancer* 15, 579.
- Heffernan, J.M., Mcnamara, J.B., Borwege, S., Vernon, B.L., Sanai, N., Mehta, S., et al., 2017. PNIPAAm-co-Jeffamine® (PNJ) scaffolds as in vitro models for niche enrichment of glioblastoma stem-like cells. *Biomaterials* 143, 149–158.
- Huang, S., He, Y.-Q., Jiao, F., 2017. Advances of particles/cells magnetic manipulation in microfluidic chips. *Chin. J. Anal. Chem.* 45, 1238–1246.
- IncuCyte, IncuCyte® S3 Multi-Spheroid Assays, <https://www.essenbioscience.com/hi/applications/cell-health-viability/multi-spheroid/> accessed 14.01.2019.
- Ingram, M., Techy, G.B., Ward, B.R., Imam, S.A., Atkinson, R., Ho, H., et al., 2010. Tissue engineered tumor models. *Biotech. Histochem.* 85, 213–229.
- Jordahl, J.H., Solorio, L., Sun, H., Ramcharan, S., Teeple, C.B., Haley, H.R., et al., 2018. 3D jet writing: functional microtissues based on tessellated scaffold architectures. *Adv. Mater.* 30, 1707196.
- King, S.M., Development of 3D bioprinted human breast cancer for in vitro screening of therapeutics targeted against cancer progression, [https://organovo.com/wp-content/uploads/2015/07/12-12-13\\_ASCB\\_Poster\\_Final\\_SMK-low-res.pdf](https://organovo.com/wp-content/uploads/2015/07/12-12-13_ASCB_Poster_Final_SMK-low-res.pdf), accessed 14.01.2019.
- Knowlton, S., Onal, S., Yu, C.H., Zhao, J.J., Tasoglu, S., 2015. Bioprinting for cancer research. *Trends Biotechnol.* 33, 504–513.
- Kruczynski, A., Hill, B.T., 2002. Classic in vivo cancer models: three examples of mouse models used in experimental therapeutics. *Curr. Protoc. Pharmacol.* Chapter 5, Unit5 24.
- Kwak, B., Lee, Y., Lee, J., Lee, S., Lim, J., 2018. Mass fabrication of uniform sized 3D tumor spheroid using high-throughput microfluidic system. *J. Control. Release* 275, 201–207.
- Lee, V.K., Guohao, D., Hongyan, Z., Seung-Schik, Y., 2015. Generation of 3-D glioblastoma-vascular niche using 3-D bioprinting. In: 2015 41st Annual Northeast Biomedical Engineering Conference (NEBEC), 17–19 April 2015. pp. 1–2.
- LifeSciences, <https://lifesciences.solutions>, accessed 14.01.2019.
- Lin, D.-G., Lin, J.-Q., Li, P.-W., Yang, N., Xu, B.-L., Liu, D.-Y., 2018. Construction of tumor tissue array on an open-access microfluidic chip. *Chin. J. Anal. Chem.* 46, 113–120.



- Lonza, Raft 3D Cell Culture System for Tissue Modeling, [https://bioscience.lonza.com/lonza\\_bs/CH/en/raft-3d-cell-culture](https://bioscience.lonza.com/lonza_bs/CH/en/raft-3d-cell-culture), accessed 14.01.2019.
- Loureiro, R., Mesquita, K.A., Magalhães-Novais, S., Oliveira, P.J., Vega-Naredo, I., 2017. Mitochondrial biology in cancer stem cells. *Semin. Cancer Biol.* 47, 18–28.
- Lü, W.-D., Sun, R.-F., Hu, Y.-R., Lu, J.-R., Gu, L., Liu, Z.-G., et al., 2018. Photooxidatively crosslinked acellular tumor extracellular matrices as potential tumor engineering scaffolds. *Acta Biomater.* 71, 460–473.
- Mahmoudzadeh, A., Mohammadpour, H., 2016. Tumor cell culture on collagen–chitosan scaffolds as three-dimensional tumor model: a suitable model for tumor studies. *J. Food Drug Anal.* 24, 620–626.
- Medema, J.P., 2013. Cancer stem cells: the challenges ahead. *Nat. Cell Biol.* 15, 338–344.
- Merckmillipore, 3D Collagen Culture Kit, [http://www.merckmillipore.com/DE/en/product/3D-Collagen-Culture-Kit,MM\\_NF-ECM675?ReferrerURL=https%3A%2F%2Fwww.google.com%2F](http://www.merckmillipore.com/DE/en/product/3D-Collagen-Culture-Kit,MM_NF-ECM675?ReferrerURL=https%3A%2F%2Fwww.google.com%2F) accessed 14.01.2019.
- Muz, B., DE La puente, P., Azab, F., Azab, A.K., 2015. The role of hypoxia in cancer progression, angiogenesis, metastasis, and resistance to therapy. *Hypoxia (Auckland, N.Z.)* 3, 83–92.
- n3DBiosciences, <http://www.n3dbio.com>, accessed 14.01.2019.
- Nietzer, S., Baur, F., Sieber, S., Hansmann, J., Schwarz, T., Stoffer, C., et al., 2016. Mimicking metastases including tumor stroma: a new technique to generate a three-dimensional colorectal cancer model based on a biological decellularized intestinal scaffold. *Tissue Eng. Part C: Methods* 22, 621–635.
- nScript, <https://www.nscript.com>, accessed on 14.01.2019.
- Ollitrault, D., Legendre, F., Drogard, C., Briand, M., Benateau, H., Goux, D., et al., 2014. BMP-2, hypoxia, and COL1A1/HtrA1 siRNAs favor neo-cartilage hyaline matrix formation in chondrocytes. *Tissue Eng. Part C Methods* 21, 133–147.
- Organovo, <https://organovo.com>, accessed 14.01.2019.
- Osaki, T., Sivathanu, V., Kamm, R.D., 2018. Vascularized microfluidic organ-chips for drug screening, disease models and tissue engineering. *Curr. Opin. Biotechnol.* 52, 116–123.
- Ozcelikkale, A., Moon, H.-R., Linnes, M., Han, B., 2017a. In vitro microfluidic models of tumor microenvironment to screen transport of drugs and nanoparticles. *Wiley Interdiscipl. Rev. Nanomed. Nanobiotechnol.* 9, e1460.
- Ozcelikkale, A., Shin, K., Noe-Kim, V., Elzey, B.D., Dong, Z., Zhang, J.-T., et al., 2017b. Differential response to doxorubicin in breast cancer subtypes simulated by a microfluidic tumor model. *J. Control. Release* 266, 129–139.
- Palomeras, S., Rabionet, M., Ferrer, I., Sarrats, A., Garcia-Romeu, M.L., Puig, T., et al., 2016. Breast cancer stem cell culture and enrichment using poly(epsilon-caprolactone) scaffolds. *Molecules* 21, 537.
- Pandya, H.J., Dhingra, K., Prabhakar, D., Chandrasekar, V., Natarajan, S.K., Vasan, A.S., et al., 2017. A microfluidic platform for drug screening in a 3D cancer microenvironment. *Biosens. Bioelectron.* 94, 632–642.
- Polley, C., Mau, R., Lieberwirth, C., Stenzel, J., Vollmar, B., Seitz, H., 2017. Bioprinting of three dimensional tumor models: a preliminary study using a low cost 3D printer. *Curr. Direct. Biomed. Eng.*
- Promocell, 3D Cell Culture, <https://www.promocell.com/portfolio/3d-cell-culture-2/> accessed 14.01.2019.



- Regenovo, Drug Discovery and Tissue Engineering, <http://regenovo.com/English/index.aspx>, accessed 14.01.2019.
- Ricci, C., Moroni, L., Danti, S., 2013. Cancer tissue engineering—new perspectives in understanding the biology of solid tumours—a critical review. *OA Tissue Eng.* 1, 4.
- Richardson, P.F., 2012. Chapter Sixteen—Nanotechnology therapeutics in oncology—recent developments and future outlook. In: Desai, M.C. (Ed.), *Annual Reports in Medicinal Chemistry*. Academic Press.
- Rijal, G., Li, W., 2017. A versatile 3D tissue matrix scaffold system for tumor modeling and drug screening. *Sci. Adv.* 3, e1700764.
- Rijal, G., Bathula, C., Li, W., 2017. Application of synthetic polymeric scaffolds in breast cancer 3D tissue cultures and animal tumor models. *Int. J. Biomater.* 2017, 9.
- Ross, A.E., Pompano, R.R., 2018. Diffusion of cytokines in live lymph node tissue using microfluidic integrated optical imaging. *Anal. Chim. Acta* 1000, 205–213.
- Schmitt, S.K., Xie, A.W., Ghassemi, R.M., Trebatoski, D.J., Murphy, W.L., Gopalan, P., 2015. Polyethylene glycol coatings on plastic substrates for chemically defined stem cell culture. *Adv. Healthc. Mater.* 4, 1555–1564.
- Schwarz, J., Bierbaum, V., Merrin, J., Frank, T., Hauschild, R., Bollenbach, T., et al., 2016. A microfluidic device for measuring cell migration towards substrate-bound and soluble chemokine gradients. *Sci. Reports* 6, 36440.
- Sears et al. Inventor; Oregon Health& Science University assignee, Three-dimensional bio-printed pancreatic tumor model, WO2016022830A1, under application since 11.02.2016.
- Serra, M., Correia, C., Malpique, R., Brito, C., Jensen, J., Bjorquist, P., et al., 2011. Microencapsulation technology: a powerful tool for integrating expansion and cryopreservation of human embryonic stem cells. *PLoS One* 6, e23212.
- Sheikholeslam, M., Wheeler, S.D., Duke, K.G., Marsden, M., Pritzker, M., Chen, P., 2018. Peptide and peptide-carbon nanotube hydrogels as scaffolds for tissue & 3D tumor engineering. *Acta Biomater.* 69, 107–119.
- Sigma-Aldrich, 3D Hydrogels, <https://www.sigmaaldrich.com/labware/labware-products.html?TablePage=119102956>, accessed 14.01.2019.
- Sigma-Aldrich, 5 Reasons Cancer Researchers Adopt 3D Cell Culture: A Review of Recent Literature. <https://www.sigmaaldrich.com/technical-documents/articles/biology/5-reasons-cancer-researchers-adopt-3d-cell-culture-white-paper.html>, accessed 14.01.2019.
- Smith, L.J., Li, P., Holland, M.R., Ekser, B., 2018. FABRICA: a bioreactor platform for printing, perfusing, observing, & stimulating 3D tissues. *Sci. Reports* 8, 7561.
- Sokol, E.S., Miller, D.H., Breggia, A., Spencer, K.C., Arendt, L.M., Gupta, P.B., 2016. Growth of human breast tissues from patient cells in 3D hydrogel scaffolds. *Breast Cancer Res.* 18, 19.
- Sun, J., Masterman-Smith, M.D., Graham, N.A., Jiao, J., Mottahedeh, J., Laks, D.R., et al., 2010. A microfluidic platform for systems pathology: multiparameter single-cell signaling measurements of clinical brain tumor specimens. *Cancer Res.* 70, 6128–6138.
- Sun, D., Liu, Y., Wang, H., Deng, F., Zhang, Y., Zhao, S., et al., 2018. Novel decellularized liver matrix-alginate hybrid gel beads for the 3D culture of hepatocellular carcinoma cells. *Int. J. Biol. Macromol* 109, 1154–1163.
- Suzuki, R., Aruga, A., Kobayashi, H., Yamato, M., Yamamoto, M., 2014. Development of a novel in vivo cancer model using cell sheet engineering. *Anticancer Res.* 34, 4747–4754.
- Tabata, Y., Horiguchi, I., Lutolf, M.P., Sakai, Y., 2014. Development of bioactive hydrogel capsules for the 3D expansion of pluripotent stem cells in bioreactors. *Biomater. Sci.* 2, 176–183.

- Tang, Y., Soroush, F., Sheffield, J.B., Wang, B., Prabhakarandian, B., Kiani, M.F., 2017. A biomimetic microfluidic tumor microenvironment platform mimicking the EPR effect for rapid screening of drug delivery systems. *Sci. Reports* 7, 9359.
- Tevidobiodevices, <http://tevidobiodevices.com>, accessed 14.01.2019.
- ThermoFisher, Algimatrix 3D Cell Culture System, <https://www.thermofisher.com/ro/en/home/references/protocols/cell-culture/3-d-cell-culture-protocol/algimatrix-3d-culture-system.html> accessed 14.01.2019.
- Trachtenberg, J.E., Santoro, M., Williams, C., Piard, C.M., Smith, B.T., Placone, J.K., et al., 2018. Effects of shear stress gradients on ewing sarcoma cells using 3D printed scaffolds and flow perfusion. *ACS Biomater. Sci. Eng.* 4, 347–356.
- Walsh, C.L., Babin, B.M., Kasinskas, R.W., Foster, J.A., McGarry, M.J., Forbes, N.S., 2009. A multipurpose microfluidic device designed to mimic microenvironment gradients and develop targeted cancer therapeutics. *Lab. Chip* 9, 545–554.
- Wang, W.-X., Liu, W.-P., Wu, B., Liang, G.-T., Liu, D.-Y., 2015. Construction of Tumor Tissue Microarray on a Microfluidic Chip. *Chinese J. Anal. Chem.* 43 (5), 637–642.
- Wang, J.-Z., Zhu, Y.-X., Ma, H.-C., Chen, S.-N., Chao, J.-Y., Ruan, W.-D., et al., 2016. Developing multi-cellular tumor spheroid model (MCTS) in the chitosan/collagen/alginate (CCA) fibrous scaffold for anticancer drug screening. *Mater. Sci. Eng. C* 62, 215–225.
- Wang, X., Dai, X., Zhang, X., Li, X., Xu, T., Lan, Q., 2018. Enrichment of glioma stem cell-like cells on 3D porous scaffolds composed of different extracellular matrix. *Biochem. Biophys. Res. Commun.* 498, 1052–1057.
- Wang, Y., Nicolas, C.T., Chen, H.S., Ross, J.J., De lorenzo, S.B., Nyberg, S.L., 2017. Recent advances in decellularization and recellularization for tissue-engineered liver grafts. *Cells Tissues Organs* 204, 125–136.
- Webmaster, CTIBiotech advances cancer treatments with state-of-the-art 3D-Bioprinting. <http://www.imodi-cancer.org/ctibiotech-advances-cancer-treatments-with-state-of-the-art-3d-bioprinting/> accessed 14.01.2019.
- Wei, Z., Nathan, J.C., Haitao, C., Xuan, Z., Benchaa, B., Robert, M., et al., 2016. A 3D printed nano bone matrix for characterization of breast cancer cell and osteoblast interactions. *Nanotechnology* 27, 315103.
- Wen, H., Gao, T., Fu, Z., Liu, X., Xu, J., He, Y., et al., 2017. Enhancement of membrane stability on magnetic responsive hydrogel microcapsules for potential on-demand cell separation. *Carbohydr. Polym.* 157, 1451–1460.
- Xingliang, D., Cheng, M., Qing, L., Tao, X., 2016. 3D bioprinted glioma stem cells for brain tumor model and applications of drug susceptibility. *Biofabrication* 8, 045005.
- Xu, H., Liu, X., Le, W., 2018. Recent advances in microfluidic models for cancer metastasis research. *TrAC Trends Anal. Chem.* 105, 1–6.
- Yoon, S.K., 2012. The biology of cancer stem cells and its clinical implication in hepatocellular carcinoma. *Gut Liver* 6, 29–40.
- Young, M., Rodenhizer, D., Dean, T., D'arcangelo, E., Xu, B., Ailles, L., et al., 2018. A TRACER 3D Co-Culture tumour model for head and neck cancer. *Biomaterials* 164, 54–69.
- Yu, Z., Rui, Y., Liliang, O., Hongxu, D., Ting, Z., Kaitai, Z., et al., 2014. Three-dimensional printing of Hela cells for cervical tumor model in vitro. *Biofabrication* 6, 035001.

- Yuhas, J.M., Li, A.P., Martinez, A.O., Ladman, A.J., 1977. A simplified method for production and growth of multicellular tumor spheroids. *Cancer Res.* 37, 3639–3643.
- Zanoni, M., Piccinini, F., Arienti, C., Zamagni, A., Santi, S., Polico, R., et al., 2016. 3D tumor spheroid models for in vitro therapeutic screening: a systematic approach to enhance the biological relevance of data obtained. *Sci. Reports* 6, 19103.
- Zhu, W., Holmes, B., Glazer, R.I., Zhang, L.G., 2016. 3D printed nanocomposite matrix for the study of breast cancer bone metastasis. *Nanomed. Nanotechnol. Biol. Med.* 12, 69–79.

# Index

*Note:* Page numbers followed by “*f*” and “*t*” refer to figures and tables, respectively.

## A

Abduction and adduction motion, 64  
Adult stem cells, 229  
Alginate, 33  
Alkaline phosphatase activity (ALP), 9, 382  
Aluminum-doped hydroxyapatite, 217–218  
Anion-doped hydroxyapatite, 220  
Antimicrobial action, 172–173  
Apatite coated titanium alloys, 32–33  
Apatites, 343  
Apligraf, 99*t*  
Artificial musculoskeletal systems, 71–72  
Artificial skin, 98, 101*f*, 104–105, 109–110  
Atomic force microscopy (AFM), 143  
Autoacceleration mechanism, 254

## B

Bacterial cellulose (BC) tubes, 6  
Beschitin, 99*t*  
17- $\beta$ -estradiol valerate, 132  
Bioactive glasses, 373–379, 401–404  
  antibacterial effect of, 403–404  
  –based scaffolds, 406–408  
    electrospinning process, 408  
    freeze-casting and freeze-drying process, 407–408  
    melt-derived processing, 406  
    polymer-foam replication, 407  
    rapid prototyping process, 408  
    sol–gel processing, 407  
  bone, 397–399  
  bone tissue engineering, 399–400, 408–426  
    bioactive glasses–based composite scaffolds, 408–419  
    bone implant materials, requirements for, 399–400  
    mixed natural and synthetic polymers/  
      bioactive glasses–based composite  
      scaffolds, 425–426  
    natural polymer/bioactive glasses–based  
      composite scaffolds, 419–422  
    synthetic polymer/bioactive glasses–based  
      composite scaffolds, 423–425  
  borate-based bioactive glass, 377–378  
  fabrication of bioactive glass scaffolds,  
    378–379  
    mechanical properties, 379

    future perspective, 426–427  
    phosphate-based bioactive glass, 377  
    response of bioactive glasses to cells, 402–403  
    silicate-based bioactive glass, 374–377  
    surface modification of bioactive glasses,  
      405–406  
  synthesis of, 404–405  
    flame-spray method, 405  
    laser-spinning method, 405  
    microemulsion method, 405  
    sol–gel method, 404–405  
  type of, 401–402  
    borate/borosilicate-bioactive glasses, 401  
    doped-bioactive glasses (DBGs), 402  
    metallic-bioactive glasses, 402  
    phosphate-bioactive glasses, 401–402  
    silicate-bioactive glasses, 401  
Bioactive glass nanoparticles (BGNPs), 404  
Bioactivity, 345  
Biobrane, 99*t*  
Bioceramics, 10–11  
Biocomposites, 121, 123–125  
  prepared by using resorbable polymeric fibers,  
    125–147  
    collagen, 142–145  
    polylactide, 125–142  
    silk, 145–147  
Biodegradation, 173  
  of polylactic acid, 129  
Biomimetic structures, 70–71  
Bionanotechnology, 12  
Bio-printing, 471–474  
Bisfenol A dimethacrylate (Bis-DMA), 253  
Bisphenol A glycerolate dimethacrylate (Bis-GMA), 252–253  
Blended polymers, for smart hybrid scaffold  
  fabrication, 7–8  
Bone, 397–399  
  biology, 333–334  
  composition of, 24*t*  
  hierarchical ordered structure of, 398*f*  
  hierarchical organization of, 334*f*  
  physical properties of, 28*t*  
  structures of, 24*f*  
Bone-forming peptide (BFP), 415–417  
Bone graft, 335–337  
  biocompatibility, 335  
  biodegradability, 336

- Bone graft (*Continued*)
    - manufacturing technology, 336–337
    - mechanical properties, 336
    - structural requirements, 336
  - Bone graft substitutes, 23–27
    - chitosan-based material for, 30–34
      - chitosan-alginate scaffolds, 33
      - chitosan–calcium phosphate based substitutes, 31–32
      - chitosan hydroxyapatite based bone graft substitutes, 32–33
      - chitosan polylactic acid substitute, 34
    - properties of, 27–30
      - biocompatibility, 27
      - mechanical stability and biodegradability, 30
      - osteinduction, 30
      - pore size, 27
      - porosity, 27
      - surface properties, 27–30
  - Bone lining cells, 333
  - Bone Marrow Stromal Cells (BMSCs), 401–402
  - Bone morphogenetic proteins (BMPs), 130
    - BMP-2, 5–6
  - Bone regeneration
    - chitosan as biomaterial for, 347–350
    - hydroxyapatite as biomaterial for, 343–347
  - Bones, cartilage, and tendon tissue regeneration
    - electrospinning (ES) process for, 82–88
  - Bone tissue engineering, 184–185, 399–400
    - applications, 408–426
      - bioactive glasses–based composite scaffolds, 408–419
      - mixed natural and synthetic polymers/bioactive glasses–based composite scaffolds, 425–426
      - natural polymer/bioactive glasses–based composite scaffolds, 419–422
      - synthetic polymer/bioactive glasses–based composite scaffolds, 423–425
    - bioactive glasses for, 400
    - bone implant materials, requirements for, 399–400
  - Borate-based bioactive glass, 377–378
  - Borate/borosilicate-bioactive glasses, 401
  - Born–Oppenheimer approximation, 307
  - Bovine bones, 23–26, 212–213
  - Bulk metallic glasses (BMGs), 402
- C**
- Calcium carbonate, 302–303
    - properties, 302–303
  - Calcium hydroxyapatite, basic structure of, 207–209
  - Calcium phosphate bone graft substitutes, 26
  - Calcium phosphate cements (CPCs), 31–32, 408–409
  - Calcium phosphates (CaPs), 251
  - Calcium polyphosphate (CPP) crystal, 224
  - Cancellous bone grafts, 336
  - Carbon nanofibers (CNFs), 8–9
  - Carbon nanotubes (CNTs), 8–9
  - Carboxyl functionalized MWCNTs, 10
  - Cartilage, 82–88
  - Cartilage tissue engineering, 182–184
  - Cellulose, 146*t*
  - Cellulose nanocrystals (CNCs), 421–422
  - Cellulose nanofibers (CNFs), 82–83
  - Ceramic NPs, 221–222
  - Ceramics, 303
  - Cetyltrimethylammonium bromide (CTAB), 410–413
  - Chemical precipitation method, 211
  - Chirality, 46
  - Chitin, structure of, 348*f*
  - Chitinase, 173
  - Chitin hydroxyapatite composite, 32–33
  - ChitoFlex PRO, 99*t*
  - ChitoPack C, 99*t*
  - ChitoPack S, 99*t*
  - Chitosan (CS), 170–171
    - based material for bone graft substitutes, 25*f*, 30–34
      - chitosan-alginate scaffolds, 33
      - chitosan–calcium phosphate based substitutes, 31–32
      - chitosan hydroxyapatite based bone graft substitutes, 32–33
      - chitosan polylactic acid substitute, 34
    - as biomaterial, 171–173
      - antimicrobial action, 172–173
      - biocompatibility, 173
      - biodegradation, 173
      - for bone regeneration, 347–350
      - hemostasis, 172
      - mucoadhesion, 171–172
    - cationic nature of, 348*f*
    - structure of, 348*f*
  - Chitosan–calcium phosphate (CCP) composites, 31
  - Chitosan/collagen/alginate (CCA) fibrous scaffolds, 468
  - Chitosan/collagen biocomposite, 105–106
  - Chitosan composites, 104–109
    - challenges, 115–116
    - characterization, 109–112
      - biocompatibility, 112
      - mechanical strength, 110–112
      - pore size and porosity, 109–110

- conductive membrane/films, 108–109
  - future perspectives, 116
  - as hydrogels, 106
  - in vivo models, 113–114
    - full thickness wound model, 114
    - split thickness model, 114
  - as nanofibers, 106–108
  - as sponges, 104–106
  - wound healing models studied for, 112–114
  - Chitosan films, 178–179
  - Chitosan/gelatin biocomposite, 104–105
  - Chitosan hydrogel, 174–177
    - cross-linked networks, 177
    - physical association network, 176–177
  - Chitosan nanocomposite, 180–181
  - Chitosan nanofibers, 179–180
  - Chitosan/poly(vinyl alcohol)/graphene oxide (GO) composite nanofibers, 85
  - Chitosan scaffolds
    - applications of, 181–191
      - drug delivery, 189–190
      - gene therapy, 190–191
      - bone tissue engineering, 184–185
      - cartilage tissue engineering, 182–184
      - liver tissue engineering, 185–186
      - nerve tissue engineering, 186–188
      - wound healing, 188–189
    - fabrication techniques for, 175*f*
  - Chitosan sponges, 178
  - Chondroitin sulfate, 4–5
  - Classical stereolithography, 472
  - Coating material, hydroxyapatite as, 231–233
  - Cold plate electrospinning (CPE), 88
  - Collagen, 4–5, 106–107, 142–145
    - based nanocomposites, 146*t*
    - for bone tissue regeneration, 8
    - COL I, 84
    - physical properties of, 28*t*
  - Collagraft, 143
  - Commercially available bone grafts, 337–342
  - Composite production techniques, 383–388
    - electrospinning, 384–385
    - freeze-drying, 387–388
    - microspheres, 386
    - solvent casting–particulate leaching (SCPL), 386–387
    - 3D printing, 388
  - Computational chemistry, 304–308
    - molecular mechanics (MM), 305–306
    - Monte Carlo technique, 308
    - quantum mechanics (QM), 306–308
  - Conductive membrane/films, 108–109
    - chitosan composites as, 108–109
  - Cortical bone, 23, 397–399
  - Coulomb interaction, 307
  - Critical micellar concentration (CMC), 212
  - Curcumin, 188–189
- ## D
- Decellularized intestinal scaffolds, 469
  - Degradable materials, physical properties of, 28*t*
  - Degree of deacetylation (DD), 168
  - Degumming, 5
  - Demineralized bone matrix (DBM), 337–338
  - Dental applications, hydroxyapatite in, 226–228
    - dental fillers, 227
    - dental implants, 227–228
    - enamel restoration, 226–227
  - Dental composites, 252–258
    - filler typologies, 255–258
    - polymerization process, 254
    - resin matrix for, 252–254
  - Deproteinized bones, 23–26
  - Dermagraft, 99*t*
  - Dexamethasone (DEX)-loaded poly (lactic-co-glycolic acid) (PLGA) microspheres, 224
  - Digital micromirror projection, 472
  - Dimethacrylate monomers, 253
  - N,N*-Dimethylacetamide, 135
  - DNA nanotechnology, 12
  - DNA origami, 12
  - Doped-bioactive glasses (DBGs), 402
  - Drop hanging method, 466
  - Drosophila melanogaster*, 180
  - Drug delivery system, 189–190
    - polylactic acid composites in, 131–132
  - Dynamic loading, 53–54, 60
- ## E
- Elastase, 129
  - Electrospinning (ES) process, 3–4, 77–81, 384–385, 408
    - melt electrospinning, 81
    - multijets
      - from multiple needles, 80
      - from needleless systems, 81
      - from a single needle, 80
    - for tissue engineering, 82–91
      - bones, cartilage, and tendon tissue regeneration, 82–88
      - skin tissue regeneration, 88–89
  - Electrospun nanofibers, 7, 79, 85, 88
  - Electrostatic potential map, 310–311, 317
  - Elemental doping role in hydroxyapatite, 216–220
    - aluminum-doped hydroxyapatite, 217–218
    - anion-doped hydroxyapatite, 220
    - iron-doped hydroxyapatite, 219

## Elemental doping role in hydroxyapatite (Continued)

- lithium-doped hydroxyapatite, 217
- magnesium-doped hydroxyapatite, 218–219
- manganese-doped hydroxyapatite, 219
- selenium-doped hydroxyapatite, 217
- silver-doped hydroxyapatite, 218
- zinc-doped hydroxyapatite, 219–220
- zirconium-doped hydroxyapatite, 218

## Embryonic stem cells (ESCs), 228

## Emulsification, 355

## Emulsion technique, 212

## Engineered composites, 123–125

## Erythrocytes coagulation, 172

## Ethoxylated bisphenol A glycol dimethacrylate (Bis-EMA), 253

## Ethylene glycol dimethacrylate (EGDMA), 251, 253

## Ethylene oxide (EtO), 360–361

## Extension motion, 64

## External anal sphincter muscle (EAS), 68

## Extracellular matrix (ECM), 1–2, 77–78, 333

## F

## Fecal incontinence (FI) treatment, 68

## Fiber filler, 447

## Fibrin–collagen combination, 144–145

## Fibroblast cells, 145

## Fickian diffusion theory, 273–274

## Filler reinforcing efficiency, 275–277

## Filler typologies, 255–258

## Finger bones, 64

## Flame-spray method, 405

## Flexion motion, 64

## Force measurement, 60–61

## Fourier transform infrared spectroscopy (FTIR), 214, 267, 310

## Freeze-casting and freeze-drying process, 407–408

## Freeze-drying, 358, 387–388

## Full thickness wound model, 114

## Futek LBS-200 load cells, 60

## G

## Galactosylated chitosan, 185–186

## Gallagher–Corrigan model, 225

## Gelatin, 4, 104–105, 107–108

## Gelatin/polycaprolactone (Gt/PCL) fibrous mats, 83

## Gelatin-tyrosine-triazole (GTT), 85

## Gene therapy, 190–191

## 3-Glycidoxypolytrimethoxysilane (GPTMS), 385

## Gold, 146*t*

## Gram-negative *Escherichia coli*, 172–173

## Gram-positive *Staphylococcus aureus*, 172–173

## Graphene, 301–302

## properties, 301–302

## structure, 301*f*

## Graphene oxide (GO), 10, 85

## Green composites, 123

## H

## Hamiltonian operator, 306–307

## HAp covered cellulose nanofiber scaffold (HAp/ CMC), 82–83

## Hartree–Fock (HF) theory, 307–308

## Hemostasis, 172

## Hexagonal HAp, 344*f*

## Higuchi model, 225

## Human amniotic membrane (HAM), 5

## Human bone marrow-derived stromal cells (hMSCs), 410–413

## Human dental pulp stem cells (HDPSCs), 419–421

## Human hand

## description, 64

## grasping and gripping, 63–64

## Hydrogels, chitosan composites as, 106

## Hydrothermal/solvothermal method, 211–212

## Hydroxyapatite (HAp), 8, 146*t*, 205, 251–252, 335*t* bioactivity of, 214–216

## bone–material interface, cellular mechanism at, 215–216

## resorption of hydroxyapatite, 216

## as biomaterial for bone regeneration, 343–347

## calcium hydroxyapatite, basic structure of, 207–209

## challenges and limitations of, 233–235

## characterizations of, 213–214

## Fourier transform infrared spectroscopy (FTIR), 214

## mechanical characterization, 214

## Raman spectroscopy, 213

## X-ray powder diffraction, 213

## as coating material, 231–233

## complications of, 234–235

## crystal structure of, 208*f*

## in dental applications, 226–228

## dental fillers, 227

## dental implants, 227–228

## enamel restoration, 226–227

## as a drug delivery vehicle for antibiotics in bone infection, 220–225

## drug release kinetics, 224–225

## hexagonal and monoclinic crystal structure of, 209*t*

- role of elemental doping in, 216–220
    - aluminum-doped hydroxyapatite, 217–218
    - anion-doped hydroxyapatite, 220
    - iron-doped hydroxyapatite, 219
    - lithium-doped hydroxyapatite, 217
    - magnesium-doped hydroxyapatite, 218–219
    - manganese-doped hydroxyapatite, 219
    - selenium-doped hydroxyapatite, 217
    - silver-doped hydroxyapatite, 218
    - zinc-doped hydroxyapatite, 219–220
    - zirconium-doped hydroxyapatite, 218
  - and stem cell differentiation, 228–230
    - adult stem cells, 229
    - embryonic stem cells, 228
    - hydroxyapatite interaction with stem cells, 229
    - mechanism of osteoblast differentiation of mesenchymal stem cells, 229–230
    - mesenchymal stem cells, 229
  - synthesis route, biomimetic techniques, 212–213
  - synthesis route, chemical methods, 211–212
    - chemical precipitation method, 211
    - emulsion technique, 212
    - hydrothermal/solvothermal method, 211–212
    - sol–gel method, 211
    - sonochemical technique, 212
  - synthesis route, physical method, 210
    - mechanochemical technique, 210
    - solid state method, 210
  - in the treatment of osteomyelitis, 230–231
  - variable phases of, 206*t*
  - Hydroxyapatite-based dental resin composites, 251
    - biocompatibility issues, 280–282
    - chemicophysical properties of HA-based composite, 266
    - degree of conversion, 266–269
    - dental composites, 252–258
      - filler typologies, 255–258
      - polymerization process, 254
      - resin matrix for, 252–254
    - future trends, 282–284
    - hydroxyapatite crystal morphologies, 258–265
      - fibers, 263
      - spheroidal particles, 258–260
      - urchin-like, 263–265
      - whiskers, 261–263
    - mechanical properties, 274–280
    - optical properties, 271–272
    - shrinkage, 269–271
    - sorption/solubility in water, 272–274
  - Hydroxyapatite/chitosan microparticles, preparation of, 354–357
  - Hydroxyapatite/chitosan nanocomposite materials, 350–354
    - sterilization, 359–361
  - Hydroxyapatite/chitosan scaffolds, preparation of, 357–359
  - 2-Hydroxyethyl methacrylate (HEMA), 253
- ## I
- iGrab orthotic device, 65*f*
  - Immature collagen fibers, 102–103
  - Implant assisted bacterial infection (IABI), 231–233
  - Inkjet bioprinting, 472
  - Inorganic–organic hybrid materials, 351
  - Integra, 99*t*
  - Interpenetrating polymer networks (IPNs), 351–352
  - In vitro tissue engineering technologies for cancer research, 465–477
    - bio-printing, 471–474
    - microchips and microfluidics, 474–476
    - 3D cell cultures, 465–471
      - liquid methods, 466
      - scaffolds, 466–471
  - Iron-doped hydroxyapatite, 219
- ## L
- L-Lactic acid, 136
  - Lactobacillus acidophilus*, 251
  - Laser guided bioprinting, 472
  - Laser induced bioprinting, 472
  - Laser-spinning method, 405
  - Linear strains, 54, 56
  - Lithium-doped hydroxyapatite, 217
  - Liver tissue engineering, 185–186
- ## M
- Magnesium-doped hydroxyapatite, 218–219
  - Magnetic levitation method, 466
  - Manganese-doped hydroxyapatite, 219
  - Mast cells, 102–103
  - Matrix metalloproteinase (MMP), 106–107
  - MC3T3-E1 preosteoblasts, 9
  - Mechanochemical technique, 210
  - Medical textiles, 71
  - Melt-derived processing, 406
  - 6-Mercaptopurine, 133
  - Mesenchymal stem cells (MSCs), 229, 333, 410–413
  - Mesoporous bioactive glass (MBG), 386, 403–404
  - Mesoporous bioactive glass nanofibers (MBGNFs), 410–413



- Mesoporous silica-based nanoparticles (MSNs), 415–417
- Mesoporous silica nanoparticles loaded with silver nanoparticles (Ag-MSNs), 89
- Metacarpophalangeal (MCP) joint, 64
- Metal and metal oxide filler, 446–447
- Metallic-bioactive glasses, 402
- Metals, 206, 303
- Methyl methacrylate, 253, 443*f*. *See also* Polymethyl methacrylate (PMMA)
- Metropolis algorithm, 308
- Microchips and microfluidics, 474–476
- Microemulsion method, 405
- Microextrusion method, 472
- Microspheres, 106, 386
- Mitomycin C (MMC)-loaded PLLA, 88
- MMC-loaded PLLA fibrous membranes, production of, 87*f*
- Molecular electrostatic potential maps (MESP), 310–311
- Molecular mechanics (MM), 305–306
- Monomers, defined, 297
- Monte Carlo method, 308, 311–313, 311*f*
- Mucin, 171–172
- Mucoadhesion, 171–172
- Multicellular tumor spheroids, 465
- Multijets
- from multiple needles, 80
  - from needleless systems, 81
  - from a single needle, 80
- Multiple needle electrospinning (MNE), 80
- Multiwalled carbon nanotubes (MWCNTs), 9–10
- functionalized MWCNTs, 10
- Musculoskeletal systems (MSs), 71–72
- N**
- N*-acetyl-D-glucosamine, 104
- Nanocrystalline forsterite (NF), 410–413
- Nanoengineered scaffolds, in regenerative medicine, 2–3
- Nanofiller-based polymethyl methacrylate composite for dentist, 448–451
- mechanical properties, 448
  - wear properties, 448–451
- Nanofillers, 444–447
- fiber filler, 447
  - metal and metal oxide filler, 446–447
- NanoHAp/poly-L-lactic acid (n-HA/PLLA) fibrous layer, 86
- Nanohydroxyapatite (n-HAp), 332, 355
- Nanohydroxyapatite/chitosan nanocomposites for bone tissue regeneration, 331
- bone biology, 333–334
  - chitosan as biomaterial for bone regeneration, 347–350
  - commercially available bone grafts, 337–342
  - hydroxyapatite as biomaterial for bone regeneration, 343–347
  - hydroxyapatite/chitosan microparticles, preparation of, 354–357
  - hydroxyapatite/chitosan nanocomposite materials, 350–354
  - sterilization, 359–361
  - hydroxyapatite/chitosan scaffolds, preparation of, 357–359
  - ideal bone graft, 335–337
  - biocompatibility, 335
  - biodegradability, 336
  - manufacturing technology, 336–337
  - mechanical properties, 336
  - structural requirements, 336
- Nanomedicine, 1, 12
- Nanostructured polymers as tissue engineering scaffolds, 3–12
- blended polymers for smart hybrid scaffold fabrication, 7–8
  - nanostrategies combined with polymeric scaffolds, 8–12
  - natural and synthetic polymers, 4–6
- Nano titanium based dental composite resin, 441
- experimental
- characterization, 452
  - materials, 452
  - preparation of Ti/polymethyl methacrylate composite, 452
- mechanical analysis, 452–454
- tensile test, 452
  - wear test, 453–454
- morphological analysis, 454–455
- nanofiller-based polymethyl methacrylate composite for dentist, 448–451
- mechanical properties, 448
  - wear properties, 448–451
- nanofillers, 444–447
- fiber filler, 447
  - metal and metal oxide filler, 446–447
  - polymethylmethacrylates, 442–444
  - thermal analysis, 458
- Natural and synthetic polymer–bioactive glass composites, 380–383
- Natural bone, 28*t*, 333
- Natural fibers' use in biocomposites, 147
- Natural muscles, 45–46
- Natural polymers, 3–6, 127*t*
- Natural sources, classification of fibers obtained from, 124*f*, 125
- Nerve tissue engineering, 186–188

Neutral hollow metal rod (NHMR), 86  
 Neutral metal disc (NMD), 86  
 Nitrogen annealing, 53  
 Nondegradable materials, physical properties of, 28*t*  
 Nonmesoporous BG, 386  
 Nonprehensile movements, 63  
 Norfloxacin, 188–189  
 Nylon 6,6, 48–50

## O

Omega LCL-010, 60  
 Orthopedic system, polylactic acid composites in, 132–133  
 Orthotic hand, 68  
   CAD model of, 65*f*  
 Osseointegration, 345  
 Osteoblasts, 32–33, 230, 333  
   characteristics and functions of, 24*t*  
 Osteocalcin (OCN), 410–413  
 Osteoclasts, 216, 333  
   characteristics and functions of, 24*t*  
 Osteoconductive graft, 335  
 Osteocytes, 333  
   characteristics and functions of, 24*t*  
 Osteogenesis, 336  
 Osteoinductive graft, 335  
 Osteomyelitis (OM), hydroxyapatite in the treatment of, 230–231

## P

Pauli's exclusion principle, 307–308  
 PEG/PCL/AgNP (PPA), 85–86  
 Permacol, 99*t*  
 Phalanges, 64  
 Phosphate-based bioactive glass, 377  
 Phosphate-bioactive glasses, 401–402  
 Plasma sorption, 172  
 PLGA (polylactic glycolic acid) silk composite nanofibrous scaffold, 147  
 Poly(3-hydroxybutyrate) (P3HB), 381–383  
 Poly(3-hydroxybutyrate-co-3-hydroxyhexanoate) (PHBV), 386–387  
 Poly( $\epsilon$ -caprolactone) (PCL), 9–10, 381–382  
 Poly( $\epsilon$ -caprolactone)/gelatin fibrous (PCL/GT) scaffolds, 84  
 Poly(ethylene glycol)/chitosan scaffold, 188–189  
 Poly(ethylene glycol)-modified chitosan, 191  
 Poly(ethylene glycol dimethyl acrylate) (PEGDMA) scaffolds, 424  
 Poly(ethylene oxide) (PEO), 81, 84  
 Poly(glycerol sebacate) (PGS), 424

Poly(glycerol sebacate)-based nanofibers, 187–188  
 Poly(glycolic acid) (PGA), 381  
 Poly(H-caprolactone) scaffolds, 83  
 Poly(lactic-coglycolic acid) (PLGA), 147, 381  
   PLGA microspheres, 224  
 Poly(L-lactic acid)-co-poly( $\epsilon$ -caprolactone) (PLLA-CL), 84  
 Poly(orthoesters), 132–133  
 Poly(vinyl alcohol) (PVA), 410–413  
 Polycaprolactone (PCL), 423  
 Polydimethylsiloxane (PDMS), 424–425  
 Polydimethylsiloxane (PDMS) modified BGNPs (MBGNPs)-poly(ethylene glycol) (PEG) (PDMS-MBGNPs-PEG) hybrid monoliths, 424–425  
 Polyethylene terephthalate (PET), 441  
 Polyethyl methacrylate (PEMA), 442  
 Poly glycolic acid, physical properties of, 28*t*  
 Polylactic acid (PLA). *See* Polylactide  
   D,L-Polylactic acid, physical properties of, 28*t*  
   L-Polylactic acid, physical properties of, 28*t*  
 Polylactic acid composites, 129–130  
 Polylactic acid (PLA)-silica nanocomposites, 136  
 Polylactide, 125–142, 380, 467  
   biodegradation of, 129  
   medical applications of, 129–133  
     drug delivery system, 131–132  
     orthopedic system, 132–133  
     tissue engineering, 129–130  
     wound management, 130–131  
   physical/mechanical properties of, 129*t*  
   polylactide based microcomposites, 133–134, 137*t*  
   polylactide based nanocomposites, 134–142, 137*t*  
   preparation of, 128*f*  
 Poly-L-lactic acid, physical properties of, 28*t*  
 Polymer–bioactive glass nanocomposites, for bone repair and substitution, 373  
   bioactive glass, 374–379  
     borate-based bioactive glass, 377–378  
     fabrication of bioactive glass scaffolds, 378–379  
     phosphate-based bioactive glass, 377  
     silicate-based bioactive glass, 374–377  
   composite production techniques, 383–388  
     3D printing, 388  
     electrospinning, 384–385  
     freeze-drying, 387–388  
     microspheres, 386  
     solvent casting–particulate leaching (SCPL), 386–387

- Polymer—bioactive glass nanocomposites, for bone repair and substitution (*Continued*)
    - natural and synthetic polymer—bioactive glass composites, 380–383
  - Polymer-foam replication, 407
  - Polymeric nanofibers, 78
  - Polymerization process, 254
  - Polymers as biomaterials, 304
  - Polymethyl methacrylate (PMMA), 300–301, 441–444
    - properties, 300–301
  - Polypyrrole, 108–109
  - Polystyrene scaffolds, 469
  - Polystyrene (PS), 410–413
  - Polyurethane, 298–299
    - applications, 299
    - properties, 298–299
  - Polyurethane/graphene polymeric nanocomposites, 297
    - computational chemistry, 304–308
      - molecular mechanics (MM), 305–306
      - Monte Carlo technique, 308
      - quantum mechanics (QM), 306–308
    - methodology, 310–312
      - determination of the effect of temperature on the nanocomposite, 311–312
      - electrostatic potential map, 311
      - Fourier-transform infrared spectroscopy (FTIR) analysis, 310
      - simulated body fluid characterization, 312
    - molecular properties, 309–310
      - electrostatic potential maps, 310
      - Fourier-transform infrared spectroscopy, 310
      - molecular energy, 309
      - optimization geometry, 309
    - quantitative structure—activity relationships
      - properties, 309
      - partition coefficient, 309
    - polymers, 297–303
      - calcium carbonate, 302–303
      - graphene, 301–302
      - polymethyl methacrylate (PMMA), 300–301
      - polyurethane, 298–299
    - polyurethane/graphene/calcium carbonate nanocomposite, 317–326
      - electrostatic potential map, 326
      - Fourier-transform infrared spectroscopy, 319–326
      - optimization geometry, minimum energy, and partition coefficient, 317–319
    - polyurethane/graphene/polymethyl methacrylate nanocomposite, 312–317
      - electrostatic potential map, 317
      - Fourier-transform infrared spectroscopy, 314–316
      - optimization geometry and partition coefficient, 312–314
  - prostheses, 303–304
    - ceramics, 303
    - metals, 303
    - polymers, 304
    - simulated body fluid (SBF), 304
  - Poly- $\epsilon$ -caprolactone (PCL), 9–10
  - Prehensile movement, 63–64
  - Pristine collagen, 4–5
  - Prosthesis, 303–304
    - materials, 303–304
      - ceramics, 303
      - metals, 303
      - polymers, 304
  - Prosthetic hands, 63–68
    - CAD model of, 65f
    - grasping capability of, 65f
    - 3D printed prototype of, 65f
- ## Q
- Quantitative structure—activity relationships (QSAR), 309
  - Quantum mechanics (QM), 306–308
- ## R
- Raman spectroscopy, 213, 267
  - Rapid prototyping process, 408
  - Rectus orthotopic suturing closure (ROSC), 234–235
  - Regenerative medicine, nanoengineered scaffolds
    - in, 2–3
  - Resin matrix for dental composites, 252–254
  - Resorbable biomaterials, 23
    - bone graft substitutes, chitosan-based material
      - for, 25f, 30–34
      - chitosan-alginate scaffolds, 33
      - chitosan—calcium phosphate based substitutes, 31–32
      - chitosan hydroxyapatite based bone graft substitutes, 32–33
      - chitosan polylactic acid substitute, 34
    - properties of substitutes to act as bone grafts, 27–30
      - biocompatibility, 27
      - mechanical stability and biodegradability, 30
      - osteinduction, 30
      - pore size, 27
      - porosity, 27
      - surface properties, 27–30

Resorbable polymer fiber reinforced composites, 121  
 biocomposites prepared by using resorbable polymeric fibers, 125–147  
 collagen, 142–145  
 polylactide, 125–142  
 silk, 145–147  
 patent literature on, 147–158, 148*t*  
 properties of, 126*t*  
 recent advances and future prospects, 159  
 Roothaan–Hall approximation, 308

## S

Salt-leaching electrospinning (SLE), 88  
 Scaffold, defined, 169–170  
 Schiff base, 177  
 Schrödinger equation, 306  
 Selenium-doped hydroxyapatite, 217  
 Self-healing composites, 70–71  
 Sepiolite, 134  
 Shape memory alloys (SMAs), 48–49  
 Shear modulus, 280  
 Si-based hydroxyapatite substitutes, 26  
 Silica, 146*t*  
 Silicate-based bioactive glass, 374–377  
 Silicate-bioactive glasses, 401  
 Silicone, TCP muscle embedded in, 71  
 Silk, 145–147  
 Silk fibroin (SF), 5  
 Silk fibroin (SF)/hydroxyapatite (HAP) scaffold, 5–6, 10–11  
 Silver coating, 49, 52  
 Silver-doped hydroxyapatite, 218  
 Silver nanoparticles, 136  
 Silver-PLA nanocomposites, 136  
 Simulated body fluid (SBF), 82–83, 212–213, 304  
 Simulated body fluid characterization, 312  
 determination of the effect of temperature and SBF on the nanocomposite, 312  
 Single-needle electrospinning (SNE), 80  
 Skin, 97–98  
 anatomy of, 101–103  
 dermis, 102–103  
 epidermis, 103  
 subcutaneous layer, 102  
 chitosan composites in artificial skin.  
   *See* Chitosan composites  
 functions of, 101–102  
 Skin tissue regeneration, 88–89  
 Smart hybrid scaffold fabrication  
 blended polymers for, 7–8  
 Sodium alginate (SA), 84

Sodium carboxy methyl cellulose (Na-CMC), 82–83  
 Soft actuators, 48–49  
 Sol–gel method, 211, 383–384, 404–405  
 Sol–gel processing, 407  
 Solid state method, 210  
 Solvent casting–particulate leaching (SCPL), 382, 386–387  
 Sonochemical technique, 212  
 Soy protein isolated (SPI), 84  
 Spheroidal particles, 258–260  
 Spinner bioreactor, 466  
 Split thickness model, 114  
 Sponges, 178  
   chitosan composites as, 104–106  
*Staphylococcus aureus*, 136, 382–383  
 Static loading, 60  
 Static suspension method, 466  
 Stem cell differentiation, hydroxyapatite and, 228–230  
   hydroxyapatite interaction with stem cells, 229  
   mechanism of osteoblast differentiation of mesenchymal stem cells, 229–230  
 Stem cells  
   hydroxyapatite interaction with, 229  
   types of, 228–229  
     adult stem cells, 229  
     embryonic stem cells, 228  
     mesenchymal stem cells, 229  
 Sterilization, 359–360  
 Stober process, 256  
 Strain and force measurement, 56–60  
 Strength retention period, 125  
*Streptococcus sobrinus*, 251  
 Stromal cells, 229  
 Supercritical CO<sub>2</sub> (scCO<sub>2</sub>), 361  
 Synthetic polyesteric polymers, 97–98  
 Synthetic polymers, 3–6, 381  
 Syvek-Patch, 99*t*

## T

Tegasorb, 99*t*  
 Tendonitis, 85  
 Tendon tissue regeneration, 82–88  
   electrospinning (ES) process for, 82–88  
 Tensile actuation strain, 57  
 Thermogravimetric analysis (TGA), 134  
 3D cell cultures, 465–471  
   liquid methods, 466  
   scaffolds, 466–471  
 3D electrospun poly( $\epsilon$ -caprolactone) scaffolds, 468–469  
 3D printing technique, 388

Ti/polymethyl methacrylate composite, preparation of, 452

Tissue engineering triad, 1

Tissue regeneration, commercial formulations for, 99*t*

Trabecular bones, 23

Training of the muscle, 53–54

Transcyte, 99*t*

TraumaStat, 99*t*

Triethylene glycol dimethacrylate (TEGDMA), 251, 253

*N,N,N*-Trimethyl chitosan, 172–173

Trypsin, 129

Twisted and coiled polymer (TCP) muscles

- 1-ply, 2-ply and 3-ply silver-coated TCP muscles, 62*f*, 72
- biomedical applications of, 63–71
  - fecal incontinence (FI) treatment, 68
  - medical textiles, 71
  - orthotic hand, 68
  - prosthetic hands, 63–68
  - self-healing composites, 70–71
  - variable stiffness actuators (VSAs), 68–70
- characteristics and properties of, 54–63
  - force measurement, 60–61
  - frequency measurement and pulsed actuation, 61
  - microscopy, 61–63
  - strain and force measurement, 56–60
- characteristics of, 51*f*
- comparison with other soft actuators, 48–49
- displacement/strain measurement of, 51*f*
- fabrication of, 46, 47*f*, 49–54, 51*f*, 55*t*
  - annealing (heat treatment), 52–53
  - coiling, 50–52
  - training, 53–54
  - twisting, 49–50
- locking mechanism for, 65*f*, 66–68
- robotic application of, 71–72

- artificial musculoskeletal systems, 71–72
- TCP muscle embedded in silicone, 71
- structures and working principles of, 46–48

## U

Urchin-like hydroxyapatite (UHA), 258, 263–265

Urethane dimethacrylate (UDMA), 253

## V

Variable stiffness actuators (VSAs), 68–70

Vascular endothelial growth factor (VEGF), 410–413

Vickers hardness (HV), 214, 268, 446–447

Viscoelasticity, 110–112

Vulnosorb, 99*t*

## W

Whiskers, 261–263

Wound healing, 106–108, 110–112, 188–189
 

- chitosan composites for, 112–114
- commercial formulations for, 99*t*
- functioning of artificial skin in, 101*f*

Wound management
 

- polylactic acid composites in, 130–131

## X

Xenograft, 337–338

X-ray powder diffraction, 213

## Y

Young's modulus, 133, 423

## Z

Zinc-doped hydroxyapatite, 219–220

Zinc oxide (ZnO) NPs, 9

Zirconium-doped hydroxyapatite, 218